

Linda M. Ernst · Eduardo D. Ruchelli · Dale S. Huff
Editors

Color Atlas of Fetal and Neonatal Histology

Color Atlas of Fetal and Neonatal Histology

Color Atlas of Fetal and Neonatal Histology

Editors

Linda M. Ernst, MD, MHS

Northwestern University, Feinberg School of Medicine
Department of Pathology, Chicago, Illinois, USA

Eduardo D. Ruchelli, MD and Dale S. Huff, MD

The Children's Hospital of Philadelphia, Department of Pathology
Philadelphia, Pennsylvania, USA

 Springer

<http://bookmedico.blogspot.com>

Editors

Linda M. Ernst, MD, MHS
Northwestern University
Feinberg School of Medicine
Department of Pathology
Chicago, Illinois
USA
linda-ernst@northwestern.edu

Eduardo D. Ruchelli, MD
The Children's Hospital of Philadelphia
Department of Pathology
Philadelphia, Pennsylvania
USA
ruchelli@email.chop.edu

Dale S. Huff, MD
The Children's Hospital of Philadelphia
Department of Pathology
Philadelphia, Pennsylvania
USA
huff@email.chop.edu

ISBN 978-1-4614-0018-9 e-ISBN 978-1-4614-0019-6
DOI 10.1007/978-1-4614-0019-6
Springer New York Dordrecht Heidelberg London

Library of Congress Control Number: 2011932987

© Springer Science+Business Media, LLC 2011

All rights reserved. This work may not be translated or copied in whole or in part without the written permission of the publisher (Springer Science+Business Media, LLC, 233 Spring Street, New York, NY 10013, USA), except for brief excerpts in connection with reviews or scholarly analysis. Use in connection with any form of information storage and retrieval, electronic adaptation, computer software, or by similar or dissimilar methodology now known or hereafter developed is forbidden.

The use in this publication of trade names, trademarks, service marks, and similar terms, even if they are not identified as such, is not to be taken as an expression of opinion as to whether or not they are subject to proprietary rights.

While the advice and information in this book are believed to be true and accurate at the date of going to press, neither the authors nor the editors nor the publisher can accept any legal responsibility for any errors or omissions that may be made. The publisher makes no warranty, express or implied, with respect to the material contained herein.

Printed on acid-free paper

Springer is part of Springer Science+Business Media (www.springer.com)

Dedication

This book is dedicated to all the families who have struggled with fetal loss or the death of a neonate. We hope that by encouraging the careful study of fetal and neonatal tissues we have contributed to their healing process.

Preface

The impetus for the writing of this book came largely from the many students and residents in pathology who spent time on the perinatal autopsy service and frequently asked us what reference they could turn to for a review of normal fetal histology.

The inspiration for this book is one of the few references that does exist, although out of print, the volume entitled *Histology of the Fetus and Newborn* by Dr. Valdes-Dapena, published in 1979. This reference served as the model for ours, and we constantly turned to it for verification and help in deciding what to include and what not to include. We hope the quality of our volume is comparable to the standards set by Dr. Valdes-Dapena.

The main goal for us was to provide an atlas of fetal and neonatal histology for use by pathology trainees and attending pathologists who have to deal with fetal tissues at autopsy. However, any scientist who might be examining fetal tissues outside of routine pathology might also find this a useful volume. Since there are dramatic changes in many of the fetal tissues over gestation, it is important for the examiner to understand normal development and histology, especially when attempting to decide if a particular finding is pathologic. We have attempted to describe the

histology of each organ in detail with particular emphasis on the changes throughout the fetal period. An embryology section is included with each chapter to briefly review the important developmental changes as they apply to the appearance of the tissues. The embryology sections are not intended to be a comprehensive review of the subject since the main goal of our book is to highlight the histology.

All the images in this book are obtained from fetal tissues that were formalin fixed and paraffin embedded, unless otherwise stated. Fetal dates were generally obtained by clinical gestational age estimates (menstrual age) and corroborated by fetal morphologic measurements. Since embryologists and embryology texts frequently refer to postfertilization dates, dates prior to 12 weeks are generally postfertilization. The magnifications listed after each image represent the objective power used when taking the photomicrograph. No attempt to calculate exact magnification is made, since most pathologists can relate to objective power more easily.

We hope this book will teach others as much as we have learned in the process of writing it, and inspire the next generation of scientists interested in the microscopic anatomy of fetal tissue

Linda M. Ernst
Eduardo D. Ruchelli
Dale S. Huff

Contributors

Scott Bourne, MD

Staff Pathologist
Department of Pathology
Physicians Regional Medical Center
Naples, USA

Linda M. Ernst, MD, MHS

Assistant Professor of Pathology
and Director of Perinatal Pathology
Department of Pathology
Northwestern University
Feinberg School of Medicine
Chicago, USA

Dale S. Huff, MD

Senior Pathologist
Department of Pathology
and Laboratory Medicine
The Children's Hospital of Philadelphia
Philadelphia, USA
Associate Professor
Department of Pathology
and Laboratory Medicine
The University of Pennsylvania
School of Medicine
Philadelphia, USA

Portia A. Kreiger, MD

Staff Pathologist
Department of Pathology
Nemours/A.I. duPont Hospital for Children
Wilmington, USA

Michele E. Paessler, DO

Hematopathologist and Medical Director
Clinical Immunology and Flow Cytometry
Laboratory, Department of Pathology and
Laboratory Medicine
The Children's Hospital of Philadelphia
Philadelphia, USA
Assistant Professor
Department of Pathology
and Laboratory Medicine
University of Pennsylvania
School of Medicine
Philadelphia, USA

Veena Rajaram, MD

Staff Pathologist/Neuropathologist
Department of Pathology
and Laboratory Medicine
Children's Memorial Hospital
Chicago, USA
Assistant Professor
Department of Pathology
Northwestern University Feinberg
School of Medicine
Chicago, USA

Eduardo D. Ruchelli, MD

Associate Pathologist and Director of
Autopsy Service
Department of Pathology
and Laboratory Medicine
The Children's Hospital of Philadelphia
Philadelphia, USA
Associate Professor
Department of Pathology
and Laboratory Medicine
University of Pennsylvania
School of Medicine
Philadelphia, USA

Pierre Russo, MD

Director
Division of Anatomic Pathology
Department of Pathology
and Laboratory Medicine
The Children's Hospital of Philadelphia
Philadelphia, USA
Professor
Department of Pathology
and Laboratory Medicine
University of Pennsylvania
School of Medicine
Philadelphia, USA

Contents

SECTION I Cardiovascular System

Chapter 1

Heart and Blood Vessels	3
Linda M. Ernst	

SECTION II Respiratory Tract

Chapter 2

Lung	21
Portia A. Kreiger	

SECTION III Digestive System

Chapter 3

Gastrointestinal Tract.	39
Dale S. Huff	

Chapter 4

Liver	67
Pierre Russo	

Chapter 5

Pancreas.	79
Eduardo D. Ruchelli	

Chapter 6

Salivary Glands	87
Eduardo D. Ruchelli	

SECTION IV Genitourinary Tract

Chapter 7

Kidney	105
Eduardo D. Ruchelli and Dale S. Huff	

Chapter 8

Urinary Bladder.	117
Eduardo D. Ruchelli and Dale S. Huff	

Chapter 9

Testis.	121
Dale S. Huff	

Chapter 10

Epididymis	143
Dale S. Huff and Eduardo D. Ruchelli	

Chapter 11

Vas Deferens	153
Linda M. Ernst, Eduardo D. Ruchelli, and Dale S. Huff	

<i>Chapter 12</i>	
Seminal Vesicle	157
Linda M. Ernst, Eduardo D. Ruchelli, and Dale S. Huff	
<i>Chapter 13</i>	
Prostate Gland	163
Linda M. Ernst, Eduardo D. Ruchelli, and Dale S. Huff	
<i>Chapter 14</i>	
Ovary	173
Eduardo D. Ruchelli and Dale S. Huff	
<i>Chapter 15</i>	
Fallopian Tubes	181
Eduardo D. Ruchelli and Dale S. Huff	
<i>Chapter 16</i>	
Uterus	187
Eduardo D. Ruchelli and Dale S. Huff	
<i>Chapter 17</i>	
Vagina	195
Eduardo D. Ruchelli and Dale S. Huff	
SECTION V Endocrine System	
<i>Chapter 18</i>	
Adrenal Gland	201
Linda M. Ernst	
<i>Chapter 19</i>	
Thyroid Gland	213
Linda M. Ernst	
<i>Chapter 20</i>	
Parathyroid Gland	225
Linda M. Ernst	
<i>Chapter 21</i>	
Pituitary Gland	231
Linda M. Ernst	
SECTION VI Hematolymphoid System	
<i>Chapter 22</i>	
Thymus Gland	241
Linda M. Ernst	
<i>Chapter 23</i>	
Spleen	251
Linda M. Ernst	

<i>Chapter 24</i>	
Lymph Nodes and Lymphatics	261
Michele E. Paessler	
<i>Chapter 25</i>	
Palatine Tonsil	267
Linda M. Ernst	
<i>Chapter 26</i>	
Bone Marrow	273
Michele E. Paessler and Scott Bourne	
SECTION VII Central Nervous System	
<i>Chapter 27</i>	
Brain and Spinal Cord	285
Veena Rajaram	
SECTION VIII Musculoskeletal System	
<i>Chapter 28</i>	
Bone	323
Linda M. Ernst	
<i>Chapter 29</i>	
Skeletal Muscle	337
Linda M. Ernst	
SECTION IX Mammary Gland	
<i>Chapter 30</i>	
Mammary Gland	347
Dale S. Huff	
SECTION X Placenta	
<i>Chapter 31</i>	
Placenta	363
Linda M. Ernst	
Appendix	389
Index	391

SECTION I

Cardiovascular System

1

Heart and Blood Vessels

Linda M. Ernst

The fetal myocardium has a distinctive histological appearance that differs from the histological appearance of adult myocardium. Familiarity with these differences is important when examining fetal tissues. In addition, there are specific vascular structures, such as the umbilical vein and ductus arteriosus, that represent components of the fetal circulation and are only normally present during gestation and in the early neonatal period. This chapter highlights the histological features of the fetal and neonatal heart, and some of these unique vascular structures during fetal life.

Embryology

Formation of the human heart is a complex developmental process that is reviewed more extensively in embryology texts [1,2]. It is reviewed briefly in this chapter for background purposes and as needed to assist in the understanding of cardiac anatomy and structure of the endocardium, myocardium, and epicardium. The heart begins to form from bilateral angiogenic clusters located in the splanchnic mesoderm of the embryo. These clusters form into the bilateral endocardial tubes that fuse with the folding of the embryo around 21 to 22 days postconception. The developing heart tube is suspended in the pericardial cavity by a dorsal mesocardium and surrounded by two mesodermal layers, the cardiac jelly and the epimyocardial mantle. Cells that invade the cardiac jelly will become the endothelium and the cardiac tube becomes divided into three layers: endocardium, myocardium, and epicardium. The cardiac tube is initially a straight tube with its cranial end attached to the branchial arches. The intrapericardial portion consists of the bulbus cordis and ventricular tissues, and the caudal end, or atrial portion, is embedded in the septum transversum.

As the heart tube elongates, it also bends, a process known as *formation of the cardiac loop*, which begins on day 23. The cephalic portion of the heart tube moves ventrally, caudally, and to the right while the caudal portion moves dorsally, cranially, and to the left. During this process of looping, which is completed around day 28, the cranial portion of the heart tube gives rise to the truncus arteriosus, the conus cordis, and the trabeculated part of the right ventricle (derived from the bulbus cordis). The ventricular portion of the heart tube gives rise to the primitive left ventricle and the atrial portion of the heart tube becomes incorporated into the pericardium as it takes its dorsal position.

Partitioning of the chambers begins around day 27 postconception. The atrial septum forms from two distinct membranes: septum primum and septum secundum. Septum primum appears first and grows downward toward the endocardial cushions but does not reach the endocardial cushions, leaving an opening known as *ostium primum* that is later closed by growth of the endocardial cushions. Fenestrations appear in the upper portion of septum primum. These openings coalesce and form an opening known as *ostium secundum*. Subsequently, septum secundum, the second interatrial membrane, begins to form to the right of septum primum. It is an incomplete septum with the upper solid portion overlapping the ostium secundum and a more inferior ovoid defect known as foramen ovale. Therefore, shunting blood from the right atrium occurs across the interatrial septum through the foramen ovale, over the free edge of septum primum, and into the left atrium.

The common atrioventricular canal, which encompasses the lower atrial and upper ventricular portions in the center of the heart, is closed by formation of the lateral, superior, and inferior endocardial cushions that appear as bulges of myocardium and fuse to form two separate left and right atrioventricular canals. The majority of the ventricular septum is formed while the two primitive ventricles are enlarging. The medial walls of the two enlarging ventricles fuse and form a nearly complete interventricular septum with a small opening just inferior to the endocardial cushions. This opening persists until conal septal formation is complete and the upper portion of the ventricular septum, also known as the *membranous septum*, is closed by the union of

portions of the right and left conal swellings and the inferior atrioventricular cushion.

The outflow of the ventricles is created by the formation of the conal swellings within the conus cordis and the truncal swellings within the truncus arteriosus. The truncal swellings appear in about the fifth week postconception as ridges that form from the right superior and left inferior truncal walls. These ridges grow toward each other and twist around one another, creating the spiral aorticopulmonary septum. Within the more proximal cordis conus, similar bilateral swellings appear and grow upward, meeting the aorticopulmonary septum. The conal swellings also fuse with the inferior atrioventricular cushion to close the upper portion of the interventricular septum.

Histology

The low-power appearance of the fetal and neonatal myocardium is quite different from the appearance of adult myocardium. The striking difference is the cellularity of the myocardium (see Fig. 1-1). The fetal myocardial cells are generally smaller than adult myocardial cells and have higher nuclear to cytoplasmic ratios. The traditional view has been that the number of cardiac myocytes is established at birth and there is little regenerative capacity among the population of terminally differentiated myocardial cells. However, this paradigm has been challenged recently with the discovery of a

cardiac stem cell population with regenerative capacity [3]. Nevertheless, the highly cellular appearance of the fetal myocardium is not maintained throughout life.

Despite these morphologic cellular differences, the basic histological structure of the fetal heart is not different from the adult heart. The majority of the heart consists of three principle layers: epicardium, myocardium, and endocardium. Additionally, there are specialized tissues such as the fibrous skeleton, valves, and conduction system that can be examined if they are specifically sampled for histological study.

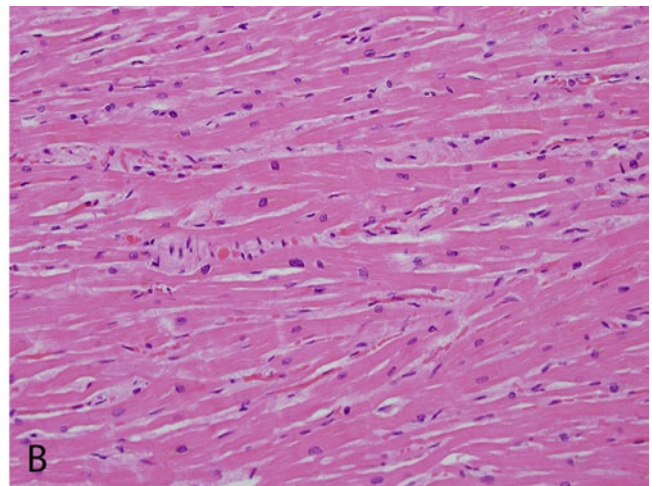
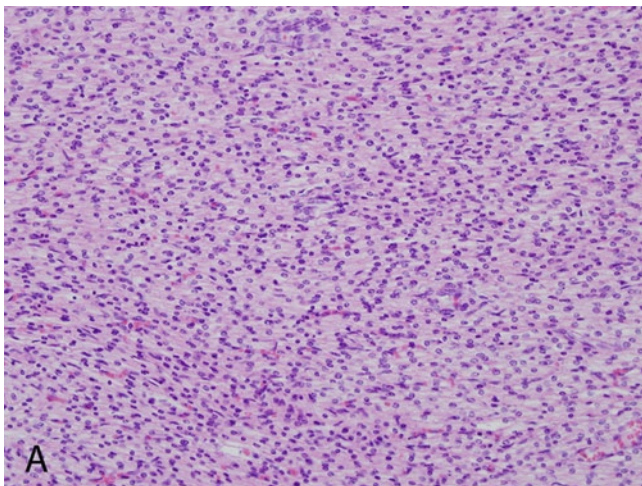


FIGURE 1-1. Comparison of fetal and adult myocardium. **A**, Fetal myocardium at 23 weeks gestation and **B**, adult myocardium is shown. Note the marked hypercellularity and higher nuclear to

cytoplasmic ratio of the fetal myocardium compared with the adult myocardium. (Hematoxylin and eosin [H&E], 20 \times .)

Pericardium

The heart is surrounded by a fibrous sac, the pericardium (parietal pericardium), which grossly is a thin membrane in the fetus. Anatomically, the parietal pericardium is in continuity with the serous (visceral) pericardium, also known as the epicardium, at the pericardial reflections over the great vessels [4]. The fibrous pericardial sac may normally contain a small amount of serous fluid in the fetal and neonatal period, and in macerated fetuses it may

contain abundant serosanguineous fluid. Histologically, the pericardial sac consists of a core of dense connective tissue and is lined on the inner surface by a flattened layer of mesothelial cells (see Fig. 1-2). In fetuses and neonates, the outer layer of the pericardium consists of loose connective tissue with occasional blood vessels and without significant adipose tissue. Heterotopic thymic or thyroid tissue can be seen in the pericardial sac [4].

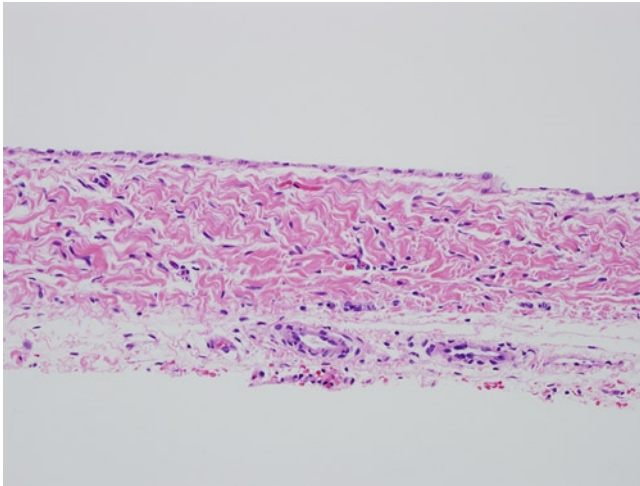


FIGURE 1-2. Fetal pericardium at 23 weeks gestation. The fetal pericardium is a delicate, membranous structure with a simple squamous epithelium and a layer of underlying dense connective tissue. In the adult, the loose connective tissue outside the pericardium can contain adipose tissue, but there is usually little adipose tissue in the fetus. (H&E, 20 \times .)

Epicardium

The external surface of the heart, known as *epicardium*, or alternatively the *visceral pericardium*, is composed of a simple squamous layer of mesothelial cells and variable amounts of underlying connective tissues (see Fig. 1-3). Early in fetal life, the amount of connective tissue is quite sparse, but becomes thicker with increasing

gestational age (see Fig. 1-4). The epicardial connective tissues consist mainly of fibrous connective tissue that contains epicardial coronary vessels. Nerves are also seen within the connective tissue. Fat is not a prominent feature of the fetal epicardium; however, some adipose tissue is seen near term.

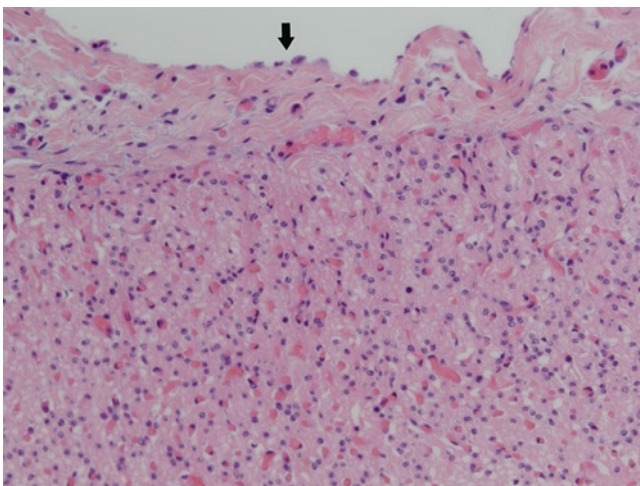


FIGURE 1-3. Fetal epicardium at 34 weeks gestation. The epicardium is composed of a connective tissue layer with flattened mesothelial layer (*arrow*). Note the fairly sharp demarcation between the underlying myocardium and the connective tissue of the epicardium. (H&E, 20 \times .)

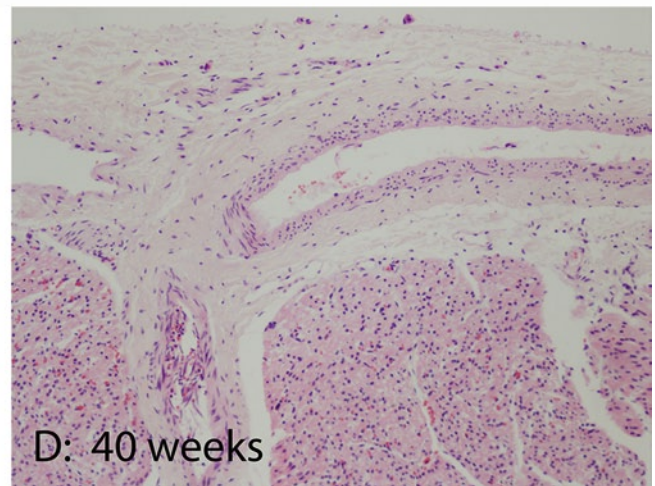
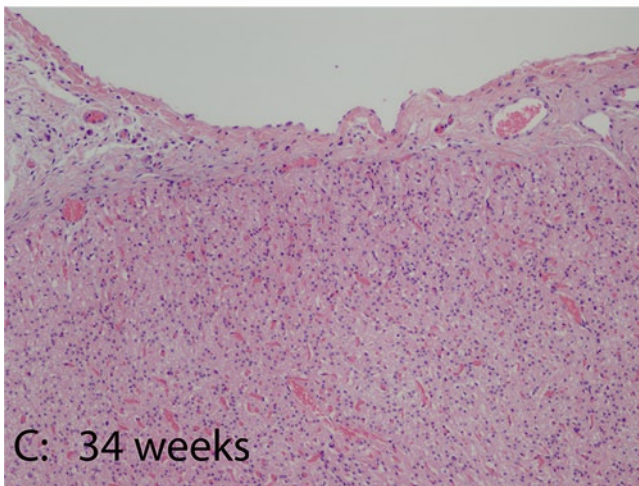
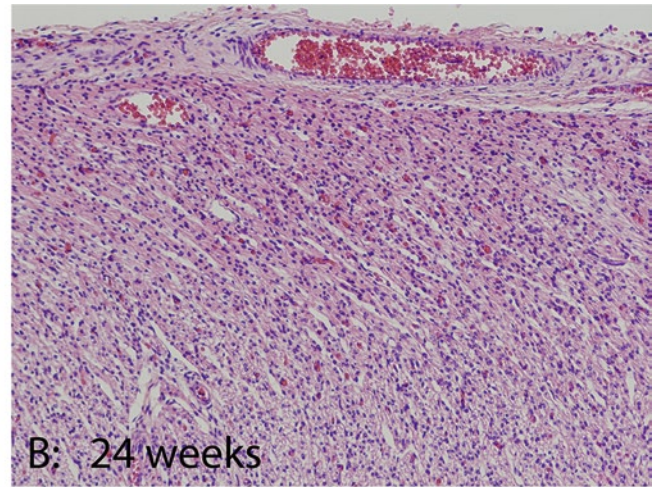
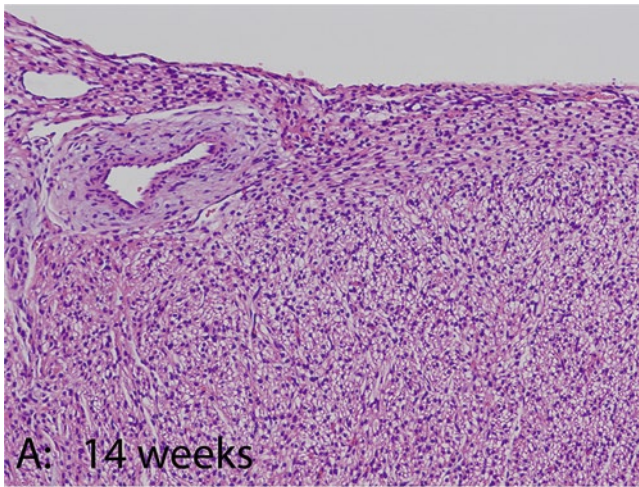


FIGURE 1-4. Epicardium of the heart during gestation. The epicardium of the heart is shown at gestational ages **A**, 14 weeks; **B**, 24 weeks; **C**, 34 weeks; and **D**, 40 weeks. Note the increasing

thickness of the epicardial connective tissue with increasing gestational age. Epicardial coronary arteries are present within the epicardium. (H&E, 10 \times .)

Myocardium

The middle, thickest histological layer of the atrial and ventricular wall is the myocardium, which is composed of cardiac-type muscle fibers with striated cytoplasm, centrally placed nuclei, and intercalated discs. Sections of the fetal myocardium show both longitudinal fibers and cross-sections of the cardiac myocytes, arranged loosely in bundles. Early fetal myocytes frequently appear to have clear, vacuolated cytoplasm secondary to high glycogen content. This change appears most prominently in the midtrimester to early third trimester (see Fig. 1-5). As the fetus approaches term, the clearing of the fetal myocyte cytoplasm is generally less prominent (see Fig. 1-6). The myocytes acquire more cytoplasm as term approaches and the cytoplasm becomes more eosinophilic.

Myocardial cell nuclei are generally ovoid to slightly elongate with smooth nuclear borders. Cells with features

of Anitschkow cells, also known as *Anitschkow nuclear structure*, have been described to occur commonly in fetal and neonatal hearts [5]. Anitschkow cells are characterized by a caterpillar-shaped nucleus in longitudinal sections and in cross-sections the nucleus shows a central condensation of chromatin with fine fibrillar chromatin extensions to the nuclear membrane. This nuclear appearance has been classically associated with rheumatic heart disease [6, 7]. While Anitschkow cells frequently represent myocytes, the Anitschkow nuclear structure has been described in other cells within the heart such as endothelium, histiocytes, and stromal cells. The significance of this particular nuclear structure is not clear, but it may represent a reactive change to stimuli such as hypoxia [5].

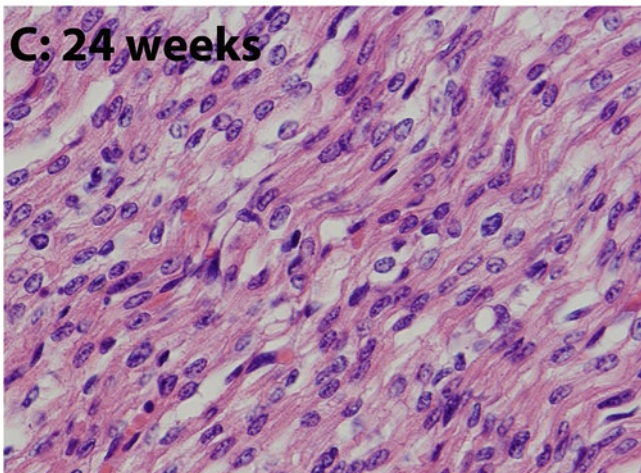
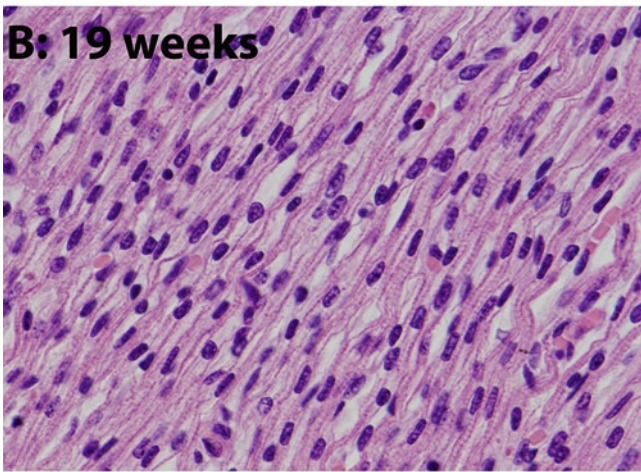
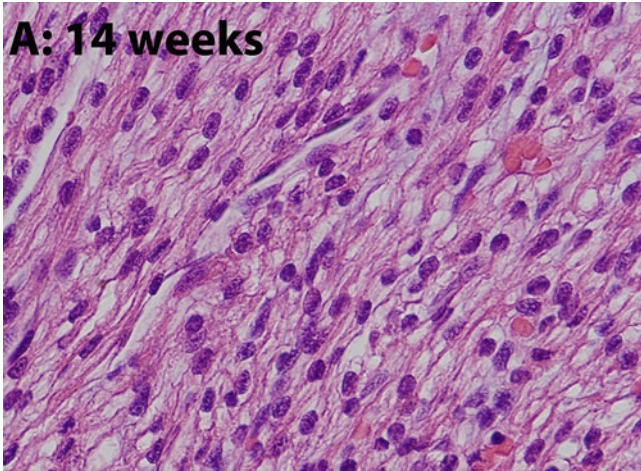
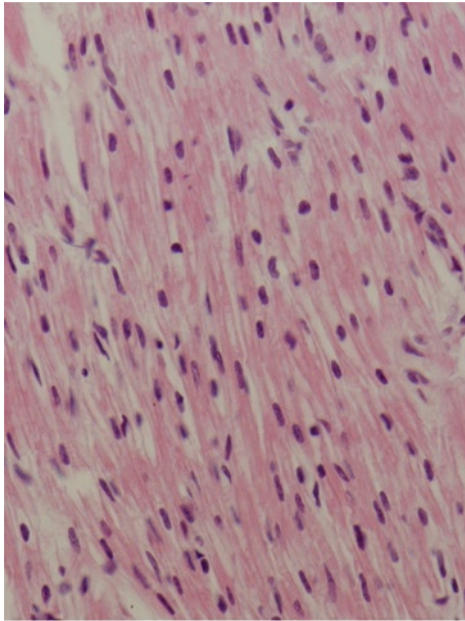
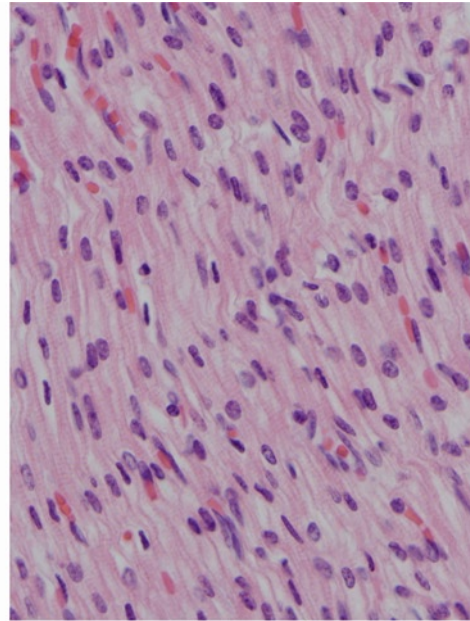


FIGURE 1-5. Myocardium in the second trimester. Myocardium is shown at gestational ages at **A**, 14 weeks; **B**, 19 weeks; and **C**, 24 weeks. (H&E, 40 \times .)



A: 34 weeks



B: 40 weeks

FIGURE 1-6. Myocardium in the third trimester. Myocardium is shown at gestational ages **A**, 34 weeks and **B**, 40 weeks. (H&E, 40 \times .)

Endocardium

The innermost layer of the heart is the endocardium, which appears as a simple squamous layer of flattened endothelial cells supported by a generally very thin, underlying connective tissue layer in the ventricle (see

Fig. 1-7). Atria are also lined by endocardium, but normally the underlying connective tissue, consisting of collagen and elastic fibers, is thicker than in the ventricle (see Fig. 1-8).

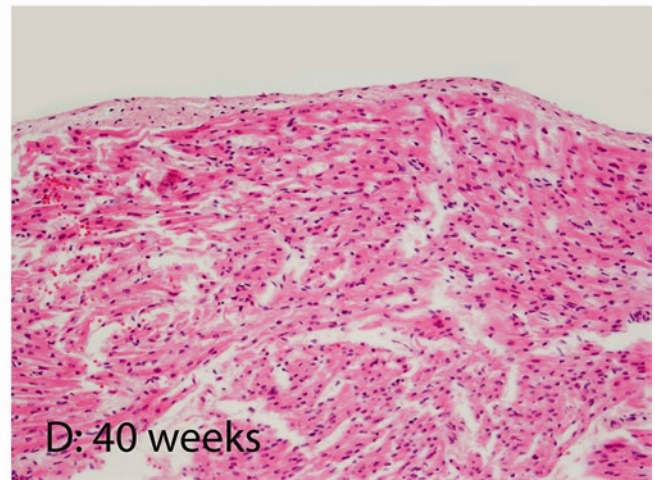
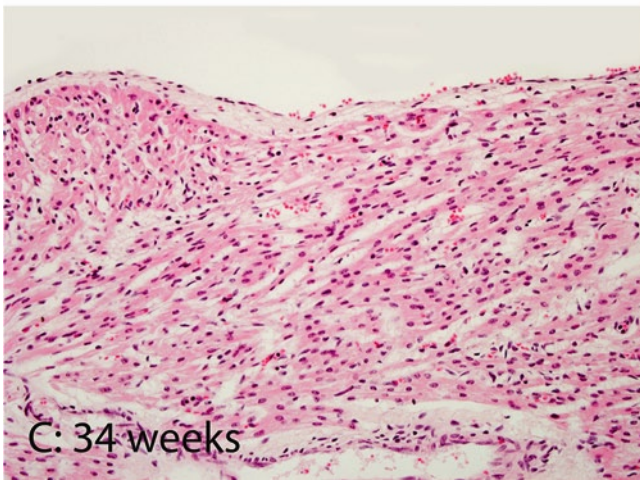
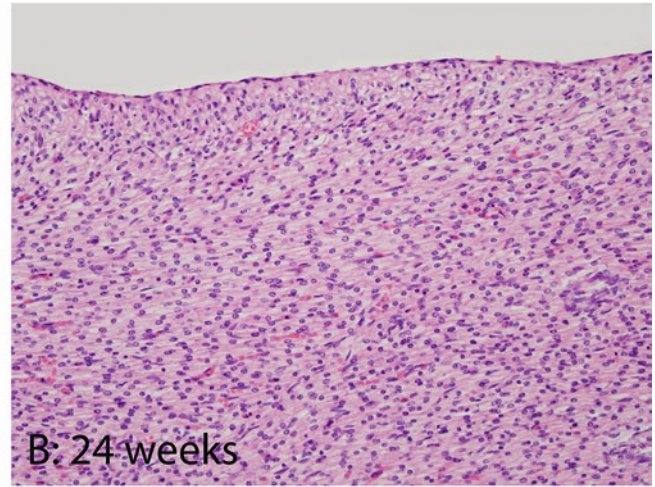
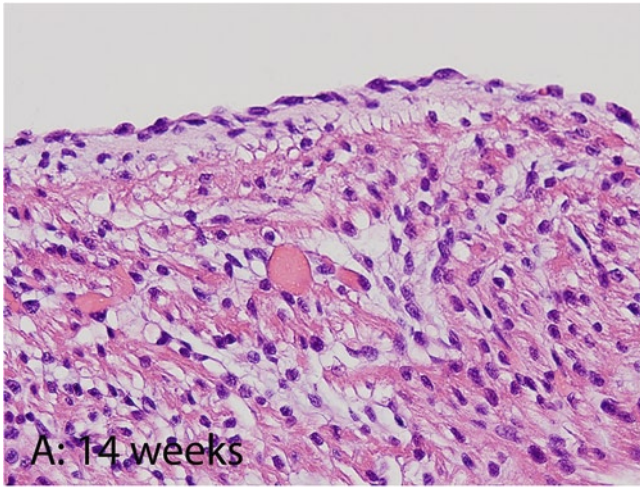


FIGURE 1-7. Endocardium of the left ventricle during gestation. Endocardium of the left ventricle is shown at gestational ages **A**, 14 weeks; **B**, 24 weeks; **C**, 34 weeks; and **D**, 40 weeks

gestation. Note the minimal increase in thickness of the endocardial connective tissue with increasing gestational age. (H&E, 20 \times .)

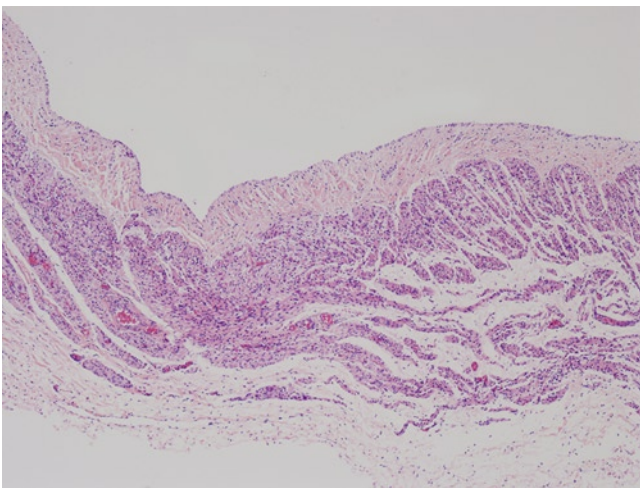


FIGURE 1-8. Right atrium at 23 weeks gestation. The full thickness of the right atrium at 23 weeks gestation, including a slightly thicker endocardium and thinner myocardial layer, is shown. (H&E, 4 \times .)

Specialized Structures of the Heart

Papillary Muscles and Cordae Tendineae

Papillary muscles are specialized cones of ventricular myocardium into which the chordae tendineae of the atrioventricular valves insert. The base of the papillary muscle has an endocardial lining on all sides surrounding the central myocardial tissue. At the tip of the papillary muscle, where the chordae tendineae insert, the myocardium is gradually replaced by fibrous tissue that

merges with the fibrous tissue of the chordae tendineae (see Fig. 1-9). The very tip of the papillary muscle may also lack its endocardial lining.

The chordae tendineae, which tether the atrioventricular valve leaflets to the papillary muscle, have a central core of densely arranged collagen fibers with peripheral, more loosely arranged, collagen fibers.

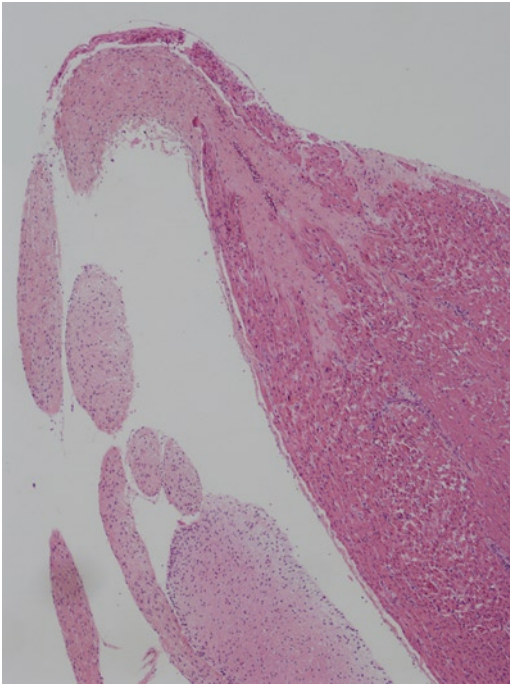


FIGURE 1-9. Papillary muscle at 40 weeks gestation. The tip of papillary muscle at 40 weeks gestation, including the transition to chordae tendineae, is shown. (H&E, 4 \times .)

Valve Leaflets and Cusps

Fetal valve leaflets and cusps are delicate structures composed predominantly of a fairly densely arranged central core of collagen fibers with the free surfaces lined by endocardium (see Figs. 1-10–1-12). Fetal valve stroma is frequently focally myxoid in character (see Fig. 1-13); however, nodular myxoid structures are considered a sign of valvular dysplasia (see Fig. 1-14). While cardiac valve tissue is not vascularized except at the base, a common finding in the fetal heart valve, especially

the mitral and tricuspid valves, is a structure known as a *congenital blood cyst*. These are small red–brown excrescences near the margin of the valve on the atrial side (see Fig. 1-15). Histologically, they consist of ovoid cystic spaces containing blood and are lined by endocardial-like cells (see Fig. 1-16). Evidence from serial sections has shown that blood cysts result from blood being pressed into the crevices of the valve tissue and retained after the mouth of the crevice fuses shut [8, 9].

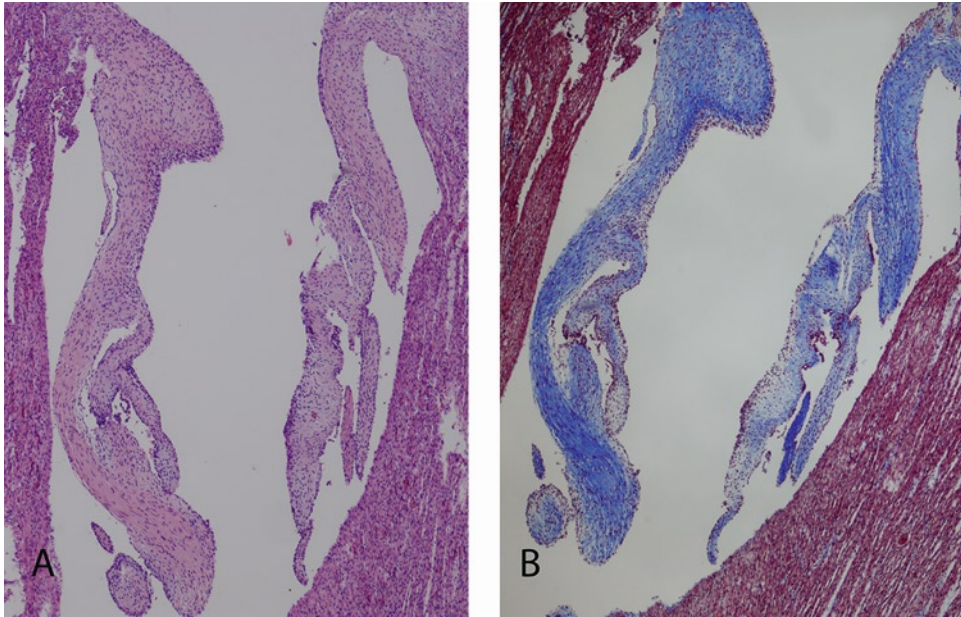


FIGURE 1-10. Atrioventricular valve at 23 weeks gestation. A low-power view of the valve leaflets of the atrioventricular valve at 23 weeks gestation is shown. (**A**, H&E, 4× and **B**, Masson trichrome, 4×.)

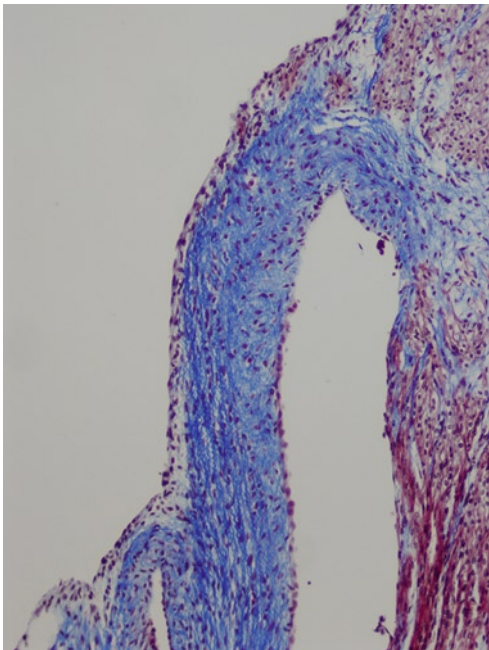


FIGURE 1-11. Atrioventricular valve at 23 weeks gestation. A higher power view of the valve leaflet of the atrioventricular valve at 23 weeks gestation is shown, including the fibrous core and the simple squamous endothelial lining on both sides of the valve leaflet. (Masson trichrome, 10×.)

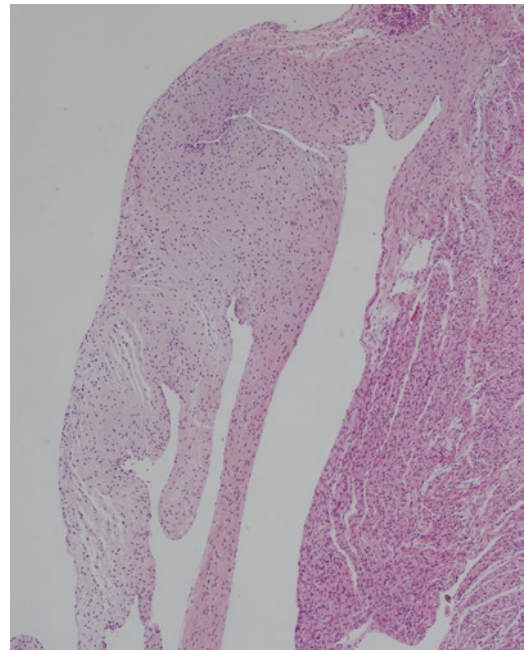


FIGURE 1-12. Atrioventricular valve at 40 weeks gestation. A low-power view of the valve leaflets of the atrioventricular valve at 40 weeks gestation is shown. (H&E, 4×.)

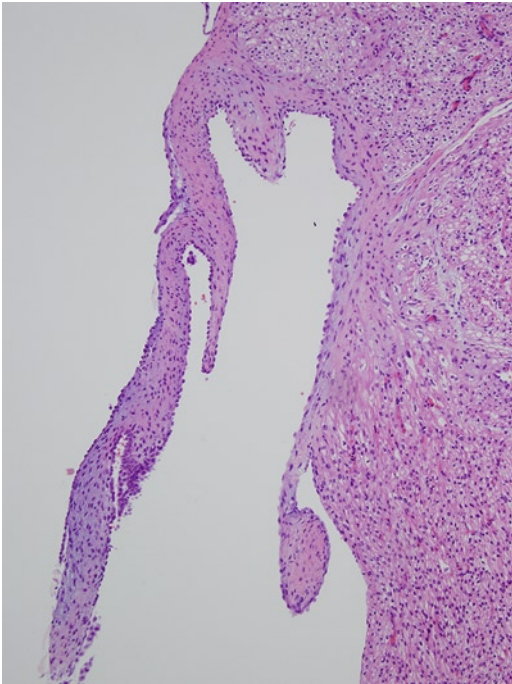


FIGURE 1-13. Atrioventricular valve at 19 weeks gestation. A low-power view of the valve leaflet of the atrioventricular valve at 19 weeks gestation, including the focally myxoid character of the fibrous stroma and flattened endothelial lining on both sides, is shown. (H&E, 10 \times .)

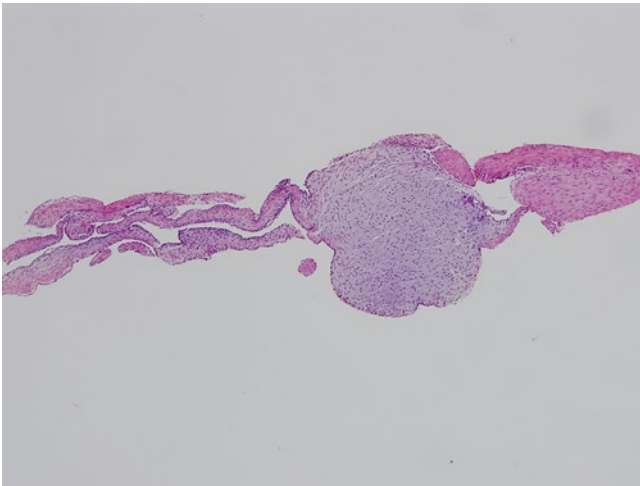


FIGURE 1-14. Atrioventricular valve at 19 weeks gestation. A tricuspid valve leaflet at 19 weeks gestation with valvular dysplasia is shown. Note the well-defined nodular myxoid excrescence on the valve leaflet. (H&E, 4 \times .)



FIGURE 1-15. Congenital blood cyst on the septal leaflet of the tricuspid valve. A gross photograph of a congenital blood cyst on the septal leaflet of the tricuspid valve is shown. These cysts are typically ovoid red-brown excrescences on the atrial side of the valve leaflet. Some can be large and bulbous, as shown here.

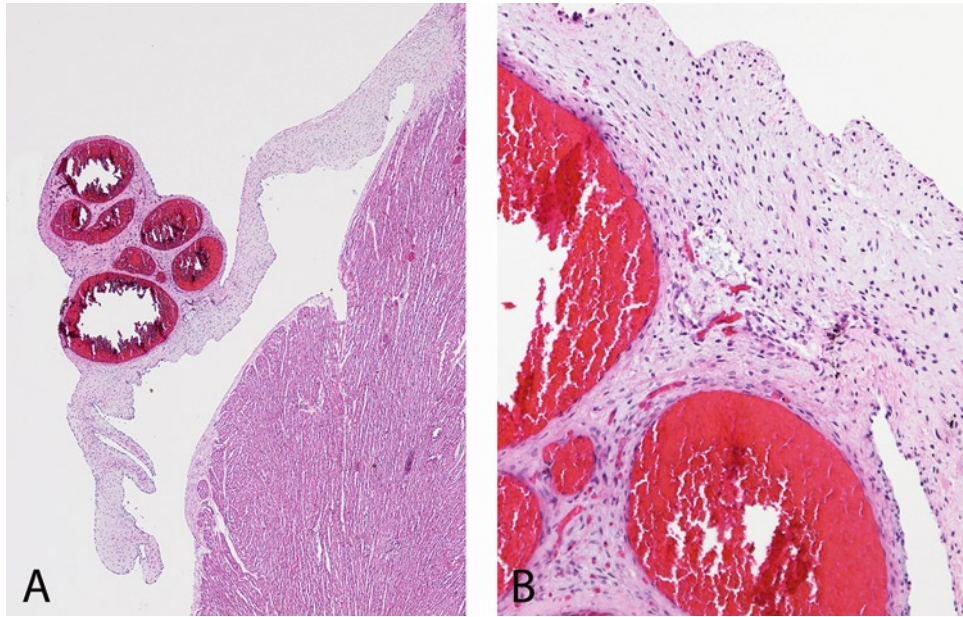


FIGURE 1-16. Blood cyst on the mitral valve. Note the blood-filled spaces lined by flattened endocardial-like cells. (H&E, **A**, 2× and **B**, 10×.)

Conduction System

The cardiac conduction system consists of specialized myocardial fibers involved in the initiation and propagation of electrical impulses within the heart. The conduction signal begins in the sinoatrial node, which is located within the right atrium at the junction with the superior vena cava, near the crista terminalis. Histologically, the sinoatrial node consists of dense connective tissue containing specialized myocardial fibers that appear paler than normal myocytes. Typically, there is a central arteriole around which these myocytes are arranged.

Several tracts from the sinoatrial node radiate through the atrium toward the atrioventricular node/bundle of

His complex, which is located at the junction of the interatrial septum and membranous portion of the interventricular septum. Histological sections in this region show a small mass of pale-staining specialized myocardial cells with scant myofibrils embedded within the connective tissue of the central fibrous body of the heart (see Figs. 1-17–1-19). In the perinatal period, the tissues of the conduction system contain loosely woven connective tissue without any evidence of active degeneration, necrosis, phagocytosis, or replacement fibrosis [10, 11]. The main His bundle branches form the right and left bundle branches, which travel downward along the endocardial surfaces of the interventricular septum.

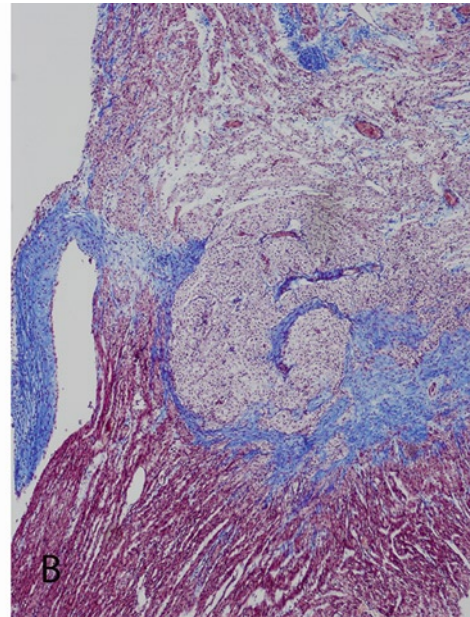
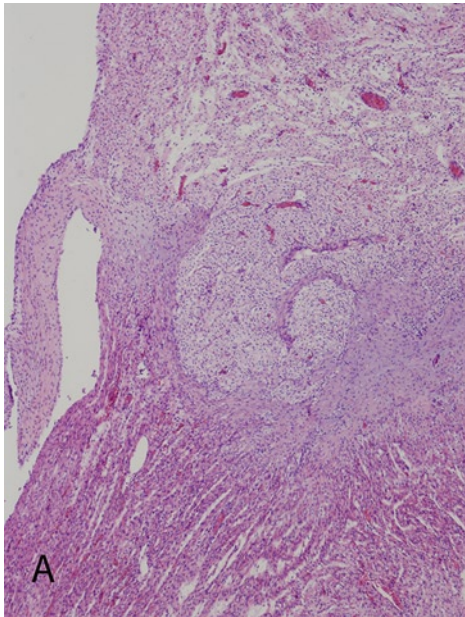


FIGURE 1-17. Atrioventricular node at 23 weeks gestation. A low-power view of the atrioventricular junction at 23 weeks gestation, including the more pale-staining atrioventricular node

embedded within the fibrous skeleton of the heart, is shown. (A, H&E, 4× and B, Masson trichrome, 4×.)

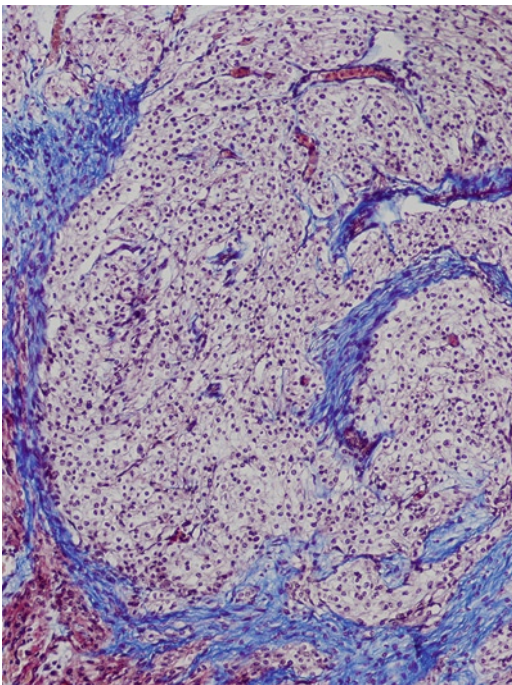


FIGURE 1-18. Atrioventricular node at 23 weeks gestation. The atrioventricular node at 23 weeks gestation, including pale-staining specialized myocardial fibers of the conduction system, is shown. (Masson trichrome, 10×.)

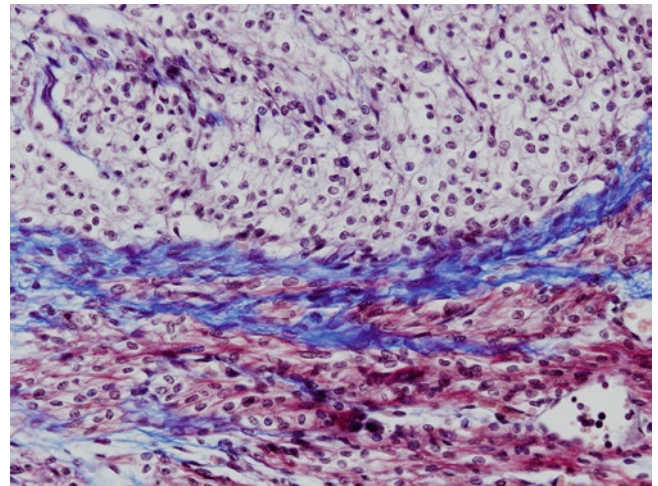


FIGURE 1-19. Atrioventricular node at 23 weeks gestation. A higher power view of the atrioventricular node at 23 weeks gestation is shown. Note the pale-staining specialized myocardial fibers of the conduction system adjacent to the more eosinophilic fibers of the myocardium at the lower half of the image. (Masson trichrome, 20×.)

Blood Vessels

Aorta

The aorta of fetuses and newborns has the same anatomical structure and mural features that are present in adulthood. The innermost layer, the tunica intima, is composed of a simple squamous layer of endothelial cells with very little additional supporting intimal fibrous tissue. The presence of fibrointimal thickening or fatty changes within the intima is considered abnormal in the fetal or newborn period. The tunica media comprises

the bulk of the aortic wall and is composed of densely packed circumferential layers of elastic tissue with intervening collagen (see Figs. 1-20 and 1-21). The nuclei present in the media consist predominantly of smooth muscle cells and fibroblasts. The wall is free of inflammatory cells in the normal state. The outermost layer is the tunica adventitia, which consists of loose fibrous connective tissue containing vessels of the vasa vasorum.

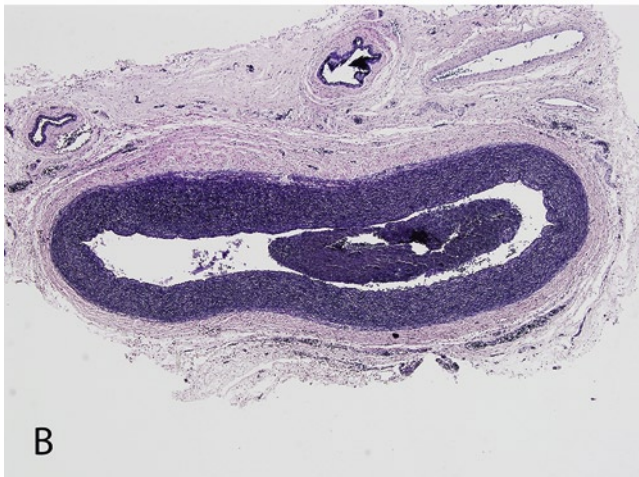
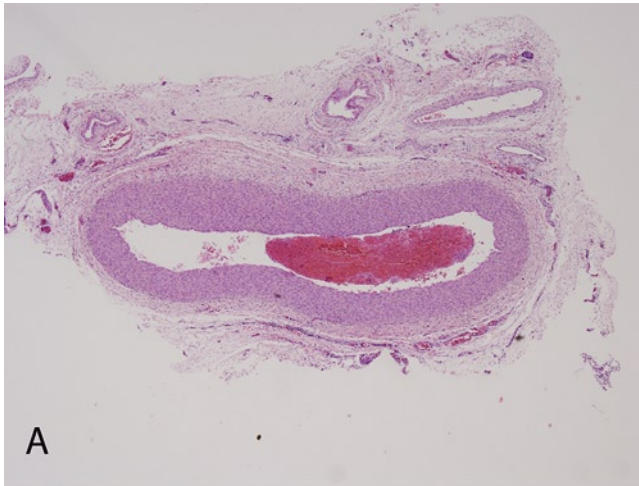


FIGURE 1-20. Fetal aorta at 23 weeks gestation. A low-power view of the fetal aorta at 23 weeks is shown. Note the bulky tunica media and the abundant elastic fibers within the tunica media. (**A**, H&E, 4 \times and **B**, Verhoeff-van Gieson, 4 \times .)

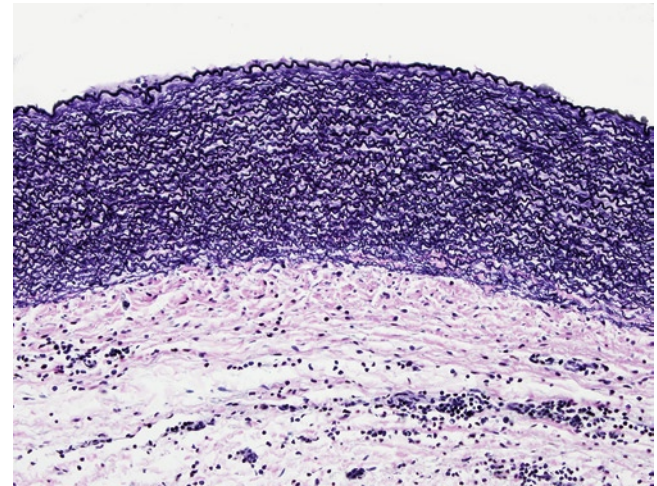


FIGURE 1-21. Fetal aorta at 23 weeks gestation. A higher power view of the fetal aorta at 23 weeks gestation is shown, highlighting the darkly stained elastic fibers within the tunica media. (Verhoeff-van Gieson, 20 \times .)

Ductus Arteriosus

The ductus arteriosus is the vascular structure in fetal life that shunts the relatively oxygenated blood from the right ventricle/pulmonary artery to the descending aorta, thus providing oxygenated blood to the systemic circulation and bypassing the pulmonary circuit. The ductus arteriosus is a muscular artery with an intima, media, and adventitia. The media of the ductus arteriosus lacks the tightly packed elastic fibers of the aorta, but does have some elastic fibers with a prominent internal elastic lamina (see Fig. 1-22). The intima of the ductus arteriosus may show slight

thickened during fetal life and it has been shown that the histological changes characteristic of closure of the ductus arteriosus begin before birth [12]. The morphological changes seen with closure of the ductus arteriosus (see Fig. 1-23) include: 1) increased thickness of the intima with formation of intimal cushions; 2) increased thickness of the media; 3) thickening and fragmentation of the internal elastic lamina; 4) increased ground substance and connective tissue in the intima and media; and 5) appearance of spaces in the inner part of the media [12].

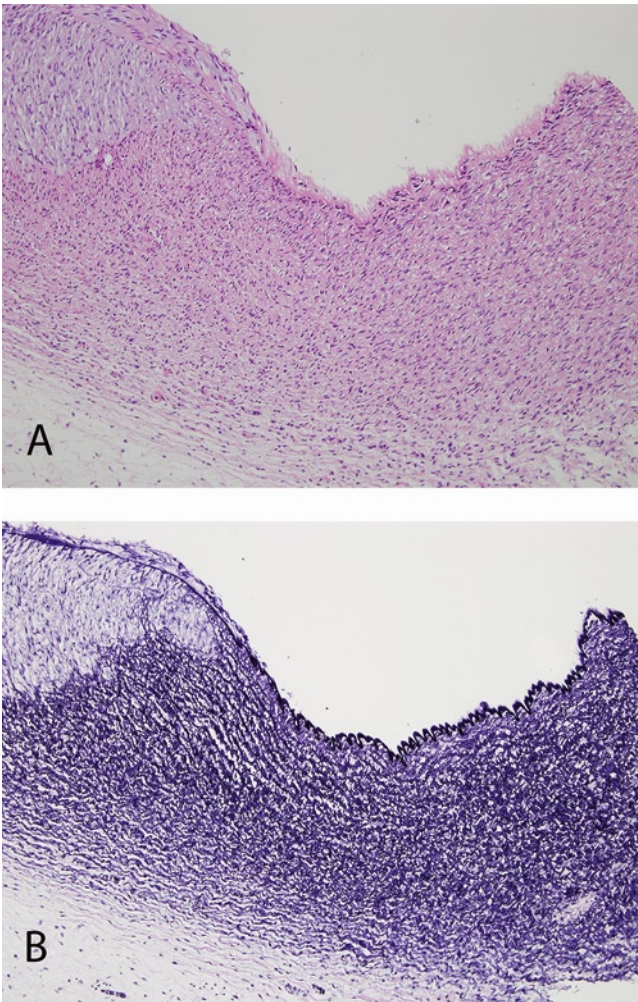


FIGURE 1-22. Ductus arteriosus in the midtrimester at 21 weeks gestation. Note the features of a muscular artery including intima, internal elastic lamina, media, and adventitia. Even at this gestational age, focal intimal thickening is present. (**A**, H&E, 10× and **B**, Verhoeff-van Gieson, 10×.)

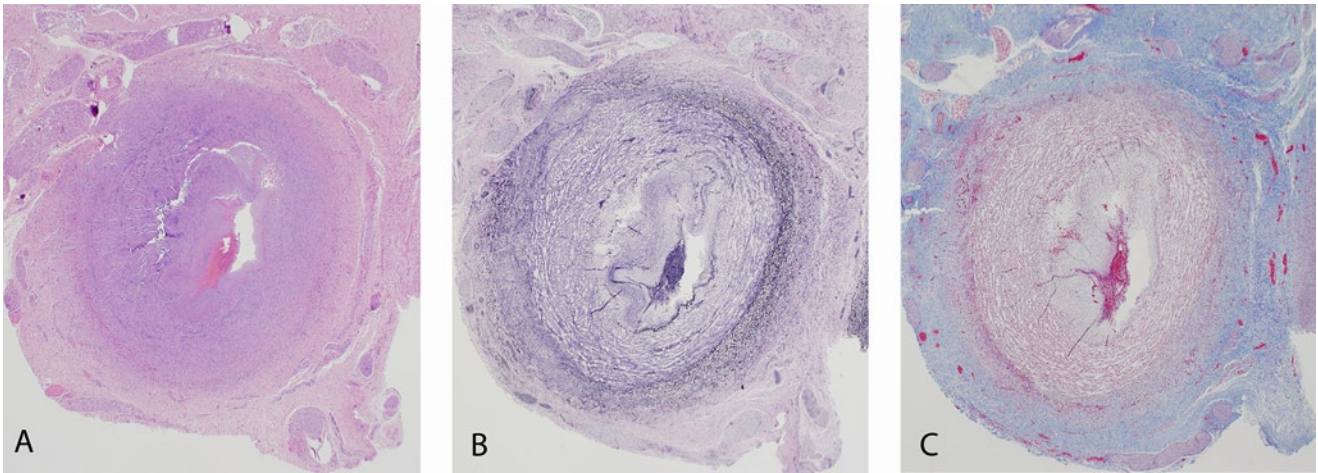


FIGURE 1-23. Ductus arteriosus after birth. The ductus arteriosus of a term infant who lived for 6 days is shown. Note the features of closure of the ductus arteriosus including **A**, increased thickness of the intima with formation of intimal cushions; **B**, fragmentation

of the internal elastic lamina; and **C**, increased connective tissue in the intima. (**A**, H&E, 2 \times ; **B**, Verhoeff-van Gieson, 2 \times ; and **C**, Masson trichrome, 2 \times .)

Umbilical Vein

While not usually seen in the examination of the adult abdomen, the umbilical vein is easily identified in the internal pathologic examination of all fetuses as the vascular structure extending from the umbilicus to the liver. In the midtrimester, the vein is a thin-walled, easily

collapsible structure, but appears thicker in fetuses near term and in neonates. The vein has an inner intimal layer, a fairly thick media composed of haphazardly arranged smooth muscle and a relatively thick adventitia (see Fig. 1-24) [10].

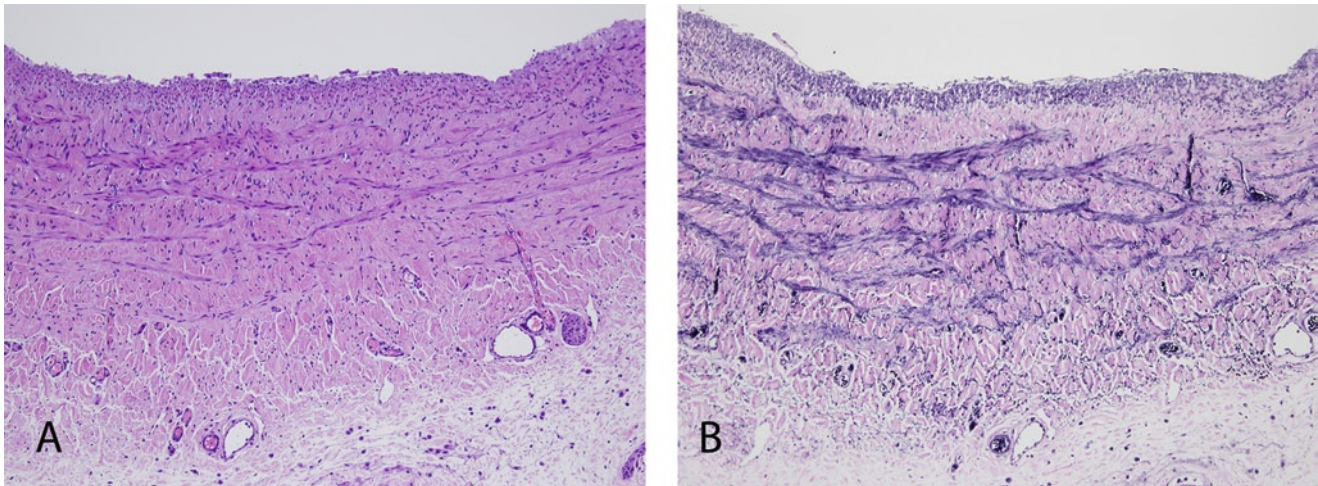


FIGURE 1-24. Umbilical vein at term. Note the features of the umbilical vein at term, including a lining endothelium, an inner intimal layer, and a fairly thick media composed of haphazardly

arranged smooth muscle. No internal elastic lamina is seen. (**A**, H&E, 10 \times and **B**, Verhoeff-van Gieson, 10 \times .)

References

1. Sadler TW, Langman J: *Langman's Medical Embryology*, edn 11. Philadelphia: Wolters Kluwer Lippincott Williams & Wilkins; 2009.
2. Schoenwolf GC, Larsen WJ: *Larsen's Human Embryology*, edn 4. Philadelphia: Elsevier/Churchill Livingstone; 2009.
3. Di Nardo P, Forte G, Ahluwalia A, Minieri M: Cardiac progenitor cells: potency and control. *J Cell Physiol* 2010, 224:590–600.
4. Bery GJ, Billingham ME: Normal heart. In *Histology for Pathologists*, edn 3. Edited by Mills SE. Philadelphia: Lippincott Williams & Wilkins; 2007:527–545.
5. Favara BE, Moores H: Anitschkow nuclear structure: a study of pediatric hearts. *Pediatr Pathol* 1987, 7:151–164.
6. Murphy GE, Becker CG: Occurrence of caterpillar nuclei within normal immature and normal appearing and altered mature heart muscle cells and the evolution of Anitschkow cells from the latter. *Am J Pathol* 1966, 48:931–957.
7. Wagner BM, Siew S: Studies in rheumatic fever. V. Significance of the human Anitschkow cell. *Hum Pathol* 1970, 1:45–71.
8. Boyd TA: Blood cysts on the heart valves of infants. *Am J Pathol* 1949, 25:757–759.
9. Zimmerman KG, Paplanus SH, Dong S, Nagle RB: Congenital blood cysts of the heart valves. *Hum Pathol* 1983, 14:699–703.
10. Valdes-Dapena MA: *Histology of the fetus and newborn*. Philadelphia: Saunders; 1979.
11. Valdes-Dapena MA, Greene M, Basavanand N, et al.: The myocardial conduction system in sudden death in infancy. *N Engl J Med* 1973, 289:1179–1180.
12. Mujahid BMGP: A study of histology of human ductus arteriosus: before and after birth. *J Anat Soc India* 2000, 49:3–5.

SECTION II

Respiratory Tract

2

Lung

Portia A. Kreiger

The process of fetal development is continuous; however, the developing lung can be subdivided into five morphologic stages (embryonic, pseudoglandular, canalicular, sacular, and alveolar). Based on various authors' observations, differing transition times from one stage to another have been proposed. This is thought to be due, at least in part, to the fact that lung development is not completely synchronous. Specifically, lung development is more rapid in cranial regions than caudal areas [1]. The five developmental stages can be identified by histology and each stage of lung development is marked by a major developmental milestone (see Fig. 2-1) [1–3].

Five Stages of Lung Formation

Developmental stage	Age range	Developmental milestone
Embryonic	3–4 wk to 6–8 wk gestational age	Proximal airways
Pseudoglandular	6–8 wk to 16 wk gestational age	Distal (pre-acinar) airways
Canalicular	16 wk to 26–28 wk gestational age	Acinus* and primitive capillary network
Saccular	26–28 wk to 32–36 wk gestational age	Maturing alveolar–capillary interface
Alveolar	32–36 wk to 2–4 y postnatal age	Increasing acquisition of alveoli

*Acinus encompasses the respiratory bronchioles, alveolar ducts, and terminal sacs.

FIGURE 2-1. Five stages of lung formation. The general time ranges and developmental milestones for the five stages of lung formation are shown here. The embryology and histology of the lung are discussed with reference to these five morphologic stages.

Embryology

The lung arises at approximately 3 to 4 weeks gestation from the foregut endoderm as a ventral diverticulum, which is destined to ultimately become the larynx and trachea proximally and the bronchi and lung parenchyma distally. This ventral foregut diverticulum develops within a mass of mesenchyme and forms the primary lung bud by 4 2/7 weeks postfertilization age (PFA) [4–6]. The primary lung bud bifurcates laterally to form right and left primary bronchial buds at about 4 4/7 weeks PFA and subsequently begins to branch asymmetrically, forming lobar buds (three right and two left) at 5 1/7 weeks PFA, segmental buds at 5 6/7 weeks PFA, and subsegmental buds at 6 2/7 weeks PFA [1,4,5]. These sequential endodermal buds carry with them coats of mesenchyme. Within this mesenchyme, islands of precartilaginous appear within proximal branches concurrent with segmental buds and will ultimately form the cartilage plates of bronchi [4,5]. In addition, this mesenchyme will ultimately form the muscular and connective tissue components of the airways and the interstitial connective tissue of the alveolar parenchyma [6]. The vascular network of the lung also arises from this mesenchyme [7]. These events correspond to the embryonic stage of lung development [1,4,6].

During the pseudoglandular stage of lung development, subsegmental buds branch rapidly and dichotomously to form sequential generations of airways [1,4,6]. By 16 weeks gestation, all pre-acinar airways (ie, airways to the level of the terminal bronchioles) have formed [4,6]. This process is accomplished largely through complex epithelial–mesenchymal interactions. Also, the epithelial lining of these endodermal buds is beginning to be organized in a proximal to distal pattern. The more proximal branches will form the airways and the more distal branches will form the alveolar parenchyma [4]. Within the accompanying mesenchyme, generations of vessels develop alongside sequential generations of

branching airways. This process of vasculogenesis forms the accompanying arteries and veins to the level of the terminal bronchiole and is complete by the end of the pseudoglandular stage [4,7]. The subsequent venous network develops synchronously but independently from the arterial and airway network [4,7]. Lymphatics arise initially within the hilar regions at approximately 8 weeks gestation and develop within the lung by about 10 weeks gestation [1].

During the ensuing canalicular stage of lung development, lung growth increases substantially. The development of the acinus, ie, respiratory bronchioles, alveolar ducts, and early airspaces (terminal sacs), occurs during this time. However, the expansion of the mesenchymal capillary network is also greatest at this time. As this capillary network expands, the mesenchymal bed in which these capillaries grow begins to thin. By the end of the canalicular stage, the formation of primitive capillary–airspace interfaces has begun [1,6].

During the saccular stage of lung development, increasingly complex airspace development occurs. The more primitive airspaces of the canalicular period are subdivided by the ingrowth of ridges of mesenchymal tissue containing capillaries, known as “secondary crests.” Vasculogenesis continues to increase and mature, and mesenchyme continues to thin. With these events, concomitant progressive differentiation of airspace lining epithelium results in a maturing surface required for postnatal blood–gas exchange [1,6].

The final, alveolar stage of lung development is characterized by the formation of increasing numbers of mature alveoli with well-formed alveolar–capillary interfaces [1,7]. The lung at birth contains a reported 24 million alveoli. However, alveologenesis continues postnatally. The majority of alveoli are thought to be formed by 2 years of age and by adulthood the lung contains between 300–600 million alveoli [1,3,6,7].

Histology

General Overview of Postnatal Pulmonary Histology

The fully formed, mature lung consists of three lobes on the right and two lobes on the left. Each lobe is invested by a thin layer of visceral pleura composed of a monolayer of mesothelium and subjacent fibroconnective tissue containing small blood vessels and lymphatics (see Fig. 2-2). Each lung is supplied by a primary bronchus and each lobe is supplied by a secondary bronchus. The pulmonary lobes are further subdivided into bronchopulmonary segments, each associated with a tertiary bronchus (see Figs. 2-3 and 2-4). Each segment is further subdivided into pulmonary lobules, each of which is supplied by a terminal bronchiole. Each bronchiole is accompanied by an arteriole. Together these two structures form a bronchovascular bundle (see Fig. 2-5), which is invested in fibroconnective tissue that also contains lymphatics and nerves. Beyond the terminal bronchiole is the pulmonary acinus. The acinus encompasses a respiratory bronchiole and all its branches, including alveolar ducts and terminal alveoli (see Figs. 2-6 and 2-7). The perimeter of each lobule is demarcated by interlobular septa (see Figs. 2-8 and 2-9), which consists of bands of fibroconnective tissue containing veins or venules and lymphatics [6].

Bronchi are supported by cartilage plates (see Figs. 2-10 and 2-11), which are larger proximally and become progressively smaller proceeding distally; bronchi are also associated with seromucinous glands. In contrast, bronchioles (see Fig. 2-12) contain neither a cartilage support structure nor associated seromucinous glands.

However, both bronchi and bronchioles are supported by smooth muscle and connective tissue. The epithelial lining of bronchi is pseudostratified ciliated respiratory in type. Bronchioles show similar ciliated respiratory-type epithelium, but this epithelium is simple rather than pseudostratified [6]. The respiratory epithelium of airways incorporates occasional goblet cells, which are more prevalent proximally than distally, and Clara cells, which are present primarily within distal bronchioles. Neuroendocrine cells are also present, though normally inconspicuous, along both airways and airspaces. Infolding of airway-lining epithelium is seen within larger bronchi and bronchioles, and is likely related to the contraction of airway smooth muscle [2,6]. Aggregates of lymphoid tissue, known as bronchus-associated lymphoid tissue (BALT), may be seen postnatally along the airways of normal infants and children (see Fig. 2-13) [6]. BALT may be first recognized in utero at approximately 16 weeks gestation; however, it is typically sparse in fetal life but may become prominent in cases of in utero infection [8,9].

Alveoli are lined predominantly by simple flattened epithelium, known as type I pneumocytes (see Figs. 2-14 and 2-15). Type I pneumocytes provide a thin air-blood interface with the abundant capillary network of the intervening alveolar septa. Alveoli also contain interspersed type II pneumocytes, which are more cuboidal in shape. Type II pneumocytes produce surfactants and represent the progenitors of type I pneumocytes [1,6].

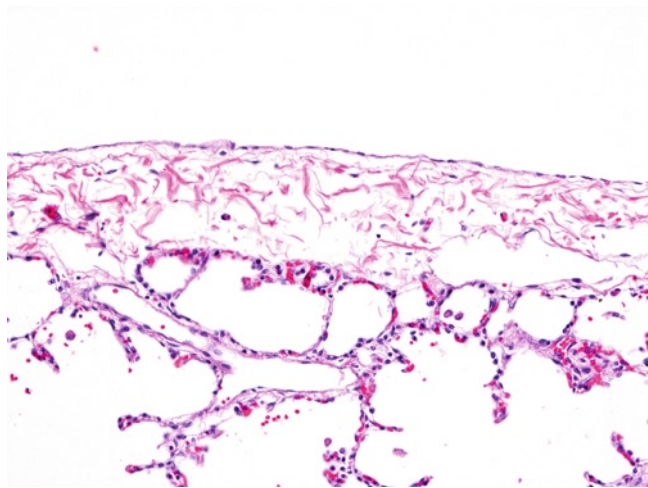


FIGURE 2-2. Normal 5-month postnatal lung I. The visceral pleural surface of the lung consists of a simple layer of mesothelium and subjacent loose fibroconnective tissue, which contains occasional small blood vessels and lymphatics. (Hematoxylin and eosin [H&E], 20 \times .)

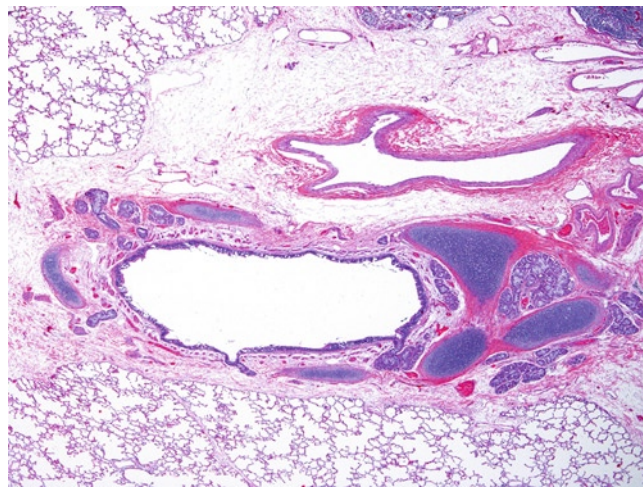


FIGURE 2-3. Normal 5-month postnatal lung II. This tertiary bronchus is surrounded by fibroconnective tissue, which contains cartilage plates, seromucinous glands, and smooth muscle. (H&E, 2 \times .)

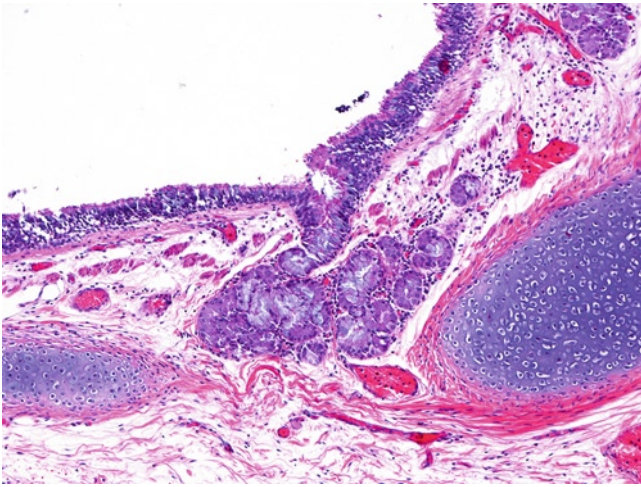


FIGURE 2-4. Normal 5-month postnatal lung III. Seromucinous glands connect to the respiratory mucosal surface in this high-power image of a tertiary bronchus; smooth muscle and cartilage are also seen. (H&E, 10 \times .)

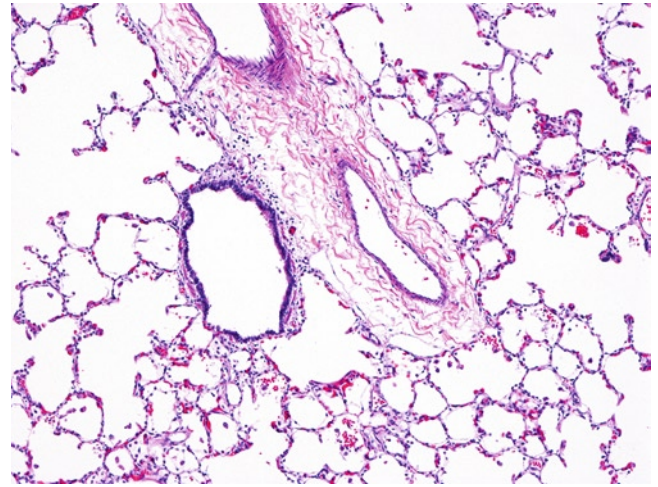


FIGURE 2-5. Normal 5-month postnatal lung IV. This bronchovascular bundle contains both a terminal bronchiole and accompanying arteriole. These structures are invested in a fibroconnective tissue sheath that also contains lymphatics but not venules. (H&E, 10 \times .)

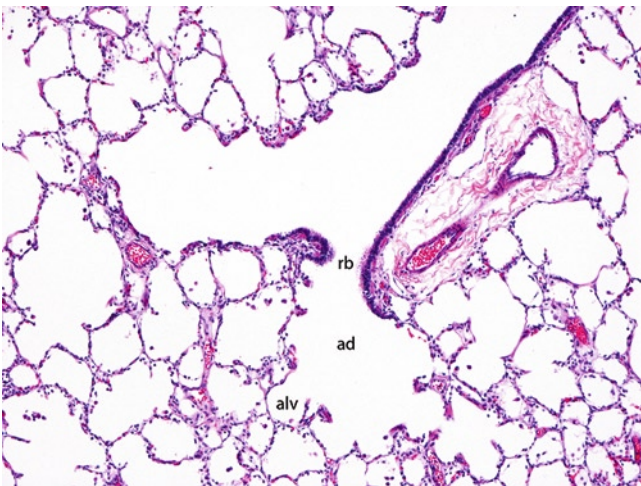


FIGURE 2-6. Normal 5-month postnatal lung V. A pulmonary acinus consists of a respiratory bronchiole (rb) with associated alveolar ducts (ad) and alveoli (alv). (H&E, 10 \times .)

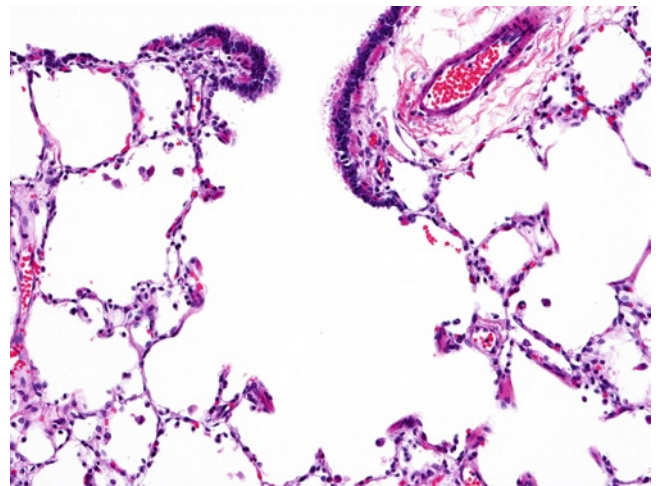


FIGURE 2-7. Normal 5-month postnatal lung VI. At high power, the transition from ciliated columnar bronchiolar epithelium to flattened alveolar epithelium can be seen in this pulmonary acinus. (H&E, 20 \times .)

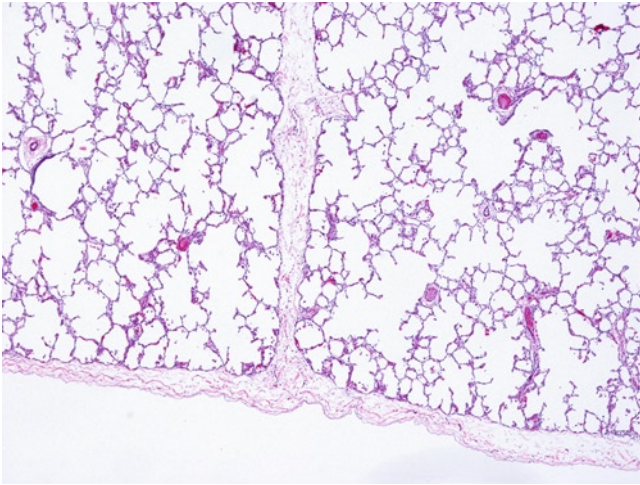


FIGURE 2-8. Normal 5-month postnatal lung VII. Interlobular septa demarcate pulmonary lobules and consist of bands of connective tissue, which intersect peripherally with the visceral pleura. (H&E, 4 \times .)

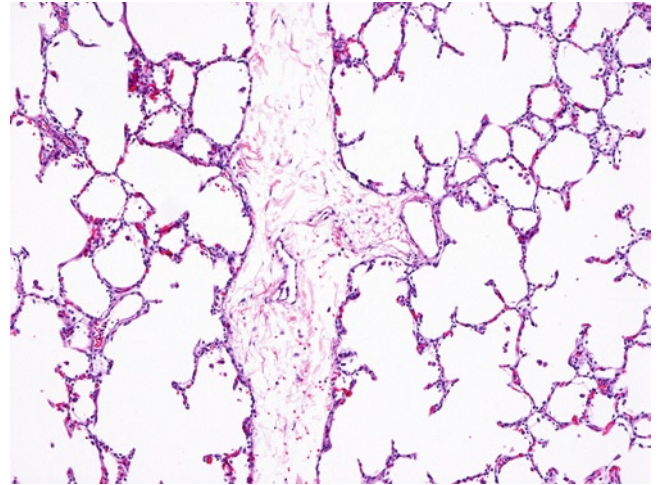


FIGURE 2-9. Normal 5-month postnatal lung VIII. Interlobular septa may contain occasional venous or lymphatic channels. (H&E, 10 \times .)

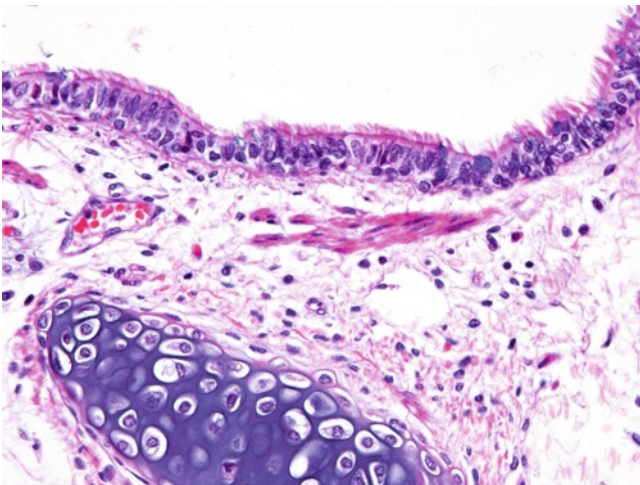


FIGURE 2-10. Normal 5-month postnatal lung IX. Bronchi are respiratory mucosal-lined and contain subepithelial connective tissue incorporating cartilage and smooth muscle, which is more abundant proximally than distally. (H&E, 20 \times .)

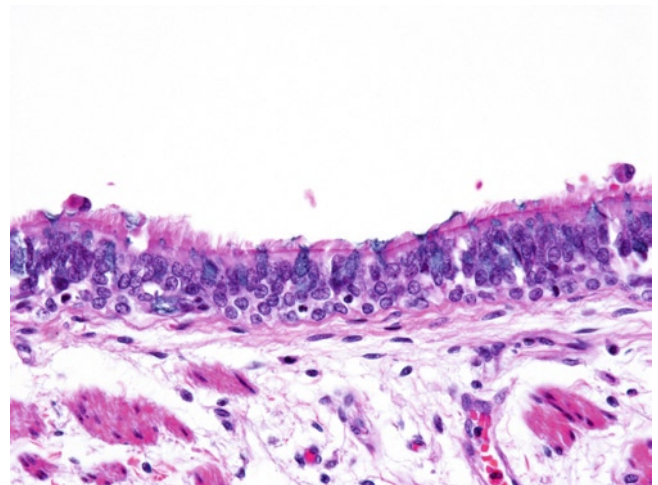


FIGURE 2-11. Normal 5-month postnatal lung X. Bronchial mucosa consists of pseudostratified ciliated columnar epithelium. (H&E, 40 \times .)

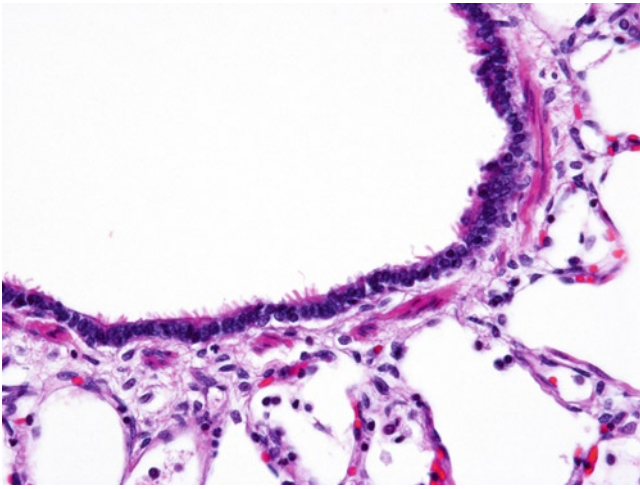


FIGURE 2-12. Normal 5-month postnatal lung XI. Bronchioles are lined by mostly simple ciliated columnar epithelium. No cartilage is present. (H&E, 40 \times .)

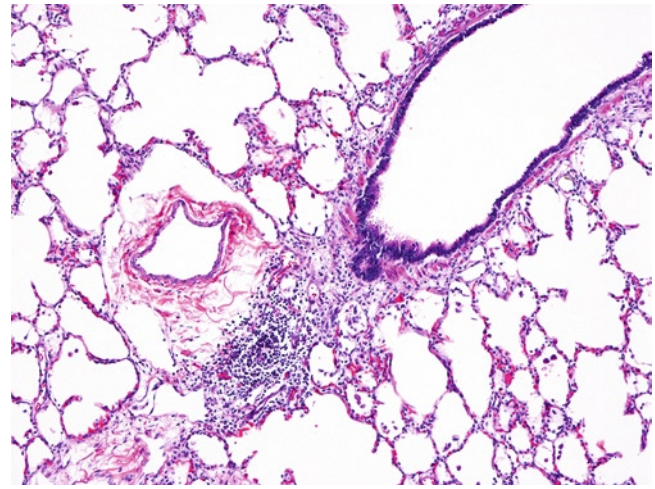


FIGURE 2-13. Normal 5-month postnatal lung XII. Bronchus-associated lymphoid tissue may be seen as small aggregates of lymphocytes along the airways in the normal postnatal lung, but is not typically prominent in the normal fetal lung. (H&E, 10 \times .)

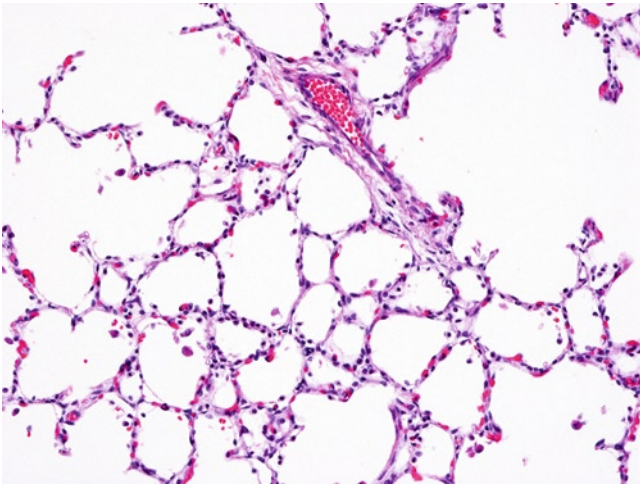


FIGURE 2-14. Normal 5-month postnatal lung XIII. Mature alveoli consist of polyhedral airspaces separated from one another by thin alveolar septa, which contain an abundant capillary network and occasional small thin-walled intra-acinar arterioles. (H&E, 20 \times .)

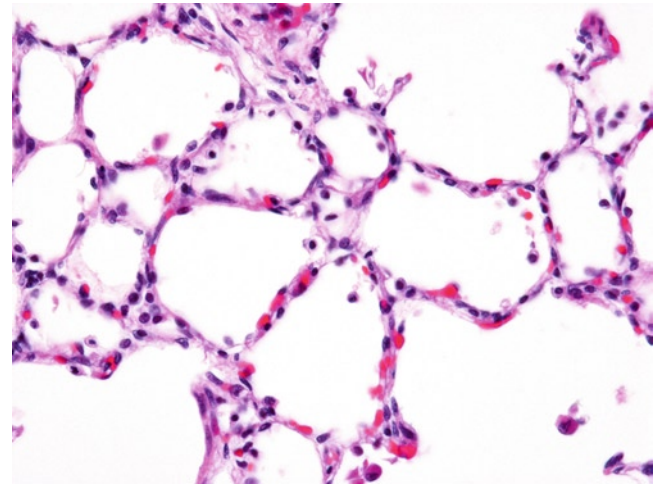


FIGURE 2-15. Normal 5-month postnatal lung XIV. Alveoli are lined by predominantly flattened type I pneumocytes. (H&E, 40 \times .)

Fetal Pulmonary Developmental Stages

Embryonic stage

During the earliest stage of lung development, the embryonic stage, the lung consists of rather primitive bronchial buds. These bronchial buds consist of small simple tubules, which are lined by a thick layer of

endoderally derived epithelium and are situated within a bed of abundant loose mesenchyme (see Figs. 2-16–2-18) [1].



FIGURE 2-16. Embryonic stage I: normal lung at 7 weeks gestation. The embryonic stage of lung development is characterized by small primitive tubules set amidst an abundant loose mesenchymal stroma. (H&E, 10 \times .)

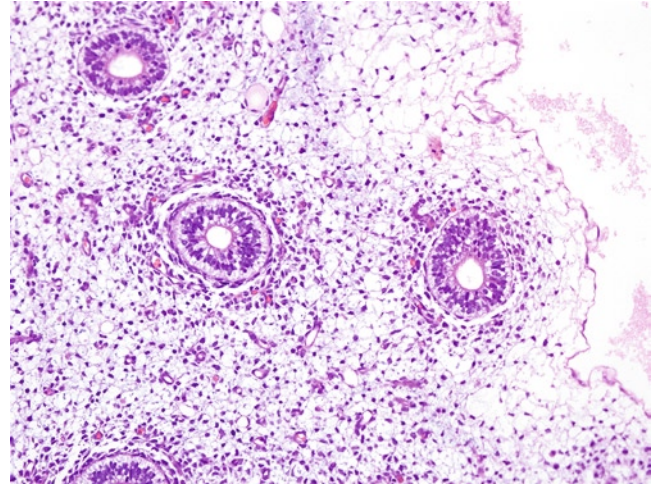


FIGURE 2-17. Embryonic stage II: normal lung at 7 weeks gestation. Mesenchyme shows some condensation around endodermal tubules. (H&E, 20 \times .)

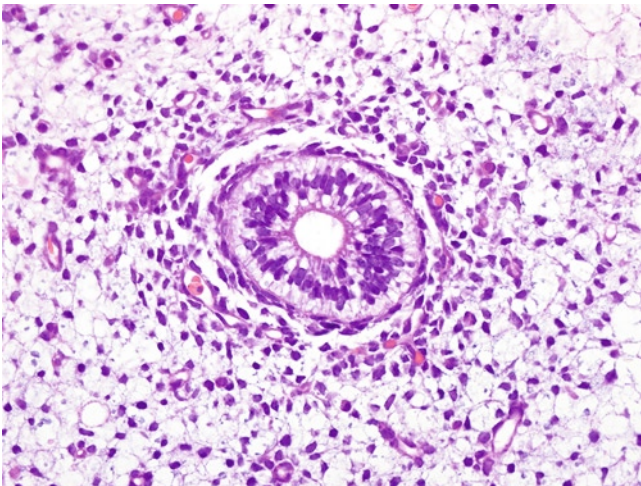


FIGURE 2-18. Embryonic stage III: normal lung at 7 weeks gestation. Tubules are lined by thick pseudostratified endodermal epithelium. (H&E, 40 \times .)

Pseudoglandular stage

During the pseudoglandular stage, progressive branching of bronchial buds gives rise to increasing generations of airways. Early in the pseudoglandular stage (see Figs. 2-19–2-21), these airways remain small simple tubules lined by pseudostratified endoderm. However, with progressive branching, by approximately 13 weeks gestation these airways enlarge and the endodermal lining thins. The more proximal airways become lined by ciliated respiratory epithelium with interspersed goblet cells. The more distal airways become lined by simple

columnar epithelium. This epithelium is notable for prominent subnuclear vacuolization, conferring a "pseudoglandular" appearance to these simple tubules (see Figs. 2-22–2-24). Similar to the embryonic period, these tubules are set amidst a relatively abundant loose interstitial mesenchyme, which appears somewhat condensed around bronchial buds [6,10]. Cartilage formation around proximal airways and smooth muscle around airways and major vessels is also first appreciable during this stage [1].

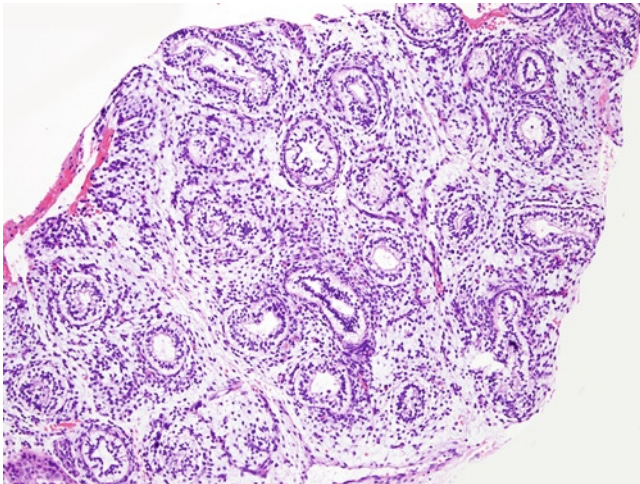


FIGURE 2-19. Early pseudoglandular stage I: lung at 10 to 11 weeks gestation. Early in the pseudoglandular stage, the lung consists of simple tubules, which are increased in number compared with the embryonic stage. (H&E, 10 \times .)

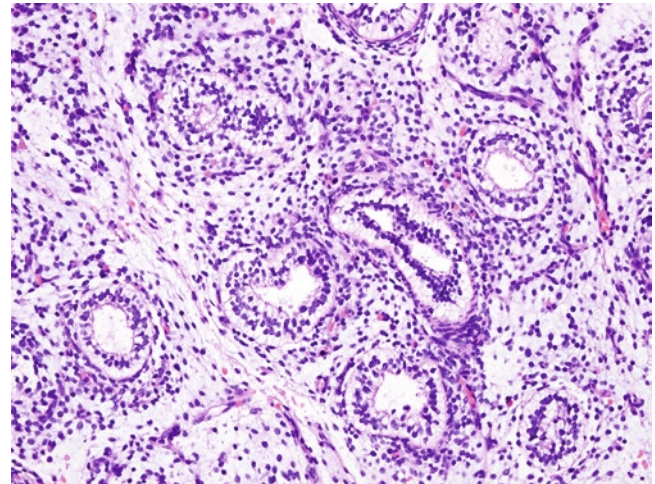


FIGURE 2-20. Early pseudoglandular stage II: lung at 10 to 11 weeks gestation. These tubules remain situated amidst a relatively abundant loose mesenchymal stroma, similar to the embryonic stage. (H&E, 20 \times .)

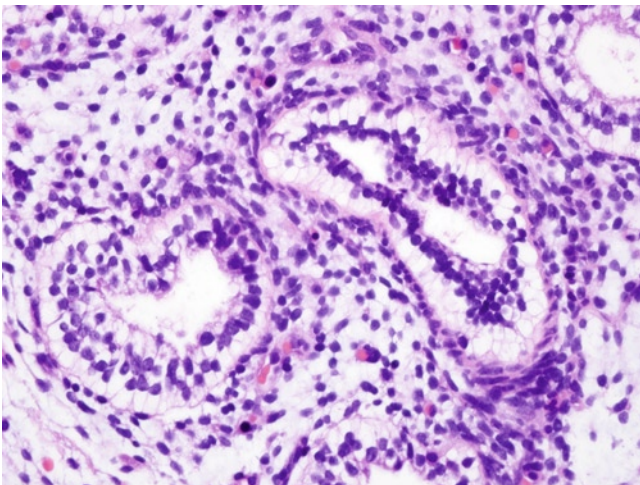


FIGURE 2-21. Early pseudoglandular stage III: lung at 10 to 11 weeks gestation. Tubules are lined by pseudostratified to simple columnar endodermal epithelium. (H&E, 40 \times .)

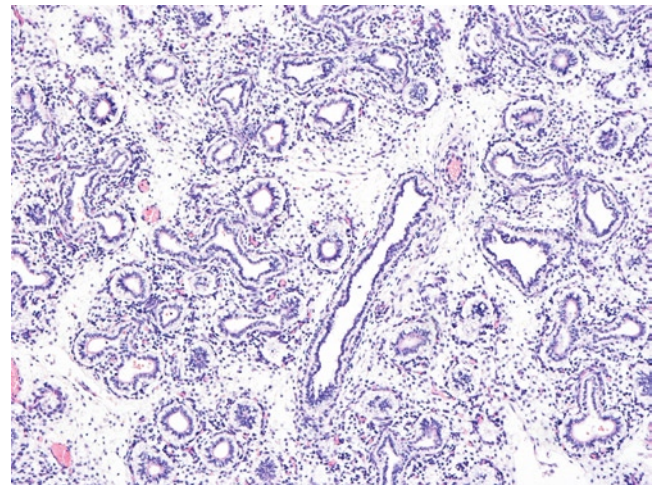


FIGURE 2-22. Late pseudoglandular stage IV: lung at 15 weeks gestation. Late in the pseudoglandular stage, the lung remains composed of simple tubules amidst a loose mesenchymal stroma. (H&E, 10 \times .)

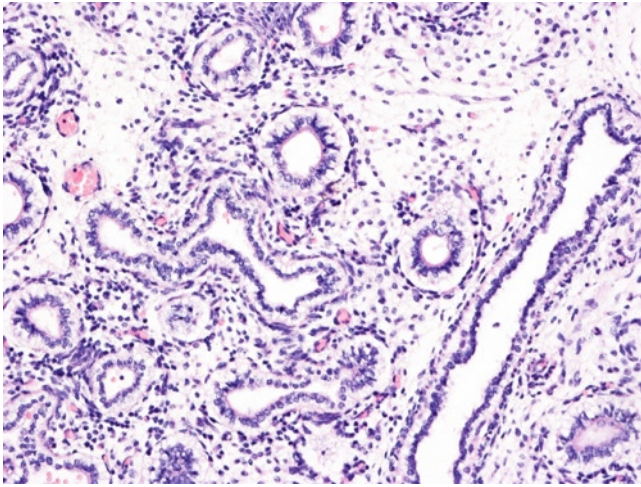


FIGURE 2-23. Late pseudoglandular stage V: lung at 15 weeks gestation. Tubules are lined by simple columnar epithelium. (H&E, 20 \times .)

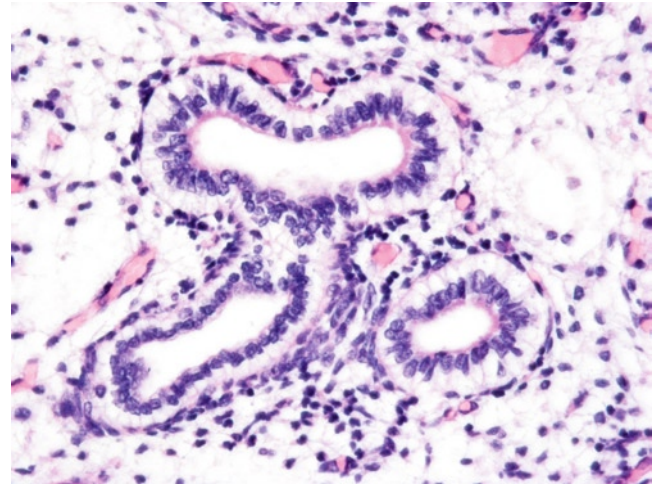


FIGURE 2-24. Late pseudoglandular stage VI: lung at 15 weeks gestation. Epithelium is notable for prominent subnuclear vacuoles. (H&E, 40 \times .)

Canalicular stage

The canalicular stage is marked by the initiation of air-space development and the beginnings of capillarization of these primitive airspaces. The onset of the canalicular stage is first recognizable as capillaries becoming apposed to and even extended between airspace epithelial cells, whereby the airspaces are "canalized." Early in the canalicular stage (see Figs. 2-25–2-27), simple tubules transition from being lined by columnar vacuolated epithelium to cuboidal nonvacuolated epithelium. A rather abundant mesenchyme remains. However, as the canalicular stage proceeds (see Fig. 2-28–2-30), there is increasing enlargement and complexity to these simple tubular structures. The outlines of these early airspaces change from tubular to rather wavy or undulating. The lining epithelium becomes

progressively simple cuboidal in type and as early as 20 to 22 weeks gestation a subset of epithelium may even become flattened. This epithelial transition represents the initiation of mature pneumocyte differentiation. Ultimately, type II pneumocytes will remain cuboidal and type I pneumocytes will be flattened. In addition, the amount of interstitial mesenchyme begins to decrease. The beginning of pneumocyte differentiation in combination with the canalization and decreasing interstitial mesenchyme of this stage results in a primitive air–capillary membrane, also as early as 20 to 22 weeks gestation. Airways show condensation of surrounding elastic tissue, and by the end of this stage the most distal airways show differentiation of lining epithelium to form ciliated respiratory epithelium and Clara cells [1,6,10].

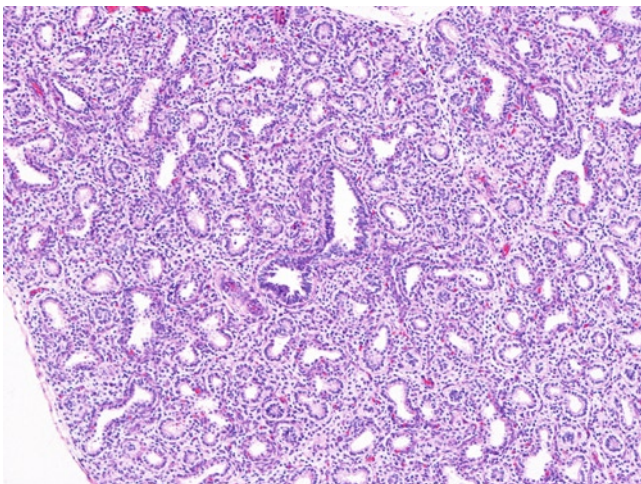


FIGURE 2-25. Early canalicular stage I: lung at 18 weeks gestation. Early in the canalicular stage, the lung is characterized by increasingly branched tubules. (H&E, 10 \times .)

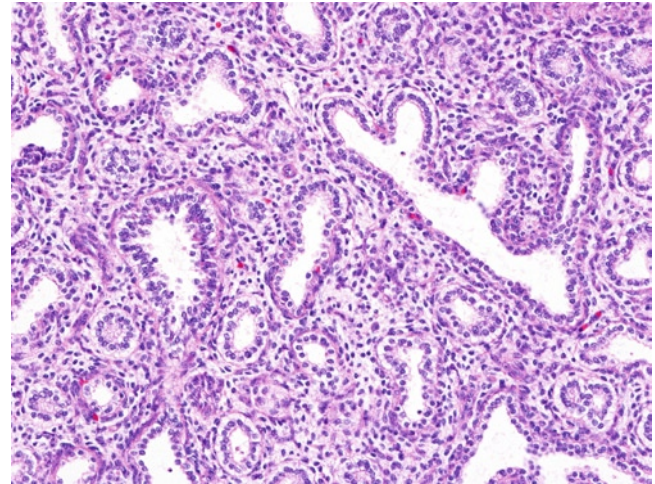


FIGURE 2-26. Early canalicular stage II: lung at 18 weeks gestation. Tubules are increasingly branched, but abundant mesenchyme remains. (H&E, 20 \times .)

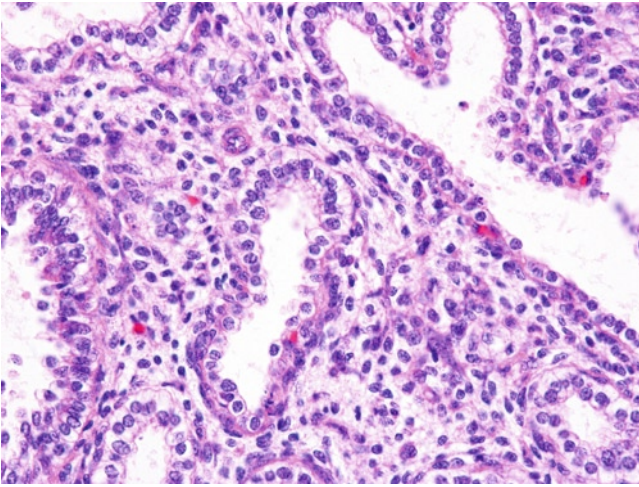


FIGURE 2-27. Early canalicular stage III: lung at 18 weeks gestation. The lining epithelium is transitioning from columnar and vacuolated to cuboidal and nonvacuolated. Capillaries are just beginning to protrude between these epithelial cells. (H&E, 40 \times .)

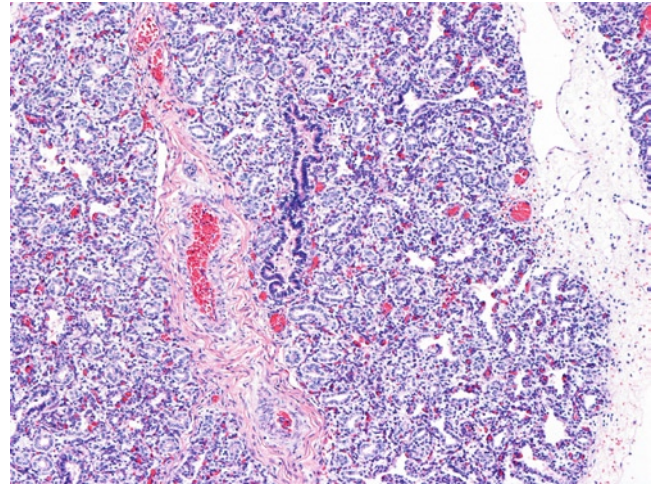


FIGURE 2-28. Late canalicular stage I: lung at 23 weeks gestation. Late in the canalicular stage the lung is characterized by more complex airspaces. The amount of interstitial mesenchyme is beginning to decrease compared with earlier gestations. Distal airways are readily recognizable among airspaces. (H&E, 10 \times .)

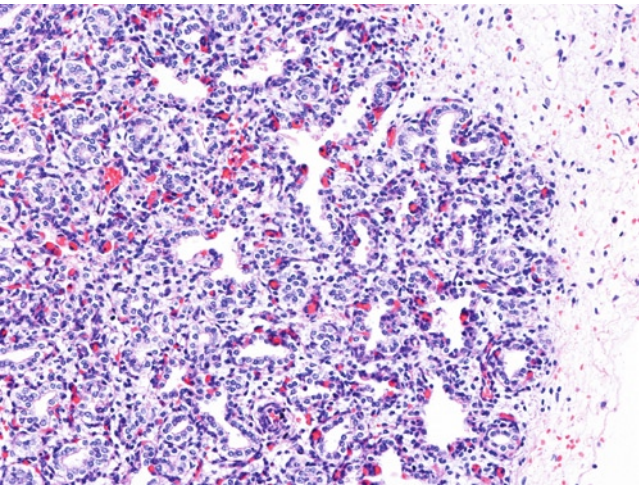


FIGURE 2-29. Late canalicular stage II: lung at 23 weeks gestation. Airspaces show slightly undulating outlines. (H&E, 20 \times .)

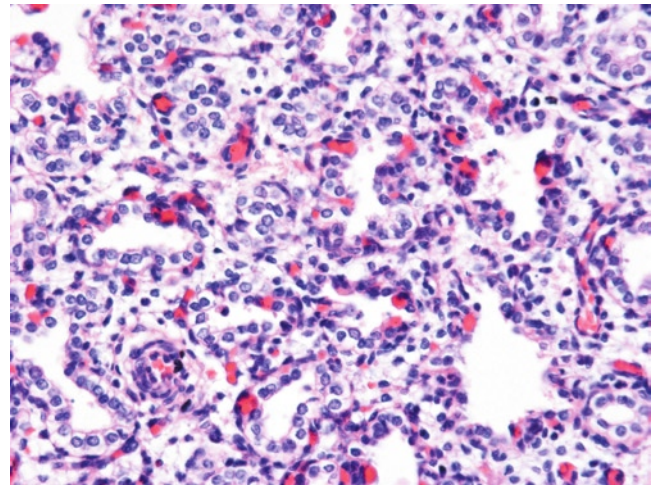


FIGURE 2-30. Late canalicular stage III: lung at 23 weeks gestation. A primitive capillary network is beginning to emerge. Airspaces are lined by predominantly cuboidal to, in areas, flattened nonvacuolated epithelium. Many capillaries are apposed to and protrude between airspace epithelial cells. (H&E, 40 \times .)

Saccular stage

The saccular stage is heralded by the formation of *secondary crests*. These ridges of epithelial-surfaced mesenchyme contain a double-layered capillary network and protrude into airspaces, subdividing them into increasingly more complex structures known as *sacculules*. With the ingrowth of secondary crests and expansion of the capillary network, the sacculules become vascularized initially with two layers of capillaries (see Figs. 2-31–2-33). The saccular stage is also marked by progressive thinning of the interstitial mesenchyme and

an increasing framework of elastic tissue around not only airways but also between airspaces. By the latter saccular stage (see Figs. 2-34–2-36), the double-layered capillary network begins to coapt into a single capillary layer. The formation of a single-layered capillary network in concert with the differentiation of airspace epithelium to flattened pneumocytes provides for the maturing capillary–airspace interface necessary for eventual postnatal respiration [1,6,10].

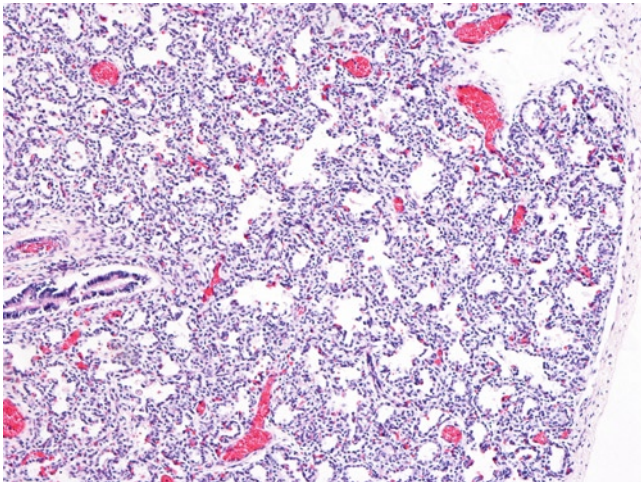


FIGURE 2-31. Early saccular stage I: lung at 28 weeks gestation. The early saccular stage is characterized by more complex airspaces with decreasing amounts of interstitial mesenchyme and an expanding capillary network. (H&E, 10 \times .)

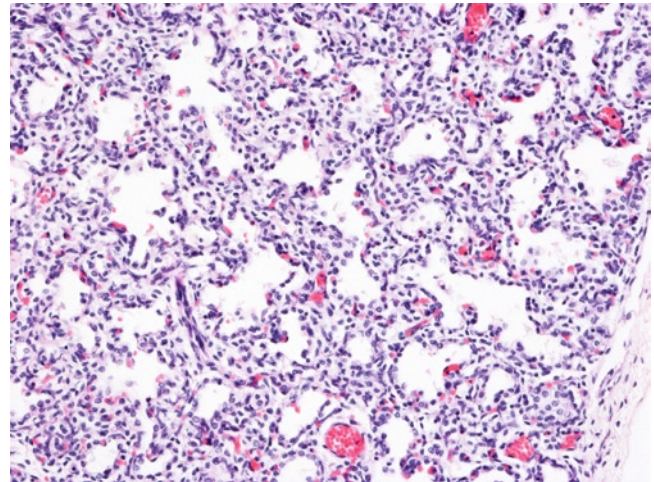


FIGURE 2-32. Early saccular stage II: lung at 28 weeks gestation. Airspaces show a wavy outline and an expanding capillary network. (H&E, 20 \times .)

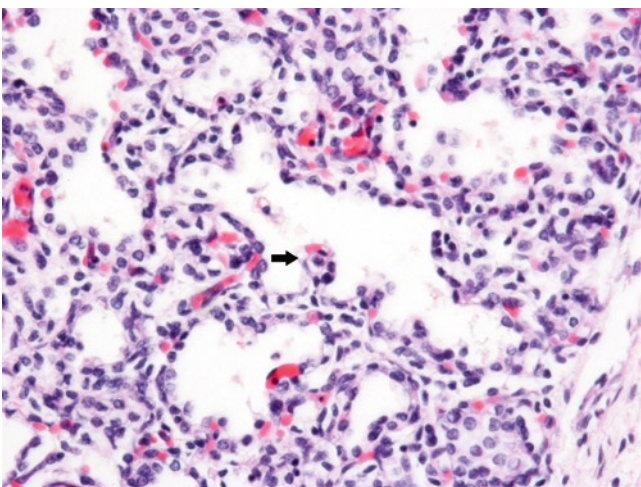


FIGURE 2-33. Early saccular stage III: lung at 28 weeks gestation. Airspaces are now becoming subdivided by "secondary crests" (arrow), to form "sacculules." These sacculules are increasingly lined by flattened epithelium. Secondary crests initially form a double capillary network within the interstitium. (H&E, 40 \times .)

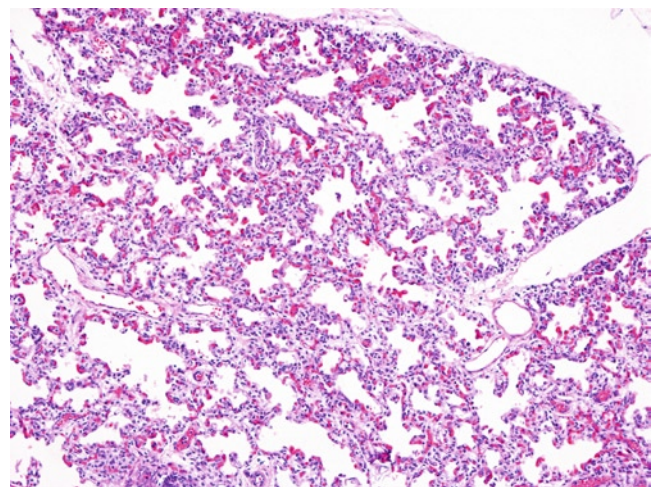


FIGURE 2-34. Late saccular stage I: lung at 31 2/7 weeks gestation. The late saccular stage is characterized by increasing numbers of sacculules. (H&E, 10 \times .)

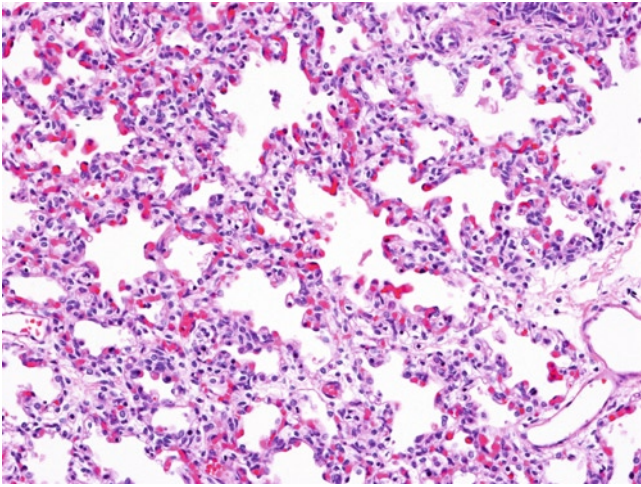


FIGURE 2-35. Late saccular stage II: lung at 31 2/7 weeks gestation. The interstitial capillary network is expanding and is also transitioning from a double-layered network to a single layer of capillaries. (H&E, 20 \times .)

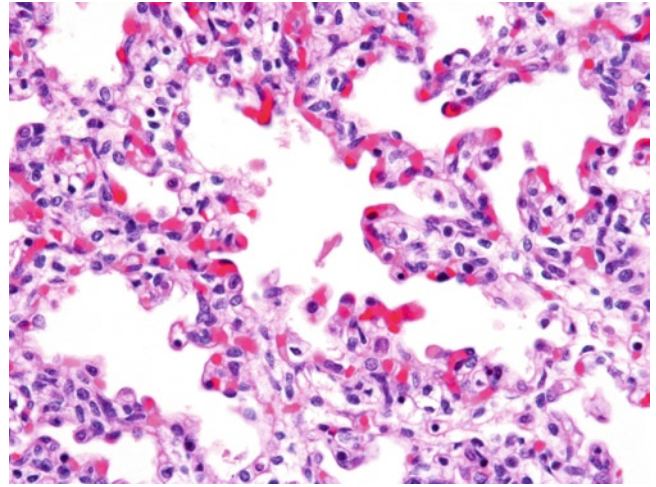


FIGURE 2-36. Late saccular stage III: lung at 31 2/7 weeks gestation. Saccules are lined by flattened epithelium with an increasingly thin interstitium. (H&E, 40 \times .)

Alveolar stage

During the alveolar stage, the amount of interstitial mesenchyme decreases substantially to form thin interalveolar septa. Alveoli now show their mature back-to-back configuration and are lined by flattened mature epithelium. Alveoli attain a more polyhedral configuration compared with the rounded sacs of the saccular stage, a process thought to be related to increasing elastin deposition within the interstitium of the lung (see

Figs. 2-37–2-39). Capillaries appear as thin single layers within alveolar septa and directly coapt with airspace-lining epithelium [1,6,7]. By the completion of the alveolar stage of lung development, the lung has attained its full complement of structures, including lymphatics, vasculature, airways, and airspaces, and a fully mature alveolar–capillary surface for postnatal respiration has been achieved [1].

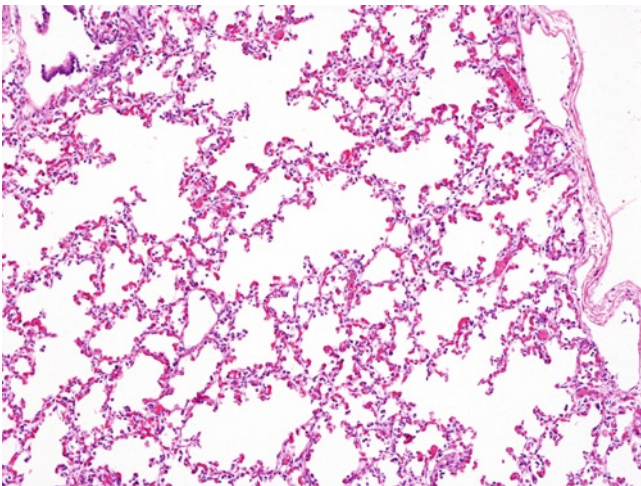


FIGURE 2-37. Alveolar stage I: lung at 36 3/7 weeks gestation. The beginnings of the alveolar stage are characterized by the attainment of thin interalveolar septa separating now back-to-back alveoli. (H&E, 4 \times .)

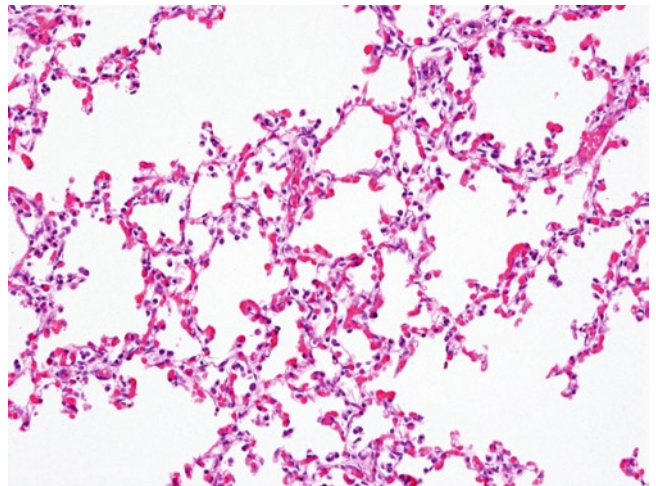


FIGURE 2-38. Alveolar stage II: lung at 36 3/7 weeks gestation. Alveolar septa contain an abundant single-layered interalveolar capillary network. (H&E, 10 \times .)

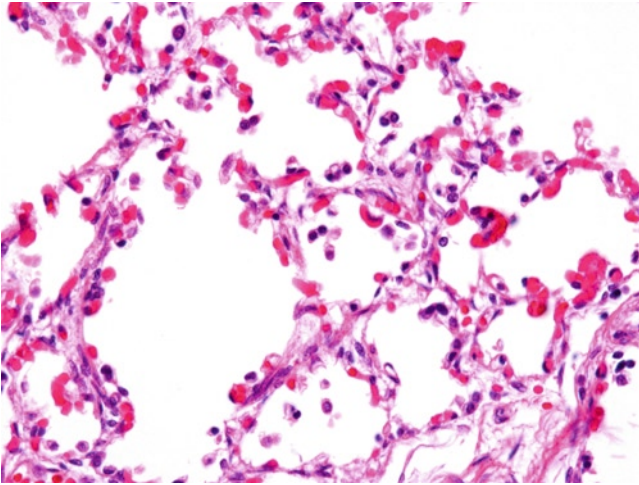


FIGURE 2-39. Alveolar stage III: lung at 36 3/7 weeks gestation. Alveoli are lined by flattened epithelium and the abundant capillaries bulge into the alveoli. (H&E, 40×.)

Special Considerations

Intra-acinar Pulmonary Arterioles

The alveolated lung parenchyma contains the most distal arterioles, which supply the alveolar capillary network. These intra-acinar precapillary arterioles are located within the interalveolar septa beyond the level of the bronchovascular bundle. These intra-acinar arterioles in the fetus and newborn normally are thin-walled

and nonmuscularized (see Figs. 2-40 and 2-41). However, in pathologic states either in utero or postnatally, these arterioles may appear thick-walled from muscularization. Smooth muscle does, however, normally extend to within these intra-acinar arterioles beginning at approximately 6 months postnatal age [1,4,6].

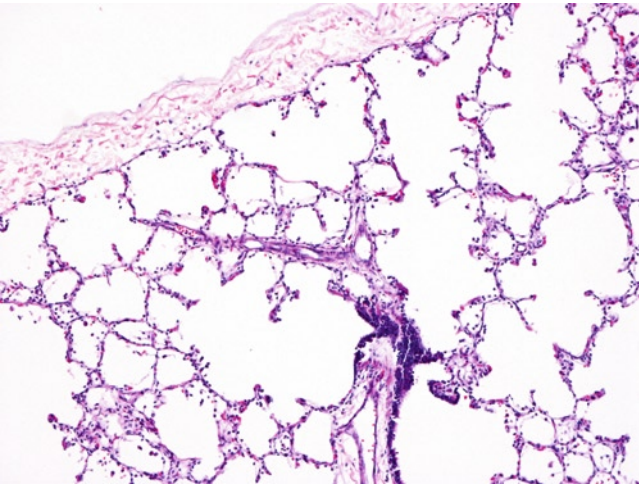


FIGURE 2-40. Intra-acinar arterioles I: normal 5-month postnatal lung. Normal intra-acinar arterioles are present within the alveolar parenchyma beyond the level of the bronchovascular bundle. (H&E, 10×.)

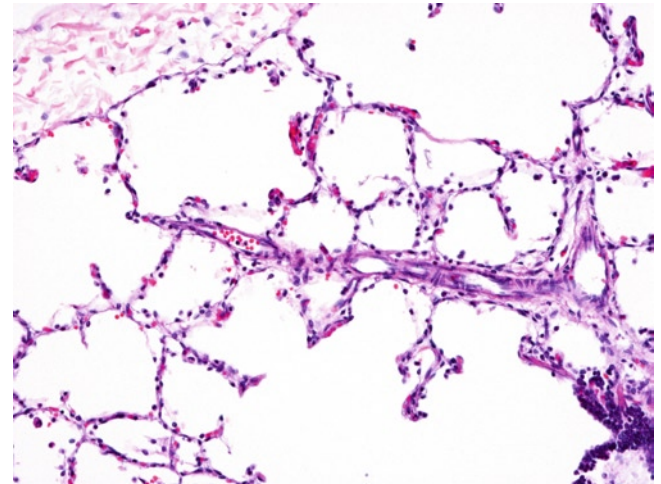


FIGURE 2-41. Intra-acinar arterioles II: normal 5-month postnatal lung. Intra-acinar arterioles normally appear to be progressively thin-walled as they extend through the parenchyma toward the pleural surface. (H&E, 20×.)

Intrapulmonary Karyorrhectic Cells

The normal fetal lung, particularly in the midtrimester, may contain prominent karyorrhectic material. This material may be the result of apoptosis, which is likely integral to the normal development of the lung [11,12].

Karyorrhectic material within fetal airways and airspaces may mimic neutrophils, an important distinction (see Fig. 2-42).

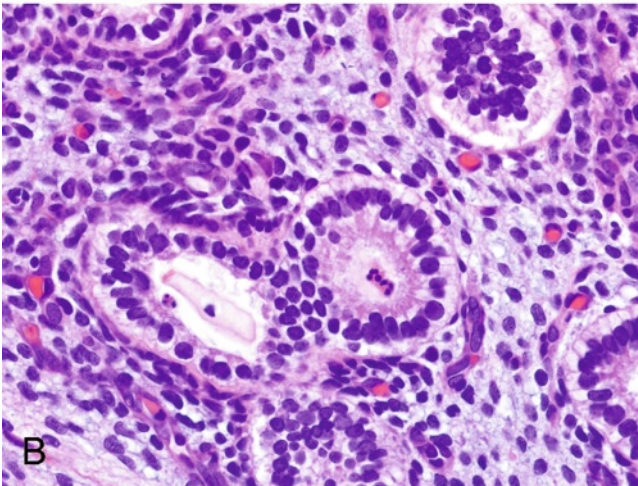
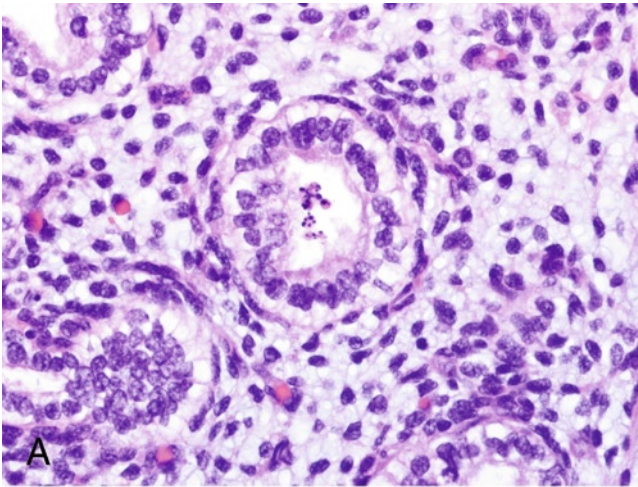


FIGURE 2-42. Karyorrhectic material: lung at 16 weeks (A) and 14 weeks (B) gestation. Karyorrhectic material (A) is present within the lung of a midtrimester fetus. This material should not be mistaken for neutrophils, which have better defined nuclear lobes as seen in B, as in utero infection. (H&E, 60 \times .)

Intrapulmonary Squamous Cells

A few scattered squamous cells within the fetal airways and airspaces of later gestations are a normal finding. These squamous cells enter the lung via fetal inspiration

of amniotic fluid. However, large numbers of squamous cells in the fetal lung are considered to be pathologic and a sign of fetal hypoxia (see Fig. 2-43) [6].

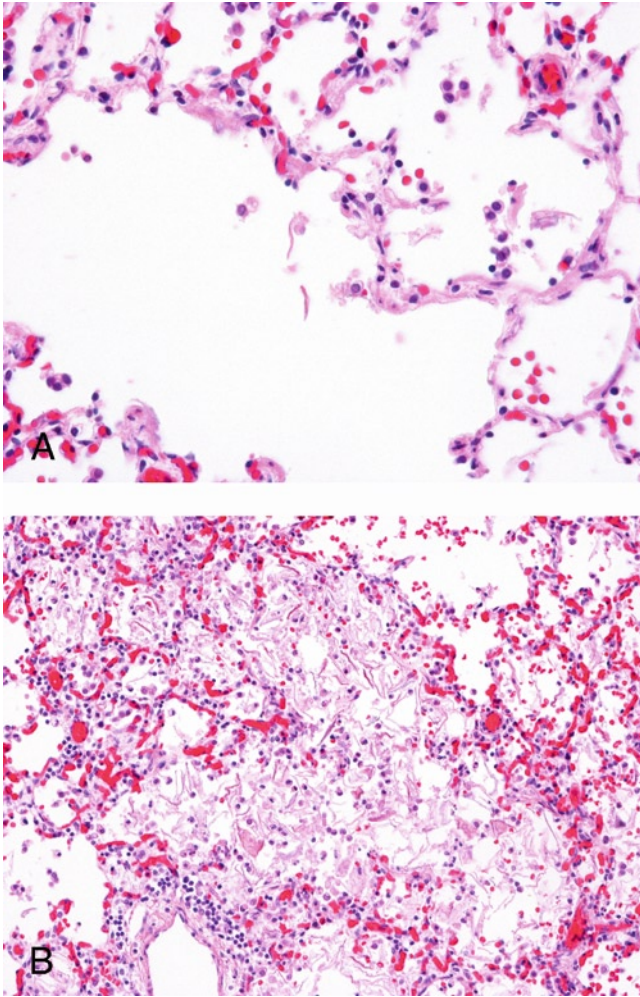


FIGURE 2-43. Squamous cells. Lung at 41 weeks gestation is shown. Occasional squamous cells are present within this late gestation lung (**A**); this is generally considered to be within normal limits. However, large numbers of squames, as seen in this late gestation lung (**B**), are considered to be pathologic. (H&E, **A**, 40× and **B**, 20×.)

References

1. dePaepe ME: Lung growth and development. In *Thurlbeck's Pathology of the Lung*, edn 3. Edited by Churg AM, Myers JL, Tazelaar HD, Wright JL. New York: Thieme; 2005:39–71.
2. Colby TV, Leslie KO, Yousem SA: Lungs. In *Histology for Pathologists*, edn 3. Edited by Mills SE. Philadelphia: Lippincott Williams & Wilkins; 2007:473–483.
3. Langston C: Prenatal lung growth and pulmonary hypoplasia. In *Pediatric Pulmonary Disease*. Edited by Stocker JT. New York: Hemisphere; 1989:1–13.
4. Kimura J, Deutsch GH: Key mechanisms of early lung development. *Pediatr Dev Pathol* 2007, 10:335–347.
5. O'Rahilly RM: *Human Embryology and Teratology*. New York: Wiley-Liss; 2001.
6. Valdes-Dapena MA: The lower respiratory tract. In *Histology of the Fetus and Newborn*. Philadelphia: WB Saunders; 1979:309–341.
7. Hislop A: Developmental biology of the pulmonary circulation. *Paediatr Respir Rev* 2005, 6:35–43.
8. Ersch J, Tschernig T, Stallmach T: Frequency and potential cause of bronchus-associated lymphoid tissue in fetal lungs. *Pediatr Allergy Immunol* 2005, 16:295–298.
9. Gould SJ, Isaacson PG: Bronchus-associated lymphoid tissue (BALT) in human fetal and infant lung. *J Pathol* 1993, 169:229–234.
10. Wigglesworth JS, ed: *Perinatal Pathology*, edn 2. Philadelphia: WB Saunders; 1996.
11. Kresch MJ, Christian C, Wu F, Hussain N: Ontogeny of apoptosis during lung development. *Pediatr Res* 1998, 43:426–431.
12. Scavo LM, Ertsey R, Chapin CJ, et al.: Apoptosis in the development of rat and human fetal lungs. *Am J Respir Cell Mol Biol* 1998, 18:21–31.

SECTION III

Digestive System

3

Gastrointestinal Tract

Dale S. Huff

The gastrointestinal tract is a tube that extends from the end of the pharynx to the anus. Its functions are the propulsion and digestion of food and the elimination of the waste products. It is divided into primary segments that are, from rostral to caudal, the esophagus, stomach, small intestine, and large intestine. The primary segments are divided into secondary segments and are, from rostral to caudal: the proximal, middle and distal parts of the esophagus; the cardia, fundus, body, and antrum or pylorus of the stomach; the duodenum (with its first, second, third, and fourth parts); jejunum and ileum of the small intestine; and the cecum, appendix, ascending, transverse, descending, sigmoid, rectum, and anal canal segments of the large intestine. The histologic junctions between the primary segments may be abrupt but those between the secondary segments are gradual transition zones. Sphincters and valves at junctions of primary segments regulate forward propulsion and prevent retrograde flow of the contents. Although the general architecture of the gastrointestinal tract is established in embryonic life, there is continued development of the layers of the wall during fetal life. Thus, the histology of the gastrointestinal tract is characterized by numerous changes in the fetal period, which are highlighted in this chapter.

Embryology

The gastrointestinal tract is composed of an epithelial lining derived from the endoderm. The epithelial tube is surrounded by concentric layers of mesenchyme derived from the splanchnic mesoderm. The development of the tube is controlled by rostral to caudal, right to left, and inside to outside (radial) molecular genetic morphogenetic gradients. The rostral to caudal division of the tube into its primary and secondary segments is completed by the end of the seventh postfertilization week. The right to left orientation is established by the 10th postfertilization week, when rotation and fixation of the stomach and intestines are completed [1–3]. There is one exception. The “descent” of the cecum, the vertical orientation of the ascending colon and the formation of the hepatic flexure, are not completed until the third trimester. The radial gradient is controlled by epithelial–mesenchymal interactions and results in the orderly development of the concentric layers of the tube and in the radial organization of the villi and crypts; it is completed by the 10th week. The histogenesis of these layers is described below.

Histology

General Considerations

Organization of the wall of the gastrointestinal tract

The wall of the gastrointestinal tract is organized into five concentric layers. From inside out these are mucosa, muscularis mucosae, submucosa, muscularis propria, and subserosa. The histology of the mucosa of each segment is unique to that segment and specific for the function of that segment. The muscularis mucosae, submucosa, muscularis propria, and subserosa or adventitia vary little from segment to segment.

The mucosa is composed of the epithelium and the lamina propria. The epithelium lies on a basement membrane. In the esophagus it is nonkeratinizing stratified squamous epithelium. In the stomach it is simple columnar mucous-producing surface epithelium with gastric pits, which give rise to simple mucous cardiac and pyloric glands, as well as serous gastric glands or crypts. In the small intestine it is villous with serous crypts between the villi. In the large intestine it is simple columnar mucous-producing surface epithelium with mucous crypts. Numerous neuroendocrine cells are scattered throughout the epithelium of the gastrointestinal tract primarily in the base of the crypts and are seen beginning at the 11th week [4]. At least 16 subtypes have been identified and each produces a different gastrointestinal peptide hormone [5]. The frequency and topographic distribution of neuroendocrine cells have been reviewed [6]. Although some can be identified in routine sections by the presence of subnuclear eosinophilic granules or, in the case of Paneth cells by supranuclear eosinophilic granules, they are difficult to see in routine sections and are best studied by immunohistochemical stains. The lamina propria is composed of loose stroma containing nerves, blood vessels, lymphatics, and the scattered lymphoid and other inflammatory cells of the diffuse gut-associated lymphoid tissue. Eosinophils and mast cells are seen in the small and large intestines beginning by the 16th to 20th weeks. The number and cell types of the diffuse gut-associated lymphoid tissue varies somewhat; otherwise, the lamina propria varies little from segment to segment.

The muscularis mucosae is a thin longitudinal layer of smooth muscle separating the mucosa from the submucosa. The muscularis mucosae is composed of smooth muscle even in the upper esophagus, where the muscularis propria is skeletal muscle. Wisps of smooth muscle extend from the muscularis mucosae into the lamina propria and attach to the basement membrane. Small nerve fibers are present.

The submucosa is composed of loose connective tissue containing nerves, ganglia, blood vessels, scattered smooth muscle fibers, lymphatics, and the solitary and aggregated lymphoid follicles of the gut-associated lymphoid tissue that are most well developed at the junctions of the primary segments such as the duodenum, terminal ileum, appendix, and the anorectal region. The submucosal neural plexuses are divided into the submucosal plexus of Meissner, located immediately below the muscularis mucosae, and the deep submucosal plexus of Henle, located along the inner surface of the inner circular layer of the muscularis propria. The submucosa of the esophagus and duodenum contain specialized glands: the esophageal submucosal mucous glands and Brunner's glands, respectively.

The muscularis propria consists of two layers of muscle, the inner circular and outer longitudinal. They are separated by a thin stromal intermuscular septum containing the myenteric or Auerbach's plexus of nerves and ganglion cells. The muscularis propria is composed of smooth muscle except in the upper esophagus, where it is skeletal muscle.

The subserosa or adventitia is loose areolar tissue containing nerves, blood vessels, lymphatics, and lymph nodes. In segments that are intraperitoneal, it is continuous with the mesentery and covered by mesothelium. The esophagus, duodenum except for its first part, rectum, and anus are retroperitoneal and have no mesothelial covering. The dorsal walls of the ascending and descending colons are retroperitoneal and only their ventral walls are covered by mesothelium.

Timing and sequence of developmental events

The gestational ages at which developmental events occur, as cited by different authors, vary considerably. The gestational ages given below are averages of different ages given for each event by several authors [1–4, 7–12] and should be considered approximations.

It is convenient to divide the development of the gastrointestinal tract into three arbitrary periods. During the first period, up to the 14th postfertilization week, the unique definitive histology of each segment is established. During the second period, between 14 and 30 weeks, a few additional histological structures appear. The third period from 30 to 40 weeks is a one of growth and continued maturation of structures and cells that

developed in the previous periods. Histogenesis in general proceeds from rostral to caudal.

Less than 14 weeks. The differentiation of the mucosa occurs in an orderly sequence that is similar in all segments. First, the simple endodermal epithelium, which is present since the formation of the bilaminar disc, develops into a stratified columnar primordial epithelium before the sixth postfertilization week. This primitive stratified epithelium is similar throughout the gastrointestinal tract. Second, during the sixth week the epithelium enters into a proliferative phase, also referred to as *vacuolization*, in which the epithelium of the entire tract becomes multilayered and thick. Third, during the eighth week the

thick proliferative epithelium differentiates into tall simple or pseudostratified columnar epithelium, which then immediately differentiates into the epithelium specific for each segment by 8 to 10 weeks. The development of the unique mucosa of each segment is described below.

Development of the muscular coats and the enteric neural system are intertwined. The muscularis propria appears first in the esophagus, beginning with the appearance of the inner circular layer during the sixth week followed by the outer circular layer during the seventh week. Differentiation spreads from rostral to caudal, and reaches the anal canal by as early as the eighth week. The outer longitudinal layer is very thin until approximately the third trimester. The muscularis mucosae is the last layer to develop. It begins in the esophagus during the 11th week, in the stomach during the 14th week, in the anal canal in the 16th week, and in the duodenum in the 21st week. It spreads from the duodenum caudally and from the anal canal rostrally to meet at the ileocecal junction during the last trimester. However, recent studies utilizing immunohistochemical stains suggest that the onset of differentiation of the muscularis propria and muscularis mucosae in the upper esophagus occur earlier in gestation and the rostral to caudal wave of differentiation of the smooth muscle coats to the rectum is more rapid than the times indicated above, which are based on routine stains [13,14].

The rostral neural crest cells, which will form the nerves and ganglion cells of the neurenteric plexuses, diffusely invade the upper esophagus during the fourth week and migrate caudally to reach the anal canal by the seventh week. The neural crest cells gather into loose bands in the connective tissue layer of the future muscularis propria to form the primordium of Auerbach's plexus in the esophagus during the fifth week. During the sixth week, the neural crest cells migrate centripetally through the developing inner circular muscle layer into the submucosa to form the primordia of the submucosal plexuses. During the seventh week, the bands of neural primordia in the esophagus form discrete nests or ganglia composed of neuroblasts. In the ninth week, interstitial cells of Cajal enter the rostral esophagus and gather around Auerbach's plexuses, then spread centripetally into the submucosa and surround the submucosal plexuses of Henle and Meissner. All of these events begin first in the muscularis propria of the upper esophagus, spread into submucosa a week or two later, and

spread caudally so that the entire enteric neural system is completed by approximately 14 weeks [13,14]. Neural crest cells from the sacral area invade the anorectal area during the 10th to 12th weeks. In the meantime, the neuroblasts of the plexuses gradually differentiate into mature ganglion cells from rostral to caudal, a process that is not complete until the neonatal period.

14 to 30 weeks. Scattered lymphoid cells appear in the lamina propria during the seventh week. Beginning in the 11th week, immunohistochemical stains identify precursors of lymphoid tissue in sites where lymphoid aggregates will develop in the future. After 14 weeks the gut-associated lymphoid tissue is visible in routine histological sections. Tiny aggregates of lymphoid and inflammatory cells in the lamina propria of the terminal ileum are infrequent at 14 weeks and more consistently seen at 16 weeks. By 19 to 20 weeks, more organized primary follicles are present and these become easily recognizable in the terminal ileum, appendix, duodenum, anorectal area, and other sites after 20 weeks postmenstrual age. By 24 weeks, large Peyer's patches are present in the submucosa of the terminal ileum and prominent submucosal solitary primary follicles are seen in the duodenum, jejunum, appendix, and distal colon [15]. The development of primary follicles and the diffuse lymphoid tissue in the lamina propria and submucosa during this period is antigen independent. Germinal centers and mature plasma cells, the development of which are dependent upon exposure to foreign antigens, are not found in normal fetuses or neonates prior to 2 weeks of age. The presence of easily identifiable submucosal lymphoid aggregates and primary follicles prior to 20 weeks, or the presence of germinal centers and mature plasma cells at any time during fetal life, may indicate fetal infection or other abnormal antigenic stimulus.

30 to 40 weeks. From 30 weeks to term, the gastrointestinal tract continues to grow and mature. Some of the major changes include maturation of the esophageal epithelium, development of the muscularis mucosae of the small and large intestines, and continued maturation of the ganglion cells of the plexuses of Auerbach, Henle, and Meissner. Maturation of some of the histologic components of the gastrointestinal tract continues into the neonatal period and infancy; this is especially true of the gut-associated lymphoid tissue and the ganglion cells of the enteric neural system.

Esophagus

Less than 14 weeks

During the seventh week, the primitive esophageal mucosa proliferates and forms multiple irregular bridges that traverse and partially occlude the lumen, leaving multiple small round lumens called *vacuoles*. At this time the inner circular layer of the muscularis propria has formed, the outer longitudinal is beginning to appear, and primitive Auerbach's plexuses populated by neuroblasts are present. The muscularis mucosae and submucosal plexuses have not appeared (see Fig. 3-1). The proliferative phase recedes and the epithelium differentiates into a primitive pseudostratified columnar type

(see Figs. 3-2–3-4) and the muscularis mucosae appears (see Fig. 3-4). The epithelium then differentiates into poorly organized stratified squamous epithelium. Columnar ciliated cells cover the surface of the middle of the esophagus and spread to cover the entire surface by the 11th week (see Figs. 3-5 and 3-6). The muscularis mucosae becomes thicker and the outer longitudinal layer of the muscularis propria remains very thin. Some of the neuroblasts in submucosal and myenteric plexuses begin to mature toward ganglion cells (see Fig. 3-5).

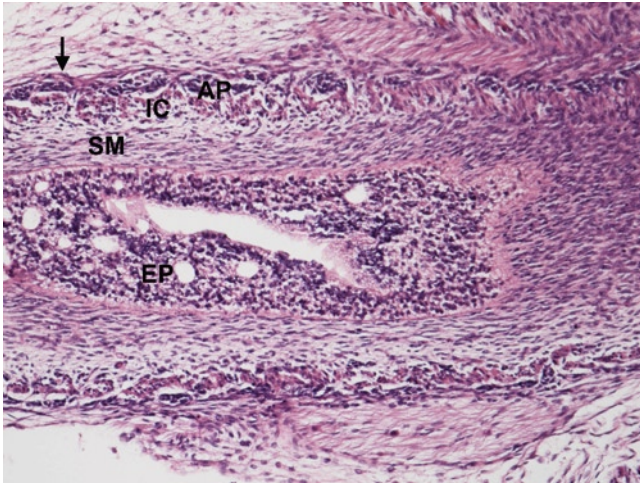


FIGURE 3-1. Esophagus at 7 weeks postfertilization. The proliferative phase of esophageal mucosal development is shown. The lumen is nearly occluded by irregular bridges of proliferative epithelium (EP) leaving several round lumens. This appearance has been referred to as *vacuolization*. The submucosa (SM) is prominent but the muscularis mucosae and submucosal neural plexuses of Meissner and Henle are not present. The inner circular (IC) layer of the muscularis propria is well formed. The outer longitudinal layer (arrow) is discontinuous and one or two cells deep. Auerbach's plexus (AP) is composed of a nearly continuous strip of undifferentiated neuroblasts. (Hematoxylin and eosin [H&E], 10 \times .)

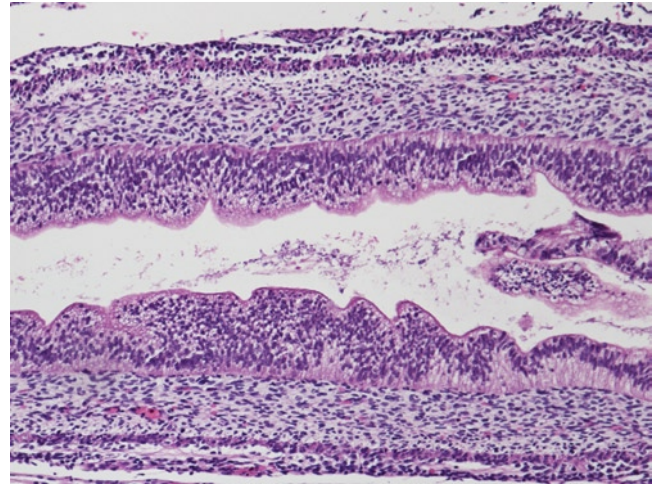


FIGURE 3-2. Esophagus at 11 weeks postfertilization. The receding proliferative phase is shown. The lumen is re-established and the epithelium is heaped up and multilayered in some areas and tall pseudostratified in others. The inner circular layer is conspicuous but the outer longitudinal layer is discontinuous and one or two cells deep. Auerbach's plexus is composed of neuroblasts. (H&E, 10 \times .)

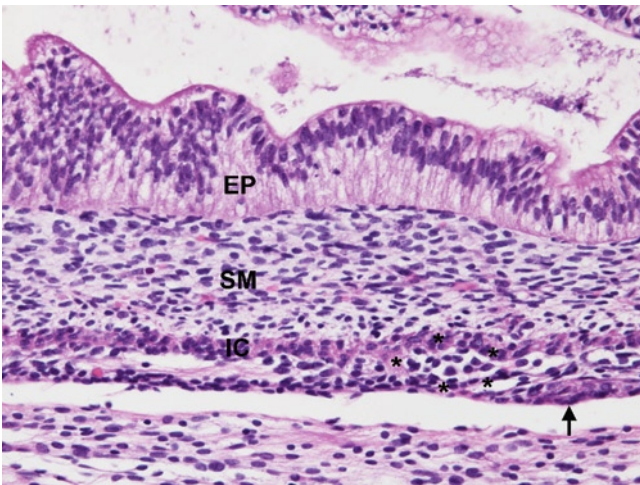


FIGURE 3-3. Esophagus at 11 weeks postfertilization. This figure is a higher magnification of Figure 3-2. The tall pseudostratified columnar epithelium (EP) is undifferentiated. The submucosa (SM) is present but the muscularis mucosae and submucosal plexuses are not. The inner circular (IC) and outer longitudinal (arrow) layers, and Auerbach's plexus (outlined by asterisks), are similar to those in Figure 3-2. (H&E, 20 \times .)

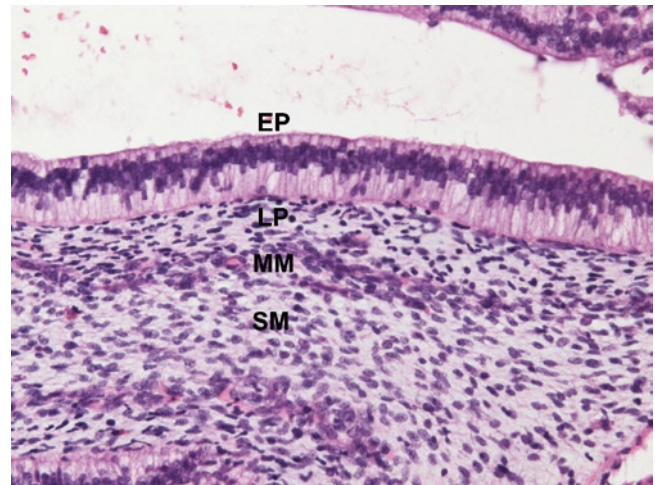


FIGURE 3-4. Esophagus at 11 weeks postfertilization. Undifferentiated pseudostratified columnar epithelium is shown. The epithelium (EP) is no longer proliferative. The muscularis mucosae (MM) is present and separates the lamina propria (LP) from the submucosa (SM). (H&E, 20 \times .)

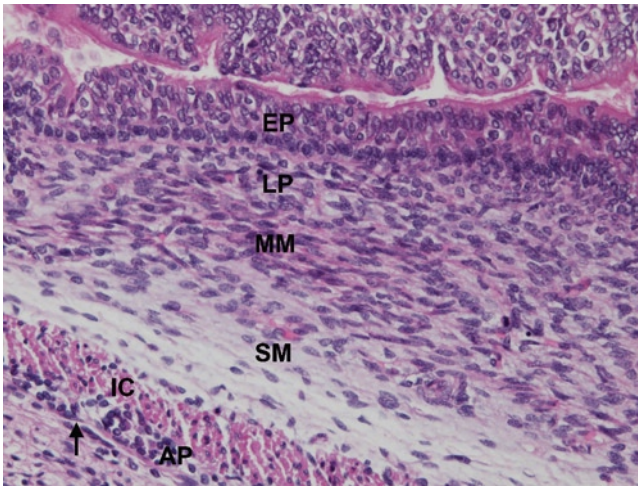


FIGURE 3-5. Esophagus at 12 weeks postfertilization. The primitive stratified squamous epithelium (EP) with ciliated columnar epithelium on the surface is shown. The epithelium is specific for the esophagus. The thickening of the muscularis mucosae (MM) and the inner circular (IC) layer continues to increase. The outer longitudinal layer (arrow) is still only one or two cells deep. Some of the neuroblasts of Auerbach's plexus (AP) have begun to differentiate into ganglion cells. (H&E, 20 \times .)

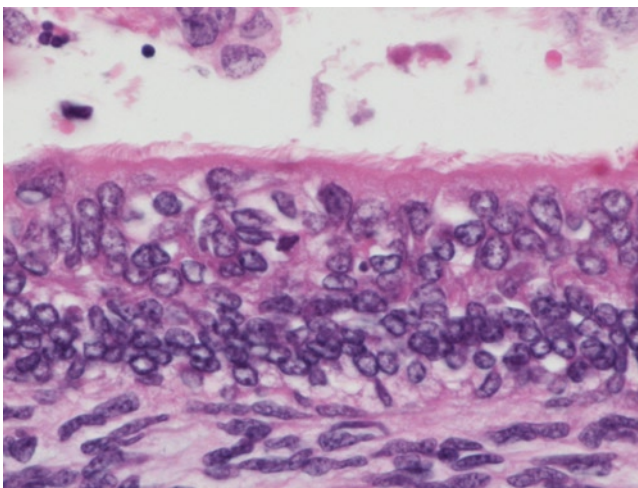


FIGURE 3-6. Esophagus at 12 weeks postfertilization. This higher magnification of Figure 3-5 shows how the stratified squamous epithelium is disorganized and the surface cells are ciliated. (H&E, 60 \times .)

14 to 30 weeks

Beginning at approximately 16 weeks, squamous epithelium gradually replaces the ciliated columnar epithelium on the surface of the mid esophagus (see Figs. 3-7 and 3-8). Esophageal cardiac glands, which are similar to gastric cardiac or pyloric glands, are mucous-producing glands in the lamina propria connected to the lumen by a duct that passes through the epithelium. Papillae of the lamina propria, which are finger-like processes of lamina propria that penetrate up into the epithelium during postnatal life and are important in the evaluation of esophagitis, are not present during fetal life (see Fig. 3-7). The esophageal muscularis mucosae rapidly increases in

thickness and becomes the thickest of all the segments of the gastrointestinal tract. The primordia of esophageal submucosal mucous glands appear at 27 weeks and are thought to be analogous to the submucosal glands of the pharynx. The outer longitudinal layer of the muscularis propria becomes slightly thicker, and the deep submucosal plexuses of Henle become more numerous and conspicuous (see Figs. 3-7 and 3-9). Ectopic gastric mucosa of the cardiac, oxyntic, or pyloric variety is often seen in the mucosa of the upper esophagus throughout fetal life (see Fig. 3-10) and may be confused with esophageal cardiac glands.

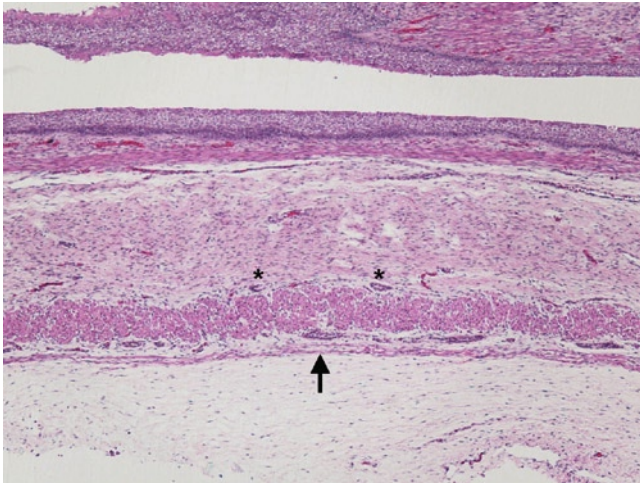


FIGURE 3-7. Esophagus at 19 weeks postmenstruation. Squamous cells are beginning to replace the ciliated columnar surface epithelium. The deep surface of esophageal epithelium is flat and papillae of the lamina propria are not present. The deep submucosal plexus of Henle (asterisks) is present. The outer longitudinal layer of the muscularis propria (arrow) is only a few cells deep and is much thinner than the inner circular layer. Auerbach's plexuses are discrete nests as opposed to the nearly continuous ribbons that are characteristic of the plexus prior to 14 weeks. (H&E, 4 \times .)

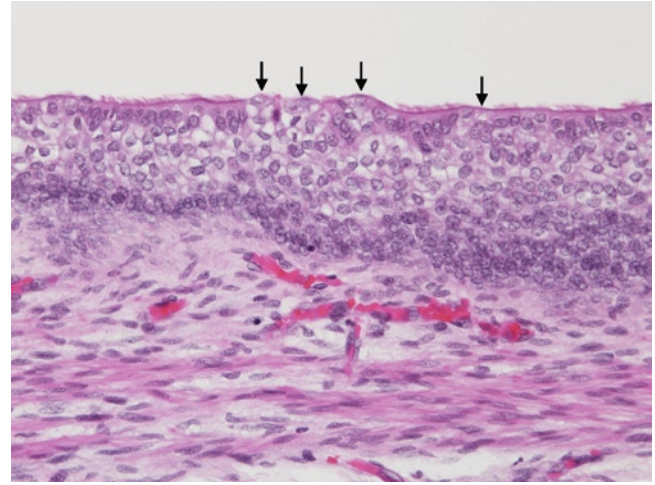


FIGURE 3-8. Esophagus at 19 weeks. This higher magnification of Figure 3-7 shows how squamous epithelium (arrows) begins to replace the ciliated columnar epithelium of the surface in focal areas. (H&E, 10 \times .)

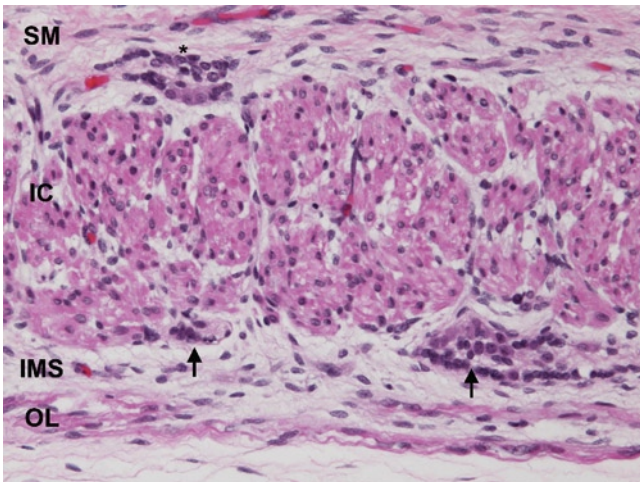


FIGURE 3-9. Esophagus at 19 weeks. Partially differentiated submucosal and myenteric plexuses are shown. The deep submucosal plexus of Henle (asterisk) and the myenteric plexus of Auerbach (arrows) are composed of a mixture of undifferentiated and partially differentiated neuroblasts. IC—inner circular layer of muscularis propria; IMS—intermuscular septum; OL—outer longitudinal layer of muscularis propria; SM—submucosa. (H&E, 20 \times .)

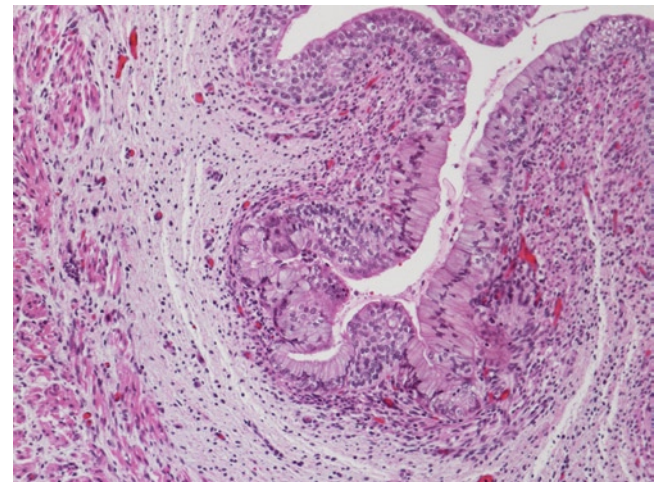


FIGURE 3-10. Ectopic gastric cardiac or pyloric mucosa in the esophagus at 19 weeks. The ectopic gastric mucosa or gastric heterotopia is composed of tall mucous-producing simple columnar epithelium that replaces the stratified squamous epithelium of the upper esophagus. (H&E, 10 \times .)

30 to 40 weeks

Figures 3-11 through 3-15 illustrate the histology of the distal and proximal esophagus near term. The squamous epithelium spreads rostrally and caudally to replace the ciliated cells and covers the surface of the entire esophagus by the 40th postmenstrual week (see Fig. 3-11). The submucosal mucous glands, the primordia of which appear by approximately 27 weeks, become well differentiated during this period. The ducts arise from the squamous mucosa and penetrate through the muscularis mucosae into the submucosa. The proximal ends of the ducts in the lamina propria

are lined by squamous cells. After they penetrate through the muscularis mucosae, the epithelium is composed of two layers of cuboidal epithelium, a luminal layer and a basal layer of myoepithelial cells (see Fig. 3-11). These ducts give rise to the mucous glands located in the submucosa (see Fig. 3-12). Some of the ganglion cells are fully mature but partially differentiated neuroblasts remain (see Fig. 3-13). Some patches of ciliated epithelium may remain at birth (see Fig. 3-15), but those disappear within a few days of birth.

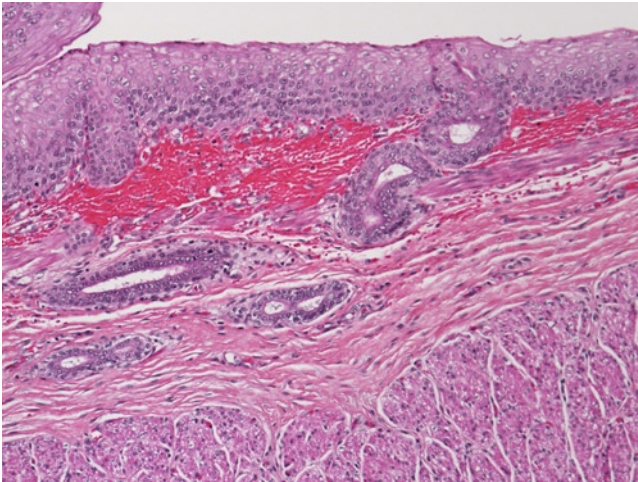


FIGURE 3-11. Esophagus at 34 weeks. Mature stratified squamous surface epithelium and ducts of esophageal submucosal mucous glands near the gastroesophageal junction are present. The epithelium is well-differentiated stratified squamous epithelium without ciliated columnar cells on the surface. The duct of the submucosal mucous gland penetrates through the muscularis mucosae into the submucosa. The bilayered cuboidal ductal epithelium is composed of a luminal layer and a basal layer. The ducts are coursing caudally toward the gastroesophageal junction, which is out of the picture to the left. (H&E, 10 \times .)

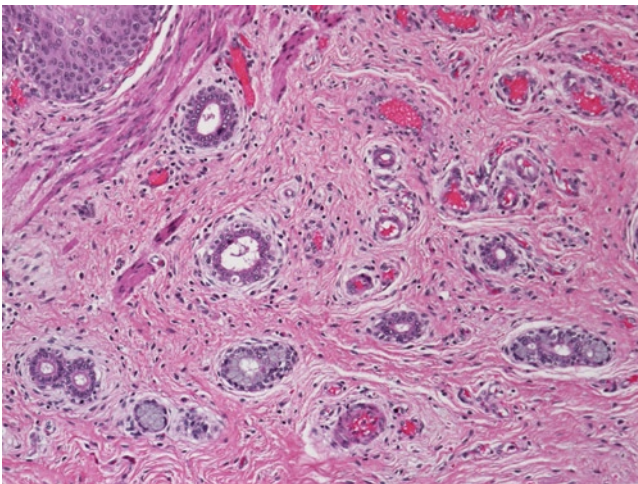


FIGURE 3-12. Esophagus at 34 weeks. The submucosal glands of the ducts, shown in Figure 3-11, are demonstrated. The esophageal epithelium and muscularis mucosae are in the upper left corner. The glands are immature and small. (H&E, 10 \times .)

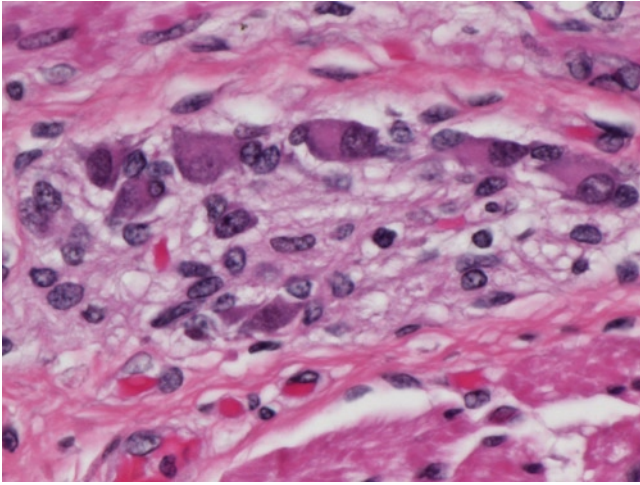


FIGURE 3-13. Auerbach's plexus in the esophagus at 34 weeks. The cells are a mixture of neuroblasts, partially differentiated neuroblasts, and mature ganglion cells. Compare with Figures 3-3 and 3-9. (H&E, 60 \times .)



FIGURE 3-14. Midesophagus at 35 weeks. There are no papillae of the lamina propria. Ducts of esophageal submucosal mucous glands are seen in the lamina propria and submucosa, and the muscularis mucosae is very thick. The muscularis propria also is very thick and, although the outer longitudinal layer has grown considerably in thickness, it is still approximately half the thickness of the inner circular layer. The intermuscular septum is distinct. (H&E, 2 \times .)

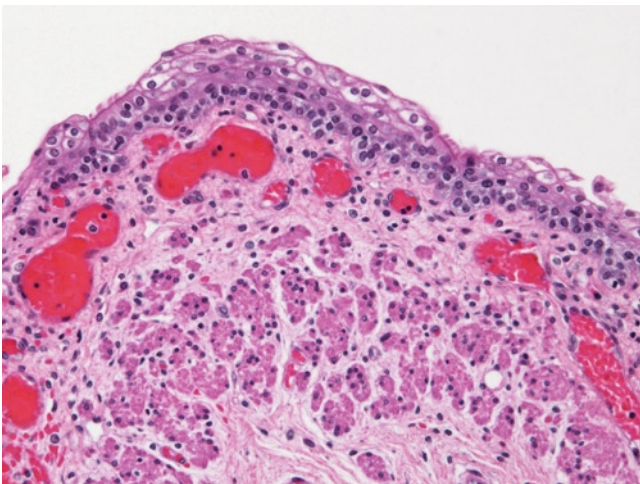


FIGURE 3-15. Esophagus at 35 weeks. This figure is a higher magnification of the esophageal mucosa shown in Figure 3-14. A few tufts of cilia remain on the surface. (H&E, 20 \times .)

Stomach

Less than 14 weeks

The unique histology of the stomach is established before the 14th postfertilization week. The multilayered pseudostratified primordial gastric epithelium (see Fig. 3-16) enters the proliferative or vacuolization phase during the sixth to seventh postfertilization week. The proliferating epithelium partially occludes the lumen of the cardia and pylorus. The unique gastric epithelium characterized by foveolar epithelium and gastric pits replaces the proliferative epithelium in the body during the seventh to eighth week [16] and lines the entire stomach by the 10th to 12th week (see Fig. 3-17). The first gastric glands with mucous neck cells, parietal cells, chief cells, and endocrine cells appear by the ninth to 10th week (see Figs. 3-18 and 3-19). Cardiac mucosa becomes distinguishable from oxyntic mucosa, although the existence of a distinct cardiac mucosa has been questioned. The embryology of the mucosa of the esophagogastric junction is the subject of continuous debate [17,18]. Specific cardiac (see Figs. 3-20–3-22) and pyloric mucosa appear

by week 13 and the mucosa of the cardia and pylorus becomes villous. The gastric muscularis propria is composed of three layers: the inner circular and outer longitudinal layers characteristic of the entire gastrointestinal tract, and an additional oblique layer internal to the inner circular layer (see Fig. 3-23). The inner circular and oblique layers appear in the cardia during the seventh week, and the outer longitudinal layer appears during the eighth week. All layers are present throughout the entire stomach by the ninth week, but the three layers may be indistinct. The circular layer is the most distinct of the three: it enlarges at the pylorus to form the pyloric sphincter during the ninth postfertilization week. The submucosal and myenteric plexuses, as well as the interstitial cells of Cajal, are formed at the same time as the muscularis propria, but the neuroblasts within the plexuses remain undifferentiated. The muscularis mucosae appears in the cardia during the 10th week and spreads throughout the entire stomach by the 14th week.

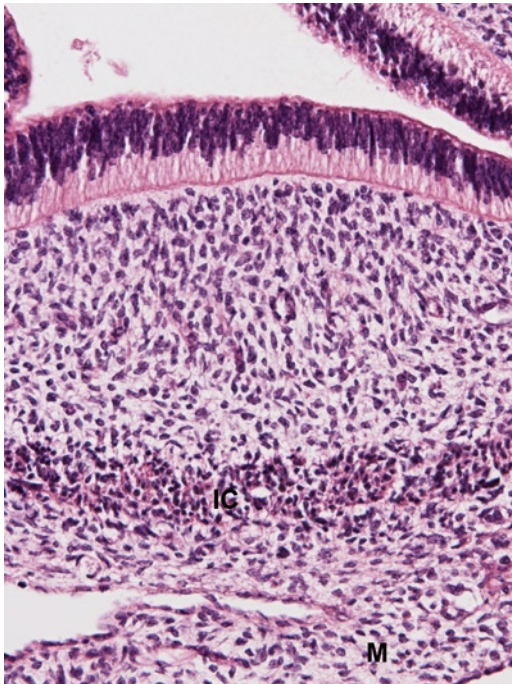


FIGURE 3-16. Stomach at 7 weeks postfertilization. The primordial multilayered pseudostratified epithelium is on the top. The inner circular (IC) layer of the muscularis propria is apparent but the outer longitudinal layer has not yet differentiated. The serosa is at the bottom and the gastric mesentery (M) is included. (H&E, 20 \times .)

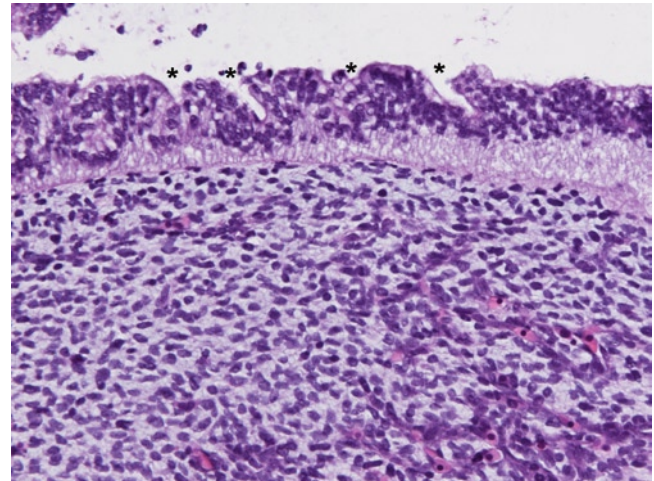


FIGURE 3-17. Formation of gastric pits in stomach at 8 weeks postfertilization. The primordial epithelium has differentiated into distinctive gastric epithelium with the formation of gastric pits (asterisks). (H&E, 20 \times .)

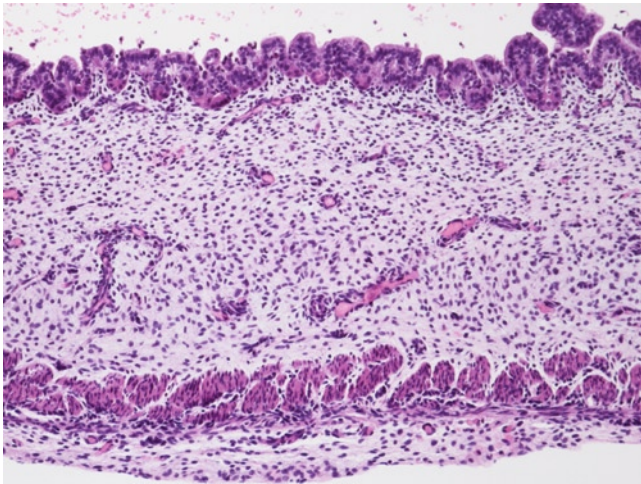


FIGURE 3-18. Formation of gastric glands in stomach at 12 weeks postfertilization. The primitive gastric pits have differentiated into gastric glands with eosinophilic parietal cells and the surface epithelium is differentiating into foveolar epithelium. The muscularis mucosae has not appeared. The muscularis propria is composed of the innermost oblique layer and inner circular layers, which are nearly indistinguishable from each other and the outer longitudinal layer of two or three cells' thickness. The nests of neuroblasts of Auerbach's myenteric plexus are visible in the intermuscular septum. (H&E, 10 \times .)

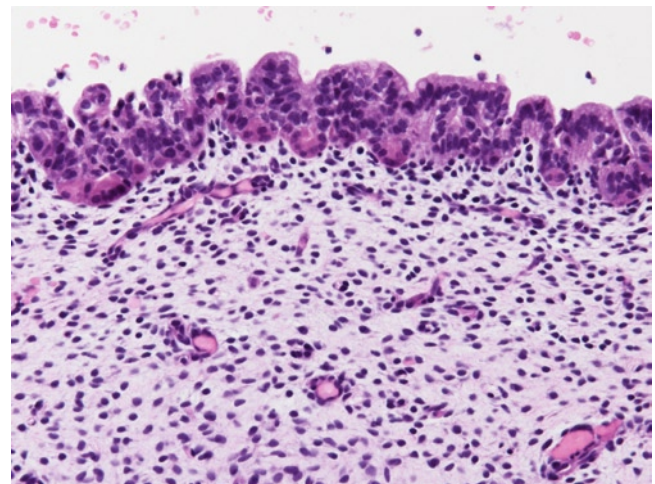


FIGURE 3-19. Stomach at 12 weeks postfertilization. This higher magnification is of the gastric glands in Figure 3-18. The parietal cells and surface epithelium are distinct, and the muscularis mucosae is not present. (H&E, 20 \times .)

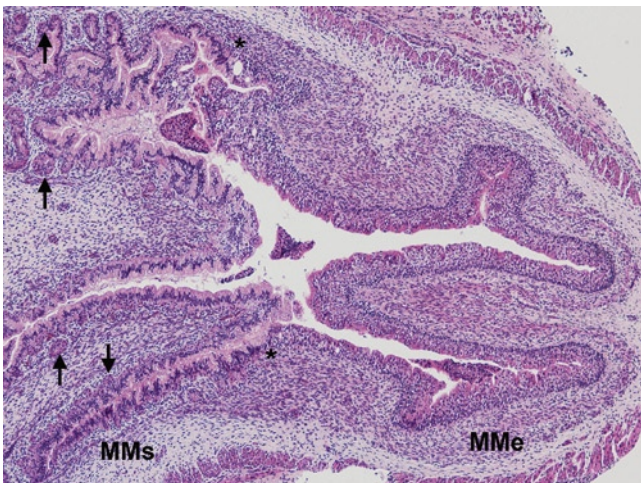


FIGURE 3-20. Esophago-gastric junction at 12 weeks postfertilization. The distal esophagus occupies the right half of the picture and the cardiac mucosa is to the left. The squamous-columnar junction is indicated by the two asterisks. The arrows indicate the junction between the cardiac mucosa and the transition to oxyntic mucosa with gastric pits and parietal cells. The distance between the squamous-columnar junction and the transitional mucosa in this specimen is less than 1 mm. The thick muscularis mucosae (MMe) of the esophagus abruptly transitions into the much thinner muscularis mucosae of the stomach (MMs). (H&E, 4 \times .)

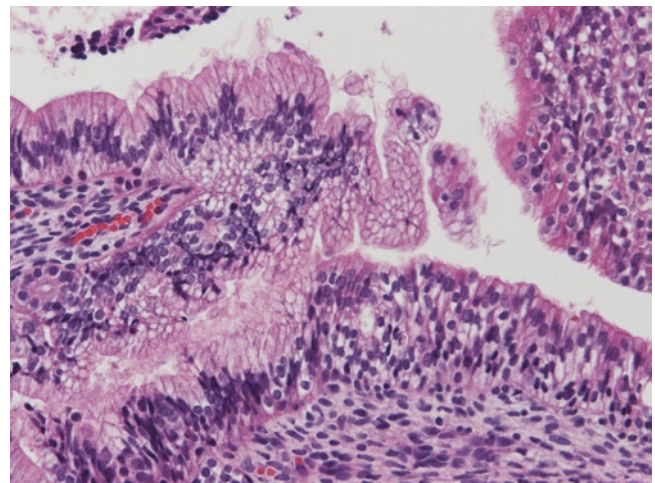


FIGURE 3-21. Stomach at 12 weeks postfertilization. This higher magnification of the squamous-columnar junction in Figure 3-20, indicated by the lower asterisk, is shown. The esophageal stratified squamous epithelium with ciliated columnar epithelium on its surface is to the right. The distinctive pseudostratified cardiac epithelium is to the left. (H&E, 20 \times .)

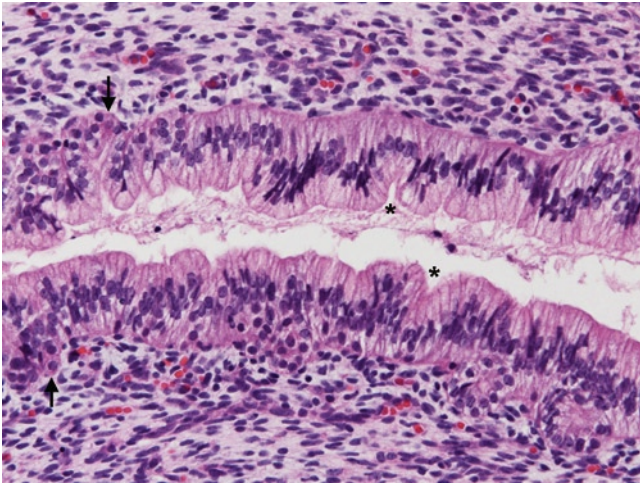


FIGURE 3-22. Gastric cardiac mucosa at 12 weeks postfertilization. This higher magnification is of the cardiac mucosa in Figure 3-20. Primitive cardiac pits (asterisks) are present in the pseudostratified columnar cardiac epithelium. Gastric pits (arrows) with primitive parietal cells indicate the junction between the cardiac and transitional epithelia. (H&E, 20 \times .)

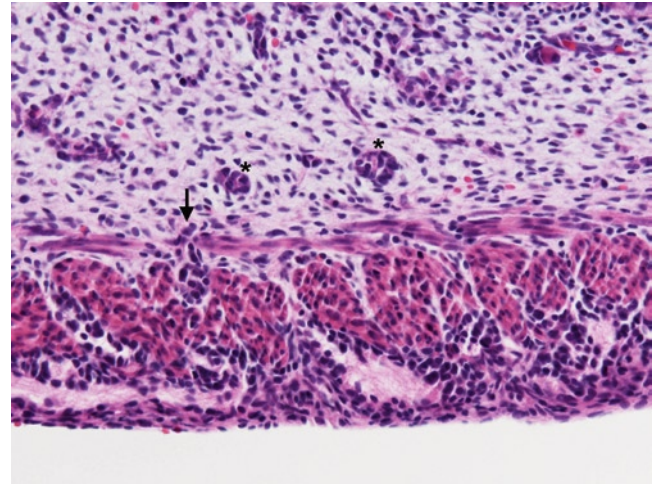


FIGURE 3-23. Muscularis propria of stomach at 11 weeks postfertilization. The submucosa occupies the top half of the picture. The three layers of the gastric muscularis propria can be identified: the thin innermost oblique layer, the thick inner circular layer, and the thin outer longitudinal layer. Auerbach's myenteric plexuses with undifferentiated neuroblasts are prominent. Neuroblasts are migrating from Auerbach's plexuses up into the submucosa (arrow) to form the deep submucosal plexuses of Henle (asterisks). (H&E, 20 \times .)

14 to 30 weeks

The cardiac and pyloric villi become prominent (see Fig. 3-24). They often disappear by 30 weeks but may persist beyond this point in some cases. The gastric glands elongate and the specific cell types of the glands continue

to differentiate (see Figs 3-25-3-27). The diffuse gut-associated lymphoid tissue develops in the lamina propria. The neuroblasts of the submucosal and myenteric plexuses continue to differentiate toward ganglion cells.

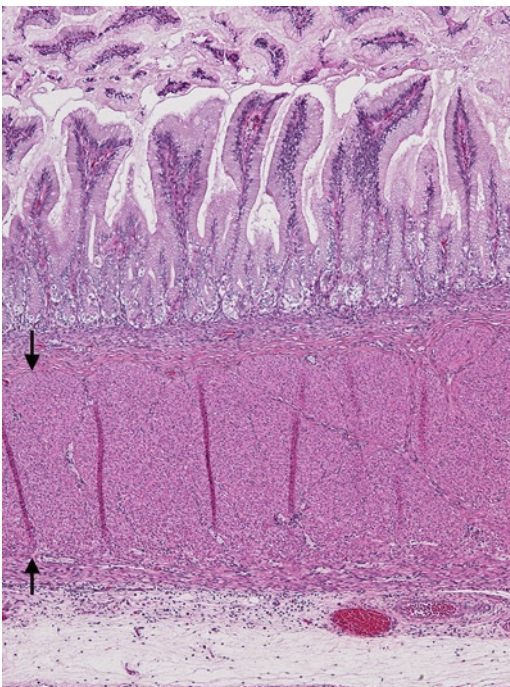


FIGURE 3-24. Gastric pyloric mucosa at 24 weeks. The pyloric mucosa is villous and its mucous glands are distinct from the gastric glands. The pyloric sphincter is formed by the inner circular layer of the muscularis propria (between the two arrows). The outer longitudinal layer is below and Auerbach's plexuses are visible between the two. The innermost oblique layer is not present in the pyloric sphincter. (H&E, 4 \times .)

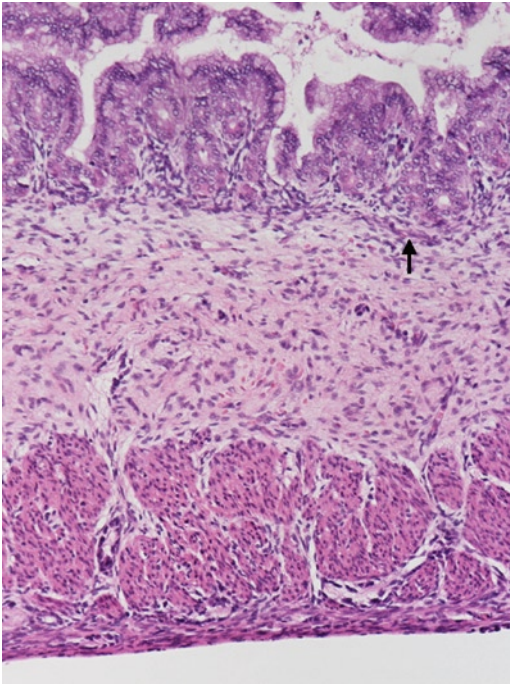


FIGURE 3-25. Stomach at 16 weeks. The full thickness of the wall of the gastric body is shown. The oxyntic mucosa has increased in thickness and the gastric glands have elongated. Compare this image with Figure 3-18 from age 12 weeks postfertilization, taken at the same magnification. Foveolar epithelium, mucous cells, and parietal cells continue to differentiate. The muscularis mucosae (arrow) is beginning to differentiate. The muscularis propria is very thick and the outer longitudinal layer, though thicker than previously, is still much thinner than the other layers. (H&E, 10 \times .)

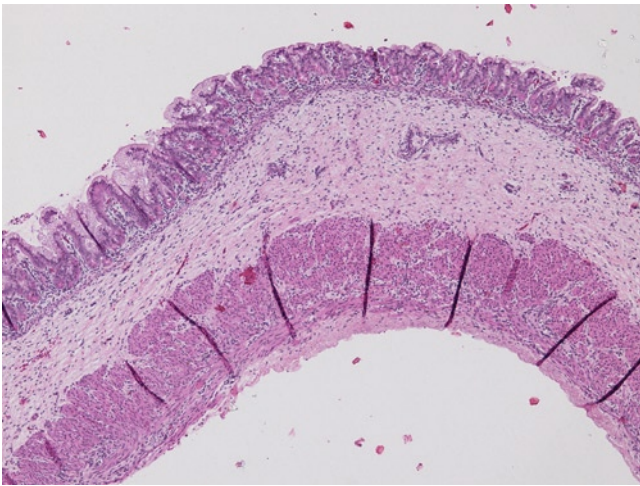


FIGURE 3-26. Stomach at 19 weeks. The full thickness of the wall of the gastric body is shown. The muscularis mucosae is well developed and the lamina propria is distinctly separated from the submucosa. (H&E, 4 \times .)

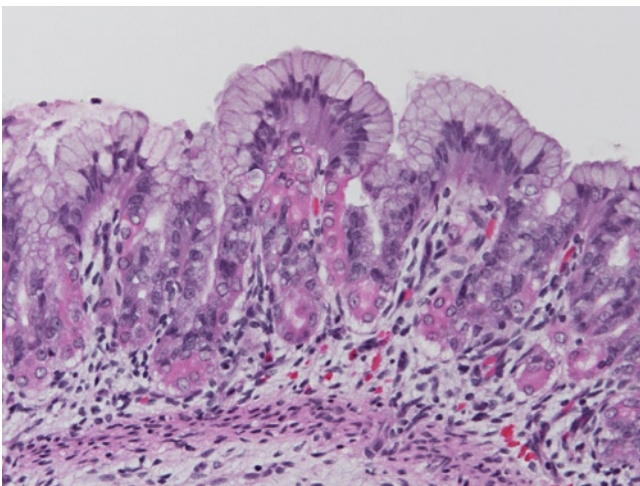


FIGURE 3-27. Stomach at 19 weeks. This image is a higher magnification of the oxyntic mucosa shown in Figure 3-26. Foveolar epithelium, mucous neck cells, chief cells, and parietal cells all are well differentiated. The basophilic cytoplasm of the chief cells is distinct from the eosinophilic cytoplasm of the parietal cells. The lamina propria contains scattered lymphoid cells. The muscularis mucosae is distinct. (H&E, 20 \times .)

30 to 40 weeks

The cardiac and pyloric villi (see Fig. 3-28) disappear. Gastric glands change little during this period (see Fig. 3-29). The diffuse gut-associated lymphoid tissue

becomes more abundant but aggregated lymphoid tissue is uncommon. Maturation of neuroblasts into ganglion cells is nearly complete.

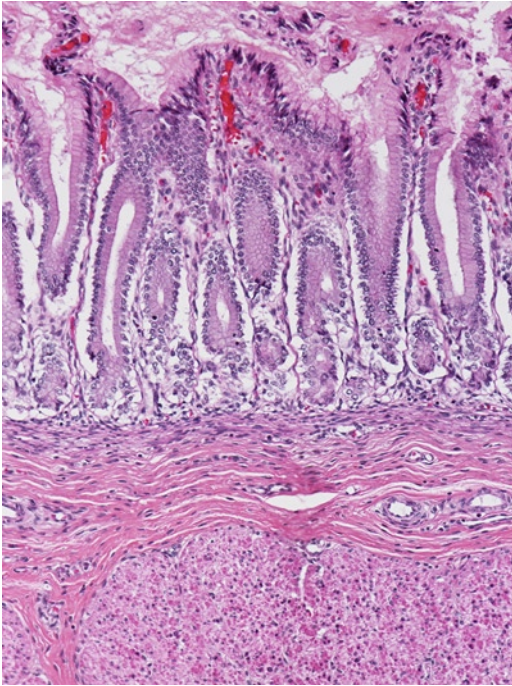


FIGURE 3-28. Gastric pyloric mucosa at 35 weeks. The pyloric mucosa is no longer villous; compare with Figure 3-24. (H&E, 10 \times .)

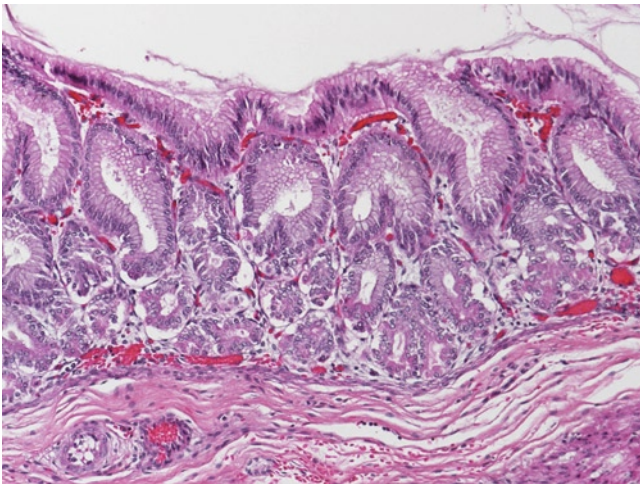


FIGURE 3-29. Oxyntic mucosa at 34 weeks. The histology of the oxyntic mucosa has not changed significantly in the last half of pregnancy, as shown; compare with Figure 3-27. (H&E, 10 \times .)

Small Intestine

Less than 14 weeks

The unique histology of the small intestine is established before the 14th week postfertilization. The multilayered primitive pseudostratified columnar epithelium enters the proliferative or vacuolization phase during the sixth week and the proliferative epithelium transiently occludes the duodenal lumen during the seventh week. The proliferative epithelium regresses, the duodenal lumen is re-established, and villi appear in the duodenum in the eighth week (see Fig. 3-30). Crypts of Lieberkühn appear in the duodenum during the ninth week (see Fig. 3-31). The villi and crypts spread from rostral to caudal and arrive at the terminal ileum in the 12th to 14th weeks (see Figs.

3-32–3-35). Some subsets of mucosal cells such as enterocytes, goblet cells, gastrin cells, and somatostatin cells differentiate prior to 14 weeks. Brunner's glands appear in the first part of the duodenum as early as the 14th week. The inner circular and outer longitudinal layers of the muscularis propria appear in the duodenum in the seventh and eighth weeks, respectively, and differentiate from rostral to caudal and arrive at the terminal ileum in the ninth to 10th weeks. The submucosal and myenteric plexuses differentiate in synchrony with the muscle coats and the myenteric plexus appears first followed by the submucosal plexuses of Henle and Meissner.

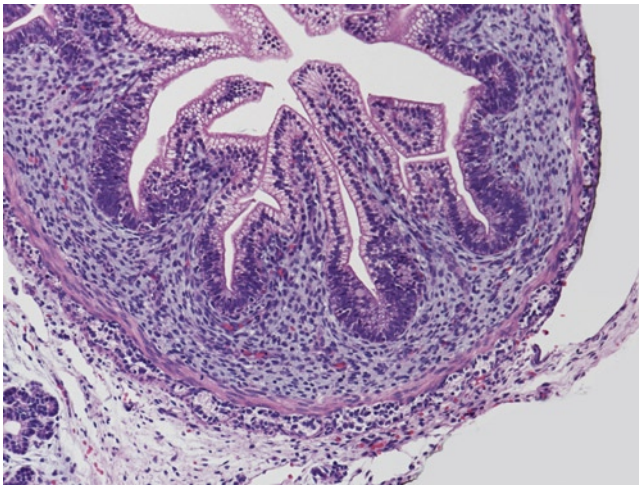


FIGURE 3-30. Duodenum at 11 weeks postfertilization. The primitive villi are covered by differentiating enterocytes. The epithelium between the villi is multilayered pseudostratified primordial epithelium, which is forming primitive crypts in some areas and will differentiate into single-layered surface epithelium in the future. The muscularis mucosae and Brunner's glands have not yet differentiated, although the inner circular layer of the muscularis propria is well differentiated. The external longitudinal layer is only one or two cells thick. Auerbach's plexus, with its undifferentiated neuroblasts, forms an almost continuous ring in the intermuscular septum. Pancreatic acini are in the left lower corner. (H&E, 10 \times .)

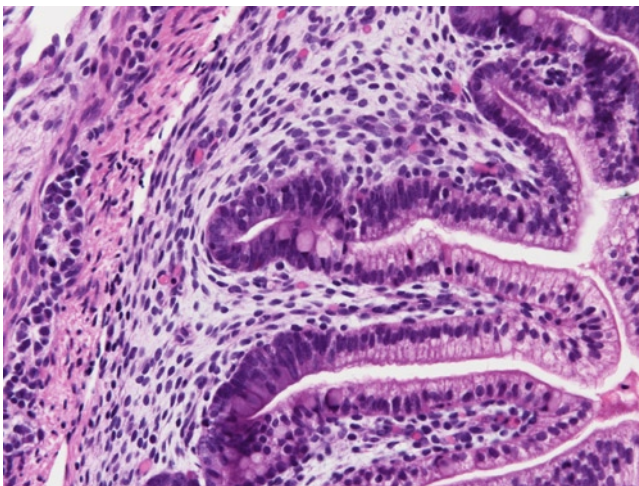


FIGURE 3-31. Duodenum at 12 weeks postfertilization. The enterocytes are more well differentiated than they were previously and goblet cells have appeared. Crypts of Lieberkühn are becoming recognizable. The primordial epithelium seen previously is differentiating into the crypts and surface epithelium. Brunner's glands have not yet differentiated. The muscularis propria is on the right and Auerbach's plexus contains sheets of neuroblasts. (H&E, 20 \times .)

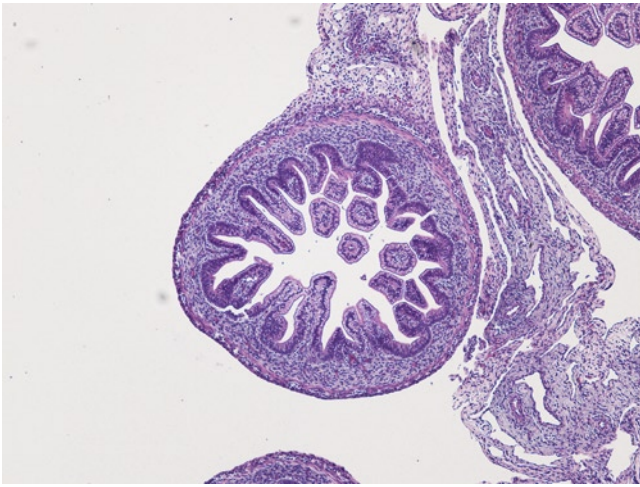


FIGURE 3-32. Small intestine (jejunum or ileum) at 11 weeks postfertilization. The jejunum and ileum cannot be differentiated histologically from the duodenum at this gestational age and the duodenum can be identified only by its attachment to the head of the pancreas. Notice the villi, intervillous primordial epithelium, primitive crypts of Lieberkühn, the two layers of muscularis propria, and the ring of Auerbach's plexus. (H&E, 4 \times .)

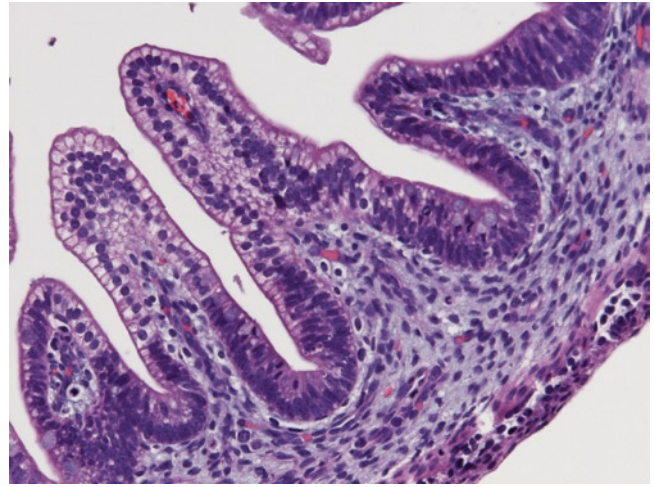


FIGURE 3-33. Small intestine at 11 weeks postfertilization. This image is a higher magnification of Figure 3-32. Note the villi, primitive crypts, muscularis propria (*lower right*), and Auerbach's plexus. The muscularis mucosae has not yet differentiated. (H&E, 20 \times .)

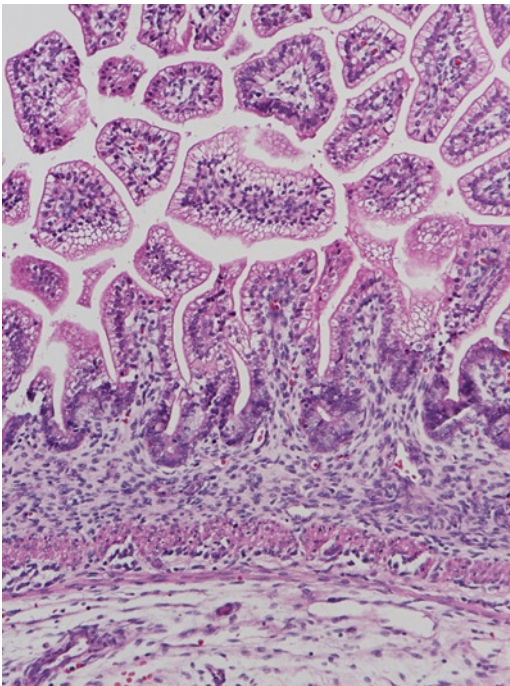


FIGURE 3-34. Small intestine (not duodenum) at 12 weeks postfertilization. The villi, enterocytes, and crypts of Lieberkühn are better differentiated than in the previous figures. The muscularis mucosa is absent, and the muscularis propria and Auerbach's plexus have changed little. (H&E, 10 \times .)

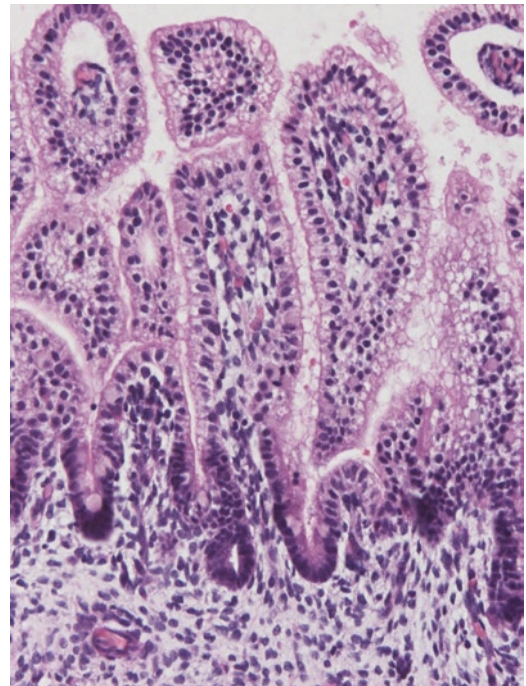


FIGURE 3-35. Small intestine at 12 weeks postfertilization. This higher magnification image is of the small intestinal mucosa. (H&E, 20 \times .)

14 to 30 weeks

Brunner's glands continue to differentiate from rostral to caudal throughout the rest of the duodenum during the 14th to 16th weeks (see Figs. 3-36–3-38). Brunner's glands are sparse distal to the papilla of Vater. The transition from pyloric to duodenal mucosa is gradual in some cases and duodenal-like villi may be found in the distal pylorus and pyloric-like epithelium may be found in the duodenum. The villi of the small intestine grow longer (see Fig. 3-39) and are covered by enterocytes with distinct brush borders, goblet cells, and a few endocrine cells. The stem cells of the intestinal mucosa reside in the base of the crypts of Lieberkühn. They proliferate and give rise to the enterocytes, goblet cells, and endocrine cells, which migrate centripetally up the crypts and to the tips of the villi where they may undergo apoptosis and slough into the lumen. Semba *et al.* state that "inclusions" are detected in the intestinal villous epithelium in the 16th week [4]; however, the authors do not describe or illustrate the inclusions. Inclusions are seen in small intestinal epithelium of some of our cases between 14 and 20 weeks. Most are brightly eosinophilic but some are orange or brown (see Figs. 3-40–3-42). They

resemble the hyaline globules or thanatosomes thought to be related to apoptosis described in adult intestinal epithelium in some conditions [19]. The intestinal mucosa is said to closely resemble that of infants by 20 weeks (see Fig. 3-43). The villi may appear shortened, blunted, or bent in segments distended by meconium (see Fig. 3-44). Clusters of basally granulated cells called Segi's caps are seen at the tips of the villi after 20 weeks; these are thought to be precursors of endocrine cells but little has been written about them [20]. Perfectly preserved tissue and special stains are needed to see them. Paneth cells are easily recognized in the bases of the crypts because of their brightly eosinophilic, coarse supranuclear granules (see Fig. 3-45). The muscularis mucosae appears in the duodenum as early as the 21st week and spreads caudally. It may arrive at the terminal ileum by 30 weeks in some cases, but not until later in others. The neuroblasts in the myenteric and submucosal plexuses continue to differentiate toward ganglion cells (see Fig. 3-46). The development of the gut associated lymphoid tissue is ongoing (see Figs. 3-47 and 3-48).

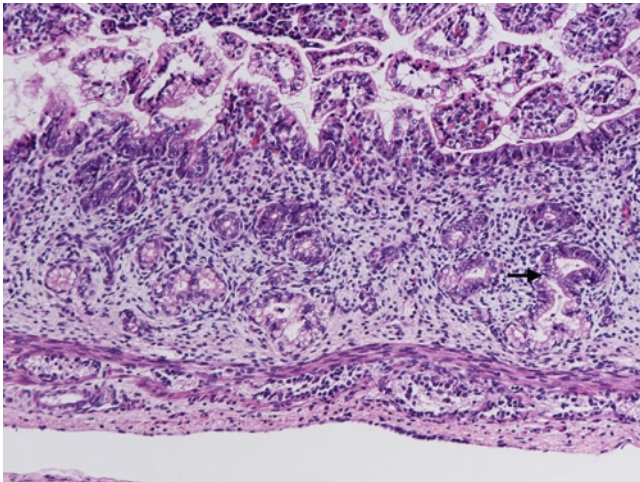


FIGURE 3-36. Duodenum at 17 weeks. Brunner's glands are budding off the crypts of Lieberkühn. The arrow at the lower right points to the junction of a crypt and a Brunner's gland. The cells of the crypts are basophilic while those of Brunner's glands are foamy and light pink. The two layers of the muscularis propria and Auerbach's plexus are at the bottom of the picture. The neuroblasts show little evidence of differentiating toward ganglion cells. The subserosa and serosa are visible below the muscularis propria. (H&E, 10 \times .)

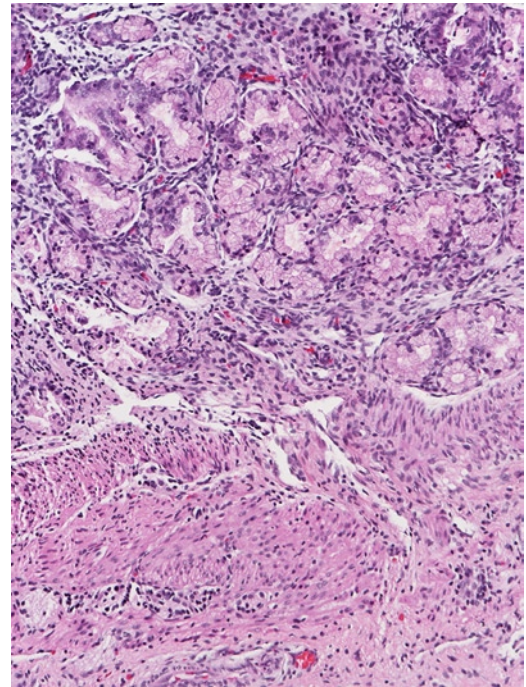


FIGURE 3-37. Duodenum (first portion) at 20 weeks. Brunner's glands are becoming more complex and larger tubuloalveolar glands, as shown here. (H&E, 10 \times .)

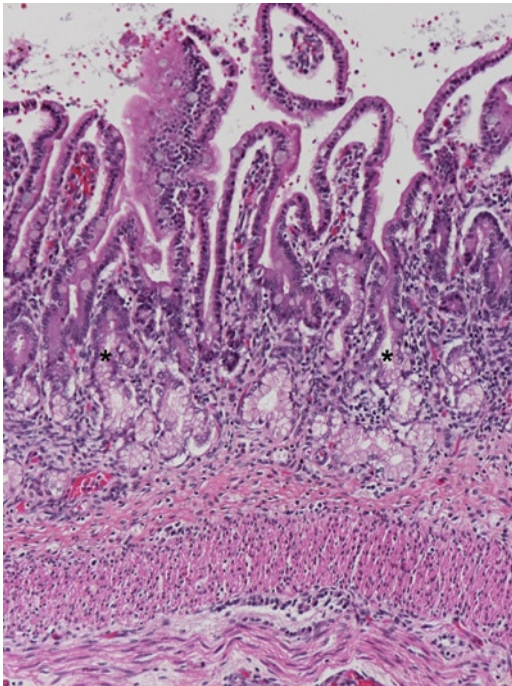


FIGURE 3-38. Duodenum (second portion) at 24 weeks. Brunner's glands are less well developed in the second portion of the duodenum of this fetus than the Brunner's glands in the first part of the duodenum of the 4-week-younger fetus shown in Figure 3-37. This is because the glands first develop near the pyloric sphincter and then progress from rostral to caudal. The junctions between two crypts and two Brunner's glands are indicated by asterisks in the lumen of the crypts. Nests of neuroblasts are visible in the deep submucosal plexus of Henle. Partially differentiated ganglion cells with a small amount of eosinophilic cytoplasm are present in Auerbach's plexus. The muscularis propria, especially the outer longitudinal layer, has grown thicker. (H&E, 10 \times .)

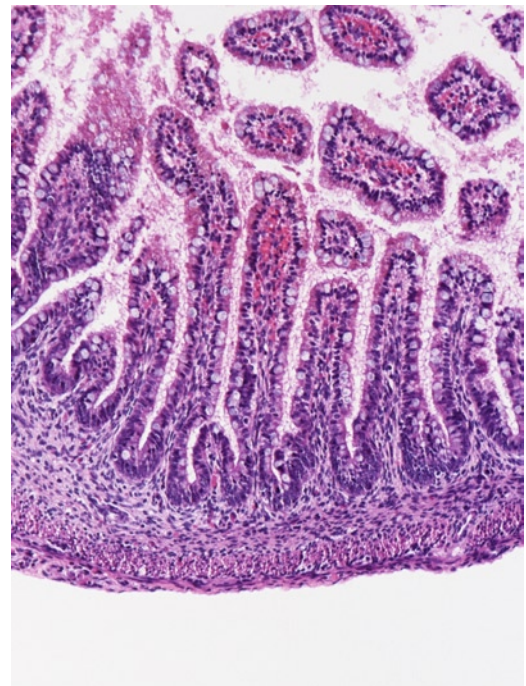


FIGURE 3-39. Small intestine at 17 weeks. Compare this image with that of the small intestinal mucosa at 12 weeks shown in Figures 3-34 and 3-35; the villi and crypts are more mature. The nuclei of all the enterocytes are located at the basal aspect of the cells and goblet cells are numerous. Note the continued absence of the muscularis mucosae. (H&E, 10 \times .)

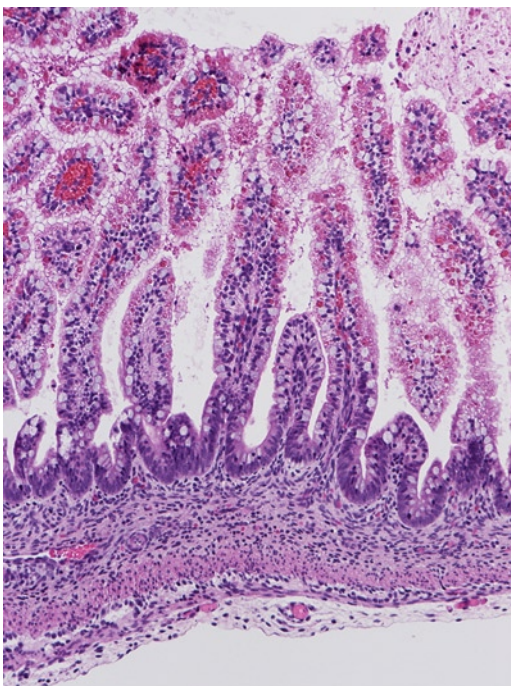


FIGURE 3-40. Small intestine at 17 weeks. Intracytoplasmic hyaline globules are shown in this image. The globules are brightly eosinophilic, round to oval, and often very large but of various sizes. They seem to be most numerous at the tips of the villi and apparently do not occur in the epithelium of the crypts. Note the other histological features of the small intestinal wall. (H&E, 10 \times .)

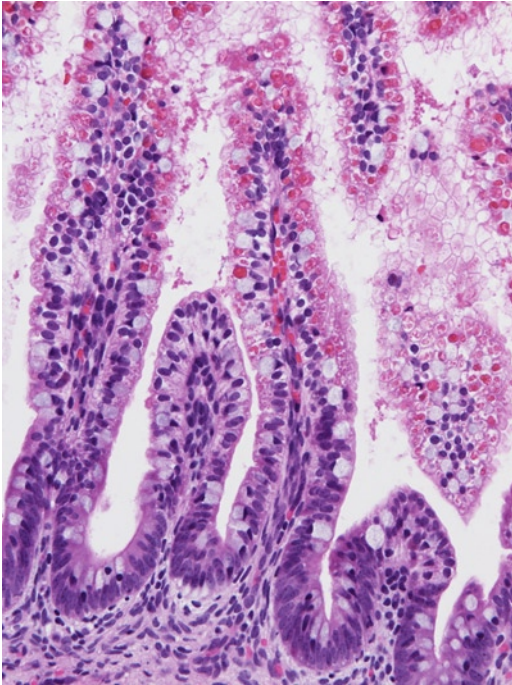


FIGURE 3-41. Small intestine at 17 weeks. In this higher power version of the hyaline globules are seen in more detail. (H&E, 20 \times .)

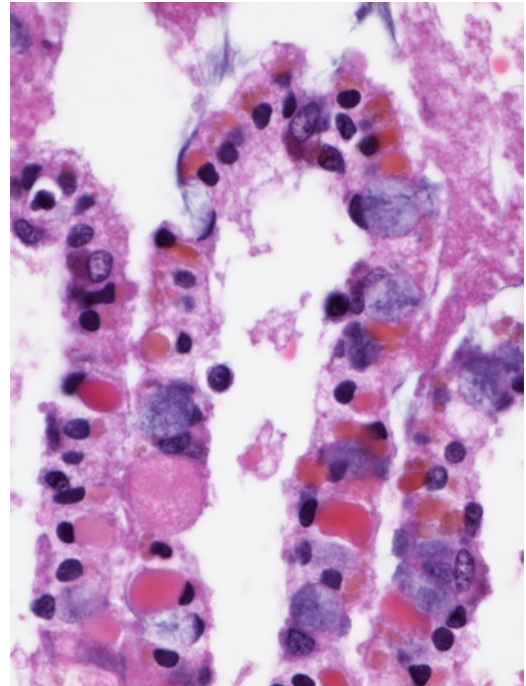


FIGURE 3-42. Small intestine at 19 weeks. In this high-power image, the hyaline globules in another case are shown. The epithelium is slightly macerated and the tips of the villi are at the top of the picture. Some globules are bright red; some are orange; and some are brown. Goblet cells are bright blue. (H&E, 60 \times .)

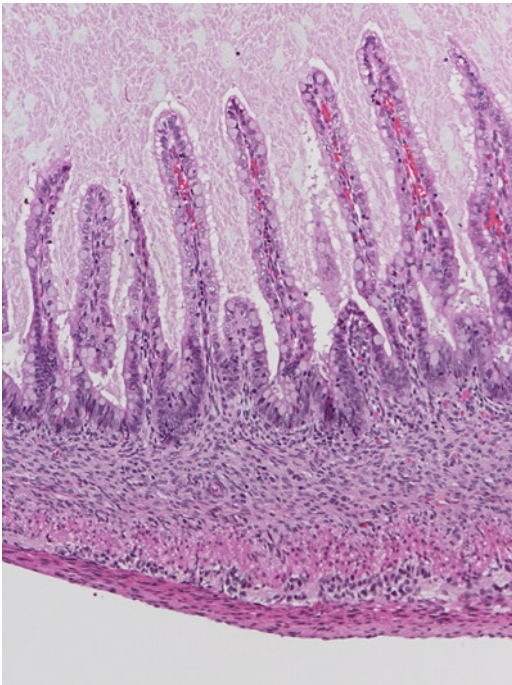


FIGURE 3-43. Small intestine at 19 weeks. The histology of the mucosa is nearly identical to that of a full-term infant and the mouths of the crypts of Lieberkühn are well illustrated. The muscularis mucosae is not present, although the muscularis propria and Auerbach's plexus are well developed. (H&E, 10 \times .)

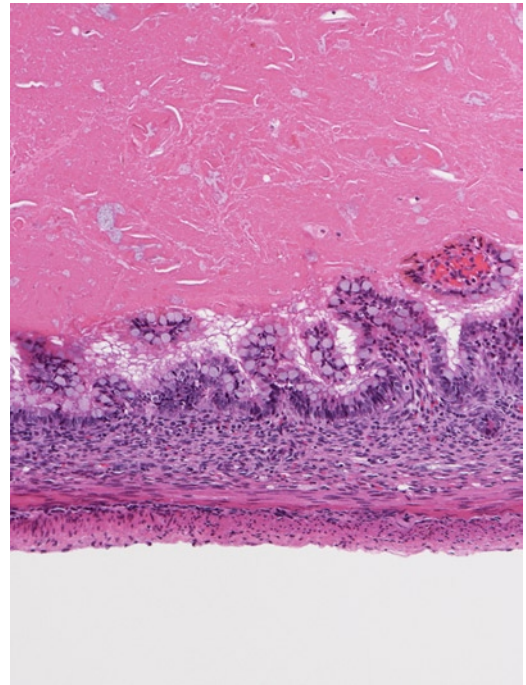


FIGURE 3-44. Small intestine at 19 weeks. This segment is distended with meconium, which flattens the mucosal surface and nearly obliterates the villi. (H&E, 10 \times .)

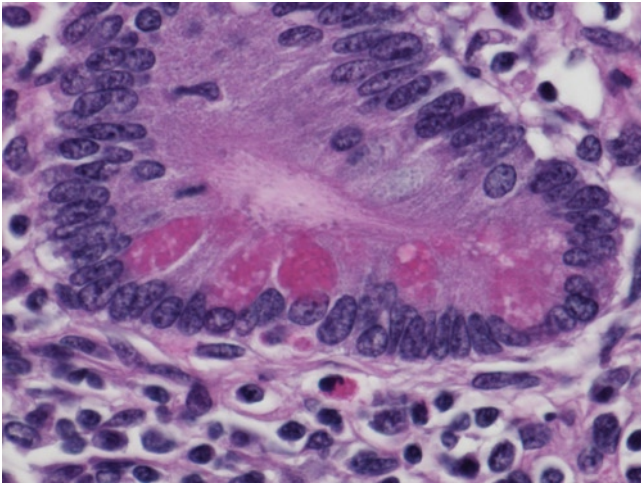


FIGURE 3-45. Small intestine (terminal ileum) at 14 days postnatal age. Paneth cells are located in the base of the crypts and are characterized by coarse, brightly eosinophilic, supranuclear granules. (H&E, 60 \times .)

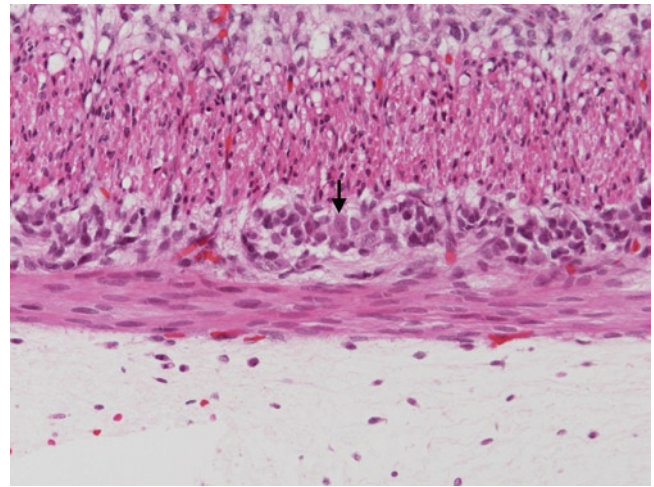


FIGURE 3-46. Auerbach's plexus in the duodenum at 19 weeks. The neuronal cells are a mixture of neuroblasts (the small round blue cells with little cytoplasm) and partially differentiated ganglion cells (the larger cells with finely granular chromatin, a small nucleolus, and eosinophilic cytoplasm, one of which is indicated by the arrow). (H&E, 20 \times .)

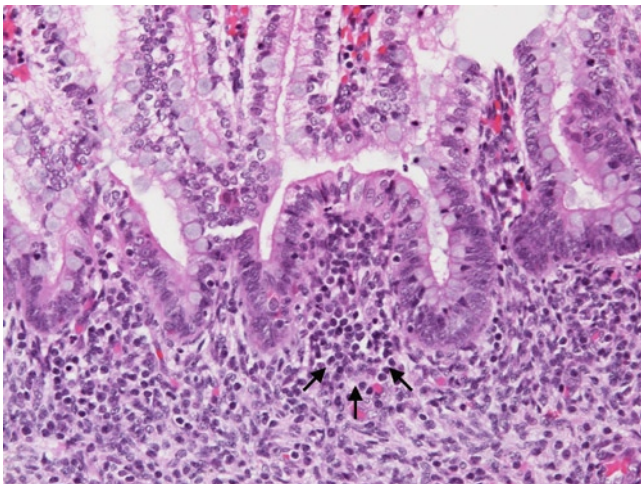


FIGURE 3-47. Gut-associated lymphoid tissue in the small intestine at 19 weeks. Prior to 20 weeks, the gut-associated lymphoid tissue is usually characterized by inconspicuous nodules of lymphoid cells in the upper lamina propria, such as the one marked by the arrows along its deep surface. Lymphoid cells are also diffusely scattered throughout the lamina propria. (H&E, 20 \times .)

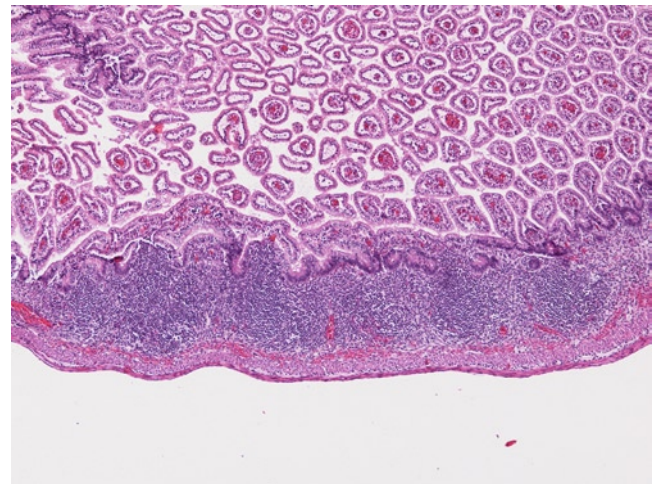


FIGURE 3-48. Gut-associated lymphoid tissue in the small intestine (terminal ileum) at 20 weeks. Peyer's patches are aggregates of multiple submucosal lymphoid follicles fused into large sheets; they are more common at 24 weeks and above than at 20 weeks, as in this instance. This slightly precocious appearance of Peyer's patches might raise the question of fetal infection or incorrect dates. (H&E, 4 \times .)

30 to 40 weeks

The subtypes of mucosal epithelial cells continue to differentiate. Brunner's glands enlarge and spread caudally but few are seen in the third and fourth portions of the duodenum. The glands are largest near the pyloric sphincter and are progressively smaller caudally (see

Figs. 3-49 and 3-50). The development of the muscularis mucosae is completed with its arrival at the ileocecal junction from the duodenum. Neuroblasts of the submucosal and myenteric plexuses continue to differentiate toward mature ganglion cells.

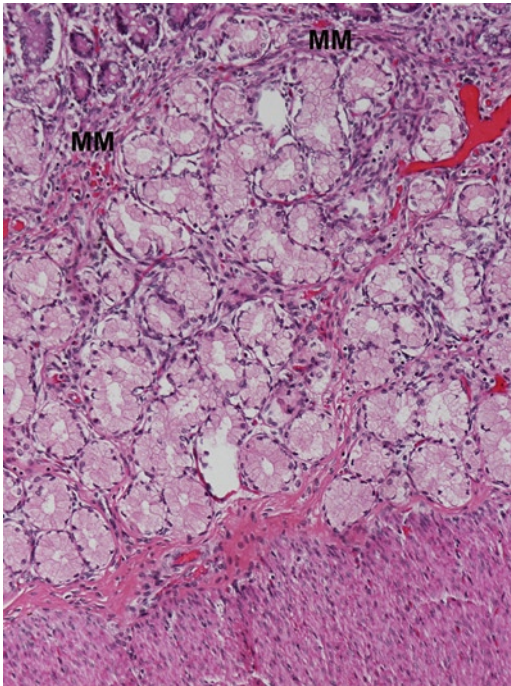


FIGURE 3-49. Duodenum (first portion) at 34 weeks. Brunner's glands are complex and large, as shown. The bulk of the glands are in the submucosa beneath the muscularis mucosae (MM), but a small portion of the glands are in the lamina propria above the muscularis mucosae among the crypts of Lieberkühn, which are the basophilic glands in the upper left-hand corner of the picture. (H&E, 10 \times .)

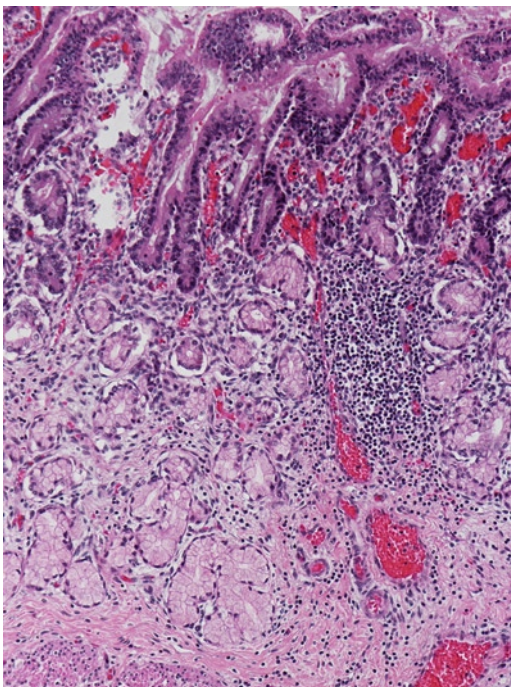
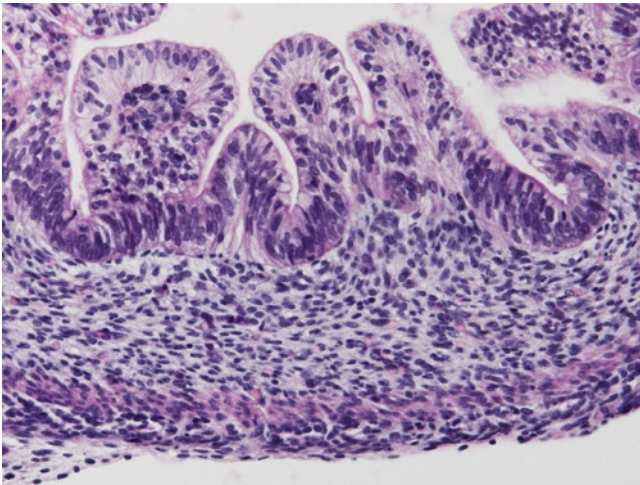


FIGURE 3-50. Duodenum (second portion) at 35 weeks. Brunner's glands are shown; compare with Figure 3-49. The gestational ages are nearly identical but the Brunner's glands in the second portion of the duodenum in this picture are smaller and less numerous than in the first portion of the duodenum in the previous picture. The mucosa is at the top and the muscularis propria is at the bottom. Note the solitary primary lymphoid follicle of the gut-associated lymphoid tissue. (H&E, 10 \times .)

Large Intestine, Appendix, and Anal Canal

Less than 14 weeks

The primordial multilayered epithelium of the large intestine and appendix enters a minor proliferative phase during the seventh postfertilization week. By the 10th to 12th week, the proliferative epithelium differentiates into colonic epithelium characterized by simple columnar mucous surface epithelial cells called colonocytes, primitive villi, and crypts (see Fig. 3-51). The colonic mucosa is villous from this point in development until the 30th week or later. Differentiating sections of colon from small intestine is difficult especially prior to 16 weeks.



Later in gestation the colonic epithelium is predominantly composed of goblet cells and differentiating it from small intestine may be easier. The muscularis propria is completely developed by the eighth or ninth week. The mucosa of the appendix is similar to that of the colon except that it lacks villi. By the eighth week the structures of the anal canal are complete. The transition from colonic mucosa to the anal transitional zone epithelium to the distal stratified squamous epithelium is distinct and the anal columns and sphincters are formed.

FIGURE 3-51. Large intestine at 12 weeks postfertilization. Primitive villi are covered by differentiating colonocytes and the surface epithelium between the villi is primordial, multilayered, and pseudostratified. Primitive crypts of Lieberkühn are beginning to evolve from the primordial epithelium. The muscularis mucosae is not yet present. The inner circular layer of the muscularis propria is well developed, but the outer longitudinal layer is only one or two cells thick. Auerbach's plexus is a continuous ring of neuroblasts in the intermuscular septum. At this gestational age the colon is difficult to distinguish histologically from the duodenum (see Fig. 3-30) or the small intestine (see Figs. 3-32 and 3-33). (H&E, 20 \times .)

14 to 30 weeks

The villi become more distinct and diffuse, and are covered by cells similar to colonocytes. The crypts deepen and the villi elongate (see Figs. 3-52 and 3-53). As in the small intestine, the villi may not be apparent in segments distended by meconium (see Fig. 3-54). The base of the crypts contains the stem cells and proliferating cells, which differentiate into colonocytes, goblet cells, endocrine cells, and Paneth cells. Colonocytes are tall columnar mucous-producing cells with basal nuclei and a brush border. The colonocytes and goblet cells migrate centripetally to the tips of the villi and undergo apoptosis or are sloughed into the lumen. The endocrine cells migrate to the midregion of the crypts and Paneth cells, which are confined to the right colon, remain in the base of the crypts. Gut-associated lymphoid tissue develops as described above and is most prominent in the cecum and rectum. The muscularis mucosae appears at the anorectal junction and grows rostrally toward the ileocecal junction. Tenia coli appear by 16 weeks.

The mucosal villi gradually disappear and are usually not seen after the 30th week. The neuroblasts in the submucosal and myenteric plexuses begin to differentiate toward ganglion cells, but this maturation lags behind that of the more proximal segments due to the rostral to caudal developmental gradient.

Prior to 20 weeks, the histology of the appendix is similar to that of the large intestine except that villi are inconspicuous and the inner circular and outer longitudinal layers of the muscularis propria are indistinct (see Fig. 3-55). Prior to 20 weeks, gut-associated lymphoid tissue is inconspicuous and composed of scattered lymphocytes and occasional small lymphoid aggregates in the lamina propria (see Fig. 3-55). Primary follicles occupying the submucosa are not common (see Fig. 3-56). Beginning at 20 weeks, larger primary follicles become common. In some cases the appendiceal crypts become microcystically dilated and push the muscularis mucosae downward, forming microdiverticula so that the deep border of the mucosa becomes irregular and disorganized (see Fig. 3-57). In 1912, Lewis described these changes in the fetal appendix [10]. The lumens of the cystic crypts contain apoptotic debris and eosinophils (see Fig. 3-58). Endocrine cells may be numerous (see Figs. 3-59 and 3-60). Polygonal and spindled myoid-like cells, eosinophils, and aggregated lymphoid follicles surround the cysts. The cystic crypts begin to regress and disappear, and may leave behind a tiny clump of calcified debris or even a small granuloma. They usually are not seen after 24 or 25 weeks and the purpose of these structures is not known. The association with lymphoid

tissue at the time when the development of aggregated gut-associated lymphoid tissue is prominent suggests an immune function.

The anal canal, which was completely formed by the eighth postfertilization week, continues to mature (see Fig. 3-61). The anal transitional zone epithelium is stratified cuboidal and columnar epithelium with peg cells on the surface and goblet cells scattered within the epithelial

membrane and on its surface. It is distinct from both the squamous epithelium of the anus and the colonic mucosa (see Figs. 3-62 and 3-63). Neuroblasts and differentiating ganglion cells of the myenteric and submucosal plexuses are present at the squamous–columnar junction and become numerous within a few millimeters of the junction. The hypoganglionic segment is less than 1 cm in most fetuses (see Fig 3-61).

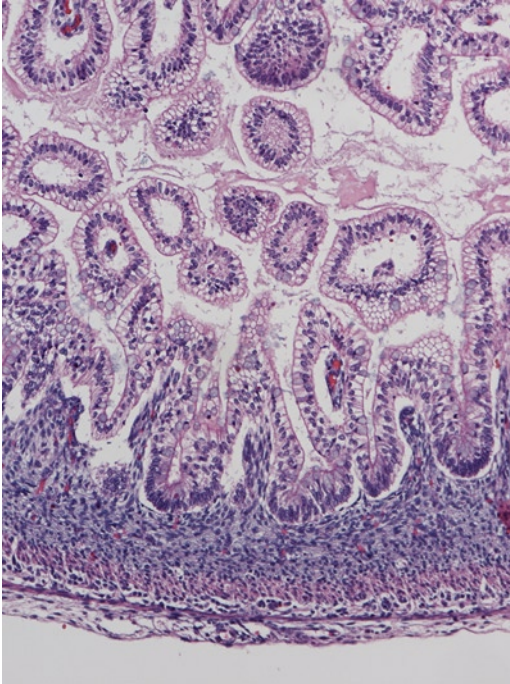


FIGURE 3-52. Large intestine at 15 weeks postfertilization. The villi are longer and most of the nuclei of the colonocytes are located basally. Goblet cells are present. The crypts of Lieberkühn are more definite. The outer longitudinal layer of the muscularis propria is very thin. (H&E, 10 \times .)

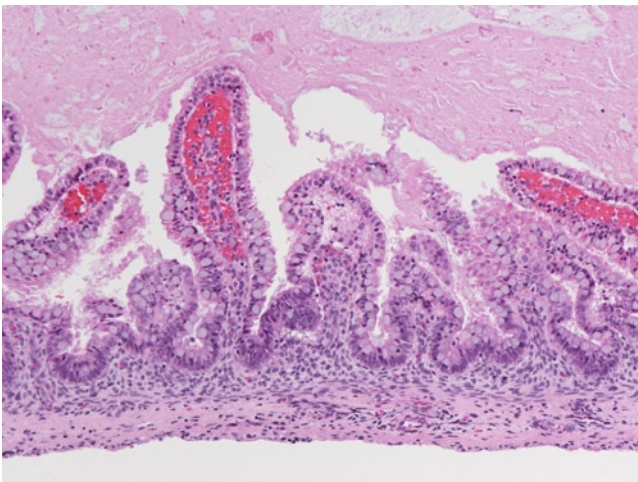


FIGURE 3-53. Large intestine at 19 weeks. The mucosal villi are well formed and long, and goblet cells are numerous. The crypts of Lieberkühn are apparent. The villous colonic epithelium may be difficult to distinguish from small intestinal mucosa. The muscularis mucosae is beginning to develop and is seen here as a thin, discontinuous longitudinal layer of spindle cells below the lamina propria. The muscularis propria is artifactually absent. (H&E, 10 \times .)

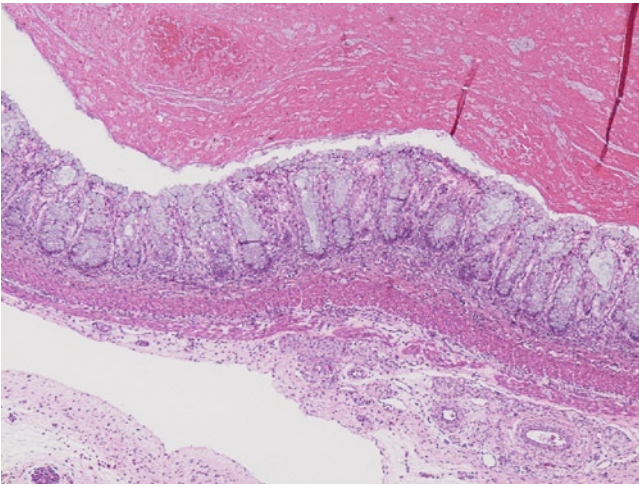


FIGURE 3-54. Large intestine at 19 weeks. Large intestine from the same fetus as in Figure 3-53 is shown. This segment is distended by meconium, which flattens the mucosa and obliterates the villi similar to the situation in the small intestine (see Fig. 3-44); compare with Figure 3-53. (H&E, 4 \times .)



FIGURE 3-55. Appendix at 19 weeks. The histology is similar to the large intestine except that villi are shorter and less frequent. Diffuse and small aggregates of gut-associated lymphoid tissue are present. (H&E, 4 \times .)

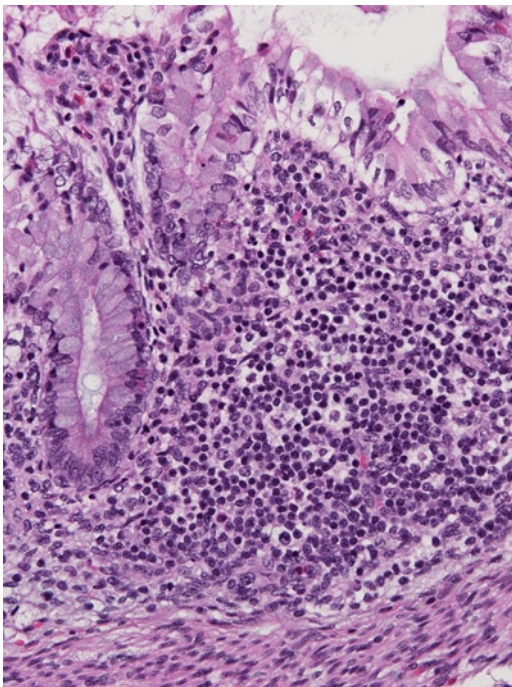


FIGURE 3-56. Gut-associated lymphoid tissue in the appendix at 19 weeks. Solitary lymphoid follicles covered by follicle-associated epithelium begin to form in the submucosa. Eosinophils are seen in the lamina propria in the upper left. Two endocrine cells with subnuclear eosinophilic granules are seen in the crypt on the left. (H&E, 20 \times .)

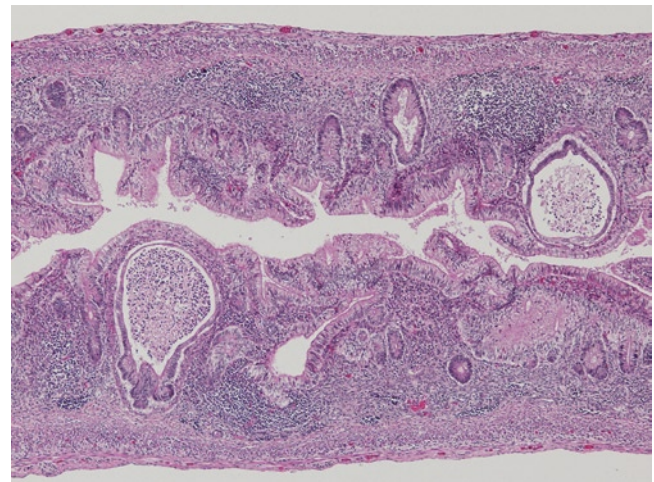


FIGURE 3-57. Appendix at 24 weeks. Microcystically dilated crypts forming microdiverticula are seen. The dilated crypts are filled with apoptotic debris and inflammatory cells, especially eosinophils, and are surrounded by polygonal and myoid cells. Follicular gut-associated lymphoid tissue is abundant. (H&E, 4 \times .)

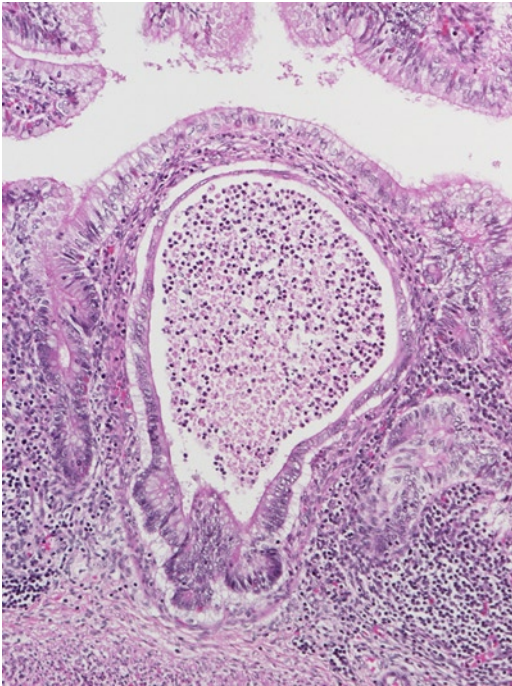


FIGURE 3-58. Appendix at 24 weeks. This higher power view is of the cystically dilated crypt seen in Figure 3-57. The cyst is filled with apoptotic and inflammatory debris but there is neither appendicitis nor neutrophils in the lumen of the appendix. (H&E, 10 \times .)

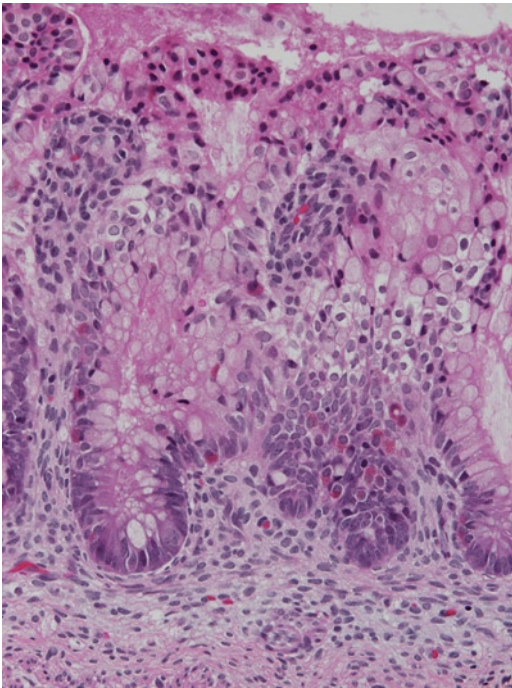


FIGURE 3-59. Appendix at 24 weeks. Endocrine cells may be common in the appendix at this gestational age. (H&E, 20 \times .)

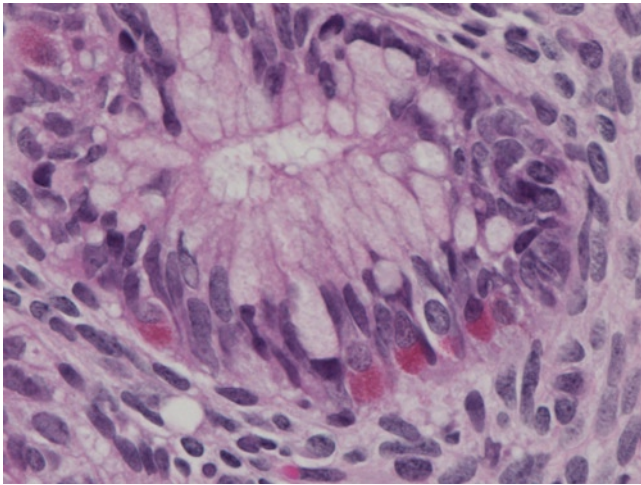


FIGURE 3-60. Appendix at 24 weeks. This image is a higher power version of Figure 3-59. The endocrine cells are characterized by brightly eosinophilic fine subnuclear granules in contrast to the coarse supranuclear granules seen in Paneth cells. Compare with Figure 3-45. (H&E, 60 \times .)

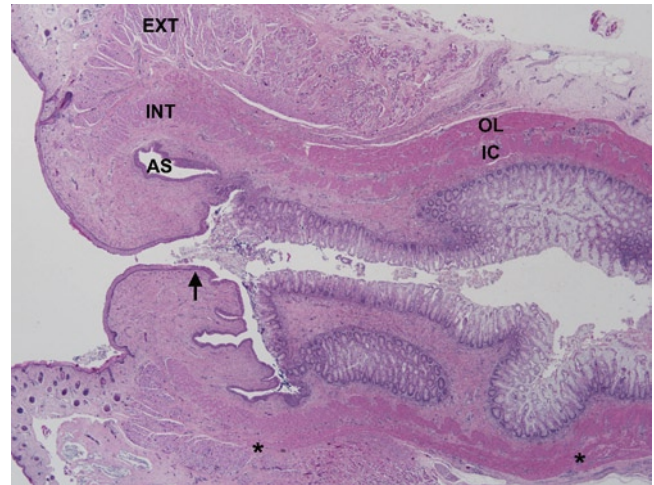


FIGURE 3-61. Anal canal at 21 weeks. The first ganglion cells of Auerbach's plexus are marked by the asterisk on the left. The asterisk on the right marks the level where the number of ganglion cells is similar to that in the rest of the rectum. Between the two asterisks is the hypoganglionic segment; it is 5 mm long in this case. The internal sphincter is formed by the inner circular layer. The arrow indicates the squamous-columnar junction. AS—anal sinus; EXT—external sphincter; IC—inner circular layer of the muscularis propria; INT—internal sphincter; OL—outer longitudinal layer of the muscularis propria. (H&E, 1 \times .)

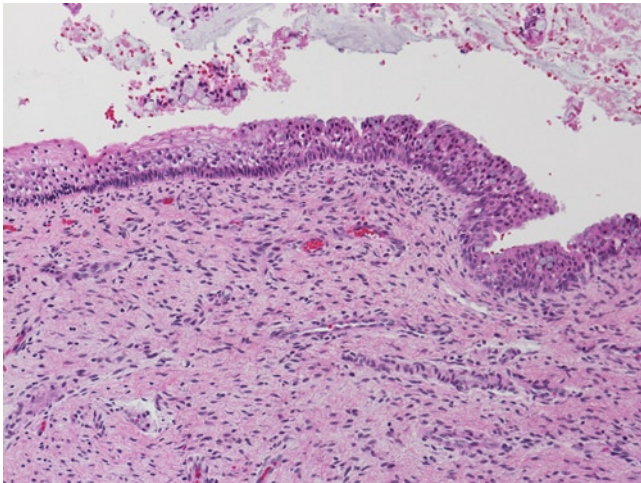


FIGURE 3-62. Anal canal at 21 weeks. This higher power view is of the squamous-columnar junction indicated by the arrow in Figure 3-61. The stratified squamous epithelium changes abruptly into the stratified columnar epithelium with intraepithelial goblet cells characteristic of the anal transitional zone epithelium. (H&E, 10 \times .)

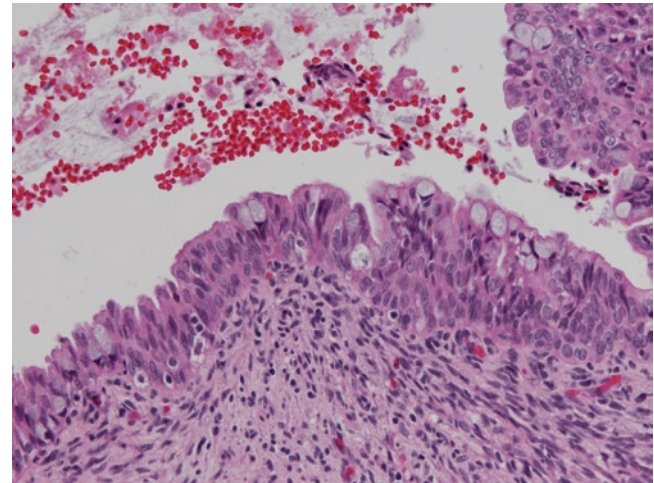


FIGURE 3-63. Anal canal at 21 weeks. This higher power view shows the anal transitional zone epithelium near the colonic mucosa. The details of this unique epithelium are demonstrated in this picture. (H&E, 20 \times .)

30 to 40 weeks

The villi have disappeared, and the crypts elongate and acquire the well-organized parallel test tube arrangement typical of postnatal colonic epithelium (see Fig. 3-64). The

neuroblasts continue to differentiate but only a few completely mature ganglion cells are seen (see Fig. 3-65). The hypoganglionic segment remains less than 1 cm long.

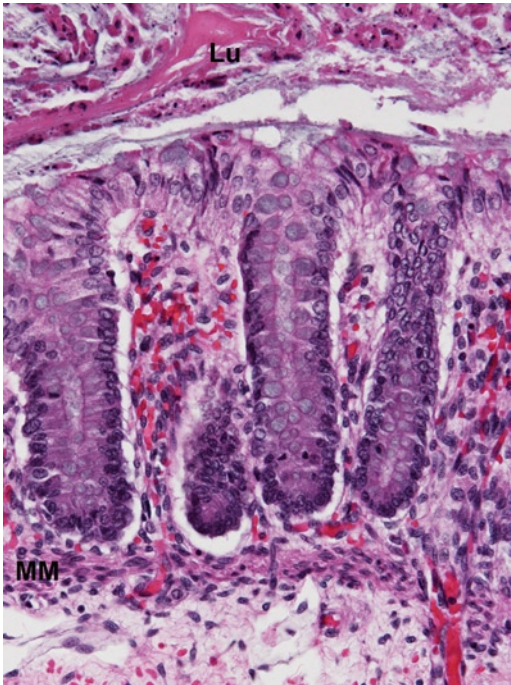


FIGURE 3-64. Large bowel at 35 weeks. The large intestinal mucosa is no longer villous. The crypts of Lieberkühn are straight, parallel, and of equal length, imparting the classical test tube appearance of the large intestinal crypts. The base of the crypts reach the muscularis mucosae (MM). Lu—lumen containing meconium. (H&E, 20 \times .)

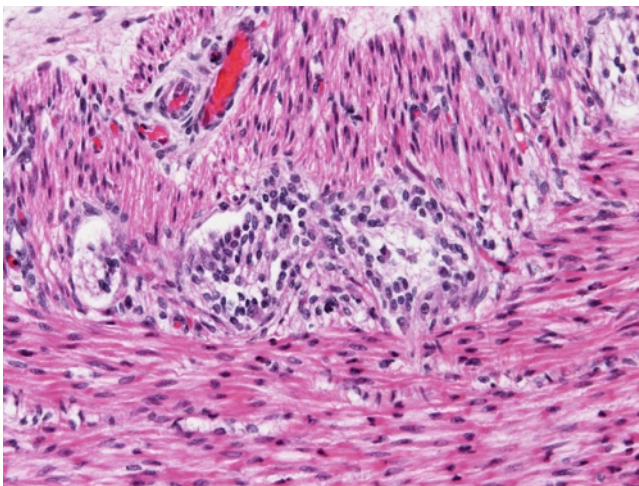


FIGURE 3-65. Auerbach's plexus in the rectum at 35 weeks. Most of the neuroblasts are undifferentiated small blue cells with little cytoplasm. A few partially differentiated ganglion cells with larger amounts of eosinophilic cytoplasm are present. Identifying these poorly differentiated cells as ganglion cells in sections of rectal mucosal biopsies to rule out Hirschsprung disease is difficult. The inner circular layer is at the top and the outer longitudinal layer is at the bottom. (H&E, 20 \times .)

Acknowledgment The author thanks Dr. Tricia R. Bhatti from The Children's Hospital of Philadelphia, Philadelphia, PA, for

invaluable assistance in selecting microscopic slides for photography, taking photographs, and editing the manuscript.

References

1. O'Rahilly R: The timing and sequence of events in the development of the human digestive system and associated structures during the embryonic period proper. *Anat Embryol (Berl)* 1978, 153:123–136.
2. Lewis F: The early development of the entodermal tract and the formation of its subdivisions. In *Human Embryology*. Edited by Keibel F, Mall FP. Philadelphia: J. B. Lippincott; 1912:295–334.
3. O'Rahilly R, Muller F: *Developmental Stages In Human Embryos*. Washington DC: The Carnegie Institution of Washington; 1987.
4. Sembra R, Tanaka O, Tanimura T: The digestive tract. In *Atlas of Prenatal Histology*. Edited by Nishimura H. Tokyo: Igaku-Shoin; 1983:193–225.
5. Moxey PC, Trier JS: Endocrine cells in the human fetal small intestine. *Cell Tissue Res* 1977, 183:33–50.
6. Sjolund K, Sanden G, Hakanson R, Sundler F: Endocrine cells in human intestine: an immunocytochemical study. *Gastroenterology* 1983, 85:1120–1130.
7. Lewis F: The development of the esophagus. In *Human Embryology*. Edited by Keibel F, Mall FP. Philadelphia: J. B. Lippincott; 1912:355–368.
8. Lewis F: Development of the stomach. In *Human Embryology*. Edited by Keibel F, Mall FP. Philadelphia: J. B. Lippincott; 1912:368–381.
9. Lewis F: Development of the small intestine. In *Human Embryology*. Edited by Keibel F, Mall FP. Philadelphia: J. B. Lippincott Company; 1912:381–393.
10. Lewis F: Development of the large intestine. In *Human Embryology*. Edited by Keibel F, Mall FP. Philadelphia: J. B. Lippincott Company; 1912:393–399.
11. Huff D: Developmental anatomy and anomalies of the gastrointestinal tract, with involvement in major malformative syndromes. In *Pathology of Pediatric Gastrointestinal and Liver Disease*. Edited by Russo P, Ruchelli E, Piccoli DA. New York: Springer; 2004:3–36.
12. O'Rahilly R, Muller F: *Human Embryology & Teratology*, edn 3. New York: Wiley-Liss; 2001.
13. Fu M, Tam PK, Sham MH, Lui VC: Embryonic development of the ganglion plexuses and the concentric layer structure of human gut: a topographical study. *Anat Embryol (Berl)* 2004, 208:33–41.
14. Wallace AS, Burns AJ: Development of the enteric nervous system, smooth muscle and interstitial cells of Cajal in the human gastrointestinal tract. *Cell Tissue Res* 2005, 319:367–382.
15. Spencer J, MacDonald TT, Finn T, Isaacson PG: The development of gut associated lymphoid tissue in the terminal ileum of fetal human intestine. *Clin Exp Immunol* 1986, 64:536–543.
16. Otani H, Yoneyama T, Hashimoto R, et al.: Ultrastructure of the developing stomach in human embryos. *Anat Embryol (Berl)* 1993, 187:145–151.
17. Zhou H, Greco MA, Daum F, Kahn E: Origin of cardiac mucosa: ontogenic consideration. *Pediatr Dev Pathol* 2001, 4:358–363.
18. De Hertogh G, Van Eyken P, Ectors N, Geboes K: On the origin of cardiac mucosa: a histological and immunohistochemical study of cyokeratin expression patterns in the developing esophagogastric junction region and stomach. *World J Gastroenterol* 2005, 11:4490–4496.
19. Dikov DI, Auriault ML, Boivin JF, et al.: Hyaline globules (thanosomes) in gastrointestinal epithelium: pathophysiologic correlations. *Am J Clin Pathol* 2007, 127:792–799.
20. Kobayashi S, Iwanaga T, Fujita T: Segi's cap: huge aggregation of basal-granulated cells discovered by Segi (1935) on the intestinal villi of the human fetus. *Arch Histol Jpn* 1980, 43:79–83.

4

Liver

Pierre Russo

The fetal liver is an important organ with synthetic and hematopoietic functions that undergoes dramatic histological change during the second and third trimesters of gestation. This chapter reviews the histological changes in the fetal liver evident in hepatocytes, the sinusoidal lining cells, the intrahepatic biliary tree, and the hematopoietic elements, as well as discusses the development of the hepatic vasculature and extrahepatic biliary tree.

Embryology

Mechanisms of Development of the Liver

Hepatobiliary morphogenesis in humans begins in the third to fourth week of development and commences from two primordia. The hepatocytes, which ultimately account for 70% of the cells in the liver, are derived from the cranial portion of the hepatic diverticulum, an outgrowth of the foregut endoderm, which invades the septum transversum, the mesodermal plate that separates the embryonic thoracic and abdominal cavities. The caudal part of the hepatic diverticulum, the portion that does not invade the septum transversum, forms the extrahepatic biliary tree and ventral pancreatic anlage (see Fig. 4-1). The stromal cells of the connective tissue elements: Kupffer's cells, stellate cells, and blood vessels are mesenchymal in origin and develop from the septum transversum, and from cells lining the coelomic cavity. The prehepatocytes or hepatoblasts proliferate within the septum transversum, organized in cords around developing sinusoids derived from branches of the vitelline veins that penetrate the septum transversum [1-3]. Development of the hepatic primordium is dependent on continuous interactions with the adjacent mesoderm and on the concerted development of the hepatic vasculature, as revealed by studies of *Klk1*^{-/-} mouse embryos, which lack mature endothelial cells, with consequent inhibition of expansion of the liver bud [4]. The molecular mechanisms that control liver development are beyond the scope of this chapter, and are the subject of several excellent reviews [5,6]. In summary, these mechanisms appear to be well conserved among various organisms and depend on the coordinated expression of transcription and signaling factors from the cardiac mesoderm, the septum transversum and the endoderm to commit the endodermal cells to a hepatic fate and to induce and regulate hepatic gene expression. Growth of the liver bud is very rapid between the fourth and tenth weeks gestation in humans, such that by 50 days, 700 portal branches from the second to the sixth order can be counted [7]. This growth requires the action of a large number of factors and downstream cascades, such as hepatocyte growth factor (HGF), transforming growth factor- β (TGF β), the *Wnt*/ β -*catenin* pathway, and tumor necrosis factor (TNF- α), that involve both proliferation and apoptosis of the hepatoblasts [5,6].

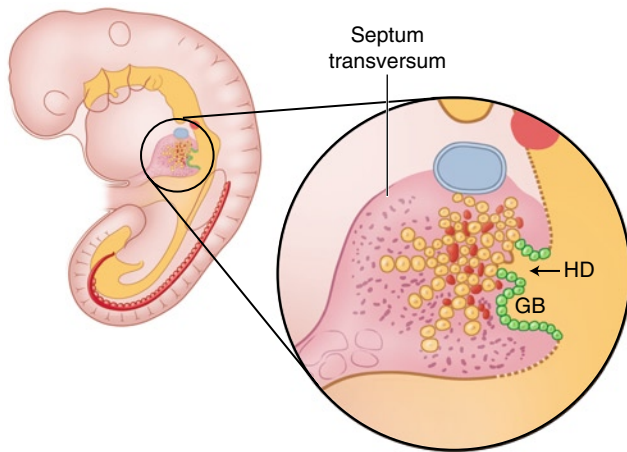


FIGURE 4-1. Hepatic morphogenesis. A 30-day embryo shows the cephalic portion of the hepatic diverticulum (HD) penetrating the septum transversum and forming cords where the endodermal cells (yellow) will differentiate into hepatoblasts. The caudal portion of the diverticulum will form the gallbladder and biliary tree. GD—gastric diverticulum. (Adapted from Ruchelli [3].)

Development of the Hepatic Vasculature

The vascular architecture of the liver is unique in that the organ receives both a venous blood supply via the portal vein from the intestines, pancreas, and spleen responsible for its functional circulation, and an arterial supply conveying nutrition and oxygenated blood from the hepatic artery. The development of the liver is closely associated with changes in the omphalomesenteric (vitelline) veins and in the umbilical veins. The definitive venous pattern within the liver is established by the seventh week [8]. The portal vein arises from anastomotic channels derived from the paired vitelline veins in the hepatic primordium. The intrahepatic segments of the portal vein and its branches become surrounded by mesenchyme, from which portal spaces will develop and within which arterial segments will grow. The proximal end of the right vitelline vein forms the terminal part of the inferior vena cava (IVC). Its remnants in the liver become the hepatic venous system, and its distal portion will form the splenic and superior mesenteric veins. The left vitelline vein forms part of the IVC. By the sixth week, the right umbilical vein disappears, and all oxygenated blood from the placenta enters the liver from the left umbilical vein. Within the liver, the umbilical vein specifically enters the caudal wall of the sinus intermedius, the future left branch of the portal vein. The ductus venosus arises from the rostral wall of the sinus

intermedius directly opposite the opening of the umbilical vein and connects the sinus intermedius to the inferior vena cava (see Fig. 4-2). Thus, the ductus venosus diverts oxygenated blood from the umbilical vein directly to the heart.

Hemodynamic studies performed during intrauterine life have confirmed that, until birth, the umbilical vein is the predominant liver vessel, and that the left lobe is supplied mainly by oxygenated blood from the umbilical vein, whereas the right lobe of the liver receives blood predominantly from the portal vein [7]. This vascular asymmetry is believed to account for differences observed between the right and left lobes of the liver in stillbirths and neonates [9,10]. At birth, the left lobe is comparably larger than in later life. Birth results in the closure of the umbilical circulation, starting with collapse of the umbilical arteries, followed by closure of the umbilical venous flow. The latter is complete by 15 to 20 days. This decrease in blood flow results in collapse of the ductus venosus and its obliteration by fibrous tissue. The umbilical vein becomes the *ligamentum teres*, whereas the ductus venosus transforms into the *ligamentum venosum*. Fetal blood flow through the hepatic artery is insignificant compared with that delivered by the umbilical and portal veins. The development of the hepatic arterial system parallels that of the bile ducts, and reaches maturity at approximately 15 years of age [8].

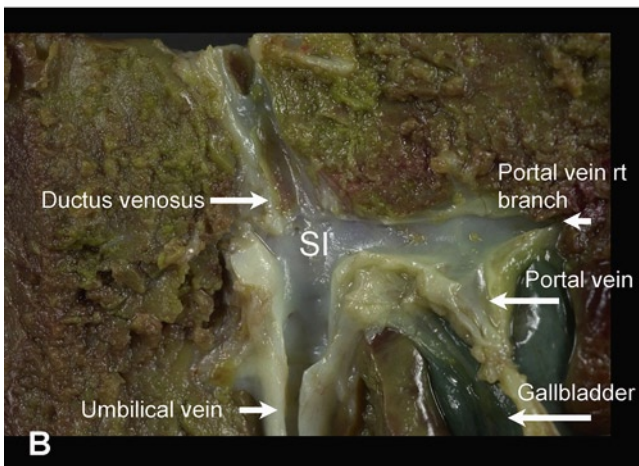


FIGURE 4-2. The ductus venosus in the fetal liver. **A**, A catheter in the umbilical vein with its tip in the sinus intermedius points toward the ductus venosus. The blood from the umbilical vein drains directly into the ductus venosus and hence into the inferior vena cava during fetal life. **B**, Cut section of the liver from a 29-week gestation fetus further illustrates the relationship between the sinus intermedius (SI), ductus venosus, umbilical vein, and portal vein. The left lobe of the liver is visible on the left side of the image. rt—right.

Histology

Hepatic Lobule

The early *hepatocyte* cords that form around the developing sinusoids remain thick throughout intrauterine life and the first few months after birth, thinning to two-cell trabeculae by 5 months of life. At 5 years of age, they adopt the single-cell cord architecture of adult life (see Fig. 4-3). Glycogen becomes plentiful in fetal hepatocytes and remains so until birth; lipofuscin is usually scanty (see Fig. 4-4). Ultrastructurally, rough endoplasmic reticulum is prominent by the seventh week, peroxisomes by the eighth week, and the Golgi apparatus moves from the perinuclear to the pericanalicular zone during the third month, as bile formation begins [11]. The lateral domains have tight junctions separating canaliculi from sinusoids. The canalicular and basolateral domains of hepatocytes contain specific transporters for organic and inorganic ions and macromolecules [12]. The canaliculus, the smallest component of the biliary system, develops by 7 to 8 weeks gestational age [13]. Enzymes of the ornithine cycle are expressed early in the human liver. It appears that the liver changes from a primarily glycolytic role during the first trimesters to a gluconeogenic role before birth [14]. Metabolic zonation, whereby periportal hepatocytes differ from peri-

central hepatocytes on the basis of differential expression of metabolism-regulating genes, begins shortly after birth, and appears to be under the control of Wnt signaling and the β -catenin pathway [5].

The *endothelial cells* that line the sinusoids are believed to originate either from the septum transversum or from the disrupted vitelline veins, and play a key role in hematopoiesis during fetal life. They undergo significant remodeling with development of fenestrations and changes in immunophenotypic features during growth of the liver, progressively losing typical endothelial markers such as CD34 and acquiring distinctive markers such as CD4 and intercellular adhesion molecule 1 (ICAM-1) as expressed by the postnatal liver (see Fig. 4-5) [7]. This fenestrated endothelium also allows fluid passing through channels between hepatocytes to enter the space of Disse and from there to drain into portal lymphatic spaces [15].

Kupffer cells are hepatic macrophages that belong to the mononuclear phagocyte system and are derived from the yolk sac, and later, from the bone marrow. Large numbers of macrophages are present in the sinusoids after 30 days of gestation, identifiable immunohistochemically by markers such as CD68, and are

characterized ultrastructurally by abundant cytoplasm, numerous filopodia, dense bodies, and prominent hemophagocytosis [16].

The liver becomes a site of *hematopoiesis* between the sixth and seventh weeks gestation. Intense hematopoietic activity is present through 20 weeks gestation (see Fig. 4-6), as the liver is the main hematopoietic organ in the body that time. Additionally, hematopoietic cells appear essential for hepatocyte maturation because they secrete oncostatin M, which activates a signaling cascade and is responsible for expression of enzymes such as glucose-6-phosphatase [5]. Hematopoiesis has a distinct zonal distribution. The production of erythroid cells occurs within the sinusoids, partly in so-called "Bessis islands," which consist of a central macrophage surrounded by erythroid cells. These macrophages are believed to play an essential role in erythroid maturation [17]. Myelopoiesis is located mainly around the vascular structures within the portal triads. Hematopoietic activity begins to decrease between 24 and 32 weeks gestation, as the bone marrow becomes hematopoietic [18]. By 36 weeks, hematopoiesis remains only as scattered islands in the hepatic parenchyma

and normally ceases within a few weeks after birth [19]. Increased erythropoiesis may be seen in cases of chronic fetal hypoxia, anemia, and in infants of diabetic mothers [20]. Erythropoiesis has been reported to decrease as a result of preeclampsia, however, suggesting that erythropoiesis in utero may also depend on factors other than just oxygen supply [21]. Fetal myelopoiesis has been observed to be elevated as a result of intrauterine infection, and this observation may help confirm a diagnosis of chorioamnionitis when the placenta is unavailable for examination [22-24]. *Hemosiderin* is normally present mainly within periportal hepatocytes and in the ductal plate in the fetal liver (see Fig. 4-7), though there is great variability in the amount of hemosiderin normally present [13,25]. When hepatocyte siderosis is abundant, it is also present within Kupffer cells. Measured iron content appears to normally increase with gestational age [25]. The distribution of the iron stores may shift from a primarily periportal to a perivenular location in cases of amniotic fluid infection [24]. Hemosiderin accumulation may increase with perinatal liver damage and also in conditions such as hemolysis without evidence of liver damage [25].

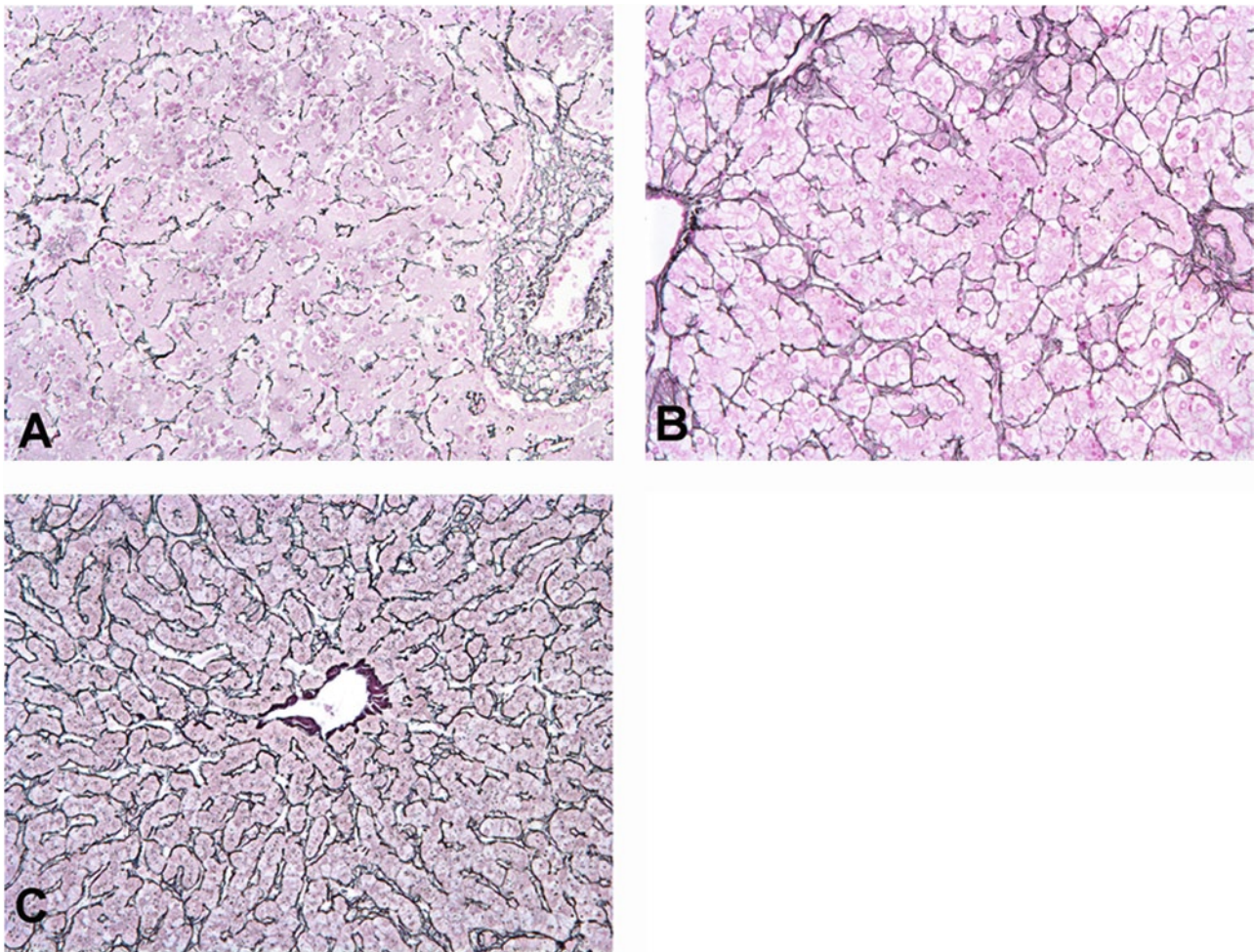


FIGURE 4-3. Reticulin staining of the hepatic cords at various ages. **A**, In the 16-week fetus, cords are poorly formed and many cell layers in thickness. **B**, In the 37-week fetus, the reticulin frame-

work is more apparent, but still several cell layers in thickness. **C**, By contrast, a single cell layer arrangement prevails in the cords of this 5-year-old boy. (**A-C**, Reticulin stain, 20 \times .)

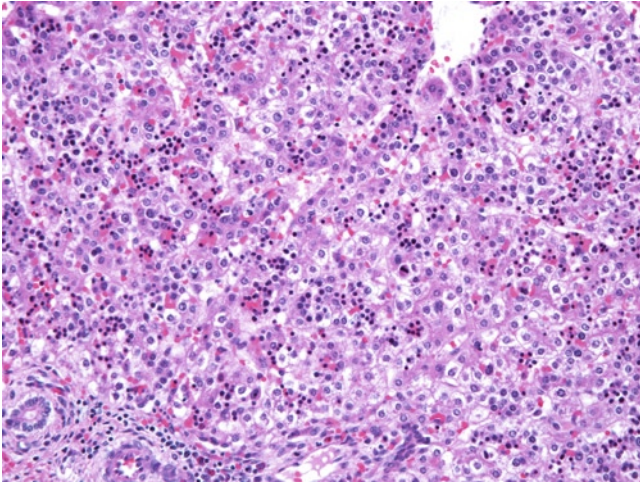


FIGURE 4-4. 20-week fetus. The alternating light and dark cell pattern, which is a feature of fetal hepatocytes, results from prominent cytoplasmic glycogen content. Note also the extensive sinusoidal hematopoiesis. (Hematoxylin and eosin [H&E], 20 \times .)

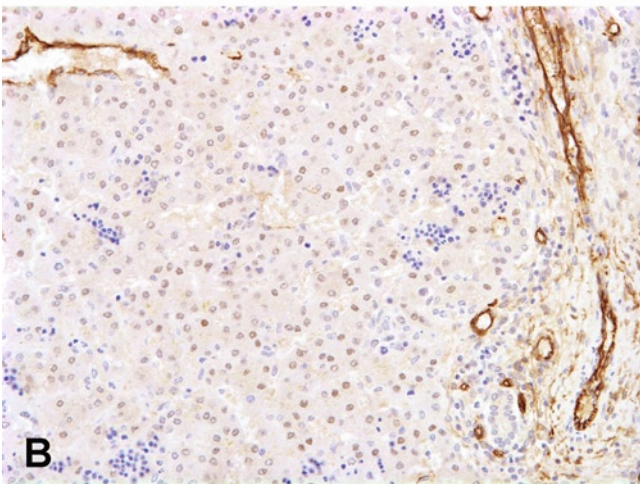
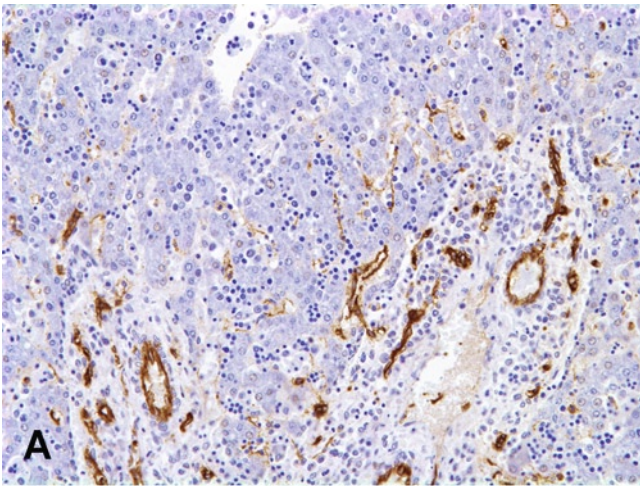


FIGURE 4-5. Endothelial sinusoids stained with CD34. **A**, In the 16-week fetus, immunohistochemical staining with CD34 highlights the vasculature of the portal tracts as well as the sinusoids of the periportal areas. **B**, In the 36-week fetus, CD34 staining has mostly disappeared from the sinusoids and is essentially limited to the portal vasculature and central veins. (**A** and **B**, CD34 immunohistochemistry, 20 \times .)

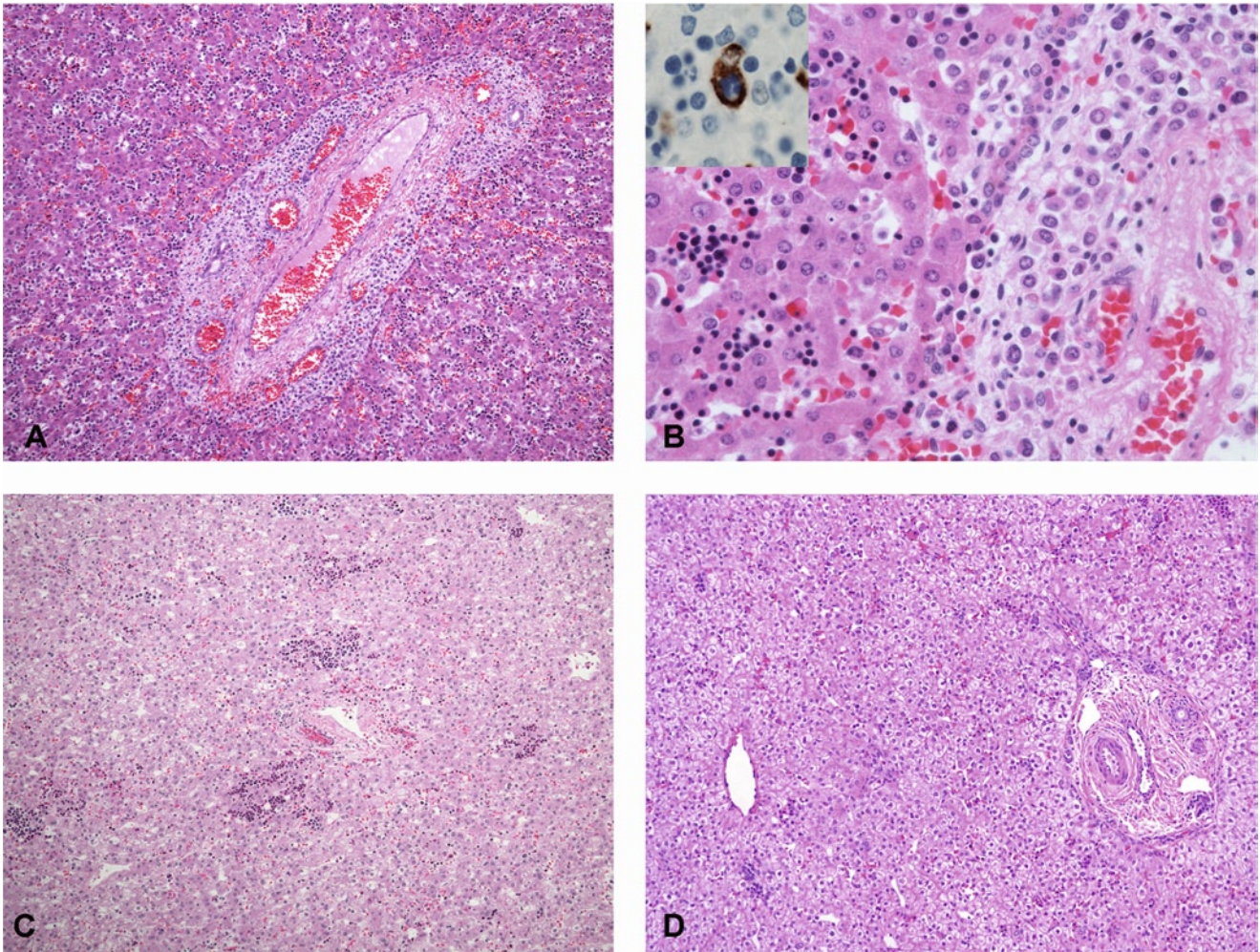


FIGURE 4-6. Hematopoiesis in the fetal liver. **A**, Hematopoietic activity is marked in the liver of an 18-week fetus. **B**, Higher-power view of **A** demonstrates erythropoiesis in the sinusoids, and myelopoiesis in the portal tract (*right*). The inset shows CD68-staining macrophage engulfing and surrounded by erythroid cells in a hepatic sinusoid, representing a so-called

"Bessis island."**C**, By 28 weeks, erythropoiesis has diminished and myelopoiesis is largely inapparent. **D**, In this 36-week fetus, erythropoiesis is present only as scattered small islands in the sinusoids. (**A**, H&E, 10×; **B**, H&E, 40× [inset, CD68 immunohistochemistry, 60×]; **C**, H&E, 4×; and **D**, H&E, 4×.)

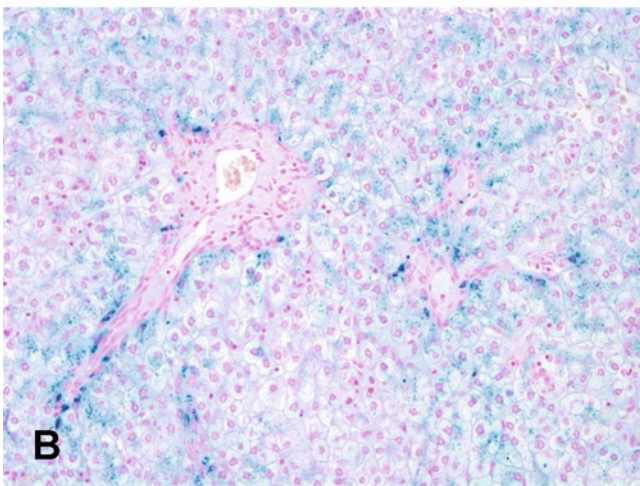
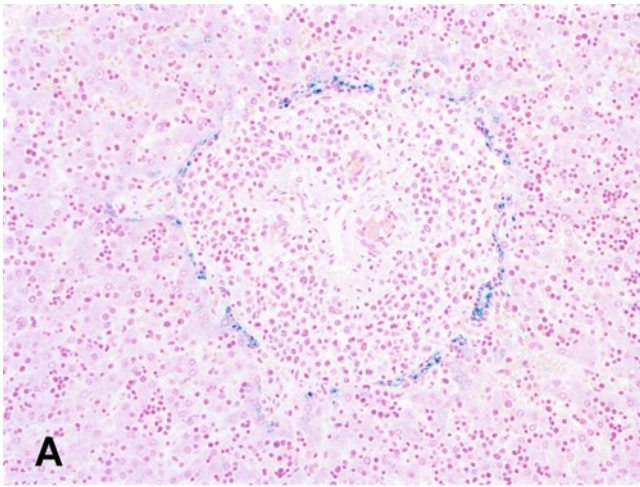


FIGURE 4-7. Hemosiderin in the fetal liver. Hemosiderin accumulation in the fetus is primarily within the ductal plate and periportal hepatocytes. **A**, 18-week fetus, Prussian Blue stain. **B**, Increased hemosiderin accumulation is noted within the periportal areas as well as in surrounding hepatocytes in this neonate born at 36 weeks gestation with severe hypoxia. (**A** and **B**, Prussian blue, 20 \times .)

Biliary Tract

The development of the *intrahepatic* biliary tree begins between the fifth and ninth week postfertilization. Biliary epithelium is believed to arise from precursor bipotential hepatoblasts that can differentiate into either hepatocytes or biliary epithelial cells [26]. Hepatoblasts at the outer boundary of the portal tracts acquire a biliary phenotype, forming the ductal plate (see Fig. 4-8) [27,28]. Biliary differentiation appears to be induced by TGF- β under the control of hepatocyte nuclear factor 6 (HNF-6) and OC-2 (One-cut 2) [5]. The downstream transcription factor HNF-1 β is required for the development of interlobular bile ducts and arteries in mice, and HNF-1 β ^{-/-} mutant mice have a paucity of intrahepatic bile ducts and absence of hepatic arteries [29,30].

Remodeling of the ductal plate, starting around week 12, involves formation of discrete tubular spaces, incorporation of the tubules more centrally into the portal tract mesenchyme and elimination of excess epithelial elements, as evidenced by staining with cytokeratin (CK)-7 and -19 (see Figs. 4-9–4-11). This process extends centrifugally from the hepatic hilum towards the periphery of the liver, and continues throughout fetal life, but with a “slow-down” period between the 20th and 32nd

weeks, when portal myelopoiesis is active [31]. Histological examination of the fetal liver thus reveals more mature ducts in the hilar region, whereas the ducts in the periphery are still in ductal plate configuration [28]. This remodeling is not complete at birth, but continues into the first month of life ex utero [32]. Thus, the “normal” bile duct/portal tract ratio is likely lower in the premature infant than in the term baby [27,31].

The *extrahepatic* biliary tree is visible as a bud on the hepatic diverticulum by the fourth week post-fertilization. By the fifth week, the gallbladder, cystic duct, hepatic ducts, common bile duct and pancreatic duct are well demarcated. The major bile ducts at the porta hepatis are fully formed by the sixteenth week of gestation (see Fig. 4-12). The anlage of the gallbladder and biliary tree have a continuously patent lumen throughout gestation, visible as early as 29 days post-fertilization, in direct continuity with converging ductules at the hepatic hilum and with the developing intrahepatic ducts, and do not have a solid stage as had been previously suggested [33,34]. Maturity of the hilar peribiliary glands and the peribiliary capillary plexus is only reached by 15 years of age [35,36].

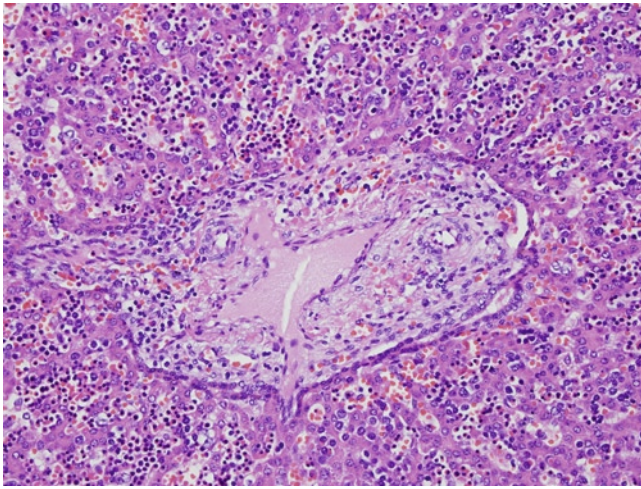


FIGURE 4-8. Biliary development. Section from a 17-week fetus illustrates the prominent focally double-layered ductal plate around this large portal tract. (H&E, 20 \times .)

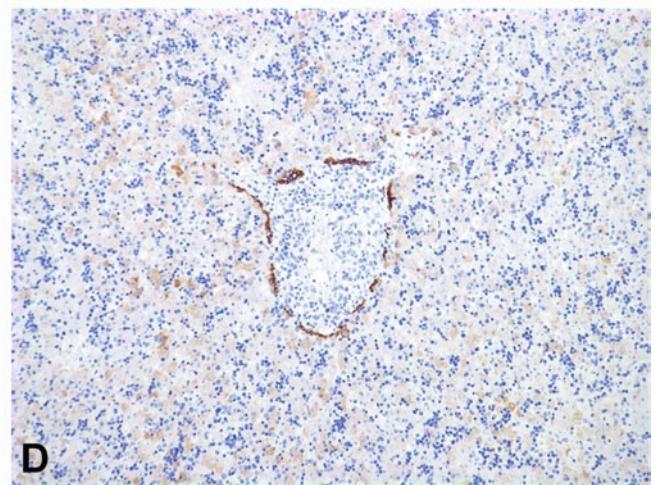
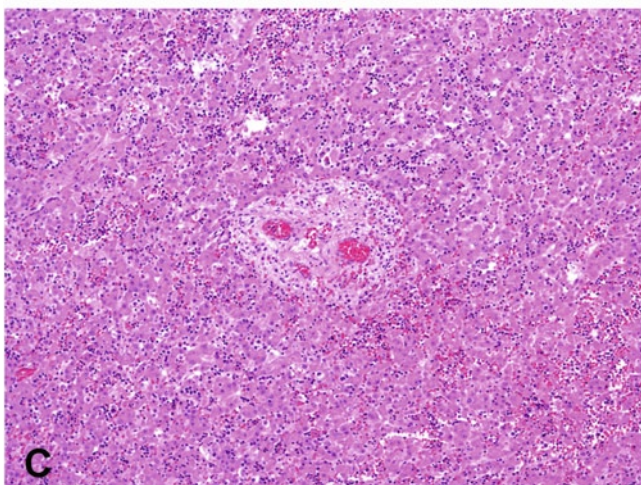
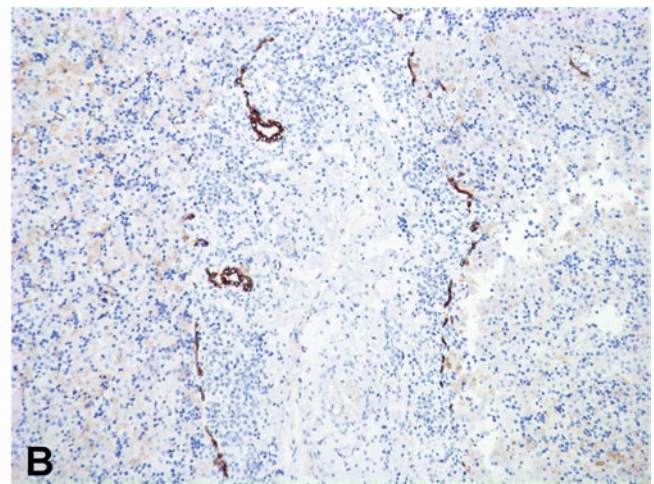
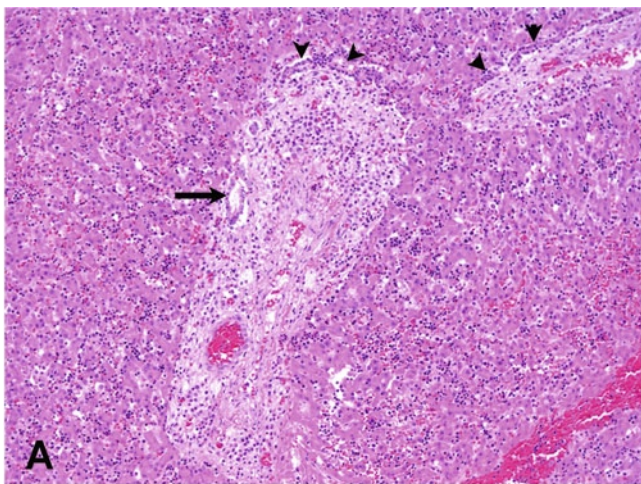


FIGURE 4-9. Biliary development in a 16-week fetus. **A.** In a larger portal tract, a bile duct lined by a cuboidal epithelium (*arrow*) is distinguishable from the ductal plate. The bilayered ductal plate is apparent in the superior portion of this portal space, as well as in an adjacent portal space to the right (*arrowheads*). **B.** Immunostaining with CK19 outlines the ductal plate, as well

as well early interlobular bile ducts being incorporated more centrally by the portal mesenchyme. **C.** By contrast, bile ducts are not apparent in a smaller more peripheral portal tract in the same liver. **D.** Immunostaining with CK19 outlines the ductal plate. (**A-D**, H&E, 10 \times .)

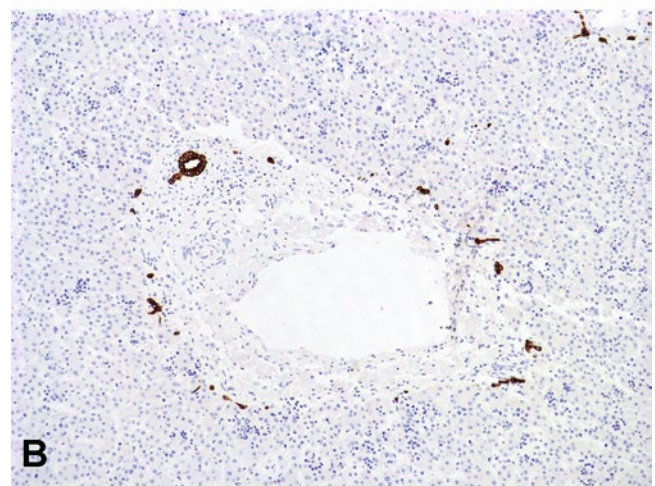
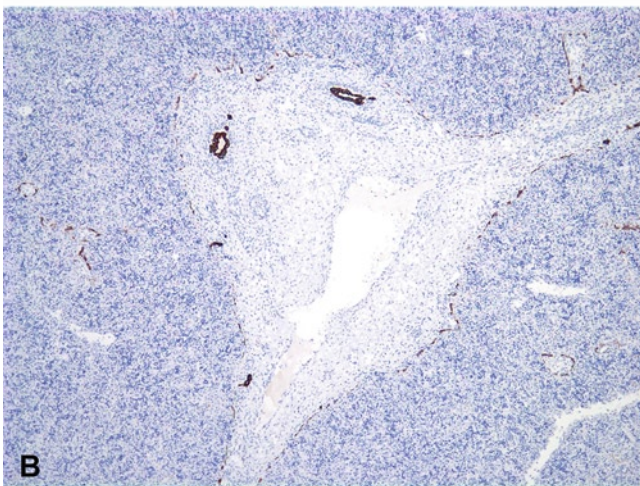
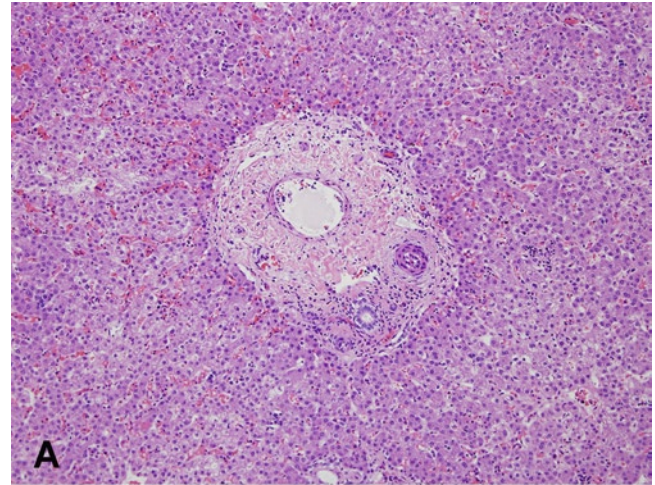
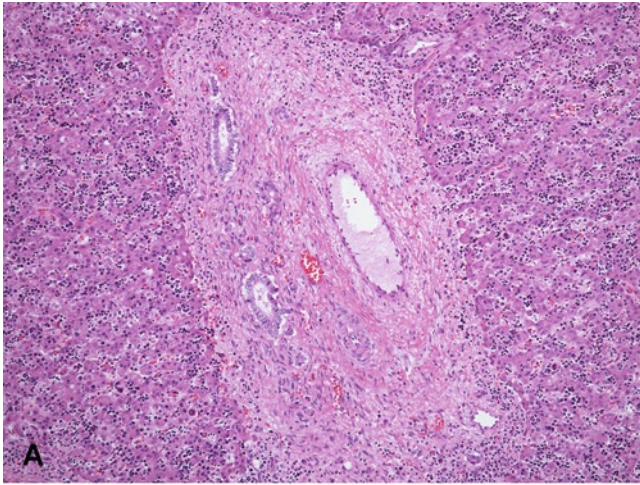


FIGURE 4-10. Biliary development in a 24-week fetus. **A**, More mature bile ducts separate from the ductal plate and begin to be incorporated more centrally in this larger portal tract. The ductal plate is recognizable at the periphery of the upper most portion of the portal tract. Note also the abundant hematopoiesis. **B**, Immunostaining with CK19 shows a more discontinuous ductal plate. (**A**, H&E, 10 \times , and **B**, CK19 immunohistochemistry, 10 \times .)

FIGURE 4-11. Biliary development in a 36-week fetus. **A**, Most portal tracts have assumed the configuration that will prevail throughout life, with a well-formed bile duct comparable in diameter to the adjacent hepatic artery. The ductal plate is no longer observable in all but the smaller more peripheral portal tracts. **B**, Immunostaining with CK19 highlights a mature bile duct and canals of Herring in the immediate periportal area. The ductal plate has become essentially inapparent. (**A**, H&E, 10 \times , and **B**, CK19 immunohistochemistry, 10 \times .)

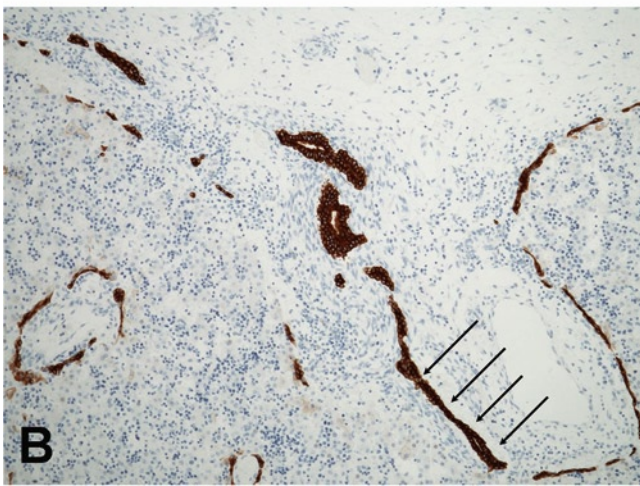
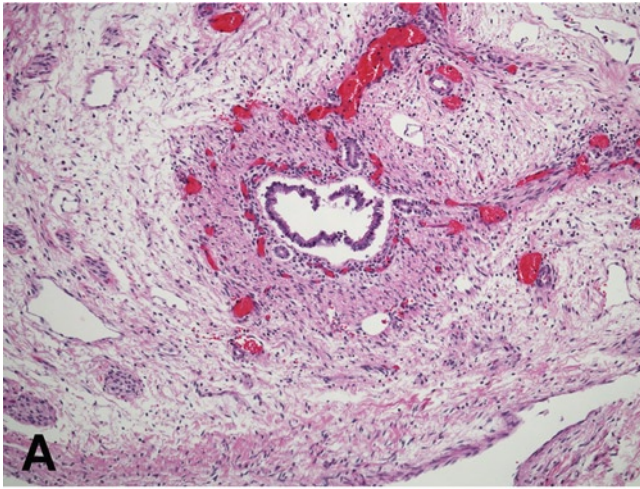


FIGURE 4-12. A, Transverse section of the hepatic duct at 23 weeks lined by columnar cells surrounded by a distinct mesenchymal collar and the presence of glands. **B**, Transverse section of the hepatic hilum in this 23-week fetus reveals that branches of the hepatic ducts close to the liver parenchyma still retain connections to peripheral ductal plate elements (arrows). (**A**, H&E, 10 \times , and **B**, CK19 immunohistochemistry, 10 \times .)

References

1. MacSween RN, Desmet V, Roskams T, Scothorne RJ: Developmental anatomy and normal structure. In *Pathology of the Liver*, edn 4. Edited by MacSween RN, Burt AD, Portman B, et al. London: Churchill Livingstone; 2002:1–67.
2. O’Rahilly R, Muller F: *Human Embryology and Teratology*, edn 3. New York: Wiley-Liss; 2001.
3. Ruchelli E: Developmental anatomy and congenital anomalies of the liver, gallbladder, and extrahepatic biliary tree. In *Pathology of Pediatric Gastrointestinal and Liver Disease*. Edited by Russo P, Ruchelli E, Piccoli D. New York: Springer; 2004:191–202.
4. Zhao R, Duncan SA: Embryonic development of the liver. *Hepatology* 2005, 41:956–967.
5. Lemaigre FP: Mechanisms of liver development: concepts for understanding liver disorders and design of novel therapies. *Gastroenterology* 2009, 137:62–79.
6. McLin VA, Zorn AM: Molecular control of liver development. *Clin Liver Dis* 2006, 10:1–25, v.
7. Collardeau-Frachon S, Scoazec JY: Vascular development and differentiation during human liver organogenesis. *Anat Rec (Hoboken)* 2008, 291:614–627.
8. Saxena R, Zucker SD, Crawford JM: Anatomy and physiology of the liver. In *Hepatology*, edn 4. Edited by Zakim D, Boyer TD. Philadelphia: Saunders; 2003:3–30.
9. Ghosh ML, Emery JL: Hypoxia and asymmetrical fibrosis of the liver in children. *Gut* 1973, 14:209–212.
10. Emery JL: Asymmetrical liver disease in infancy. *J Pathol Bacteriol* 1955, 69:219–224.
11. Dimmick J, Jevon G: Liver disease in the perinatal infant. In *Textbook of Fetal and Perinatal Pathology*, edn 2. Edited by Wigglesworth JS, Singer DB. Oxford: Blackwell Science; 1998:865–899.
12. Hutchins GF, Gollan JL: Recent developments in the pathophysiology of cholestasis. *Clin Liver Dis* 2004, 8:1–26 v.
13. Dimmick J: Hepatobiliary System. In *Developmental Pathology of the Embryo and Fetus*. Edited by Dimmick J, Kalousek D. Philadelphia: JB Lippincott; 1992:545–578.
14. Sadava D, Frykman P, Harris E, et al.: Development of enzymes of glycolysis and gluconeogenesis in human fetal liver. *Biol Neonate* 1992, 62:89–95.
15. Ohtani O, Ohtani Y: Lymph circulation in the liver. *Anat Rec (Hoboken)* 2008, 291:643–652.

16. Naito M, Hasegawa G, Takahashi K: Development, differentiation, and maturation of Kupffer cells. *Microsc Res Tech* 1997, 39:350–364.
17. Timens W, Kamps WA: Hemopoiesis in human fetal and embryonic liver. *Microsc Res Tech* 1997, 39:387–397.
18. Naus GJ, Amann GR, Macpherson TA: Estimation of hepatic hematopoiesis in second and third trimester singleton gestations using flow cytometric light scatter analysis of archival autopsy tissue. *Early Hum Dev* 1992, 30:101–107.
19. Roskams T, Desmet V, Verslype C: Development, structure and function of the liver. In *MacSween's Pathology of the Liver*, edn 5. Edited by Burt AD, Portman B, Ferrell L. Philadelphia: Churchill Livingstone Elsevier; 2007:1–74.
20. Singer DB: Hepatic erythropoiesis in infants of diabetic mothers: a morphometric study. *Pediatr Pathol* 1986, 5:471–479.
21. Stallmach T, Karolyi L, Lichtlen P, et al.: Fetuses from preeclamptic mothers show reduced hepatic erythropoiesis. *Pediatr Res* 1998, 43:349–354.
22. Bendon RW, Coventry S: Non-iatrogenic pathology of the preterm infant. *Semin Neonatal* 2004, 9:281–287.
23. Miranda RN, Omurtag K, Castellani WJ, et al.: Myelopoiesis in the liver of stillborns with evidence of intrauterine infection. *Arch Pathol Lab Med* 2006, 130:1786–1791.
24. Pfisterer C, Faber R, Horn LC: Chorioamnionitis-induced changes of fetal extramedullary hematopoiesis in the second trimester of gestation. Is diagnosis from fetal autopsy possible? *Virchows Arch* 2005, 446:150–156.
25. Silver MM, Valberg LS, Cutz E, et al.: Hepatic morphology and iron quantitation in perinatal hemochromatosis. Comparison with a large perinatal control population, including cases with chronic liver disease. *Am J Pathol* 1993, 143:1312–1325.
26. Spagnoli FM, Amicone L, Tripodi M, Weiss MC: Identification of a bipotential precursor cell in hepatic cell lines derived from transgenic mice expressing cyto-Met in the liver. *J Cell Biol* 1998, 143:1101–1112.
27. Van Eyken P, Sciot R, Desmet V: Intrahepatic bile duct development in the rat: a cytokeratin-immunohistochemical study. *Lab Invest* 1988, 59:52–59.
28. Desmet VJ: Ludwig symposium on biliary disorders—part I. Pathogenesis of ductal plate abnormalities. *Mayo Clin Proc* 1998, 73:80–89.
29. Coffinier C, Gresh L, Fiette L, et al.: Bile system morphogenesis defects and liver dysfunction upon targeted deletion of HNF1beta. *Development* 2002, 129:1829–1838.
30. Lemaigre FP: Development of the biliary tract. *Mech Dev* 2003, 120:81–87.
31. Sergi C, Adam S, Kahl P, Otto HF: The remodeling of the primitive human biliary system. *Early Hum Dev* 2000, 58:167–178.
32. Crawford JM: Development of the intrahepatic biliary tree. *Semin Liver Dis* 2002, 22:213–226.
33. Nakanuma Y, Hosono M, Sanzen T, Sasaki M: Microstructure and development of the normal and pathologic biliary tract in humans, including blood supply. *Microsc Res Tech* 1997, 38:552–570.
34. Tan CE, Vijayan V: New clues for the developing human biliary system at the porta hepatis. *J Hepatobiliary Pancreat Surg* 2001, 8:295–302.
35. Terada T, Nakanuma Y: Pancreatic lipase is a useful phenotypic marker of intrahepatic large and septal bile ducts, peribiliary glands, and their malignant counterparts. *Mod Pathol* 1993, 6:419–426.
36. Terada T, Kida T, Nakanuma Y: Extrahepatic peribiliary glands express alpha-amylase isozymes, trypsin and pancreatic lipase: an immunohistochemical analysis. *Hepatology* 1993, 18:803–808.

5

Pancreas

Eduardo D. Ruchelli

In contrast to the adult pancreas, the fetal pancreas does not undergo rapid postmortem autolysis and usually is relatively well preserved at autopsy, except for stillborn fetuses with prolonged retention in utero. Samples should be obtained from the head (including the duodenum), body, and tail. Evaluation of the fetal and neonatal pancreas, particularly its endocrine component, requires familiarity with the normal changes that the stromal, exocrine, and endocrine components undergo throughout gestation. The unique features of the endocrine tissue of the fetal and neonatal pancreas must be considered before drawing conclusions as to their possible causative role in either presumed or clinically established hyperinsulinism.

Embryology

The pancreas develops from two primordia, a dorsal larger bud and a smaller ventral bud [1,2]. The pancreas begins to develop on day 26 when the dorsal pancreatic bud starts to grow out of the duodenum into the dorsal mesentery just opposite the hepatic diverticulum. Over the next few days, the ventral pancreatic bud, adjacent to the hepatic diverticulum, grows into the ventral mesentery. Due to the close proximity of the ventral bud and the developing extrahepatic bile ducts, the main duct of the ventral pancreatic bud becomes connected to the proximal end of the common bile duct by day 32. When the duodenum rotates to the right, the mouth of the common bile duct and ventral pancreatic bud migrate posteriorly toward the dorsal mesentery. Late in the sixth week, the two pancreatic buds fuse to form the definitive pancreas. The dorsal pancreatic bud gives rise to a small part of the head, and to the entire body and tail of the pancreas, whereas the ventral pancreatic bud gives rise to most of the head and the uncinata process. The duct systems of the pancreatic buds fuse to form the main pancreatic duct in 90% to 95% of the population.

Branching of the pancreatic buds occurs differently from the classic branching of other organs such as the developing lung [3]. Rather than expanding and folding the epithelium, the originally solid epithelial clusters of the pancreatic buds develop central lumina. These soon coalesce to generate a continuous lumen, forming an epithelial tree that drains exocrine products into the duodenum. The pancreatic ductal cells, exocrine cells, and endocrine cells in the islets of Langerhans all differentiate from the endoderm of the pancreatic buds. The acinar cells first appear as small groups of cells along the sides and tips of the ducts. They are penetrated by duct cells that become the centroacinar cells. Other duct cells elongate to form the intercalated ducts, which serve as the connection between the acini and the larger ducts.

The endocrine cells are seen first during the seventh week as small clusters of cells on the outer surface of the ducts [4,5]. They then detach from the ducts and lie in clusters in the adjacent fibrous septa. The term *nesidioblastosis* was initially used to describe this normal developmental process [6]. Unfortunately, over the last few decades, nesidioblastosis has been used erroneously in the literature to describe the pathologic changes of congenital hyperinsulinism. This has created much confusion regarding the distinction between the

normal features of pancreatic development and the true histologic abnormalities of congenital hyperinsulinism. A second generation of endocrine cells arises from centroacinar cells in the fourth month of gestation and these cells lie individually or in small clusters in the center

of the lobules. Both generations of endocrine cells continue to be present throughout gestation, and both α and β cells can be recognized even in the earliest developing islets.

Histology

Microscopically, the pancreas is arranged in lobules. The lobular architecture is particularly prominent during the midtrimester due to the relatively abundant connective tissue present between the lobules (see Fig. 5-1). This normal feature should not be misdiagnosed as fibrosis. As the pancreas matures, the amount of connective tissue between and within the lobules is

proportionally decreased. At term, the connective tissue is markedly diminished while in the normal adult pancreas there is little connective tissue between the lobules and almost none within them. The epithelial component of the pancreas includes exocrine elements (acini and ducts) and endocrine elements (islets of Langerhans).

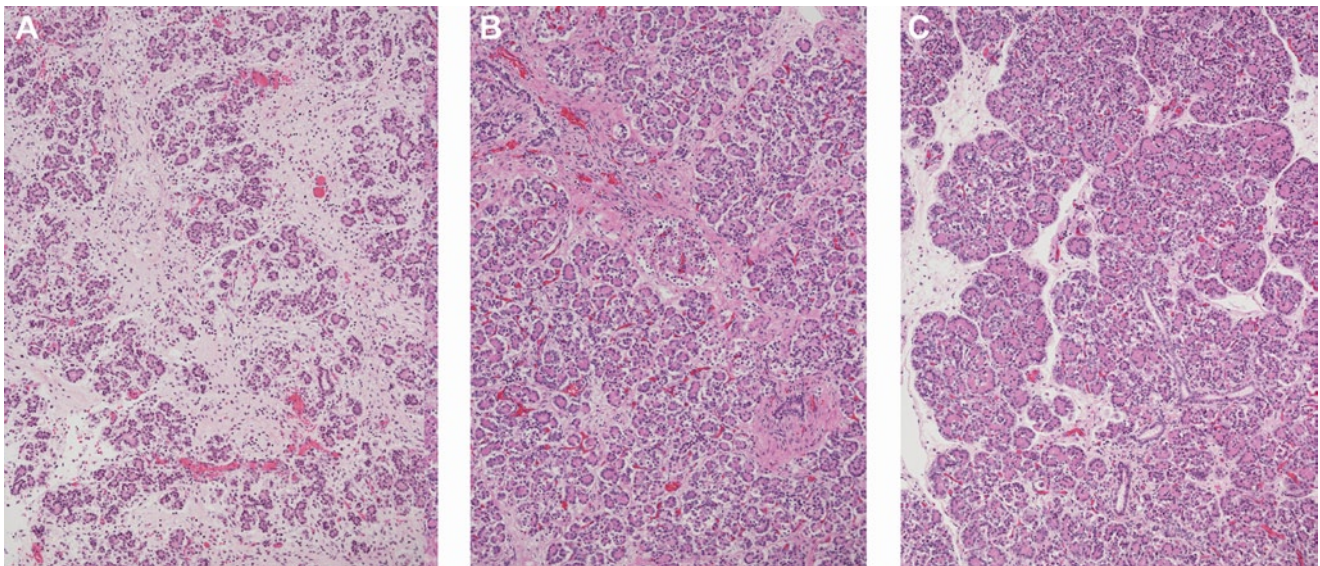


FIGURE 5-1. Pancreatic stroma. **A**, Pancreas at 16 weeks. Note the abundant connective tissue within and between lobules, which is characteristic of the midtrimester pancreas. **B**, Pancreas at 32 weeks. The relative amount of connective tissue has diminished as the glandular elements increase. Intralobular connective

tissue still remains visible in contrast to the minimal amount present in the fully mature pancreas. **C**, Pancreas at 38 weeks. Lobules are more compact with little intervening intralobular connective tissue. All figures are shown at the same magnification for comparison. (Hematoxylin and eosin [H&E], 10 \times .)

Exocrine Pancreas

Acinar cells are arranged in a single layer surrounding a minute central lumen. They have basally situated round nuclei and apical granular eosinophilic cytoplasm. In contrast, endocrine cells have central round nuclei and pale amphophilic cytoplasm and do not form acini (see Fig. 5-2). Although these cytologic features can be appreciated at any gestational age, in the fetal pancreas many endocrine cells are arranged individually or in small clusters and can be difficult to distinguish from exocrine cells on routine stains. Centroacinar cells are flat to cuboidal cells with pale or lightly eosinophilic cytoplasm and central oval nuclei, located between the acinar cell and the intercalated duct. Centroacinar

cells usually are inconspicuous, but they can occasionally be prominent and mistakenly interpreted as endocrine cells (see Fig. 5-3). If necessary, an immunostain for cytokeratins can be used to distinguish them from endocrine cells, which generally are not reactive for keratins. The lumen surrounded by acinar and centroacinar cells drains into the intercalated ducts, which in turn join together to form the intralobular ducts (see Fig. 5-4). As the ducts leave the lobules, their epithelial lining cells become slightly taller and they become enveloped by a thicker coat of collagenous tissue. These interlobular ducts gradually enlarge as they approach the main excretory ducts.

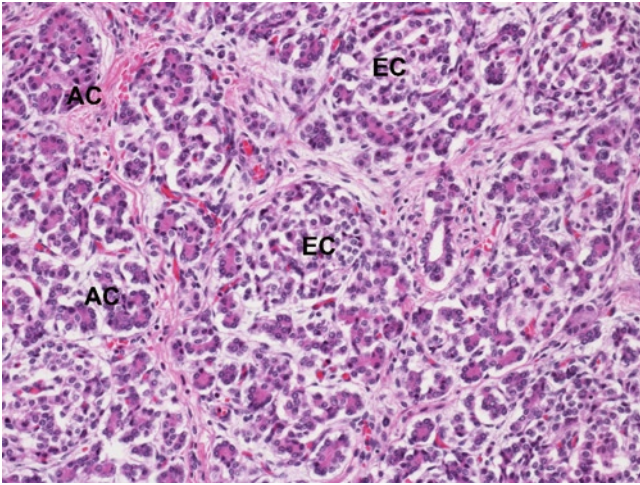


FIGURE 5-2. Exocrine and endocrine cells. An acinar cell (AC) is clearly distinguished by its basally located nuclei and apical bright eosinophilic cytoplasm surrounding a central small lumen, in contrast to the paler endocrine cell (EC) with a central nucleus and a cord-like arrangement within the islets. Pancreas at 35 weeks is shown. (H&E, 20 \times .)

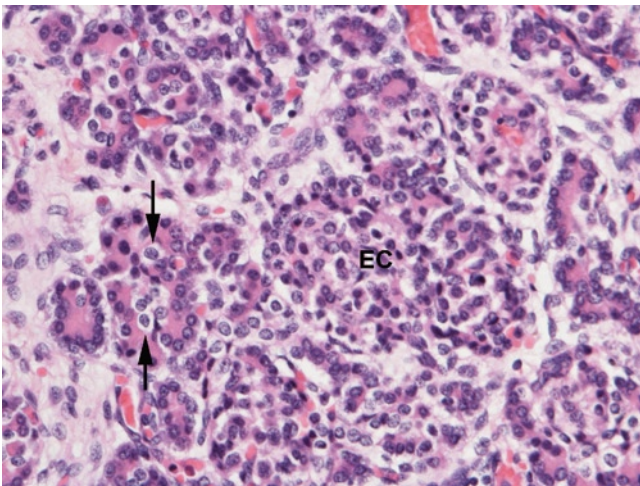


FIGURE 5-3. Centroacinar cells. Prominent centroacinar cells are seen within acini on the left (*arrows*). They may be difficult to distinguish from an endocrine cell (EC) when singly arranged. A distinct islet on the right is composed of ECs with slightly more eosinophilic cytoplasm but otherwise cytologic features are similar to centroacinar cells. Pancreas at 23 weeks is shown. (H&E, 40 \times .)

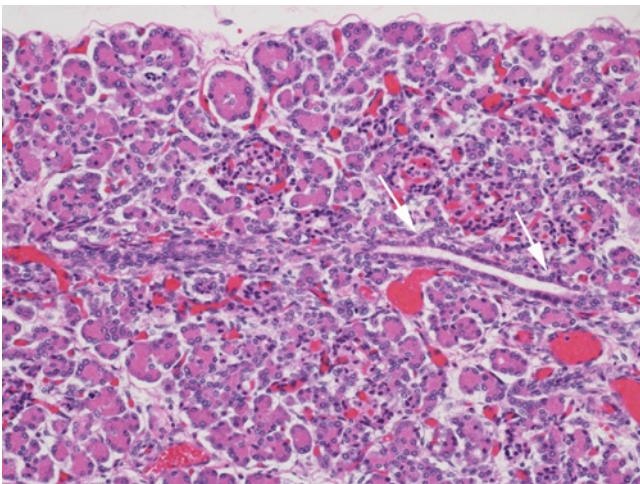


FIGURE 5-4. Ducts. The intralobular ducts (*center*) are surrounded by little connective tissue and receive innumerable intercalated ducts (*arrows*) draining the acini. Pancreas at 32 weeks is shown. (H&E, 20 \times .)

Endocrine Pancreas

Although endocrine cells constitute only 1% to 2% of the volume of the adult pancreas, about 10% of the neonatal pancreas is comprised of endocrine cells [7]. In spite of this relatively large proportion of endocrine tissue in the fetal pancreas, endocrine cells can be difficult to distinguish with certainty in routinely stained sections because so many of them occur as single cells or tiny nests rather than as the traditionally compact, larger islets (see Fig. 5-5). These extrainsular endocrine cells become much less abundant later in life and constitute less than 10% of the total endocrine cell population in the adult. The quantification of endocrine tissue is also complicated by the considerable variation that exists in the concentration of islets from one lobule to the next (see Figs. 5-6 and 5-7). The size and shape of the islets can also vary significantly (see Fig. 5-8). Fetal islets generally are not as compact and well circumscribed as islets in individuals who are several months old. Endocrine

cells arising in the ducts are particularly difficult to identify on routine stains and the immunohistochemistry for various neuroendocrine markers is necessary in order to outline their pattern of growth (see Fig. 5-9). Although most islets are surrounded by acinar elements and tend to have a centrilobular location, septal islets are not uncommon in the fetus and newborn (see Fig. 5-10). These normal features of the fetal and neonatal pancreas should not be mistaken for evidence of presumed or clinically established hyperinsulinism. Islet cells with nucleomegaly (nuclei three to four times the size of their neighbors) are the most reliable evidence for congenital hyperinsulinism (see Fig. 5-11). Similar cells may be seen in the pancreases of infants of diabetic mothers, Beckwith-Wiedemann syndrome, trisomy 13, and other anomalies, but are rarely seen in otherwise normal fetuses and newborns. They are occasionally seen in asymptomatic adults.

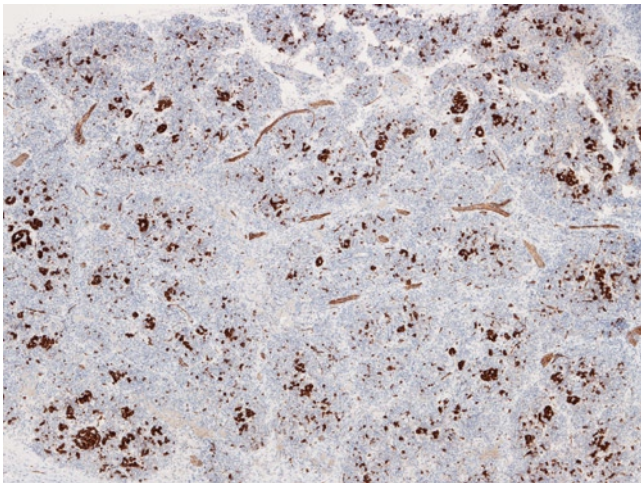


FIGURE 5-5. Endocrine pancreas. The immunostain for synaptophysin demonstrates innumerable small clusters and single endocrine cells, which are very difficult to recognize on routine stain. Pancreas at 19 weeks is shown (10 \times).

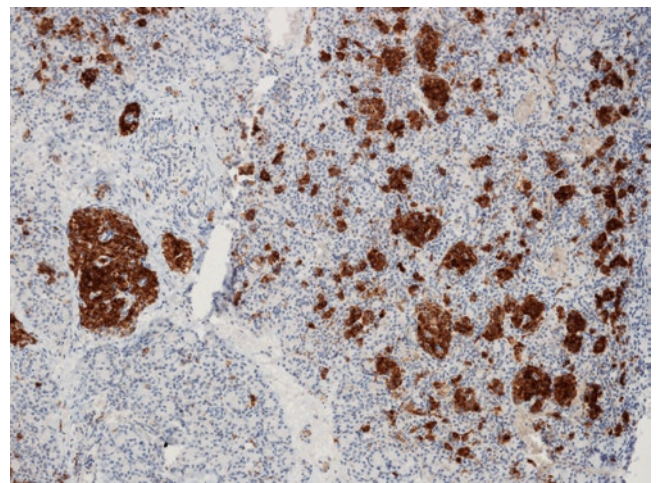


FIGURE 5-6. Endocrine pancreas. Note the variable density of endocrine tissue within neighboring lobules. Pancreas at 19 weeks is shown. (Synaptophysin immunostain, 10 \times .)

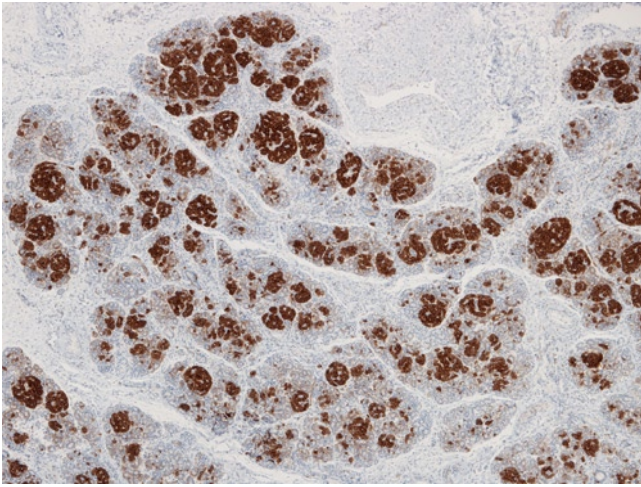


FIGURE 5-7. Endocrine pancreas. The fetal and neonatal pancreas can contain areas with a large proportion of endocrine tissue; however, this finding by itself should not be considered pathologic. Pancreas at 35 weeks is shown. (Synaptophysin immunostain, 4 \times .)

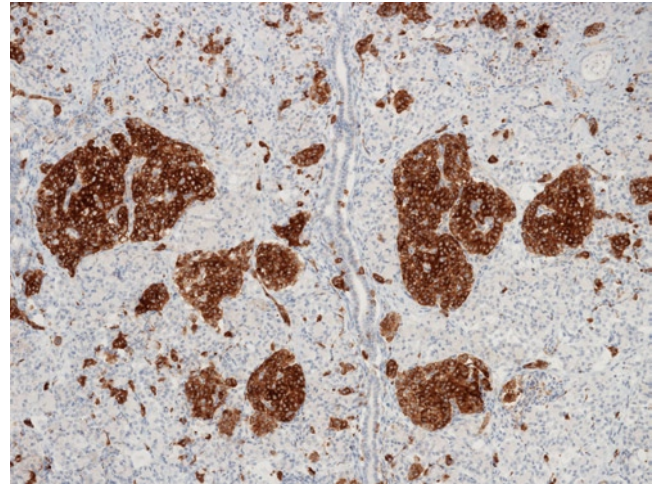


FIGURE 5-8. Endocrine pancreas. Note the variable size and shape of the developing islets. Pancreas at 24 weeks is shown. (Synaptophysin immunostain, 10 \times .)

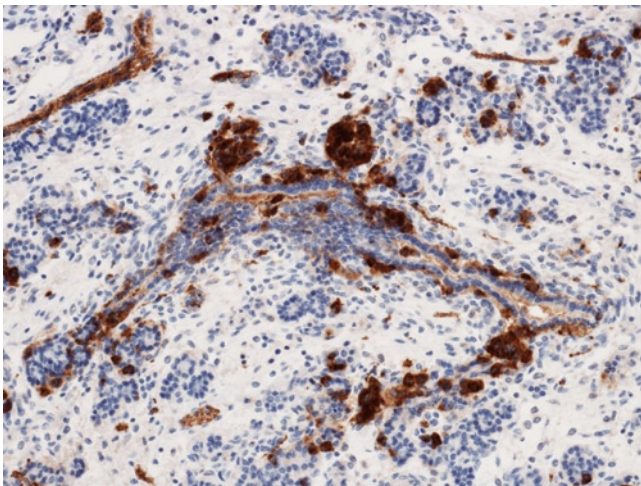


FIGURE 5-9. Nesidioblastosis. The endocrine cells are first seen as small clusters of cells on the outer surface of the ducts. Budding and the subsequent detachment of islets from ducts can be seen in this field. After detaching from the ducts, the endocrine cells lie in clusters in the adjacent fibrous septa. Pancreas at 16 weeks is shown. (Synaptophysin immunostain, 10 \times .)

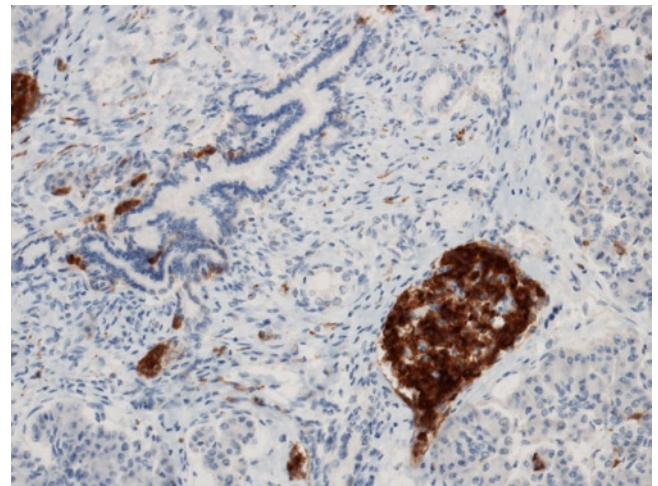


FIGURE 5-10. Septal islets. Some islets originating from large ducts (see Fig. 5-3) can remain in a septal location. Pancreas at 36 weeks is shown. (Synaptophysin immunostain, 20 \times .)

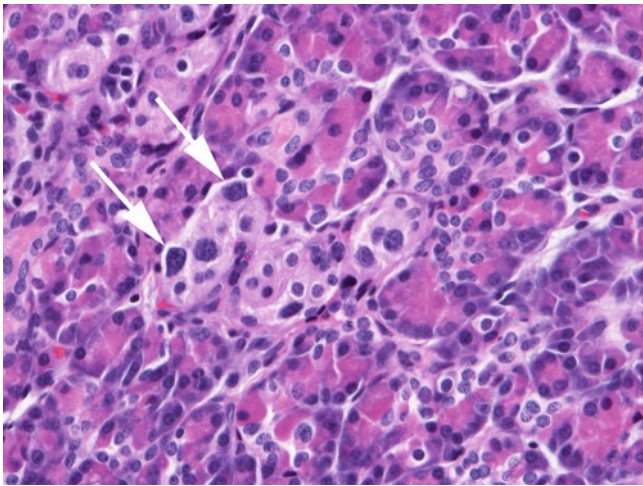


FIGURE 5-11. Endocrine cell nucleomegaly. β Cells with enlarged nuclei (arrows) are frequently seen in various types of congenital hyperinsulinism, but they are extremely rare among normal fetuses and newborns. (H&E, 40 \times .)

Other Histologic Features

Small and large lymphocytic infiltrates are frequently encountered within the fetal pancreas. These infiltrates lack follicle formation and are characterized by small mature lymphocytes intermingled with acini and ducts (see Fig. 5-12). Most lymphoid aggregates are seen in otherwise normal individuals and are thought to represent lymphoid heterotopias. However, if such infiltrates are accompanied by a significant infiltrate of plasma cells or the destruction of parenchyma or ducts, infections such as cytomegalovirus should be considered. Extramedullary hematopoiesis is also com-

monly encountered in the fetal pancreas, particularly during the midtrimester (see Fig. 5-13).

Nodular splenic heterotopias are occasionally seen in the tail of the pancreas (see Fig. 5-14) and are usually incidental findings. However, if they are extensive or accompanied by pancreatic splenic fusion, they may be part of multiple congenital anomalies such as trisomy 13. Pancreatic heterotopias are found in locations such as the site of esophageal atresia, in the wall of the stomach, on the antimesenteric border of the small intestine, or in the wall of a Meckel's diverticulum (see Fig. 5-15).

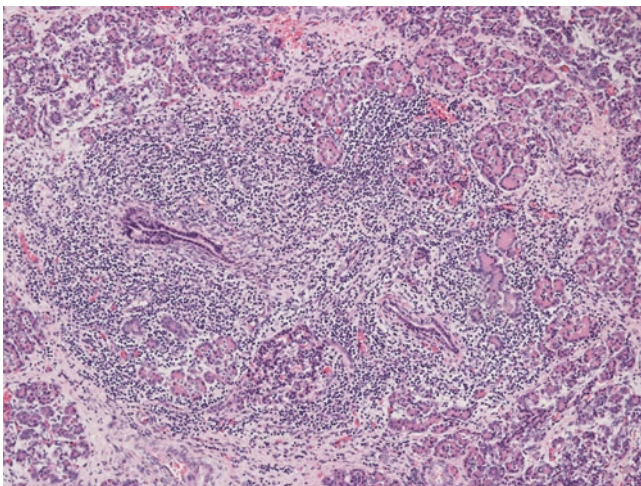


FIGURE 5-12. Lymphoid tissue. Lymphocytic aggregates around ducts and also extending between acini are common in the preterm pancreas and have no pathologic significance. They become less frequent toward term. Pancreas at 23 weeks is shown. (H&E, 10 \times .)

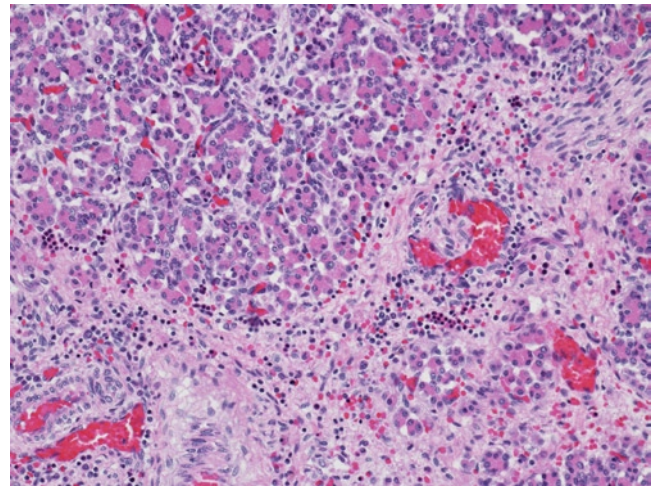


FIGURE 5-13. Hematopoiesis. Although hematopoiesis in the pancreas is never as prominent as in the liver, it is a fairly constant feature during the second and early third trimesters. Pancreas at 24 weeks is shown. (H&E, 20 \times .)

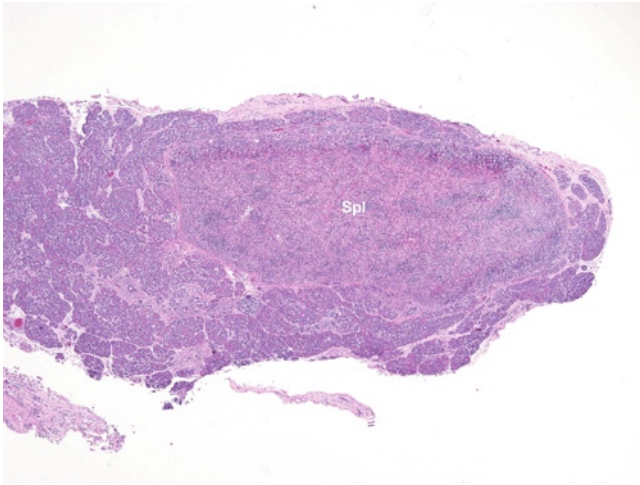


FIGURE 5-14. Nodular splenic heterotopia. A splenic nodule (Spl) is completely surrounded by pancreatic parenchyma in the tail of the pancreas. (H&E, 2 \times .)

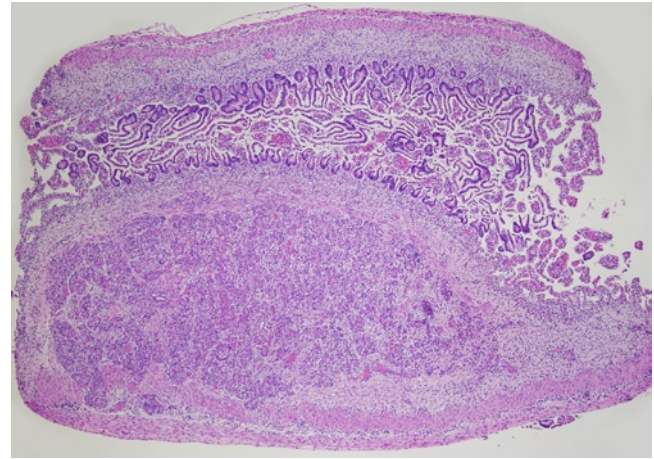


FIGURE 5-15. Small bowel pancreatic heterotopia. Heterotopic pancreatic nodule within the wall of the small bowel is shown. This is one of the most common locations of heterotopic pancreatic tissue. (H&E, 4 \times .)

References

1. Moore KL, Persaud, TVN: *The Developing Human Clinically Oriented Embryology*, 8th edn. Philadelphia: Saunders; 2008.
2. Bock P, Abdel-Moneim M, Egerbacher M: Development of pancreas. *Microsc Res Tech* 1997, 37:374–383.
3. Schoenwolf GC, Bleyl SB, Brauer PR, Francis-West PH: *Larsen's Human Embryology*, 4th edn. Philadelphia: Churchill Livingstone Elsevier; 2009.
4. Peters J, Jurgensen A, Kloppel G: Ontogeny, differentiation and growth of the endocrine pancreas. *Virchows Arch* 2000, 436:527–538.
5. Hill DJ: Development of the endocrine pancreas. *Rev Endocr Metab Disord* 2005, 6:229–238.
6. Jaffe R, Hashida Y, Yunis EJ: The endocrine pancreas of the neonate and infant. *Perspect Pediatr Pathol* 1982, 7:137–165.
7. Rahier J, Wallon J, Henquin JC: Cell populations in the endocrine pancreas of human neonates and infants. *Diabetologia* 1981, 20:540–546.

6

Salivary Glands

Eduardo D. Ruchelli

The three major salivary glands (parotid, sublingual, and submandibular) can be examined at autopsy during dissection of the neck to evaluate the presence of developmental anomalies or cytomegalovirus infection. The submandibular glands are easier to dissect at autopsy than the other two glands, and can be routinely sampled before removal of the neck block by exposing the tissues between the angle of the mandible and the base of the tongue. Thus, this chapter focuses on the development and histology of the submandibular gland.

Embryology

During the sixth and seventh weeks, the salivary glands begin as solid epithelial buds from the primordial oral cavity [1]. Five stages of development have been described in the mouse [2]. In the first stage, known as the pre-bud stage, the oral epithelium thickens and then protrudes into the underlying mesenchyme (bud stage). The bud then undergoes branching (pseudoglandular stage). These branches are initially solid but later develop a lumen and become ducts (canalicular stage). Subsequently the terminal buds are also hollowed out to form the acini (terminal bud stage). The parotid glands are the first to appear early in the sixth week and are derived from the ectoderm of the primitive oral cavity. The submandibular glands appear late in the sixth week and probably develop from endodermal buds in the floor of the stomodeum, although their exact derivation remains somewhat obscure [3]. Acini begin to form at 12 weeks and secretory activity begins at 16 weeks. The sublingual glands appear in the eighth week, approximately 2 weeks later than the other salivary glands. Unlike rat or mouse salivary glands that differentiate predominantly in postnatal life, human salivary glands appear to achieve complete maturation by the end of gestation [3]. However, the full details of the development of human salivary glands have yet to be elucidated.

Histology

The mature salivary glands have a secretory lobular component (acini, intercalated ducts, and striated ducts) and an excretory component (interlobular ducts) [4]. The acini of the submandibular glands are mixed including both mucous cells and serous cells. Mucous cells have abundant clear cytoplasm, whereas serous cells have basophilic cytoplasm and are arranged in a crescent-shaped formation around the mucous cells. The intercalated duct lies between the acinus and the striated duct. It is lined by a single layer of cuboidal epithelium and it is typically very short in the submandibular gland. In contrast, the striated duct is longer and its single layer of columnar epithelium with eosinophilic cytoplasm and characteristic striations stands out on routine sections. The interlobular ducts are lined by pseudostratified epithelium with sparse goblet cells. A layer of myoepithelial cells surround the acini and intercalated ducts, but they are difficult to identify on

routine sections. The histology of the acini and ducts changes during fetal life, as described in the following section.

During the early midtrimester the submandibular gland architecture is already lobular in nature but abundant loose mesenchyme separates the epithelial elements and constitutes the main tissue component (see Fig. 6-1). The epithelial component consists of tubules and terminal buds with a two-cell layer structure (see Figs. 6-2-6-4). Acinar differentiation is primitive at this time; however, ducts and terminal units typically contain secretions within the lumen in the second trimester (see Figs. 6-3 and 6-4). Near the end of the midtrimester the striated ducts become more distinct as the cytoplasm grows larger and eosinophilic, whereas the intercalated ducts and primitive acini remain smaller 1 to 2-cell layer tubular structures (see Fig. 6-5).

During the third trimester as the gland matures the epithelial structures become more numerous and

crowded with a relative decrease in intervening stroma (see Fig. 6-6). The interlobular ducts (excretory ducts) thicken and adopt a multilayer-cell structure (see Fig. 6-7). At the same time, striated ducts elongate becoming more prominent and mucous differentiation becomes evident in the acini (see Figs. 6-8 and 6-9). Although we have observed mucous acini during the third trimester, others consider the development of mucous acini a postnatal event [5,6]. In contrast to the parotid and sublingual salivary glands, which have short striated ducts, the submandibular gland has long striated ducts that become very distinct during the third trimester (see Fig. 6-10). The two-cell layer structure of these ducts during the second trimester gradually changes to a single layer of columnar cells with occasional cuboidal cells in the basal area (see Fig. 6-11). It is unclear whether the outer layer of cells of the intralobular ducts differentiates into myoepithelial cells (see Fig. 6-4). At term the acini display complete differentiation (see Fig. 6-12) [3].

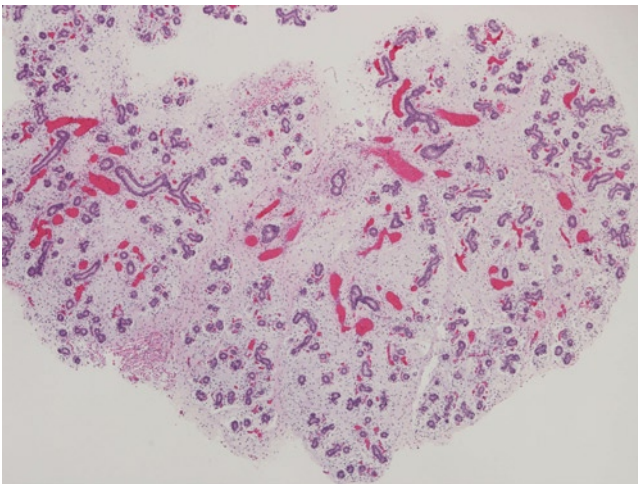


FIGURE 6-1. Submandibular gland at 16 weeks. Abundant loose mesenchyme constitutes the major tissue component at this age. The branching epithelial cords have already developed lumina throughout forming tubular structures. Larger vessels are associated with the more proximal ducts. (Hematoxylin and eosin [H&E], 4 \times .)



FIGURE 6-2. Submandibular gland at 16 weeks. Proximal and distal tubular structures are all lined by a 2-cell epithelial layer. Acinar differentiation is not evident at this time. (H&E, 10 \times .)

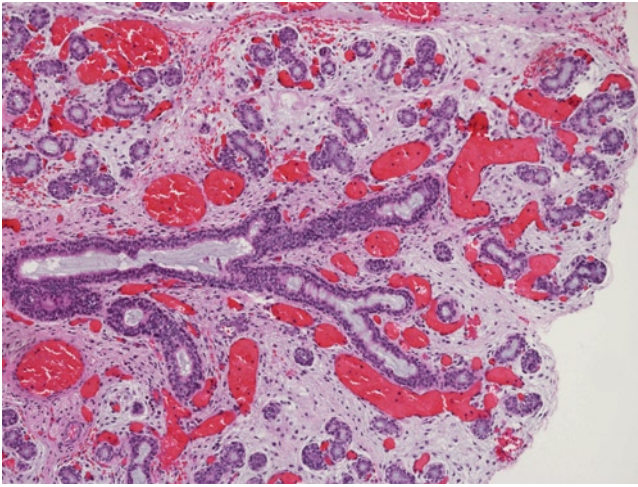


FIGURE 6-3. Submandibular gland at 19 weeks. The gland has a distinct lobular organization. Interlobular and intralobular tubular structures continue to have a 2-cell epithelial layer and secretions are present in their lumen. (H&E, 10 \times .)

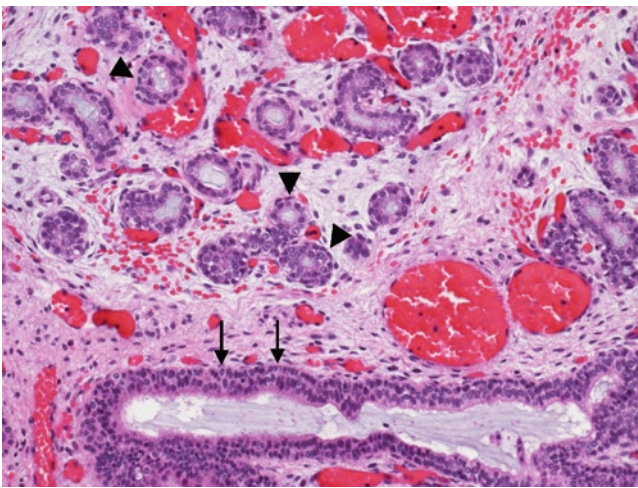


FIGURE 6-4. Submandibular gland at 19 weeks. The proximal ducts have a 2-cell structure with low columnar inner cells and cuboidal outer cells (*arrows*). The distal tubular structures have a cuboidal inner cell layer and an outer cuboidal or flattened cell layer (*arrowheads*). It is unclear whether these cells differentiate into myoepithelial cells (H&E, 20 \times .)

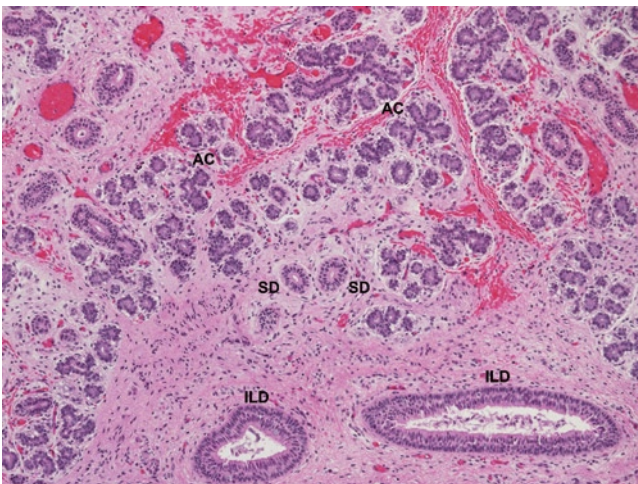


FIGURE 6-5. Submandibular gland at 23 weeks. The intralobular striated ducts (SD) become more distinct as the cytoplasm gets larger and becomes more eosinophilic. The columnar cells of the interlobular ducts (ILD) become taller, whereas the intercalated ducts and primitive acini (AC) remain smaller 1- to 2-cell layer tubular structures. (H&E, 10 \times .)

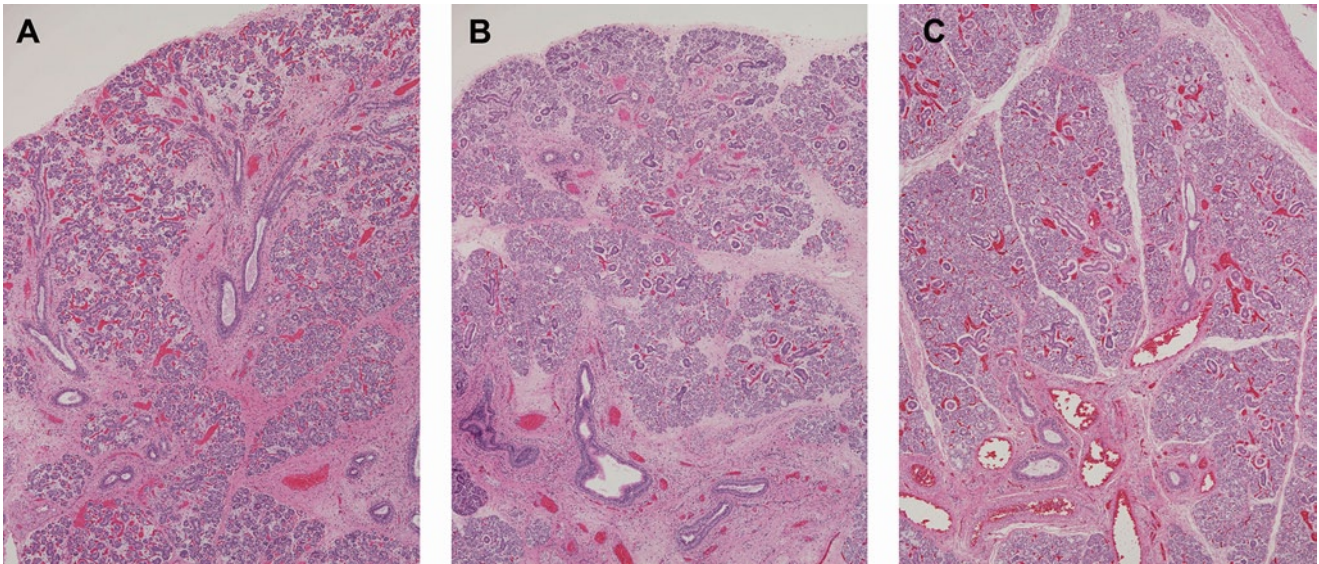


FIGURE 6-6. **A**, Submandibular gland at 27 weeks. The lobular architecture becomes more pronounced as the density of the interlobular connective tissue increases. Loose mesenchyme is still focally present within the lobules separating the epithelial elements. (Compare with Fig. 6-1.) **B**, Submandibular gland at 32 weeks. During the third trimester, the gland becomes

progressively more compact as the result of an increase in the number of acini and relative decrease in stroma. **C**, Submandibular gland at 41 weeks. The lobules have a compact appearance whereas the interlobular connective tissue is dense fibrous. (**A-C**, H&E, 4 \times .)

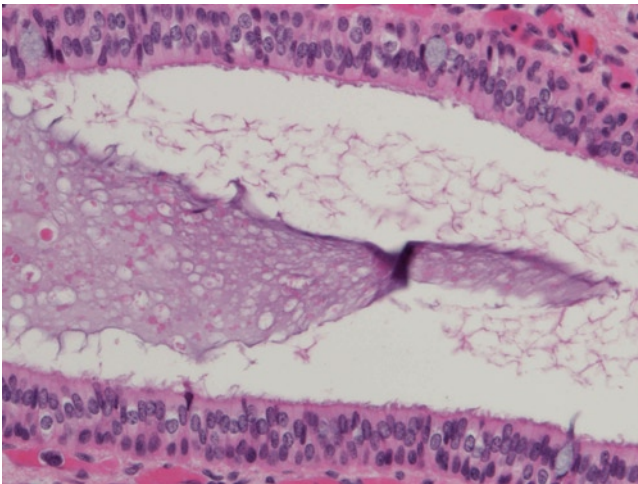


FIGURE 6-7. Submandibular gland at 27 weeks. The interlobular ducts thicken and develop a multilayer-cell structure with scattered goblet cells. (H&E, 40 \times .)

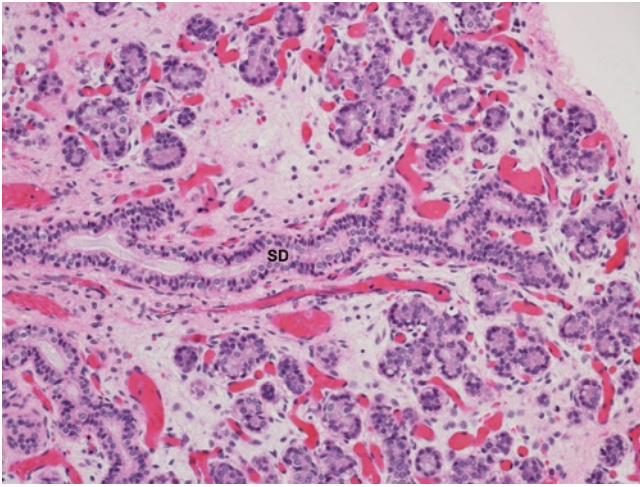


FIGURE 6-8. Submandibular gland at 27 weeks. Striated ducts (SD) elongate and the outer cell layer becomes discontinuous. Long striated ducts are characteristic of the submandibular gland in contrast to the shorter striated ducts of the other major salivary glands. Note the relatively abundant loose mesenchyme within the lobules which is still present at this age. (H&E, 20 \times .)

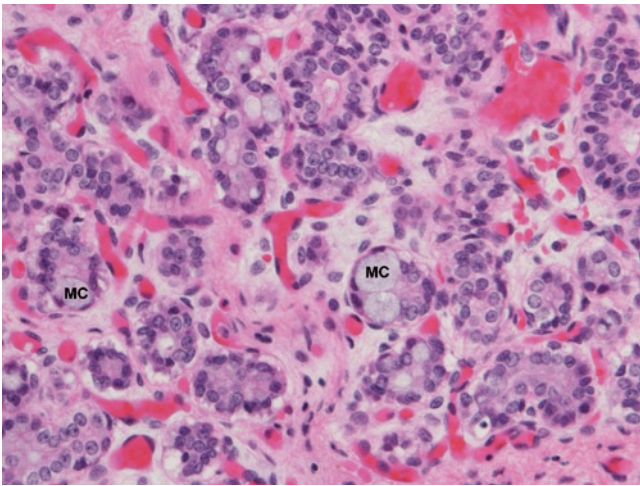


FIGURE 6-9. Submandibular gland at 27 weeks. Acini show evidence of mucous differentiation (MC), which continues to progress during the third trimester. (H&E, 40 \times .)

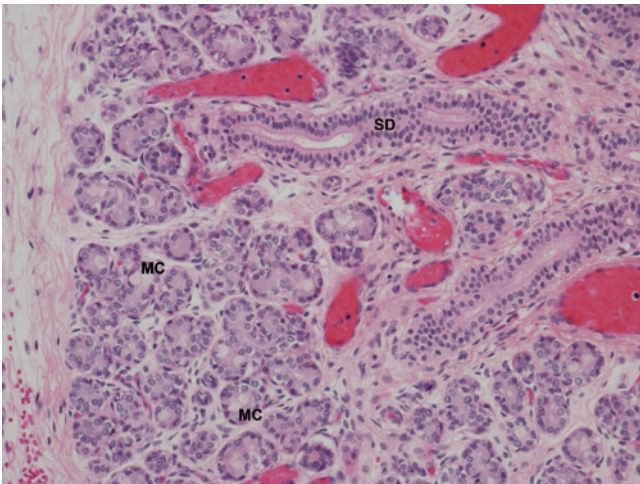


FIGURE 6-10. Submandibular gland at 35 weeks. Acini contain mucous cells (MC). The striated ducts (SD) are long and very distinct, whereas the intercalated ducts are short and difficult to visualize in the submandibular gland. (H&E, 20 \times .)

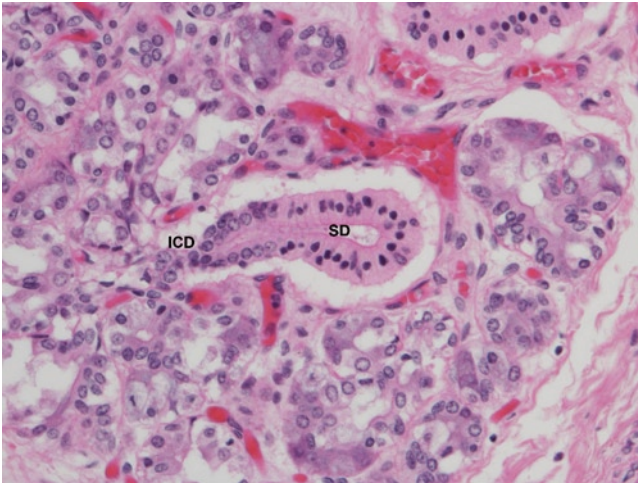


FIGURE 6-11. Submandibular gland at 41 weeks. The striated ducts (SD) lose the two-cell layer structure seen earlier in gestation and the mature wall consists of a single layer of columnar cells with eosinophilic cytoplasm and barely visible basal striations. The intercalated duct (ICD) is very short as it enters the acinus. (H&E, 40 \times .)

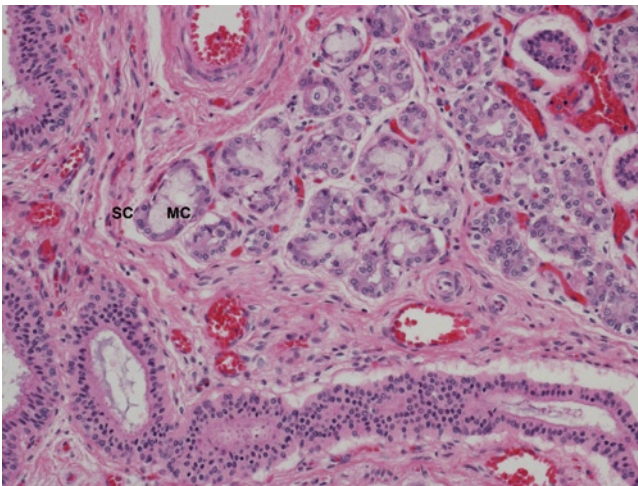


FIGURE 6-12. Submandibular gland at 41 weeks. Mucous cells (MC) become focally more abundant in the acini and are surrounded by serous cells (SC). (H&E, 20 \times .)

References

1. Moore KL, Persaud TVN: *The Developing Human Clinically Oriented Embryology*, edn 8. Philadelphia: Saunders; 2008.
2. Tucker AS: Salivary gland development. *Semin Cell Dev Biol* 2007, 18:237–244.
3. Chi JG: Prenatal development of human major salivary glands. Histological and immunohistochemical characteristics with reference to adult and neoplastic salivary glands. *J Korean Med Sci* 1996, 11:203–216.
4. Martinez-Madrígal BJ, Casiraghi O: Major salivary glands. In *Histology for pathologists*, edn 3. Edited by Mills SE. Philadelphia: Lippincott Williams & Wilkins; 2007:445–470.
5. el-Mohandes EA, Botros KG, Bondok AA: Prenatal development of the human submandibular gland. *Acta Anat (Basel)* 1987, 130:213–218.
6. Scott J: Qualitative and quantitative changes in the histology of the human submandibular salivary gland during post natal growth. *J Biol Buccale* 1979, 7:341–352.

SECTION IV

Genitourinary Tract

Early Embryology of the Genitourinary Tract

Dale S. Huff

The embryology of the genital and urinary tracts are inextricably interrelated and will therefore be described together. The development of the genitourinary tract can be divided into three phases. First, the primitive genitourinary tract develops in the early part of the fifth postfertilization week. Second, in the middle of the fifth week even before the first phase is completed, the definitive urinary tract and the bipotential genital tract begin to be superimposed upon the primitive genitourinary tract. Before the second phase is completed, the third phase, sexual differentiation of the bipotential genitourinary tract, begins when the bipotential genital tract begins to differentiate into either a male or female definitive genital tract beginning in the sixth week, a process that is not completed until the 12th week. The postfertilization gestational ages are assigned following the revised data of O'Rahilly and Muller [1, Appendix 2].

Primitive Genitourinary Tract

General

The primitive genitourinary tract is composed of the paired mesonephric bodies, the paired mesonephric ducts, and the midline cloaca. The cloaca first appears in the middle of the fourth week when the caudal curl of the embryo and the caudal intestinal portal define the hindgut from which the cloaca develops. The urorectal septum will divide the cloaca into a ventral half, which will become the urogenital sinus, and a dorsal half, which will become the rectum. The urogenital sinus will become the bladder and urethra, and, in the female, the introitus. The mesonephric bodies are composed of multiple mesonephric nephrons that are arranged in single file from rostral to caudal. Each mesonephric nephron connects to the mesonephric duct, also called the *primary excretory duct*, which connects to the ventral or urogenital part of the cloaca. The mesonephric nephrons produce urine, which drains through the collecting ducts into the mesonephric duct and into the cloaca. A mesonephric body is also called the *mesonephros*. The mesonephros is the functional part of the primitive genitourinary tract and its development is described next.

Mesonephros and Mesonephric Duct

The mesonephros develops from the intermediate mesoderm. Its development is simultaneous with the rostral to caudal wave of differentiation of the somites from the paraxial mesoderm [2] and the differentiation of the overlying ectodermal ring within the ectoderm. In the middle of the fourth week, the first somite appears in the paraxial mesoderm of the occipital region. Every few hours another pair of somites differentiates caudally to the previous pair. Simultaneously, the adjacent intermediate mesoderm differentiates into the nephrogenic cord. By the end of the fourth week, the occipital and upper cervical somites appear, and the nephrogenic cord adjacent to these somites differentiates into primitive nephric structures called *nephrotomes*, which rapidly disappear. The nephrotomes are somewhat analogous to the pronephros of lower vertebrates, but a true pronephros does not exist in humans [3].

By the beginning of the fifth week, the middle and lower cervical somites appear. The mesonephric duct arises from the dorsolateral border of the nephrogenic cord adjacent to somite C4 at the level of the upper limb bud. The first mesonephric nephron immediately differentiates within the nephrogenic cord adjacent to C6. Mesonephric nephrons are analogous to metanephric nephrons and each is attached to the mesonephric duct by its connecting tubule [4]. The mesonephric duct separates from the nephrogenic cord and grows caudally between the dorsolateral border of the nephrogenic cord and the ectoderm by elongation of its proliferating blind tip. Every few hours a new somite differentiates caudal to its predecessor [5] and new mesonephric nephrons differentiate caudally to their predecessors and attach to the independently elongating mesonephric duct. The caudal growth of the mesonephric duct is faster than the rostral to caudal differentiation of mesonephric nephrons. As the duct elongates caudally, it is attached to the ectoderm at multiple sites. It follows the caudal curl of

the embryo to the mid lumbar region at approximately the level of L2 to L3, where its most caudal attachment to the ectoderm is located. From this point of attachment it curves ventromedially away from the ectoderm and attaches to the urogenital portion of the cloaca, at the level of L4 to L5, before the caudal growth of the mesonephros is completed. The caudal end of the mesonephros reaches only to the level of L2 to L3, the site of the curve of the mesonephric duct and its attachment to the ectoderm. The mesonephric nephrons are not metameric and there are more nephrons than somites. As new nephrons are added caudally, the rostral nephrons and mesonephric duct degenerate. A total of over 80 nephrons develop but, due to the simultaneous degeneration of the rostral nephrons, when the last nephron differentiates and attaches to the curve of the mesonephric duct at the level L2 to L3 only approximately 32 nephrons remain. The mesonephric duct is attached to the mesonephros by a common investing mesenchyme and the attachments of the connecting tubules of the mesonephric nephrons to the mesonephric duct. The attachment of the caudal end of the mesonephros to the curve of the mesonephric duct and the attachment of the curve of the mesonephric duct to the ectoderm are the beginnings of the development of the inguinal canal and the caudal gonadal ligaments. This coordinated rostral to caudal differentiation of somites, mesonephros, and mesonephric duct is so rapid that within 1 to 2 days, early in the middle of the fifth week, all of the thoracic and lumbar somites have been added [6], the development of the mesonephric bodies and mesonephric duct is complete, the mesonephric duct has attached to the cloaca, and the development of the inguinal canal and caudal gonadal ligaments has begun [2] (see Figs. IV-1 and IV-2). The continued development of the inguinal region and the caudal gonadal ligaments is described below.

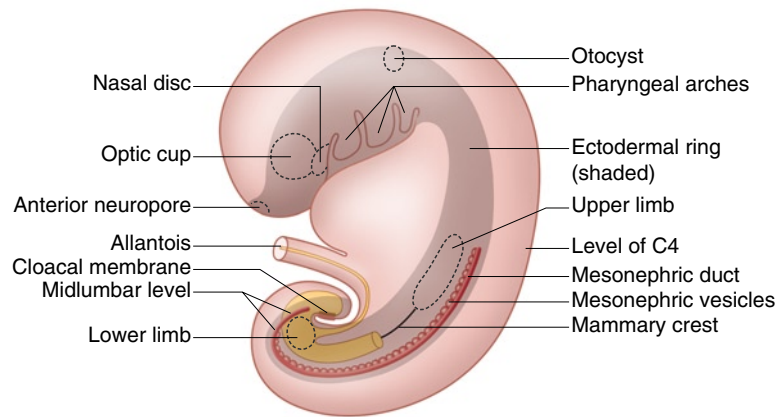


FIGURE IV-1. Left lateral view of the embryo at the beginning of the fifth postfertilization week. The mesonephros extends from the midcervical to the midlumbar area and follows the caudal curl of the embryo. The caudal development of the mesonephros is complete and the caudal end of the mesonephros is at the mid lumbar area. The mesonephric duct curves ventromedially around the distal end of the mesonephros at the midlumbar area where it is attached to the ectodermal ring at the future site of the internal inguinal ring and canal. This is the first curve of the mesonephric duct. The common mesen-

chyme, which invests the mesonephros and mesonephric duct, is not shown in this figure so that the individual mesonephric nephrons can be seen. The lower limb bud has appeared within the ectodermal ring at the midlumbar area in continuity with the cloacal membrane. The precursors of the caudal attachments of the gonads and gonadal ducts to the inguinal canal at the midlumbar area are already established. Several developmental fields within the ectodermal ring are depicted (*shaded area*).

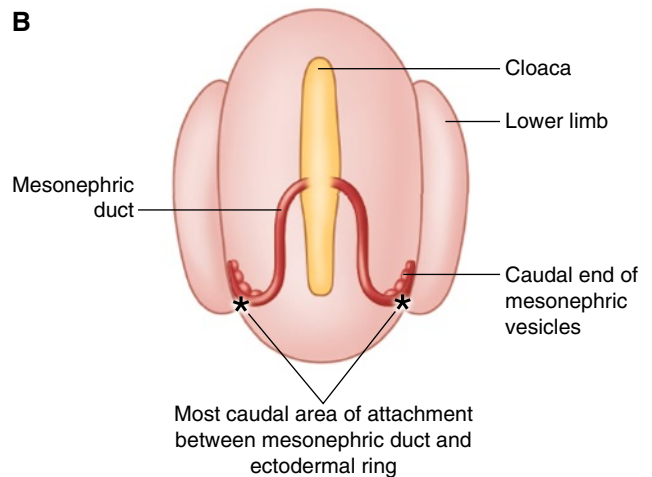
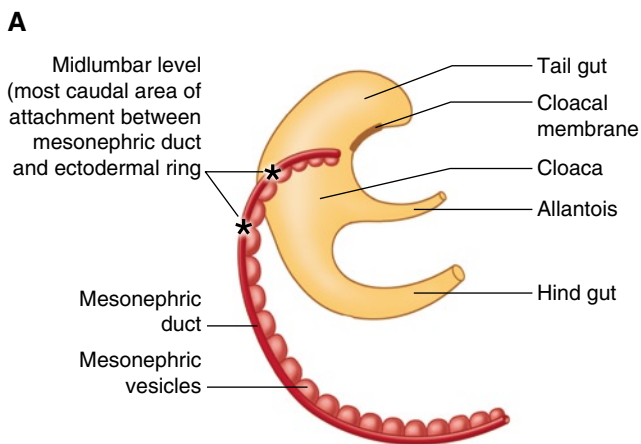


FIGURE IV-2. Closer views of the caudal end of the primitive genitourinary tract early in the fifth week. **A**, Left lateral view. The mesonephros follows the caudal curl of the embryo. At the midlumbar area, the first curve of the mesonephric duct is attached to the overlying ectodermal ring (not shown) between the asterisks at the future site of the internal inguinal ring and canal. **B**, Dorsal view of the caudal curl. The first curve

of the mesonephric seen on end is attached the ectodermal ring at the asterisks at the future site of the internal inguinal ring and canal at the origin of the lower limb. The ureteric bud will arise from the segment of the mesonephric duct between its attachment to the ectodermal ring and its entrance into the cloaca.

Ectodermal Ring

The ectodermal ring is a placodal strip of thickened ectoderm that encircles the embryo in the boundary between the dorsal and ventral halves of the body. It first appears during the end of the fourth postfertilization week in the face and extends caudally on both sides of the embryo like an inverted U to cover the lateral head, neck, thorax, abdomen, and the inguinal areas at the same time as the somites, mesonephros, and mesonephric duct are differentiating [7]. The two limbs of the inverted U meet caudally in the ventral midline over the cloacal membrane to complete the ring on the second day of the fifth week at the same time that the development of the somites, mesonephros, and mesonephric duct reaches the midlumbar region.

The ectodermal ring is in intimate contact with the underlying mesenchyme of the intermediate mesoderm, mesonephros, and especially the mesonephric duct. The rich epithelial-mesenchymal connections between the ectodermal ring and the underlying mesoderm are the histologic basis for molecular epithelial-mesenchymal interactions, which are features characteristic of developmental fields. The ectodermal ring is thought to play an important role in directing the growth and development

of the entire embryo of all vertebrates, both nonmammalian and mammalian [8]. Developmental fields arise within the ectodermal ring and the underlying specialized mesoderm for the nose, eyes, ears, pharyngeal apparatus, upper limbs, mammary glands, lower limbs, inguinal region, external genitalia, and anus (see Fig. IV-1).

The mesonephric duct is in contact with the ectodermal ring at various points from the midcervical to the midlumbar regions. Its attachment to the ectodermal ring at the level of C4 through C8, the site of the upper limb bud, is so close that some believe the duct arises in whole or in part from the epithelium of that part of the ectodermal ring rather than entirely from the nephrogenic cord [9]. The most caudal attachment is the one described above, between the first curve of the mesonephric duct (the future tail of the epididymis) and the ectodermal ring in the midlumbar region at the site of the future inguinal ring. It is possible that the epithelial mesenchymal interactions between the ectodermal ring and the first curve of the mesonephric duct at this site induce the formation of a developmental field within which the gubernaculum, inguinal canal, and gonadal ligament develop.

Inguinal Region and Caudal Gonadal Ligaments

The inguinal region is defined as the junction between the lower limb and the abdomen. The apical ectodermal ridge of the lower limb bud arises within the ectodermal ring in the midlumbar area early in the fifth week. The caudal end of the lower limb bud is adjacent to the cloacal membrane. The appearance of the lower limb bud establishes the embryonic inguinal region.

The internal structures of the inguinal area are the inguinal canal and the bipotential caudal gonadal ligaments. These structures develop rapidly beginning in the middle of the fifth week when the mesoderm of the body wall grows between the ectodermal ring and the mesonephric duct, breaking the epithelial mesenchymal attachments between the ectodermal ring and the mesonephric duct, beginning rostrally and progressing caudally. The last attachment to be broken is the one between the first curve of the mesonephric duct and the ectodermal ring at the level of L2 to L3. At the site of this broken attachment, a placode of primitive mesenchyme forms a pyramidal nodule within the mesoderm of the anterior abdominal wall [10]. The tip of the nodule protrudes into the peritoneal cavity. This mesenchymal nodule is the inguinal crest and it is located at the site of the inguinal canal. The mesenchyme around the first curve of the mesonephric duct attaches to the tip of the inguinal crest (see Fig. IV-3). The caudal end of the mesonephros, as described above, is attached to the first curve of the mesonephric duct by the common mesenchyme investing the

mesonephros and mesonephric duct. The mesenchymal attachment of the caudal end of the mesonephros to the first curve of the mesonephric duct is the bipotential gonadal ligament. The inguinal crest becomes the gubernaculum. The abdominal wall develops around the gubernaculum forming the inguinal canal. The first curve of the mesonephric duct is therefore attached to the gubernaculum in the inguinal canal and to the caudal end of the mesonephros by the gonadal ligament. The gonad will replace the mesonephros in the near future (see Fig. IV-4) and, during this process, the attachment of the gonadal ligament to the caudal end of the mesonephros gradually shifts to the caudal end of the gonad.

In the male the first curve of the mesonephric duct becomes the tail of the epididymis, the gonadal ligament becomes the testicular ligament, and the gubernaculum remains as the gubernaculum. In the female the paramesonephric duct develops beside the mesonephric duct. The first curve of the paramesonephric duct develops within the gonadal ligament. As the mesonephric duct degenerates, the gonadal ligament remains attached to the paramesonephric duct and becomes the ovarian ligament. The gubernaculum becomes the round ligament and the inguinal canal becomes the canal of Nuck.

Thus, by the middle of the fifth week the basic blue print of the primitive urinary tract is laid down

[11,12]. The mesonephric bodies are the largest visceral organs of the embryo. They extend from the midcervical to the midlumbar region as large raised, parallel, parasagittal ridges protruding from the posterior abdominal wall near the midline (see Fig. IV-5). They follow the line of the caudal curl of the embryo. The precursors of the caudal gonadal ligaments fix the caudal ends of the mesonephric bodies and the mesonephric ducts to the future inguinal ring and inguinal canal,

a relationship that will never vary. The lower limb bud is present. The mesonephric bodies will begin to produce urine during the sixth week but will then degenerate in a rostral to caudal wave. The bodies will be replaced by the gonads and will disappear by the end of the eighth week [13]. At the middle of the fifth week, this primitive urinary system is ready for the beginning of the development of the bipotential genital tract and the definitive urinary tract.

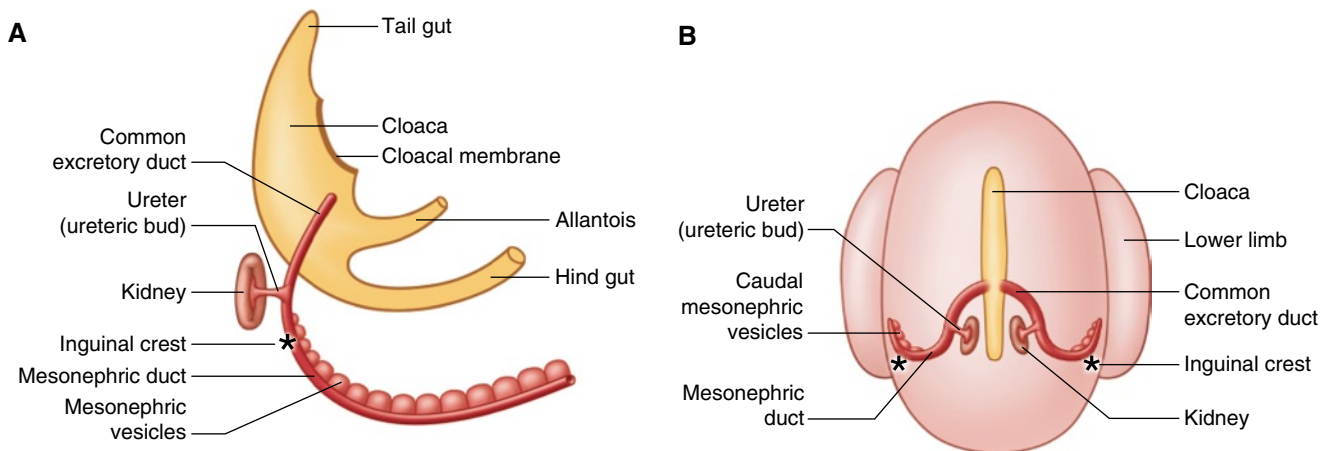


FIGURE IV-3. View of the caudal primitive genitourinary tract in the middle of the fifth week approximately 2 days later than Figure IV-2. **A**, Left lateral view. **B**, Dorsal view of the caudal curl. The ureteric bud and primitive kidney have appeared. The first curve of the mesonephric duct has separated from the ectodermal ring. The inguinal crest (asterisks) has appeared in the

future site of the inguinal ring and canal to which the first curve of the mesonephric duct is now attached. The segment of the mesonephric duct between the inguinal crest and ureteric bud will become the vas deferens. The segment between the ureteric bud and the entrance to the cloaca is the common excretory duct.

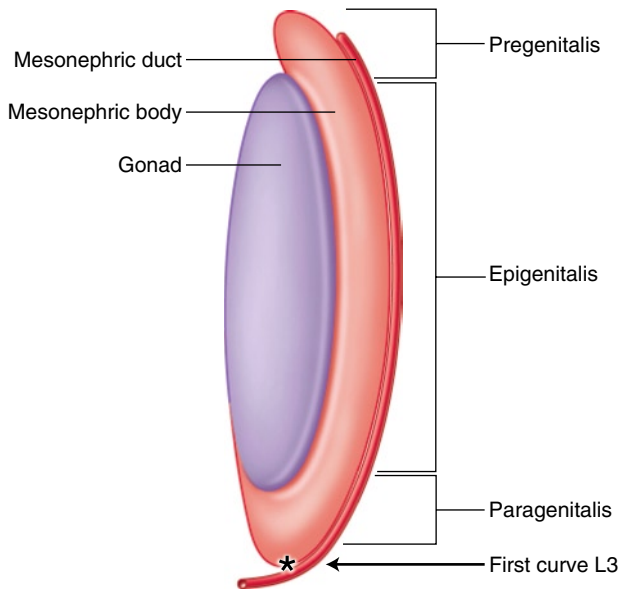


FIGURE IV-4. Left lateral view of the mesonephros and gonad at approximately the middle of the sixth postfertilization week. The individual mesonephric nephrons are hidden by the investing mesenchyme of the mesonephros and mesonephric duct. The enlarging gonad gradually replaces the regressing mesonephros. The mesonephros extends from approximately T1 to L3. The gonad extends from approximately T3 to T12. The caudal ends of the mesonephros and gonad are not separated, and the caudal end of the gonad is indirectly attached to the first curve of the mesonephric duct through its continuity with the caudal end of the mesonephros. The mesonephros is divided into three parts: the part cranial to the gonad, the pregenitalis; the part adjacent to the gonad, the epigenitalis; and the part caudal to the gonad, the paragenitalis. The embryonic remnants of the mesonephros and mesonephric duct are named according to this nomenclature. The asterisk is at the site of the developing gubernaculum, inguinal ring, and inguinal canal.

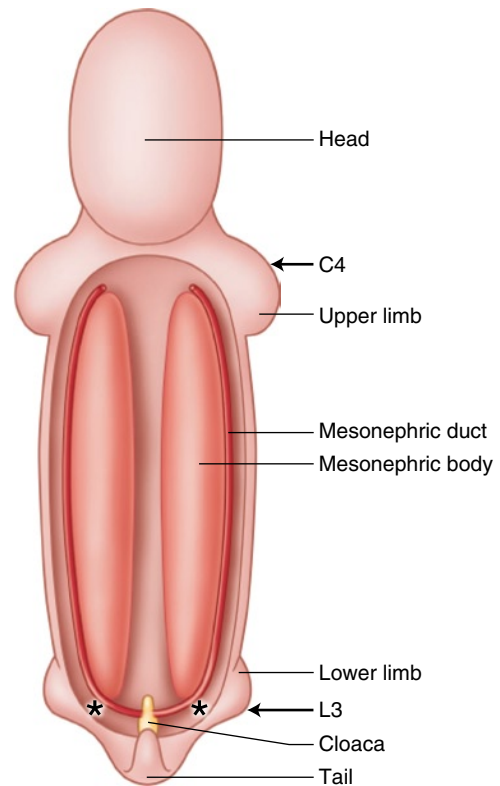


FIGURE IV-5. Mesonephric bodies in the early to mid fifth week. The investing mesenchyme of the mesonephros and mesonephric duct is included in this figure, and hide the underlying mesonephric nephrons. The mesonephric bodies are the largest organs in the embryo. They extend from the midcervical to the midlumbar area. The first curve of the mesonephric duct, the future tail of the epididymis, and indirectly the caudal end of the mesonephric bodies are attached to the inguinal crest, indicated by the *asterisk*, at the future site of the gubernaculum, internal inguinal ring, and inguinal canal.

Bipotential Genital Tract

The bipotential genital tract is superimposed upon the primitive urogenital tract. It begins with development of the bipotential gonad on the ventromedial surface of the mesonephros during the fifth week and ends with completion of the paramesonephric duct at the end of the eighth week. The differentiation of the bipotential gonads into testes and ovaries begins before the development of the paramesonephric ducts is completed.

Bipotential Gonads

The development of the gonads begins with the primordial germ cells. The primordial germ cells may be first identifiable in the inner cell mass of the blastocyst in the first postfertilization week [1,14]. There is good evidence that they are in the amniotic ectoderm at the junction of the amnion with the epiblast at the caudal end of the bilaminar disc early in the second week [15]. During the dissolution of the primary yolk sac and the formation of the definitive yolk sac, they migrate by amoeboid action through the extraembryonic mesenchyme of the body stalk and reach the endoderm of the caudal yolk sac near its junction with the allantois in the third week. During the fourth week they continue to migrate through the wall and mesentery of the proximal hindgut and toward the adjacent ventromedial side of the mesonephric bodies [16].

In the middle of the fifth week, shortly after the appearance of the ureteric bud and crista inguinalis, the primordial germ cells enter the ventromedial border of the mesonephric bodies. At the same time, the mesonephric mesoderm proliferates, differentiates into gonadal mesoderm, and induces the coelomic epithelium to proliferate and form a thickened layer. The thick coelomic epithelium and the enlarging underlying nest of

differentiating mesoderm form the early gonadal ridge on the ventromedial surface of the mesonephric body [17].

The subsequent events are somewhat controversial. One view proposes that primordial germ cells and coelomic epithelium migrate into the differentiating mesoderm, and that these three components form the gonadal blastema [15]. The coelomic epithelium serves as a scaffolding around which the other components of the gonadal blastema are organized. The mesodermal tissue forms a network of poorly defined, irregular gonadal cords in the deep portion of the gonad near its border with the mesonephric body. The coelomic epithelium, primordial germ cells, and local mesenchyme lie between the cords.

A recent study utilizing serial semithin sections of Epon-embedded gonads from human embryos and fetuses proposes that gonadal cords arise from mesonephric glomerular and tubular epithelium. These cords grow through the mesorchium into the hilum of the gonad and, hence, into the cortex. These primitive mesonephric cords never intermingle with coelomic epithelium and give rise to the rete and definitive sex cords [18].

The gonadal blastema, whatever its origin, rapidly enlarges and forms a long oval gonad with a broad attachment to the ventromedial surface of the mesonephric body [11]. It does not reach either the upper or lower pole of the mesonephric body (see Fig. IV-4). At the junction between the gonad and the mesonephric body, the gonadal blastema pushes deeply into the mesonephros.

By the middle of the sixth week, the bipotential period of gonadal development ends. The mesonephros extends from the midcervical to the midlumbar regions while the gonad extends from approximately T1 to T10 (see Fig. IV-4). A groove forms along the length of the junction between the gonad and mesonephros, and the two begin to separate. This separation continues during the following period of testicular and ovarian differentiation.

Bipotential Mesonephric and Paramesonephric Ducts

The development of the bipotential mesonephric (Wolffian) ducts is completed early in the fifth week when they reach the cloaca. Subsequent remodeling occurs [2]. In the seventh week, the pelvis begins to form medial to the developing inguinal ring and gubernaculum. As the developing urogenital sinus sinks into the deepening pelvis, the mesonephric duct curves caudally over the lip of the pelvic inlet and into the pelvis. This is the second mesonephric curve [6]. The two curves divide the mesonephric duct into three segments. First, there is a rostral vertical segment attached to the dorsolateral border of the mesonephros extending to the first curve at the caudal end of the mesonephros. This will become the epididymis. The first curve will become the tail of the epididymis. The second is a horizontal segment extending from the first to the second curve and the third is a vertical segment from the second curve to the entrance of the duct into the urogenital sinus, which will become the vas deferens.

The bipotential paramesonephric (Müllerian) ducts begin in the mid to late sixth postfertilization week as invaginations of thickened areas of the coelomic epithelium at the rostral ends of the mesonephric bodies and are probably under the inductive influence of the mesonephric duct [6]. They grow caudally along the lateral margins of the mesonephric ducts with which

they are in contact. The paramesonephric ducts may arise in part from the mesonephric ducts. By the end of the seventh week, the paramesonephric ducts reach the caudal ends of the mesonephric bodies and as they follow the first curve of the mesonephric ducts medially under the caudal end of the mesonephric bodies they cross over the ventral surfaces of the mesonephric ducts and come to lie medial to the mesonephric ducts [12]. In the female the paramesonephric duct replaces the mesonephric duct and assumes its caudal attachments.

At the start of the eighth week, the paramesonephric ducts meet in the midline and follow the second curve of the mesonephric ducts caudally into the developing pelvis. Because of the crossing over, the paramesonephric ducts are medial to the mesonephric ducts. They fuse to form a single solid duct. By the end of the eighth week, the solid blind end of the fused paramesonephric ducts meets the mesenchyme of the posterior wall of urethral part of the vesicle urethral canal at the site of the sinusal (Müllerian) tubercle between the openings of the mesonephric ducts (see Fig. IV-6). This ends the period of the bipotential genital ducts. Sexual differentiation of the ducts will begin shortly with the regression of the paramesonephric duct in the male and the mesonephric duct in female.

Fate of the Paramesonephric Duct in the Male

In the 10th week, the Sertoli cells secrete Müllerian-inhibiting substance, which diffuses along the mesonephric duct and causes the regression of the ipsilateral paramesonephric duct beginning at the site at which the paramesonephric duct crosses in front of the mesonephric duct. The regression proceeds cranially and caudally from this point. The action of Müllerian

inhibitory substance is local, not systemic, and does not effect the opposite paramesonephric duct. The regression of the duct cranial to the cross-over point is complete except that a remnant may remain attached to the upper pole of the testis as the appendix testis. The caudal portion often persists as the prostatic utricle at the veru montanum.

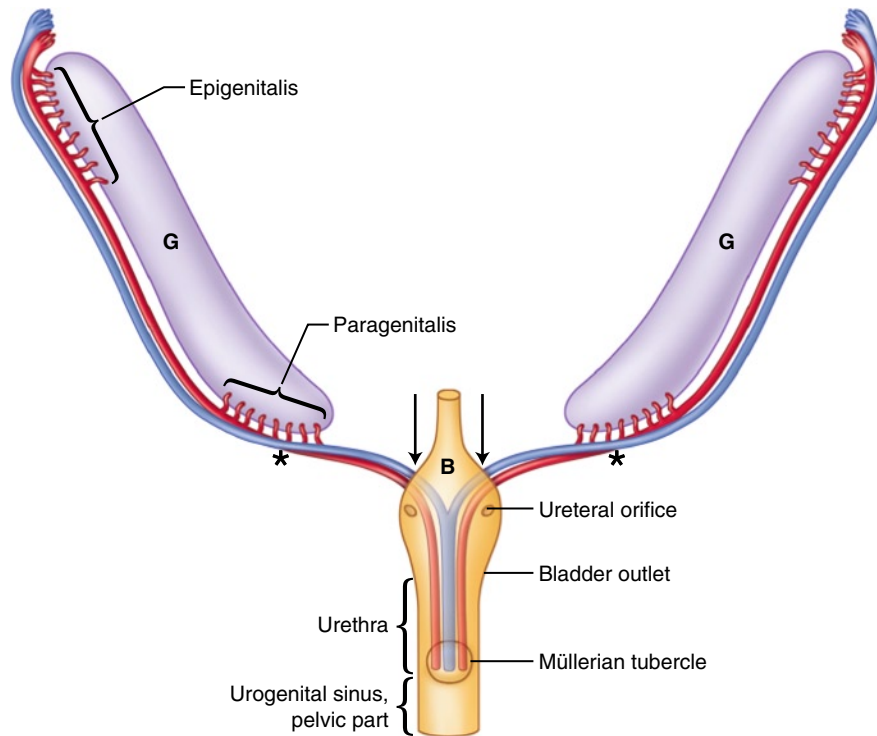


FIGURE IV-6. Bipotential genitourinary tract in the eighth week. The gonads (G) have replaced the mesonephric bodies. The mesonephric (red) and paramesonephric ducts (blue) are parallel, curve medially under the gonad (the first curve is at the *asterisks*), curve caudally (the second curve is at the *arrows*) over the pelvic inlet into the pelvis and fuse to the dorsal wall of the urogenital sinus at the Müllerian tubercle. The paramesonephric ducts cross in front of the mesonephric ducts at the first curve and fuse in the pelvic midline medial to the mesonephric ducts. The caudal gonadal ligaments and inguinal canal develop at the *asterisks*. The point of fusion of the mesonephric and paramesonephric ducts with the urogenital sinus at the Müllerian tubercle marks the division of the urogenital sinus into the vesicle urethral canal rostrally and the definitive urogenital sinus caudally. The vesicle urethral canal becomes the bladder and urethra. In the male the urethra

from the bladder outlet to the rostral edge of the Müllerian tubercle becomes the proximal prostatic urethra and the Müllerian tubercle becomes the veru montanum. In the female the urethra from the bladder outlet to the rostral edge of the Müllerian tubercle greatly elongates and forms the entire length of the urethra except for its distal end and in the process the Müllerian tubercle migrates to the distal end of the urethra and becomes the hymen. The mesonephric nephrons have all degenerated except for the remnants labeled *epigenitalis* and *paragenitalis* in this figure. In the male, the epigenitalis becomes the efferent ductules and the paragenitalis persist as embryonic remnants in the distal spermatic cord. In the female, the epigenitalis remnants become the epoophoron along the hilum of the ovary and the paragenitalis remnants become the paroophoron between the medial end of the ovary and the uterus. B—bladder.

References

1. O'Rahilly R, Muller F: *Human Embryology & Teratology*, edn 3. New York: Wiley-Liss; 2001.
2. Felix W: The development of the urinogenital organs. In *Human Embryology*. Edited by Keibel F, Mall FP. Philadelphia: JB Lippincott; 1912:752–979.
3. Torrey TW: The early development of the human nephros. *Contrib Embryol* 1954, 25:199–240.
4. Shikunami J: Detailed form of the Wolffian body in human embryos of the first eight weeks. *Contrib Embryol* 1926, 28:49–61.
5. O'Rahilly R, Muller F: *Developmental Stages in Human Embryos*. Washington, DC: Carnegie Institution of Washington; 1987.
6. O'Rahilly R, Muecke EC: The timing and sequence of events in the development of the human urinary system during the embryonic period proper. *Z Anat Entwickl Gesch* 1972, 138: 99–109.
7. O'Rahilly R, Muller F: The origin of the ectodermal ring in staged human embryos of the first 5 weeks. *Acta Anat* 1985, 122:145–157.
8. Hughes ESR: The development of the mammary gland. *Ann R Coll Surg* 1950, 122:3–23.
9. Jirásek JE: *Development of the Genital System and Male Pseudohermaphroditism*. Baltimore: The Johns Hopkins Press; 1971.
10. Barteczko KJ, Jacob MI: The testicular descent in human. *Adv Anat Embryol Cell Biol* 1999, 156:1–98.
11. Steding G: *The Anatomy of the Human Embryo*. Basel, Switzerland: Karger; 2009.
12. Jirásek JE: *An Atlas of Human Prenatal Morphogenesis*. Boston: Martinus Nijhoff; 1983.
13. Hamilton WJ, Mossman HW: *Human Embryology*, edn 4. Baltimore: William & Wilkins; 1972.
14. Hertig AT: *Human Trophoblast*. Springfield, IL: Charles C. Thomas; 1968.
15. Jirásek JE: *An Atlas of Human Prenatal Developmental Mechanics*. London And New York: Taylor & Francis; 2004.
16. Witschi E: Migration of the germ cells from the yolk sac to the primitive gonadal fields. *Contrib Embryol* 1948, 32:67–80.
17. van Wagenen G, Simpson ME: *Embryology of the Ovary and Testis*. New Haven, CT: Yale University Press; 1965.
18. Satoh M: Histogenesis and organogenesis of the gonad in human embryos. *J Anat* 1991, 177: 85–107.

7

Kidney

Eduardo D. Ruchelli and Dale S. Huff

The histological appearance of the fetal kidney is significantly different than that of the adult kidney, mostly because it is an organ that continues to develop almost until the end of gestation, when the formation of nephrons (nephrogenesis) comes to an end. Furthermore, the neonatal kidney is still immature and significant changes occur as the kidney continues to grow and mature during infancy and childhood. A lack of familiarity with these differences may lead to mistakenly considering normal findings as pathologic ones, or to overlooking abnormalities of renal development, such as impaired nephrogenesis with reduced number of nephrons (as seen in intrauterine growth restriction) or abnormal tubular differentiation (as seen in renal tubular dysgenesis). The aim of this chapter is to review the dramatic changes in renal development in the fetal and neonatal period and highlight the important differences at various gestational ages.

Embryology

Early in the fifth postfertilization week, the sacral intermediate mesoderm differentiates into the sacral nephrogenic cord, which separates completely from the mesonephros and differentiates into the metanephric blastema. The ureteric bud arises from the dorso-medial aspect of that segment of the mesonephric duct between its attachment to the inguinal crest and its attachment to the cloaca [1]. The blind end of the bud grows dorsally toward the ventral surface of the metanephric blastema and by the end of the fifth week it becomes dilated and pushes into the ventral surface of the metanephric blastema. The metanephric blastema surrounds the dilated blind end of the ureteric duct forming the metanephric cap. The straight duct-like segment of the ureteric bud becomes the ureter and its dilated blind end becomes the rudimentary pelvis. The metanephric cap becomes the renal parenchyma. The segment of the mesonephric duct between the origin of the ureter and the cloaca is now referred to as the *common excretory duct*. Thus, at the end of the fifth week the primitive kidney has formed.

At the beginning of the sixth week, the blind end of the ureteric bud, which is buried within the ventrally facing hilum of the metanephric cap, dilates to form the cone-shaped ampulla [1,2]. The ampulla is the actively proliferating and elongating end of the ureteric bud. The ampulla continues to grow into the metanephric cap by dichotomous branching morphogenesis. The first branching produces an upper pole branch and a lower pole branch of the primitive pelvis. This causes an elongation of the primitive kidney in the rostral-caudal direction and the kidney becomes reniform [1]. The lower pole is closer to the midline than the upper pole. This explains why a horseshoe kidney is formed by the fusion of the lower poles. During the second branching, each polar branch of the pelvis divides into a secondary polar branch and an interpolar branch. This results in four primitive major calyces, each surrounded by its lobe of metanephric blastema. The interpolar branches are perpendicular to the polar branches. The polar branches subsequently branch more rapidly than the interpolar branches, causing the polar lobes to be complex

with two or more papillae emptying into one minor calyx and the interpolar lobes to remain simple with only one papilla emptying into a minor calyx. The next few branches form additional primitive major and minor calyces, the cribriform plates of the future papillae, and the first collecting ducts. The primitive pelvis and calyces are narrow tubes that will later be remodeled and become dilated. Therefore, by the end of the sixth week, primitive lobes are recognizable. Although some of the early ureteric bud branches that will be subsequently remodeled into minor calyces induce rudimentary nephrons, many of these early nephrons degenerate and disappear. The rest become detached from the ampulla that induced their formation and may persist as rudimentary glomeruloid structures in the renal sinus.

During the beginning of the seventh week postfertilization, the metanephric blastema surrounding the tips of the branching collecting ducts will be induced to form nephrons [1–3]. Each branch has a straight ductal stem and a dilated tip, the ampulla. The blastema around the ampulla will differentiate into nephrons while that around the stems will differentiate into specialized renal interstitium. Each ampulla of the first generation of collecting ducts induces its surrounding metanephric blastema to form a nephrogenic vesicle that becomes an “S”-shaped tubule within a few days. The fate map of the “S”-shaped tubule has been well established (see Fig. 7-1).

In the eighth week, the first generation consisting of 18 nephrons is completed [2]. By the end of the week, the characteristic histology of each part of the nephron is well developed (see Fig. 7-2). The proximal convoluted tubular epithelium has a well-developed brush border. The descending, thin, and ascending limbs of the loops of Henle are identifiable. The epithelial cells of the macula densa, the granular cells of the afferent and efferent arterioles, and the Goormaghtigh cells (also called “laci cells” or “extraglomerular mesangial cells”) of the juxtaglomerular apparatus are differentiated. Renin activity is identifiable in the afferent arterioles. The distal convoluted tubular epithelium is well differentiated. Principal and intercalated epithelial cells of the collecting ducts are identifiable. Metanephric urine production begins. The pelvis and major calyces are remodeled, begin to dilate, and assume their definitive form, but the minor calyces remain as narrow tubes. The nephrogenic zone, definitive cortex, and medulla begin to be recognizable. By the 12th week, the renal pelvis, major and minor calyces, and papillary tips have developed their definitive forms. By the 13th week, the nephrogenic zone, definitive cortex, and medullary pyramids have attained their final appearance (see Fig. 7-3).

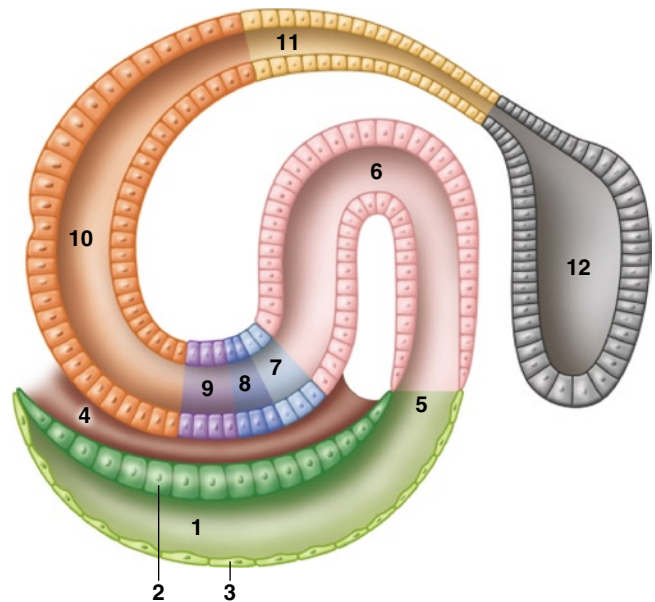


FIGURE 7-1. Diagrammatic fate map of the “S”-shaped nephron: seventh week. The lower limb (green, 1), will become the glomerulus. The dark green (2) cells will become the visceral epithelium of the glomerular tuft. The light green (3) cells will become the parietal epithelium of Bowman’s capsule. The middle limb (pink, 6) will become the proximal convoluted tubule and is attached to the margin of the future glomerulus (5). The junction between the middle and upper loops (blue and purple) will become the descending loop of Henle (light blue, 7), the ascending loop of Henle (dark blue, 8), and the macula densa (purple, 9), respectively. One view holds that these precursors of the loop of Henle and the macula densa are the proximal part of the upper limb. The upper limb will become the distal convoluted tubule (orange, 10) and the arched connecting duct (yellow, 11). The arched connecting duct joins the collecting duct (black, 12) at the previous site of the ampulla, which induced the differentiation of the nephron. The brown tissue (4) between the macula densa and the glomerulus is the anlage of the vascular mesenchyme of the future vascular pole of the glomerulus. It will push into the glomerular visceral epithelium and become the glomerular capillary loops, glomerular mesangium, extraglomerular mesangium (Goormaghtigh cells) of the juxtaglomerular apparatus, and the afferent and efferent arterioles. The segment that will become the macula densa is anchored to this position at the vascular pole and will never move.

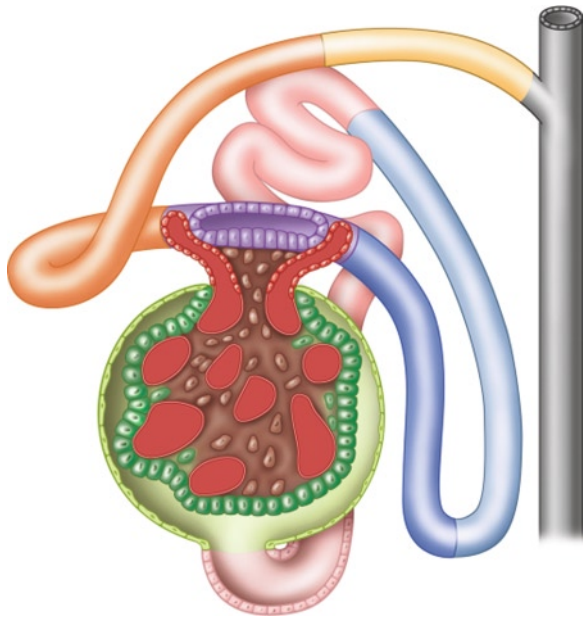


FIGURE 7-2. Nephron: eighth week. The color scheme is the same as in Figure 7-1. The junction of the proximal convoluted tubule (pink) and the glomerulus (green) has shifted from the edge of the glomerulus to a site opposite the vascular pole. The proximal convoluted tubule passes behind, to the right, and above the glomerulus. The descending loop of Henle (light blue) lies adjacent to its collecting tubule of origin (black). The macula densa (purple) remains in its original position at the vascular pole. The distal convoluted tubule (orange) passes to the left and in front of the glomerulus. The arching connecting duct (yellow) passes in front of the proximal convoluted tubule and joins its collecting duct of origin (black). The afferent and efferent arterioles have appeared, and the juxtaglomerular apparatus is well differentiated. The glomerular mesangium and the Goormaghtigh cells (both brown) arise from the same primitive tissue. Compare with Figure 7-17.

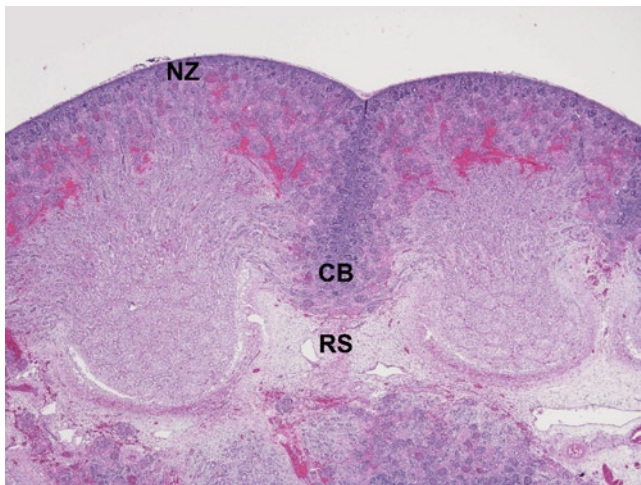


FIGURE 7-3. Renal lobe: kidney at 19 weeks gestation. This low-power view demonstrates two well-demarcated lobes. Although the cortex is thin at this age, it is already well defined, as is the underlying medullary pyramid. The nephrogenic zone (NZ) can be seen at the periphery of the cortex as a basophilic band of developing nephrons under the capsule and in the column of Bertin (CB) where the two adjacent lobes meet. The renal sinus (RS) consists of loose mesenchymal tissue and is devoid of fat at this age. (Hematoxylin and eosin [H&E], 2 \times .)

Histology

Anatomically, the human kidney is organized in lobes (see Fig. 7-3) [4]. Each lobe consists of a medullary pyramid and its surrounding cortex. These lobes account for the characteristic gross appearance of the external surface of the fetal kidney, which shows prominent fissures between adjacent lobes that divide the kidney into polygons. During the third trimester, partial lobar and calyceal fusion occurs and the number of fissures, papillae, and calyces decreases. The fissures usually disappear during the first few years of life secondary to renal growth. The peripheral portion of the lobe consists of the cortex, which surrounds the central portion, the medullary pyramid. While a portion of the cortex lies under the renal capsule, where two adjacent lobes meet laterally, the two layers of cortex from each lobe (septal cortex) become confluent and form the so-called *column of*

Bertin (see Fig. 7-3). The tips of the medulla drain into the papillae and calyceal system, and the columns of Bertin are in direct continuity with the mesenchymal tissues of the renal sinus, between the calyces.

Both cortex and medullary elements are primarily formed in the nephrogenic zone. The nephrogenic zone is easily recognized at low power in renal sections of all preterm fetuses as a band situated in the most outer portion of the cortex (see Fig. 7-4). During the midtrimester, abundant undifferentiated blastema cells can be seen in the background of the developing nephrons, which impart a deeply basophilic appearance to the nephrogenic zone (see Fig. 7-5). The number of blastema cells decreases after 30 weeks and, as nephrogenesis comes to an end between weeks 32 and 36, the nephrogenic zone is no longer present in

the normal term fetus. At term, mature tubules should be seen between the last generation of glomeruli and the capsule. By the end of gestation, the full complement of nephrons is attained and subsequent renal growth reflects enlargement and maturation of the existing nephrons.

During fetal life, subsequent generations of nephrons formed in the nephrogenic zone are added to the underlying developing cortex in ill-defined "layers." These "layers" are histologically represented by rows of glomeruli. As the result of this pattern of growth, the oldest (first-formed) glomeruli are those in the inner cortex, whereas the youngest (last-formed) glomeruli are those in the outer cortex, immediately under the nephrogenic zone (see Fig. 7-5). The timing of a developmental disturbance can sometimes be presumed based on whether abnormalities involve the entire cortex (early event) or only the outer cortex (late event). A few studies [5,6] have proposed a histologic method to evaluate nephrogenesis by counting the number of "layers" of glomeruli as representative of nephrons, from inner to outer cortex. These estimates need to be performed on well-oriented sections in which the medullary rays are seen extending longitudinally from a well-defined corticomedullary junction to the outer cortex (see Fig. 7-5). Unfortunately, such well-oriented areas are not necessarily common on routine autopsy sections and some interobserver variability may also exist in the process of identifying "layers." Nevertheless, based on these studies, an estimate of the average number of layers is shown in Figure 7-6.

The stages of individual nephron development as described in the embryology section can be observed histologically in the nephrogenic zone until 36 weeks gestation (see Figs. 7-7–7-11). Once formed, fetal glomeruli resemble adult glomeruli but are smaller and the podocytes have a typical cuboidal appearance. This cuboidal appearance is continuous around the glomerulus at birth but podocytes gradually flatten during the first year of life and remnants of the cuboidal layer are usually not seen in normal glomeruli after 12 months of age [7]. Glomeruli experience a decrease in size between 12 and 20 weeks gestation (see Fig. 7-5) [8], remain the same size until birth, and then increase in diameter postnatally. Regional differences in glomerular size also exist within the cortex of the fetus and newborn. Juxtamedullary glomeruli are larger than more

immature glomeruli under the nephrogenic zone or capsule (see Fig. 7-12). A small percentage of glomeruli (usually 1%–2%) undergo involutonal sclerosis in otherwise normal kidneys of fetuses and children (see Fig. 7-13) [9].

As the glomeruli differentiate on one end of the developing nephron, tubular differentiation can be recognized histologically relatively early (see Fig. 7-14). Proximal tubule differentiation is evident immediately beneath the S-shaped bodies. The characteristic deep eosinophilia of the cytoplasm of proximal tubular epithelial cells allows for easy identification of the tubules, except for those cases with severe autolysis. As the tubules differentiate, they also elongate and increase in diameter, separating the glomeruli from one another. This separation is more pronounced in the deeper cortex (see Fig. 7-15). Postnatally, tubular growth is also responsible for the separation of the outermost glomeruli from the capsule and the formation of a subcapsular zone largely devoid of glomeruli (see Fig. 7-16) [7].

Development of the juxtamedullary apparatus starts very early in gestation (see Fig. 7-17). The renin-angiotensin system plays a critical role in kidney development and the activity of the intrarenal renin-angiotensin system is high during fetal and neonatal life, declining during postnatal maturation [10]. The juxtamedullary apparatus is not easily identified on routine sections of fetal kidneys but renin expression can be demonstrated by immunohistochemistry (see Fig. 7-18).

In the medulla the loops of Henle are relatively short in the fetus and significant lengthening occurs after birth. The last formed nephrons (outer cortex) are the shortest whereas the earliest formed nephrons (juxtamedullary) are the longest. In the fetus, thin portions of loops of Henle are only present in the earliest formed nephrons and only in the descending limb (not in the ascending limb) [7]. Early in the midtrimester the medulla contains primarily immature collecting ducts surrounded by abundant loose stroma (see Fig. 7-19). As the number of nephrons increase and the cortex thickens, the medulla becomes denser and occupied by collecting ducts and elongating loops of Henle from the juxtamedullary nephrons (see Fig. 7-20). Like the mature kidney, the fetal medulla displays more abundant interstitium toward the papillae between the ducts of Bellini (distal segment of the collecting duct) (see Figs. 7-21 and 7-22).

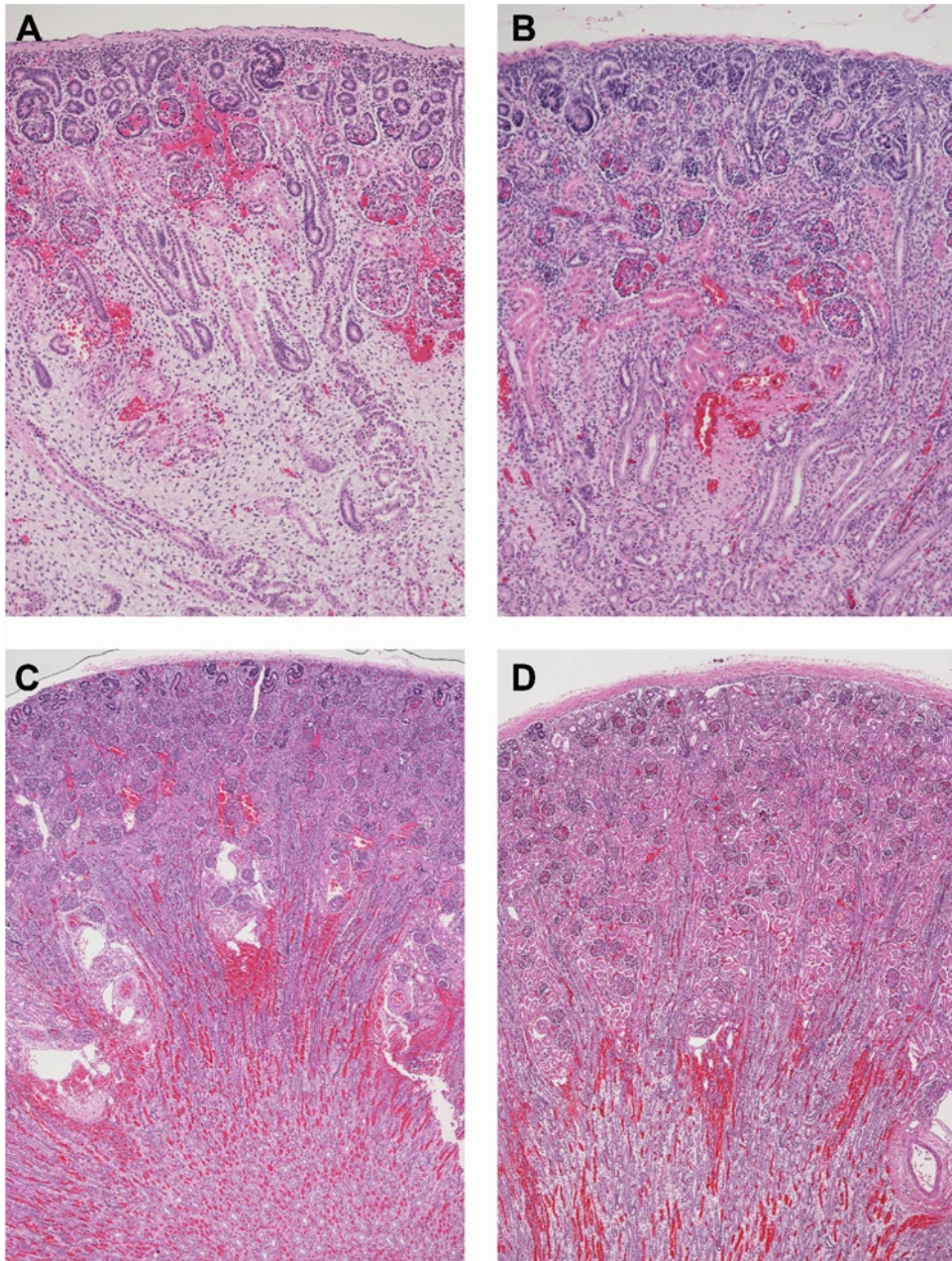


FIGURE 7-4. Renal cortex during gestation. **A**, 16; **B**, 21; **C**, 27; and **D**, 35 weeks gestation. The cortex becomes thicker as the number of nephrons formed in the nephrogenic zone increases until shortly before term. Notice that the nephrogenic zone is

present at all ages except for the kidney at 35 weeks, which shows only a few foci of discontinuous nephrogenesis (see Fig. 7-5 for details). (H&E: **A** and **B**, 10 \times ; **C** and **D**, 4 \times .)

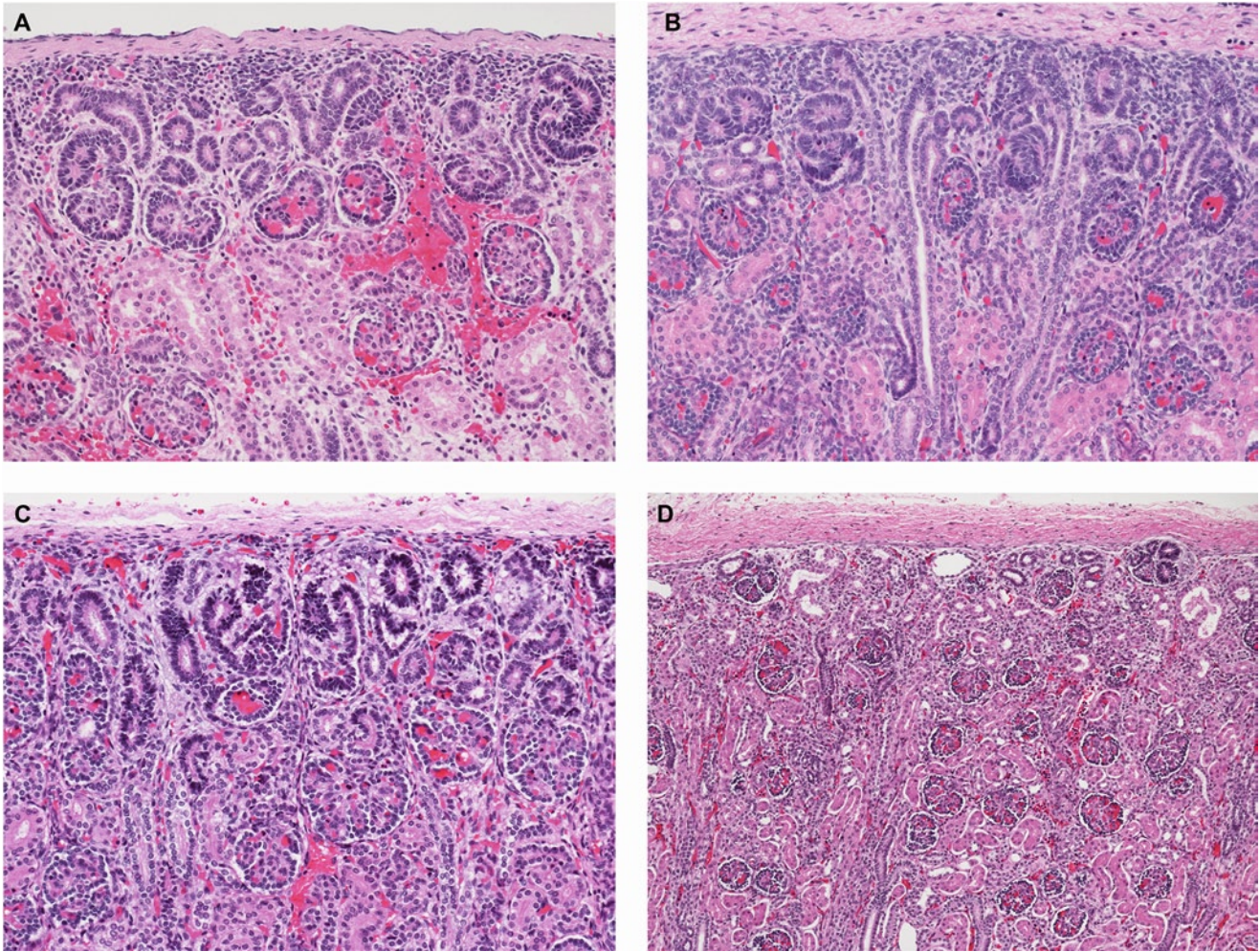


FIGURE 7-5. Nephrogenic zone during gestation. **A**, 16; **B**, 21; **C**, 27; and **D**, 35 weeks gestation. The nephrogenic zone is continuous and readily observed under the capsule at 16, 21, and 27 weeks gestation. At 35 weeks gestation it is almost completely absent and only rare foci of immature nephrons are present. Also notice the high density of undifferentiated blastema cells in the background of the nephrogenic zone at gestational ages 16

and 21 weeks. At gestational age 27 weeks the number of undifferentiated cells has diminished in the background but developing nephrons are still present. The number of glomeruli has substantially increased from 16 to 35 weeks. Proximal convoluted tubules with distinct cytoplasmic eosinophilia are seen at all gestational ages. (H&E: **A, B** and **C**, 20 \times ; **D**, 10 \times .)

Development of Glomeruli During Gestation

Gestational age, wk	Rows of glomeruli
23 or less	3
24	5–7
28	8–9
32	9–10
36	10–14

Data from Clapp and Croker [7] and from Dorovini-Zis and Dolman [5]

FIGURE 7-6. Development of glomeruli during gestation.

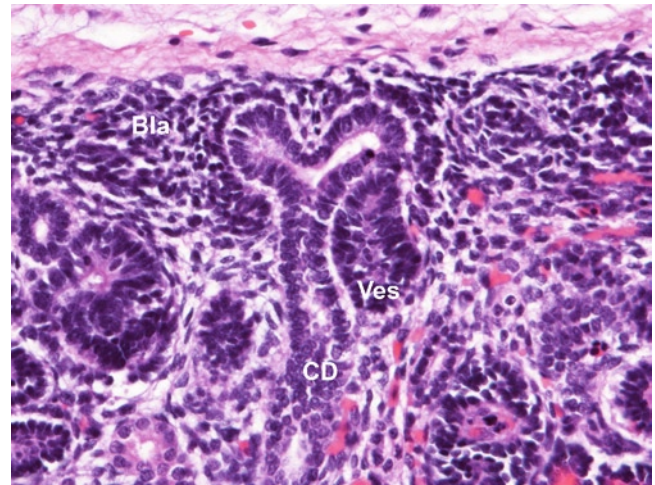


FIGURE 7-7. Nephrogenesis. The branches of the ureteric bud form the collecting ducts (CD), seen here as a T-shaped structure. These ureteric bud branches induce the metanephric blastema (Bla) to condense around their tips (ampulla) and then to differentiate into a vesicle (Ves), which develops a lumen and fuses to the end of the T-shaped structure (one on each side). This vesicle will form the entire nephron. (H&E, 40 \times .)

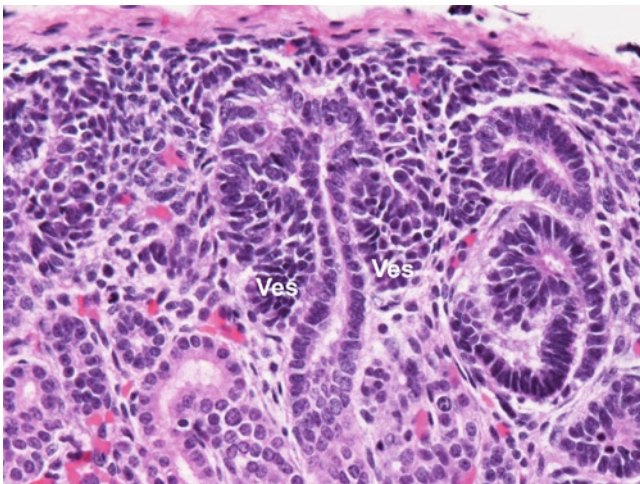


FIGURE 7-8. Nephrogenesis. Vesicles (Ves) have fused to the T-shaped ends of the ureteric bud branches and start to elongate to form the S-shaped body. (H&E, 40 \times .)

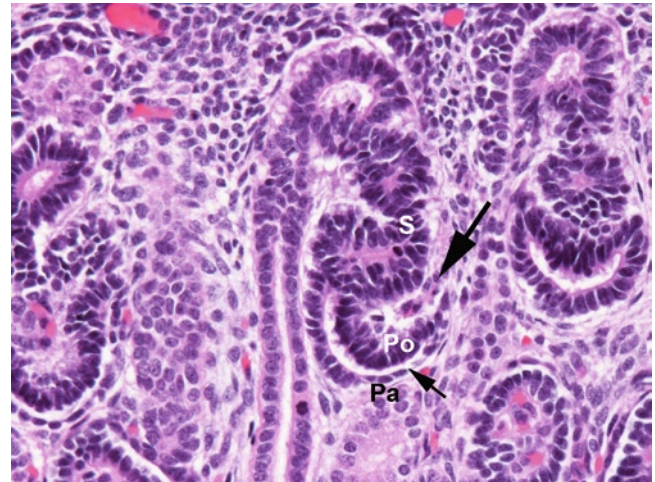


FIGURE 7-9. Nephrogenesis. The S-shaped body (S) has formed and a vascular cleft (*large arrow*) develops at the site where the glomerular capillaries will emerge. Below the cleft, the lower limb of the S-shaped body, most distant from the ureteric bud, differentiates into the parietal (Pa) and visceral (podocytes; Po) epithelium of the glomerulus. The future Bowman's space (*small arrow*) can be seen between the two. The middle limb generates the proximal convoluted tubule and the upper limb forms the loop of Henle, macula densa, and distal convoluted tubule. (H&E, 40 \times .)

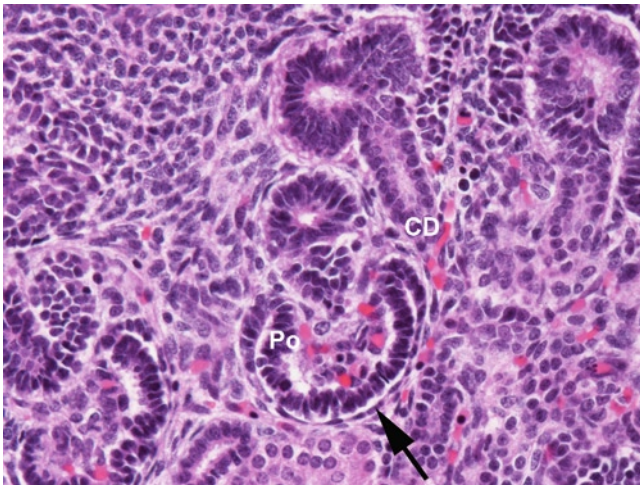


FIGURE 7-10. Nephrogenesis. The developing glomerulus is now better defined as the capillary loops covered by the podocytes (Po) start to fill out into an expanding Bowman's space (arrow). Above the glomerulus, cross-sections of the developing tubules can be seen connected to the collecting duct (CD). (H&E, 40 \times .)

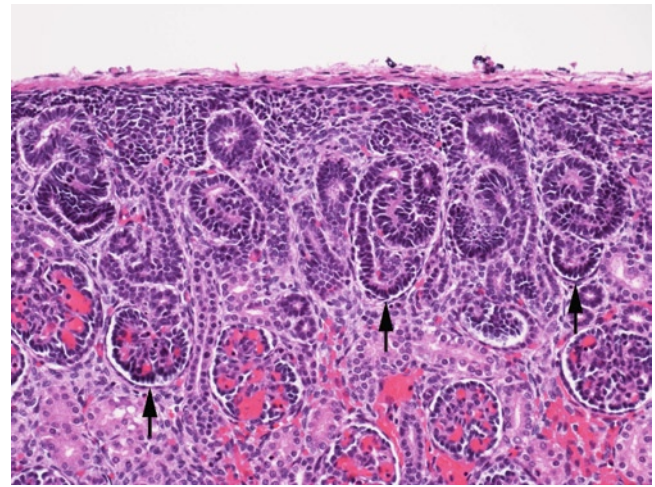


FIGURE 7-11. Nephrogenesis. Nephrons in various stages of development can be seen within the nephrogenic zone. Developing glomeruli are indicated by arrows. (H&W, 20 \times .)

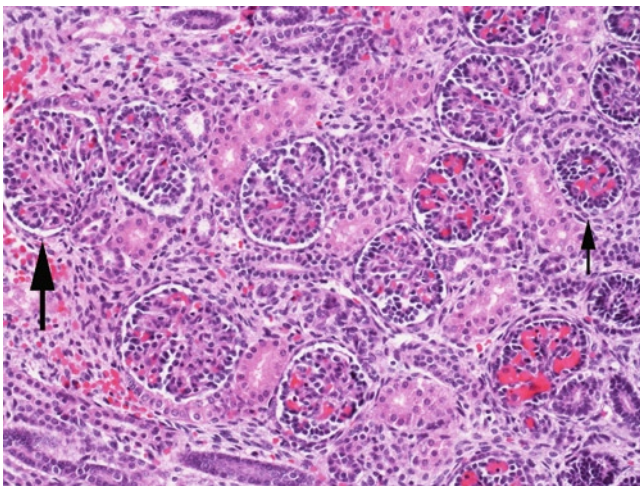


FIGURE 7-12. Glomeruli: kidney at 19 weeks gestation. The most recently formed glomeruli increase in size as they become incorporated into the developing cortex under the nephrogenic zone (right, small arrow). Thus, the older juxtamedullary glomeruli (left, large arrow) are larger than more superficial ones in fetuses and infants. All glomeruli retain the cuboidal appearance of podocytes through the end of gestation. (H&E, 20 \times .)

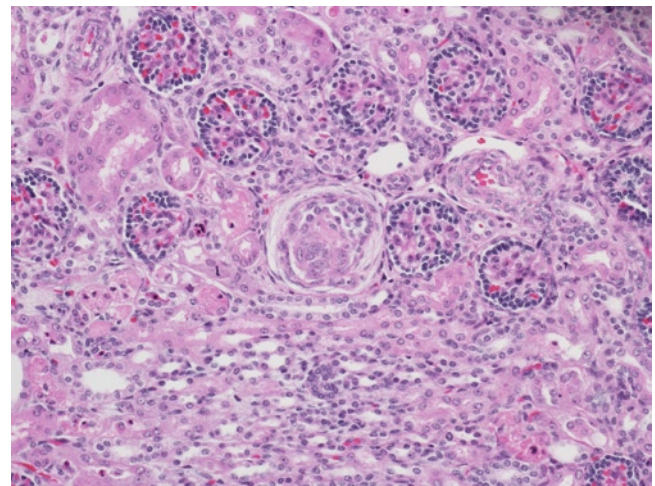


FIGURE 7-13. Sclerotic glomeruli: kidney at 37 weeks gestation. Scattered sclerotic glomeruli are commonly observed in fetuses and neonates. When present in small numbers (usually 1%–2%, occasionally up to 10%), they should not be considered pathologic changes in the absence of other abnormalities. (H&E, 20 \times .)

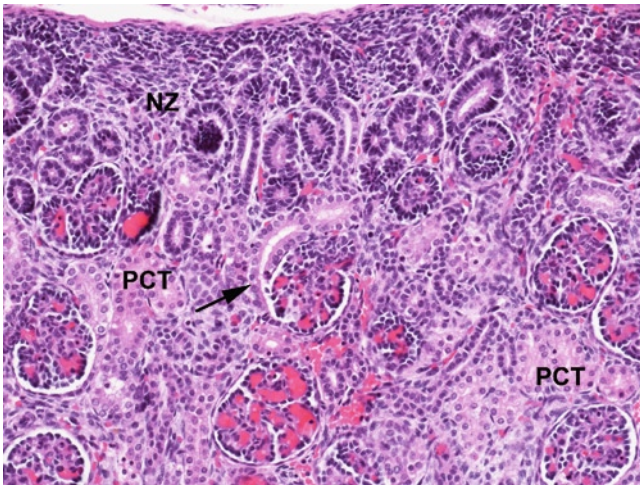


FIGURE 7-14. Proximal convoluted tubules: kidney at 19 weeks gestation. Proximal convoluted tubules (PCT) differentiate very early in nephrogenesis and can readily be identified under the nephrogenic zone (NZ) due to their distinct cytoplasmic eosinophilia. A proximal convoluted tubule can be seen draining the Bowman's space of a young glomerulus (arrow). (H&E, 20 \times .)

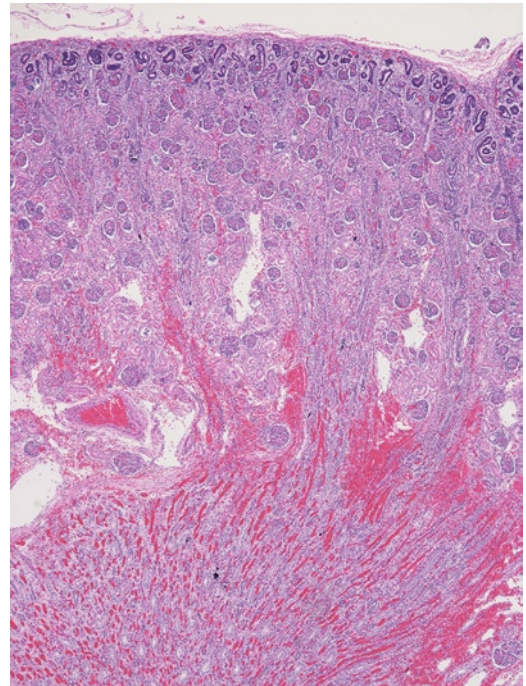


FIGURE 7-15. Tubular growth and maturation: kidney at 35 weeks gestation. The young glomeruli are more crowded in the outer cortex whereas the older glomeruli are more widely separated near the medulla as the result of tubular elongation and increase in diameter. (H&E, 4 \times .)

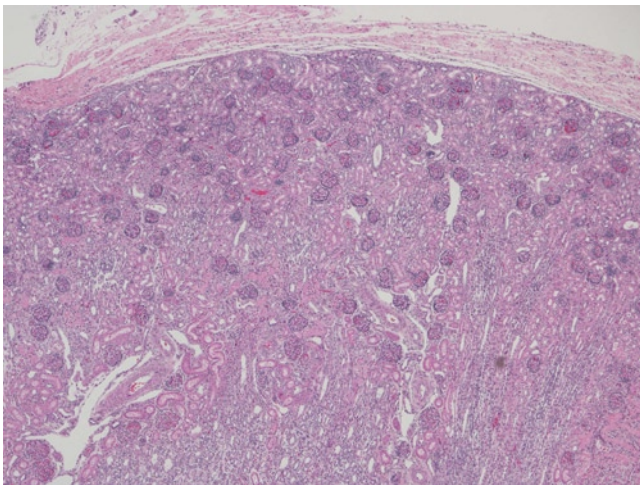


FIGURE 7-16. Cortex at term. The nephrogenic zone is no longer present and the full complement of nephrons is attained at this age. Glomeruli in the neonate are typically very close to the capsule before further tubular growth separates them and creates a subcapsular zone devoid of glomeruli ("cortex corticis") during infancy. (H&E, 4 \times .)

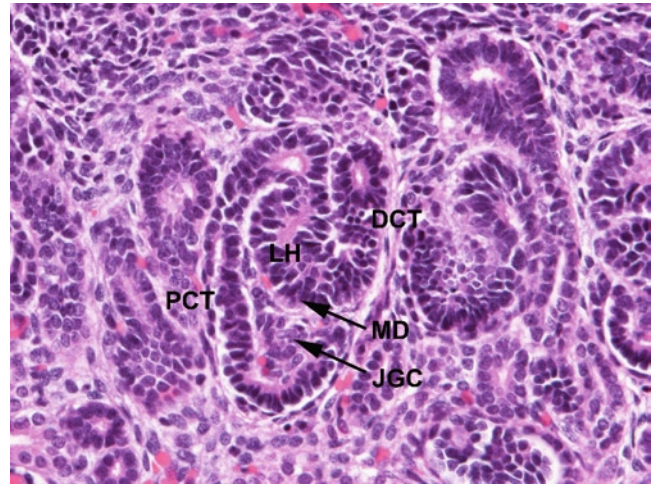


FIGURE 7-17. Juxtaglomerular apparatus. The different segments of the S-shaped body are committed to become specific portions of the nephron very early in the differentiation process. At the same time, the cells that form the juxtaglomerular apparatus can be identified next to the glomerulus. DCT—distal convoluted tubule; JGC—juxtaglomerular cells; LH—loop of Henle; MD—macula densa; PCT—proximal convoluted tubule. (H&E, 40 \times .)

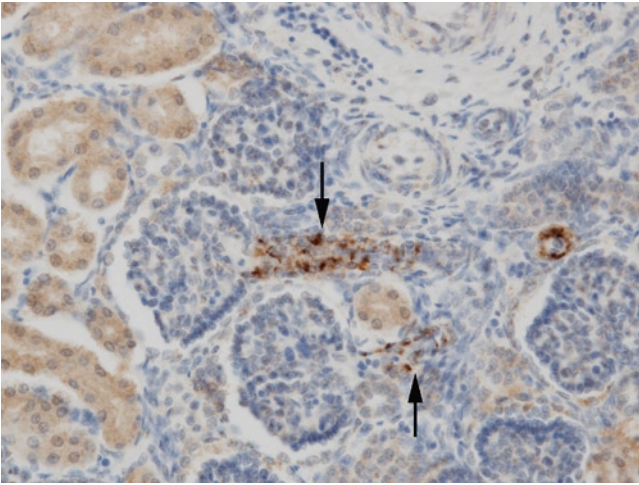


FIGURE 7-18. Renin-expressing cells (granular cells): kidney at 27 weeks gestation. Renin expression is high in the fetus and can be demonstrated by immunohistochemistry, primarily in the terminal afferent arteriole (arrows). The juxtaglomerular apparatus is otherwise not readily evident on routine stains of fetal kidneys. (Renin immunohistochemistry, 20 \times .)

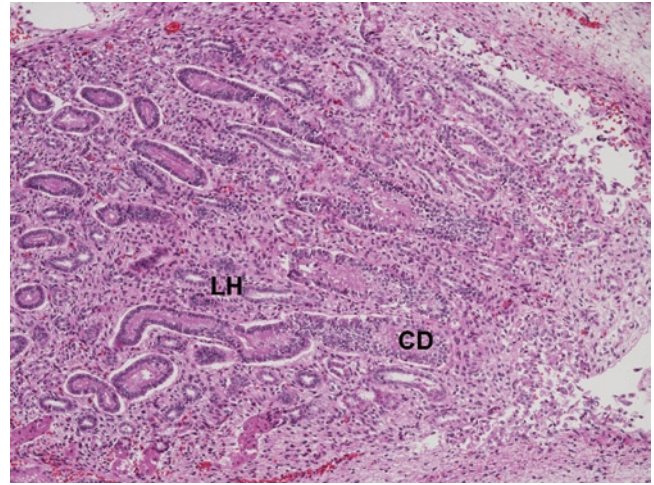


FIGURE 7-19. Medulla: kidney at 17 weeks gestation. Loose stroma separates immature collecting ducts (CD) and loops of Henle (LH). Thin segments of the loop of Henle are not evident at this age. (H&E, 10 \times .)

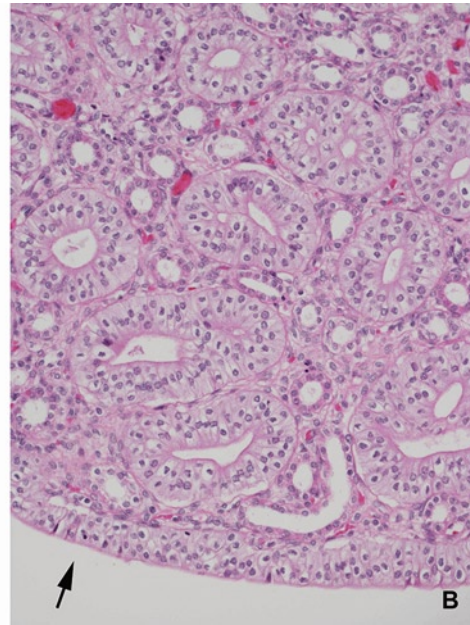
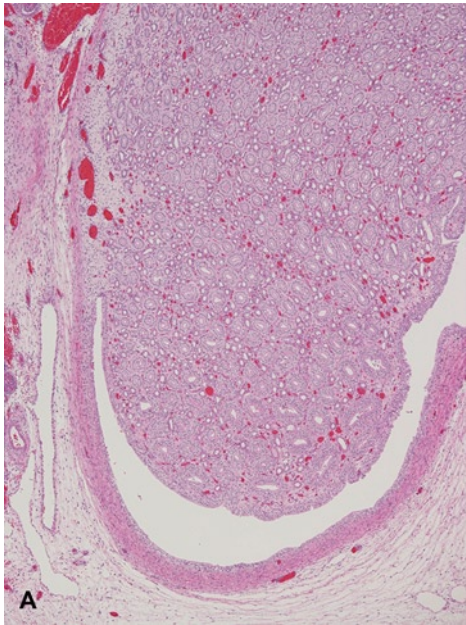


FIGURE 7-20. Medulla: kidney at 21 weeks gestation. **A**, As the tubules elongate and increase in diameter, the medulla becomes denser. **B**, Closeup view of the papilla (arrow) show-

ing maturing collecting ducts (ducts of Bellini) and loops of Henle. (H&E: **A**, 2 \times and **B**, 20 \times .)

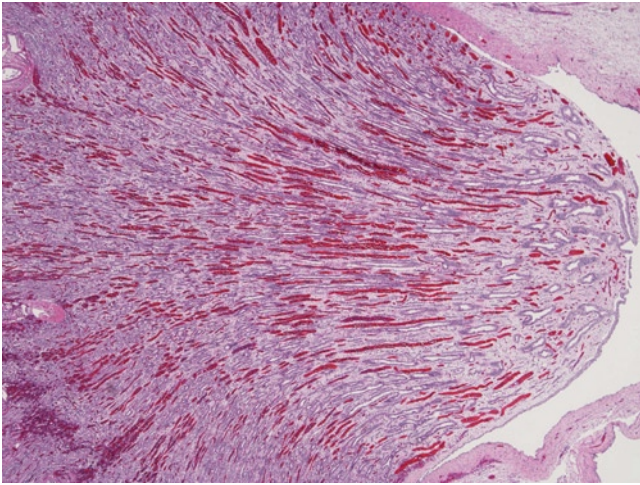


FIGURE 7-21. Medulla: kidney at 35 weeks gestation. The interstitium is normally more abundant near the papilla and this should not be mistakenly interpreted as fibrosis. (H&E, 2 \times .)

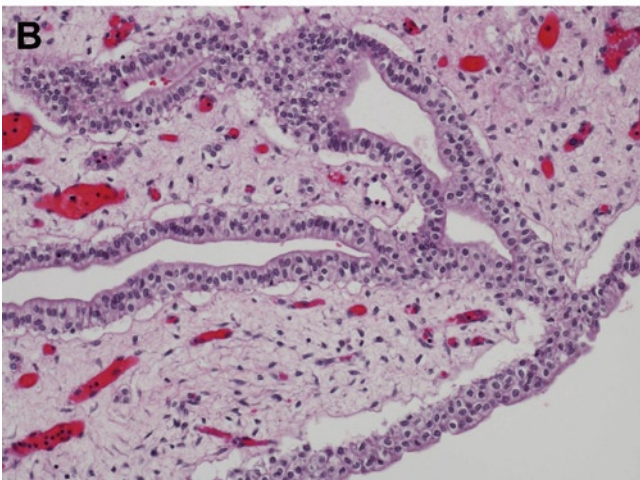
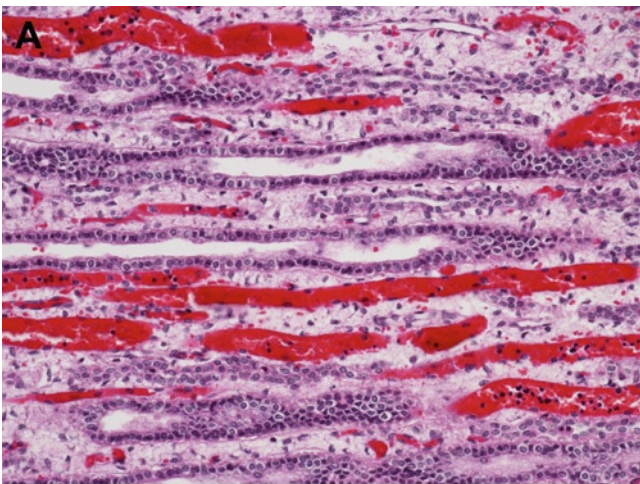


FIGURE 7-22. Collecting ducts: kidney at 35 weeks gestation. The collecting ducts in the outer medulla (**A**) are lined by cuboidal epithelium whereas the collecting ducts in the inner medulla (ducts of Bellini), near the papilla (**B**), are lined by columnar epithelium. (H&E: **A** and **B**, 20 \times .)

References

1. O'Rahilly R, Muecke EC: The timing and sequence of events in the development of the human urinary system during the embryonic period proper. *Z Anat Entwicklungsgesch* 1972, 138:99–109.
2. Potter EL: *Normal and Abnormal Development of the Kidney*. Chicago: Year Book Medical; 1972.
3. O'Rahilly R, Muller F: *Developmental Stages in Human Embryos*. Washington DC: Carnegie Institution Of Washington: 1987.
4. Sykes D: The morphology of renal lobulations and calices, and their relationship to partial nephrectomy. *Br J Surg* 1964, 51:294–304.
5. Dorovini-Zis K, Dolman CL: Gestational development of brain. *Arch Pathol Lab Med* 1977, 101:192–195.
6. Hinchliffe SA, Sargent PH, Chan YF, *et al.*: "Medullary ray glomerular counting" as a method of assessment of human nephrogenesis. *Pathol Res Pract* 1992, 188:775–782.
7. Clapp WL, Croker BP: Kidney. In *Histology for Pathologists*, edn 3. Edited by Mills SE. Philadelphia: Lippincott Williams & Wilkins; 2007:839–907.
8. Souster LP, Emery JL: The sizes of renal glomeruli in fetuses and infants. *J Anat* 1980, 130:595–602.
9. Emery JL, Macdonald, MS: Involuting and scarred glomeruli in the kidneys of infants. *Am J Pathol* 1960, 36:713–723.
10. Yosypiv IV: A new role for the renin-angiotensin system in the development of the ureteric bud and renal collecting system. *Keio J Med* 2008, 57:184–189.

8

Urinary Bladder

Eduardo D. Ruchelli and Dale S. Huff

The fetal urinary bladder extends high into the abdomen even when empty, compared to the adult bladder, which is found entirely within the pelvis minor. The fetal bladder is flanked by the two umbilical arteries, one on each side, and it is anchored to the umbilicus by the cord-like remnant of the urachus. In fact, the dome of the fetal bladder tapers off into the urachal remnant, giving the organ an almond-like shape. Bladder development is dependent on urine production; therefore, any condition that impairs the latter (ie, renal agenesis, severe renal cystic disease, renal tubular dysplasia) will result in hypoplasia of the bladder. Conversely, the fetal bladder becomes enlarged and hypertrophic in the presence of prolonged bladder outlet or urethral obstruction. These pathologic changes should be distinguished from the normal variability of physiologic dilatation, which will also affect the thickness of the wall and its histological appearance.

Embryology

The urinary bladder and urethra develop from the urogenital portion of the cloaca. The simple columnar epithelium of the entire cloaca is derived from endoderm whereas the mesenchyme is derived from the splanchnopleuric mesoderm [1]. In the early part of the fifth postfertilization week, when the ureteric bud first appears, the site of the urorectal septum becomes visible on the external surface of the cloaca. By the early part of the sixth week, the urorectal septum delineates the primary urogenital sinus from the anorectum.

The mesonephric duct distal to the takeoff of the ureteric bud is the common excretory duct, which enters the ventral or urogenital sinus portion of the cloaca. The entrance of the common excretory ducts divides the primary urogenital sinus into the vesico-urethral canal rostrally and the definitive urogenital sinus caudally. The vesico-urethral canal will form the bladder and proximal prostatic urethra in the male, and the bladder and most of the urethra in the female [2]. The definitive urogenital sinus is divided into pelvic and phallic parts. The pelvic part will form the distal prostatic and membranous urethra in the male and the distal urethra in the female. By the end of the sixth week, the urorectal septum completely separates the urogenital sinus from the anorectum.

During the seventh week, the common excretory duct gradually becomes incorporated into the posterior wall of the vesico-urethral canal, and the ureters and mesonephric ducts enter the vesico-urethral canal separately [3]. The ureteral orifices come to lie cranially and laterally to the openings of the mesonephric ducts, which migrate caudally and remain near the midline. The bladder outlet forms just cranially to the openings of the mesonephric ducts. The bladder enlarges and becomes distinct from the urethra. The trigone becomes defined. The trigone and the dorsal midline of the proximal prostatic urethra down to the orifices of the mesonephric ducts are thought to be of mesonephric origin, but a contribution from the urogenital sinus has been suggested.

The simple columnar epithelium of the urethra, except at the sinual tubercle, becomes stratified during the seventh week and is composed of several layers. The epithelium of the bladder remains simple and later differentiates into stratified epithelium two or three layers

thick [2,4]. During the eighth week, beginning at the dome of the bladder, the undifferentiated mesenchyme begins to differentiate into lamina propria and muscularis propria [2]. Full maturation of the epithelium and muscularis propria is completed in fetal life.

Histology

The four layers of the bladder wall from the lumen outward consist of the urothelium, lamina propria, muscularis propria, and adventitia (see Figs. 8-1 and 8-2) [5,6]. Some authors describe a muscularis mucosae of the urinary bladder, which may be indistinct and composed of a thin, discontinuous layer of smooth muscle [7]. The urothelium becomes well differentiated early in the midtrimester (see Fig. 8-3) and has a similar appearance to the adult urothelium, consisting of a variable number of cellular layers depending on the degree of bladder dilatation. The urothelium is usually up to six to seven layers thick in the contracted bladder. However, in autopsy specimens the urothelium frequently is poorly preserved and its layers may be incomplete or completely absent (see Fig. 8-1). The lamina propria is

composed of dense connective tissue in which there are blood vessels, lymphatics, and nerves (see Figs 8-1 and 8-3). The major changes in fetal life in the histological appearance of the urinary bladder occur in the muscularis propria, which is relatively poorly developed in the early midtrimester (see Fig. 8-1) and becomes progressively thicker during the third trimester (see Figs. 8-4–8-6). Similarly to the adult bladder, the layers of smooth muscle that constitute the muscularis propria frequently have no definite orientation and three distinct layers cannot be identified with the exception of the area of the bladder neck (see Figs 8-4–8-6) [6]. The adventitia is a relatively thin fibrous tissue layer containing large vessels and nerves (see Figs. 8-2 and 8-4).

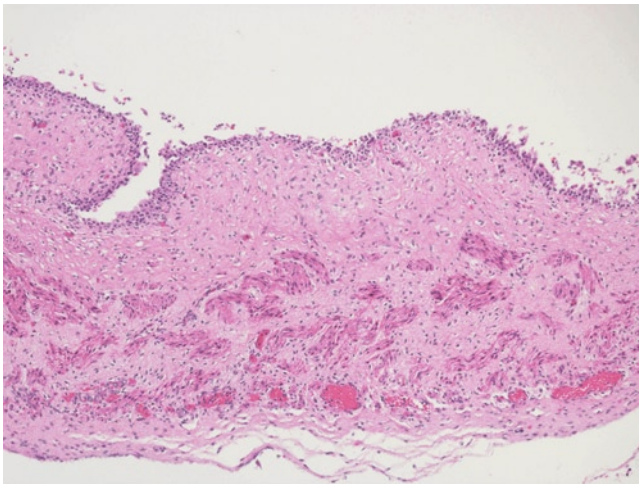


FIGURE 8-1. Urinary bladder at 16 weeks. A full-thickness section of the bladder wall is shown. The urothelium is frequently poorly preserved in autopsy specimens. The underlying lamina propria is relatively thick, depending on the degree of dilatation. The dense connective tissue of the lamina propria blends with the relatively abundant stroma that separates the smooth muscle fascicles of the immature muscularis propria. The adventitia consists of a thin layer of connective tissue, which may be covered by peritoneum in sections of the superior bladder. (Hematoxylin and eosin [H&E], 10 \times .)

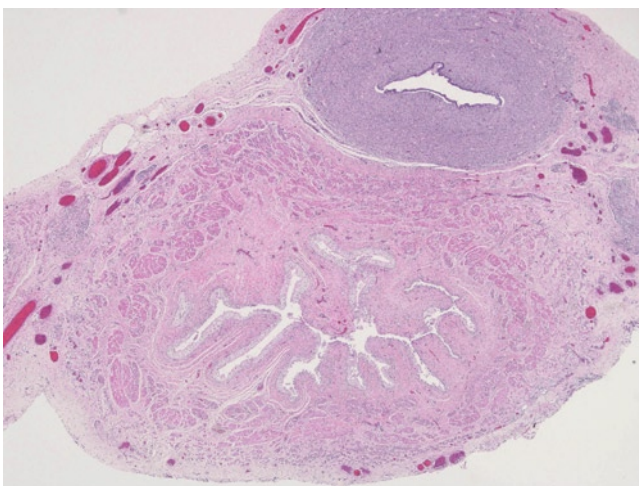


FIGURE 8-2. Urinary bladder and uterus (top) at 19 weeks. This cross-section of bladder demonstrates the typical mucosal folds in the empty, contracted state. The muscularis propria is better developed than in Figure 8-1, but the smooth muscle fascicles still remain separated by relatively abundant stroma. (H&E, 2 \times .)

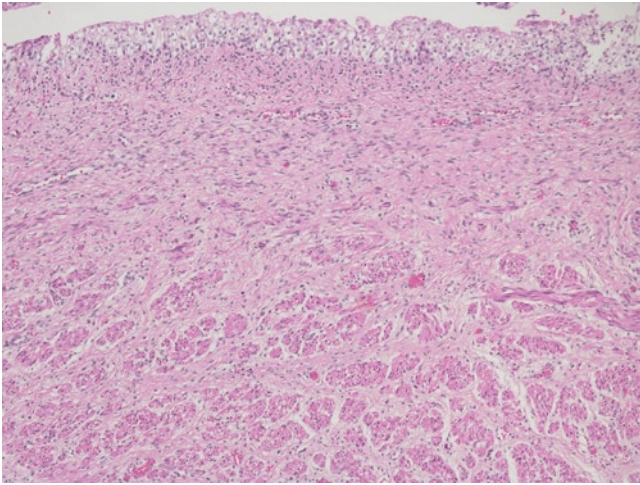


FIGURE 8-3. Urinary bladder at 19 weeks. The epithelium is relatively well preserved in this field, as shown here. This figure clearly exhibits urothelial differentiation and the epithelium will remain unchanged throughout gestation. (H&E, 10 \times .)

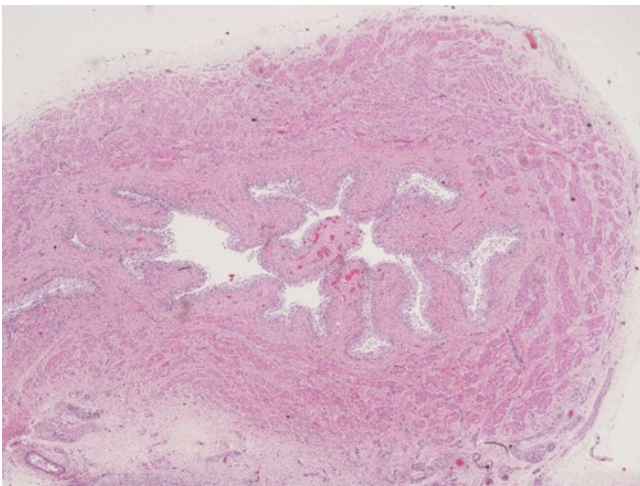


FIGURE 8-4. Urinary bladder at 23 weeks. The muscularis propria continues to thicken, as is shown here. The layers of the muscular coat (inner, central, and outer) have no definite orientation and are imperfectly separated. (H&E, 2 \times .)

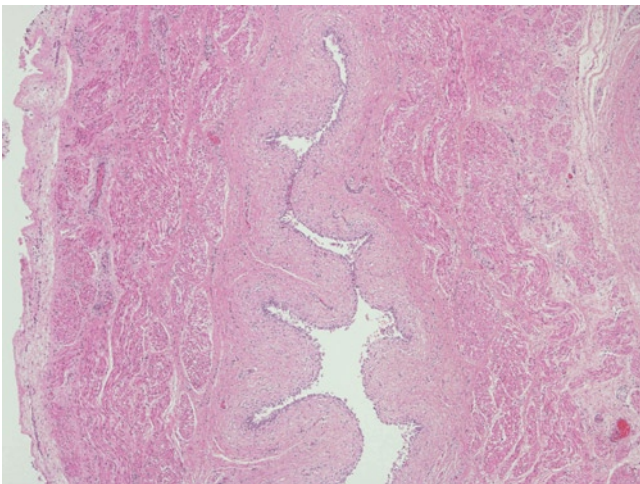


FIGURE 8-5. Urinary bladder at 32 weeks. The muscularis propria occupies most of the bladder wall, but the smooth muscle fascicles normally remain separated by some connective tissue. (Compare to Fig. 8-1.) The other layers remain unchanged. (H&E, 4 \times .)

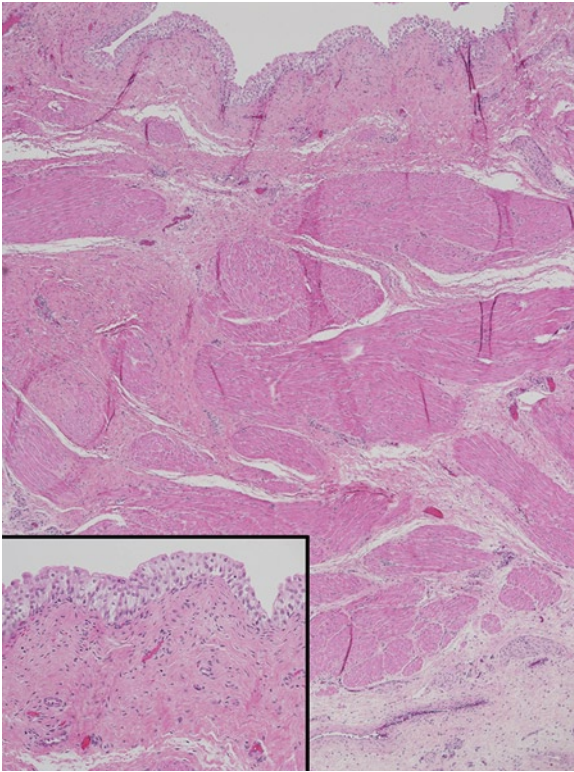


FIGURE 8-6. Urinary bladder at 35 weeks. This full-thickness view of the bladder wall near term illustrates how little the microscopic features of the bladder wall change during the second and third trimesters of gestation, except for an increase in smooth muscle in the muscularis propria. (Compare to previous figures.) The urothelium (*inset*) is fully differentiated prenatally. (H&E, 4×; inset, ×20.)

References

1. O'Rahilly R, Muecke EC: The timing and sequence of events in the development of the human urinary system during the embryonic period proper. *Z Anat Entwicklungsgesch* 1972, 138:99–109.
2. Felix W: The development of the urinogenital organs. In *Human Embryology*. Keibel F, Mall FP, eds. Philadelphia: JB Lippincott; 1912:752–979.
3. O'Rahilly R, Muller F: *Human Embryology and Teratology*, 3rd. ed. New York: Wiley-Liss; 2001, 264.
4. Yasuda Y: Genital system. In *Atlas of Human Prenatal Histology*. Nishimura H, ed. Tokyo: Igaku-Shoin; 1983:147–169.
5. Valdes-Dapena MA: *Histology of the Fetus and Newborn*. Philadelphia: Saunders; 1979:469–477.
6. Reuter VE: Urinary bladder, ureter and renal pelvis. In *Histology for Pathologists*, 3rd ed. Mills SE, ed. Philadelphia: Lippincott Williams & Wilkins; 2007:909–922.
7. Weaver MG, Abdul-Karim FW: The prevalence and character of the muscularis mucosae of the human urinary bladder. *Histopathology* 1990, 17:563–566.

9

Testis

Dale S. Huff

During the embryonic period, the microscopic anatomy of the testis is formed. The first step in the maturation of germ cells, the transformation of primordial germ cells into gonocytes, takes place. Sertoli cells and Leydig cells differentiate from their progenitors. The Sertoli cells produce Müllerian-inhibiting substance, which will cause regression of the paramesonephric ducts. The Leydig cells produce testosterone, which will cause masculinization of the internal and external genitalia. The embryonic testis begins its control of male sexual differentiation.

During the fetal period between 10 and 20 weeks postmenstrual age, the fetal step in testicular differentiation causes a dramatic change in testicular histology. Fetal Leydig cells rapidly increase in size and number, become the dominant histological feature of the testis, and make up half or more of the volume of the testis. The testosterone secreted by maturing fetal Leydig cells triggers the second step in the maturation of the male germ cells, the transformation of gonocytes into fetal spermatogonia. This event, though very important, causes no noticeable alteration in routine testicular histology during the fetal period.

The main histologic change between 20 weeks gestation and birth is the regression, dedifferentiation, and disappearance of Leydig cells. Although maturation of germ cells as seen by routine histology does not advance any further after 20 weeks gestation, the successful completion of the embryonic and fetal steps in the maturation of germ cells is essential. Without them, the postnatal steps in the maturation of germ cells cannot occur. During embryonic and fetal life, the two major functions of the testis—secretion of hormones and the development of germ cells—are established.

Embryology

Toward the end of the sixth postfertilization week in the presence of SRY, the primitive gonadal cords of the bipotential gonad transform into solid testicular seminiferous cords [1]. This process is the first histological evidence of testicular differentiation. The origin of the cords is controversial. One view is that the cords are formed by coelomic epithelium invading the mesoderm [2] and another is that the cords arise from mesonephric glomerular and tubular mesodermal epithelium [1]. The cords lack lumens but as soon as they become sharply outlined structures some refer to them as *seminiferous tubules*.

During the seventh week, the testis is attached to the remnants of the mesonephros by a thick mesorchium [3]. The capsule first appears at this stage; it is composed of a simple cuboidal epithelium that covers the surface and is derived from the visceral layer of the tunica vaginalis and, underlying it, the primitive tunica albuginea [4]. Each seminiferous tubule forms a loop similar to an inverted “U” with the two ends of the “U” at the hilum, the two straight parallel limbs radiating toward the periphery and the arch of the “U” under the capsule. The two hilar ends of the looped seminiferous tubules are narrow, delicate, and solid, and are composed of small dark cells. These are the precursors of the straight tubules and rete testis [5]. The opposite arched ends of the tubules may blend

into the tunica albuginea [4], which explains the occasional inclusion of remnants of primitive testicular blastema or individual germ cells in the tunica albuginea in later fetal or postnatal life [6]. These inclusions should not be mistaken for testicular dysgenesis [7]. The cells in the tubules differentiate into fetal Sertoli cells, which are small, basophilic, and spindle shaped. The long axis of the Sertoli cells are perpendicular to the long axis of the seminiferous tubules [4]. Primordial germ cells migrate by amoeboid action from the coelomic epithelium and interstitium into the center of the tubules and transform into gonocytes [8,9]. The transformation of primordial germ cells into gonocytes is the first step in the maturation of male germ cells [10,11] (see Fig. 9-1). At 7 weeks postfertilization, gonocytes are difficult to recognize in routine sections stained with hematoxylin and eosin (H&E), but are demonstrated by immunohistochemical stains for several markers of early germ cells such as OCT 4, PLAP, and C-Kit. Rising maternal plasma levels of human chorionic gonadotropin stimulate precursors of Leydig cells in the interstitium to differentiate into fetal Leydig cells. Testosterone production begins and Sertoli cells begin to produce Müllerian-inhibiting substance.

By the eighth postfertilization week, the shape of the testis has changed from a long and flat structure typical of a bipotential gonad to a short, ovoid, and smooth-surfaced structure typical of a testis. The simple cuboidal surface epithelium may be focally multilayered and the tunica albuginea increases in thickness.

The mesonephric body has nearly completely degenerated. Five to twelve of the epigenital nephrons adjacent to the hilum of the testis do not completely degenerate (see Fig. IV-4). The collecting ducts of these nephrons remain. The blind ends of these degenerating collecting ducts lie adjacent to the tubules of the rete testis but do not connect with them. The opposite ends are attached to the mesonephric duct. The remnants of these mesonephric nephrons will become the efferent ductules of the head of the epididymis [3]. The seminiferous tubules become more sharply outlined by a distinct basement membrane [4] and their peripheral looped ends are distinctly separated from the tunica albuginea. Gonocytes become recognizable in some well-preserved and well-prepared routine sections and they occupy the center of the tubule. The levels of human chorionic gonadotropin reach their peak. The gradual differentiation of fetal Leydig cells continues, but their numbers remain relatively low and the cells are only moderately enlarged with increasingly eosinophilic cytoplasm [4,12]. They are not a prominent histological feature of the embryonic testis. The interstitium from local mesonephric mesenchyme extends between the seminiferous tubules in the hilum. This loose interstitium contains fibroblasts, vessels, nerves, mast cells, and pre-Leydig cells. By the end of the eighth postfertilization week, the germ, Sertoli, and Leydig cell lines are present and the production of Müllerian-inhibiting substance and testosterone is established.

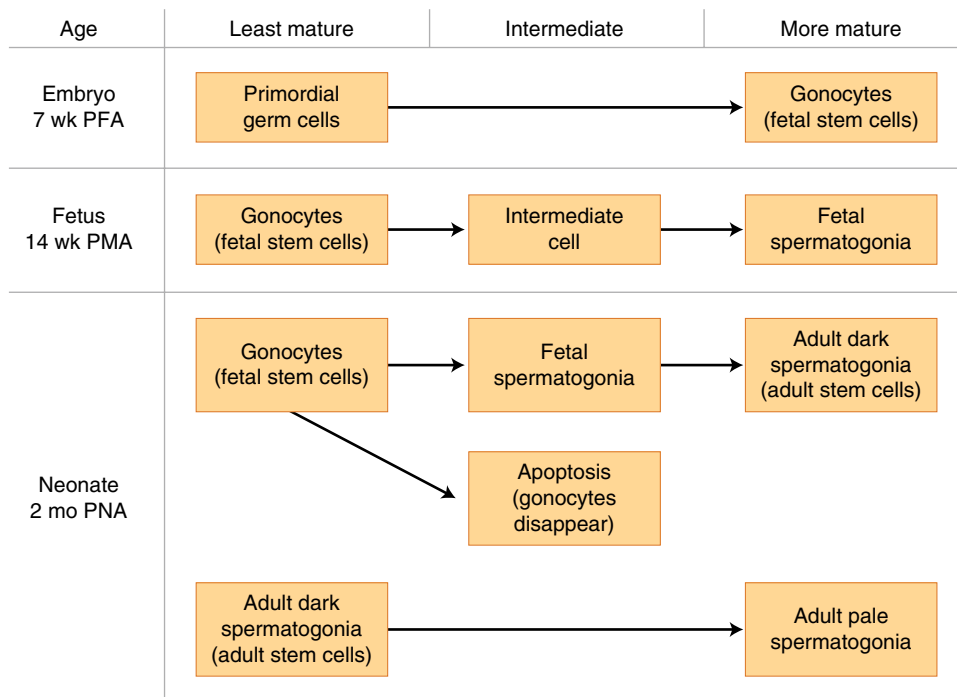


FIGURE 9-1. Maturation process of germ cells. Three steps in the maturation of germ cells during the embryonic, fetal, and neonatal periods are shown. PFA—postfertilization age; PMA—postmenstrual age; PNA—postnatal age.

Histology

General Overview

At term, the testis is covered by a thick, smooth capsule except at the hilum. The capsule is composed of three layers that are, from outside in: a layer of simple epithelium on the surface (tunica vaginalis), beneath that a layer of dense connective tissue (tunica albuginea), and the deepest layer composed of loose vascular connective tissue (tunica vasculosa). The tunica vaginalis and tunica albuginea are present when the testis first differentiates from the bipotential gonad. The tunica vasculosa gradually develops between 20 and 30 weeks gestation. The parenchyma is composed of seminiferous tubules and interstitium. The seminiferous tubules are tightly

coiled. The tubules contain Sertoli cells and germ cells, and are surrounded by a basement membrane, a layer of peritubular myoid cells, and a layer of peritubular fibroblastic spindle cells. Interlobular septa divide the seminiferous tubules into approximately 250 lobules, each containing one to four looped seminiferous tubules. The interstitium contains Leydig cells, spindled stromal cells, vessels, nerves, mast cells, and macrophages. The hilar ends of the seminiferous tubules become straight tubules that connect to the mediastinal component of the rete testis, which in turn connects to the head of the epididymis through the efferent ductules.

10 to 20 Weeks Postmenstrual Age (Figs. 9-2–9-10)

The histology of the fetal testis changes dramatically between the 10th and 20th postmenstrual weeks due to the appearance of large numbers of fetal Leydig cells. Most of the transformation occurs by the 14th to 16th weeks of gestation. By the 11th week, the hormonal control of testicular differentiation switches from placental human chorionic gonadotropin to fetal pituitary gonadotropins. Fetal pituitary luteinizing hormone

initiates the dramatic fetal step in testicular differentiation. Two important events occur during fetal testicular differentiation. The first is the rapid proliferation and maturation of fetal Leydig cells, which produce increasing amounts of testosterone. The second is the transformation of gonocytes to fetal spermatogonia, which is triggered by the increasing levels of testosterone (see Fig. 9-1).

Maturation of fetal Leydig cells

The most dramatic histological manifestation of fetal testicular differentiation is the rapid increase in the number and size of fetal Leydig cells [12]. Fetal luteinizing hormone stimulates pre-Leydig cells in the interstitium to begin to mature into fetal Leydig cells. Pre-Leydig cells are spindle cells, which are difficult to distinguish from other spindle cells in the stroma and are derived either from coelomic epithelium or from mesonephric mesodermal epithelium. In the process of transforming into fetal Leydig cells, they acquire a large amount of bright pink cytoplasm and become round to polygonal cells with sharp cytoplasmic borders. Their nuclei become large and contain a large, round central nucleolus. Mature fetal Leydig cells are identical to adult Leydig

cells except that they lack the Reinke crystalloids of the adult form. Fetal Leydig cells resemble fetal adrenal cortical cells, to which they are closely related. By 14 weeks gestation, fetal Leydig cells constitute half the volume of the testis. Longitudinal sections through the hilum demonstrate straight seminiferous tubules separated by broad bands of fetal Leydig cells (see Fig. 9-2). Many of the bands of Leydig cells are broader than the seminiferous tubules [13]. Sections perpendicular to the long axis of the tubules demonstrate widely scattered tubular cross-sections in a sea of Leydig cells (see Fig. 9-3). The relative number and size of fetal Leydig cells (see Figs. 9-2–9-10) and the levels of testosterone are greatest between 14 and 19 weeks gestation.

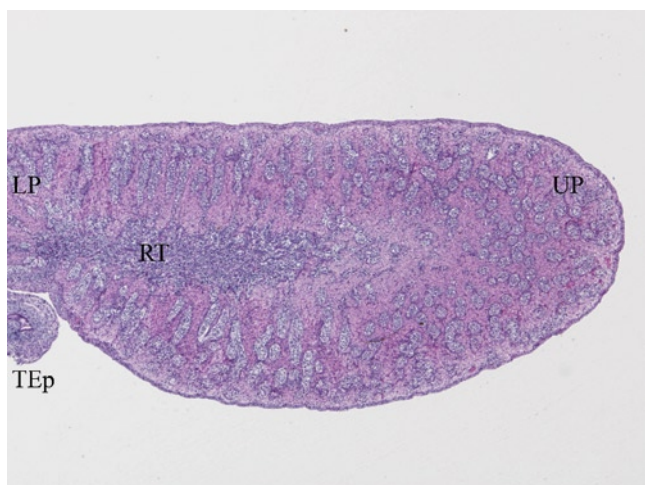


FIGURE 9-2. Fetal testis at 15 weeks gestation. The straight loops of the uncoiled seminiferous tubules in the left half are cut longitudinally; those in the right half are cross-sectioned. The hilar ends of the seminiferous tubules abruptly become the narrow, straight tubules. The narrow zone that contains the short, straight tubules is the septal compartment of the rete testis. The straight tubules connect the seminiferous tubules with the mediastinal portion of the rete testis. The broad bands of pink tissue between the tubules are fetal Leydig cells. The tunica albuginea of the capsule is apparent. LP—lower pole of testis; RT—mediastinal compartment of the rete testis; TEp—tail of the epididymis; UP—upper pole of testis. (H&E, 2 \times .)

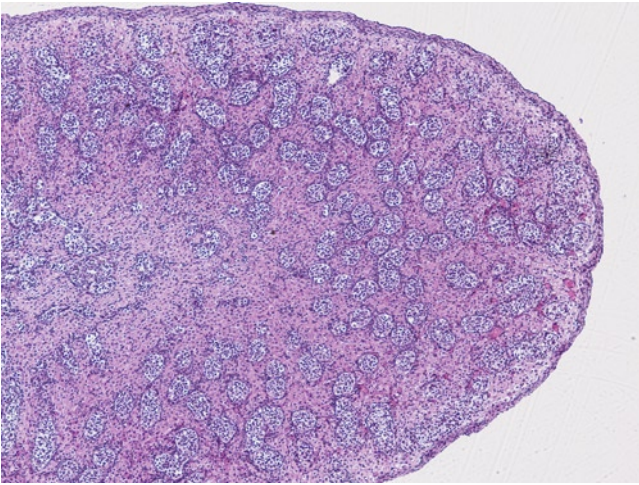


FIGURE 9-3. Fetal testis at 15 weeks gestation. This is a higher magnification of Figure 9-2. Fetal Leydig cells constitute approximately half of the volume of the testis. (H&E, 4 \times .)

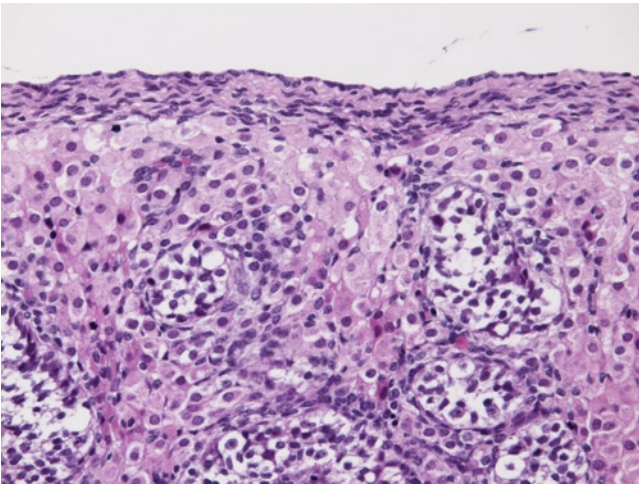


FIGURE 9-4. Capsule of the fetal testis at 15 weeks gestation. This is a higher magnification of Figure 9-2. The capsule consists of two layers. The visceral epithelium of the processus vaginalis forms the flat to low cuboidal epithelium that covers the surface and is called the tunica vaginalis. The second layer, the tunica albuginea, is a uniformly thick homogeneous band composed of several horizontal parallel layers of spindled fibroblasts and collagen. Its deep surface is sharply demarcated from the underlying Leydig cells and is parallel to the surface of the testis. The fetal Leydig cells form broad sheets between the tubules and between the tips of the tubules and the tunica albuginea. In contrast to the situation during the embryonic period, the tips of the tubules no longer blend into the tunica albuginea. The ends of the loops of seminiferous tubules are not coiled. (H&E, 20 \times .)

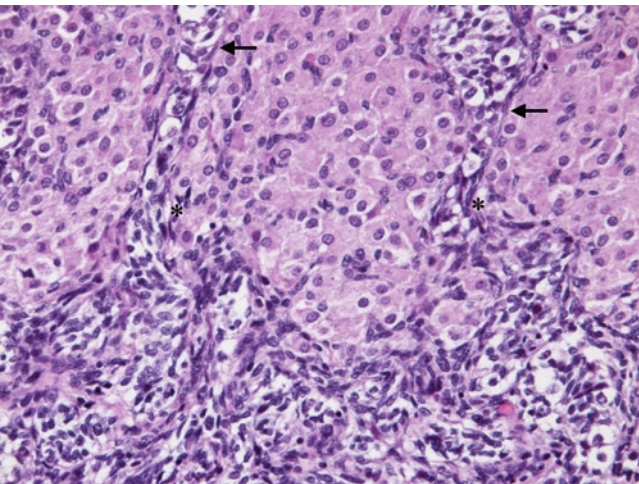


FIGURE 9-5. Rete testes at 15 weeks gestation. This is a higher magnification of Figure 9-2. This image shows details of the septal compartment of the rete. At the top of the figure, the hilar ends of two seminiferous tubules abruptly become narrow and form two straight tubules (*arrows*). Collectively, the straight tubules constitute the septal compartment of the rete testis. In the middle of the figure, the two straight tubules join the mediastinal compartment of the rete testis (*asterisks*), which occupies the lower half of the figure. In adults, at the junctions of the seminiferous tubules and straight tubules, the Sertoli cells are oriented parallel to the long axis of the tubule with the apices of the cells pointing downstream toward the straight tubules. The tips of the cells extend into the rete testis to form a valve that prevents retrograde flow of fluid and cells from the rete testis back into the seminiferous tubules. This structure is either not yet developed or very difficult to identify in the fetus. The rete testis is not yet canalized. In the septal compartment of the rete testis, fetal Leydig cells fill the area between the straight tubules. (H&E, 20 \times .)

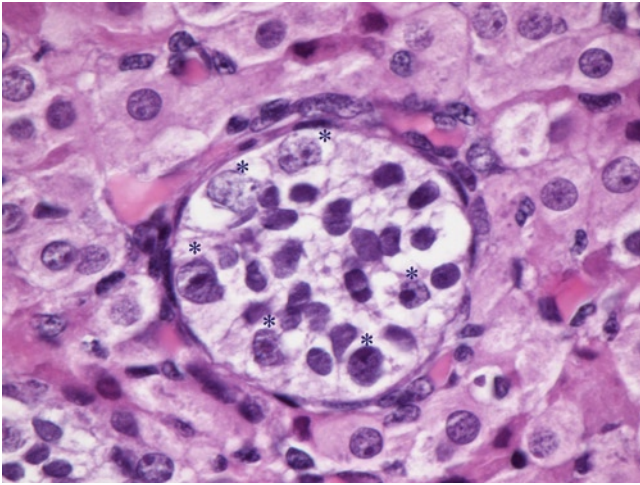


FIGURE 9-6. Seminiferous tubule of the fetal testis at 15 weeks gestation. This image is a high-power view of a cross-section of one seminiferous tubule from the same testis shown in Figure 9-2. The tubule is surrounded by one or two layers of peritubular myoid and fibroblastic cells. The tubule contains six or eight large germ cells with large, round nuclei, some of which contain one or two large nucleoli (asterisks). It is difficult to distinguish between gonocytes, intermediate cells, and fetal spermatogonia. The germ cells have a large amount of clear cytoplasm and several are located on the basement membrane. The smaller cells with oval or elongate nuclei and little cytoplasm are fetal Sertoli cells. The large fetal Leydig cells surrounding the tubule have large amounts of eosinophilic cytoplasm similar to adult Leydig cells but Reinke crystalloids are not seen. (H&E, 60 \times .)

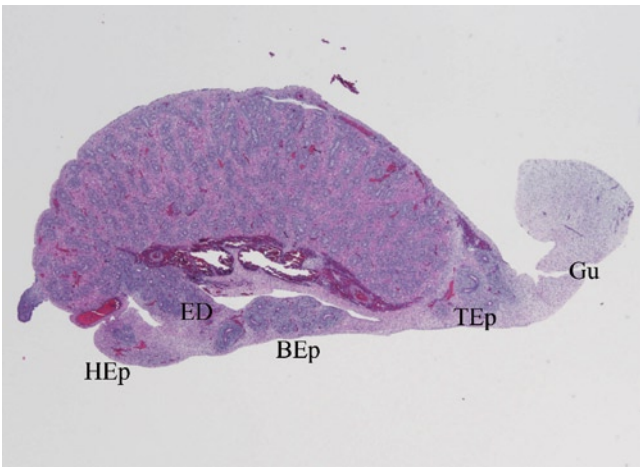


FIGURE 9-7. Fetal testis at 17 weeks gestation. This low-power view is of a testis that is 2 weeks older than the above testis in Figures 9-2 through 9-6. The upper pole with an attached solid appendix testis is to the left. The epididymis is at the bottom of the testis. The efferent ductules (ED) extend from the rete testis to the epididymis. The tail of the epididymis (TEp) is embedded in the gubernaculum (Gu). The bright red Leydig cells constitute much of the volume of the testicular tissue. BEp—body of epididymis; HEp—head of epididymis. (H&E, 1 \times .)

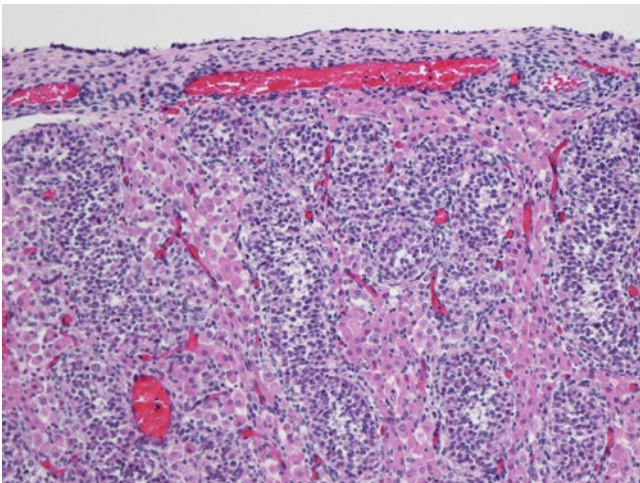


FIGURE 9-8. Fetal testis at 17 weeks gestation. This is a higher power view of Figure 9-7. The capsule is composed of the visceral epithelium of the tunica vaginalis on the surface and the tunica albuginea. A third layer of loose vascular connective tissue is beginning to form deep the tunica albuginea, and will become the tunica vasculosa. The most distal portions of the seminiferous tubules are slightly coiled. The fetal Leydig cells are beginning to dedifferentiate and regress in size and number. The columns of Leydig cells between the tubules become progressively more narrow. There are very few Leydig cells between the tips of the tubules and the tunica albuginea. Some of the fetal Leydig cells are becoming smaller and spindle shaped, especially in the column closest to the right edge of the figure. This change indicates that fetal Leydig cells are regressing into juvenile Leydig cells. (H&E, 10 \times .)

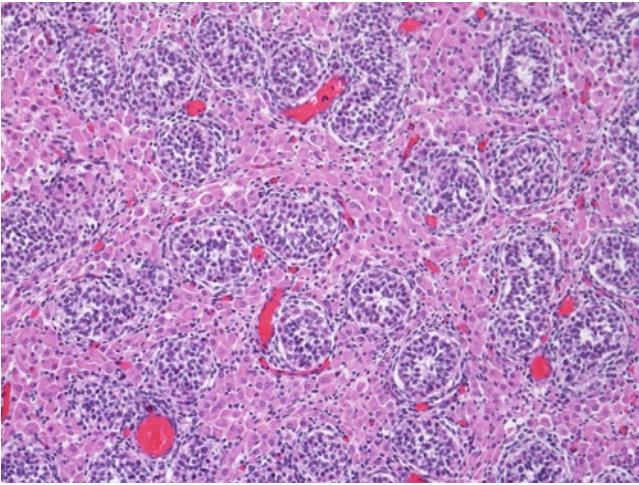


FIGURE 9-9. Fetal testis at 17 weeks gestation. This is a higher magnification of Figure 9-7. This image shows cross-sections of seminiferous tubules and early regression of fetal Leydig cells. The fetal Leydig cells constitute a large portion of the volume of the testis but some are dedifferentiating into smaller, spindle-shaped juvenile Leydig cells. (H&E, 10 \times .)

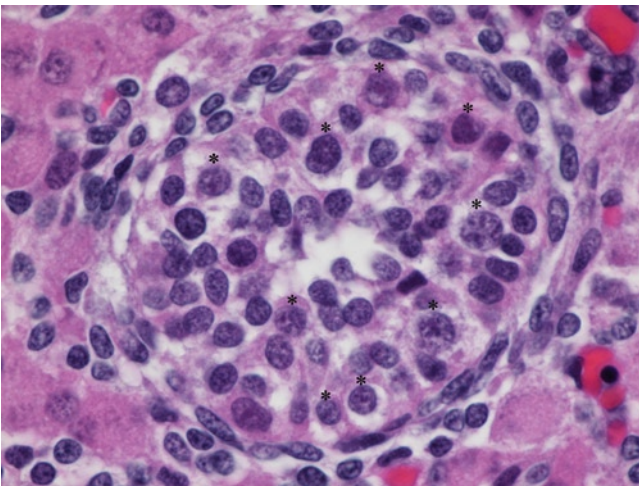


FIGURE 9-10. Seminiferous tubule of the fetal testis at 17 weeks gestation. This image shows a seminiferous tubule of Figure 9-7 at high power. The peritubular myoid and fibroblastic cells are one or two cells thick. At least nine germ cells are present and are marked with asterisks above their nuclei. Even in this well-preserved specimen, the germ cells are difficult to differentiate from Sertoli cells. Identification of subtypes of germ cells is impossible in most autopsy specimens. In the right lower quadrant of the tubule, three large germ cells on or near the basement membrane are easily distinguished from the smaller elongated or oval Sertoli cells between them. Some of the Leydig cells closest to the tubule, especially at approximately 3 o'clock, are small and spindle shaped. These cells are dedifferentiating juvenile Leydig cells and will form a pool from which fetal and adult Leydig cells will differentiate in the future. (H&E, 60 \times .)

Maturation of germ cells: transformation of gonocytes into fetal spermatogonia

By 14 to 15 weeks gestation, rapidly increasing levels of testosterone in the fetal testis and plasma trigger the second step in the maturation of germ cells: the transformation of gonocytes into fetal spermatogonia (see Fig. 9-1) [14]. During this transformation, the gonocytes in the center of the tubule extend a pseudopod that attaches to the basement membrane. The gonocytes migrate toward the basement membrane and transform into intermediate cells. On arrival at the basement membrane, the intermediate cells transform into fetal spermatogonia. Because gonocytes are the stem cells of the fetal male germ cell line, they not only proliferate to produce increasing numbers of fetal spermatogonia, but they also maintain their own numbers. The classification of the subtypes of germ cells used in this chapter is from Fukuda and Hedinger [9] and Wartenberg, Holstein, and Vossmeier [15]. Several confusing nomenclatures have been used in the classification of the subsets of fetal germ cells (see Fig. 9-11) [16].

In contrast to the dramatic change in testicular histology caused by the maturation of Leydig cells, this step in the maturation of germ cells causes very little change in the histology of the testis [13]. Distinguishing between gonocytes, intermediate cells, and fetal spermatogonia is very difficult in routine sections from autopsies (see Fig. 9-6). Gonocytes occupy the center of the tubules. They have a large, round central nucleus; one

or two large round nucleoli; and a scant amount of clear glycogen-rich, PAS-positive cytoplasm. Intermediate cells are larger than gonocytes, round to oval, and are close to or on the basement membrane. They have a large amount of clear glycogen-rich cytoplasm. Fetal spermatogonia are larger than intermediate cells. They are oval, lie flat on the basement membrane, and have a large round nucleus and an inconspicuous or absent nucleolus. The distinction between the cell types is more easily made in very fresh tissue obtained within an hour of death, in 0.5 to 1.0 μm -thick semi-thin sections of epon-embedded samples, and in electron micrographs. The immunophenotypes of the morphological subsets of germ cells in the fetal and neonatal periods are beginning to be worked out [17,18]. The maximal mean number of germ cells per tubular cross-section of six is reached by 14 weeks gestation [13] (Fig. 9-6). The second type of cell in the tubule is the fetal Sertoli cell. Fetal Sertoli cells are the most numerous cells in the tubule. They are small, oval, dark cells with very little cytoplasm. They are oriented perpendicularly to the basement membrane and fill up the tubule around the germ cells. Their microscopic appearance does not change during fetal life. Although they look unimportant, they play vital roles in the maintenance of the germ cells and the regulation of the maturation of germ cells.

Nomenclature for Subsets of Germ Cells	
Names used in this chapter	Alternate names
Primordial germ cells	Gonocytes
Gonocytes	Primitive germ cells
Intermediate cells	Primordial germ cells
Fetal spermatogonia	Prespermatogonia
	M, T1, or T2 prespermatogonia
	Prespermatogonia
	M, T1, or T2 prespermatogonia
	Gonocytes (for all three)

FIGURE 9-11. Alternative nomenclature for subsets of germ cells in the embryo and fetus. Each alternate name may refer to any of the four names used in this chapter or to any combination of the four. Pre- or prospermatogonia have been subdivided into three subtypes: M (multiplying), T1 (transitional nonproliferating), and T2 (transitional proliferating).

Other changes

At between 10 and 20 weeks gestation, the capsule begins to change. The tunica albuginea continuously increases in thickness and becomes a layer of dense fibrous tissue beneath the surface epithelium of the tunica vaginalis. A loose inner layer of connective tissue, the tunica vasculosa, forms on the deep surface of the tunica albuginea (see Figs. 9-4 and 9-8). Septa begin to form from the tunica vasculosa and the fibrous septa in the hilum begin to extend peripherally. The seminiferous tubules begin to elongate and their peripheral ends

begin to coil (see Figs. 9-7–9-10). The median tubular diameter increases to 59 μm [13] (see Figs. 9-6 and 9-10). Peritubular myoid cells appear before 15 weeks gestation and become more prominent thereafter (see Figs. 9-6 and 9-10). Some of the collecting tubules of the epigenetic mesonephric nephrons begin to form a solid junction with the rete to form efferent ductules. This union is called the *urogenital union* [3] (see Fig. 9-7). The solid junctions become canalized late in fetal life or early in postnatal life.

20 to 40 Weeks Postmenstrual Age (Figs. 9-12–9-32)

Regression and dedifferentiation of fetal Leydig cells

The most dramatic histologic change in this period is the regression, dedifferentiation, and apparent disappearance of fetal Leydig cells that become smaller, vacuolated, and finally revert to spindle-shaped cells similar to pre-Leydig cells, which are difficult to distinguish from other connective tissue cells of the interstitium [4,12,13]. These are juvenile Leydig cells that, along with pre-Leydig cells, form a pool from which more fetal and adult Leydig cells can be recruited. Some may undergo apoptosis. Because they are difficult to identify in routine histological sections from autopsies, Leydig cells

have been said to be virtually absent in some near-term fetuses. However, they are recognizable in semi-thin sections of epon-embedded tissue and in electron micrographs. As fetal Leydig cells regress, the seminiferous tubules become more and more crowded. Compare the appearance of the testis at 21 weeks gestation (see Figs. 9-12 and 9-13), 23 weeks gestation (see Figs. 9-14–9-16), 26 weeks gestation (see Figs. 9-17–9-22), 39 weeks gestation (see Figs. 9-23–9-28), and 41 weeks gestation (see Figs. 9-29–9-32).

Maturation of germ cells

The appearance of germ cells does not change in routine histological sections (see Figs. 9-13, 9-20, 9-25, and 9-31). However, the immunohistochemical phenotypes of germ cells may change and additional subsets of

germ cells at between 20 and 40 weeks gestation may be identified in the future. Apoptosis of germ cells is an important feature in their maturation [19].

Other changes

The next most obvious histological change is the increased coiling of the seminiferous tubules due to their increasing length [4,13]. Coiling becomes maximal by approximately 30 weeks gestation. The increased coiling adds to the effect of the regression of Leydig cells to result in the tightly packed appearance of the tubules. Compare the appearance of the tubules at the various gestational ages given above. The tunica albuginea continues to increase in thickness and the third layer of loose connective tissue, the tunica vasculosa, increases in thickness and vascularity (see Figs. 9-12, 9-14, 9-15, 9-17, 9-18, 9-23, and 9-29). The fibrous septa extend from the hilum to the tunica vasculosa (see Figs. 9-17, 9-23,

and 9-29). The septal, mediastinal, and extratesticular portions of the rete become more recognizable. The septal portion is composed of the straight tubules (also known as tubuli recti) and the mediastinal portion is the labyrinth of anastomosing clefts. In the extratesticular portion, the labyrinth coalesces into five to 12 tubules that join with the efferent ductules. Lumens begin to form in the rete at approximately 24 weeks gestation [20] and are prominent by 40 weeks gestation. Canalization of the rete–efferent ductular junction may not be complete until postnatal life (see Figs. 9-21, 9-22, 9-26–9-28, and 9-32). Extramedullary hematopoiesis and lipochrome pigment increase with increasing gestational age [13].

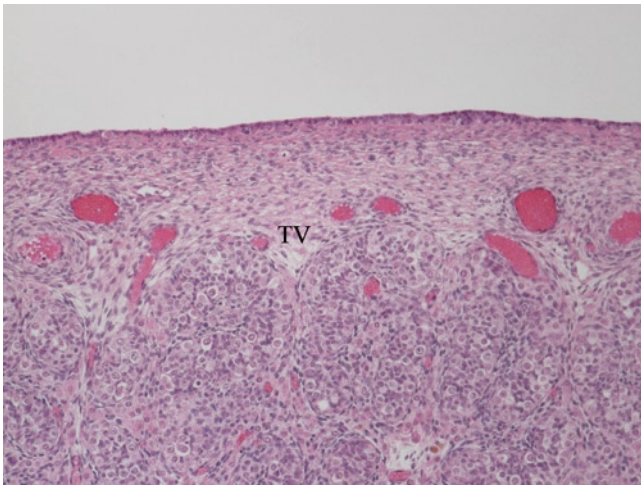


FIGURE 9-12. Fetal testis at 21 weeks gestation. This testis is dramatically different from the 17-week testis shown above. This image shows the capsule and peripheral ends of the seminiferous tubules. The fetal Leydig cells have almost completely disappeared and the tubules are extensively coiled and packed back to back. The tunica vasculosa (TV) is more distinct; its deep surface is scalloped because fibrovascular septa arise from it and extend down into the parenchyma, dividing it into lobules. The surface epithelium, the tunica vaginalis, is cuboidal and contains nests of germ cells. The germ cells and Sertoli cells are unusually well preserved and distinct. (H&E, 10 \times .)

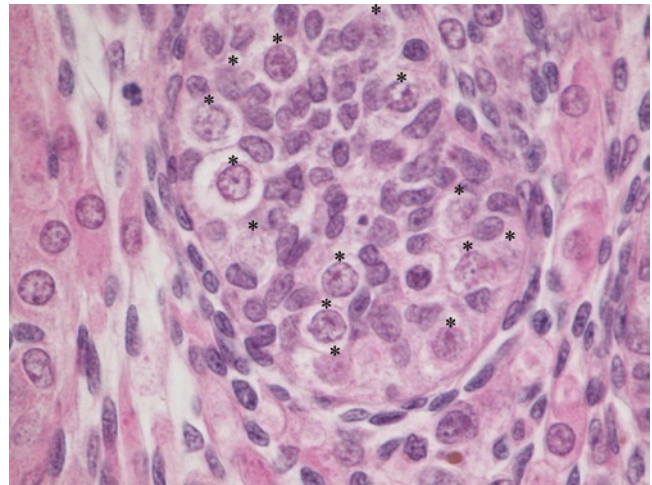


FIGURE 9-13. Seminiferous tubule of the fetal testis at 21 weeks gestation. This high-power view is of a cross-section of one seminiferous tubule from the same testes as seen in Figure 9-12. The peritubular myoid and fibroblastic cells are more numerous than in the testes at earlier gestational ages. The germ cells and Sertoli cells have not changed and are unusually distinct in this specimen. A total of 14 germ cells are marked with asterisks above their nuclei. The Leydig cells are mostly juvenile forms and blend into the peritubular spindle cells. (H&E, 60 \times .)

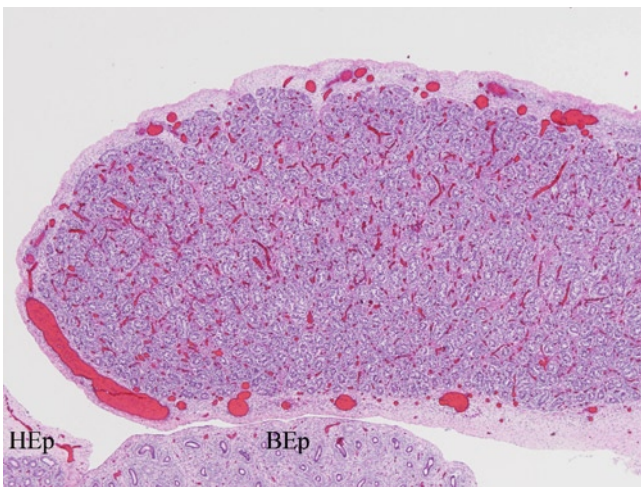


FIGURE 9-14. Fetal testis at 23 weeks gestation. The tunica vasculosa is very vascular and the fibrovascular interlobular septa extend more deeply into the parenchyma toward the hilum than in earlier specimens. The seminiferous tubules are extensively coiled. Fetal Leydig cells are less numerous than in the testis at 21 weeks gestational age. The timing of the maturational changes varies from fetus to fetus by several weeks. BEp—body of epididymis; HEp—head of epididymis. (H&E, 2 \times .)

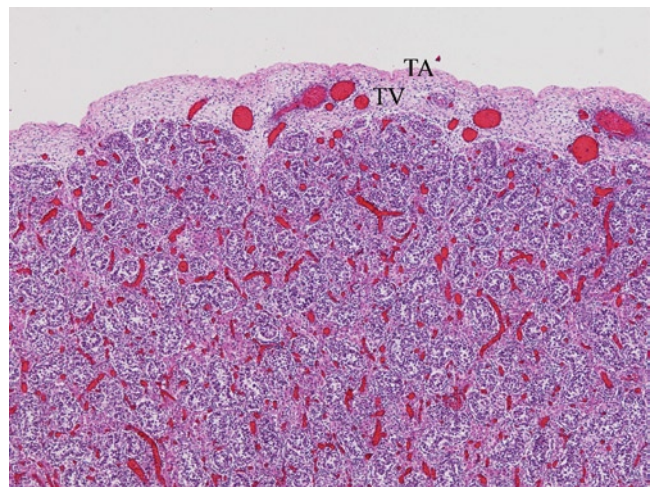


FIGURE 9-15. Fetal testis at 23 weeks gestation. This is a higher power view of Figure 9-14. The fetal Leydig cells are partially regressed into smaller elongate juvenile Leydig cells. TA—tunica albuginea; TV—tunica vasculosa. (H&E, 4 \times .)

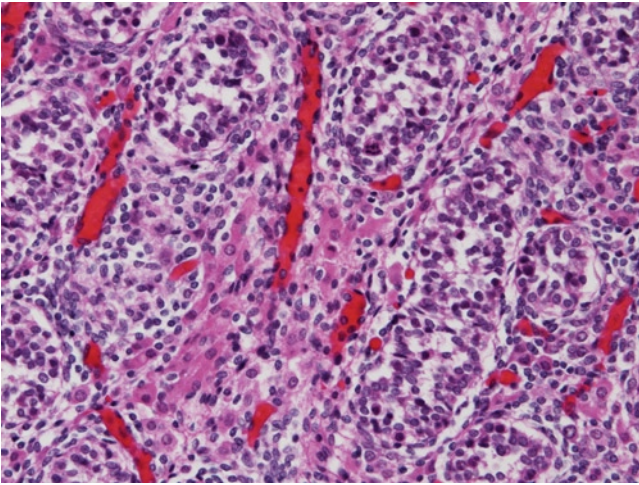


FIGURE 9-16. Fetal testis at 23 weeks gestation. This is a higher power view of Figures 9-14 and 9-15. Most of the Leydig cells are regressing, small, spindle-shaped juvenile forms. The germ cells are almost impossible to identify even in this relatively well-preserved section. (H&E, 20 \times .)

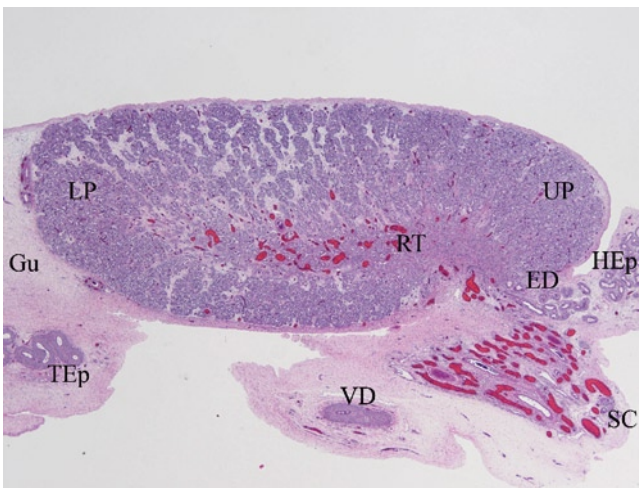


FIGURE 9-17. Fetal testis at 26 weeks gestation. In this low-power view of the entire testis, the extratesticular portion of the epididymis, seen at the lower border of the upper pole (UP), joins with the efferent ductules (ED) that stream into the head of the epididymis (HEp). The vas deferens (VD) is joining the spermatic cord (SC). There are no visible Leydig cells and the interlobular septa, which are accentuated due to edema, extend from the tunica vaginalis to the hilum. Gu—gubernaculum; LP—lower pole of testis; RT—mediastinal compartment of the rete testis; TEp—tail of the epididymis. (H&E, 1 \times .)

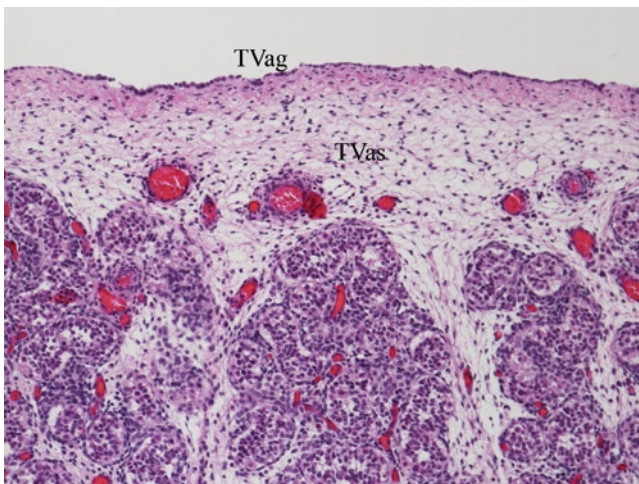


FIGURE 9-18. Fetal testis at 26 weeks gestation. This image is a higher magnification of the capsule and peripheral loops of the seminiferous tubules. The capsule is composed of the simple cuboidal epithelium of the visceral layer of the tunica vaginalis (TVag) on the surface, the outer dense fibrous layer called the tunica albuginea, and the inner loose highly vascular layer that gives rise to the interlobular septa, now called the tunica vasculosa (TVas). The peripheral loops of the seminiferous tubules are tightly coiled and back to back. The fetal Leydig cells have all regressed into small, spindled juvenile forms that cannot be distinguished from the stromal fibroblasts. (H&E, 10 \times .)

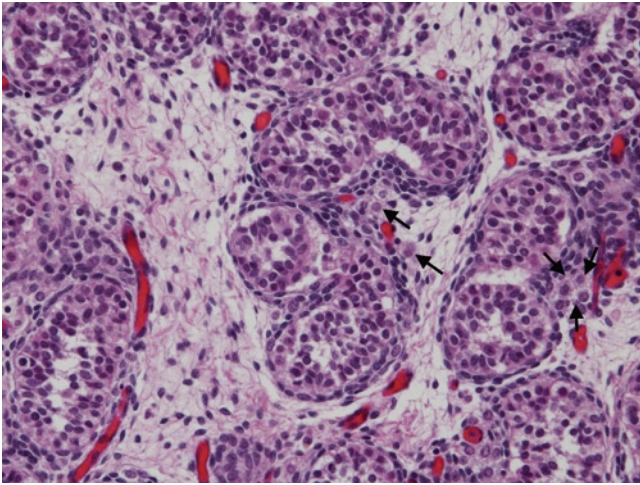


FIGURE 9-19. Seminiferous tubules of the fetal testis at 26 weeks gestation. This is a higher magnification of [Figure 9-18](#). Leydig cells are extremely difficult to identify. A few possible single juvenile Leydig cells and clusters of Leydig cells are indicated by arrows. The layers of peritubular spindle cells are very thick and the outer layers of these spindle cells are thought to be composed of completely regressed Leydig cells that can be referred to as *pre-Leydig cells*. Germ cells are difficult to identify in this section. (H&E, 20 \times .)

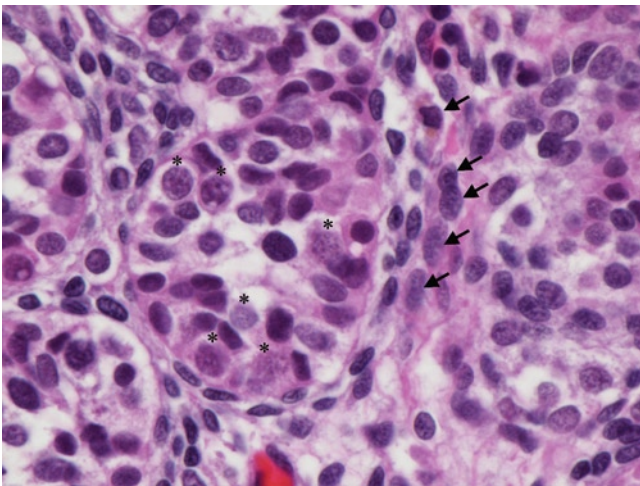


FIGURE 9-20. Seminiferous tubule at 26 weeks gestation. This image is a high magnification of a single tubule from [Figure 9-18](#). Regressed spindle-shaped juvenile Leydig cells are marked by arrows. Germ cells within the tubule in the center are marked by asterisks above their nuclei. (H&E, 60 \times .)

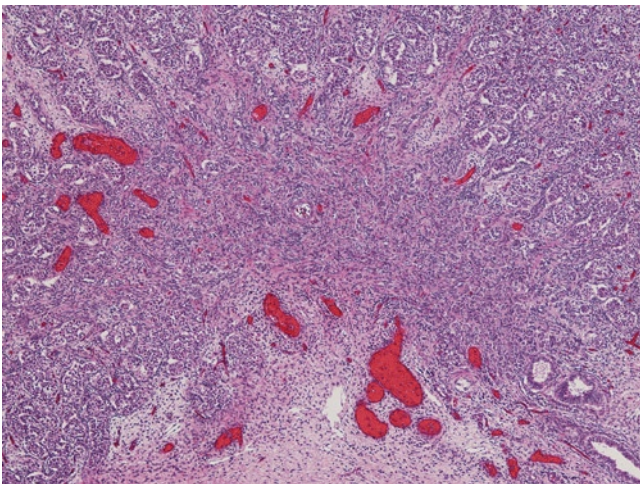


FIGURE 9-21. Rete testis at the hilar aspect of the upper pole of the testis at 26 weeks gestation. This is from the same testis as shown in [Figure 9-17](#). The seminiferous tubules surround the top and two sides of the rete testis and the bottom of the rete testis is at the hilar surface. The septal compartment of the rete testis is composed of the straight tubules, which are the short narrow tubules connecting the hilar ends of the seminiferous tubules to the mediastinal compartment. The mediastinal compartment is the largest compartment of the rete testis. The extratesticular compartment, which connects the mediastinal compartment to the efferent ductules, is in the right lower border of the rete testis. Two cross-sections and one oblique section of efferent ductules are in the right lower corner of this figure. The efferent ductules are heading toward the head of the epididymis, which is to the right, not shown here. Lumens are not present in the rete testis. (H&E, 20 \times .)

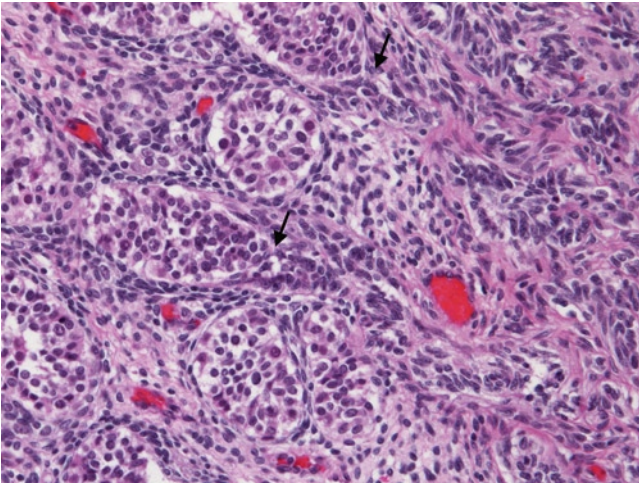


FIGURE 9-22. Septal compartment of the rete testis at 26 weeks gestation. This is a higher magnification of [Figure 9-21](#). The junctions between two seminiferous tubules and two straight tubules are marked by *arrows*. The straight tubules are narrow and short, and they join the mediastinal compartment that is at the extreme right edge of this figure. (H&E, 20 \times .)

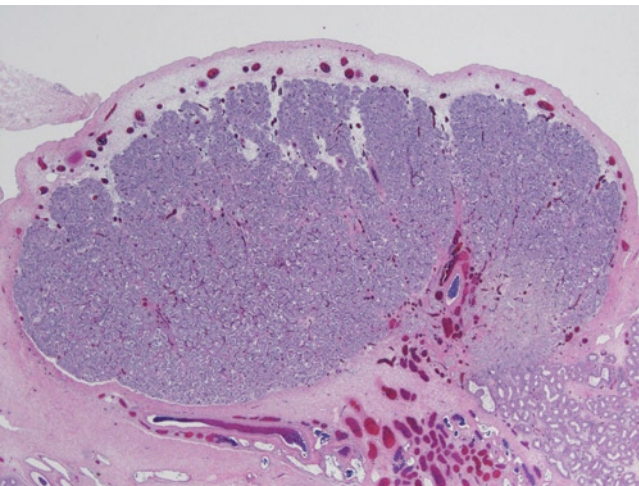


FIGURE 9-23. Fetal testis at 39 weeks gestation. In this low-power view of the testis, the three layers of the capsule—the tunica vaginalis, the tunica albuginea, and the tunica vasculosa—are sharply defined. The interlobular septa extend from the tunica vasculosa to the hilum. The seminiferous tubules are tightly coiled and back to back. Leydig cells are not recognizable at this magnification. (H&E, 1 \times .)

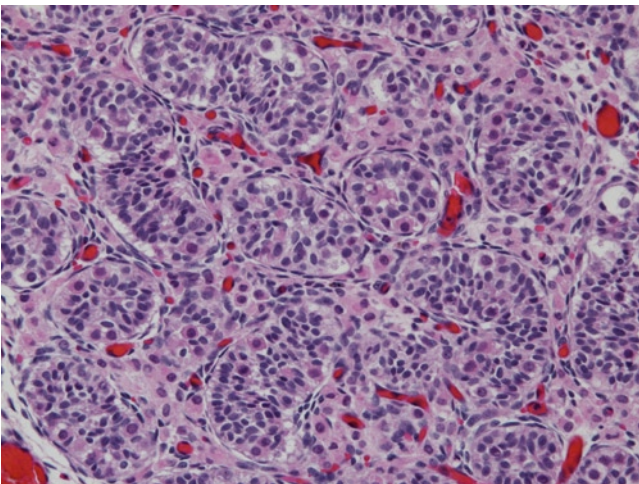


FIGURE 9-24. Seminiferous tubules and Leydig cells at 39 weeks gestation. This is a higher magnification of [Figure 9-23](#). Although Leydig cells are not recognizable at low magnification, numerous partially regressed and dedifferentiated juvenile Leydig cells are present between the tubules. Many of the germ cells are apparently undergoing apoptosis. Note the difference between the testis shown here at 39 weeks gestation, in which Leydig cells are easily identified, with the previous image of one at 26 weeks gestation, in which Leydig cells are difficult to identify even at high power. The timing of maturational changes in the testis varies widely from fetus to fetus. (H&E, 20 \times .)

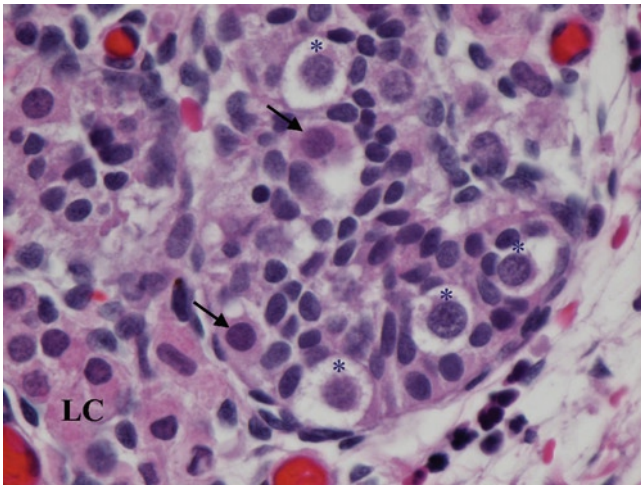


FIGURE 9-25. Single seminiferous tubule at 39 weeks gestation. This is a high-power view of [Figure 9-23](#). Four viable germ cells are marked with asterisks above their nuclei and two apoptotic germ cells are marked with arrows. Partially regressed juvenile Leydig cells (LC) are seen in the interstitium. (H&E, 60 \times .)

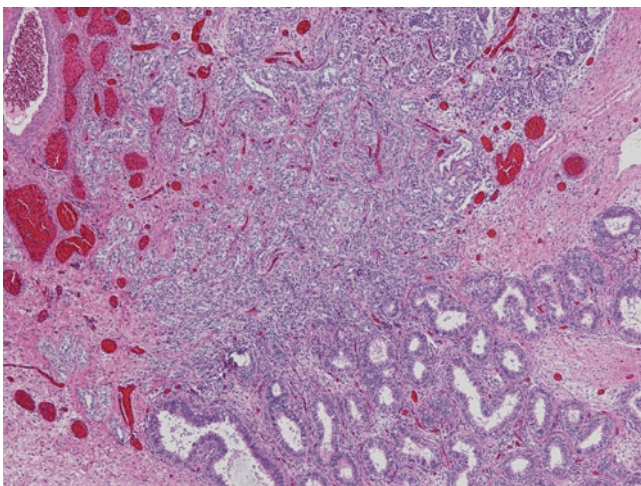


FIGURE 9-26. Rete testis at 39 weeks gestation. This is a higher magnification of [Figure 9-23](#). In this medium-power image of the rete testis, seminiferous tubules are present along the upper edge. Efferent ductules are at the lower right and are streaming toward the head of the epididymis, which is out of the picture to the right. The septal, mediastinal, and extratesticular compartments are visible, but only a few lumens are present. (H&E, 4 \times .)

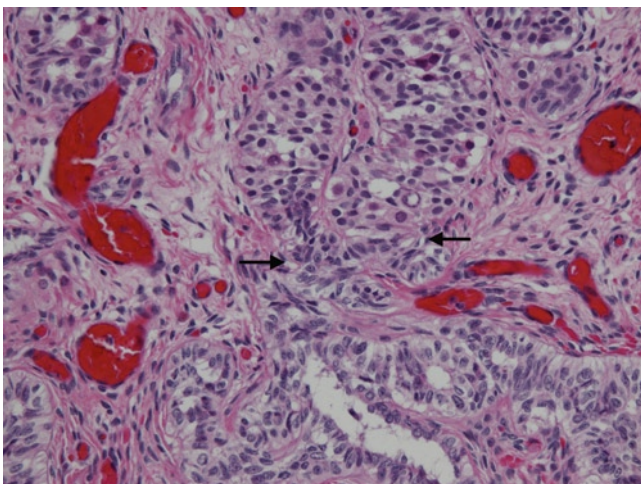


FIGURE 9-27. Septal compartment of the rete testis at 39 weeks gestation. This is a higher magnification of [Figure 9-26](#). The junctions between two seminiferous tubules and two straight tubules are marked with arrows, and lumens are present in some straight tubules. The irregular cuboidal to columnar epithelium of the rete testis is becoming recognizable. Irregular bundles of dense collagen appear between the channels of the rete testis. (H&E, 20 \times .)

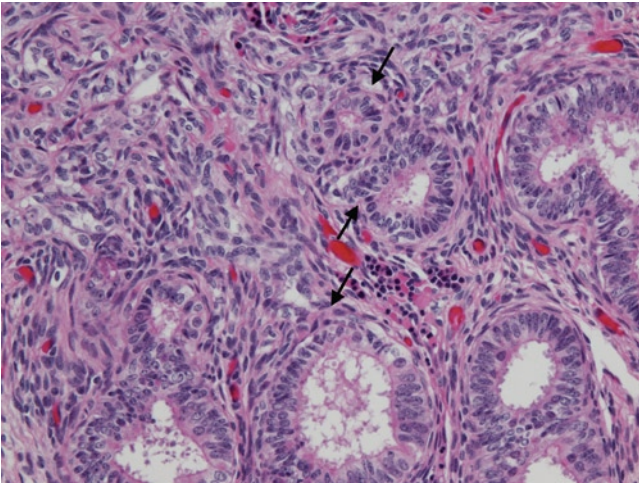


FIGURE 9-28. Extratesticular compartment of the rete testis at 39 weeks gestation. This is a higher magnification of [Figure 9-26](#). The large, round efferent ductules occupy the right lower half of the picture. The efferent ductules are lined by pseudostratified columnar and cuboidal epithelium with apical blebs. The arrows point to three sites at which the blind ends of efferent ductules abut against the blind ends of extratesticular tubules of the rete testis. These junctions have not yet canalized. Nests of erythroid extramedullary hematopoiesis are present. (H&E, 20 \times .)

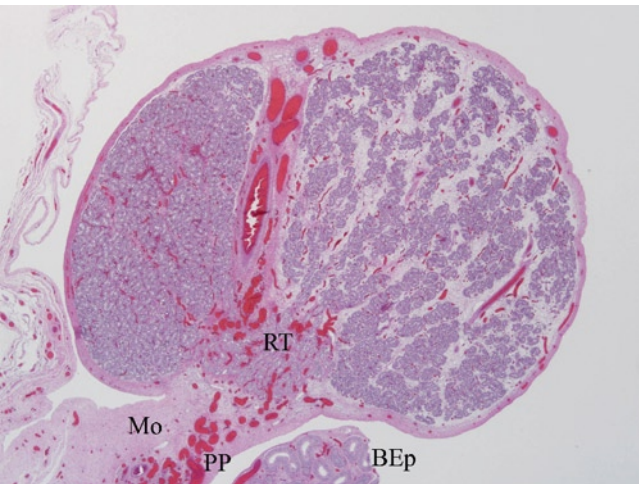


FIGURE 9-29. Fetal testis at 41 weeks gestation. This low-power view shows a cross-section of the testis. The cause of the interstitial edema localized to the right half of the testis is not known, but it accentuates the interlobular septa. BEp—body of epididymis; Mo—mesorchium; RT—mediastinal compartment of the rete testis. (H&E, 1 \times .)

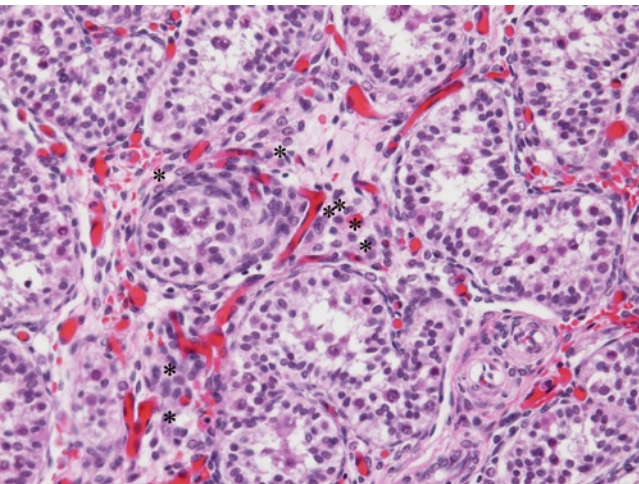


FIGURE 9-30. Fetal testis at 41 weeks gestation. This image is a medium-power view of seminiferous tubules and interstitium from [Figure 9-29](#). The small roundish cells with frayed pink cytoplasm in the interstitium are juvenile Leydig cells (asterisks). (H&E, 20 \times .)

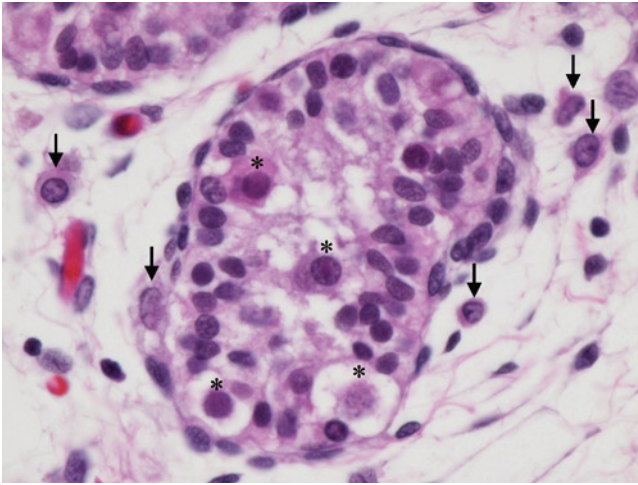


FIGURE 9-31. One seminiferous tubule at 41 weeks gestation. Four germ cells are marked by asterisks above their nuclei. The cell in the upper left of the tubule is undergoing apoptosis. The arrows point to five juvenile Leydig cells. The spindle-shaped one on the right side of the tubule blends in with the peritubular myoid and fibroblastic cells. (H&E, 60 \times .)

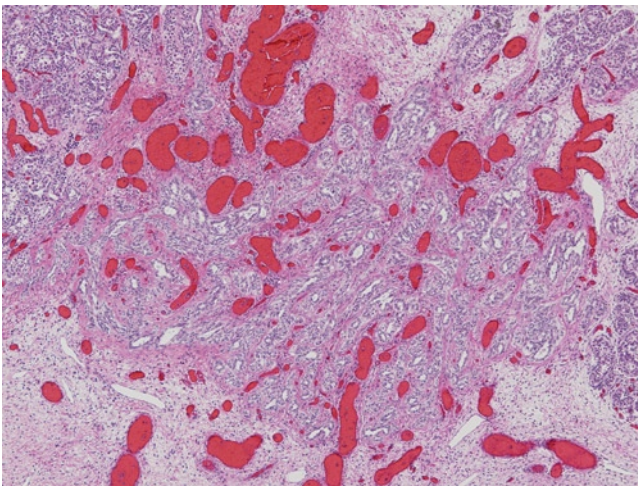


FIGURE 9-32. Rete testis at 41 weeks gestation. The rete testis fills the center of the image. The seminiferous tubules are around the right, upper, and left sides of the rete testis. The hilum is at the bottom of the image. The septal compartment is at the right upper edge of the mediastinal compartment. The rete testis is completely canalized, and the irregular squamoid and cuboidal lining epithelium of the rete testis can be appreciated. (H&E, 4 \times .)

Two Months Postnatal Age: Mini Puberty (Figs. 9-33–9-35)

A "mini puberty" occurs at 2 months of age. At the onset of this event, the seminiferous tubules contain numerous germ cells that are gonocytes, intermediate cells, and fetal spermatogonia (see Figs. 9-33 and 9-34). The mini puberty is initiated by a transient surge in luteinizing hormone secretion, which stimulates the recruitment and maturation of fetal Leydig cells from pre-Leydig cells and from the regressed juvenile Leydig cells. Secretion of testosterone triggers the third step in the maturation of germ cells: the transformation of gonocytes, the fetal stem cells, into adult dark spermatogonia, the adult stem cells (see Fig. 9-1) [21]. It is not clear whether gonocytes transform directly into adult dark spermatogonia, indirectly through fetal spermatogonia, or both. Future immunohistochemical studies may more accurately identify the stem cells of the germ cell line. Gonocytes either transform into adult dark spermatogonia or undergo apoptosis. Adult dark spermatogonia then transform into adult pale spermatogonia. Fetal spermatogonia remain but may have a different immunophenotype than those present during the fetal period. As stem cells, the adult dark spermatogonia also maintain their own numbers.

The mini puberty and the transformation of gonocytes into adult dark spermatogonia last for several weeks, then begin to recede by the third or fourth postnatal month. Secretion of luteinizing hormone falls, fetal Leydig cells again regress to juvenile Leydig cells, and secretion of testosterone falls. When this surge in activity is over, gonocytes have disappeared and are replaced by adult dark and adult pale spermatogonia. The number of germ cells per tubular cross-section falls from six to two because of the apoptosis. Juvenile Leydig cells are difficult to identify in routine sections but are identifiable in 0.5- μ m sections (see Fig. 9-35). In normal testes, gonocytes should be absent by 6 months of age [14]. The presence of some cells positive for PLAP, OCT 4, C-Kit, and other markers of immature germ cells during the first 6 months of life is normal and not necessarily diagnostic of carcinoma in situ. The successful completion in this step in germ cell maturation is essential for the development of normal fertility. Figures 9-33 through 9-35 are biopsies that were immediately fixed in glutaraldehyde, embedded in epon, sectioned at 0.5- μ m thickness, and stained with toluidine blue.

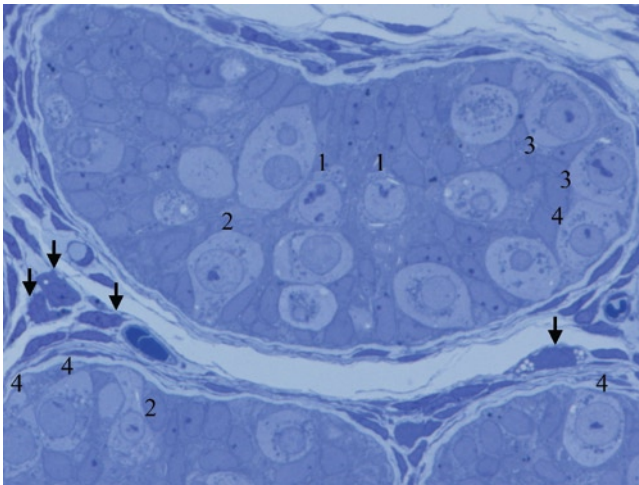


FIGURE 9-33. Postnatal testis, 2 months. This high-power view is of a seminiferous tubule from an infant prior to the onset of the mini puberty at 2 months postnatal age. The cytology of the germ cells and Leydig cells is distinct. Approximately 18 germ cells are present. The two germ cells in the center of the tubule labeled "1" are gonocytes. The one labeled "2" is a gonocyte that has attached itself to the basement membrane by a pseudopod. The two on the basement membrane at the right end of the tubule (labeled "3") are intermediate cells. The one on the basement membrane at the right end of the tubule and the one in the lower right corner are fetal spermatogonia (both labeled "4"). The tubule in the lower left corner contains a gonocyte migrating to the basement membrane ("2") and two fetal spermatogonia ("4") on the basement membrane. The other germ cells are not further classified. The arrows point to juvenile Leydig cells. (Toluidine blue, 60 \times .)

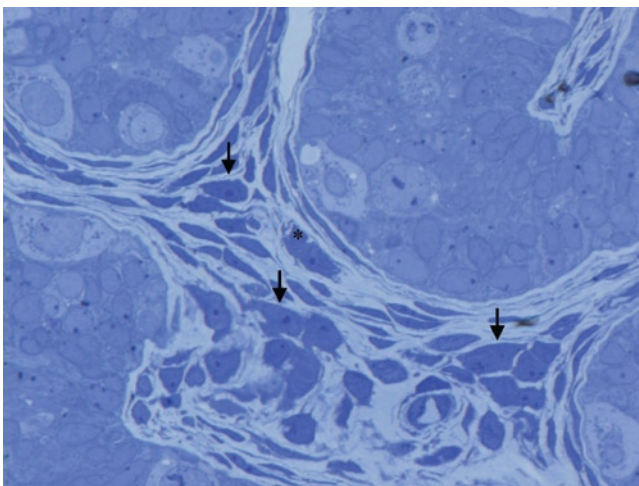


FIGURE 9-34. Postnatal testis, 2 months. Shown here is the same testis as in Figure 9-33. The interstitium is filled with juvenile Leydig cells. The arrows point to clusters of Leydig cells that, in routine autopsy sections, would look like those in Figures 9-17, 9-18, 9-28, and 9-29. In routine autopsy sections, the elongated Leydig cell marked with an asterisk would look like the long cell next to the tubular basement membrane in Figure 9-31. (Toluidine blue, 60 \times .)

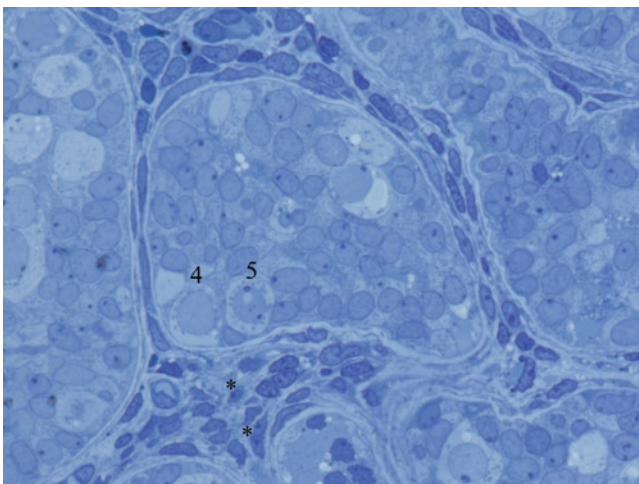


FIGURE 9-35. Postnatal testis, 6 months. Shown here is the seminiferous tubule from an infant after completion of the mini puberty at 6 months of age. The number of germ cells is greatly reduced and gonocytes are no longer present. Adult dark spermatogonia labeled "5" are present. A few fetal spermatogonia labeled "4" remain. Leydig cells (asterisks) are difficult to identify even in this preparation: they are hidden among the peritubular and interstitial spindle cells. (Toluidine blue, 60 \times .)

Special Considerations

Paramesonephric and mesonephric embryonic remnants are often described as being distinctly different. Paramesonephric remnants (appendix testis) are said to be solid and covered by prominent cuboidal and columnar epithelium. Mesonephric remnants (appen-

dix epididymis) are said to be cystic and covered by flat, inconspicuous mesothelium. Although these definitions are sometimes true, the descriptions below emphasize that the two may be impossible to differentiate by their histologic appearances.

Paramesonephric remnants

The appendix testis, sometimes called the *hydatid of Morgagni*, is thought to be a remnant of the paramesonephric duct and is described as the homologue of the fimbriated end of the Fallopian tube by some (see Figs. 9-36–9-38). It is attached to the upper pole of the testis and it may be polypoid or filiform, sessile or pedunculated. It is usually solid but may be cystic or contain a tubule. The cyst or tubule may communicate with the

surface similar to a fimbria. The appendix is often covered by cuboidal to columnar, focally ciliated, and basophilic epithelium. If cystic, the cyst is usually lined by similar epithelium. The surface epithelium is sometimes flat mesothelium. The stroma may contain scattered smooth muscle fibers and, if tubular, may demonstrate a muscularis [3,22,23].

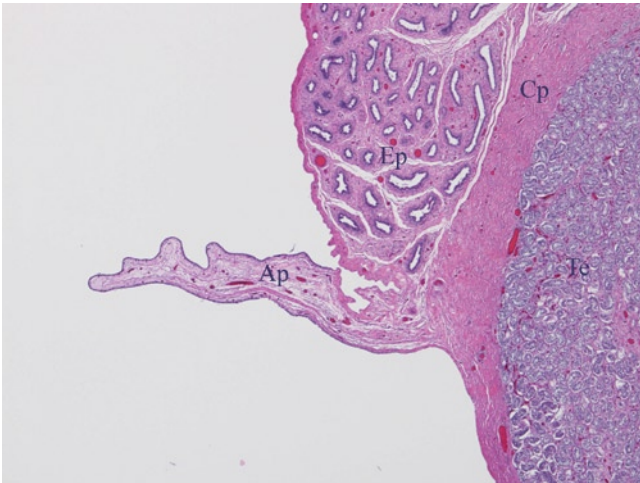


FIGURE 9-36. Solid filiform appendix testis. The finger-like appendix is attached to the testicular capsule and points to the left. It is covered with simple, low-cuboidal epithelium. Ap—appendix testis; Ep—head of epididymis; Cp—capsule of testis; Te—upper pole of testis. (H&E, 4×.)

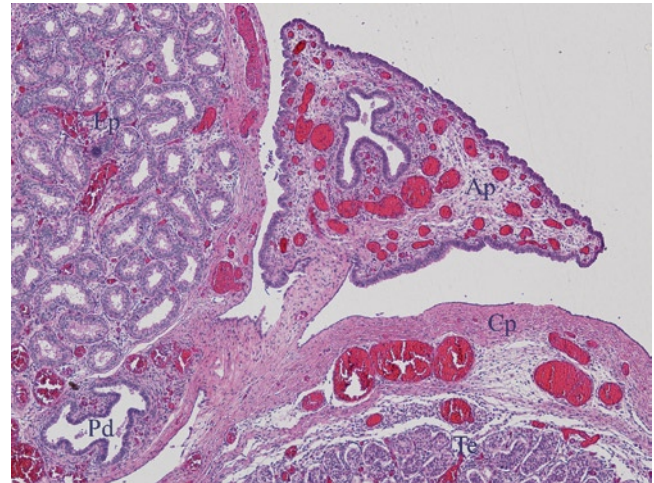


FIGURE 9-37. Cystic appendix testis. The appendix contains a central cyst and is attached by a thin pedicle to the capsule of the testis. The epithelium covering the surface and lining the cyst is similar and shown in Figure 9-38. The capsule of testis includes the tunica vaginalis, the tunica albuginea, and the tunica vasculosa. Ap—appendix testis; Cp—capsule of testis; Ep—head of epididymis; Pd—remnant of paramesonephric duct; Te—upper pole of testis. (H&E, 4×.)

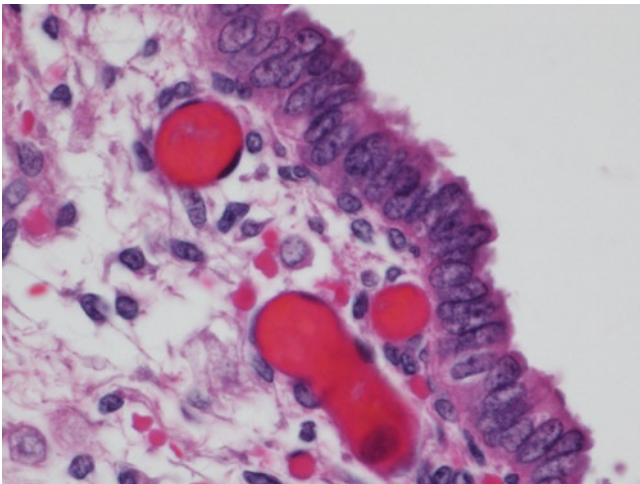


FIGURE 9-38. Epithelium of the appendix testis. This higher power image of the epithelium covers the surface of the appendix testis shown in Figure 9-37. The epithelium is pseudostratified columnar and cuboidal with patches of cilia. (H&E, 60×.)

Mesonephric remnants

Several mesonephric remnants are often present [3,22,23]. The appendix epididymis is attached to the head of the epididymis and is thought to be a remnant of the blind rostral end of the mesonephric duct (see Figs. 9-39–9-41). It is polypoid or filiform, pedunculated or sessile. It is usually cystic or contains a rudimentary tubule that usually does not communicate with the surface. It is usually covered by simple flat epithelium similar to the adjacent covering of the tunica albuginea, but may be covered by an epithelium identical to that typical of an appendix testis. If cystic, the cyst is lined by simple cuboidal or columnar epithelium that may be focally ciliated. This description is almost identical to that of the appendix testis. Differentiation between an appendix testis and an appendix epididymis may be impossible by histological criteria alone and may depend on location. Some appendages are attached at the junction between the epididymis and the testis; these may be difficult to classify.

Blind-ended remnants of mesonephric collecting ducts, which remain attached to the mesonephric duct near the upper and lower poles of the testis, are called *superior* and *inferior aberrant ducts*, respectively, or organs of Haller. They are analogous to epoophoron in the female. These are inconspicuous. Ductular remnants seen between the epididymis and

testis may be either mesonephric or paramesonephric in origin. Ductular remnants associated with the vas deferens in the distal end of the spermatic cord are the remnants of the paragenital mesonephric nephrons and have been called the paradidymis or organ of Giraldez (see Fig. 9-42). They are analogous to the paroophoron, lined by simple cuboidal or columnar epithelium, and are accompanied by sparse smooth muscle fibers. In our material, some of the embryonic remnants in the pampiniform plexus near the hilum, adjacent to the head of the epididymis, or in the distal spermatic cord appear to arise from partially degenerated epigenitalis mesonephric nephrons, which stream from the testicular hilum into the pampiniform plexus rostrally toward the spermatic cord. Any of these mesonephric ductular remnants may be associated with mesonephric glomeruloid structures (see Figs. 9-43 and 9-44).

Similar embryonic remnants are found in the spermatic cord and in the wall of hernia sacs, where they may be confused with vas deferens or epididymis. Recent evidence that mesonephric epithelium may be positive for CD 10 while paramesonephric epithelium is not may provide an immunohistochemical method for determining the origin of all the embryonic remnants discussed above [24].

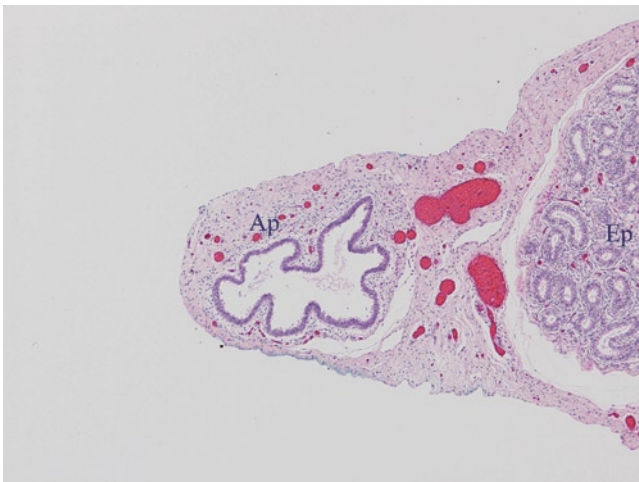


FIGURE 9-39. Cystic, sessile appendix epididymis. The appendix (Ap) is attached to the head of the epididymis (Ep). The epithelium lining the cyst is similar to that in Figures 9-38 and 9-41. (H&E, 4 \times .)

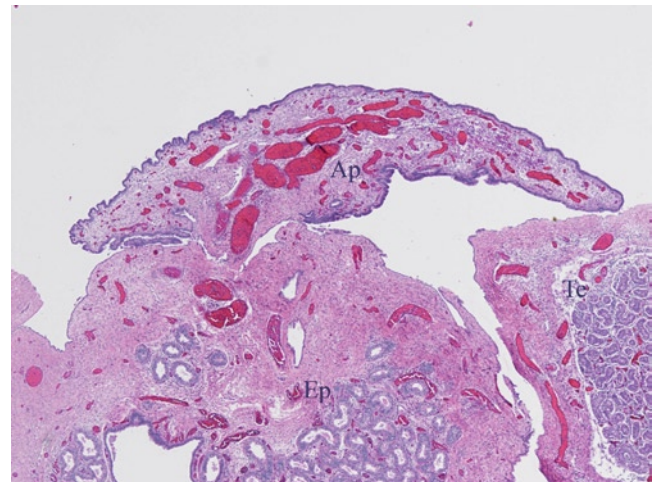


FIGURE 9-40. Solid, pedunculated appendix epididymis. The appendix (Ap) is attached to the head of the epididymis (Ep) by a short pedicle. The surface epithelium is shown in Figure 9-41. Te—upper pole of testis. (H&E, 2 \times .)

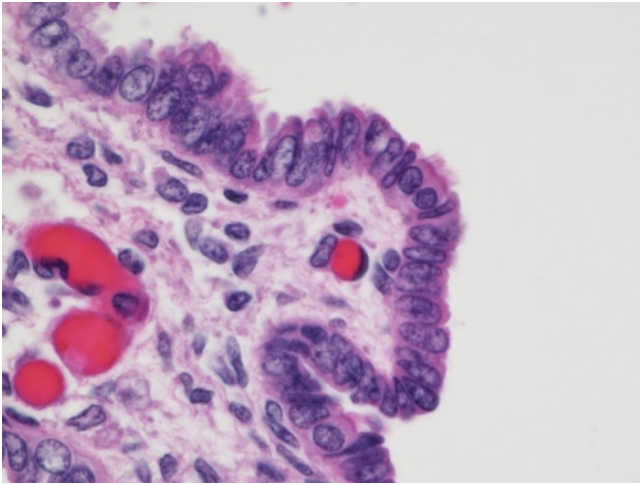


FIGURE 9-41. Surface epithelium of the appendix epididymis. The surface epithelium of the appendix epididymis in Figure 9-40 is shown here. This epithelium is identical to that of the cystic appendix testis seen in Figure 9-38. (H&E, 60 \times .)

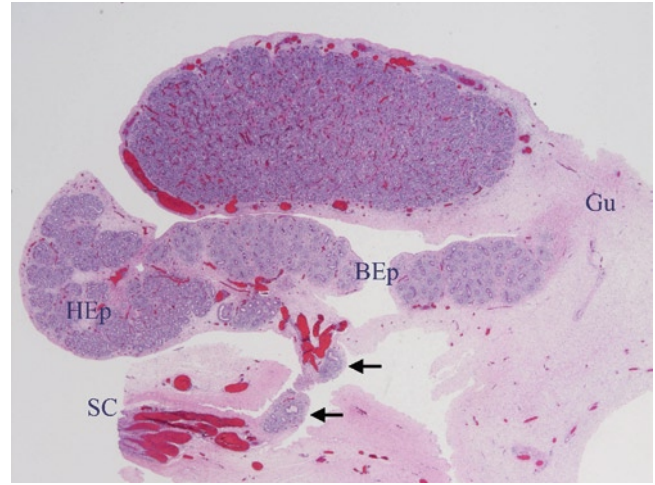


FIGURE 9-42. Embryonic rests in the distal spermatic cord. These mesonephric embryonic rests (arrows) are found in the distal spermatic cord adjacent to or rostral to the head of the epididymis. In this fetus they appear to arise from the epigenital mesonephric nephrons related to those that form the efferent ductules. These rests are intermingled with the vessels of the pampiniform plexus entering the distal spermatic cord. BEp—body of epididymis; Gu—gubernaculum; HEP—head of epididymis; SC—cut end of spermatic cord. (H&E, 1 \times .)

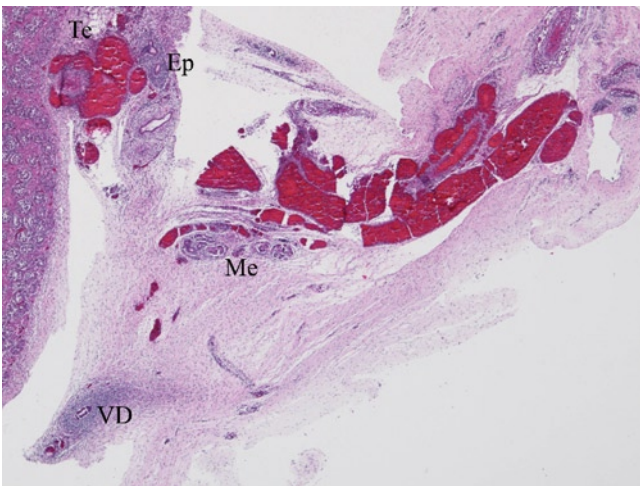


FIGURE 9-43. Embryonic rests with glomeruloid structures. Embryonic rests with glomeruloid structures in the distal spermatic cord are shown. Ep—edge of the epididymis; Me—a nest of tubular and glomeruloid mesonephric embryonic remnants at the edge of the pampiniform plexus in the distal end of the spermatic cord; Te—hilum of the testis; VD—vas deferens as it nears the distal end of the spermatic cord. (H&E, 2 \times .)

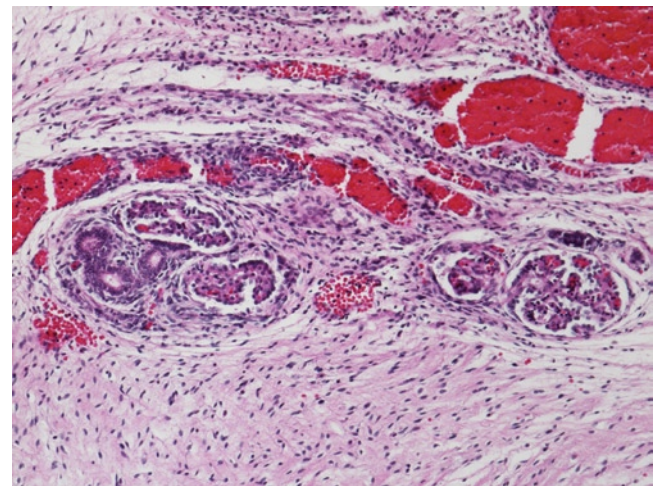


FIGURE 9-44. Higher magnification of the embryonic rests in Figure 9-43. The rest is composed of mesonephric tubular and glomerular structures. (H&E, 10 \times .)

Adrenal cortical rests

Adrenal cortical rests or ectopic adrenal nodules of Marchand may be found in the testis, the rete testis (see Fig. 9-45), the testicular hilum, the epididymis, the paratesticular soft tissue, or the spermatic cord. They are encapsulated and composed of definitive and fetal cortex without medulla. They may arise from a rostral

area of mesonephric mesodermal epithelium, which gives rise to both adrenal and testicular epithelium. They may be affected by the same lesions as fetal adrenal cortex such as adrenal cortical cytomegaly, cytomegalic inclusion disease, and other infections.

Testicular embryonic remnants

Several embryonic remnants may be found in and around the testis. Nests of testicular blastema or clusters of seminiferous tubules are occasionally present in the tunica albuginea [6,7]. On occasion, these may extend onto the surface as grossly visible reddish brown spots, giving the testis an appearance similar to a speckled bird's egg. Whether these remnants should be considered congenital anomalies or variations of normal is unclear. They should be distinguished from testicular

dysgenesis. Solitary germ cells may be found in the tunica albuginea (see Fig. 9-46), testicular interstitium, or in the rete testis. They are seen infrequently, but more likely during midpregnancy than at other periods of fetal life. Ectopic Leydig cells may be present in the tunica albuginea or in paratesticular connective tissue and nerves (see Fig. 9-47); these are often numerous in conditions associated with hyperplasia of Leydig cells. They may mimic ganglion cells.

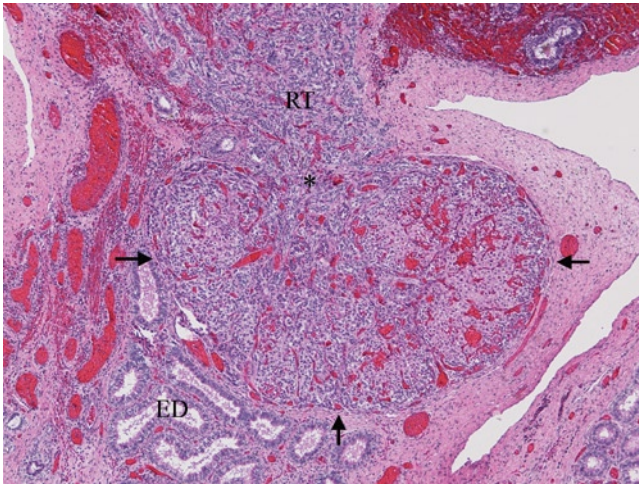


FIGURE 9-45. Adrenal cortical rest of Marchand at the junction of the rete testis and the efferent ducts. The adrenal rest is outlined by the arrows; it is composed of definitive and fetal adrenal cortex. At the asterisk, the channels of the extratesticular compartment of the rete testis intermingle with the adrenal rest. ED—efferent ductules; RT—extratesticular compartment of the rete testis. (H&E, 4x.)

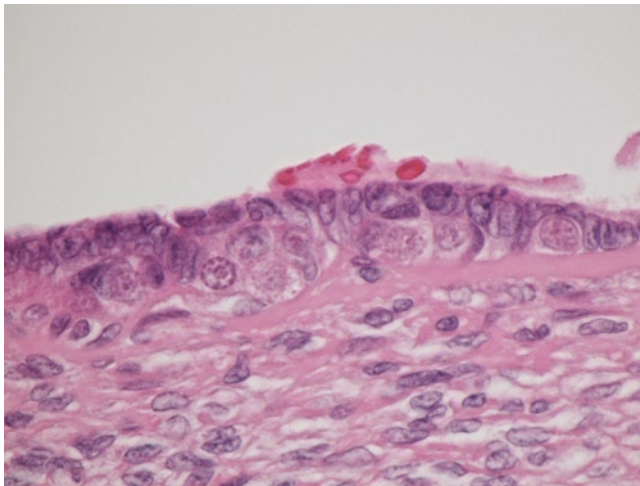


FIGURE 9-46. Ectopic germ cells in the cuboidal epithelium of the tunica vaginalis and in the tunica albuginea. The ectopic germ cells sometimes form clusters or may be single. They disappear with advancing gestational age. (H&E, 60x.)

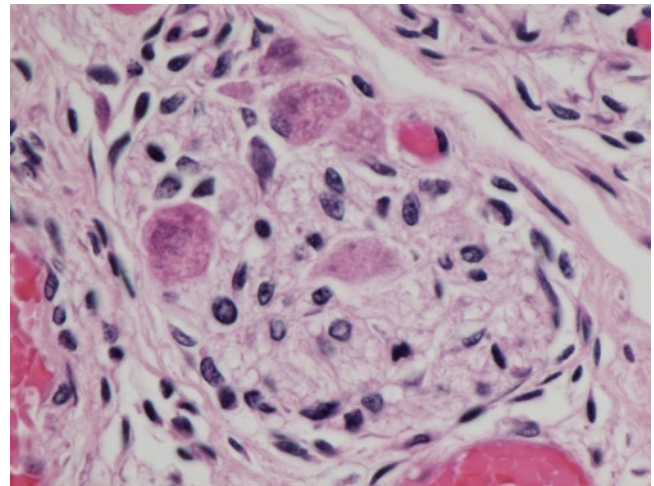


FIGURE 9-47. Ectopic Leydig cells in nerves of the paratesticular soft tissue near the hilum. These may be confused with ganglion cells. (H&E, 60x.)

Acknowledgments The author thanks Dr. Catherine T.-S. Chung from The Hospital for Sick Children, Toronto, Canada, for invaluable assistance in selecting microscopic slides for

photography, taking photomicrographs, and editing the manuscript.

References

1. Satoh M: Histogenesis and organogenesis of the gonad in human embryos. *J Anat* 1991, 177:85–107.
2. Jirásek JJ: *An Atlas of Human Prenatal Developmental Mechanics: Anatomy and Staging*. Boca Raton, FL: Parthenon; 2004.
3. Felix W: The development of the urinogenital organs. In *Human Embryology*. Edited by Keibel F, Mall, FP. Philadelphia: JB Lippincott; 1912:752–979.
4. van Wagenen G, Simpson, M: *Embryology of the Ovary and Testis Homo sapiens and Macaca mulatta*. New Haven, CT: Yale University Press; 1965.
5. O’Rahilly R: The timing and sequence of events in the development of the human reproductive system during the embryonic period proper. *Anat Embryol (Berl)* 1983, 166:247–261.
6. Cajaiba MM, Garcia-Fernandez E, Reyes-Mugica M, Nistal M: The spectrum of persistence of testicular blastema and ectopic testicular parenchyma: a possible result of focal delay in gonadal development. *Virchows Arch* 2007, 451:89–94.
7. Nistal M, Panigua, R: Non-neoplastic diseases of the testes. In *Urologic Surgical Pathology*, edn 2nd. Edited by Bostwick D, Cheng L. Philadelphia: Elsevier; 2008:616–755.
8. Falin LI: The development of genital glands and the origin of germ cells in human embryogenesis. *Acta Anat (Basel)* 1969, 72:195–232.
9. Fukuda T, Hedinger C, Groscurth P: Ultrastructure of developing germ cells in the fetal human testis. *Cell Tissue Res* 1975, 161:55–70.
10. Culty M: Gonocytes, the forgotten cells of the germ cell lineage. *Birth Defects Res C Embryo Today* 2009, 87:1–26.
11. Hermo L, Pelletier RM, Cyr DG, Smith CE: Surfing the wave, cycle, life history, and genes/proteins expressed by testicular germ cells. Part 1: background to spermatogenesis, spermatogonia, and spermatocytes. *Microsc Res Tech* 2010, 73:241–278.
12. Svechnikov K, Landreh L, Weisser J, et al.: Origin, development and regulation of human Leydig cells. *Horm Res Paediatr* 2010, 73:93–101.
13. Waters BL, Trainer TD: Development of the human fetal testis. *Pediatr Pathol Lab Med* 1996, 16:9–23.
14. Hadziselimovic F: *Adult and Pediatric Urology*, edn 2. Edited by Gillenwater J, Grayhack JT, Howards SS, Duckett JW. St Louis: Mosby; 1987:2173–2188.
15. Wartenberg H, Holstein AF, Vossmeier J: [Cytology of the prenatal development of human gonads. II. Electronmicroscopic studies on the cytogenesis of gonocytes and foetal spermatogonia in the testis]. *Z Anat Entwicklungsgesch* 1971, 134:165–185.
16. Wartenberg H: Human testicular development and the role of the mesonephros in the origin of a dual Sertoli cell system. *Andrologia* 1978, 10:1–21.
17. Gaskell TL, Esnal A, Robinson LL, et al.: Immunohistochemical profiling of germ cells within the human fetal testis: identification of three subpopulations. *Biol Reprod* 2004, 71:2012–2021.
18. Franke FE, Pauls K, Rey R, et al.: Differentiation markers of Sertoli cells and germ cells in fetal and early postnatal human testis. *Anat Embryol (Berl)* 2004, 209:169–177.
19. Helal MA, Mehmet H, Thomas NS, et al.: Ontogeny of human fetal testicular apoptosis during first, second, and third trimesters of pregnancy. *J Clin Endocrinol Metab* 2002, 87:1189–1193.
20. Yasuda Y: Testis. In *Atlas of Prenatal Histology*. Edited by Nishimura H. Tokyo: Izaku-Shoin; 1983:148–151.
21. Clermont Y: Renewal of spermatogonia in man. *Am J Anat* 1966, 118:509–524.
22. Willis R: *The Borderland of Embryology and Pathology*. London: Butterworth; 1958.
23. Hamilton W, Mossman HW: *Hamilton, Boyd, and Mossman’s Human Embryology*, edn 4. Baltimore: Williams and Wilkins; 1972.
24. Cerilli LA, Sotelo-Avila C, Mills SE: Glandular inclusions in inguinal hernia sacs: morphologic and immunohistochemical distinction from epididymis and vas deferens. *Am J Surg Pathol* 2003, 27:469–476.

10

Epididymis

Dale S. Huff and Eduardo D. Ruchelli

The primary function of the epididymis is to provide a conduit for the transport of sperm and seminiferous fluid from the rete testis to the vas deferens. However, the epididymis performs much more elaborate functions including the resorption of some of the fluid by the head of the epididymis, final maturation and development of motility in the body, and storage of sperm in the tail. Performance of these functions requires the development of an elaborate rostral to caudal gradient of epithelial specialization from the efferent ductules to the beginning of the vas deferens, which is not completed until puberty. Knowledge of the changing fetal histology described in this chapter aids in the understanding of the congenital anomalies of the epididymis that are seen in association with cryptorchidism [1], renal and ureteral anomalies, cystic fibrosis, and other underlying conditions.

Embryology

The early embryology of the genitourinary system and the mesonephric duct is described in Section IV, and the development of the rete testis and efferent ductules is described in Chapter 9. The development of the epididymis is one part of the rostral to caudal segmental differentiation of the mesonephric duct into its various components: the head, body, and tail of the epididymis; the vas deferens; the ampulla of the vas deferens; the seminal vesicles; and the ejaculatory ducts. This segmental differentiation is similar to that seen in the gastrointestinal tract and is under elaborate genetic control. The viability and maturation of all the structures is androgen dependent.

The efferent ductules and head of the epididymis are derived from the collecting ductules of five to 12 of the most rostral degenerating epigenital mesonephric nephrons. The body and tail of the epididymis are derived from the mesonephric duct. When the embryonic period closes at the end of the 10th postmenstrual week, the rudimentary epididymis is composed of five to 12 straight efferent ductules that will form the head. Each efferent ductule is attached to the rostral part of the mesonephric duct, which descends along the postero-lateral hilar border of the testis to the lower pole, then curves medially under the lower pole. The segment of the mesonephric duct from the junction with the efferent ducts to the lower pole of the testis will become the body of the epididymis. The segment that curves under the lower pole of the testis will become the tail of the epididymis.

Histologically, the mesonephric duct is lined by simple, nonciliated, columnar epithelium [2] and its wall is composed of concentric layers of undifferentiated mesenchyme that will become the circular muscular coat. In fetuses at 11 weeks gestation, the undifferentiated mesenchyme of the caudal end of the mesonephric duct becomes organized into concentric layers and this transformation extends rostrally into the epididymis. Cilia begin to appear in fetuses at approximately 11 to 12 weeks gestation [2].

During the fetal period, the simple straight efferent ductules and straight ductus epididymis become elaborately coiled with a rostral to caudal gradient in the degree of coiling, epithelial specialization, and thickness of the muscular coat. At 11 weeks gestation, the solid tubules of the epigenital mesonephric collecting ductules connect with the solid cords of the rete. This is called the *urogenital union*. The epigenital ductules are

now called the *efferent ductules* and the mesonephric duct is called the *ductus epididymis*. Each efferent ductule connects to the upper end of the ductus epididymis. The efferent ductules and their connections to the rete testis and to the ductus epididymis begin to develop lumens in the third trimester, a process that is not complete until after birth.

Histology

General Overview

The epididymis is the first segment of the excretory system of the testis. It is "C" shaped and fits around the upper pole, the postero-lateral or hilar margin, and the lower pole of the testis. The bulbous head (*caput*) of the epididymis is tightly attached to and pressed into the upper pole of the testis. The body (*corpus*) is joined to the hilar margin of the testis by a short mesentery, the *mesorchium*. The tail (*cauda*) curves under and is tightly fused to the lower pole of the testis by the fibrous remains of the testicular ligament and gubernaculum. The head is joined to the rete testis by the efferent ductules and the tail is continuous with the vas deferens. The head and all but the most caudal end of the body are intraperitoneal and are covered with a fibrous capsule similar to, but not as well developed as, the tunica albuginea of the testis. The capsule is covered by simple flat mesothelial epithelium derived from the visceral epithelium of the *processus vaginalis*. The caudal end of the body and the tail are retroperitoneal and are buried in the connective tissue remnants of the testicular ligament and gubernaculum [3,4]. The head is composed of five to 12 lobules called *coni vasculosi* and a second ill-defined region that connects the *coni vasculosi* with the body. Each of the *coni vasculosi* is composed of one extensively coiled efferent ductule. One end of each efferent ductule is connected to the extratesticular portion of the rete testis and the other end is connected to the ductus epididymis formerly the mesonephric duct. The *coni vasculosi* are separated by fibrous septa and the coils of the efferent ductules within the *coni vasculosi* are embedded in an interstitium of connective tissue. The body and tail of the epididymis are composed of the single coiled ductus epididymis, which is continuous caudally with the vas

deferens. The coils of the efferent ductules and ductus epididymis in the body and tail are all set in an interstitium of connective tissue.

The histology of the adult human epididymis has been extensively described [5–7]. The rostral to caudal gradient in specialization of epithelial histology and function in adults has been shown to be much more elaborate than previously thought and has been divided into eight segments: anterior and posterior efferent ductules; anterior, middle, and posterior body; and anterior and posterior tail [5]. The histological organization is similar throughout all the multiple segments of the epididymis. The epithelium lining the ductules lies upon a basement membrane that is surrounded from the inside out by spindle-shaped periductular myoid cells, an inconspicuous lamina propria, and a circular layer of smooth muscle. The epithelium is pseudostratified cuboidal to columnar and has stereocilia, but the epithelium varies in a rostral to caudal gradient. In the head the pseudostratified epithelium is composed of short cuboidal nonciliated cells and tall columnar cells with stereocilia. Five ultrastructurally distinct zones have been described within the ciliated epithelium lining the efferent ductules [6]. In the body, the pseudostratified columnar epithelium consists of four types of cells: tall columnar stereociliated principal cells, tall slender apical mitochondria-rich cells, clear cells, and basal cells. The length of the stereocilia varies gradually in a rostral to caudal gradient. They are longest at the rostral end of the ductus epididymis, where they nearly fill the lumen, and shortest at the caudal end of the tail. The thickness of the circular muscle coat varies in a rostral to caudal gradient; it is thinnest in the head and thickest in the tail. Longitudinal fibers appear in the tail [8].

Fetal Histology

The changing histology of the fetal epididymis is due to increased coiling, maturation of the epithelium, and development of the muscular coat, each of which varies in a rostral to caudal gradient. The histological plan of the fetal epididymis is similar to that of the adult. The primitive pseudostratified columnar epithelium lies on a basement membrane that is surrounded by one or two layers of spindle-shaped myoid or myofibroblastic cells, which is in turn surrounded by a cuff of swirled primitive mesenchyme. The primitive mesenchyme differentiates into the lamina propria, the circular smooth muscle coat, and the adventitia. The lamina propria and adventitia are inconspicuous but the smooth muscle becomes prominent and important. Immunohistochemical studies of inhibin [9], androgen and estrogen receptors [10], epithelial membrane antigen, cytokeratins, and estradiol-related protein receptors [11] in the fetal epididymis have been reported. The histology of the fetal epididymis in a large series of cases from multiple gestational ages has not been reported.

At 13 weeks through the developmental process known as tubulogenesis [12], the distal ends of the efferent ducts close to their attachment to the ductus epididymis begin to coil and form the *coni vasculosi*. The proximal ends at the rete remain straight and parallel. Each coiled duct forms a pyramidal lobule with its apex at the testicular hilum and its base toward the mesonephric duct. These are the *coni vasculosi* and collectively they form the head of the epididymis.

The body and tail begin as the uncoiled mesonephric duct, which becomes the uncoiled ductus epididymis. When the efferent ductules begin to coil, the ductus epididymis of the body and tail also elongates and coils through coiling tubulogenesis. The coiling follows a rostral to caudal gradient and is most extensive in the efferent ductules, less extensive in the body, and least extensive in the tail. This coiling results in a rostral to caudal gradient in the diameter of the epididymis so that of the head is the largest and that of the tail is the smallest. The coiling of the epididymis continues throughout fetal life and postnatal life, and causes a dramatic increase in the length of the tube. Histologically increased coiling results in increased numbers of ductular cross-sections that become more closely packed.

Prior to approximately the middle of the second trimester, coiling is not extensive. The diameter of the head is small, only slightly larger than that of the body. It is bent away from the upper pole of the testis and is not attached to it. The ductus epididymis of the body and tail shows even less coiling and is gently undulating. The simple ciliated columnar epithelium of the embryonic efferent ductules and ductus epididymis has differentiated into primitive pseudostratified stereociliated cuboidal and columnar epithelium, which is similar from the head to the tail. The primitive periductular mesenchyme is thinnest in the head and thickest in the tail, but shows no evidence of smooth muscle differentiation (see Figs. 10-1-10-4).

After the middle of the second trimester, the size of the head of the epididymis grows rapidly due to the extensive coiling of the efferent ductules. Within a few weeks the head enlarges into a cap-shaped structure that is bent over and pressed into the upper pole of the testis to which it becomes tightly attached. The gestational age at which the head is attached to the upper

pole of the testis has not been established with certainty; the attachment probably varies by several weeks from fetus to fetus but in some cases occurs shortly after 20 weeks gestation. The attachment of the head of the epididymis to the upper pole of the testis is best visualized in complete longitudinal sagittal sections of the testis and epididymis. The increased coiling results in more numerous and more tightly packed ductular cross-sections. The epithelium continues to mature but remains primitive and similar throughout the length of the epididymis. Smooth muscle has been reported to appear in the primitive periductular mesenchyme at approximately 19 to 20 weeks gestation [2]. However, the time of appearance of smooth muscle differentiation may be variable and in some cases is not seen until later in gestation (see Figs. 10-5-10-11).

During the second trimester, coiling continues to increase throughout the epididymis. By the end of the second or beginning of the third trimester, the primitive epithelium differentiates into epithelium that is characteristic of epididymis. The epithelium throughout the epididymis increases in thickness. Principal cells and apical mitochondria-rich cells are present in the head, body, and tail of the epididymis by 24 to 27 weeks gestation [11]. Basal cells and clear cells may be difficult to recognize in routine histological sections. In the head, the outline of the lumen becomes irregular and the epithelium is pseudostratified cuboidal and columnar. The tall columnar cells have stereocilia while the cuboidal surface cells are not ciliated. Smooth muscle differentiation within the primitive periductular mesenchyme is not typically recognizable in routine sections of the head. In the body, the outline of the lumen is smooth and round. The mucosa is thicker than in the head and the epithelium is composed of tall, wide stereociliated principal cells and tall, slender, dark apical mitochondria-rich nonciliated cells. As is the case in the head, smooth muscle differentiation within the primitive periductular mesenchyme is usually not recognizable in the body. In the tail, the mucosa is similar to but thinner than that in the body. The periductular cuff of primitive mesenchyme is thicker than in the body and head. Circular smooth muscle cells that are thin and delicate differentiate within the periphery of the primitive periductular mesenchyme. Longitudinal bundles of large smooth muscle cells appear around the tail of the epididymis and the proximal vas deferens. These longitudinal bundles are, for the most part, separate from the smooth muscle differentiating within the periductular mesenchyme. However, in some areas they swirl around and blend into the periductal and vascular smooth muscle. These longitudinal bundles are not much discussed or illustrated in the literature, but may be the longitudinal muscle referred to above (see Figs. 10-12-10-18) [8].

By the end of the third trimester the epithelial maturation has increased. The dramatic rostral to caudal gradient in the length of cilia, with very long cilia rostrally and short cilia caudally, seen in adults is not prominent in fetuses. Differentiation of smooth muscle within the primitive periductal mesenchyme of the tail and caudal portion of the body continues. Smooth muscle differentiation may not be present in the mid and rostral body and head of the epididymis at the end of the third trimester (see Figs. 10-19-10-24).

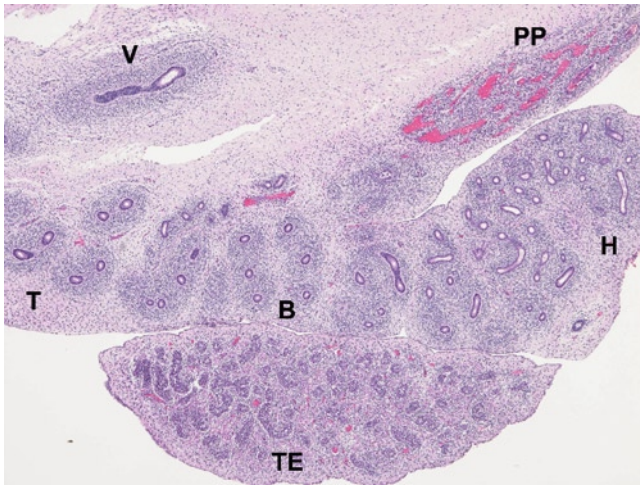


FIGURE 10-1. Epididymis at 17 weeks gestation. This image is a longitudinal section of the epididymis and testis. The epididymis is very primitive and the thin connective tissue capsule is visible. The head of the epididymis (H) is bent away from the testis (TE). The lobules formed by the individual efferent ductules are faintly visible in the head. The efferent ductules are slightly coiled. The body (B) and tail (T) of the epididymis are even less coiled than the efferent ductules and the path of the gently curved mesonephric duct, which is differentiating into the epididymis, can be seen in the body and tail. The vas deferens (V) is straight. The peritubular swirls of dark blue primitive mesenchyme, which will become the stroma and smooth muscle of the epididymis, are seen around the tubules. PP—pampiniform plexus. (Hematoxylin and eosin [H&E], 4 \times .)

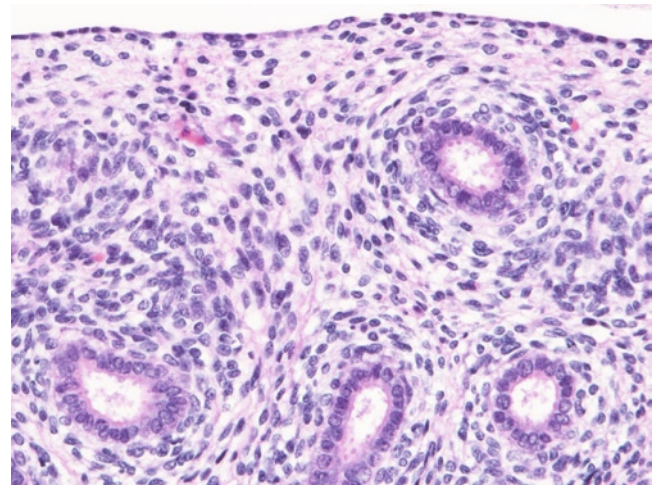


FIGURE 10-2. Efferent ductules forming the head of the epididymis at 17 weeks gestation. The visceral mesothelial epithelium of the processus vaginalis covers the thin fibrous capsule, similar to the visceral mesothelial epithelium of the tunica vaginalis covering the tunica albuginea of the testis seen in Figure 10-1. The ductules are lined by crowded simple columnar epithelium and are surrounded by concentric swirls of primitive mesenchyme. The luminal surface is slightly irregular, and apical blebs and occasional stereocilia are recognizable in this imperfectly preserved section. (H&E, 40 \times .)

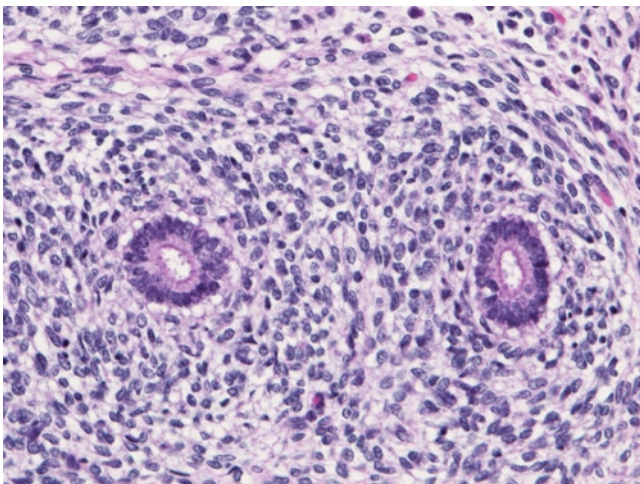


FIGURE 10-3. Body of the epididymis at 17 weeks gestation. This image is a higher magnification of the body of the epididymis shown in Figure 10-1. The histology of the body is nearly identical to that of the head. The cross-sections of the tubule are slightly smaller and more round than those of the head. The simple cuboidal epithelial cells are very crowded. The luminal surface is sharply outlined and terminal bars appear. (H&E, 40 \times .)

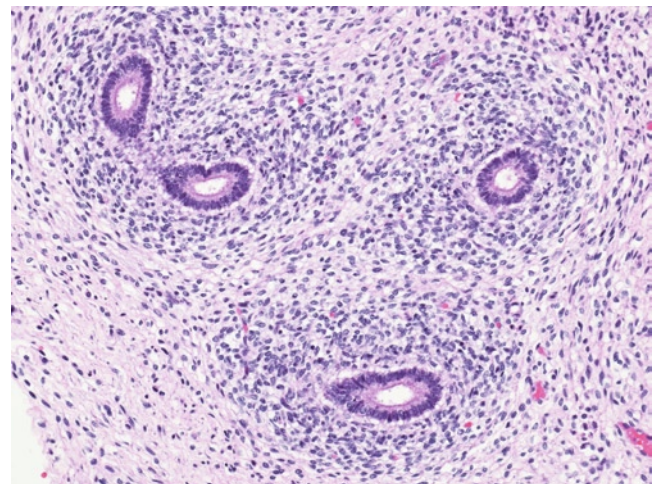


FIGURE 10-4. Tail of the epididymis at 17 weeks gestation. This image is a higher magnification of the tail seen in Figure 10-1. The histological appearance of the tail is identical to that of the body. (H&E, 20 \times .)

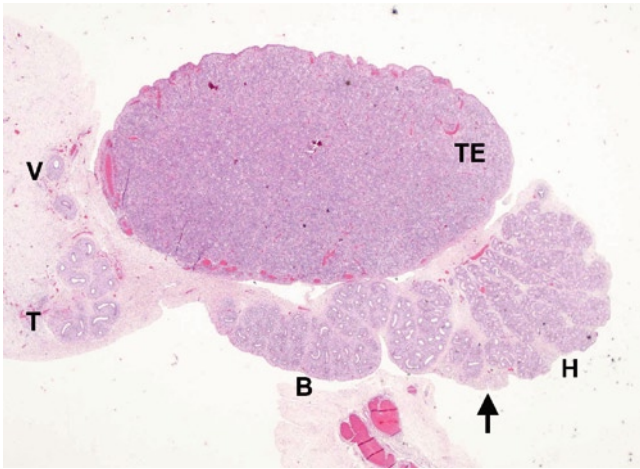


FIGURE 10-5. Epididymis at 22 weeks gestation. This image shows a longitudinal section of the entire epididymis and testis. The enlarged head (H) is bent around and pressed against the upper pole of the testis (TE). Coiling of the efferent ductules in the head has increased dramatically. The pyramidal coni vasculosi of five or six efferent ductules are sharply outlined by septa. The testicular end of each is only slightly coiled and, therefore, narrow while the opposite end is very coiled and, therefore, wide. The periductular mesenchymal cuffs are indistinct. The demarcation (*arrow*) between the head and body (B) is vague. The coiling of the body has increased but not so dramatically as that in the head. The peritubular mesenchymal cuffs are thick and condensed. Due to the extensive coiling, the diameters of the head and body have increased. The tail (T) is less coiled than the body but the peritubular mesenchymal cuffs of the tail and the vas deferens (V) are thicker and more condensed than in the body. (H&E, 1 \times .)

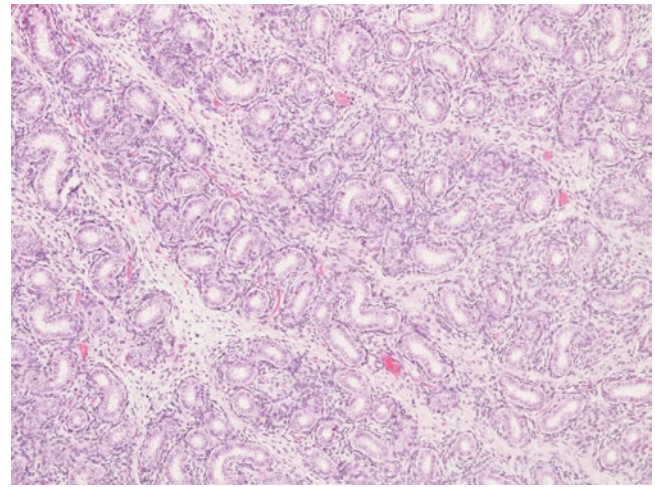


FIGURE 10-6. Coni vasculosi of the head of the epididymis at 22 weeks gestation. This image is a higher magnification of the coni vasculosi shown in Figure 10-5. The cross-sections of the tightly coiled efferent ductules are closely packed and back to back. The periductular primitive mesenchyme is thin. (H&E, 10 \times .)

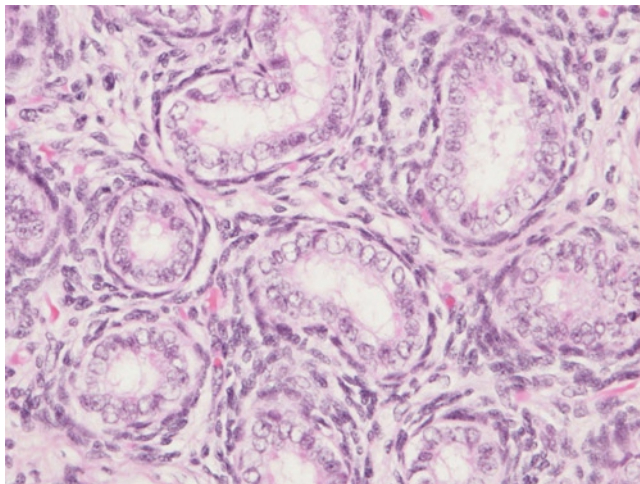


FIGURE 10-7. Coni vasculosi of head of epididymis at 22 weeks gestation. This is image a higher magnification of the efferent ductules shown in Figure 10-6. The nuclei of the cuboidal epithelial cells are irregular in size and shape, and are becoming pseudostratified. A layer of spindled myoid cells one or two cells thick surrounds the epithelium and a thin irregular layer of primitive mesenchyme surrounds the layer of myoid cells. (H&E, 40 \times .)

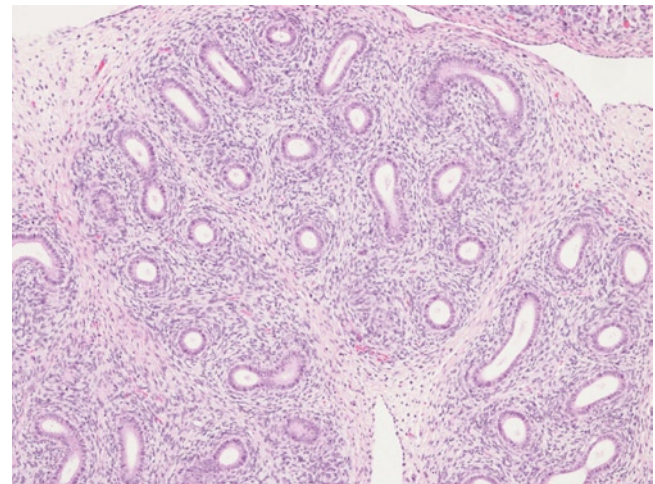


FIGURE 10-8. Body of the epididymis at 22 weeks gestation. This image is a higher magnification of the body shown in Figure 10-5. The cross-sections of the ductus epididymis are more widely spaced than those of the efferent ductules because the ductus epididymis is less coiled than the efferent ductules. The primitive periductular mesenchyme is much thicker than that of the efferent ductules. (H&E, 10 \times .)

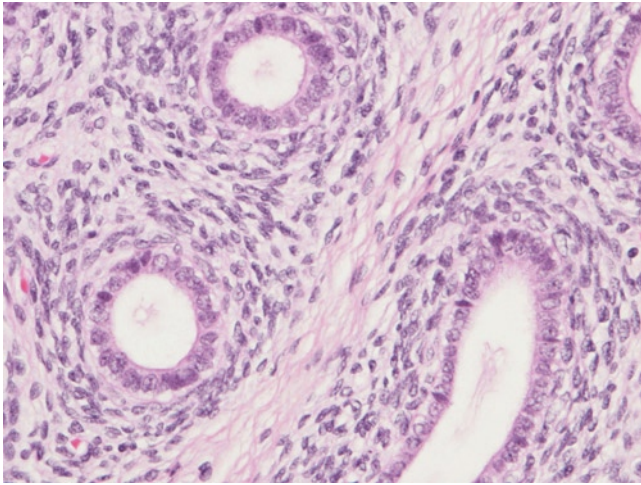


FIGURE 10-9. Body of epididymis at 22 weeks gestation. This image is a higher magnification of the body shown in Figure 10-8. Occasional tall thin columnar cells are interspersed between the tightly packed cuboidal cells, especially in the tubule in the right lower corner. These cells may be primitive apical mitochondria-rich cells. The peritubular mesenchyme is composed of spindle cells but smooth muscle differentiation is not seen (H&E, 40 \times .)

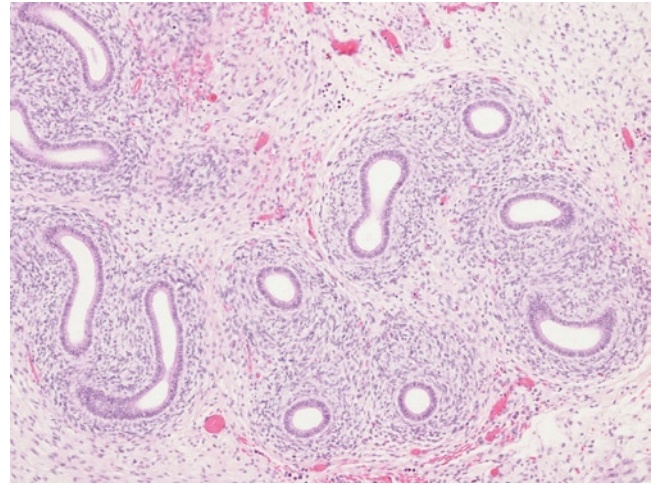


FIGURE 10-10. Tail of epididymis at 22 weeks gestation. This image is a higher magnification of the tail shown in Figure 10-5. The tail is less coiled than the body and peritubular mesenchyme is thicker than that of the body. (H&E, 10 \times .)

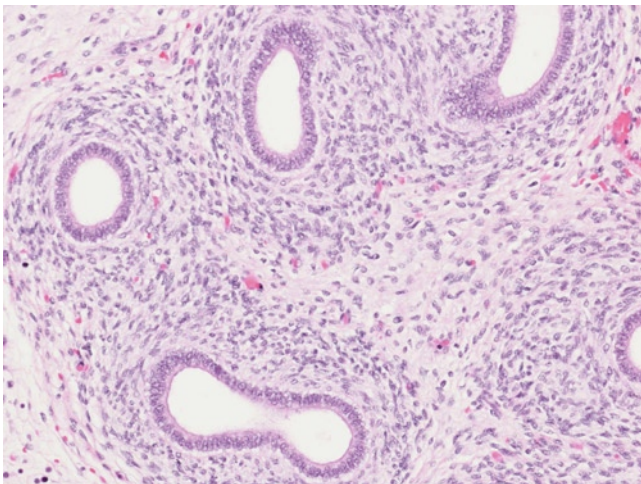


FIGURE 10-11. Tail of the epididymis at 22 weeks gestation. This image is a higher magnification of the tail shown in Figure 10-10. The epithelium is similar to that of the body but lacks the tall thin columnar cells seen in the body. (H&E, 40 \times .)

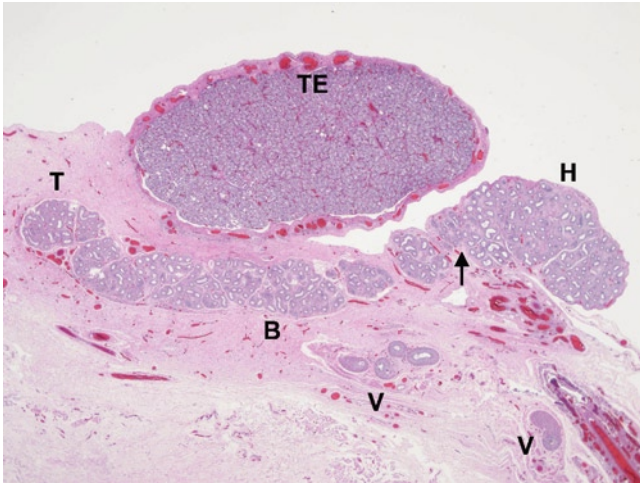


FIGURE 10-12. Epididymis at 34 weeks gestation. This image shows a longitudinal section of the entire epididymis and testis. The head (H) of the epididymis is bent away from the upper pole of the testis. The head of this epididymis is less well developed than the epididymis at 22 weeks gestation, shown in Figure 10-5. This figure illustrates the wide range of the timing of developmental events. Otherwise, little has changed with the low-magnification appearance of the epididymis. The arrow indicates the indistinct junction between the head and body of the epididymis. B—body of epididymis; T—tail of epididymis; TE—testis; V—vas deferens. (H&E, 1×.)

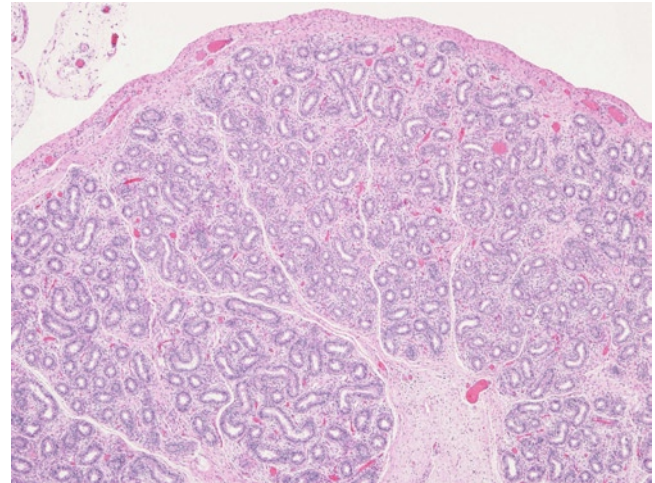


FIGURE 10-13. Head of epididymis at 34 weeks gestation. This image is a longitudinal section of the head shown in Figure 10-12. The coni vasculosi are separated by fine interlobular septa. The efferent ductules are more extensively coiled than previously and their profiles are curved. (H&E, 4×.)

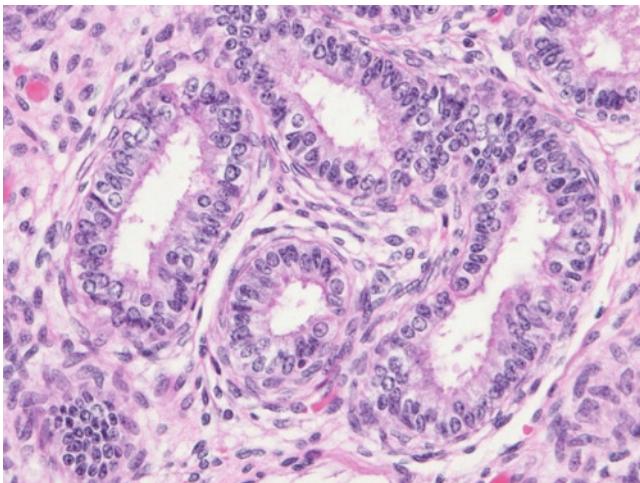


FIGURE 10-14. Efferent ductules at 34 weeks gestation. This image is a higher magnification of the efferent ductules shown in Figure 10-13. The epithelium is becoming more columnar and pseudostratified. The broad columnar cells are principal cells and occasional tall thin columnar cells reach from the basement membrane to the lumen. These cells are apical mitochondrial-rich cells. Some stereocilia are preserved and the outline of the lumen is slightly irregular. There is a peritubular layer of spindle-shaped myoid cells and a substantial layer of peritubular mesenchyme. (H&E, 40×.)

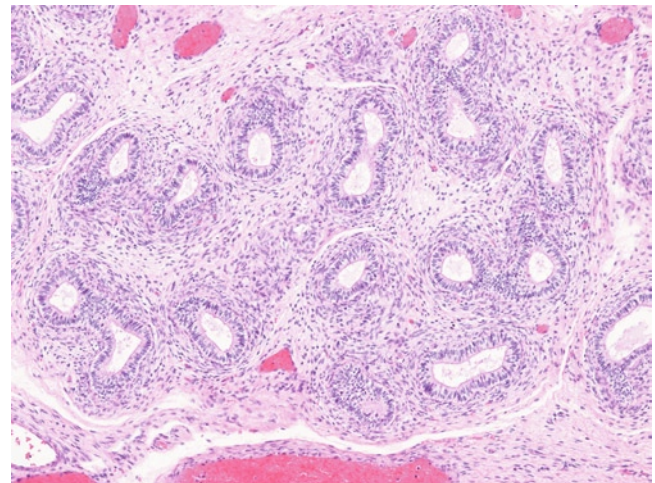


FIGURE 10-15. Body of epididymis at 34 weeks gestation. This image is a higher magnification of the body seen in Figure 10-12. The ductule is lined by pseudostratified columnar epithelium. The mesenchyme forms a dense layer of spindle cells, but histologically identifiable smooth muscle is not present. (H&E, 10×.)

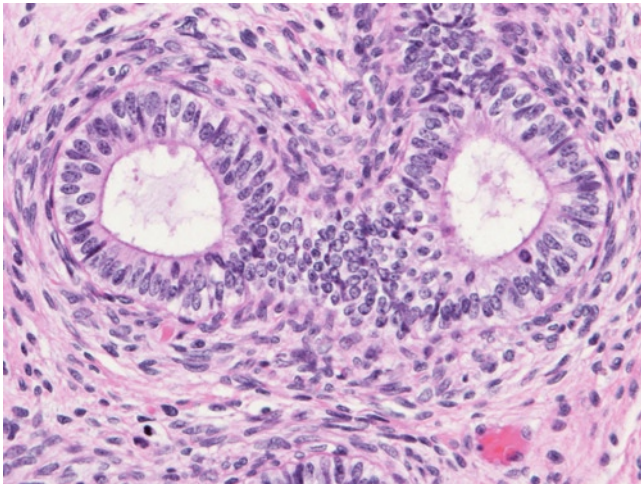


FIGURE 10-16. Body of epididymis at 34 weeks gestation. This image is a higher magnification of the body seen in Figure 10-15. Compared with efferent ductules of the head, the ductus of the body has a more regular round lumen, a taller pseudostratified columnar epithelium with the nuclei mostly confined to the lower half of the thickness of the epithelium, and more apical mitochondria-rich cells. The pseudostratified tall columnar epithelium rests on a thin basement membrane. Of the four types of epithelial cells described in the adult, principal cells and apical mitochondria-rich cells are present. Two types of apical-mitochondria rich cells are seen: the tall slender dark cells that extend from the basement membrane to the lumen and the small cells at the lumen that contain dark oval nuclei in the upper half of the epithelium. The remainder are principal cells. Clear cells and basal cells are difficult to identify in this preparation. Smooth muscle is not present. (H&E, 40 \times .)

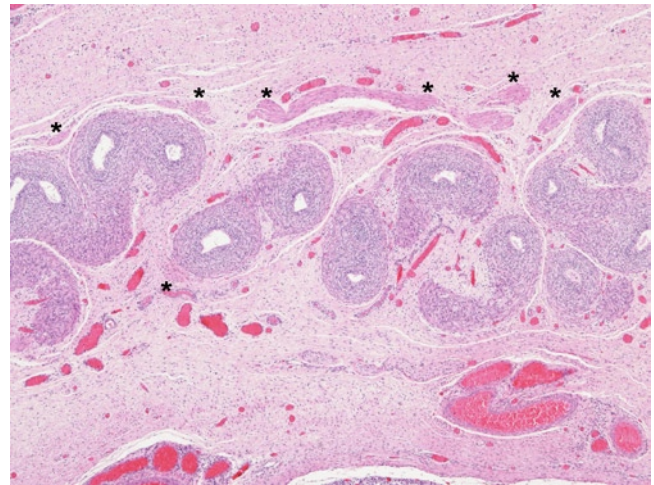


FIGURE 10-17. Tail of epididymis at 34 weeks gestation. This image is a higher magnification of the tail seen in Figure 10-12. This photomicrograph is from the distal end of the tail close to its junction with the vas deferens; therefore, it is only slightly coiled. Smooth muscle is present. The most well-differentiated smooth muscle is organized into broad bundles (asterisks) that partially surround the outside of the epididymis like a capsule and extend around the outside of the proximal vas deferens. The muscle cells forming the bundles are unusually large. They sometimes swirl around the ductule and adjacent vessels, and blend in with the outer layers of the periductular mesenchyme and the vascular smooth muscle. The significance of this smooth muscle is not clear. The peritubular cuffs of spindled mesenchymal cells are very condensed and much thicker than those in the body but only the outer layers are recognizable smooth muscle. (H&E, 10 \times .)

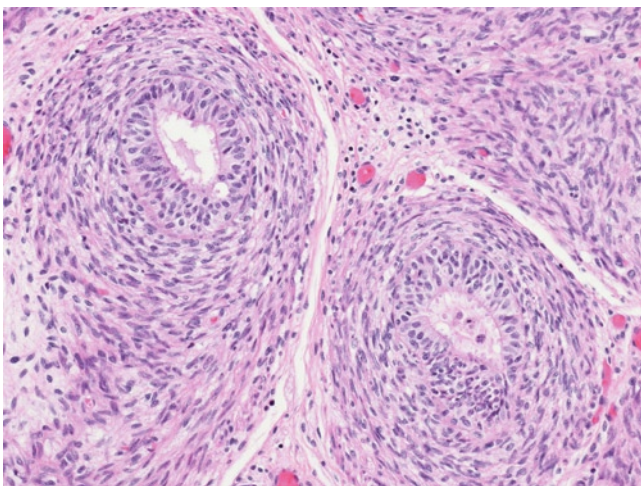


FIGURE 10-18. Tail of epididymis at 34 weeks gestation. This image is a higher magnification of the tail seen in Figure 10-17. The multilayered pseudostratified epithelium is cuboidal rather than columnar, as in the body. Numerous stereocilia are preserved in this section. The peritubular mesenchyme is vaguely divided into two or three layers, the outer layer of which is recognizable as smooth muscle. (H&E, 40 \times .)

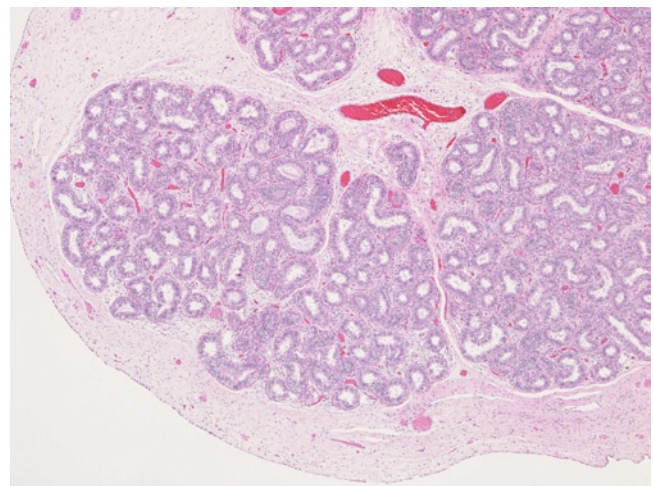


FIGURE 10-19. Head of epididymis at 39 weeks gestation. The epididymis is surrounded by a fibrous capsule that is covered by a layer of simple flat mesothelial epithelium. The conical vasculosa are separated by connective tissue septa and the efferent ductules are tightly coiled. The periductular mesenchymal cuffs are thicker and more condensed than in younger fetuses. (H&E, 4 \times .)

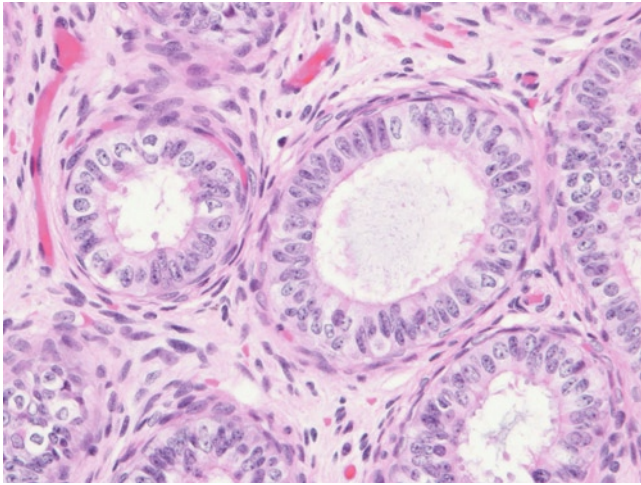


FIGURE 10-20. Efferent ductules of the head of the epididymis at 39 weeks gestation. This image is a higher magnification of the efferent ductules seen in Figure 10-19. The lumens are large and slightly irregular. The epithelium is thin and single layered in some foci. A few apical mitochondria-rich cells of both types are present. Smooth muscle differentiation is recognizable in the peritubular mesenchyme. (H&E, 40 \times .)

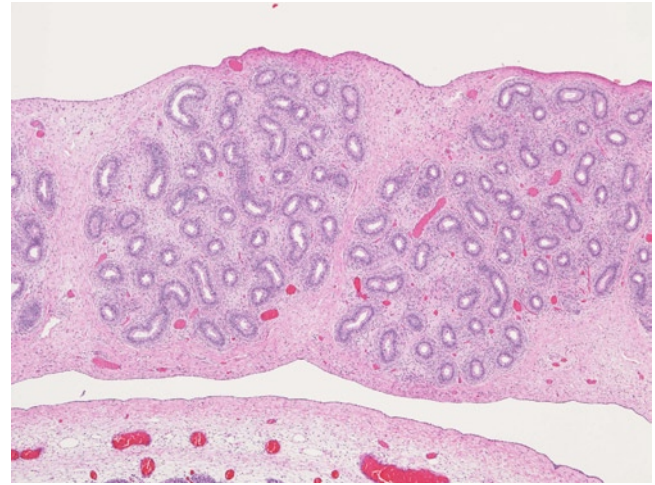


FIGURE 10-21. Body of epididymis seen at 39 weeks gestation. This image of the body is from the same specimen shown in Figures 10-19 and 10-20. The fibrous capsule is thick and covered by mesothelium. The duct of the epididymis is more tightly coiled than previously and the lobules are separated by septa. (H&E, 4 \times .)

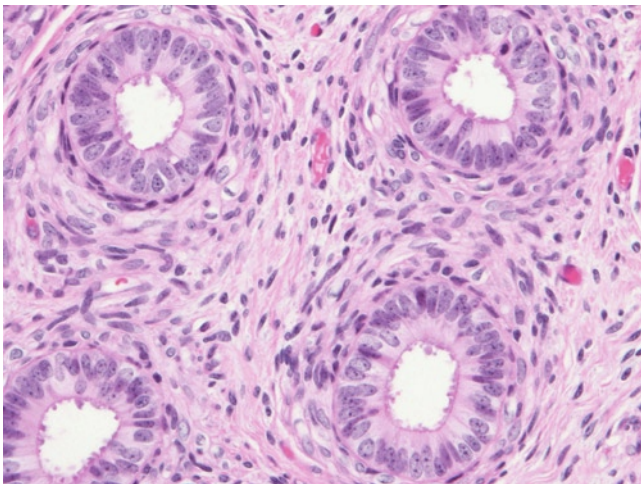


FIGURE 10-22. Body of the epididymis at 39 weeks gestation. This image is a higher magnification of the head seen in Figure 10-21. The lumens are smaller and more round than those in the head. Principal, apical mitochondria-rich cells, and basal cells are present. The basement membrane and peritubular myoid cells are prominent and smooth muscle cells are recognized in the peritubular mesenchyme. (H&E, 40 \times .)

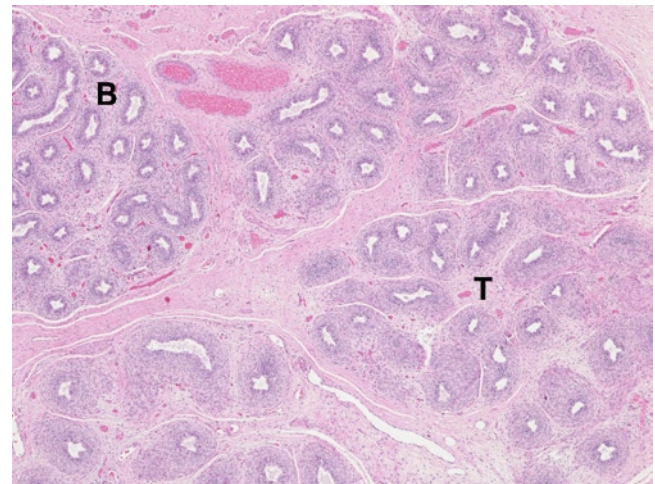


FIGURE 10-23. Tail of epididymis at 39 weeks gestation. This image of the tail is from the same case seen in Figure 10-19. This section is from the gradual transition from the body (B) in the upper left to the tail (T) in the lower half of the picture. Smooth muscle is seen in the periphery of the periductular mesenchyme of some cross-sections of the duct. (H&E, 4 \times .)

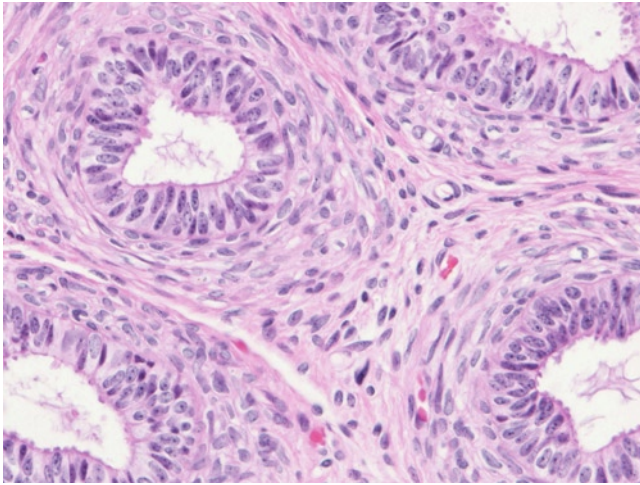


FIGURE 10-24. Tail of epididymis at 39 weeks gestation. This image is a higher magnification of the tail seen in Figure 10-23. The lumen is lined by pseudostratified cuboidal and columnar epithelium with stereocilia. The distinction between principal and apical mitochondria-rich cells is not as clear as in the body. (H&E, 40 \times .)

References

1. De Miguel MP, Marino JM, Gonzalez-Peramato P, *et al.*: Epididymal growth and differentiation are altered in human cryptorchidism. *J Androl* 2001, 22:212–225.
2. Felix W: The development of the urinogenital organs. In *Human Embryology*. Edited by Keibel F, Mall FP. Philadelphia: JB Lippincott; 1912:752–979.
3. Hadziselimovic F: *Cryptorchidism*. Berlin: Springer-Verlag; 1983.
4. Hadziselimovic F, Kruslin E: The role of the epididymis in descensus testis and the topographical relationship between the testis and epididymis from the sixth month of pregnancy until immediately after birth. *Anat Embryol (Berl)* 1979, 155:191–196.
5. Dacheux JL, Belghazi M, Lanson Y, Dacheux F: Human epididymal secretome and proteome. *Mol Cell Endocrinol* 2006, 250:36–42.
6. Yeung CH, Cooper TG, Bergmann M, Schulze H: Organization of tubules in the human caput epididymidis and the ultrastructure of their epithelia. *Am J Anat* 1991, 191:261–279.
7. Trainer T: The testis and excretory duct system. In *Histology for Pathologists*, edn 3. Edited by Mills SE. Philadelphia: Lippincott Williams & Wilkins; 2007:943–963.
8. Ladman A: The male reproductive system. In *Histology*, edn 3. Edited by Greep RO, Weiss L. New York: McGraw-Hill; 1973: 847–890.
9. Nistal M, Gonzalez-Peramato P, De Miguel MP: Immunodetection of inhibin in the human testis and epididymis during normal development and in non-tumoural testicular lesions. *Reprod Fertil Dev* 2010, 22:558–563.
10. Shapiro E, Huang H, Masch RJ, *et al.*: Immunolocalization of androgen receptor and estrogen receptors alpha and beta in human fetal testis and epididymis. *J Urol* 2005, 174:1695–1698; discussion 8.
11. Regadera J, Cobo P, Paniagua R, *et al.*: Immunohistochemical and semiquantitative study of the apical mitochondria-rich cells of the human prepubertal and adult epididymis. *J Anat* 1993, 183:507–514.
12. Joseph A, Yao H, Hinton BT: Development and morphogenesis of the Wolffian/epididymal duct, more twists and turns. *Dev Biol* 2009, 325:6–14.

11

Vas Deferens

Linda M. Ernst, Eduardo D. Ruchelli, and Dale S. Huff

The vas deferens, also known as the *ductus deferens* or *spermatic duct*, is a tubular conduit that begins at the tail of the epididymis and ends by joining the excretory duct of the seminal vesicle to form the ejaculatory duct. During the in situ inspection on an autopsy of a preterm infant or fetus, prior to testicular descent, the vas deferens is grossly recognized as a thin structure traveling from the tail of the epididymis over the ipsilateral umbilical artery toward the midline and terminating posterior to the urinary bladder at the base of the prostate. After testicular descent, the vas deferens can be seen emanating from the internal inguinal ring and terminating again at the prostatic base.

The histology of the vas deferens in the fetus and neonate is not well studied. However, there are some significant changes, especially in the structure of the muscular wall, that occur over the fetal period. This chapter reviews the development and histological changes in the vas deferens over gestation.

Embryology

The vas deferens is derived from the mesonephric duct. As reviewed in the embryology section at the beginning of Section IV, at approximately the seventh gestational week, two curves divide the mesonephric duct into three segments. The two most caudal segments, distal to the tail of the epididymis, become the vas deferens and terminate in the urogenital sinus.

Histology

The fetal vas deferens is a tubular structure with an epithelial-lined lumen and a mesenchymal or muscular coat. In the adult vas deferens, a thin layer of connective tissue containing elastic fibers is seen beneath the epithelium, but these fibers are lacking in infants and children [1]. On hematoxylin and eosin (H&E)-stained sections of the fetal vas deferens, the epithelium appears to be in close contact with the muscular coat, with little to no intervening connective tissue present.

In the early midtrimester, the vas deferens is thin with a round to ovoid lumen (see Figs. 11-1 and 11-2). The epithelium is well developed and appears as a columnar to pseudostratified columnar epithelium. The apical border of the lining cells displays a prominent eosinophilic terminal bar, a marker of the stereocilia present on the surface of these cells. Unfortunately, the stereocilia may appear sloughed or are not easily seen in sections from autopsy material, as preservation is typically suboptimal. The muscular coat of the vas deferens in this early stage of gestation is present; however, it appears as concentric layers of closely packed, spindle-shaped mesenchymal cells without significant smooth muscle differentiation (see Figs. 11-1 and 11-2). As gestation progresses into the late midtrimester to early third trimester, the muscular coat develops further and thickens (see Figs. 11-3 and 11-4). The vas deferens widens in diameter. The epithelium remains unchanged; however, the mesenchyme of the muscle wall begins to take on a more eosinophilic appearance

as smooth muscle differentiation progresses. Near term, the muscular wall of the vas deferens becomes quite thick and spindle-shaped cells show definitive smooth muscle differentiation. The formation of distinct layers of muscle also becomes apparent (see Figs. 11-5 and 11-6), although some research has stated that evidence of separate layers of muscle is not apparent until after birth [2]. In the mature, adult vas deferens, there are inner and outer longitudinal muscle layers and a middle

oblique or circular layer [1]. The appearance of the lining epithelium of the vas deferens remains constant throughout gestation as a columnar to pseudostratified-columnar epithelium with stereocilia (see Fig. 11-7). A layer of basal cells is described as present in the mature vas deferens [1], but they are difficult to appreciate in routine fetal sections. Ultrastructural studies have identified at least four different cell types within the epithelium of the mature vas deferens [1].

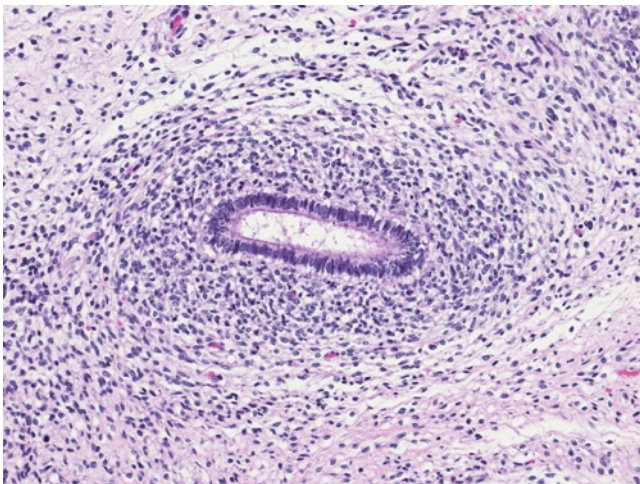


FIGURE 11-1. Vas deferens at 17 weeks gestation. Early in the midtrimester, the vas deferens is characterized by a central lumen surrounded by mesenchyme with very little well-defined smooth muscle differentiation. The lining of the vas deferens consists of a columnar epithelium with a well-defined terminal bar and cilia on the apical surface. (H&E, 20 \times .)

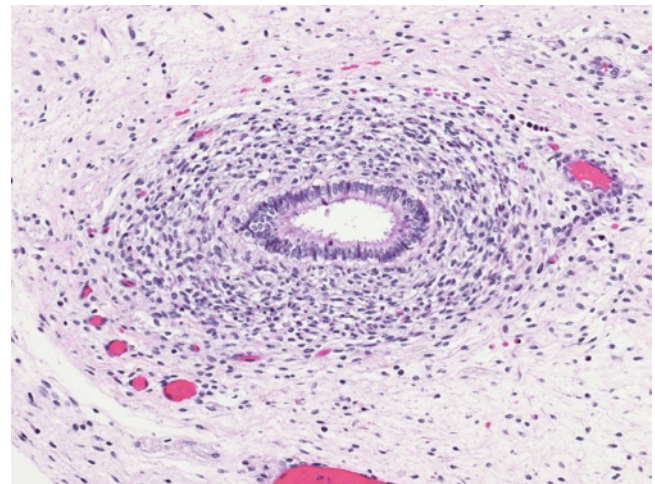


FIGURE 11-2. Vas deferens at 20 weeks gestation. The epithelial lining has not changed significantly, but the surrounding mesenchyme is slightly more organized with increased cytoplasm noted in the spindle-shaped cells. (H&E, 20 \times .)

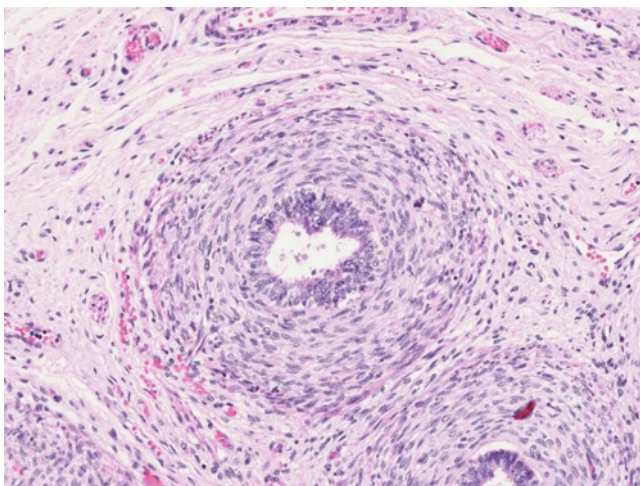


FIGURE 11-3. Vas deferens at 24 weeks gestation. By the late midtrimester, the wall of the vas deferens appears more organized and shows clear smooth muscle differentiation. The epithelium appears as pseudostratified columnar epithelium with cilia. (H&E, 20 \times .)

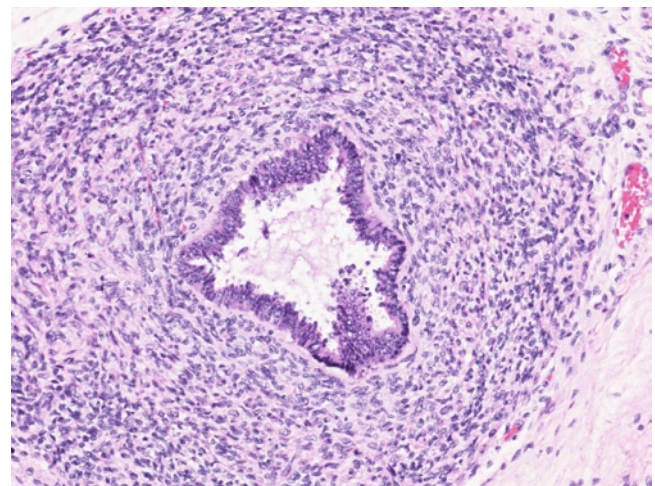


FIGURE 11-4. Vas deferens at 29 weeks gestation. This section is from the ampullary region of the vas deferens and the lumen is slightly larger and irregular. The epithelium is pseudostratified columnar and cilia are not well preserved. The muscular coat is thick and smooth muscle differentiation can be seen. (H&E, 20 \times .)

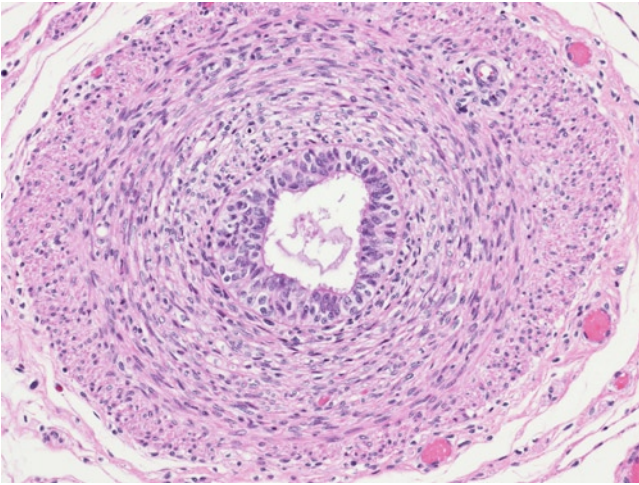


FIGURE 11-5. Vas deferens at 34 weeks gestation. At this gestational age, the wall of the vas deferens exhibits well-developed smooth muscle and the beginning of different layers can be identified. The epithelium is pseudostratified columnar with cilia noted on the apical surface. Basal cells can be seen along the basement membrane. (H&E, 20 \times .)

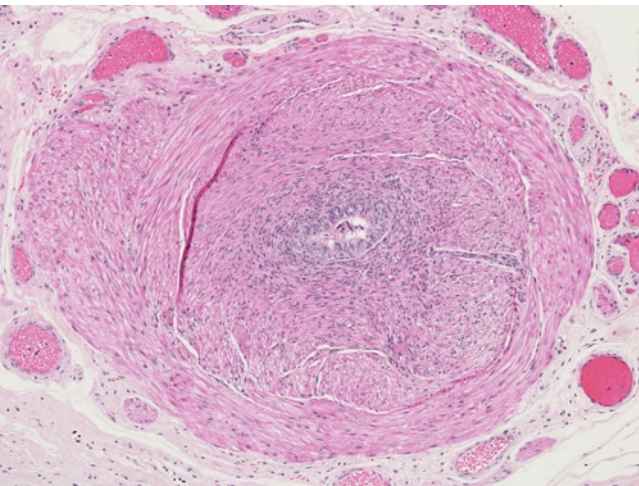


FIGURE 11-6. Vas deferens at 38 weeks gestation. This lower power image shows that the vas deferens is larger at term. Note the well-defined smooth musculature of the wall, now divided into distinct layers. (H&E, 10 \times .)

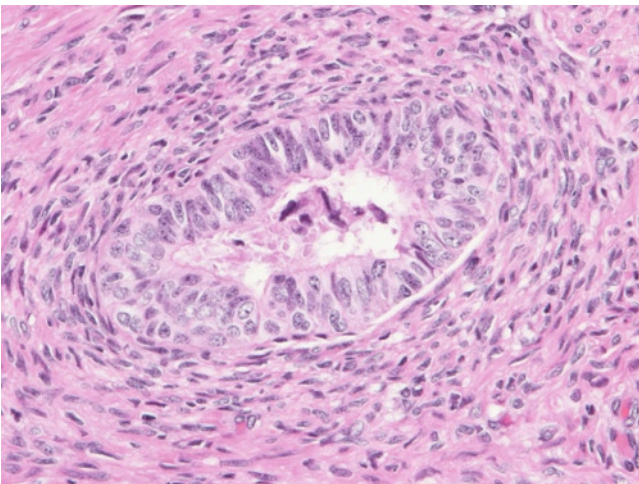


FIGURE 11-7. Vas deferens at 38 weeks gestation. This higher power image shows the luminal lining characterized by a pseudostratified columnar epithelium with poorly preserved cilia. (H&E, 40 \times .)

The proximal portion of the vas deferens has a round to ovoid lumen (see Figs. 11-1–11-3) but, distally, in the area anatomically known as the ampulla, the lumen of the vas deferens widens. In sections of the distal vas deferens, this

wider lumen can be appreciated with small outpouchings of the lumen, imparting a somewhat stellate appearance to the shape of the lumen (see Figs. 11-4, 11-8, and 11-9, and compare with 12-8).

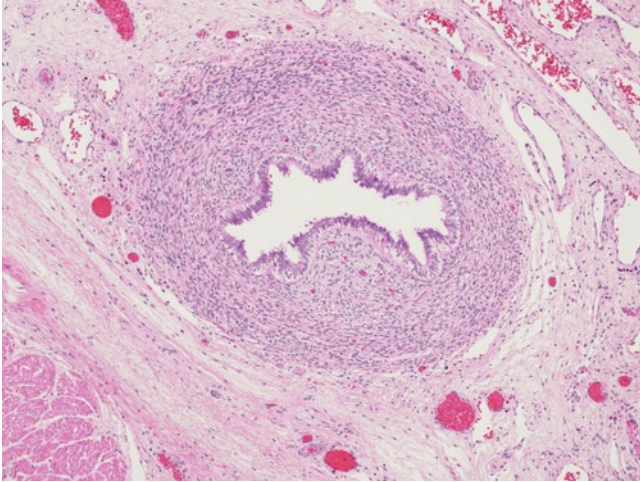


FIGURE 11-8. Ampulla of the vas deferens at 34 weeks gestation. This low-power image shows the larger, wider lumen of the vas deferens in the ampullary region. Note the outpouchings of the lumen characteristic of the ampulla. (H&E, 10 \times .)

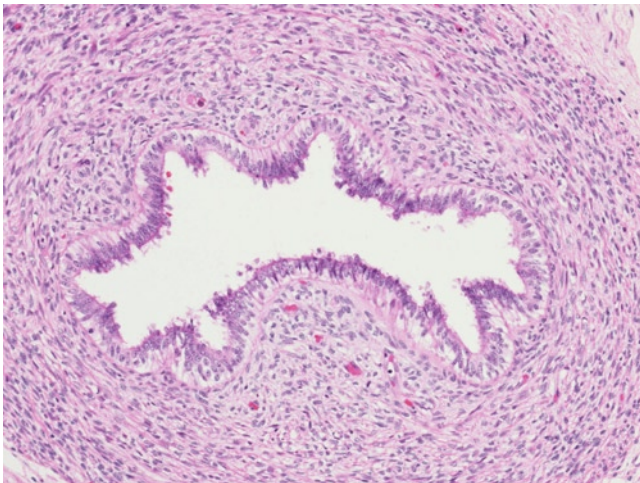


FIGURE 11-9. Ampulla of the vas deferens at 34 weeks gestation. This higher power image shows the widened and more complex ampullary lumen. Note that the epithelium is not distinctly different from the more proximal vas deferens. Basal cells and stereocilia can be appreciated. (H&E, 20 \times .)

References

1. Trainer T: Testis and excretory duct system. In *Histology for Pathologists*, edn 3. Edited by Mills SE. Philadelphia: Lippincott Williams & Wilkins; 2007:943–963.
2. Dixon JS, Jen PY, Gosling JA: Structure and autonomic innervation of the human vas deferens: a review. *Microsc Res Tech* 1998, 42:423–432.

12

Seminal Vesicle

Linda M. Ernst, Eduardo D. Ruchelli, and Dale S. Huff

There are three accessory glands of the male genital system: the seminal vesicles, the prostate and the bulbourethral glands. The seminal vesicles are paired structures on the posterolateral aspect of the base of the bladder. Their main function is to secrete fluid that will form part of the semen; secretions of the seminal vesicles contain nutrients for the spermatozoa such as fructose, as well as other proteins, enzymes, and mucus [1]. In fetal life, since spermatozoa are not yet developed, the physiological functions of the seminal vesicles are not necessary for the maintenance of life, but proper development of all the components of the male genital tract is important for future fertility. Aberrations of the proper development of the seminal vesicles such as agenesis, fusion, duplication, hypoplasia, diverticulum, and cysts [2] can be seen during fetal life, and can occur in association with other genitourinary tract anomalies due to the close embryological origin of these complex tissues. Therefore, knowledge of the normal development and histological appearance of the seminal vesicle during fetal life can be useful. This chapter reviews the embryology of the seminal vesicles and highlights the histological features of the fetal seminal vesicles at various points in gestation.

Embryology

The three accessory glands of the male genital system—the seminal vesicles, the prostate, and the bulbourethral glands—originate at the most caudal end of the mesonephric duct, where it joins the endodermally-derived pelvic urethra. The seminal vesicles begin to develop in the 10th to 12th weeks as bilateral, dorsolateral outpouchings from the mesonephric duct proximal to the prostatic outpouchings, at the angle between the vertical and horizontal portions of the duct [3,4]. By the 13th week, the outpouchings enlarge and distal constrictions are visible that represent the beginning of the developing ejaculatory ducts [4], which will receive both the ampulla of the distal vas deferens and ipsilateral seminal vesicle. Further development of the seminal vesicles occurs in fetal life as described below.

Histology

General Overview

The overall appearance of the seminal vesicle is that of a coiled, tubular structure. The wall is composed of an epithelial layer, lamina propria, and muscularis. The mucosa of the adult seminal vesicle is extensively folded and alveolus-like [5]. While these mucosal convolutions do begin to develop in fetal life and appear fairly significant by term, they

do not reach the complexity seen in adulthood. The mature seminal vesicle epithelium consists of a layer of luminal columnar, secretory cells with microvilli and an underlying layer of basal cells. Adult columnar epithelial cells contain lipofuscin pigment [5], which is not a feature seen in fetal seminal vesicles. The lamina propria is

the connective tissue layer beneath the basement membrane of the epithelium and contains connective tissue elements and blood vessels. The outer coat of the mature seminal vesicle is comprised of a thin external, longitudinal smooth muscle layer and a thicker, internal circular smooth muscle layer[5].

Fetal Development/Histology

By 15 weeks gestation, the seminal vesicle anlage becomes “kinked” and consists of a medial, horizontal portion and a lateral, vertical portion [4]. In the early midtrimester, the lumen of the seminal vesicle shows only occasional diverticula, folding, or outpouchings, but significant folding of the epithelium has not occurred yet (see Fig. 12-1 and 12-2). The surrounding mesenchyme appears to be undifferentiated and consists of haphazardly arranged spindle-shaped cells (see Fig. 12-2). Later in the midtrimester, the seminal vesicle is more coiled and the lumen develops more epithelial convolutions, especially noticeable in the distal half (see Fig. 12-3) [4]. In addition, the mesenchyme surrounding the lumen matures and early formation of the lamina propria and muscularis is seen (see Fig. 12-4). The epithelium appears as a simple columnar to pseudostratified columnar type (see Fig. 12-5).

In the early third trimester, the coiling of the seminal vesicle and folding of the epithelium increases (see Fig. 12-6). The surrounding muscularis thickens and takes on a more eosinophilic appearance as smooth muscle differentiation also increases. The lamina propria is distinct beneath the epithelium, containing tightly packed spindle cells without eosinophilia in their cytoplasm (see Fig. 12-7). The epithelium may still appear pseudostratified, but the formation of two distinct layers can be seen as some cells along the basement membrane take on the appearance of basal cells (see Fig. 12-8). As the third trimester progresses toward term, the epithelial folding increases to involve the majority of the organ with the most prominent folding seen at term (see Figs. 12-9–12-12). The epithelial differentiation into basal and columnar cells also becomes more apparent late in gestation.

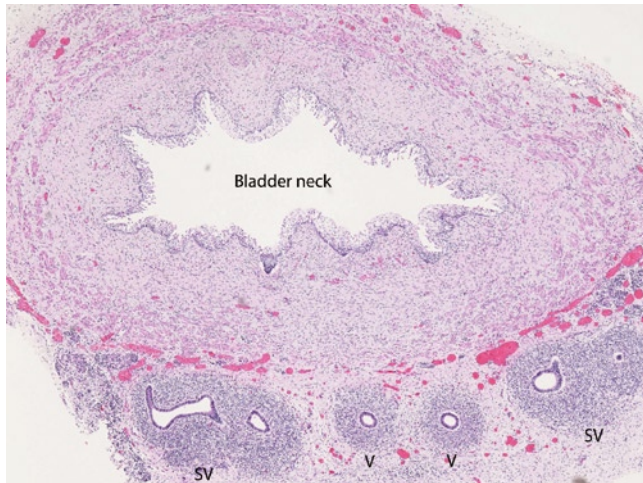


FIGURE 12-1. Seminal vesicle at 17 weeks gestation. The architecture of the seminal vesicles (SV) appears to be similar to the ampulla of the vas deferens (V). The lumen shows minimal outpouchings. The surrounding mesenchyme is immature with little definitive smooth muscle differentiation. (Hematoxylin and eosin [H&E], 4×.)

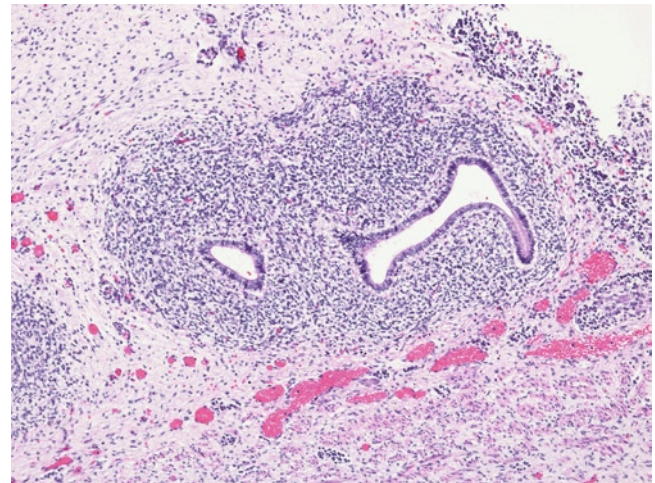


FIGURE 12-2. Seminal vesicle at 17 weeks gestation. This image shows a higher power view of the seminal vesicle. The lumen shows minimal outpouchings and the surrounding mesenchyme is immature with little definitive smooth muscle differentiation. (H&E, 10×.)



FIGURE 12-3. Seminal vesicle at 24 weeks gestation. This low-power image shows the overall architecture of the seminal vesicles (SV) with increased coiling, especially distally. U—urethra. (H&E, 1 \times .)

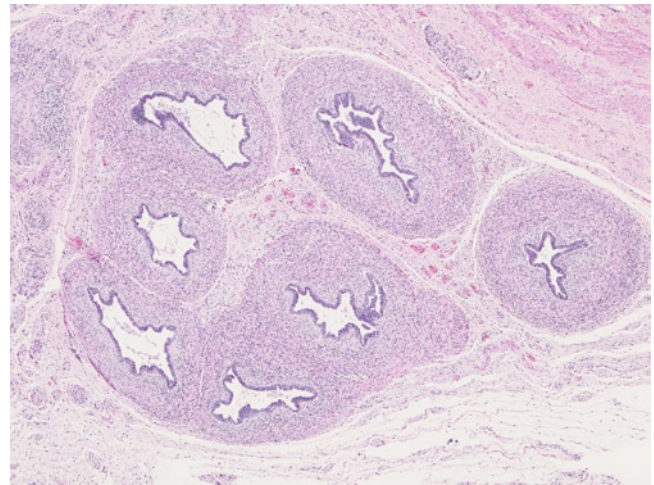


FIGURE 12-4. Seminal vesicle at 24 weeks gestation. This low-power image shows the overall architecture of the seminal vesicle with increased coiling. The epithelium shows increased outpouchings as well. The surrounding mesenchyme appears to show two indistinct layers with an inner, less-differentiated mesenchyme layer (lamina propria) and the outer layer showing more smooth muscle differentiation (muscularis). (H&E, 4 \times .)

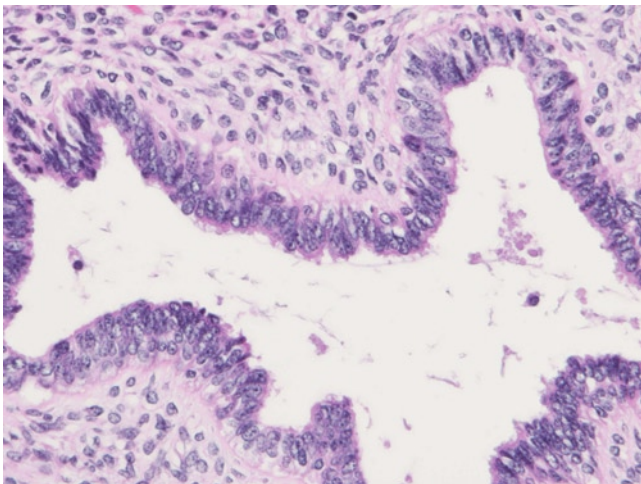


FIGURE 12-5. Seminal vesicle at 24 weeks gestation. This high-power image highlights the epithelium of the seminal vesicle, which appears columnar and pseudostratified. (H&E, 40 \times .)

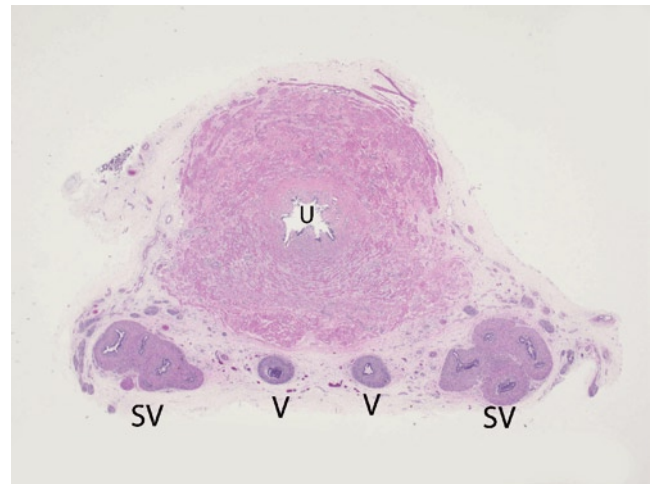


FIGURE 12-6. Seminal vesicle at 29 weeks gestation. This low-power image shows the overall coiled architecture of the seminal vesicles (SV), the increasing definition of the wall, and the relationship with the vas deferens (V) and urethra (U). (H&E, 1 \times .)

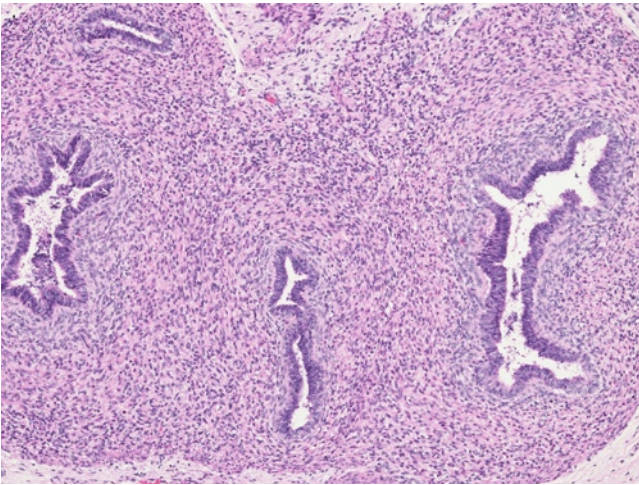


FIGURE 12-7. Seminal vesicle at 29 weeks gestation. This image highlights the development of the wall of the seminal vesicle. The lamina propria and muscularis are more easily appreciated, and the epithelium continues to show folds. (H&E, 10 \times .)

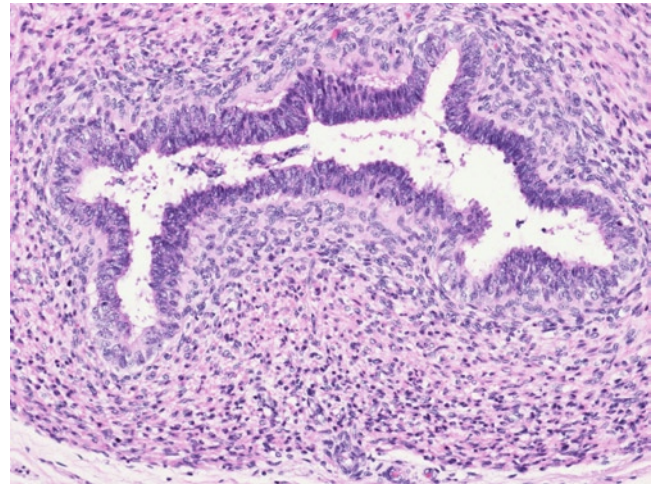


FIGURE 12-8. Seminal vesicle at 29 weeks gestation. This higher power view highlights the epithelium, which still appears partially pseudostratified. A hint of two populations of epithelial cells with a basal layer, and a more superficial layer, is seen. (H&E, 20 \times .)

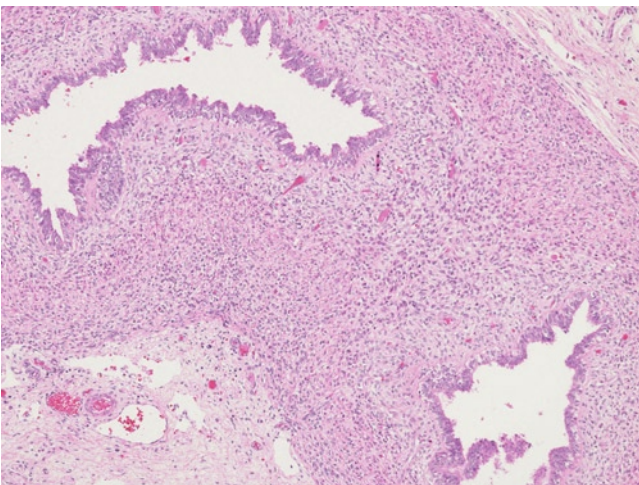


FIGURE 12-9. Seminal vesicle at 34 weeks gestation. This low-power image shows the coiled seminal vesicle with slightly more complex epithelial folding. (H&E, 10 \times .)

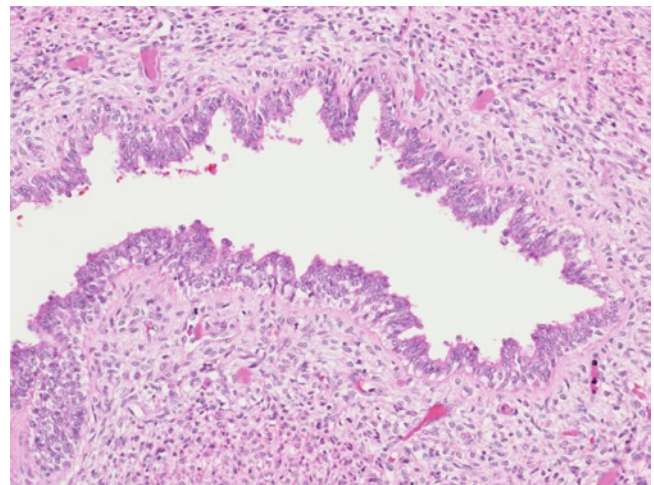


FIGURE 12-10. Seminal vesicle at 34 weeks gestation. Epithelial folding is more complex and the distinction between basal epithelial cells and apical cells is more obvious. (H&E, 20 \times .)

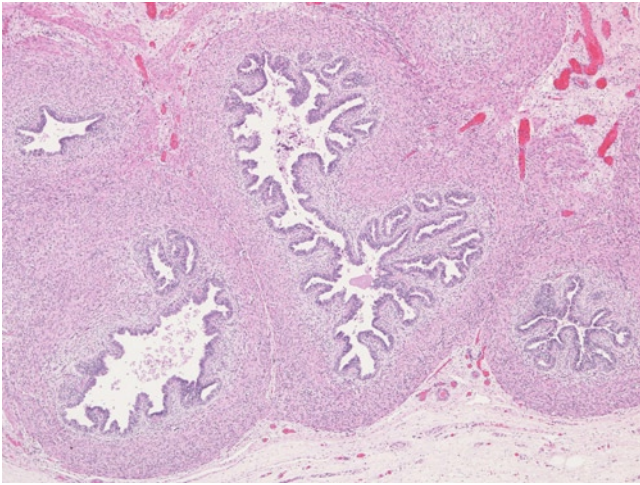


FIGURE 12-11. Seminal vesicle at 38 weeks gestation. This low-power image shows the coiled nature of the seminal vesicle and, by term, the most complex folding of the epithelium is appreciated. Note the eosinophilic appearance of the muscularis and the paler appearing lamina propria. (H&E, 4 \times .)

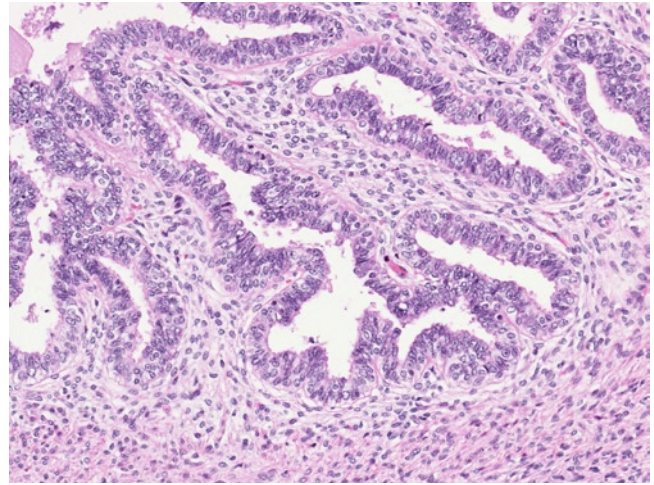


FIGURE 12-12. Seminal vesicle at 38 weeks gestation. In this higher power image of the epithelium, note the paler basal cells and columnar luminal cells with secretions present in the lumen. (H&E, 20 \times .)

References

1. Huggins C, Scott W, Heinen JJ: Chemical composition of human semen and of the secretions of the prostate and seminal vesicles. *Am J Physiol* 1942, 136:467–473.
2. Arora SS, Breiman RS, Webb EM, et al.: CT and MRI of congenital anomalies of the seminal vesicles. *AJR Am J Roentgenol* 2007, 189:130–135.
3. Schoenwolf GC, Larsen WJ: *Larsen's Human Embryology*, edn 4. Philadelphia: Churchill Livingstone/Elsevier; 2009.
4. Brewster SF: The development and differentiation of human seminal vesicles. *J Anat* 1985, 143:45–55.
5. Trainer T: Testis and excretory duct system. In *Histology for Pathologists*, edn 3. Mills SE, ed. Philadelphia: Lippincott Williams & Wilkins; 2007:943–963.

13

Prostate Gland

Linda M. Ernst, Eduardo D. Ruchelli, and Dale S. Huff

There are three accessory glands of the male genital system: the seminal vesicles, the prostate gland, and the bulbourethral glands. The prostate gland is the largest of these three glands. Its main purpose is to store prostatic secretions and, when needed, expulse those secretions, which form part of the ejaculate. In fetal life, the physiological functions of the prostate gland are not necessary for the maintenance of life, but proper development of all the components of the male genital tract is important for future fertility.

The prostate gland has both epithelial and stromal components that can be recognized histologically, and the early development of these components is seen during fetal life. Aberrations of the proper development of the prostate gland can be seen in some syndromes, such as androgen insensitivity syndrome, prune belly syndrome, and posterior urethral valves [1]. Therefore, knowledge of the proper development and histological appearance of the prostate gland during fetal life can be useful. This chapter highlights the histological features of the fetal prostate at various points in gestation.

Embryology

The three accessory glands of the male genital system—the seminal vesicles, the prostate gland, and the bulbourethral glands—originate at the most caudal end of the mesonephric duct, where it joins the endodermally derived pelvic urethra. Under the inductive influence of the surrounding mesenchyme, multiple evaginations of the urethral endoderm begin the formation of the prostate gland in the 10th week [2]. These epithelial evaginations elongate and bifurcate in a tightly regulated process known as *branching morphogenesis* [3], which produces the ducts and acini of the prostate gland. The factor or factors secreted by the mesenchyme that induce prostatic development are still the subject of scientific investigation, but the process of prostatic development and growth is known to be androgen-dependent [4]. Initially, there are at least five endodermal outgrowths consisting of solid cords of epithelial tissue [2]. The cords develop lumens in the 11th week and, by branching morphogenesis, form the ducts and acini. By the 15th week, secretory activity of the prostate gland begins. The prostatic fibromuscular stroma is derived from the mesenchyme surrounding the epithelial components that differentiates into the smooth muscle and connective tissue of the prostate [2].

The paramesonephric ducts largely regress in the male, except for the cranial and caudal ends. The caudal end of the fused paramesonephric ducts frequently remains and is incorporated into the developing prostate, where it is known as the *prostatic utricle*. The definitive embryological origin of the prostatic utricle is a matter of scientific debate. Origin from the urogenital sinus alone or urogenital sinus in combination with the paramesonephric ducts has been considered [5,6]. The prostatic utricle can appear as a solid cord of cells; however, it frequently acquires a lumen and can be cystically dilated [7,8]. The lining cells typically appear as a stratified squamous epithelium.

The bilateral bulbourethral glands, also known as Cowper's glands, further develop caudal to the prostatic origin as additional endodermal buds from the pelvic urethra. The surrounding mesenchyme gives rise to the connective tissue and smooth muscle elements of the glands.

Histology

General Overview

The prostate gland is situated anatomically at the distal end of the bladder, surrounding the prostatic urethra, and in fetuses it is typically recognized as a small, firm, ovoid structure at the base of the bladder. On cross-section, the fetal prostate gland has a discoid to round shape and is surrounded by an ill-defined capsule. Skeletal muscle can be seen at the anterior aspect of the gland and likely contributes to the capsule (see Fig. 13-1) [1]. The prostate is composed of epithelial and

mesenchymal/stromal elements. The stroma generally is more prominent in the anteromedial portions of the gland, producing the convexity of the gland anteriorly. Epithelial elements consist of ducts in the central portion of the gland and acini more peripherally. As gestation progresses, the ducts and acini continue to develop by increasing in number and volume within the prostate gland.

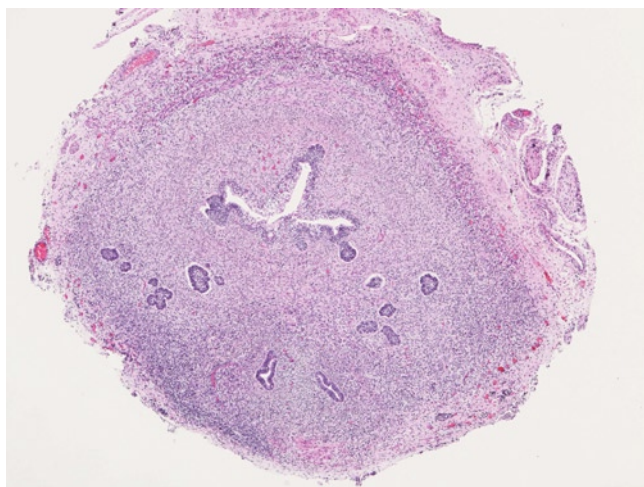


FIGURE 13-1. Prostate gland at 17 weeks gestation. This low-power image of the fetal prostate gland shows a paucity of epithelial elements in the anterior portion (*upper*) and a few simple ductal structures posteriorly (*lower*). The prostatic urethra is present in the center of the gland. The stroma appears to be basophilic and shows minimal smooth muscle differentiation. An ill-defined connective tissue capsule is present with a band of skeletal muscle noted anteriorly. The bilateral ejaculatory ducts can be seen in the lower aspect of the section. (Hematoxylin and eosin [H&E], 4 \times .)

Epithelial Elements

The most centrally located, endodermally derived, epithelial-lined structures in the prostate gland are the ductal elements of the prostate gland, which drain to the prostatic urethra. The ducts consist of the branching epithelial structures that predominate in the central portion of the prostate gland around the prostatic urethra. In fact, in the early midtrimester, ducts compose most of the epithelial elements and are most prominent in the posterior aspect of the prostate (see Fig. 13-1) [1]. The ducts are canulated and have a double-layered epithelium consisting of a cuboidal basal cell layer and a cuboidal to columnar luminal cell lining (see Fig. 13-2).

The prostatic urethra is the largest epithelial-lined lumen that can be seen in cross-sections including the central portion of the gland. Within the prostatic urethra, there is an elongated median elevation or ridge that protrudes into the lumen known as the *verumontanum* or *seminal colliculus*. The verumontanum produces the inverted-U shape of the prostatic urethra seen on cross-sections (see Fig. 13-3). The verumontanum is an important area of the urethra that receives the ejaculatory ducts and can be seen in most fetal specimens (see Figs. 13-3 and 13-4). Also seen at the verumontanum is the prostatic utricle, which appears typically as an ovoid,

tubular structure with a stratified squamous epithelium, believed to be squamous metaplasia related to estrogen-related hormone effect (see Fig. 13-5) [1]. Squamous metaplasia is also seen in the urethra, especially along the posterior wall (see Fig. 13-6) [9] and is also seen in ducts (see Fig. 13-7). As the prostate gland matures, foci of squamous metaplasia become less prominent.

As gestation progresses, the epithelial component of the prostate gland occupies a larger proportion of the gland, increasing the gland-stroma ratio. In one histologic study of 107 fetal prostates at various gestational ages, three stages for the development of the ductal and acinar structures are described [9]. The bud stage from approximately 20 to 30 weeks gestation is characterized by simple solid cellular buds at the ends of the ducts (see Figs. 13-8–13-14). The next stage, between 31 and 36 weeks gestation, is known as the bud-tubular stage, in which cellular buds and acinar structures in small collections are identified (see Figs. 13-15–13-17). Near term, the acinotubular stage is recognized by acinotubular clusters arranged in lobules. Acinar development is seen best at the periphery of the gland, while ductal elements are still seen in the central regions (see Figs. 13-18–13-20).

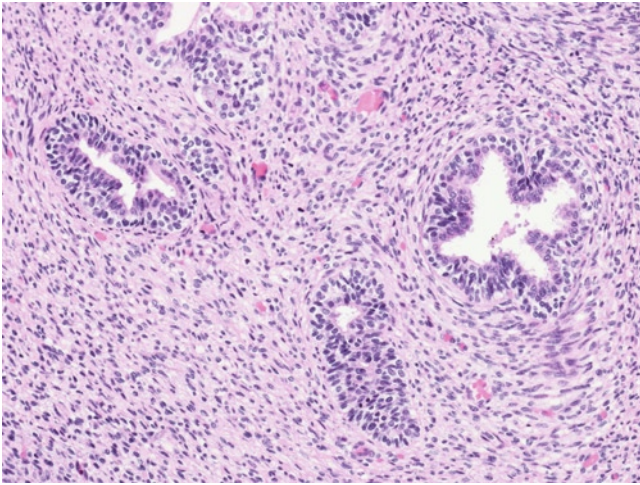


FIGURE 13-2. Prostate gland at 17 weeks gestation. This higher power image of the prostate gland highlights the ductal elements. They are mostly round to focally stellate in shape and lined by a double-layered epithelium consisting of cuboidal basal cells and slightly more columnar apical cells. The surrounding mesenchymal stroma is composed of ovoid to spindle-shaped cells in a sheet-like arrangement with minimal smooth muscle differentiation. (H&E, 20 \times .)

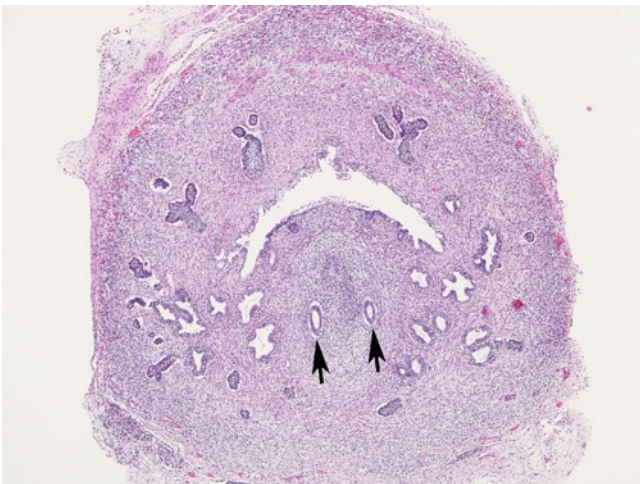


FIGURE 13-3. Verumontanum at 17 weeks gestation. This low-power image of the prostate gland shows the verumontanum, which bulges into the prostatic urethra. The bilateral ejaculatory ducts (arrows) are visible within the verumontanum. (H&E, 4 \times .)



FIGURE 13-4. Ejaculatory ducts at 17 weeks gestation. This higher power image shows the ejaculatory ducts with a pseudostratified columnar epithelium. (H&E, 20 \times .)

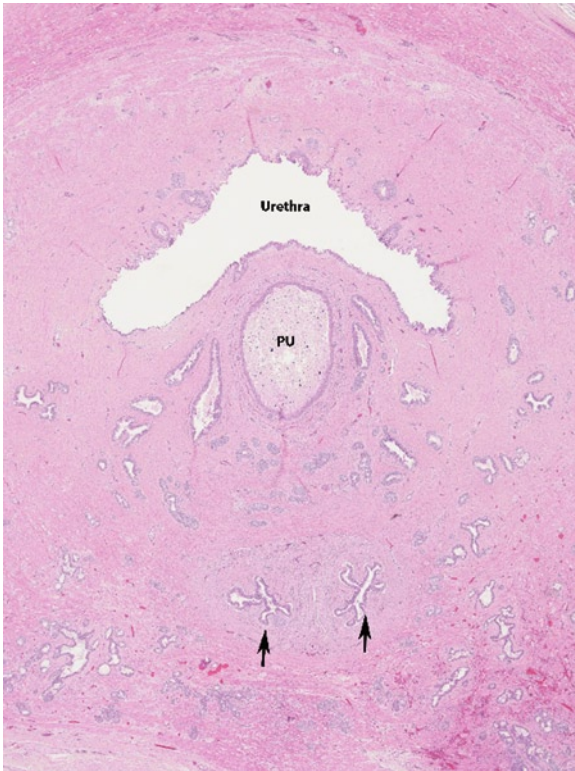


FIGURE 13-5. Prostatic utricle at verumontanum. This low-power image shows the inverted-U-shaped urethra and the protruding prostatic utricle (PU) at the verumontanum. The prostatic utricle is somewhat dilated and cystic, and is frequently lined by squamous epithelium. Note the adjacent prostatic ducts coursing toward the urethra and the ejaculatory ducts (*arrows*) located more posteriorly. (H&E, 2 \times .)

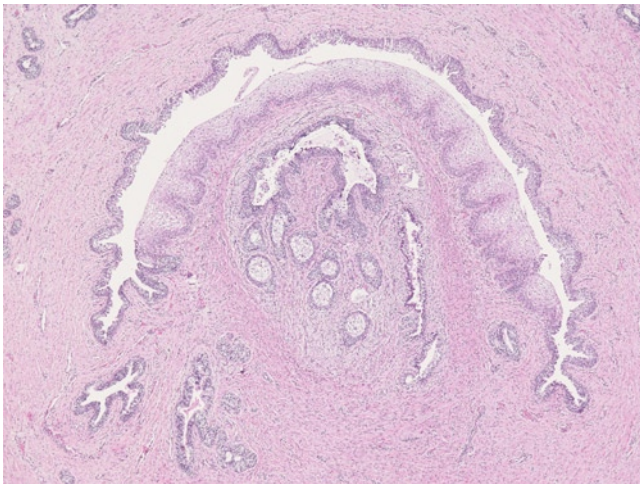


FIGURE 13-6. Prostatic urethra with squamous metaplasia. This low-power image shows the prostatic urethra with its inverted-U shape. Note that it is lined by urothelium along the anterior (*upper*) wall and that there is squamous metaplasia of the epithelium along the posterior (*lower*) wall. (H&E, 4 \times .)

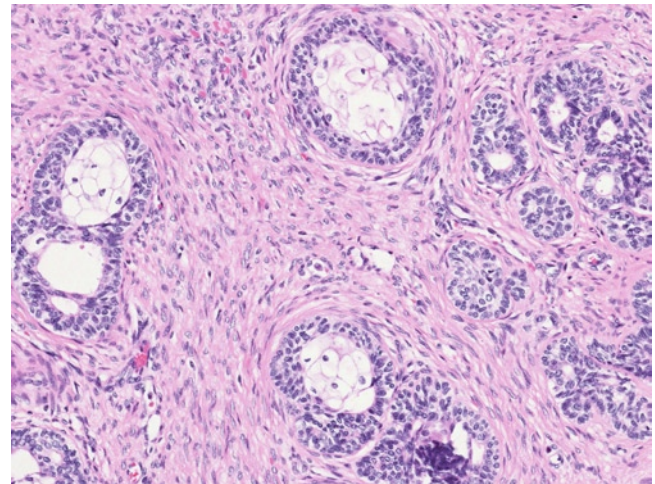


FIGURE 13-7. Squamous metaplasia of prostatic ducts. Squamous metaplasia of ducts is shown in this fetal prostate at 29 weeks gestation. This change becomes less frequent as gestation progresses. (H&E, 20 \times .)



FIGURE 13-8. Prostate gland at 20 weeks gestation. At this gestational age the prostate gland appears larger than at 17 weeks (compare with Fig. 13-1) and the central prostatic urethra is larger. The epithelial elements are still somewhat sparse and consist predominantly of ducts. The prostatic utricle is present posteriorly, between the ejaculatory ducts, and is lined by stratified squamous epithelium. The cross-sectional level is more proximal to the verumontanum, which is not shown here. (H&E, 4 \times .)

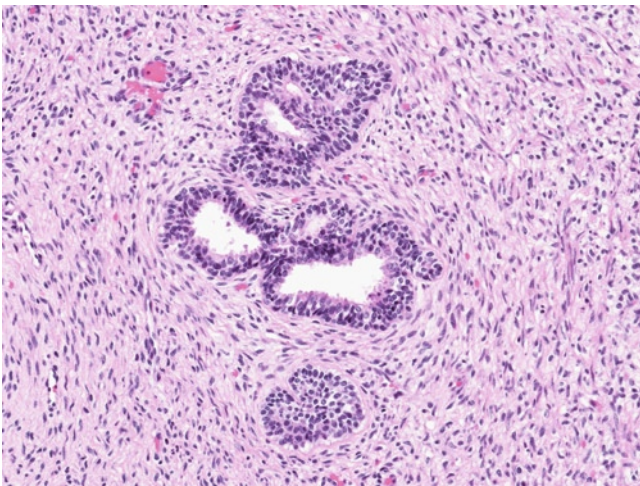


FIGURE 13-9. Prostate gland at 20 weeks gestation. In this higher power view, the prostatic ducts, which are slightly more complex than at 17 weeks, have similar double-layered epithelium. (H&E, 20 \times .)

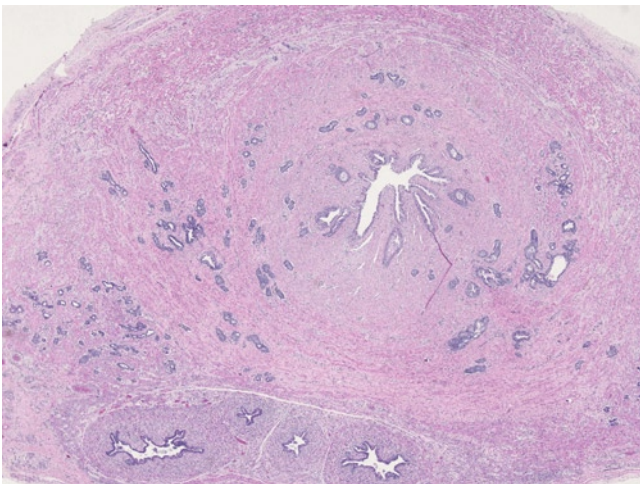


FIGURE 13-10. Prostate gland at 24 weeks gestation. At this gestational age the gland is larger still and this low-power image shows an increase in epithelial elements. Note the seminal vesicles located posteriorly. (H&E, 2 \times .)

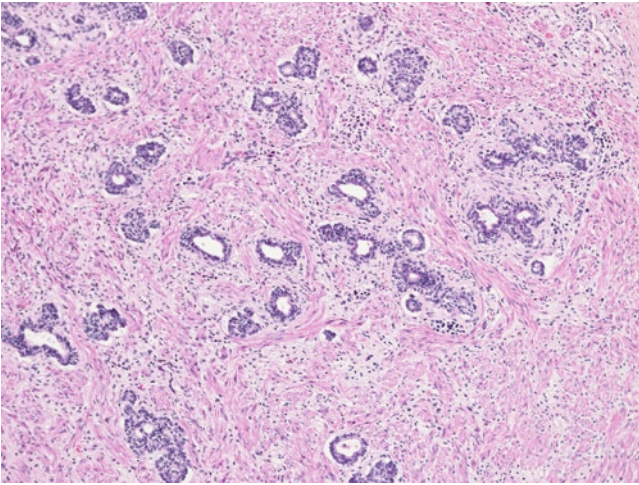


FIGURE 13-11. Prostate gland at 24 weeks gestation. The epithelial elements at the periphery appear in the bud stage with solid buds at the ends of the ducts. The fibromuscular stroma shows more differentiation of the smooth muscle component. (H&E, 10 \times .)

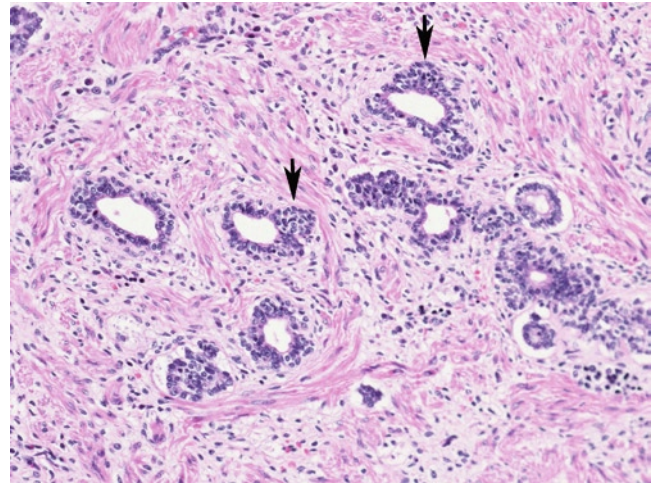


FIGURE 13-12. Prostate gland at 24 weeks gestation. This higher power image shows the basal cells and more apical cells of the ductal lining epithelium. Note the small cellular buds emanating from the ends of the ducts (*arrows*), which is characteristic of the bud stage. (H&E, 20 \times .)

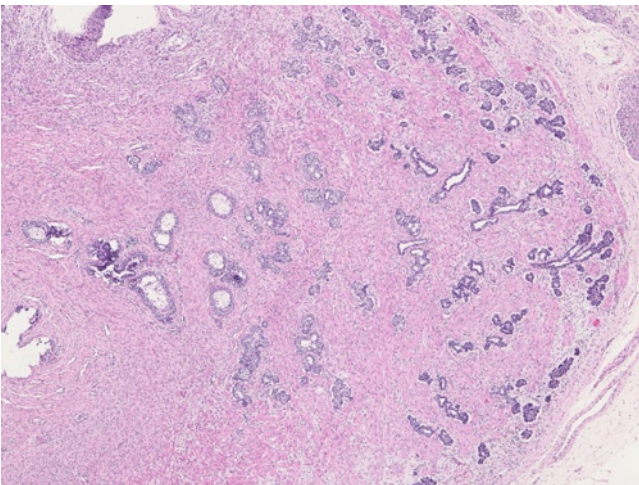


FIGURE 13-13. Prostate gland at 29 weeks gestation. At this gestational age, still more epithelial development is appreciated. Note the ductular structures centrally and the beginning of acinar collections peripherally. (H&E, 4 \times .)

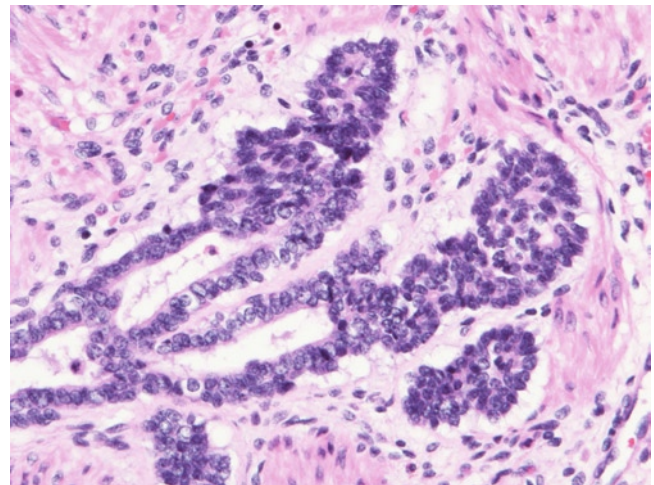


FIGURE 13-14. Prostate gland at 29 weeks gestation. This higher power image shows the epithelial elements near the periphery of the gland. The ducts terminate in buds that are just beginning to form acinar structures. Note the obvious smooth muscle differentiation in the stroma surrounding the epithelial elements. (H&E, 40 \times .)

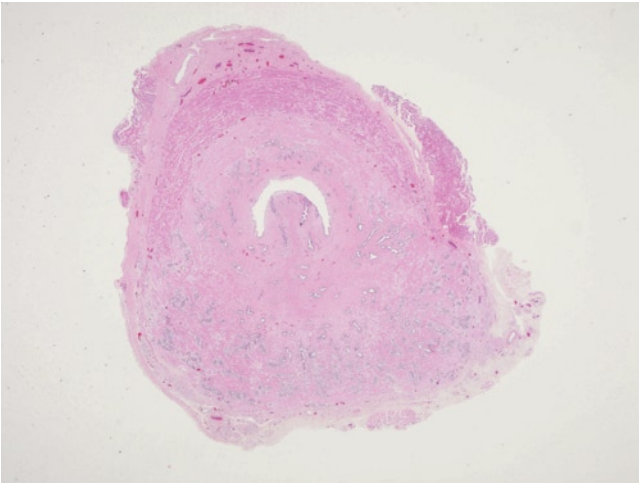


FIGURE 13-15. Prostate gland at 34 weeks gestation. Overall, the gland is larger still and the epithelial elements are quite prominent, especially in the posterior aspect of the gland. The verumontanum is seen protruding into the prostatic urethra. Prostatic ducts drain into the urethra at this level. The connective tissue capsule is present with a band of skeletal muscle incorporated anteriorly. (H&E, 1×.)

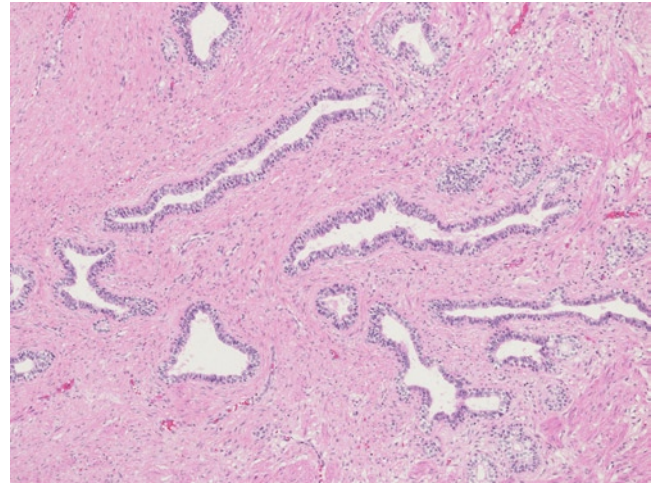


FIGURE 13-16. Prostate gland at 34 weeks gestation. This higher power image shows the epithelial components of the gland. The ducts now terminate in more well-formed small acinar structures (bud-tubule stage). Note the obvious smooth muscle differentiation in the stroma surrounding the epithelial elements. (H&E, 10×.)

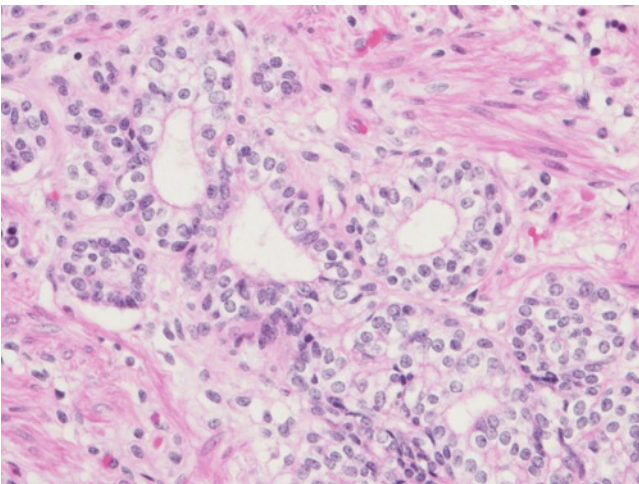


FIGURE 13-17. Prostate gland at 34 weeks gestation. This image is a higher power view of the acinar structures at the terminus of the duct. (H&E, 40×.)

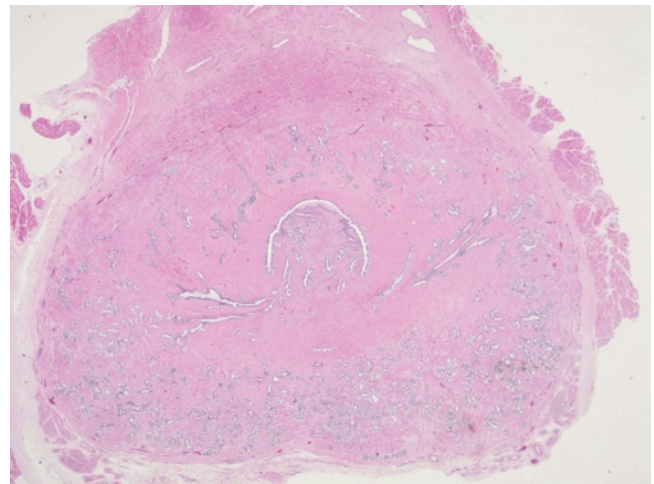


FIGURE 13-18. Prostate gland at 39 weeks gestation. In this low-power image, the prostate gland is larger still. Note the prominence of the epithelial elements, involving the majority of the gland. The verumontanum is seen protruding into the prostatic urethra with numerous ductal structures entering the urethra. A connective tissue capsule is seen around the majority of the gland. (H&E, 1×.)

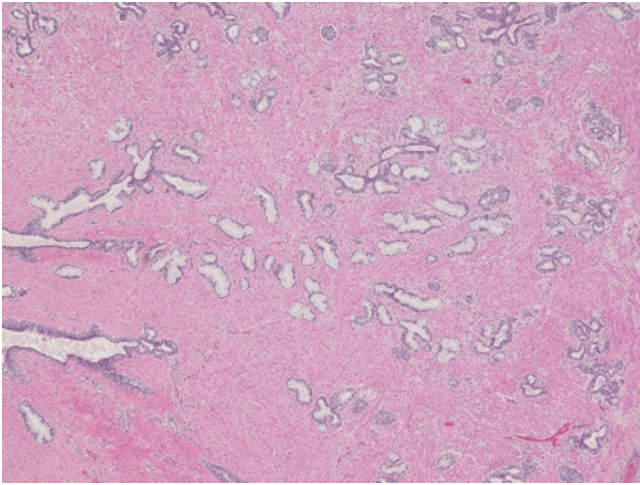


FIGURE 13-19. Prostate gland at 39 weeks gestation. This image shows ducts at the left and the formation of small lobules of acini (acinotubular stage) in the center. The acinar-lining cells show a clearing of apical cytoplasm with secretions. The elongated ducts present on the left side of the picture drain toward the urethra. The stroma has obvious smooth muscle differentiation. (H&E, 4 \times .)

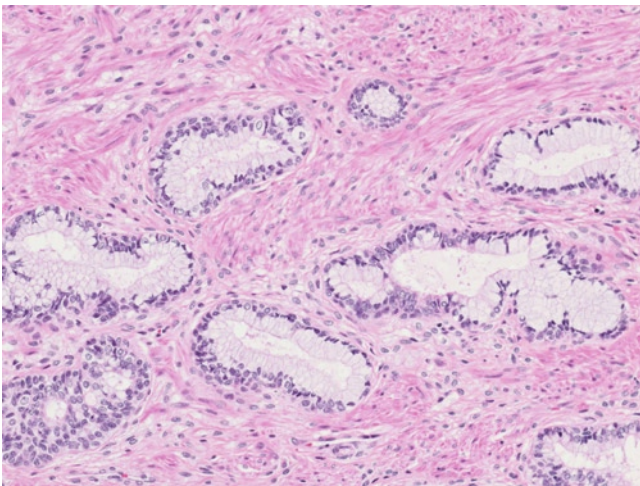


FIGURE 13-20. Prostate gland at 39 weeks gestation. This higher power image shows the secretions by the apical cells. Basal cells remain present along the basement membrane of the glands. (H&E, 20 \times .)

Stromal Elements

The stromal elements of the prostate include the fibromuscular tissue that intervenes between the epithelial elements and the capsule. In the early midtrimester, the stroma of the fetal prostate gland has an immature appearance composed of spindle-shaped cells without much smooth muscle differentiation and the capsule is an ill-defined connective tissue layer. Skeletal muscle bands are often seen in the anterior prostate (see Figs

13-1 and 13-15). As gestation progresses, the stroma develops a more eosinophilic appearance as some of the stromal cells acquire the cytoplasmic properties of smooth muscle, with numerous spindle-shaped cells with a fibroblastic phenotype intermixed (see Figs. 13-11, 13-13, 13-16, and 13-20). Near term, the capsule is also thicker and a more well-defined connective tissue layer (see Figs. 13-15 and 13-18).

References

1. Popek EJ, Tyson RW, Miller GJ, Caldwell SA: Prostate development in prune belly syndrome (PBS) and posterior urethral valves (PUV): etiology of PBS—lower urinary tract obstruction or primary mesenchymal defect? *Pediatr Pathol* 1991, 11:1–29.
2. Schoenwolf GC, Larsen WJ: *Larsen's Human Embryology*, edn 4. Philadelphia: Churchill Livingstone/Elsevier; 2009.
3. Risbridger GP, Almahbobi GA, Taylor RA: Early prostate development and its association with late-life prostate disease. *Cell Tissue Res* 2005, 322:173–181.
4. Thomson AA, Cunha GR, Marker PC: Prostate development and pathogenesis. *Differentiation* 2008, 76:559–564.
5. Shapiro E, Huang H, McFadden DE, *et al.*: The prostatic utricle is not a Mullerian duct remnant: immunohistochemical evidence for a distinct urogenital sinus origin. *J Urol* 2004, 172:1753–1756, discussion 1756.
6. Wernert N, Kern L, Heitz P, *et al.*: Morphological and immunohistochemical investigations of the utriculus prostaticus from the fetal period up to adulthood. *Prostate* 1990, 17:19–30.
7. Glenister TW: The development of the utricle and of the so-called 'middle' or 'median' lobe of the human prostate. *J Anat* 1962, 96:443–55.
8. Valdés-Dapena MA: *Histology of the Fetus and Newborn*. Philadelphia: Saunders; 1979.
9. Xia T, Blackburn WR, Gardner WA Jr: Fetal prostate growth and development. *Pediatr Pathol* 1990, 10:527–537.

14

Ovary

Eduardo D. Ruchelli and Dale S. Huff

The ovary is much smaller during fetal life than in adulthood (30 times lighter at birth than at puberty). Yet, the number of germ cells is several times higher before birth than during the reproductive years (6–7 million at 20 weeks gestation, 0.5–1 million at birth, 300,000 at puberty, and less than 1000 at the end of menopause [1]). Thus, it is not surprising that the gross and microscopic features of the ovary continue to change throughout life, reflecting the steady decline of germ cells and the differences in folliculogenesis during fetal development, childhood, and after puberty. This chapter focuses on the histological features of the fetal ovary and highlights the differences from the adult ovary.

Embryology

Ovarian differentiation of the bipotential gonad occurs at the end of the sixth week postfertilization, a day or two after testicular differentiation [2]. In the female, rather than forming testicular cords, the gonadal cords in the hilar area become indistinct. This area is called the *central zone* and will become the medulla of the ovary. The gonadal blastema surrounding the hilar area becomes thicker and is called the *peripheral zone*, which will become the ovarian cortex. The peripheral zone is composed of a monotonous sheet of cells, which include small primordial germ cells and slightly smaller oval interstitial cells, the precursors of granulosa and theca cells. The two cell types may be nearly indistinguishable except in very well-preserved specimens. The cell of origin of the interstitial cells is controversial and may be the coelomic epithelial cells [3] or the mesonephric epithelial cells [4]. The ovary is long, oval, has an irregular surface, and is distinct from the mesonephros at this age, but it is attached to the mesonephric body along its ventromedial border by a broad mesovarium. The ovarian tissue pushes into the mesonephros and abuts the mesonephric glomeruli; this may explain the occasional embryonic mesonephric glomeruloid remnants found in the ovarian hilus. Mesonephric mesenchyme begins to invade the central zone through the mesovarium.

During the seventh week postfertilization, the peripheral zone becomes thick and develops very broad and indistinct cords. The enlargement of the peripheral zone is caused by rapid proliferation by mitosis of all cells, especially the primordial germ cells. In the central zone, remnants of the fragmented gonadal cords form broad epithelial cords (sex cords) that contain rare germ cells. The central cords extend as narrow strands of dark cells into the mesovarium; these narrow strands will become the rete ovarii. A study based on serial semithin sections of Epon-embedded ovaries suggests that central and peripheral cords arise from mesonephric glomerular and tubular epithelium, and that coelomic epithelium does not contribute to the cords [4].

During the eighth week postfertilization, the peripheral and central zones become definite cortex and medulla, respectively. The ingrowth of stroma from the mesovarium into the medulla breaks up the medullary cords except for those of the rete. The deep margin of

the thickening cortex becomes lobulated. The primordial germ cells in the deep cortex begin to differentiate into oogonia and the differentiation into oogonia gradually spreads up from the deep cortex into more superficial cortex.

Histology

The fetal ovary is tan, elongated, and flattened in contrast to the adult ovary, which is pink–white, ovoid, and becomes increasingly convoluted during reproductive life. In near-term fetuses, follicular cysts may cause a lobulated external appearance. Although the neonatal ovary only weighs 0.3 g (compared to 5–8 g in the adult), it is relatively long compared to the length of the fallopian tube, which is only slightly longer. The ovary is attached at the hilus to the posterior aspect of the broad ligament by the mesovarium (see Fig. 14-1). The peritoneum of the mesovarium is contiguous with the surface epithelium of the ovary at the hilus. From the hilus, the blood supply of the ovary penetrates through an ill-defined medulla into the cortex. The main cellular components of the ovary include the surface epithelium, the stroma and its derivatives, the germ cells, and the sex cord-derived granulosa cells, which will surround the germ cells and form the follicles.

The surface epithelium consists of a single, focally pseudostratified layer of modified cuboidal peritoneal cells, which focally lacks a distinct basement membrane (see Fig. 14-2). The tunica albuginea, a thin fibrous layer located under the surface epithelium, is not as distinct as in the testis (see Fig 14-3). In contrast

to the adult ovary, the stroma of the fetal ovary is very scanty, as 90% of the cortex consists of crowded germ cells (see Fig. 14-4). Primordial germ cells begin to differentiate into oogonia during the early fetal period [5,6]. Oogonia are premeiotic germ cells that represent the mitotically active pool from which meiotic oocytes develop and differentiate. The series of mitosis preceding meiosis results in a syncytium of clusters of oogonia, which are intermingled with groups of pregranulosa cells (see Fig. 14-5). Oogonial mitotic activity peaks at 20 weeks gestation, when the largest number of germ cells can be observed, and then declines through week 28 [1]. Simultaneously, starting at 12 to 13 weeks gestation, some oogonia in the inner cortex enter meiosis and become oocytes (see Figs. 14-2 and 14-6). Oocytes are arrested in the very last stage of prophase for as long as 40 years or more, and only a small fraction will complete the first meiotic division at the time of ovulation (approximately 400). Between 14 and 18 weeks gestation, individual oocytes lose the intercellular bridges that kept them in a syncytial arrangement and become surrounded by a layer of flattened pregranulosa cells to form primordial follicles.

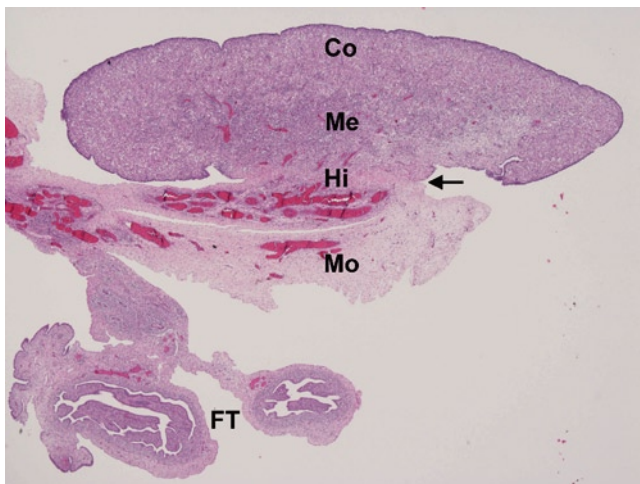


FIGURE 14-1. Ovary at 19 weeks gestation. Most of the ovary is comprised of the cortex (Co), which overlies the medulla (Me). Crowded germ cells occupy 90% of the cortex. At the hilus (Hi), the ovary is attached to the mesovarium (Mo). The entire ovary is covered by a distinct, single layer of cuboidal surface epithelium and the surface is irregular. The surface epithelium is contiguous with the peritoneal mesothelium of the mesovarium at the hilus (arrow). FT—fallopian tube. (Hematoxylin and eosin [H&E], 2 \times .)

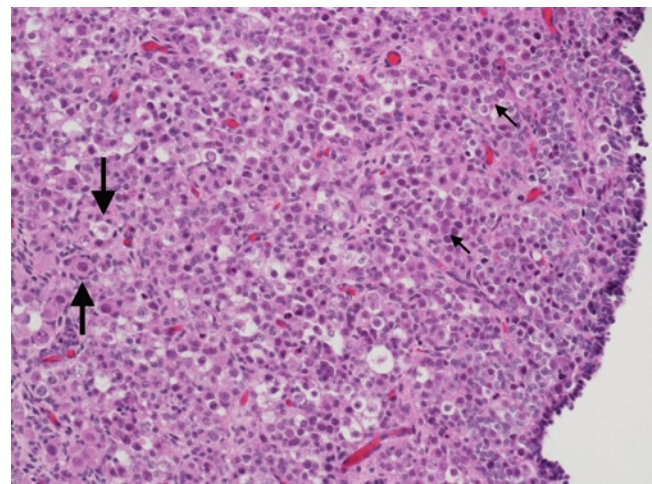


FIGURE 14-2. Surface epithelium: ovary at 21 weeks gestation. This closer view of the surface epithelium (*right*) demonstrates a single layer of cuboidal cells that focally lack a distinct basement membrane. The tunica albuginea is not developed at this age. The outer cortex is primarily occupied by a syncytium of oogonia (*small arrows*) and occasional primordial follicles (*large arrows*). (H&E, 20 \times .)

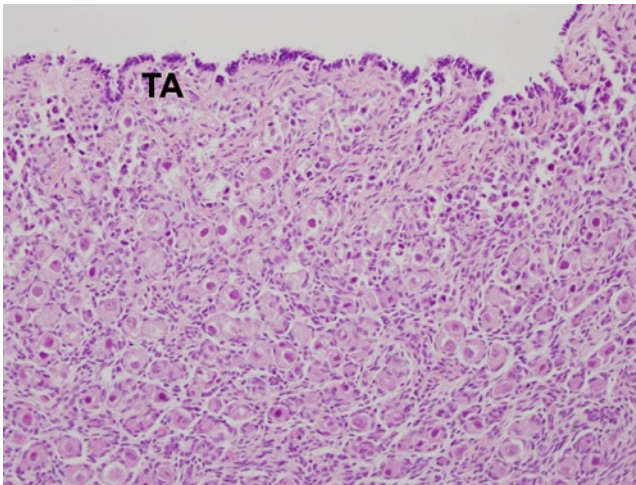


FIGURE 14-3. Tunica albuginea (TA): ovary at 28 weeks gestation. In contrast to Figure 14-2, the tunica albuginea is better developed at this age. Also notice the larger number of primordial follicles with a layer of flattened granulosa cells and slightly increased spindle-shaped stromal cells. (H&E, 20 \times .)

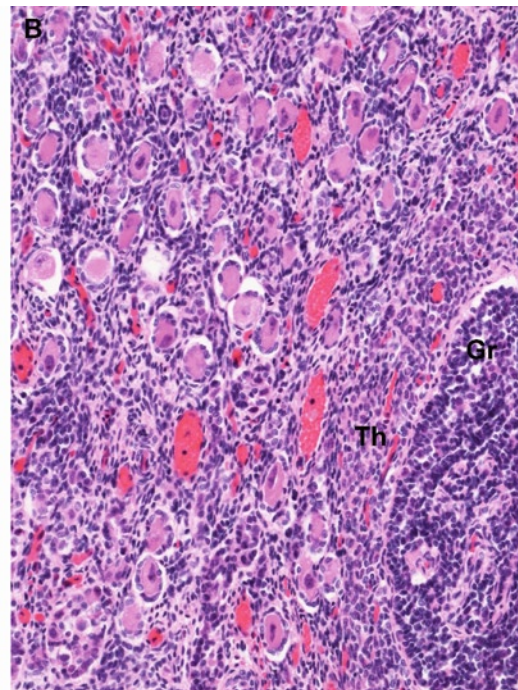
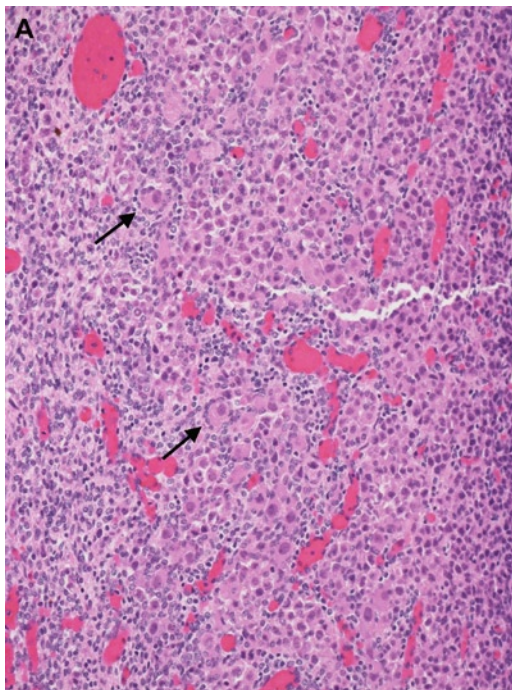


FIGURE 14-4. Stroma: ovary at 19 (A) and 35 (B) weeks gestation. Although spindle-shaped stromal cells remain a minor component of the ovary throughout fetal life (in contrast to the adult ovary), they become better developed during the third trimester

(B). Notice the marked increase in primordial and primary follicles (arrows). The edge of a secondary follicle, probably undergoing atresia, with a stratified layer of granulosa cells (Gr) and a rim of theca cells (Th) can be seen to the right in B. (H&E, 20 \times .)

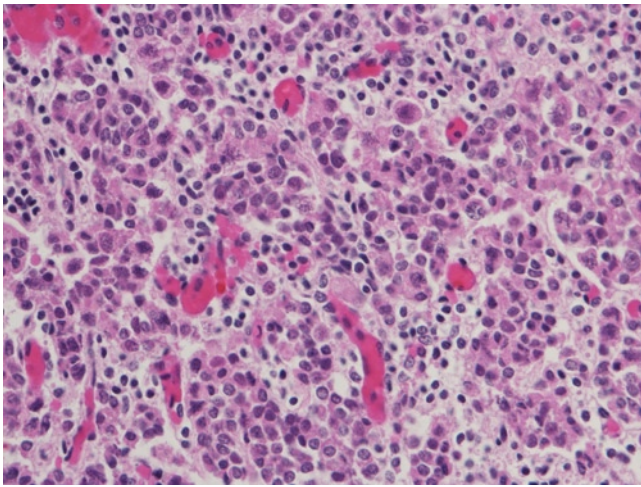


FIGURE 14-5. Oogonia: ovary at 16 weeks gestation. Mitotically active oogonia comprise the majority of cells in the cortex as the ovary approaches the stage with the largest number of germ cells throughout prenatal and postnatal life. The groups of oogonia represent a syncytium kept together by intercellular bridges between the germ cells. Pregranulosa cells and germ cells may be nearly indistinguishable except in very well-preserved specimens. (H&E, 40 \times .)

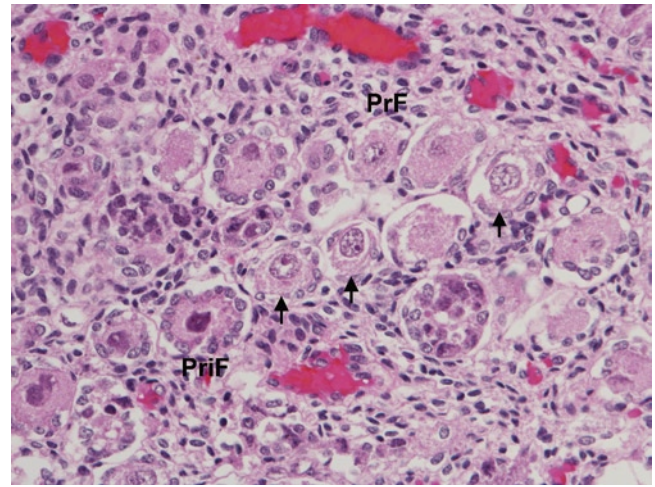


FIGURE 14-6. Oocytes and follicles: ovary at 24 weeks gestation. Oocytes (arrows) are larger than oogonia and display a characteristic nucleus arrested in the last stage of prophase of the first meiotic division. In this field they can be seen within primordial follicles (PrF) with a layer of flattened granulosa cells and within primary follicles with a layer of cuboidal granulosa cells (PriF). (H&E, 40 \times .)

Folliculogenesis

Follicles are the functional unit of the ovary. Each follicle consists of an oocyte surrounded by at least one, and up to several layers of somatic granulosa cells (see Figs. 14-6 and 14-7). The follicle is separated from the surrounding stroma by a basement membrane and the granulosa cells are devoid of any vascular supply. Folliculogenesis refers to the continuous process whereby primordial follicles undergo maturation. During reproductive life, only one follicle achieves complete maturation each month, culminating in ovulation. The other follicles that have begun simultaneous maturation undergo atresia at earlier stages of their development. Atresia accounts for the normal, steady decline in germ cells starting at 20 weeks gestation, when the loss of oogonia outpaces the mitotic activity of the remaining oogonia. Folliculogenesis and atresia occur prenatally and throughout childhood following the same stages that can be seen in the adult ovary, but the majority of these follicles will not reach the pre-ovulatory stage. The maturational stages that can be observed prenatally and during childhood include the primordial follicle; the primary follicle; the secondary or preantral follicle; the tertiary or antral follicle; and, less commonly, the mature or Graafian follicle.

Primordial follicles are dormant quiescent follicles that represent the ovarian reserve. Histologically, they are characterized by a single oocyte or, less commonly, multiple oocytes surrounded by a single layer of flattened, mitotically inactive, granulosa cells resting on a basement membrane. The oocyte measures 40 to 70 μm in diameter (see Fig. 14-8). Primordial follicles should

be observed in the normal ovary by 18 weeks gestation [7]. However, autolysis frequently impairs the evaluation of folliculogenesis and ovarian dysgenesis in autopsy specimens, and caution should be used when tissues are not well preserved.

Primary follicles represent the first morphological evidence of follicular maturation (see Fig. 14-9). In contrast to their flattened appearance in the primordial follicle, the granulosa cells assume a cuboidal to columnar shape and the oocyte enlarges.

Secondary or preantral follicles are characterized by stratification of the granulosa cells into three to five concentric layers around the oocyte (see Fig. 14-10). In addition, the oocyte becomes surrounded by an eosinophilic, homogeneous, acellular layer, known as the *zona pellucida*. Secondary follicles measure from 50 to 400 μm in diameter. Simultaneously, the surrounding stromal cells begin to become specialized into several layers of theca interna cells and an ill-defined layer of theca externa cells (see Fig. 14-11).

Tertiary or antral follicles are seen when the secretion of fluid by granulosa cells results in the formation of fluid-filled clefts that eventually coalesce to form a single cavity lined by several layers of granulosa cells (see Fig. 14-12). The oocyte continues to enlarge and may adopt an eccentric position at one pole of the follicle. When granulosa cells proliferate around the oocyte and form the so-called *cumulus oophorus*, the follicle is known as a mature or Graafian follicle (see Fig. 14-13). In the near-term fetus, multiple grossly visible Graafian follicles may be present.

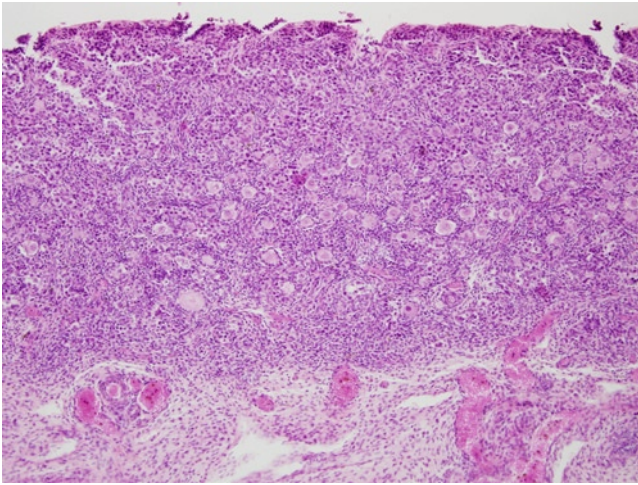


FIGURE 14-7. Follicles: ovary at 28 weeks gestation. Initially, primordial and primary follicles are more numerous in the inner cortex. The surface epithelium, as shown here, is frequently denuded in autopsy specimens due to poor preservation or handling. (H&E, 10 \times .)

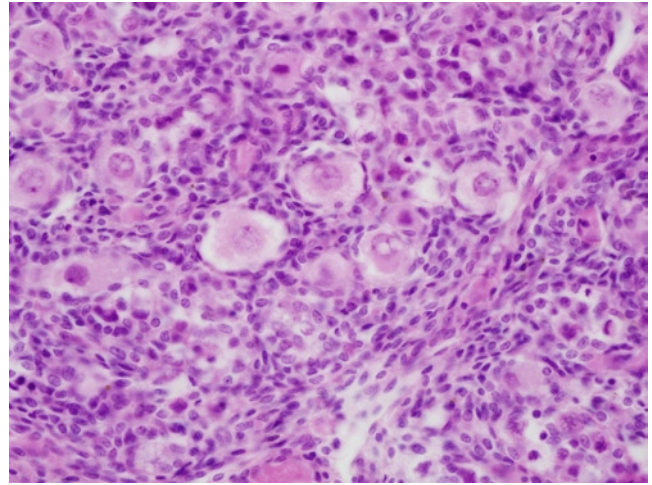


FIGURE 14-8. Primordial follicles: ovary at 28 weeks gestation. Primordial follicles consist of an oocyte measuring 40 to 70 μm in diameter, surrounded by a single layer of flattened granulosa cells. The nucleus of the oocyte displays chromosomes arrested in the dictyate stage of prophase and one or more nucleoli. Rare oocytes may have multiple nuclei. (H&E, 40 \times .)

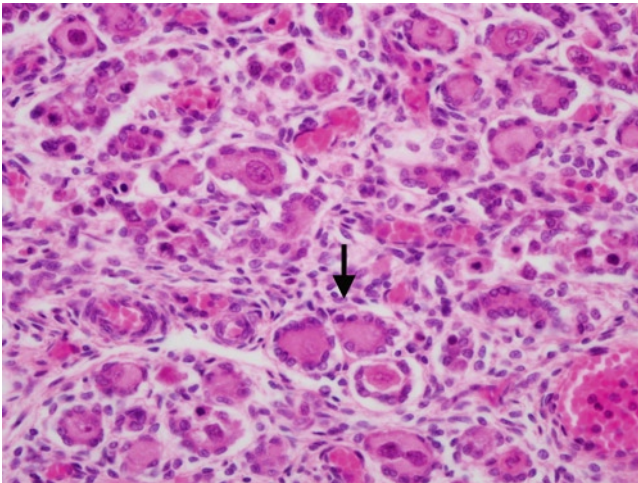


FIGURE 14-9. Primary follicles: ovary at 30 weeks gestation. As the granulosa cells begin to become mitotically active they assume a cuboidal shape, which characterizes the primary follicle (arrow). (H&E, 40 \times .)

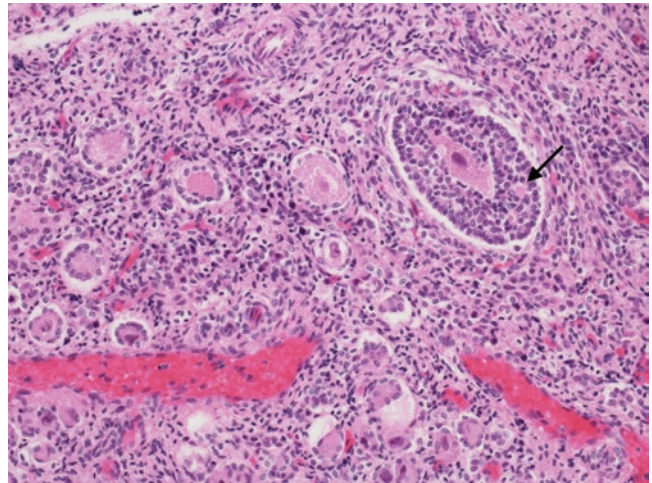


FIGURE 14-10. Secondary follicle: ovary at 32 weeks gestation. Mitotic activity in the granulosa cells results in the formation of multiple layers around the central oocyte. A Call-Exner body (arrow) can be seen within the layers of granulosa cells. The oocyte enlarges and the stromal cells surrounding the follicle begin to differentiate into theca cells. (H&E, 20 \times .)

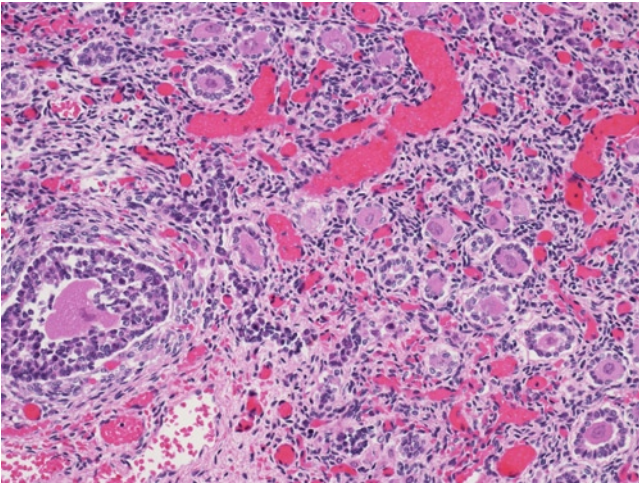


FIGURE 14-11. Secondary follicle: ovary at 38 weeks gestation. This secondary follicle (*left*) is already surrounded by several layers of differentiating theca cells. The theca interna has three to four layers of plump cells while the theca externa is ill defined and merges with the adjacent ovarian stroma. Elsewhere in the field there are numerous primordial and primary follicles. (H&E, 20 \times .)

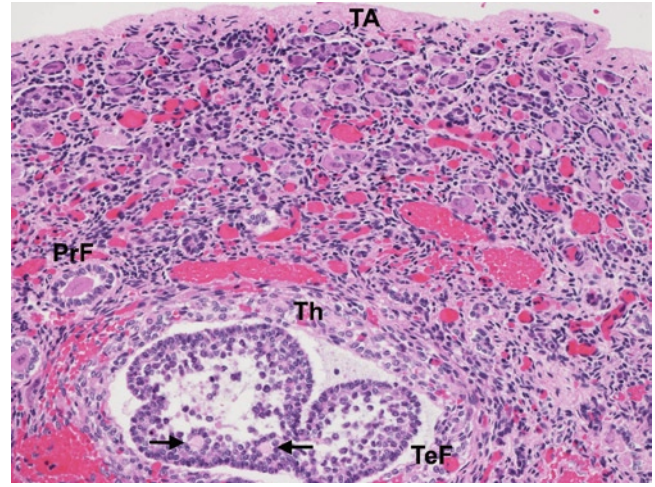


FIGURE 14-12. Tertiary or antral follicle: ovary at 38 weeks gestation. Granulosa cells begin to secrete fluid and create spaces that coalesce to form a single cavity. The tertiary follicle (TeF) is surrounded by better differentiated theca cells (Th). Two Call-Exner bodies (*arrow*) can be seen within the layers of granulosa cells. A primary follicle can be seen to the left, whereas the outer cortex under the tunica albuginea (TA) contains mostly primordial follicles (PrF). (H&E, 20 \times .)

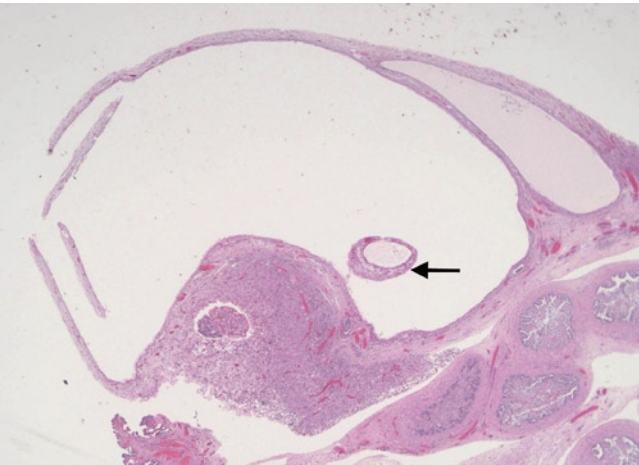


FIGURE 14-13. Graafian follicle: ovary at 32 weeks gestation. The oocyte has adopted an eccentric position and is surrounded by a mantle of granulosa cells, the cumulus oophorus (*arrow*). This tertiary follicle is undergoing atresia as the granulosa cell layers at the periphery of the cystic follicle have thinned out and exfoliated. (H&E, 1 \times .)

Follicular Atresia

Follicular atresia may begin at any stage of follicular maturation. Atresia of primordial and primary follicles is characterized by pyknosis and nuclear fragmentation of the oocyte and by cytoplasmic vacuolation. The granulosa cells degenerate and the follicle disappears without a trace [8]. In contrast, atresia of antral follicles usually results in the formation of a scar, the corpus fibrosum.

Some follicles do not become completely obliterated and remain as atretic cystic follicles for an indefinite period of time (see Fig. 14-13). Follicles that exceed 3 cm are designated as *follicular cysts* [8]. Structures resembling microscopic gonadoblastomas and sex cord tumors with annular tubules have been identified within atretic follicles in up to 35% of normal fetuses and infants [8].

Hilus Cells

Ovarian hilus cells are morphologically identical to testicular Leydig cells. Similarly to Leydig cells, they can be recognized during fetal life but become inconspicuous after birth, only to reappear at the time of puberty. Clusters of hilus cells are typically found in the hilus and mesovarium, but can be found within the ovary at

some distance from the hilus (see Fig. 14-14). The cells are 15 to 25 μm in diameter and are round to oval, with abundant eosinophilic cytoplasm. Hilus cells should be distinguished from adrenal cortical rests, which are usually found in the mesovarium (see Chapter 18, Fig. 18-19).

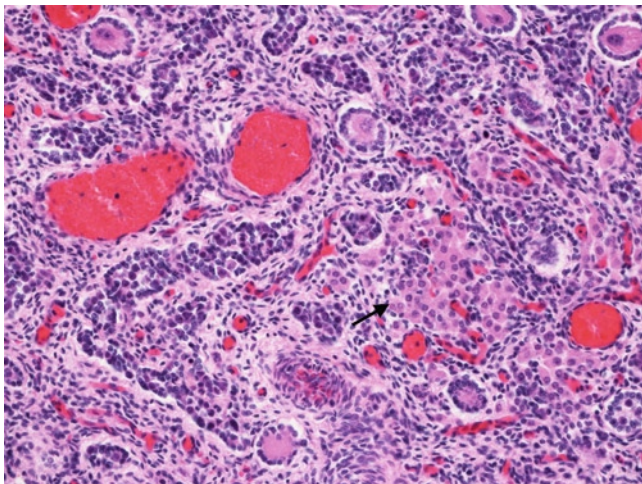


FIGURE 14-14. Hilus cells: ovary at 35 weeks gestation. Hilus cells (arrow) are morphologically identical to Leydig cells. Although typically seen at the hilus, they can be observed in clusters within the inner cortex, as in this case. The eosinophilic cytoplasm is very distinct in the fetus, but it becomes inconspicuous after birth and cannot be readily identified until they reappear after puberty. (H&E, 20 \times .)

Rete Ovarii and Mesonephric Duct Remnants

The rete ovarii, the female analog of the rete testis, is found at the hilus of the ovary. It consists of a network of clefts, tubules, and cysts with focal intraluminal papillae, lined by cuboidal to columnar epithelium. A cuff of spindle-shaped stromal cells surround the rete structures. The rete may juxtapose and communicate with mesonephric remnants within the mesovarium. Mesonephric remnants are commonly found in the vicinity of the ovary in fetal autopsies (see Figs. 14-15 and 14-16). The remnants usually consist of tubules lined by cuboidal to columnar epithelium and are surrounded by concentric

layers of spindle cells. Those found in the mesovarium next to the ovary are known as *epoophoron*, which consists of a few blind tubules and a duct that correspond to the efferent ductules and epididymis in the male. Closer to the uterus, some rudimentary tubules may persist as the paroophoron and remnants corresponding to the vas deferens and ejaculatory duct in the male may persist as Gartner duct cysts between the layers of the broad ligament along the lateral wall of the uterus and in the lateral wall of the entire length of the vagina to the introitus [9].

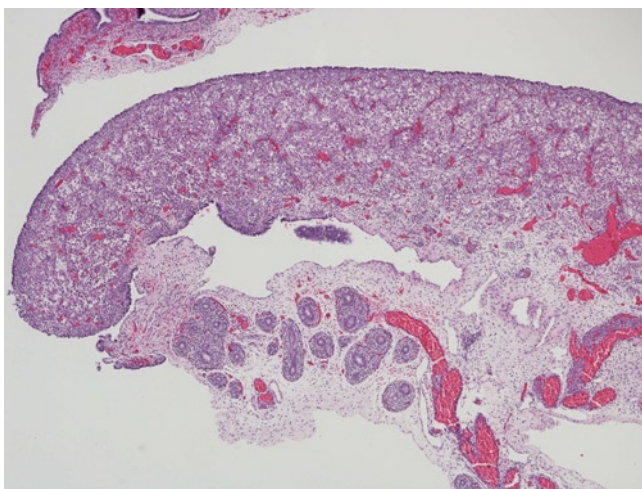


FIGURE 14-15. Mesonephric remnants: ovary at 19 weeks gestation. Blind-ending tubules in the mesovarium, corresponding to the efferent ductules and epididymis in the male, are known as *epoophoron*. This is a common finding in autopsy sections of the fetal ovary or fallopian tube. (H&E, 4 \times .)

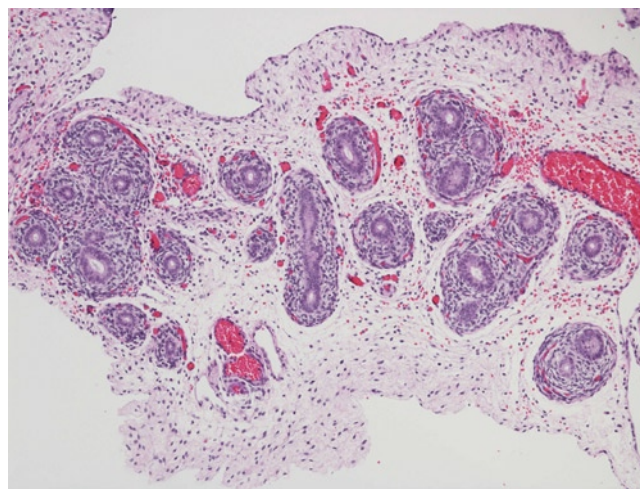


FIGURE 14-16. Mesonephric remnants: ovary at 19 weeks gestation. This closer view of the epoophoron demonstrates tubules lined by cuboidal to columnar epithelium, surrounded by a concentric layer of loose spindle-shaped cells. Due to their common mesonephric origin, these structures are reminiscent of the fetal vas deferens in the male. (H&E, 10 \times .)

References

1. O Oktem, Oktay K: The ovary: anatomy and function throughout human life. *Ann N Y Acad Sci* 2008, 1127:1–9.
2. Van Wagenen G, Simpson ME: *Embryology of the Ovary and Testis: Homo sapiens and Macaca mullata*. New Haven, CT: Yale University Press; 1965.
3. Jirásek JE: *Development of the Genital System and Male Pseudohermaphroditism*. Baltimore, MD: Johns Hopkins University Press; 1971.
4. Satoh M: Histogenesis and organogenesis of the gonad in human embryos. *J Anat* 1991, 177:85–107.
5. Motta PM, Nottola SA, Makabe S: Natural history of the female germ cell from its origin to full maturation through prenatal ovarian development. *Eur J Obstet Gynecol Reprod Biol* 1997, 75:5–10.
6. Motta PM, Makabe S, Nottola SA: The ultrastructure of human reproduction. I. The natural history of the female germ cell: origin, migration and differentiation inside the developing ovary. *Hum Reprod Update* 1997, 3:281–295.
7. McFadden DE, Pantzar T: Genital system. In *Developmental Pathology of the Embryo and Fetus*. Edited by Dimmick JE, Kalousek DK. Philadelphia: Lippincott; 1992.
8. Clement PB: Ovary. In *Histology for Pathologists*, edn 3. Edited by Mills SE. Philadelphia: Lippincott Williams & Wilkins; 2007:1063–1094.
9. Moore KL, Persaud TVN: *The Developing Human Clinically Oriented Embryology*, edn 8. Philadelphia: Saunders; 2008.

15

Fallopian Tubes

Eduardo D. Ruchelli and Dale S. Huff

The fallopian tubes and uterus have a common embryologic origin; thus, it is not surprising that they have a similar anatomic organization. The layers of the wall of the fallopian tubes mature and differentiate in a similar fashion to the uterus during fetal life. During the second and third trimesters, the fallopian tubes typically exhibit a markedly convoluted gross appearance. Similarly to the adult, the fetal fallopian tube can be divided into four segments: the intramural segment within the wall of the uterine cornu; the adjacent isthmus with a thick, stout wall and narrow lumen; the ampulla, which is thin walled and tortuous; and the infundibulum, which opens into the peritoneal cavity by way of the fimbriated end.

Embryology

The fallopian tubes, uterus, and much of the vagina are derived from the paramesonephric (Müllerian) duct, the development of which is described in Section IV. The duct has two curves that divide it into three segments. The first segment, the most rostral, is vertical and extends from the abdominal ostium (the future fimbriated end) caudally along the posterolateral border of the ovary and mesonephros to the first curve [1]. This segment becomes the fallopian tube. The first curve, which bends medially under the caudal end of the ovary, is attached to the caudal end of the ovary by the ovarian ligament and by the round ligament to the inguinal canal. The second segment is horizontal and extends medially from the first curve to the midline where it meets, fuses with the opposite duct, and curves (the second curve) caudally. This segment becomes incorporated into the ipsilateral lateral wall of the uterus. The third segment is vertical and, after fusing with the opposite duct, it extends caudally to its attachment to the posterior wall of the urogenital sinus at the level of the Müllerian tubercle. This segment becomes the uterus and vagina.

The fallopian tube immediately develops a lumen that is continuous with that of the abdominal ostium. The epithelium of the abdominal ostium derives from the coelomic epithelium, while that of the remainder of the tube is of paramesonephric origin. The undifferentiated mesenchyme of the wall is derived from paramesonephric mesoderm and possibly partially from mesonephric mesoderm. The mucosa and muscularis remain undifferentiated until later in fetal life[1,2].

Histology

Three layers can be identified in sections of the mature fallopian tube: the mucosa, muscularis (myosalpinx), and serosa [3]. The tubal mucosa is invaginated into the lumen, forming longitudinal branching folds or plicae that increase in complexity from the isthmus to the infundibulum (see Fig. 15-1). During the early midtrimester, the mucosal stroma blends into the muscularis and there is no clear distinction between the two (see Figs. 15-2–15-5). The lumen is lined by undifferentiated simple or slightly pseudostratified cuboidal to columnar epithelium [4]. Cilia can be observed in well-preserved specimens but not all cells are ciliated. Two other cell types have been described: secretory cells and intercalated cells. However, secretory cells are difficult to discern in

the immature epithelium of the fetus and intercalated cells are modified secretory cells seen during the menstrual cycle after puberty [5,6]. Toward the end of the midtrimester, the muscularis gradually becomes distinct (see Fig. 15-6). The muscular layer is composed of an external longitudinal layer and an internal circular layer arranged in a basket-weave fashion (see Figs. 15-6–15-8). The muscular coat is always thicker toward the uterine end of the tube (see Fig. 15-9). The serosa is comprised of the peritoneum and underlying loose connective tissue. This layer is particularly thick during the midtrimester (see Figs. 15-2 and 15-4), but also remains relatively prominent at term. The mucosal epithelium changes little during gestation (see Fig. 15-10).

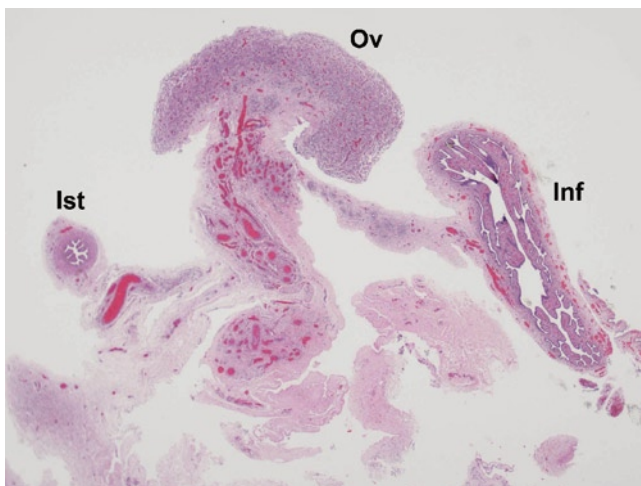


FIGURE 15-1. Fallopian tube at 23 weeks. This slide includes two cross-sections of the fallopian tube and the ovary (Ov) in the middle. On the left is the isthmus (Ist) whereas on the right is the infundibulum (Inf). Notice how the complexity of the plicae increases while the thickness of the muscular coat decreases from the isthmus to the infundibulum (see Fig. 15-9). (Hematoxylin and eosin [H&E], 1×.)

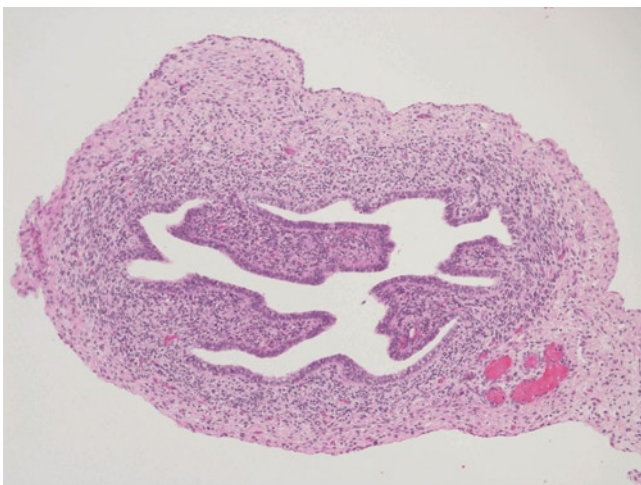


FIGURE 15-2. Fallopian tube at 19 weeks. Plicae are already developed, but the muscular layer is indistinct and blends with the stroma of the mucosa. Note the relatively thick connective tissue of the serosal layer. (H&E, 10×.)

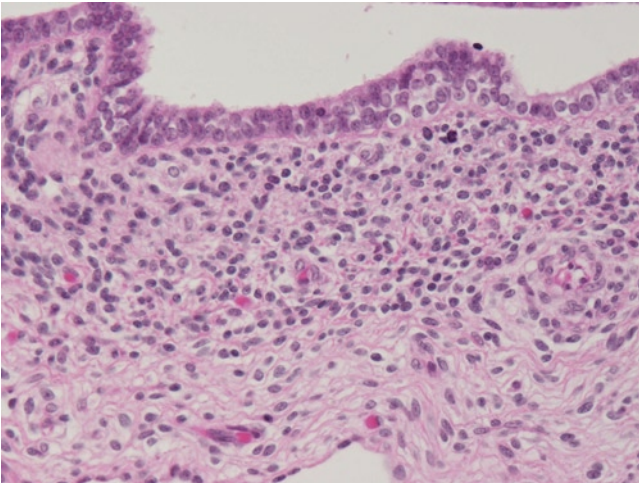


FIGURE 15-3. Fallopian tube at 19 weeks. This closer view shows a single layer of columnar cells with focally crowded nuclei along the mucosal surface. Cilia are barely discernible in some cells. The mucosal stroma blends into the developing muscular layer. (H&E, 40 \times .)

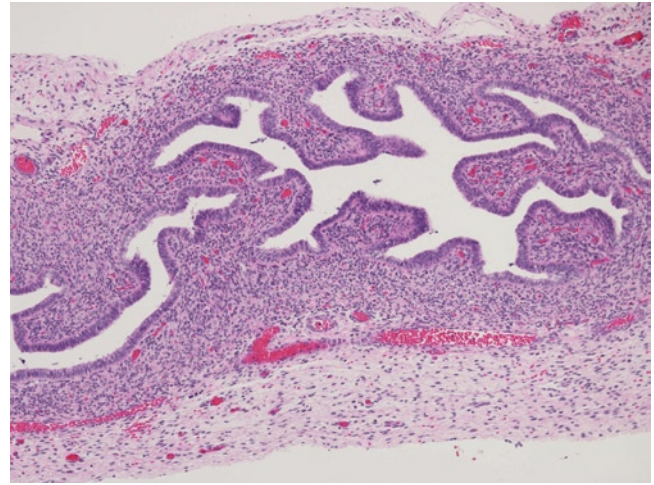


FIGURE 15-4. Fallopian tube at 21 weeks. The demarcation between mucosal stroma and smooth muscle remains indistinct, as shown. Note the relatively thick connective tissue of the serosal layer. (H&E, 10 \times .)

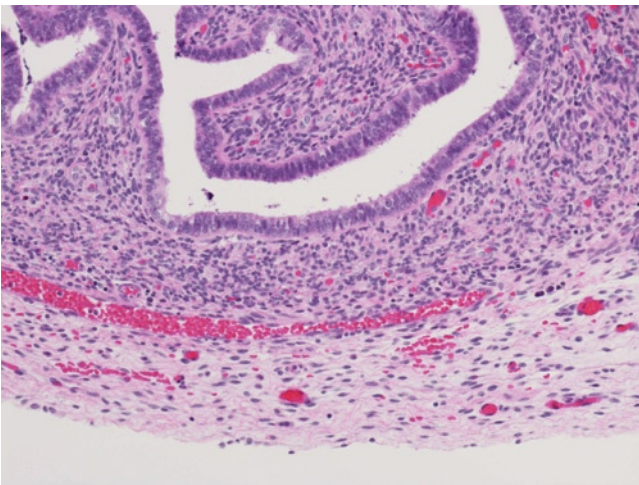


FIGURE 15-5. Fallopian tube at 21 weeks. This closer view shows no significant smooth muscle differentiation. The epithelium consists of a single layer of columnar cells. (H&E, 20 \times .)

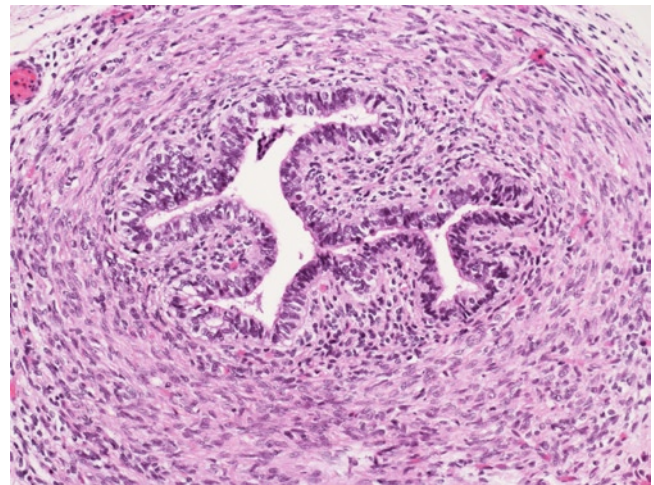


FIGURE 15-6. Fallopian tube at 23 weeks. The myosalpinx becomes more distinct as the smooth muscle fibers show better differentiation. The epithelium between plicae now almost rests on top of the muscular coat. (H&E, 20 \times .)

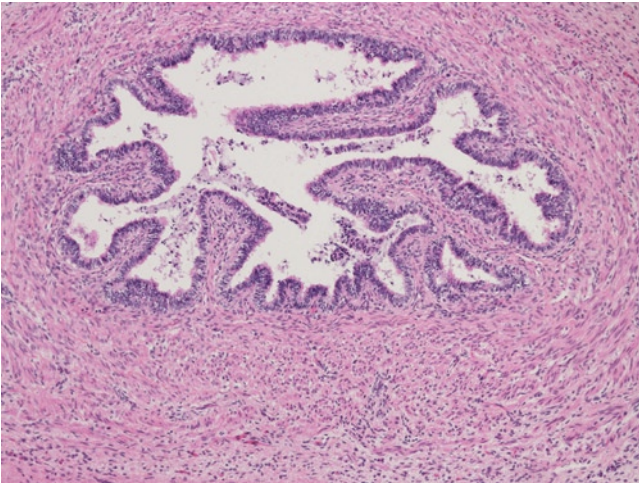


FIGURE 15-7. Fallopian tube at 32 weeks. The mucosal stroma has more collagen and the smooth muscle fibers begin to be oriented in different directions. (H&E, 10 \times .)

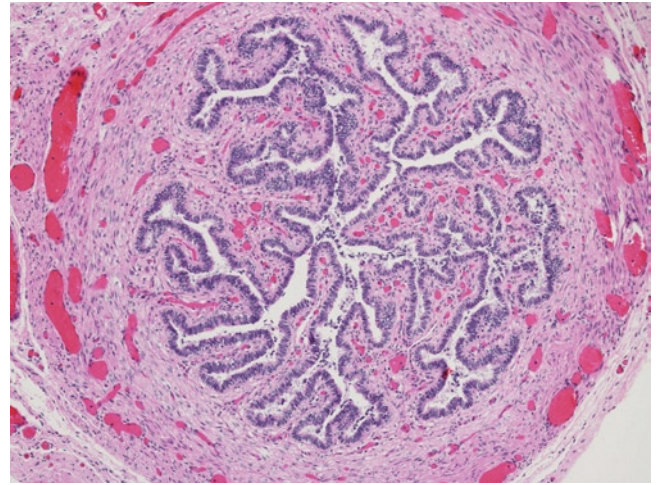


FIGURE 15-8. Fallopian tube at 38 weeks. This section closer to the ovarian end of the tube demonstrates increased complexity of the plicae and thinning of the muscular coat. (H&E, 10 \times .)

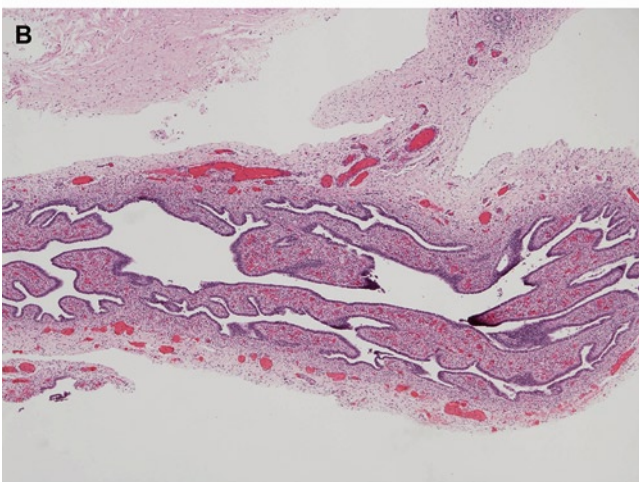
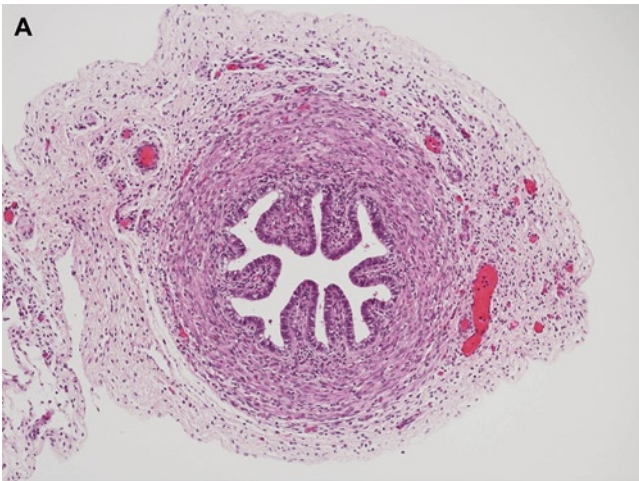


FIGURE 15-9. Fallopian tube at 23 weeks. This closer view is of the same segments of fallopian tube as depicted in Figure 15-1. The muscularis is thicker in the isthmus (**A**) than the infundibulum (**B**). (H&E: **A**, 10 \times and **B**, 4 \times .)

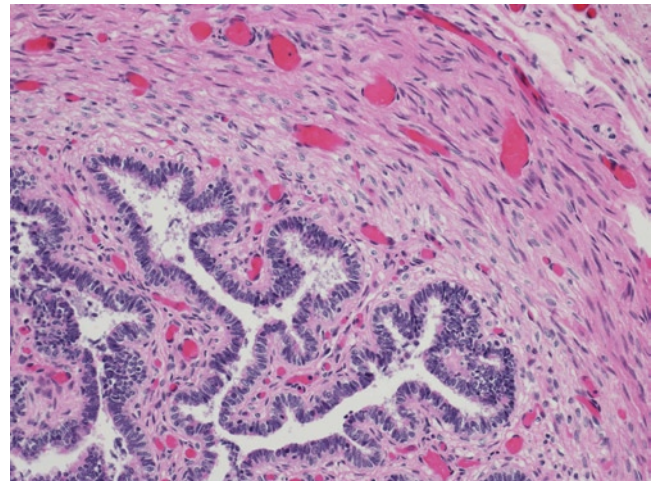


FIGURE 15-10. Fallopian tube at 38 weeks. As shown, the epithelium changes little during gestation, remaining a single layer of columnar cells. Compare to Figures 15-3 and 15-5. (H&E, 20 \times .)

References

1. Felix W: The development of the urinogenital organs. In *Human Embryology*. Edited by Keibel F, Mall FP. Philadelphia: J.B. Lippincott Company; 1912:752–979.
2. Hamilton WJ, Mossman HW: *Human Embryology*. Baltimore: Williams & Wilkins; 1972.
3. Valdes-Dapena MA: *Histology of the Fetus and Newborn*. Philadelphia: Saunders; 1979:469–477.
4. Jirásek JE: *An Atlas of Human Prenatal Developmental Mechanics*. New York: Taylor & Francis; 2004.
5. Hendrickson MR, Atkins KA, Kempson RL: Uterus and fallopian tubes. In *Histology for Pathologists*, edn 3. Edited by Mills SE. Philadelphia: Lippincott Williams & Wilkins; 2007:1011–1062.
6. Anderson MC, Robboy SJ, Russell P: The fallopian tube. In *Pathology of the Female Reproductive Tract*. Edited by Robboy SJ, Anderson MC, Russell P. Philadelphia: Elsevier; 2002:415–444.

16

Uterus

Eduardo D. Ruchelli and Dale S. Huff

The uterus of the fetus is relatively small, particularly when compared to the ovaries, which have about the same length as the fallopian tube. The relative size of the corpus and the cervix is the reverse of the adult uterus, the corpus being about a fifth to a third of the length of the cervix during gestation. This cervicocorpus disproportion is maintained into childhood.

Most developmental anomalies of the uterus are the result of insufficient development of one or both Müllerian (paramesonephric) ducts or incomplete fusion, which results in different types of anomalous uterovaginal septation. Whenever the dome of the uterus is noticed not to be round or flat, serial cross-sections of the corpus and cervix should be submitted for microscopic examination in order to evaluate the extent of septation of the lumen. The lumen of the fetal uterus is a slit-like potential space with a smooth lining, whereas the lining of the much larger cervix displays numerous delicate mucosal folds toward the end of gestation. The histological characteristics of the fetal uterine corpus and cervix are the focus of this chapter.

Embryology

In the middle of the eighth postfertilization week, the paramesonephric ducts meet in the midline at an acute, "V"-shaped angle where the rostral wall of the uterine fundus will develop [1]. The ducts fuse and grow caudally to end in the posterior wall of the urogenital sinus at the site of the sinusal (Müllerian) tubercle at the end of the eighth week [2]. This fused segment of the paramesonephric ducts is the uterovaginal canal and it will form the uterus and the rostral four-fifths of the vagina [1]. Each of the two fused ducts immediately develops a lumen that is lined by undifferentiated simple, to slightly pseudostratified cuboidal, to low columnar epithelium derived from the paramesonephric mesodermal epithelium. The epithelium becomes thick, columnar, and stratified. The undifferentiated mesenchyme of the uterovaginal canal forms a wall that is distinctly thicker than that of the developing fallopian tube [3]. The mesenchyme is derived from the paramesonephric mesoderm and, to some extent, from mesonephric mesoderm of the mesonephric ducts that are embedded in the outer layers of the mesenchymal wall of the uterovaginal canal. The "V"-shaped point of fusion of the paramesonephric ducts is remodeled partly by retrograde fusion of the ducts in a rostral direction, so that the top of the uterine fundus becomes flat and then finally acquires its definitive domed shape.

During approximately the 11th and 12th postmenstrual weeks, the common wall between the two paramesonephric ducts disappears and the uterovaginal canal has a single lumen. During approximately the 13th and 14th postmenstrual weeks, the uterine corpus becomes anatomically distinct from the uterine cervix, and the anterior and posterior vaginal fornices appear and form a distinct demarcation between the uterine cervix and the vagina. Not until the 16th postmenstrual week does the vaginal epithelium become stratified squamous and distinct from the uterine stratified columnar epithelium [3].

Histology

The corpus and cervix change little histologically until the beginning of the third trimester [4]. Both the endometrium and endocervix are devoid of glands until the

end of the midtrimester when cervical glands start to develop (see Figs. 16-1–16-3).



FIGURE 16-1. Uterine corpus at 19 weeks: low magnification. The slit-like lumen of the uterus is lined by columnar epithelium, which is devoid of glands. The endometrial stroma is very cellular and blends into the myometrium with little demarcation. The serosa is thin and extends laterally into the broad ligament on each side of the uterus (arrows). (Hematoxylin and eosin [H&E], 4 \times .)

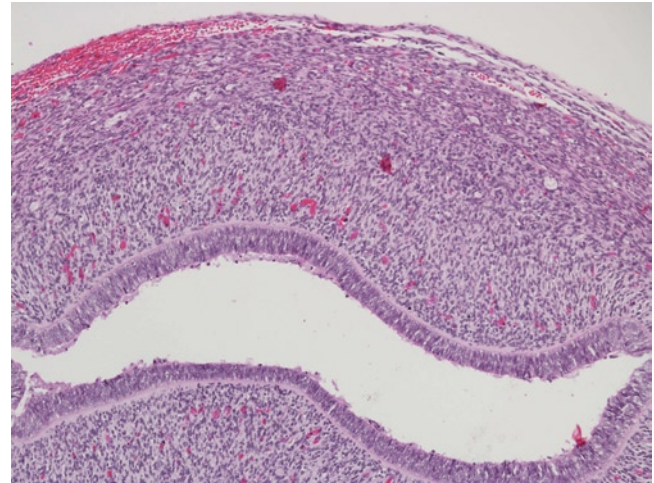


FIGURE 16-2. Uterine corpus at 19 weeks: higher magnification. This higher magnification shows the smooth endometrial lining without glands. The epithelium retains the appearance of the early uterovaginal canal with a stratified or pseudostratified columnar architecture. The basement membrane is usually prominent in the fetal and neonatal endometrium, while the stroma is poorly demarcated from the outer myometrium. (H&E, 10 \times .)

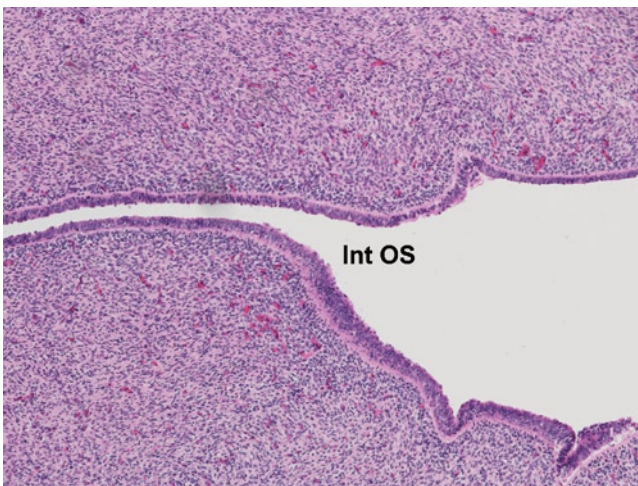


FIGURE 16-3. Uterus at 19 weeks. This longitudinal section shows the internal os (Int OS). The endometrial (right) and endocervical (left) epithelial lining are very similar at this age and both are devoid of glands. (H&E, 10 \times .)

Uterine Corpus

During the midtrimester, the surface epithelium of the endometrium retains the appearance of the early uterovaginal canal with a stratified or pseudostratified columnar architecture. The underlying stroma is very cellular and composed of ovoid cells with scanty cytoplasm. The endometrial stroma is poorly demarcated from the myometrium (see Fig. 16-2). Late in the midtrimester, the first few glands begin to appear in the endocervix but the appearance of endometrial glands is very variable [5] and, when present, they are short, straight, simple, and wide-mouthed (see Figs. 16-4 and 16-5). The endometrial stroma and myometrium begin to become more distinct but the thickness of the endometrium is about the same as that of the myometrium at this age (see Figs. 16-5 and 16-6). The endometrial glands

remain simple in nature and basically unchanged until late in the third trimester (see Fig. 16-7). The smooth muscle cells gradually develop more eosinophilic cytoplasm and are clearly spindle-shaped in contrast to the more rounded endometrial stromal cells, which have less cytoplasm (see Figs. 16-8 and 16-9). The fascicular nature of the myometrium becomes more prominent during the third trimester and the myometrium becomes thicker than the endometrium (see Figs. 16-8 and 16-10). Under the influence of maternal hormones, the endometrium of the near-term fetus may develop rapidly and may have a transient proliferative appearance or, less commonly, a weak secretory appearance at birth (see Figs. 16-8–16-10). These changes regress during the first 2 weeks after birth (see Fig. 16-11) [6].



FIGURE 16-4. Uterine corpus at 21 weeks: low magnification. A few simple glands can be seen at this age. These early glands are rather simple, straight, and wide-mouthed; compare them to branching cervical glands at a similar gestational age as shown in Figure 16-12. The thickness of the endometrium equals that of the myometrium, which is becoming slightly more eosinophilic; compare to Figure 16-1. (H&E, 4 \times .)

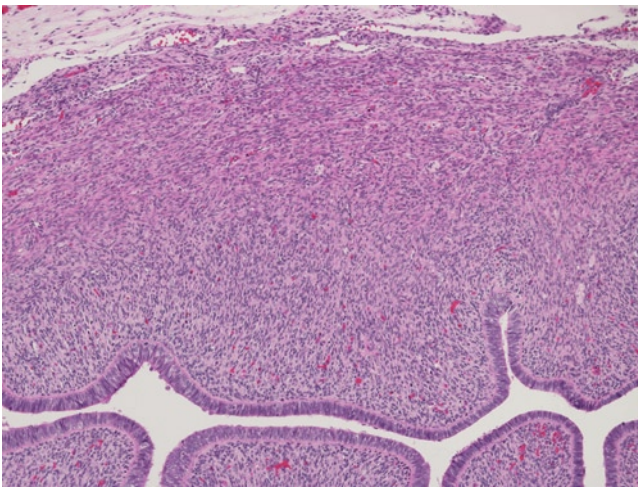


FIGURE 16-5. Uterine corpus at 21 weeks: higher magnification. This closer view of the early endometrial glands shows that they represent simple invaginations of the surface epithelium. The endometrial stroma in the inner half of the wall blends into the outer myometrium. The latter begins to have a predominantly concentric smooth muscle fiber arrangement. (H&E, 10 \times .)

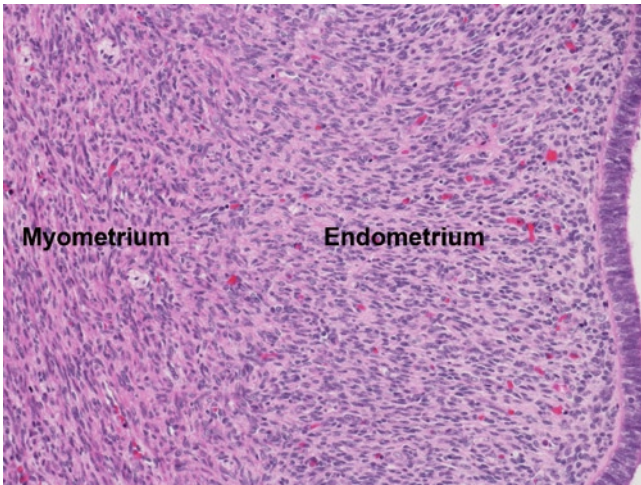


FIGURE 16-6. Endometrium at 21 weeks. This closer view shows the junction between the endometrial stroma and myometrium. The surface epithelium is stratified or pseudostratified columnar. (H&E, 20 \times .)

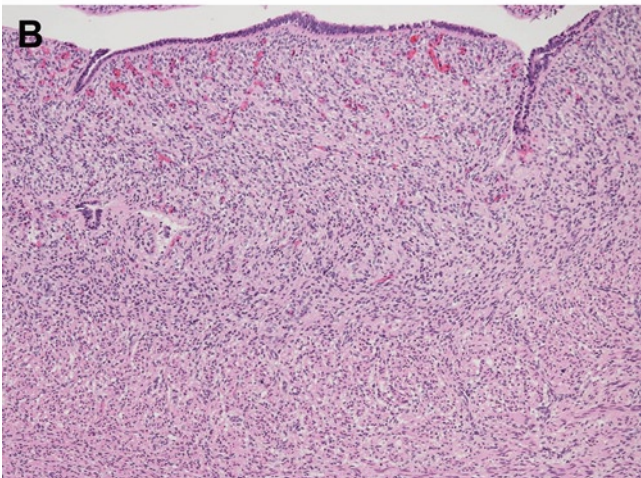
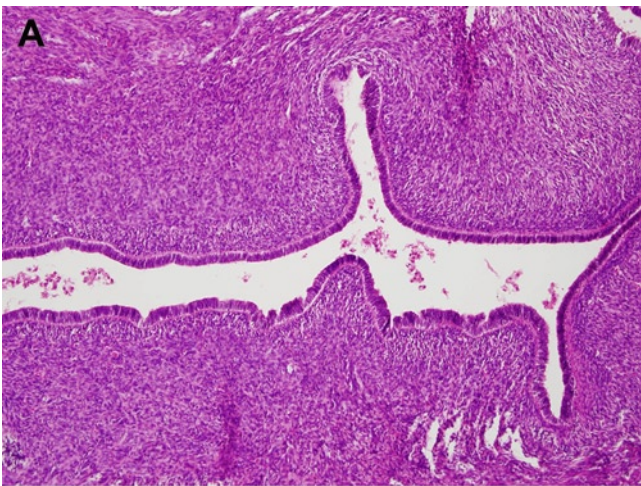


FIGURE 16-7. Endometrium at 28 (A) and 32 (B) weeks. The endometrial glands remain simple and scanty. (H&E, 10 \times .)

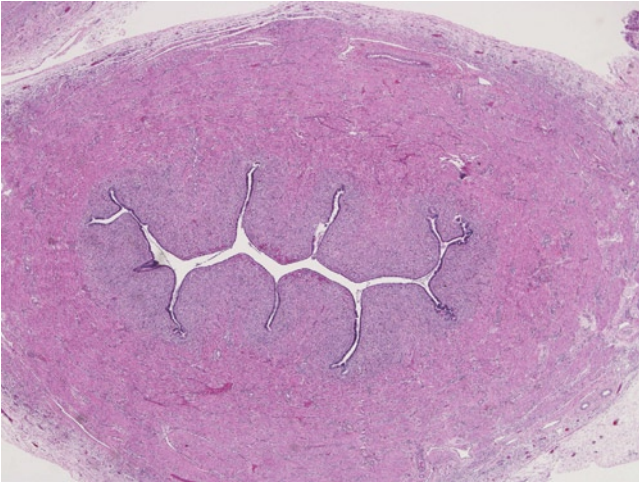


FIGURE 16-8. Uterine corpus at 35 weeks. The endometrial glands begin to branch and occupy the full depth of the mucosa. The endometrial stroma is well demarcated from the myometrium and the latter has become thicker than the endometrium; compare to Figure 16-4. (H&E, 2 \times .)

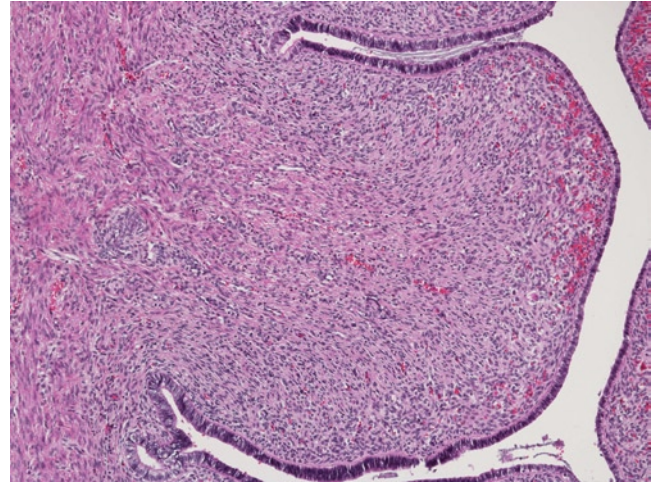


FIGURE 16-9. Endometrium at 35 weeks. This closer view of the endometrium shows the glands with simple branches reaching the myometrium (*left*). (H&E, 10 \times .)

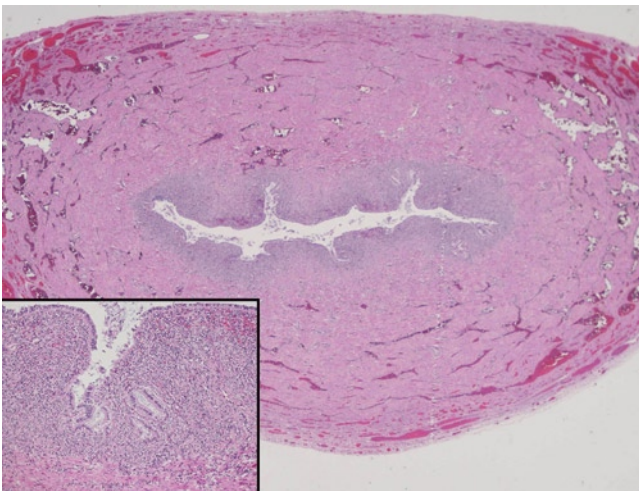


FIGURE 16-10. Uterine corpus at 38 weeks. This cross-section of the corpus shows a thick wall primarily occupied by the well-developed myometrium. The closer view of the endometrium (*inset*) demonstrates glands with mild secretory activity, a feature that can be observed in term fetuses. (H&E, 1 \times ; *inset*, 10 \times .)

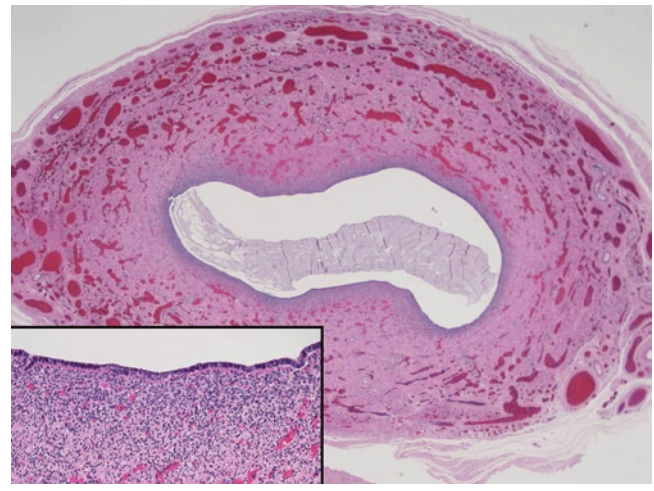


FIGURE 16-11. Uterine corpus 18 days after birth. This cross-section of the corpus shows a thinner endometrium with very rare, shallow glands and a single layer of low columnar epithelial cells on the surface (*inset*). Compare to Figure 16-10. (H&E, 1 \times ; *inset*, 20 \times .)

Uterine Cervix

During the early midtrimester, the endocervical lining is similar to the endometrium (see Fig. 16-3). Toward the end of the midtrimester, a few glands can be seen in the endocervical canal (see Fig. 16-12) and the endocervical glands develop a more complex branching pattern earlier than the endometrium (see Fig. 16-13). Mucus production becomes evident during the third trimester (see Fig. 16-14) and continues to be progressively more abundant toward the end of gestation as the glands enlarge, become longer, and exhibit a more complex branching pattern (see Figs. 16-15–16-17).

The vaginal portion of the cervix is known as the ectocervix or exocervix. It is covered by stratified squamous epithelium, which is identical to the mucosa of the vaginal fornices. Late in gestation, as the result of high mater-

nal estrogen levels, the squamous epithelium matures and accumulates glycogen in its upper layers in a fashion similar to the vaginal mucosa. The external os is the anatomical opening of the endocervical canal into the ectocervix; the opening is usually slit-like, side to side, at birth. The squamocolumnar junction between the endocervical and ectocervical mucosa does not always lie at the external os. In fact, this junction shifts throughout life [7]. The junction tends to "move" outward in the latter part of pregnancy and usually resides in the ectocervix in two-thirds of fetuses at birth (see Fig 16-16) [6]. After birth, the epithelial junction usually moves back into the endocervical canal and remains in that position until near menarche. In some fetuses, particularly near term, a large portion of ectocervix may be covered by columnar epithelium,



FIGURE 16-12. Uterine cervix at 23 weeks. A few glands can be seen in the endocervical canal, as shown. The glands begin branching relatively early, but otherwise the overall appearance of the endocervical wall is similar to corpus of the uterus at this age. Compare to Figure 16-4. (H&E, 4 \times .)

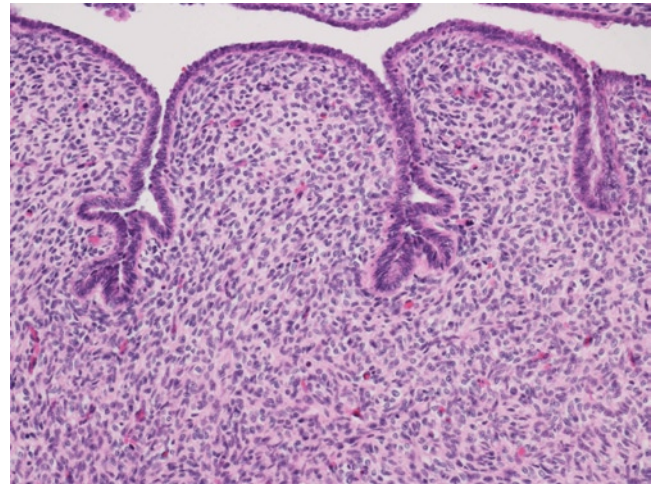


FIGURE 16-13. Uterine cervix at 24 weeks. The cervical surface and glandular epithelium is low columnar, as shown. Mucin production is not evident at this age. Note the more complex branching pattern of glands compared to the straight endometrial glands at the same gestational age. (H&E, 20 \times .)

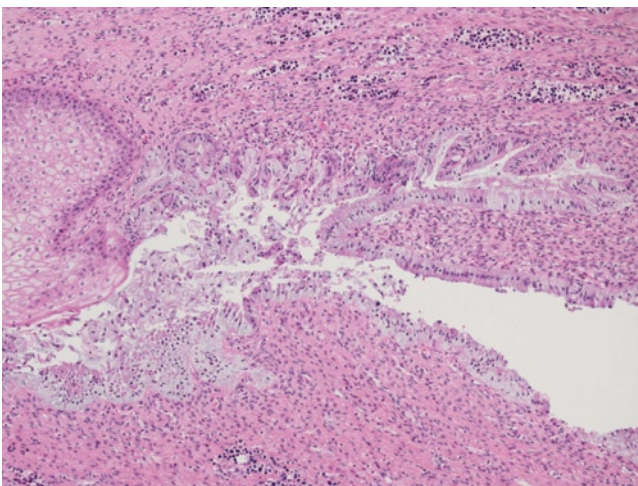


FIGURE 16-14. Uterine cervix at 32 weeks. At this age, mucus production by endocervical glands is scanty, as shown here. (H&E, 10 \times .)

sometimes including endocervical glands (see Fig 16-18). The replacement of the stratified squamous epithelium by columnar epithelium causes a grossly visible, sharply demarcated patch of brighter pink mucosa around

the os. This normal variant has been erroneously called "congenital erosion" because it does not represent a true erosion but the gross appearance of the thinner columnar epithelium.



FIGURE 16-15. Uterine cervix at 32 weeks. A few glands can be seen in the endocervical canal (Endoc). The glands are typically slanted, almost parallel to the lumen, and pointing to the fundus. The lips of the external os (Ext Os) are completely covered by stratified squamous epithelium. Vag—vagina. (H&E, 1×.)

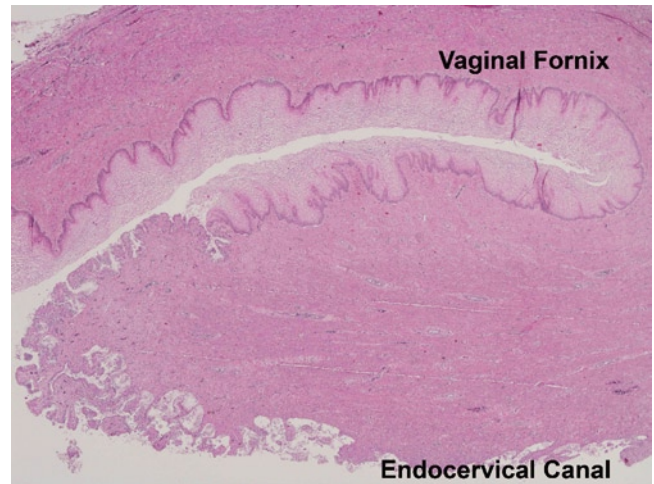


FIGURE 16-16. Uterine cervix at 35 weeks. Endocervical glands become more numerous and branching, particularly near the external os, as is shown here. Mucus production increases and the glands may become distended. The endocervical epithelium extends beyond the external os and covers the entire convexity of the portio vaginalis; compare to Figure 16-15. (H&E, 2×.)

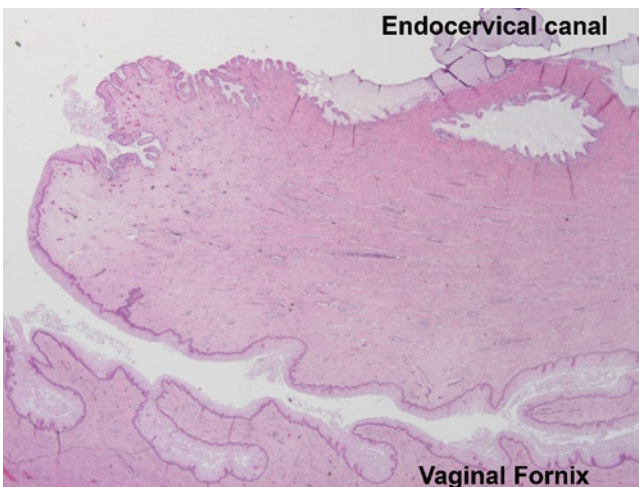


FIGURE 16-17. Uterine cervix at 38 weeks. Mucus production is abundant at term and the lumen of the endocervical glands becomes distended, as shown here. (H&E, 1×.)

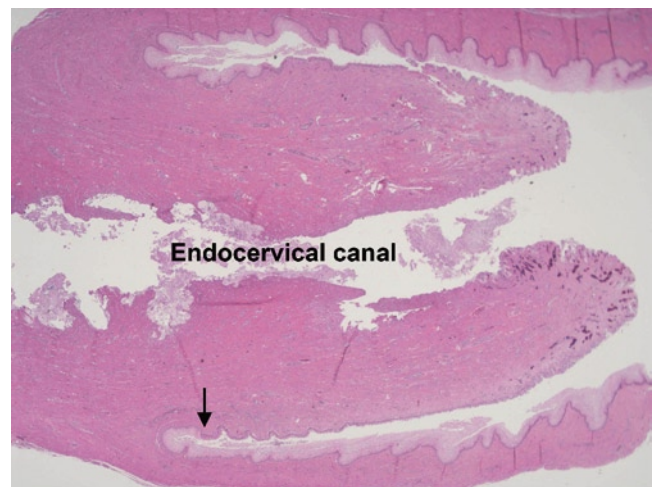


FIGURE 16-18. Uterine cervix at 37 weeks. In some neonates the entire or part of the vaginal portion of the cervix is covered by columnar epithelium; this is called the *congenital erosion*. The squamocolumnar junction is at the vaginal fornix on one side in this example (arrow). (H&E, 1×.)

References

1. Jirásek JE: *An Atlas of Human Prenatal Developmental Mechanics*. New York: Taylor & Francis; 2004.
2. O&'Rahilly R, Muecke EC: The timing and sequence of events in the development of the human urinary system during the embryonic period proper. *Z Anat Entwicklungsgesch* 1972, 138:99–109.
3. Yasuda Y: Genital system. In *Atlas of Human Prenatal Histology*. Edited by Nishimura H. Tokyo: Igaku-Shoin; 1983:147–169.
4. Valdes-Dapena MA: *Histology of the Fetus and Newborn*. Philadelphia: Saunders; 1979:469–477.
5. Felix W: The development of the urinogenital organs. In *Human Embryology*. Edited by Keibel F, Mall FP. Philadelphia: Lippincott; 1912:752–979.
6. Hendrickson MR, Atkins KA, Kempson RL: *Uterus and Fallopian Tubes*. In *Histology for Pathologists*, edn 3. Edited by Mills SE. Philadelphia: Lippincott Williams & Wilkins; 2007:1011–1062.
7. Wright TC, Ferenczy A: Anatomy and histology of the cervix. In *Blaustein&s Pathology of the Female Genital Tract*. Edited by Kurman RJ. New York: Springer; 2002:207–224.

17

Vagina

Eduardo D. Ruchelli and Dale S. Huff

The vagina undergoes complex embryologic changes during the first and part of the second trimesters, which result in significant histological transformations. The histological appearance of the fetal vagina is also affected by placental and maternal hormonal influences that are unique to prenatal life. Those histological features are the focus of this chapter.

Embryology

The developing vagina is derived from the fused paramesonephric ducts and the paired sinovaginal bulbs. At the end of the eighth postfertilization week, the fused paramesonephric ducts join the posterior wall of the urogenital sinus at the site of the sinual (Müllerian) tubercle [1]. The tubercle is a thickened plaque on the posterior wall of the urogenital sinus between the orifices of the mesonephric ducts. It is composed of epithelium derived from the urogenital sinus, mesonephric ducts, and paramesonephric ducts together with the underlying mesoderm. The fused paramesonephric ducts each have a lumen except at their caudal ends, where they join the posterior wall of the urogenital sinus. At approximately the 11th or 12th postmenstrual week, two solid cords of epithelium from the urogenital sinus, the sinovaginal bulbs, arise at the posterolateral junctions of the mesonephric ducts with the sinual tubercle [2]. They grow rostrally and join the solid caudal ends of the paramesonephric ducts to form the solid vaginal plate. The rostral four-fifths of the vagina derives from the paramesonephric ducts and the caudal one-fifth derives from the urogenital sinus through the sinovaginal bulbs [3]. At the same time, the common wall between the fused paramesonephric ducts disappears and the single uterovaginal canal forms. The anterior and posterior vaginal fornices appear and establish the transition between the uterine cervix and the vagina.

The short urethral portion of the vesicourethral canal, immediately rostral to the orifices of the mesonephric ducts and the sinual tubercle, begins to rapidly elongate caudally to form the female urethra and to displace the sinual tubercle more and more caudally. By the 20th postmenstrual week the urethral orifice and the tubercle are at the introitus, and the tubercle differentiates into the hymenal ring [3].

Histology

The vaginal wall consists of three layers: the mucosa, muscularis propria, and adventitia. Starting at 16 postmenstrual weeks, the pseudostratified columnar vaginal epithelium differentiates into stratified squamous epithelium [2]. After the squamous epithelium replaces the Müllerian columnar epithelium, it proliferates and progressively occludes the

developing vagina (see Figs 17-1 and 17-2) [4]. Desquamation of the maturing epithelium leads to canalization of the vaginal plate (see Fig 17-3). By the 18th to 20th week, the development of the vagina is complete and the original Müllerian columnar epithelium of the uterovaginal canal is entirely replaced by stratified squamous epithelium from the urogenital sinus [5, 6]. Starting at 16 weeks gestation, the squamous epithelium begins to mature and accumulate glycogen, under the influence of placental estrogens (see Figs 17-4-17-8). The abundant intracytoplasmic glycogen in the superficial layers of the fetal vaginal epithelium will disappear after birth, when estrogen levels drop. Without hormonal stimulation the cells atrophy and postnatally the vaginal epithelium remains in an atrophic state until

puberty (see Fig. 17-9). The squamous epithelium rests on the lamina propria. During the early midtrimester the lamina propria blends into the muscularis propria, from which it is almost indistinguishable (see Fig 17-2). As the mesenchyme of the lamina propria matures, it becomes less cellular and more collagenized (see Fig 17-7). The muscularis propria is continuous with that of the uterus; thus, it is not surprising that the smooth muscle fascicles in both organs become more distinct during the third trimester (see Figs. 17-6 and 17-7). The outer layers of muscle of both uterus and vagina run longitudinally, extending to the region of the hymenal ring [5], whereas the inner muscle layer has a spiral-like course (see Fig. 17-8). The adventitia is a thin layer of connective tissue that merges with the stroma of the adjacent structures.

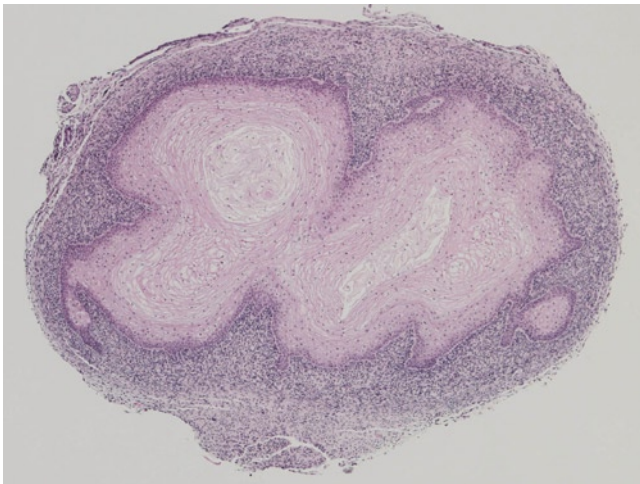


FIGURE 17-1. Vagina at 18 weeks gestation. This cross-section illustrates how the lumen at this age is occluded by proliferating squamous epithelium, which has replaced in the previous weeks the original Müllerian columnar epithelium of the uterovaginal canal. (Hematoxylin and eosin [H&E], 4×).

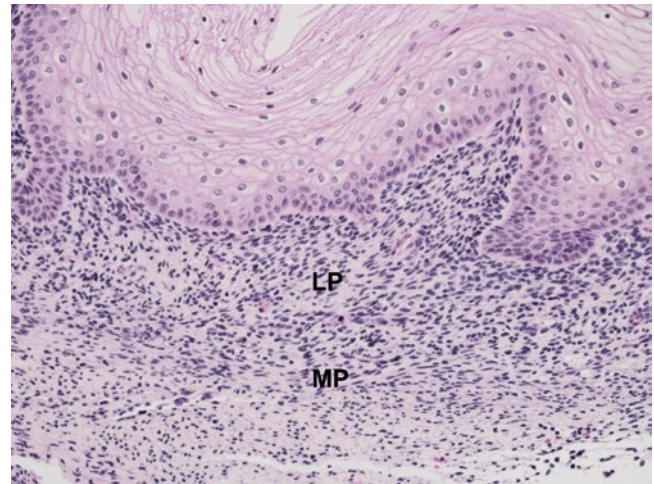


FIGURE 17-2. Vagina at 18 weeks gestation. The lamina propria (LP) consists of cellular mesenchyme and the muscularis propria (MP) is beginning to become distinct. (H&E, 20×.)

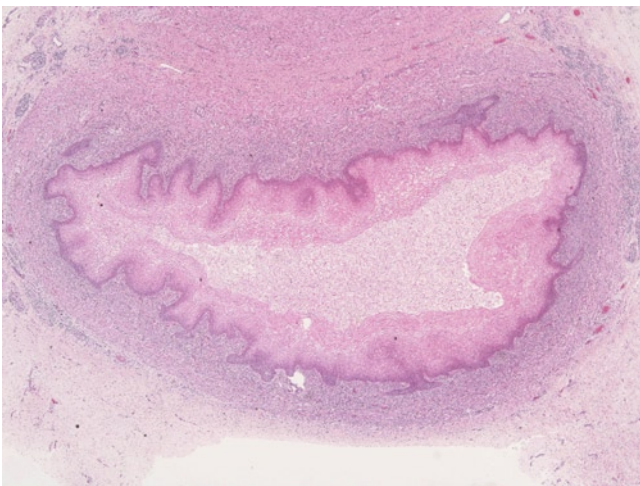


FIGURE 17-3. Vagina at 23 weeks gestation. Maturation of the epithelium under estrogen effect is accompanied by extensive desquamation, which leads to canalization of the vaginal plate (compare to Fig. 17-1). (H&E, 2×.)

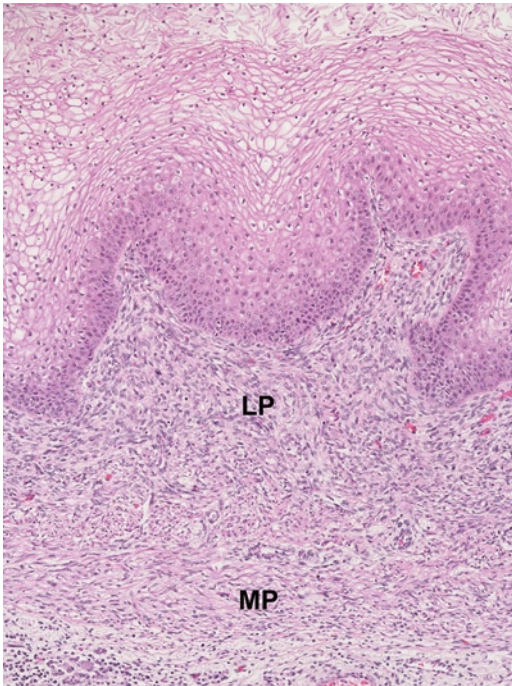


FIGURE 17-4. Vagina at 23 weeks gestation. The superficial layers of the squamous epithelium are rich in glycogen and the cells show abundant clear cytoplasm surrounding small pyknotic nuclei. Notice the cells desquamating into the lumen (*top*). The underlying cellular lamina propria (LP) is still poorly demarcated from the muscularis (MP). (H&E, 10 \times .)

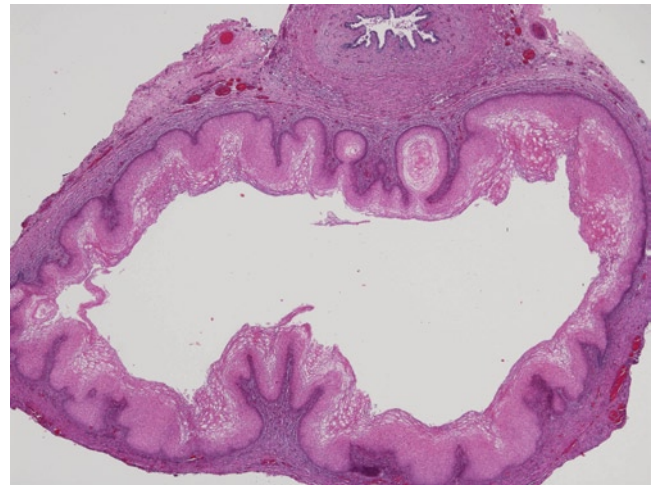


FIGURE 17-5. Vagina at 25 weeks gestation. The vaginal mucosa has an undulating appearance in contrast to the flat surface of the cervix. Notice the urethra (*top*) displacing the muscularis propria along the anterior wall of the vagina. (H&E, 2 \times .)

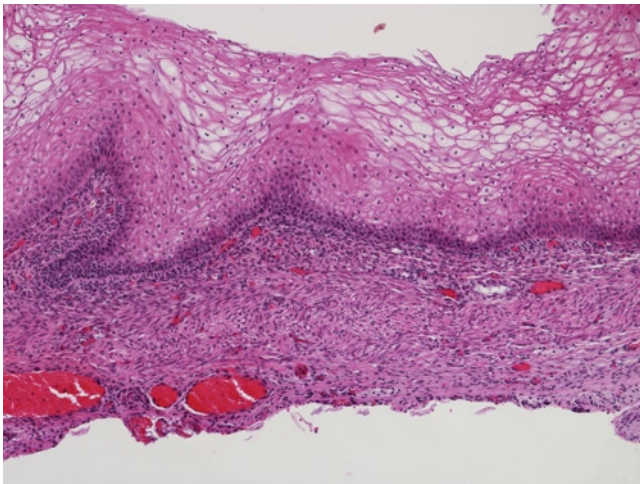


FIGURE 17-6. Vagina at 25 weeks gestation. The muscularis propria becomes more distinct but an inner layer is not evident yet. (H&E, 10 \times .)

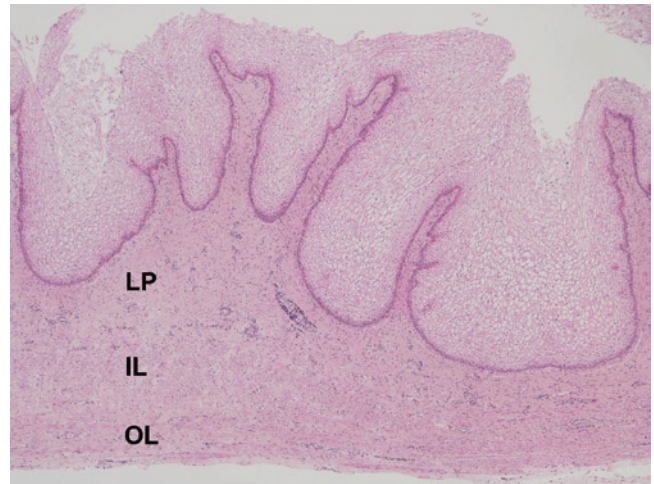


FIGURE 17-7. Vagina at 32 weeks gestation. The epithelium thickens and accumulates abundant glycogen in the latter part of gestation. The lamina propria (LP) becomes less cellular, more collagenized, and more distinguishable from the muscularis propria, which has now an inner layer (IL) and an outer layer (OL). (H&E, 4 \times .)

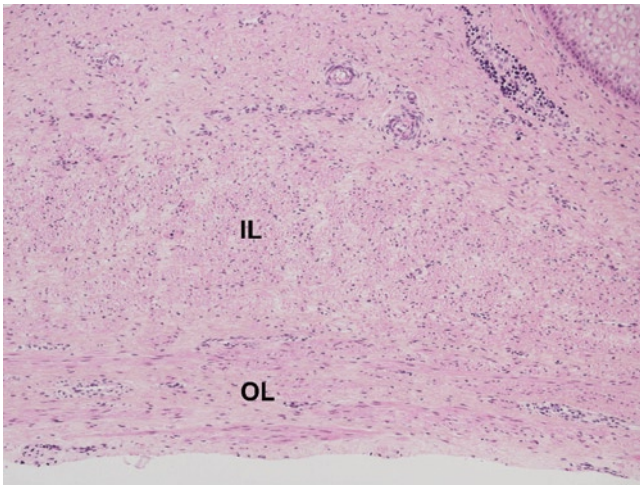


FIGURE 17-8. Vagina at 32 weeks gestation. The outer layer (OL) of the muscularis is continuous with the longitudinal fibers of the uterus. The inner muscle layer (IL) has a spiral-like configuration. (H&E, 10 \times .)

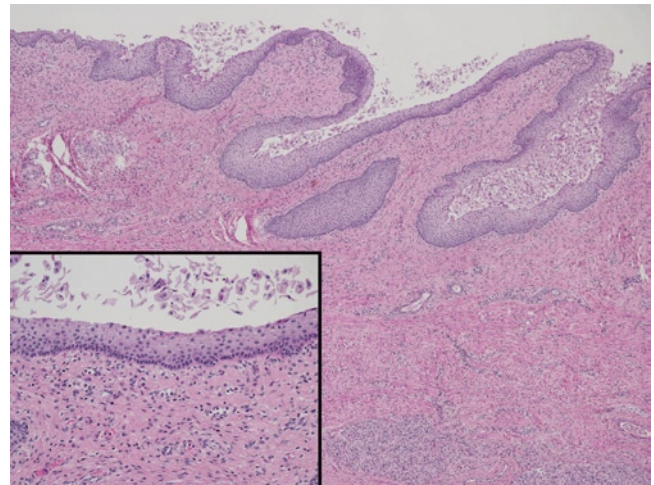


FIGURE 17-9. Vagina at 18 days of postnatal life. After birth, estrogen levels drop and the epithelium adopts an atrophic appearance with cells devoid of intracytoplasmic glycogen. Compare the inset with Figure 17-7. (H&E, 4 \times ; inset, 20 \times .)

References

1. O'Rahilly R, Muecke EC: The timing and sequence of events in the development of the human urinary system during the embryonic period proper. *Z Anat Entwicklungsgesch* 1972, 138: 99–109.
2. Yasuda Y: Genital system. In *Atlas of Human Prenatal Histology*. Edited by Nishimura H. Tokyo: Igaku-Shoin; 1983:147–169.
3. Jirásek JE: *An Atlas of Human Prenatal Developmental Mechanics*. New York: Taylor & Francis; 2004.
4. Forsberg JG: Cervicovaginal epithelium: its origin and development. *Am J Obstet Gynecol* 1973, 115:1025–1043.
5. Robboy SJ, Bentley RC: Vagina. In *Histology for Pathologists*, edn 3. Edited by Mills SE. Philadelphia: Lippincott Williams & Wilkins; 2007:999–1010.
6. Bulmer J: The development of the human vagina. *J Anat* 1957, 91:490–509.

SECTION V
Endocrine System

18

Adrenal Gland

Linda M. Ernst

The fetal adrenal gland is structurally significantly different from the adult adrenal gland. One of the obvious differences noted when performing fetal dissection is that the fetal adrenal gland is proportionately large, appearing nearly as large as the kidney in the early midtrimester. The normal adrenal gland weight in adults is about 5% of the normal kidney weight and, combined, the adrenals represent 0.02% of total adult body weight. The adrenal/kidney weight and adrenal/body weight ratios in fetuses are much higher throughout fetal life (see Fig. 18-1) [1,2]. The bulk of the fetal adrenal gland is largely due to the presence of the fetal adrenal cortex, or fetal zone, that produces dehydroepiandrosterone (DHEA) and DHEA-sulfate. These weak androgens are important precursors of placental estrogens. Later in gestation the fetal adrenal gland will also produce aldosterone and cortisol. Therefore, the fetal adrenal gland is an organ of immense importance for maintenance of pregnancy and fetal homeostasis. The hormone production also promotes organ maturation late in gestation and may assist in the timing of labor [3]. After birth, the fetal zone of the adrenal gland involutes and the adrenal weight is markedly reduced.

Adrenal Weight and Proportions of Kidney and Body Weight

Gestational age (wks)	Adrenal weight, combined (g)	Percentage of Kidney weight	Percentage of Body weight
12	0.1	62.5	5
13	0.15	71.4	5
14	0.22	62.9	4
15	0.33	54.1	4
16	0.48	49.5	4
17	0.65	48.9	4
18	0.83	47.4	4
19	1.03	45.2	4
20	1.23	42.6	4
21	1.43	41.3	4
22	1.64	39.0	4
23	1.83	36.5	4
24	2.02	35.7	3
25	2.19	33.6	3
26	2.35	31.3	3
27	2.5	29.1	3
28	2.7	27.8	3
29	3.0	27.5	3
30	3.3	26.8	3
31	3.7	27.0	3
32	4.1	27.0	3
33	4.6	27.3	3
34	5.1	27.6	3
35	5.6	27.9	3
36	6.1	28.1	3
37	6.6	28.3	3
38	7.1	28.6	3
39	7.4	28.4	3
40	7.7	28.2	3

(Data from Hansen *et al.* [1] and Siebert [2].)

FIGURE 18-1. Adrenal weight and proportions of kidney and body weight.

Embryology

The adrenal glands develop as bilateral structures within the intermediate mesoderm in intimate association with the dorsal root mesentery medially and the mesonephros and gonad laterally [4,5]. The first cells to populate that mesodermal area in approximately the fifth week of gestation are derived from the overlying mesothelial/celomic lining. These mesothelial cells proliferate and penetrate into the underlying tissue forming the first cells of the adrenal gland, the fetal cortical cells. As the cells differentiate, they become large polygonal cells with abundant eosinophilic cytoplasm. Within a short period of time, a second layer of cells, which also originate from the mesothelial lining cells, surrounds the developing fetal cortex. These cells will form the definitive cortex, and as they differentiate will be generally smaller and

less eosinophilic than the fetal cortical cells. The position of the developing adrenal glands relative to adjacent structures shifts caudally whereas that of the kidneys shifts cranially and the two meet to take their final positions.

The cells of the adrenal medulla are derived from neural crest cells. Initially, the neuroblastic cells, derived from the neural crest, form collections along the aorta that will become the paravertebral sympathetic ganglia. Nerve fibers from the sympathetic ganglia penetrate the developing adrenal gland, and neuroblastic cells migrate along these tracts. The final destination of these neural crest derivatives is the central portion of the gland, but migrating neuroblastic-type cells can be seen singly or in small groups within the fetal cortex throughout fetal life and even into the neonatal period [6,7].

Histology

General Overview

The fetal adrenal gland is an encapsulated organ composed of two main areas—the outer cortex and the central medulla—similar to the adult organ. However, the cortex of the fetal adrenal gland is much thicker than the adult gland and consists of at least two

histologically distinct layers: the definitive zone and the fetal zone (see Fig. 18-2). It is the fetal zone, recognized by its large eosinophilic cells, that contributes to the large size of the fetal adrenal and will undergo involution after birth.

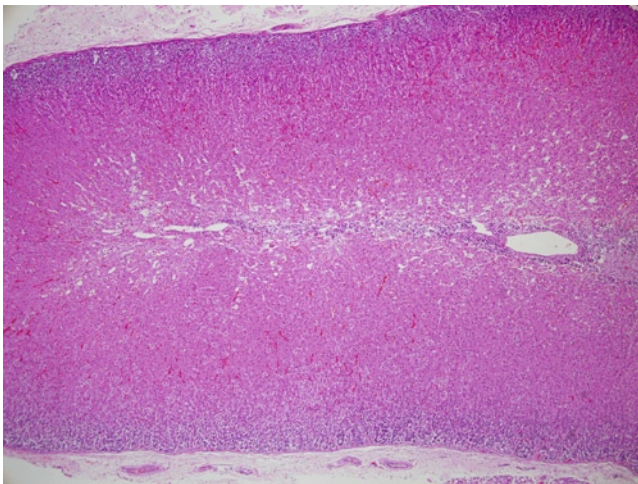


FIGURE 18-2. Adrenal gland at 39 weeks gestation. Low-power view of term adrenal gland. Note the thin capsule. The definitive zone of the cortex is the most superficial layer with the more closely packed, darkly stained cells. The much thicker fetal zone of the cortex has the more eosinophilic appearance. In the center, large thin-walled vessels are noted, surrounded by medullary cells (H&E, 4 \times .)

Capsule

The capsule is thin and not very prominent in the second trimester, consisting only of thin layers of collagen and

elastic tissue. By the late third trimester, the capsule is only slightly thicker (compare in Figures 18-3–18-7).

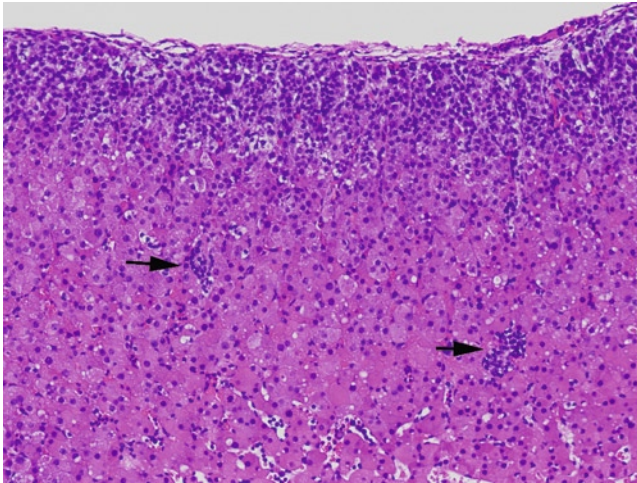


FIGURE 18-3. Adrenal gland at 12 weeks gestation. Note the thin capsule. The definitive zone of the cortex is the most superficial layer, with the more closely packed, darkly stained cells. The deeper layer with the more eosinophilic appearance is fetal zone. Small clusters of migrating neuroblasts on their path to the medulla are seen within the fetal cortex (arrows). (H&E, 10 \times .)

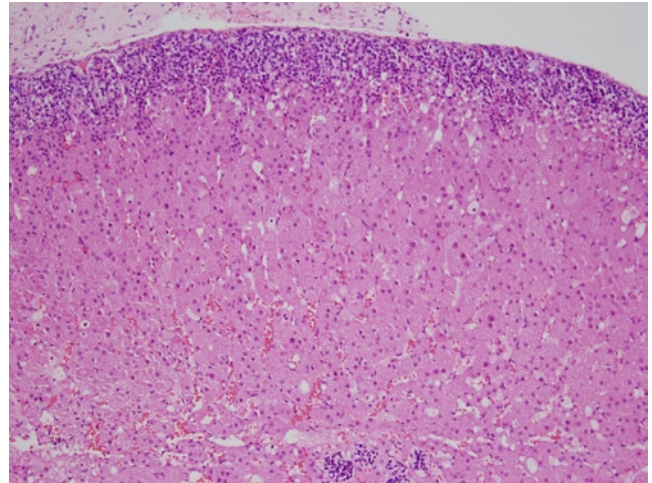


FIGURE 18-4. Adrenal gland at 17 weeks gestation. Overall, the organization and appearance of the definitive zone of the cortex (most superficial layer) and the deeper fetal zone have not changed since 12 weeks. (H&E, 10 \times .)

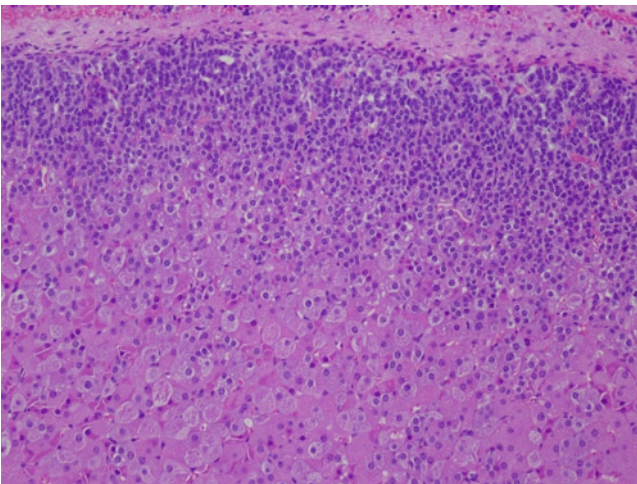


FIGURE 18-5. Adrenal gland at 20 weeks gestation. Low-power view of the superficial definitive zone of the cortex and deeper fetal zone. (H&E, 10 \times .)

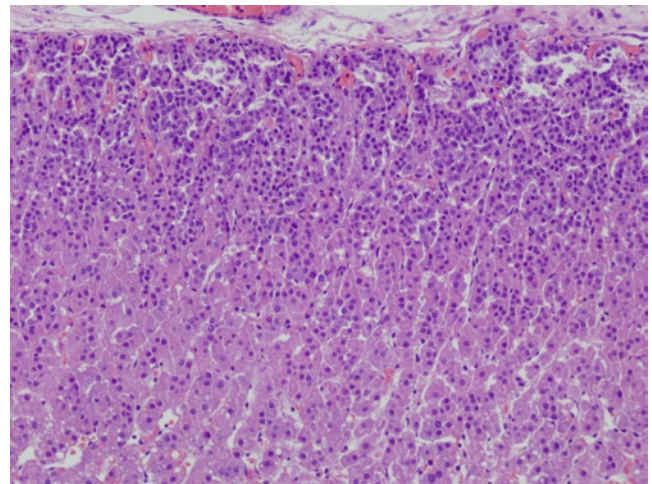


FIGURE 18-6. Adrenal gland at 26 weeks gestation. Adrenal cortex showing the distinction between the superficial definitive zone and the deeper fetal zone. Note the nature of the cortical cells arranged in cords with vascular sinusoids between them. (H&E, 10 \times .)

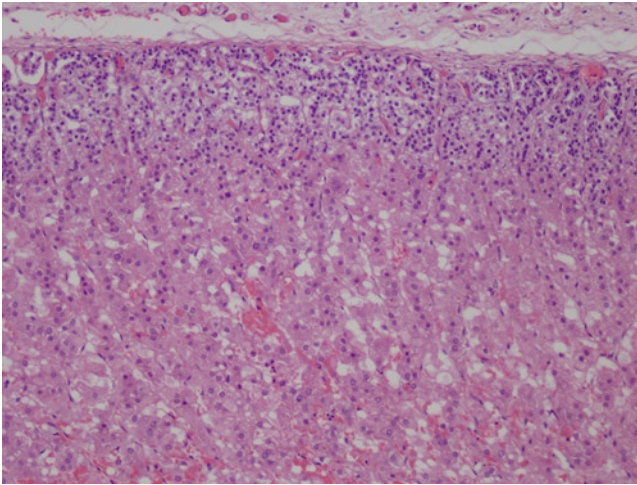


FIGURE 18-7. Adrenal gland at 35 weeks gestation. Low-power view of the adrenal cortex showing the distinction between the superficial definitive zone and the deeper fetal zone. Note the nature of the cortical cells arranged in cords with vascular sinusoids between them. (H&E, 10 \times .)

Cortex

The adrenal cortex is composed of two histologically distinct layers in fetal life (see Figs. 18-3–18-7). The most superficial layer of the cortex, located directly beneath the capsule, is known as the definitive zone, adult zone, or neocortex. It is recognizable by its basophilic appearance on hematoxylin and eosin (H&E)-stained sections. This definitive zone is thin (10–20 cells thick), and in the fetal adrenal represents only a small fraction of the entire cortical layer. The layer is composed of nonoverlapping polygonal cells with round nuclei and scant eosinophilic to pale, sometimes vacuolated, cytoplasm (see Figs. 18-8–18-10). The tightly packed cells with scant cytoplasm give the overall basophilic appearance to the definitive cortex. During fetal life, the stratification that is present in adult adrenal cortex into zona glomerulosa, fasciculata, and reticularis is not visible. However, near term, the beginnings of this zonation may be seen as the zona glomerulosa becomes organized into small clusters distinct from the cords of the zona fasciculata (see Fig. 18-11). All three layers of the definitive cortex are well-developed within the first few months of life.

The fetal zone, also known as provisional cortex or transitional cortex, constitutes the remainder and majority of the adrenal cortex in fetal life. The fetal zone of the adrenal gland is not present in most mammals, but is seen in humans and a few nonhuman primates [3,8,9]. It is distinguished histologically from the definitive zone by its large size and eosinophilic appearance

(see Fig. 18-2, 18-4, 18-11). The epithelial cells of the fetal zone are large polygonal cells with round nuclei and abundant eosinophilic, sometimes vacuolated, cytoplasm (see Fig. 18-12). These cells are generally arranged in columns separated by sinusoidal vascular spaces, although sometimes the fetal cortical cells appear so tightly packed that the sinusoidal spaces are difficult to appreciate. The fetal zone represents the majority of the adrenal gland in fetal life, but begins to involute rapidly after birth. Involution of the fetal cortex involves loss of the eosinophilic fetal cortical cells and is typically associated with some hemorrhage within the fetal cortex (see Figs. 18-13 and 18-14). Loss of this layer of the adrenal gland leads to a greater than 50% decrease in the gland size during the first months of neonatal life [3]. The involutional process and reorganization is generally completed by 4 to 6 weeks after birth [7].

A third zone, known as the transitional zone, has been described using immunohistochemical studies [10]. This zone lies between the definitive zone and the fetal zone. Its role is to produce cortisol late in gestation and will become the zona fasciculata in the infant [3,10]. This zone appears to have a similar thickness (10–20 cells) as the definitive zone and contains tightly packed cells, which are only slightly larger than those in the definitive zone. These features may make the transitional zone hard to recognize as a distinct layer on routine H&E-stained sections.

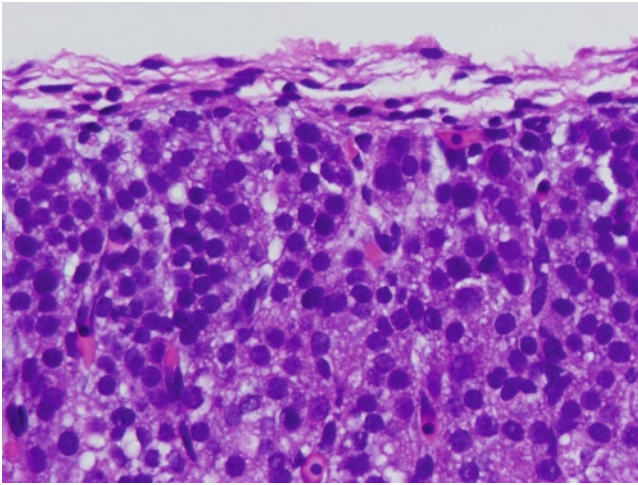


FIGURE 18-8. Adrenal gland at 12 weeks gestation, capsule and definitive zone. The capsule is composed of a few layers of collagen and elastic tissue. Note there is no distinction between separate layers of the definitive cortex. Cells of the definitive zone are small, with hyperchromatic round nuclei, arranged in cords. (H&E, 40 \times .)

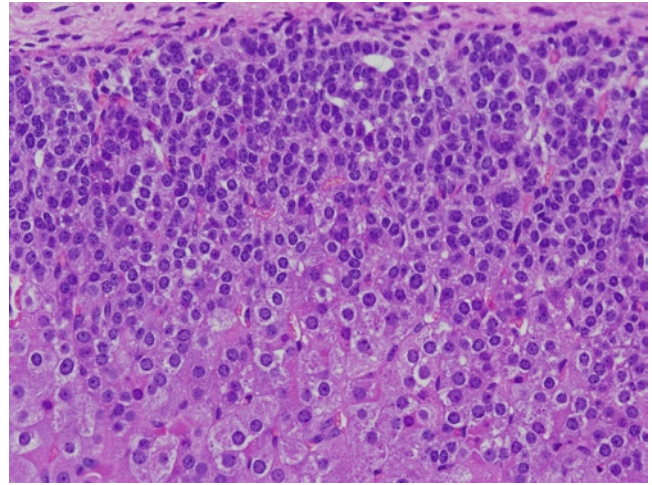


FIGURE 18-9. Adrenal gland at 20 weeks gestation, junction between definitive and fetal zones. Although there is no distinction of layers in the definitive cortex, a small pseudoglandular space is present. (H&E, 20 \times .)

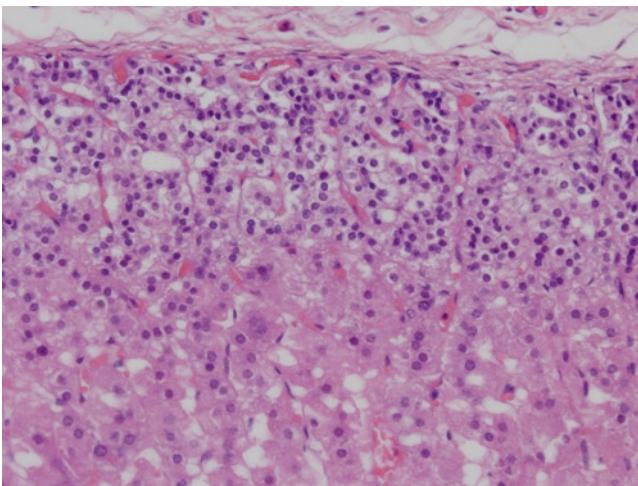


FIGURE 18-10. Adrenal gland definitive zone at 35 weeks gestation. The definitive zone is still arranged in cords, but now newly forming small clusters are suggested superficially, the beginnings of the zona glomerulosa. (H&E, 20 \times .)

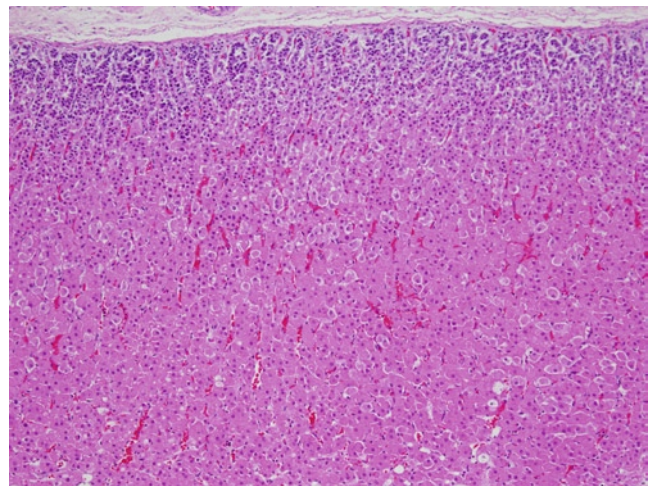


FIGURE 18-11. Adrenal gland at 39 weeks gestation. Low-power view of term adrenal gland cortex. Note the early organization of the definitive zone with clusters of cells in the zona glomerulosa. The lower two-thirds of the image is occupied by the eosinophilic-appearing fetal zone. (H&E, 10 \times .)

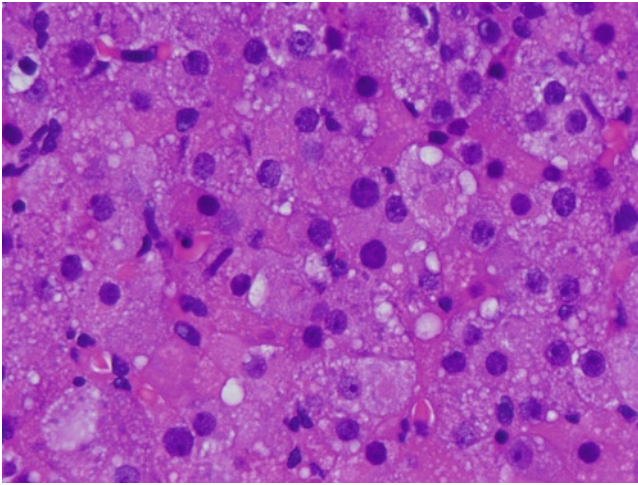


FIGURE 18-12. Adrenal gland at 12 weeks gestation. Higher-power view of the fetal zone. Larger polygonal cells with abundant eosinophilic cytoplasm and focal fine vacuolation make up the fetal cortex. Nuclei are uniformly round. (H&E, 40 \times .)

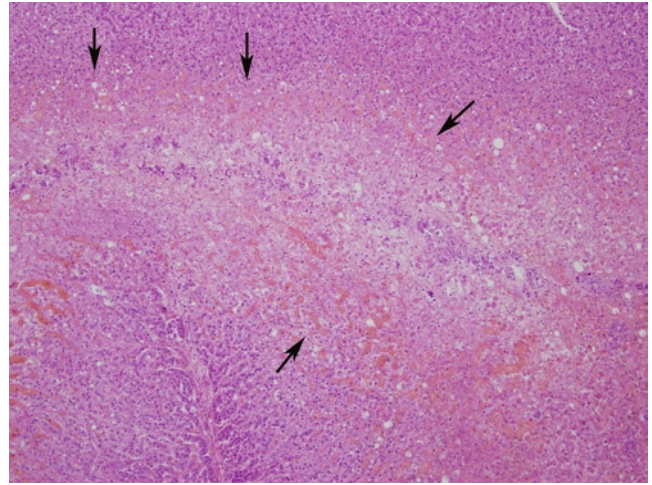


FIGURE 18-13. Involution of fetal cortex/zone. Adrenal gland from a pre-term infant who lived for 6 weeks postnatally. The fetal zone (outlined by arrows) is markedly reduced in thickness and cellularity. Congestion and hemorrhage are also present. (H&E, 10 \times .)

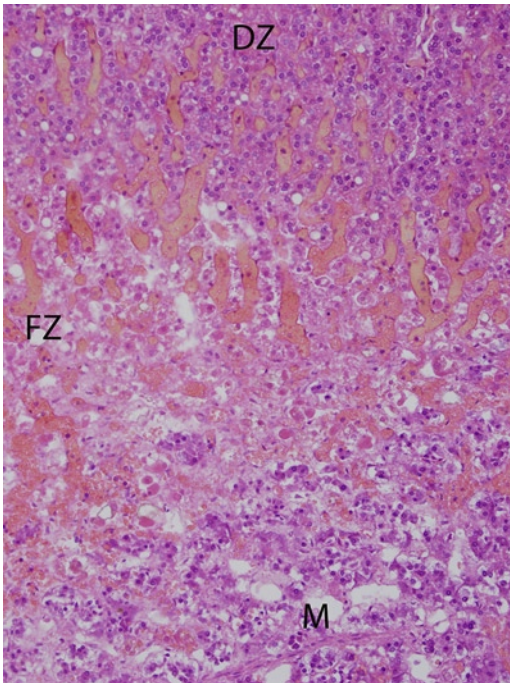


FIGURE 18-14. Involution of fetal cortex/zone. Higher-power view of the adrenal gland from a pre-term infant who lived for 6 weeks postnatally. The involuting fetal zone (FZ) is seen between the definitive zone (DZ) and medulla (M). The polygonal epithelial cells of the fetal zone show degenerative/involucional changes. Congestion and hemorrhage are also present. (H&E, 20 \times .)

Medulla

The fetal adrenal medulla is not the well-formed chromaffin cell mass that is seen in the center of the adult adrenal gland. As reviewed in the embryology section, the cells of the adrenal medulla are neural crest-derived, and in fetal life these neuroblastic cells migrate into the adrenal gland from the cortex inward. Their route of migration can be seen in sections of the fetal adrenal gland, as single neuroblastic cells or small groups within the cortex. Neuroblastic nodules are unencapsulated groups of densely packed cells with high nuclear/cytoplasmic ratios, scanty cytoplasm, and nuclei with dense granular chromatin. Therefore, they are easily differentiated from the large eosinophilic cells of the fetal zone of the cortex. Turkel *et al.* [7] provide a detailed histological study of the size, location, and histological appearance of neuroblastic nodules in fetal adrenal glands from 10 to 30 weeks gestation. Neuroblastic cells are seen in both superficial/subcapsular and deep locations. Superficial groups are seen at the youngest gestational ages and decline with increasing gestational age. Superficial neuroblasts are rare after 20 weeks gestation. However, deep groups are seen throughout gestation (see Figs. 18-15 and 18-16), including the presence of even a few nodules at the time of birth [11]. Later in gestation, the neuroblastic nodules are present in the center of the gland surrounding central veins of the medulla (see Fig. 18-17).

The size of the neuroblastic nodules also varies over gestational age with the increasing size of nodules until the peak size is attained between 17 and 20 weeks gestation. The size of the neuroblastic nodules decreases thereafter with the smallest nodules noted late in

gestation. Differentiation of the neuroblastic cells to chromaffin cells is likely the reason for the decrease in number and size of the neuroblastic nodules over gestation. Chromaffin cells appear at the periphery of the neuroblastic nodules and can be recognized as cells that are larger than the neuroblasts with larger nuclei showing a finely granular chromatin pattern and cytoplasm containing brownish granules (see Fig. 18-18). Therefore, chromaffin cells are seen in greater numbers in later gestational ages.

In the past, there has been controversy about how to deal with neuroblastic cells seen in the adrenal gland after birth. Is this a normal variant? Are these developmental remnants? Does it represent a precursor to malignancy? Is it a frank malignancy? The presence of incidentally encountered microscopic nodules of neuroblastic cells with cytological features of neuroblastoma in the adrenal glands of children led to the concept of *in situ* neuroblastoma of the adrenal gland [12]. Beckwith and Perrin [12] noted that these lesions were seen only microscopically, had no associated metastases, and were otherwise clinically insignificant. The prevalence of the lesions at autopsy suggested to the authors that the majority of *in situ* neuroblastomas may actually regress or differentiate into normal or hyperplastic chromaffin cells. Shimada [13] also noted that, to date, no clonal proliferation has been demonstrated in these lesions, and that the photomicrographs provided of *in situ* neuroblastoma in the original manuscript had the morphologic characteristics of favorable histology neuroblastoma, a lesion now known to be in the process of regression or undergoing age appropriate maturation.

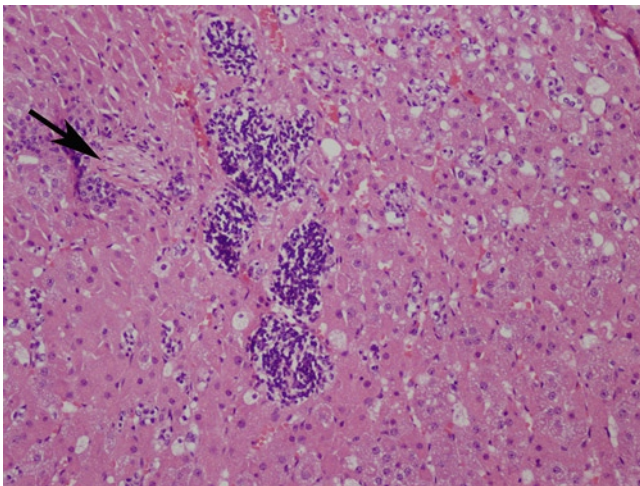


FIGURE 18-15. Adrenal gland at 17 weeks gestation. Section from near the center of the gland to show irregular clusters of neuroblastic cells, characterized by their small, round, hyperchromatic nuclei and scant cytoplasm located within the fetal zone of the cortex. Note the adjacent small nerve twig (arrow) close to the cluster of neuroblastic cells. (H&E, 10 \times .)

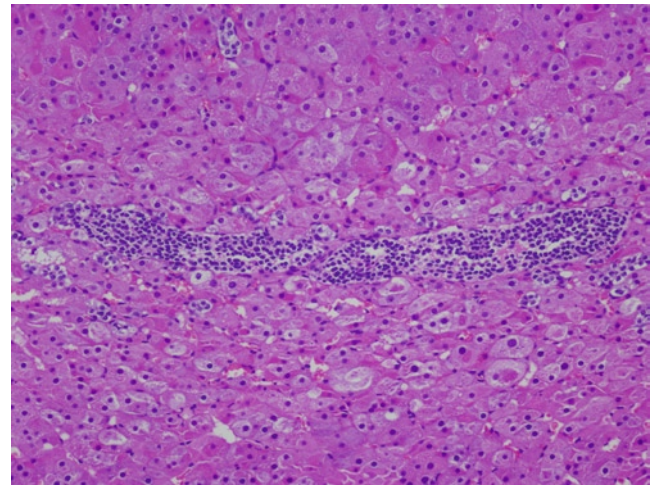


FIGURE 18-16. Adrenal gland at 20 weeks gestation. Center of the gland showing the clusters of neuroblastic cells that have migrated through the cortex and come to rest in the center of the gland. (H&E, 10 \times .)

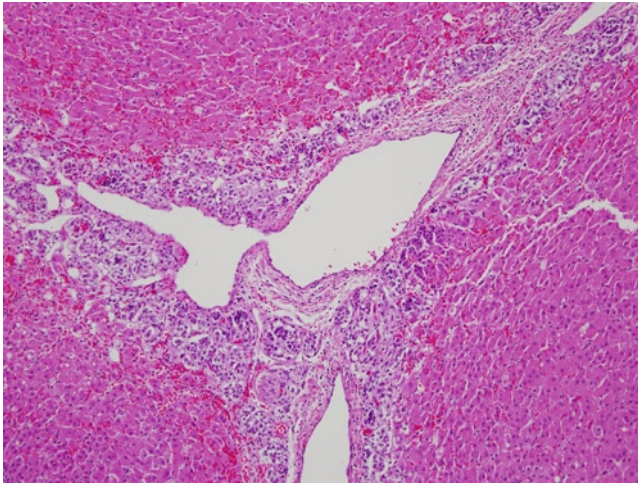


FIGURE 18-17. Adrenal gland at 39 weeks gestation. Low-power view of central region of term adrenal gland. Note the neuroblastic cells are seen mostly surrounding the central adrenal vein. (H&E, 10 \times .)

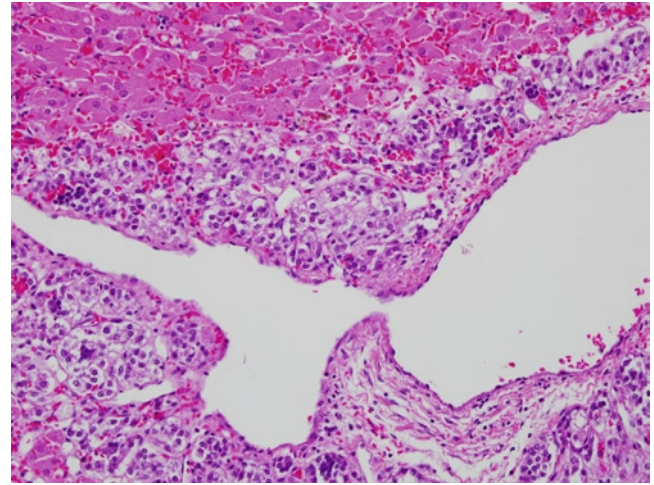


FIGURE 18-18. Adrenal gland at 39 weeks gestation. Higher-power view of the center of the term adrenal gland. Medullary cells appear less neuroblastic and take on a more chromaffin-like appearance, with more abundant, granular cytoplasm. (H&E, 20 \times .)

Special Considerations

Heterotopic Adrenal Tissue

Small nodules of cortical tissue are frequently seen adjacent to the adrenal gland and are generally not considered to represent an abnormality (see Fig. 18-19). They may be a reflection of the plane of section and/or irregularity of the gland. However, the finding of normal-appearing adrenal tissue in an abnormal location is not infrequent in fetal autopsy material (see Fig. 18-20). The most frequent locations are adjacent to the kidney, gonads, gonadal vessels, Fallopian tube, epididymis, and vas deferens. The intimate association of the developing adrenal gland with the mesonephros and gonad

accounts for the most common locations of adrenal heterotopias. In our experience, the heterotopic adrenal tissue usually consists only of cortical tissue. These small nodules of adrenal cortex contain both fetal and definitive cortex, and are likely embryonic remnants that have followed an aberrant migratory course. In most instances, these adrenal heterotopias have no clinically significant effects on the fetus. More remote sites for heterotopic adrenal tissue have been reported, such as the liver [14], central nervous system [15–17], lung [18], and placenta [19,20].

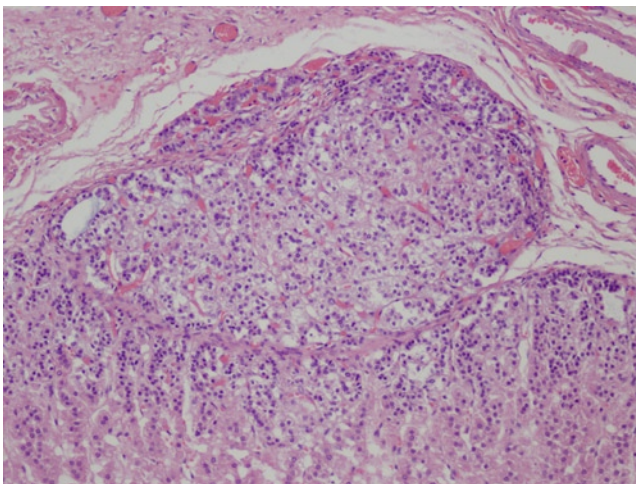


FIGURE 18-19. Nodule of adrenal cortical tissue adjacent to the capsule at 35 weeks gestation. Note that it has components of both definitive and fetal cortex. (H&E, 10 \times .)

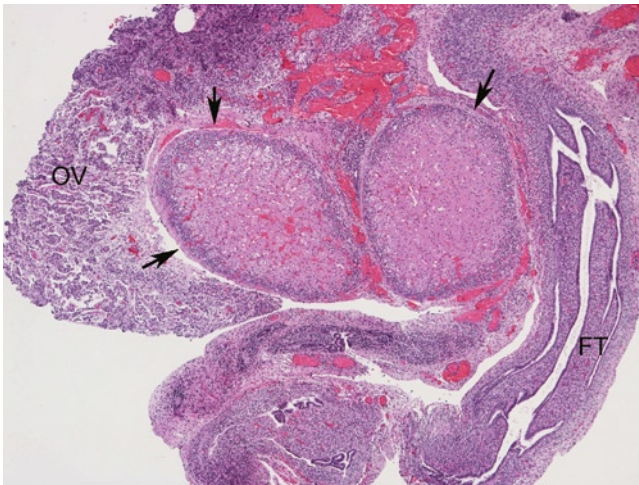


FIGURE 18-20. Heterotopic adrenal tissue in perigonadal location. Two nodules of normal-appearing adrenal tissue are noted (arrows) between the Fallopian tube (FT) and ovary (OV). Note the adrenal tissue consists of cortical tissue from the definitive zone and fetal zone. (H&E, 4 \times .)

Adrenal Cytomegaly

The fetal cortex occasionally contains cells with markedly enlarged nuclei (≥ 3 times the size of the adjacent fetal cortical cells). They also appear hyperchromatic, with nuclear atypia and occasional intranuclear cytoplasmic pseudoinclusions (see Figs. 18-21 and 18-22). The presence of these cells is not specific for a single

condition, and has been described in patients with Beckwith-Weidemann syndrome [21,22], the cytomegalic type of congenital adrenal hypoplasia [23], trisomy 13, and infants of diabetic mothers. Adrenal cytomegaly may also be seen as an unexpected finding without any clinical correlation.

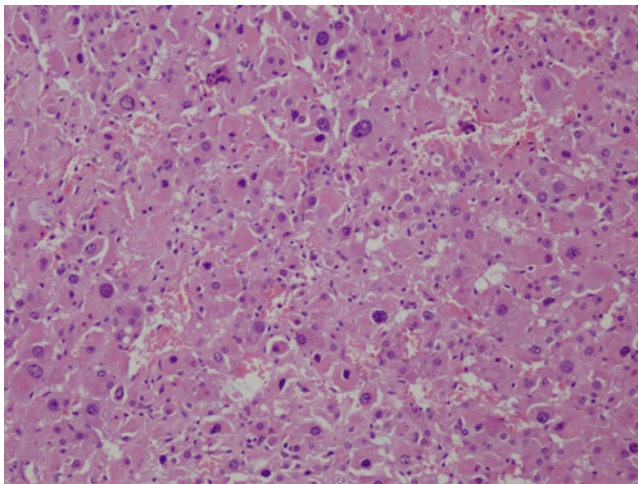


FIGURE 18-21. Adrenal cytomegaly. Low-power view of fetal adrenal gland at 22 weeks gestation showing adrenal cytomegaly within the fetal cortical cells. Note the patchy enlargement of nuclei at least three times larger than normal adjacent fetal cortical nuclei. (H&E, 10 \times .)

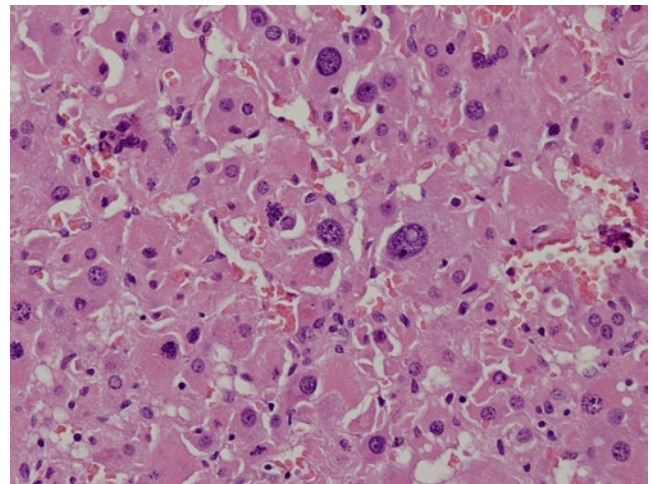


FIGURE 18-22. Adrenal cytomegaly. Higher-power view of fetal adrenal gland at 22 weeks gestation showing adrenal cytomegaly within the fetal cortical cells. Note the intranuclear cytoplasmic pseudoinclusion. (H&E, 20 \times .)

Adenoid Change in the Definitive Zone of the Cortex

The definitive cortical zone in fetal life frequently is not homogeneous and shows cystic spaces within the layer. These round to irregular spaces are lined by the resident cortical cells that surround a slightly basophilic-appearing proteinaceous fluid (see Fig. 18-23). This has been referred to adenoid change or pseudofollicular change,

and its pathogenesis is uncertain. It may represent cytolysis of cortical cells that experience oxidative stress from hypoxic ischemic injury [24,25], but this finding should be interpreted with caution because it may also represent a normal developmental process, especially in very immature fetuses [26,27].

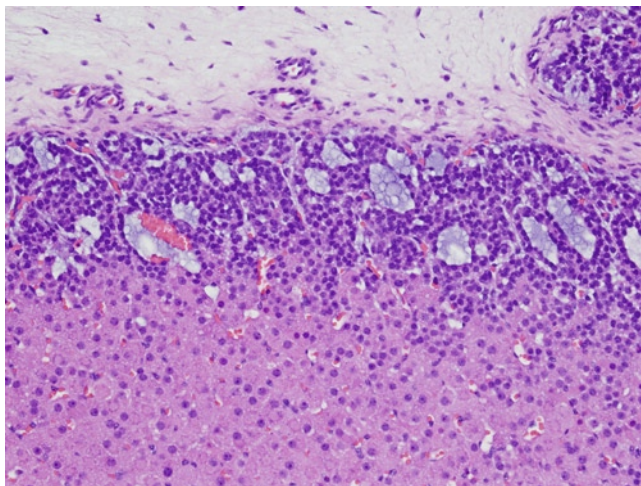


FIGURE 18-23. Adenoid change in the fetal adrenal gland. Adrenal gland at 18 weeks gestation showing definitive adrenal cortex with adenoid change. Note the round to irregular spaces containing basophilic material. (H&E, 20 \times .)

Calcifications

Calcifications of the adrenal gland are generally not a feature of the normal adrenal gland.

Extramedullary Hematopoiesis

Occasional islands of extramedullary hematopoiesis may be found in the normal fetal adrenal gland. These likely represent secondary areas of extramedullary

expansion and, if more than occasional, should be interpreted as evidence of hypoxic stress or fetal anemia.

References

1. Hansen K, Sung CJ, Huang C, *et al.*: Reference values for second trimester fetal and neonatal organ weights and measurements. *Pediatr Dev Pathol* 2003, 6:160–167.
2. Siebert J: Perinatal, fetal and embryonic autopsy. In *Potter's Pathology of the Fetus, Infant, and Child*, edn 2. Edited by Gilbert-Barnes E. Philadelphia: Mosby Elsevier; 2007:726–727.
3. Rainey WE, Rehman KS, Carr BR: Fetal and maternal adrenals in human pregnancy. *Obstet Gynecol Clin North Am* 2004, 31:817–835, x.
4. Sadler TW, Langman J: *Langman's Medical Embryology*, edn 11. Philadelphia: Wolters Kluwer Lippincott Williams & Wilkins; 2010.
5. Schoenwolf GC, Larsen WJ: *Larsen's Human Embryology*, edn 4. Philadelphia, PA: Elsevier/Churchill Livingstone; 2009.
6. Hervonen A: Development of catecholamine—storing cells in human fetal paraganglia and adrenal medulla. A histochemical and electron microscopical study. *Acta Physiol Scand Suppl* 1971, 368:1–94.
7. Turkel SB, Itabashi HH: The natural history of neuroblastic cells in the fetal adrenal gland. *Am J Pathol* 1974, 76:225–244.
8. Mesiano S, Jaffe RB: Developmental and functional biology of the primate fetal adrenal cortex. *Endocr Rev* 1997, 18:378–403.
9. Pepe GJ, Albrecht ED: Regulation of the primate fetal adrenal cortex. *Endocr Rev* 1990, 11:151–176.
10. Suzuki T, Sasano H, Takeyama J, *et al.*: Developmental changes in steroidogenic enzymes in human postnatal adrenal cortex: immunohistochemical studies. *Clin Endocrinol (Oxf)* 2000, 53:739–747.
11. Coupland RE: The natural history of the chromaffin cell—twenty-five years on the beginning. *Arch Histol Cytol* 1989, 52:331–341.
12. Beckwith JB, Perrin EV: In situ neuroblastomas: a contribution to the natural history of neural crest tumors. *Am J Pathol* 1963, 43:1089–1104.
13. Shimada H: In situ neuroblastoma: an important concept related to the natural history of neural crest tumors. *Pediatr Dev Pathol* 2005, 8:305–306.
14. Vestfrid MA: Ectopic adrenal cortex in neonatal liver. *Histopathology* 1980, 4:669–672.
15. Drut R, Quijano G, Altamirano ME, *et al.*: Vascular malformation and choroid plexus adrenal heterotopia: new findings in Beckwith-Wiedemann syndrome? *Fetal Pediatr Pathol* 2006, 25:191–197.
16. Kepes JJ, O'Boynick P, Jones S, *et al.*: Adrenal cortical adenoma in the spinal canal of an 8-year-old girl. *Am J Surg Pathol* 1990, 14:481–484.
17. Mitchell A, Scheithauer BW, Sasano H, *et al.*: Symptomatic intradural adrenal adenoma of the spinal nerve root: report of two cases. *Neurosurgery* 1993, 32:658–661; discussion 61–62.
18. Marchevsky AM: Lung tumors derived from ectopic tissues. *Semin Diagn Pathol* 1995, 12:172–184.
19. Guschmann M, Vogel M, Urban M: Adrenal tissue in the placenta: a heterotopia caused by migration and embolism? *Placenta* 2000, 21:427–431.
20. Labarrere CA, Caccamo D, Telenta M, *et al.*: A nodule of adrenocortical tissue within a human placenta: light microscopic and immunocytochemical findings. *Placenta* 1984, 5:139–143.
21. Beckwith J: Macroglossia, omphalocele, adrenal cytomegaly, gigantism, and hyperplastic visceromegaly. *Birth Defects* 1969, 5:188–196.
22. Wiedemann HR: Familial malformation complex with umbilical hernia and macroglossia—a "new syndrome"? *J Genet Hum* 1964, 13:223–232.
23. Mamelle JC, David M, Riou D, *et al.*: Congenital adrenal hypoplasia of cytomegalic type. Recessive, sex-linked form. Apropos of 3 cases [in French]. *Arch Fr Pediatr* 1975, 32:139–159.
24. de Sa DJ: Adrenal changes in chorioamnionitis. *Arch Dis Child* 1974, 49:149–151.
25. de Sa DJ: Stress response and its relationship to cystic (pseudofollicular) change in the definitive cortex of the adrenal gland in stillborn infants. *Arch Dis Child* 1978, 53:769–776.
26. Lacson A, Desa DJ: Endocrine glands. In *Potter's Pathology of The Fetus, Infant, and Child*, edn 2. Edited by Gilbert-Barnes E. Philadelphia: Mosby Elsevier; 2007:1630.
27. Rodin AE, Hsu FL, Whorton EB: Microcysts of the permanent adrenal cortex in perinates and infants. *Arch Pathol Lab Med* 1976, 100:499–502.

19

Thyroid Gland

Linda M. Ernst

By the beginning of the fetal period, the thyroid gland has attained its proper anatomical position anterior to the laryngeal and tracheal structures and has acquired its bilobed shape with the two lobes connected by a narrow isthmus. However, the histological appearance of the fetal thyroid gland is quite different from the mature adult thyroid gland, especially early in the second trimester of gestation. Therefore, the tissues of the fetal thyroid gland may be overlooked or mischaracterized. This chapter reviews the histological changes in the thyroid gland over the fetal period and discusses the two main functional components of the thyroid gland: the thyroid follicles that produce colloid and the parafollicular C cells that produce calcitonin.

Embryology

The primordium of the thyroid gland begins to form in the posterior portion of the primitive tongue in the fourth week of gestation as an endodermal mass at the apex of the foramen cecum, a depression or shallow diverticulum in the midline of the sulcus terminalis [1,2]. After formation, the endodermal mass begins migrating caudally in the midline anterior to the pharynx and remains connected to the foramen cecum by the thyroglossal duct. By approximately the fifth week of gestation, the thyroglossal duct begins to break down and the thyroid mass becomes isolated from the tongue. As the thyroid mass descends, it begins to develop a bilobed shape. It migrates anterior to the hyoid bone and larynx to reach its final destination in front of the trachea by the seventh week of gestation. By this time, the thyroid gland has also acquired its final shape with two lateral lobes connected inferiorly by a thin isthmus. This endodermal tissue derived from the foramen cecum gives rise to the numerous follicles of the thyroid gland. The fetal thyroid follicular cells begin to produce colloid as early as the 10 to 12 weeks of gestation [3–5].

The parafollicular C cells of the thyroid gland migrate from an anatomically and embryologically distinct source, the ultimobranchial bodies, derived from the somewhat controversial fifth pharyngeal pouch (immediately inferior to the fourth pharyngeal pouch). The cells that populate the paired ultimobranchial bodies are derived from the neural crest [6] and, once populated by these cells, the ultimobranchial bodies detach from the pharynx and migrate caudally to become embedded into the upper lateral aspect of the thyroid gland.

Histology

The fetal thyroid gland is best examined by sampling sequential transverse sections of the "neck block," which includes all the soft tissues of the neck, posterior to the strap muscles, from the soft palate to the trachea (see Figs. 19-1 and 19-2). This will allow for examination of the laryngeal tissues, pharyngeal tissues, and thyroid gland resting anterior to the thyroid cartilage.

A thin fibrous capsule surrounds the thyroid gland and is sometimes closely approximated to the strap muscles of the neck. On low-power histological examination, the fetal thyroid gland frequently displays a

more cellular appearance than the adult thyroid gland because thyroid follicles are generally smaller in the fetus and colloid is less abundant. In addition, the fetal thyroid gland undergoes postmortem autolytic changes relatively quickly, which can lead to a collapse of the glandular architecture and the appearance of a nearly solid sheet of epithelium (see Fig. 19-3). However, in well-preserved second- and third-trimester fetal thyroid tissue, tightly packed round follicular elements containing colloid can be appreciated throughout the gland.



FIGURE 19-1. Fetal neck organs including the thyroid gland. This anterior view of fetal neck organs shows the horseshoe-shaped fetal thyroid gland resting over the thyroid and cricoid cartilages.

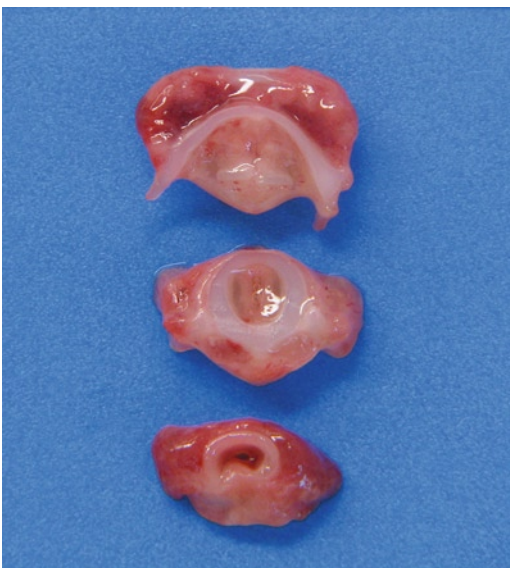


FIGURE 19-2. Fetal neck organs after serial sectioning in the transverse plane. Note the beefy red thyroid gland anterior to the laryngeal cartilages. All of these tissue sections can be submitted for histological examination.

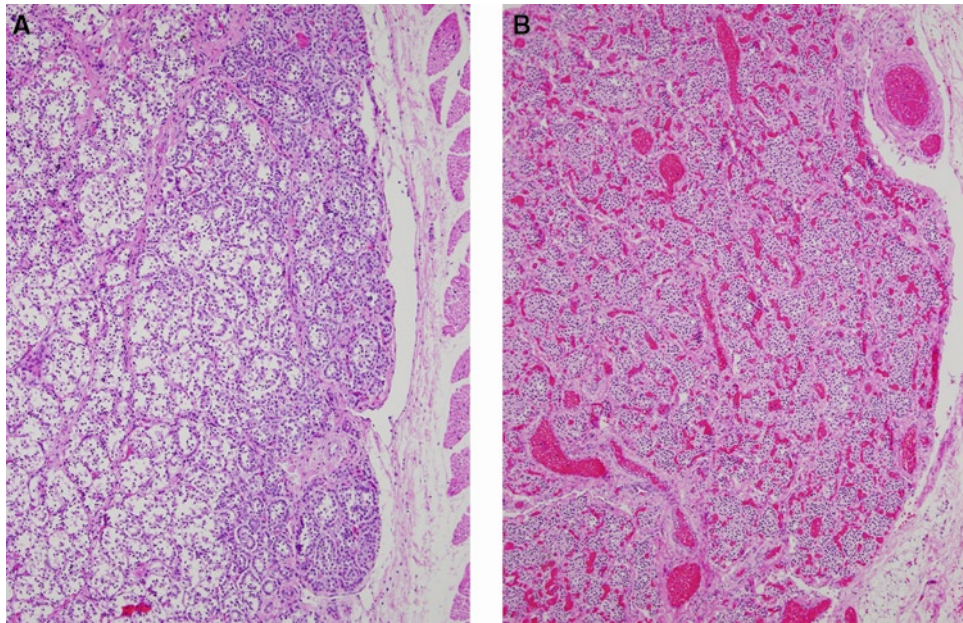


FIGURE 19-3. Autolysis of the fetal/neonatal thyroid gland. Rapid autolysis of the thyroid gland is a frequent problem in fetal autopsy specimens. There frequently is a collapse of the glandular architecture and nearly solid appearance of the gland,

which does not reflect the normal expected follicular development. **A**, Thyroid gland from a 27-week liveborn infant. **B**, Thyroid gland from a 32-week liveborn infant. (Hematoxylin and eosin [H&E], 10 \times .)

Thyroid Follicles

The follicles of the thyroid gland produce colloid, which contains the thyroid hormones necessary for proper fetal development, especially brain development. Thyroid follicles are formed by predominantly cuboidal epithelial cells. With increased secretory activity, the follicular cells may become slightly taller with more visible apical cytoplasm, which appears lightly eosinophilic. The lipofuscin pigment sometimes seen in adult thyroid follicular cells [7] is not identified in fetal follicular cells. Brown pigment within the fetal thyroid gland should raise suspicion for extrahepatic iron deposition, as seen in neonatal hemochromatosis, and should be confirmed by Prussian blue stain. The follicular cells rest their base on the follicular basement membrane. Their nuclei are round to oval and a small nucleolus can sometimes be seen.

Although fetal colloid production begins around 11 weeks gestation, intraluminal colloid is not a prominent

feature of the fetal thyroid gland in the late first trimester to early second trimester (see Figs. 19-4–19-7) and hormone production is limited until 18 to 20 weeks gestation [8]. Lightly stained eosinophilic secretions are seen within the follicles in the previable stage (see Figs. 19-8 and 19-9) and in the early third trimester colloid becomes more prominent within follicles (see Figs. 19-10 and 19-11). In general, thyroid follicles in the fetus appear larger toward the periphery of the gland, which may represent a progressive maturation of the follicles from center to periphery. Histochemical studies have shown that thyroid colloid stains with periodic-acid Schiff and toluidine blue stains and the colloid in the larger follicles demonstrates slightly more toluidine staining than small ones [9]. By near term (see Figs. 19-12 and 19-13) to term (see Figs. 19-14 and 19-15), there is enough colloid present to distend some of the follicles, especially at the periphery of the gland.

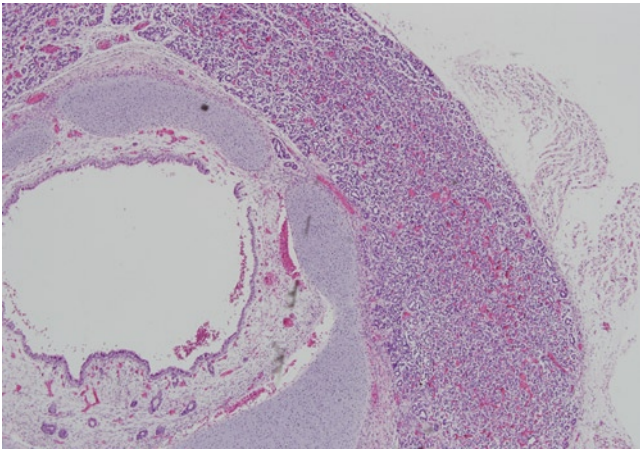


FIGURE 19-4. Low-power view of well-preserved fetal thyroid gland at 15 weeks gestation. Note that at low power early fetal thyroid has a cellular, almost solid appearance. However, on close inspection, the follicular development can be seen with the largest follicles at the periphery of the gland. Note the thin fibrous thyroid capsule. This section also includes a segment of laryngeal cartilages posterior to the gland. (H&E, 4×.)

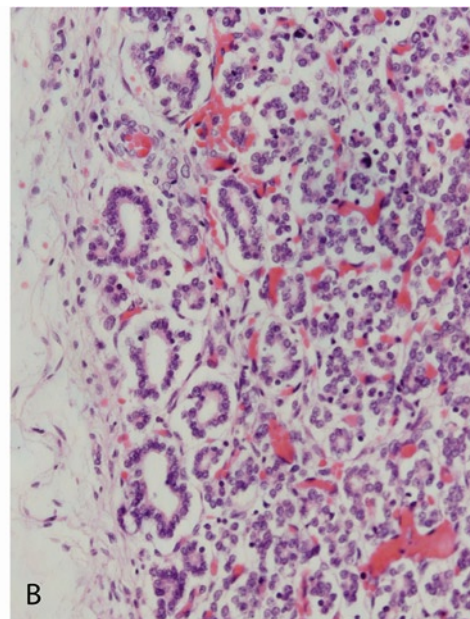
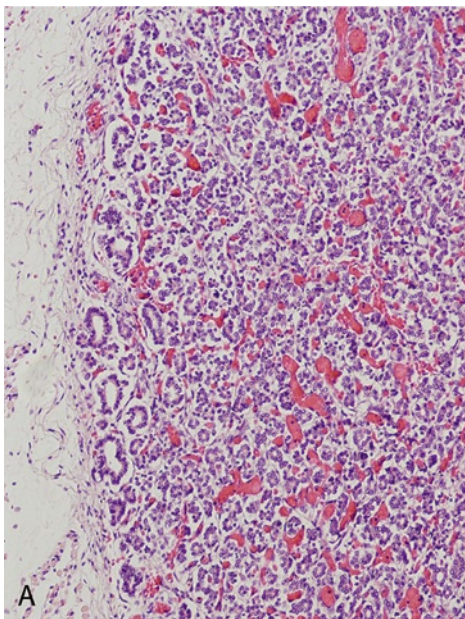


FIGURE 19-5. Higher power views of the fetal thyroid gland at 15 weeks gestation. Note the small follicular formation throughout the gland. At the periphery, the follicles are slightly larger and

intrafollicular colloid is scanty. Also note the rich capillary network in the interfollicular interstitial tissues and the delicate fibrous capsule. (H&E: **A**, 10× and **B**, 20×.)

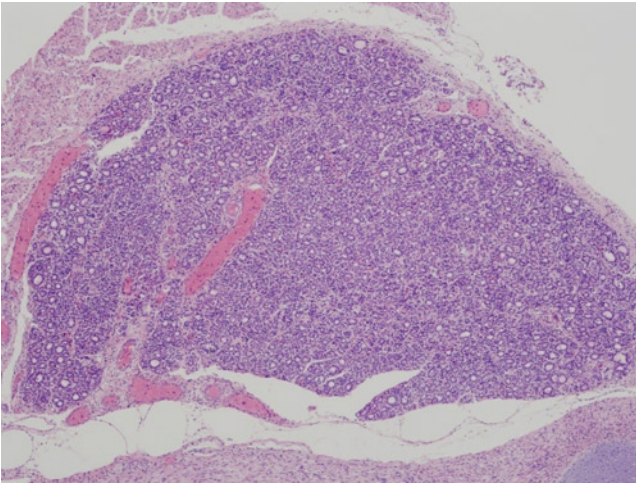


FIGURE 19-6. Low-power view of the fetal thyroid gland at 18 weeks gestation. (H&E, 4 \times .)

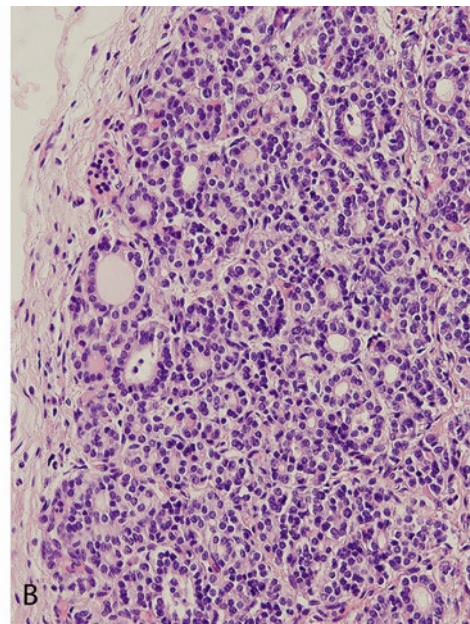
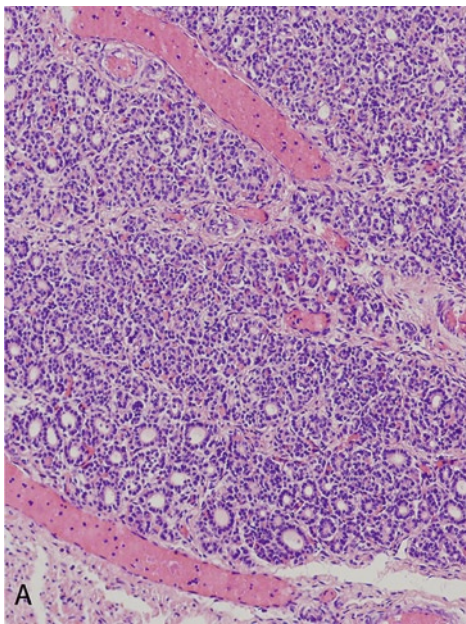


FIGURE 19-7. Higher power views of the fetal thyroid gland at 18 weeks gestation. Note the small follicular formation throughout the gland. At the periphery, the follicles are slightly larger.

Intrafollicular colloid is slightly more prominent than at 15 weeks gestation. (H&E: **A**, 10 \times and **B**, 20 \times .)

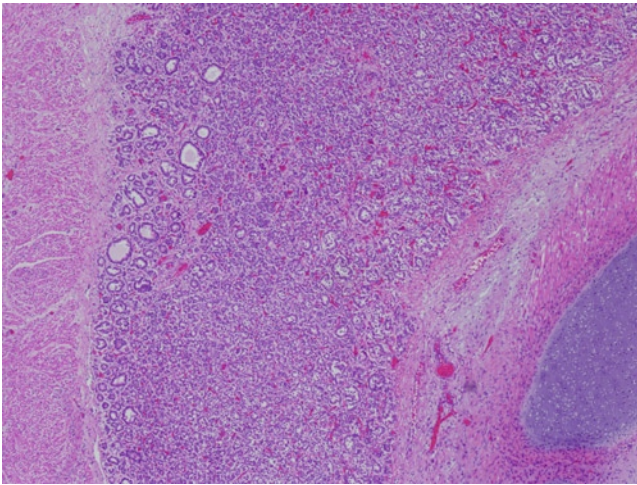


FIGURE 19-8. Low-power view of the fetal thyroid gland at 21 weeks gestation. (H&E, 4 \times .)

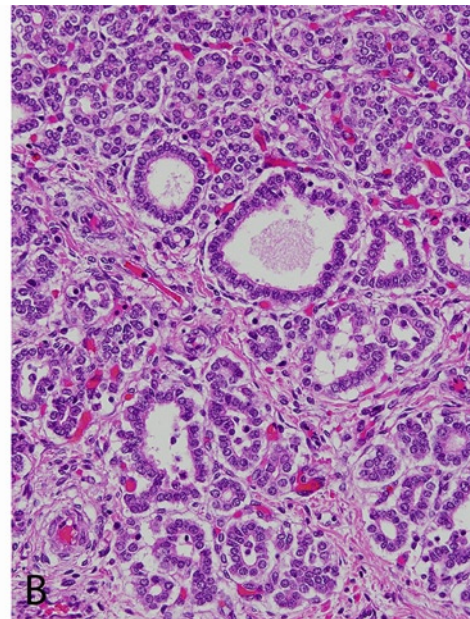
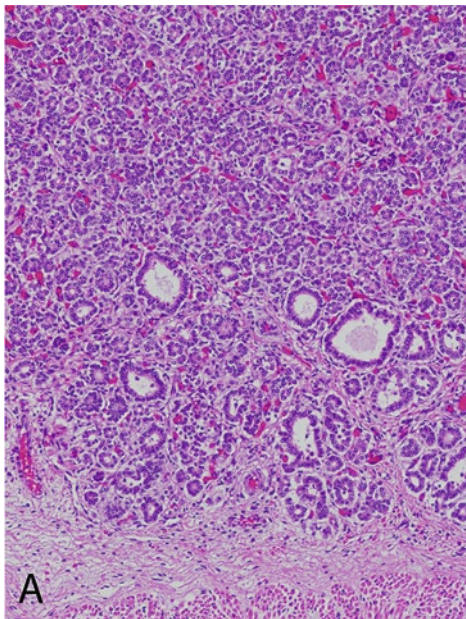


FIGURE 19-9. Higher power views of the fetal thyroid gland at 21 weeks gestation. Follicular formation and intrafollicular colloid continues to increase. (H&E: **A**, 10 \times and **B**, 20 \times .)

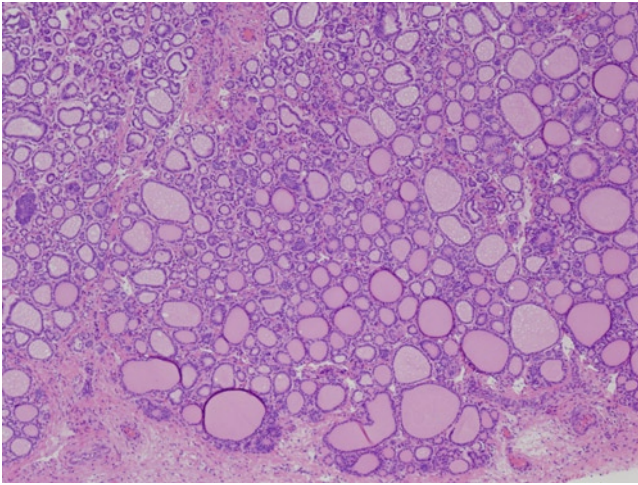


FIGURE 19-10. Low-power view of the fetal thyroid gland at 26 weeks gestation. (H&E, 4 \times .)

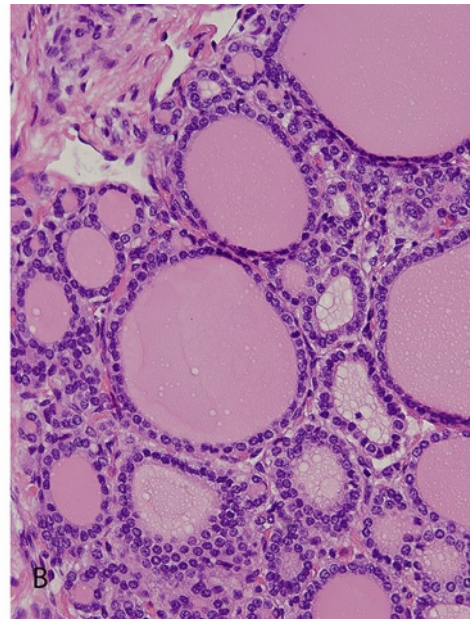
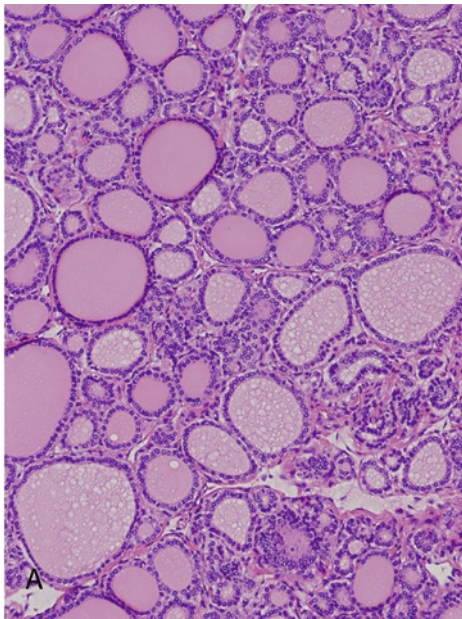


FIGURE 19-11. Higher power views of the fetal thyroid gland at 26 weeks gestation. Follicular formation and intrafollicular colloid continues to increase. (H&E: **A**, 10 \times and **B**, 20 \times .)

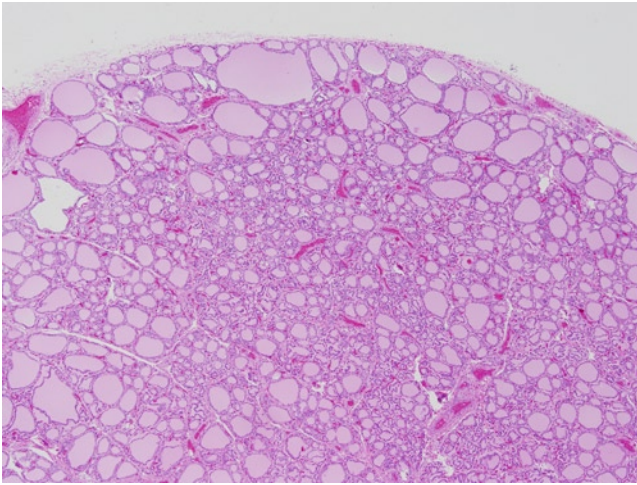


FIGURE 19-12. Low-power view of the fetal thyroid gland at 34 weeks gestation. (H&E, 4 \times .)

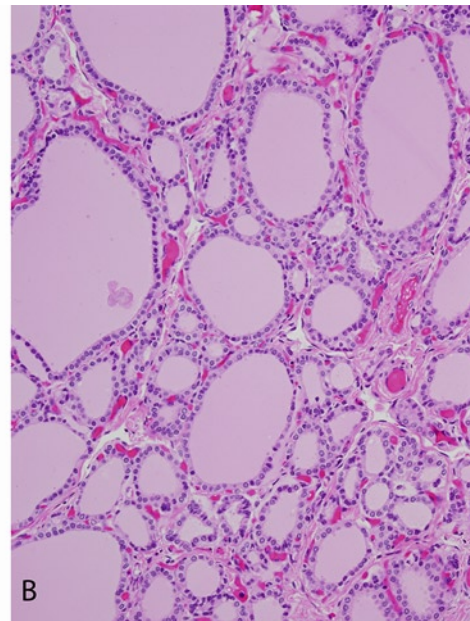
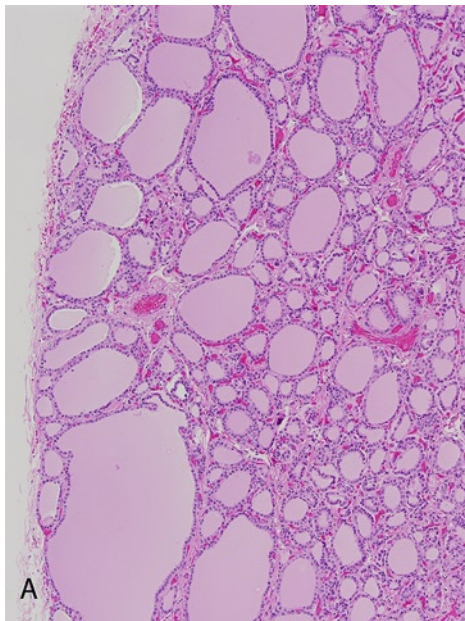


FIGURE 19-13. Higher power views of the fetal thyroid gland at 34 weeks gestation. Note how follicular formation and intrafollicular colloid continues to increase. (H&E: **A**, 10 \times and **B**, 20 \times .)

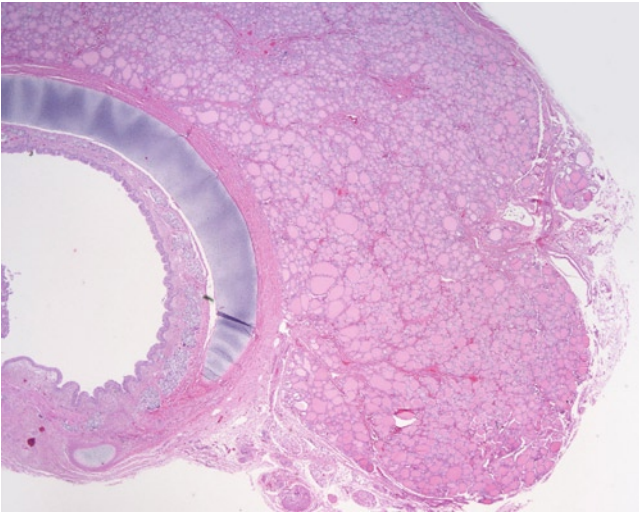


FIGURE 19-14. Fetal thyroid gland at term. This low-power view shows nearly all follicles with colloid and some distension of follicles. (H&E, 1 \times .)

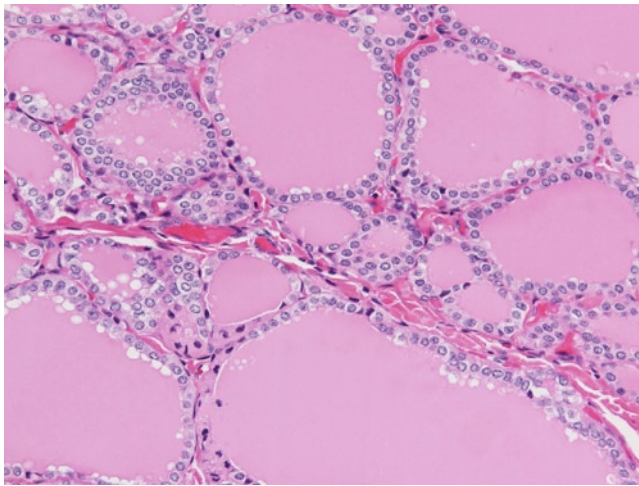


FIGURE 19-15. Fetal thyroid gland at term. This higher power view shows the details of the predominantly cuboidal follicular cells with oval nuclei and a characteristic coarsely granular chromatin pattern. Focal colloid scalloping is noted. (H&E, 20 \times .)

C Cells

The parafollicular C cells, responsible for calcitonin production, are not easily recognized with routine H&E stains, especially in the fairly cellular-appearing fetal thyroid. When recognized, C cells are described as polygonal with a more pale eosinophilic cytoplasm than the follicular cells and a round to oval nucleus with a central nucleolus [7]. To aid in their recognition, C cells can be highlighted by staining their secretory granules with the Grimelius silver nitrate argyrophil

method. Calcitonin immunohistochemistry is also a convenient method to highlight the C cells and distinguishes small groups or single cells within the deep, central region of the middle third of the lateral lobes (see Fig. 19-16). C cells are closely associated with the thyroid follicle (see Figs. 19-17 and 19-18) and by ultrastructural analysis most C cells are found within the basement membrane of the follicle and separated from the colloid by the follicular cell [10].

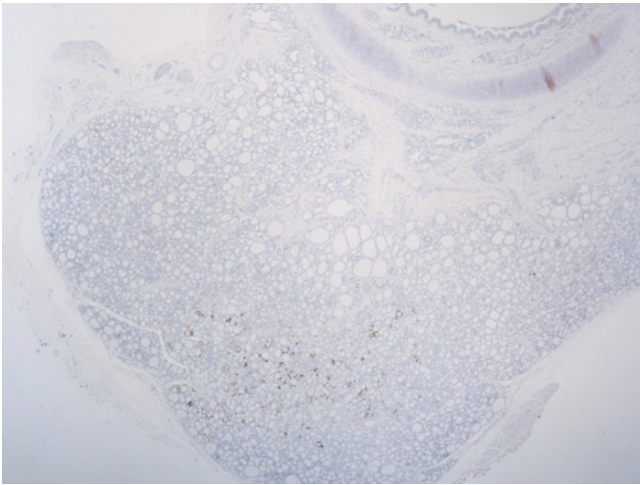


FIGURE 19-16. C cells within the lateral lobe of thyroid gland. This low-power view of the lateral lobe of the thyroid gland at term shows calcitonin stain–positive cells within the middle portion of the lobe. (Calcitonin immunohistochemistry, 1×.)

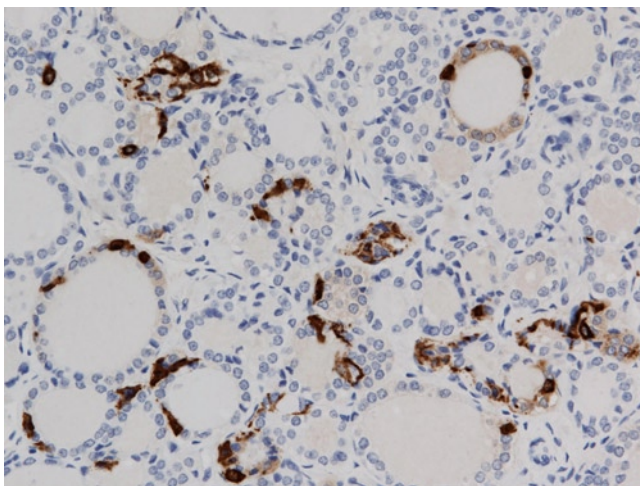


FIGURE 19-17. C cells in the fetal thyroid gland. A higher power view of term thyroid gland with darkly stained parafollicular C cells highlighted is shown. Note how intimately associated the C cells are with the basement membrane of the thyroid follicle and how they occur as single cells or in small clusters. (Calcitonin immunohistochemistry, 20×.)

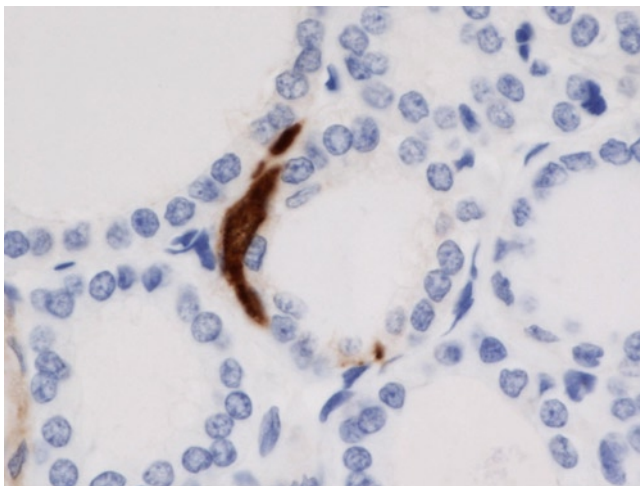


FIGURE 19-18. C cell in the fetal thyroid gland. This close-up view is of one C cell that appears to be intrafollicular. (Calcitonin immunohistochemistry, 60×.)

Stroma

The fetal thyroid is composed overwhelmingly of closely packed follicles, but between the follicles there is a small amount of interstitial fibrous tissue and numerous blood

vessels. Inflammatory cells are usually not a feature of the fetal or neonatal thyroid stroma.

Special Considerations

Intrathyroidal Inclusions

In the 1970s, Emery and colleagues examined the thyroid glands of hundreds of fetal, neonatal, and pediatric thyroid glands. In this review, the authors described numerous inclusions of nonthyroidal tissue within the thyroid gland [11]. The inclusions that have been described within the thyroid include: parathyroid, thymus, cartilage, ciliated epithelium, fat, and striated muscle. The presence of most of these ectopic tissues within the thyroid gland was considered a normal finding by the authors, related to the pharyngeal origin of the thyroid gland, as well as its descent with thymus and parathyroid glands. Striated muscle may represent disorganization of cervical tissues or, as the authors suggest, a possible association with

myopathies. The pyramidal lobe is often admixed with skeletal muscle. From this large review of thyroid glands, Emery *et al.* also introduced the concept of "perinatal thyroid discharge" [12], which is characterized by the reduction or loss of colloid (not postmortem-related), vacuolation or detachment of epithelial cells, irregular and pyknotic nuclei, and nuclear knots. The authors felt that these changes represented pathologic changes and did not consider them normal or related to autolysis. However, these sorts of studies have not been repeated and sorting out autolytic changes from true pathologic changes in the thyroid gland can be extremely difficult in the examination of the stillborn fetus.

Ultimobranchial Body Remnants

Also known as "solid cell nests," ultimobranchial body remnants are small well-defined collections of cells found in the same location as the C cells interspersed between thyroid follicles. They are considered to contain two cell types: "main cells" and "C cells." The main cells are the more abundant cell type in solid cell nests and consist of polygonal epithelial cells with abundant eosinophilic cytoplasm demonstrating a squamoid

appearance (see Fig. 19-19). These main cells are positive for p63. The C cells of the solid cell nests are less conspicuous, but do mark with calcitonin immunohistochemistry. The nature of the solid cell nest is still controversial, but some investigators believe the main cells may represent a stem cell population and suggest a link between solid cell nests and thyroid carcinoma [7, 13-15].

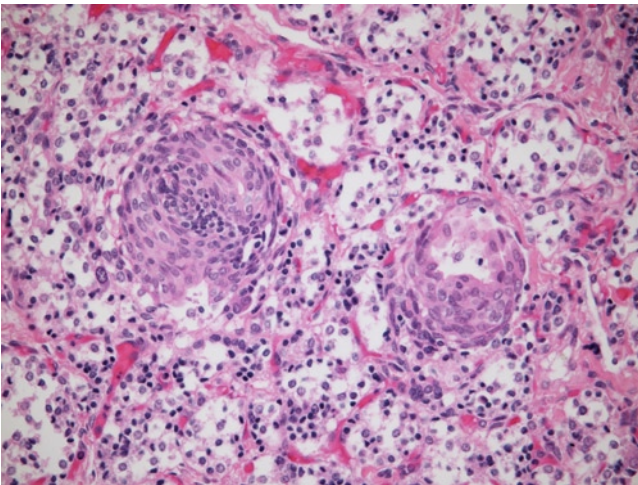


FIGURE 19-19. Solid cell nests/ultimobranchial body remnants in the thyroid. Note the interfollicular cluster of polygonal cells with squamoid features. C cells are not easily recognized. (H&E, 20 \times .)

References

1. Schoenwolf GC, Larsen WJ: *Larsen's Human Embryology*, edn 4. Philadelphia, PA: Elsevier/Churchill Livingstone; 2009.
2. Sadler TW, Langman J: *Langman's Medical Embryology*, edn 11. Philadelphia, PA: Wolters Kluwer Lippincott Williams & Wilkins; 2010.
3. Zoeller RT, Crofton KM: Thyroid hormone action in fetal brain development and potential for disruption by environmental chemicals. *Neurotoxicology* 2000, 21:935–945.
4. Park SM, Chatterjee VK: Genetics of congenital hypothyroidism. *J Med Genet* 2005, 42:379–89.
5. Contempre B, Jauniaux E, Calvo R, et al.: Detection of thyroid hormones in human embryonic cavities during the first trimester of pregnancy. *J Clin Endocrinol Metab* 1993, 77:1719–1722.
6. De Felice M, Di Lauro R: Thyroid development and its disorders: genetics and molecular mechanisms. *Endocr Rev* 2004, 25:722–746.
7. Carcangiu M: Thyroid. In *Histology for Pathologists*, edited by Mills SE. Philadelphia, PA: Lippincott Williams & Wilkins; 2007:1137–1138.
8. Fisher D, Greuters A: Disorders of the thyroid in the newborn and infant. In *Pediatric Endocrinology*, 3rd edn. Philadelphia, PA: Saunders/Elsevier; 2008:200.
9. Shepard TH, Andersen H, Andersen HJ: Histochemical studies of the human fetal thyroid during the first half of fetal life. *Anat Rec* 1964, 149:363–379.
10. Hazard JB: The C cells (parafollicular cells) of the thyroid gland and medullary thyroid carcinoma. A review. *Am J Pathol* 1977, 88:213–250.
11. Carpenter GR, Emery JL: Inclusions in the human thyroid. *J Anat* 1976, 122:77–89.
12. Sagreya K, Emery JL: Perinatal thyroid discharge. A histological study of 1225 infant thyroids. *Arch Dis Child* 1970, 45:746–754.
13. Cameselle-Teijeiro J, Preto A, Soares P, Sobrinho-Simoes M: A stem cell role for thyroid solid cell nests. *Hum Pathol* 2005, 36:590–591.
14. Burstein DE, Unger P, Nagi C, Wang BY: Thinking "out of the nest"—a reply to "a stem-cell role for thyroid solid cell nests [letter]". *Hum Pathol* 2005, 36:591–592.
15. Burstein DE, Nagi C, Wang BY, Unger P: Immunohistochemical detection of p53 homolog p63 in solid cell nests, papillary thyroid carcinoma, and hashimoto's thyroiditis: a stem cell hypothesis of papillary carcinoma oncogenesis. *Hum Pathol* 2004, 35:465–473.

20

Parathyroid Gland

Linda M. Ernst

Studies in mammals have shown that the fetus maintains a plasma calcium concentration that is higher than that of the mother. This high fetal calcium level is essential for the proper development and mineralization of the fetal skeleton, and the fetal parathyroid glands play an important role in this process. Hormones elaborated by the fetal parathyroid gland, including parathyroid hormone-related protein, are required to maintain the fetal calcium gradient created through active placental transport of calcium by syncytiotrophoblast [1]. This chapter focuses on the histological features of the fetal parathyroid glands.

Embryology

The parathyroid glands are derived from the third and fourth pharyngeal pouches beginning in the fifth week of gestation. Although one might expect the more cephalad pharyngeal pouch to give rise to the superior parathyroid gland and the more caudal pouch to give rise to the inferior gland, the reality is actually reversed. The two paired inferior parathyroid glands are derived from the bilateral dorsal buds of the third pharyngeal pouches while the two superior parathyroid glands originate from the fourth pharyngeal pouches. The nodular primordia of the parathyroid glands separate from the pharyngeal pouches, descend into the neck, and take their usual positions on the dorsal aspect of the thyroid. Descent is typically completed by approximately 7 weeks gestation [2,3].

Histology

Parathyroid glands can be difficult to identify grossly in fetuses, even with the aid of a dissecting microscope, but can be identified histologically if the eviscerated neck organs are serially sectioned in the transverse plane and entirely submitted from the base of the tongue to just below the thyroid gland (see Chapter 19, Figs. 19-1 and 19-2).

The parathyroid gland is surrounded by a thin connective tissue capsule from which septa extend into the parenchyma of the gland conveying blood vessels, nerves, and lymphatics. The fetal and neonatal parathyroid glands are composed of only one parenchymal cell type, the chief cell [2,4]. Oxyphil cells are not present until later in childhood (4.5–7 y) [2]. The chief cells within the parenchyma of the fetal parathyroid gland are polygonal cells with well-defined cell borders, a key feature in differentiating them from

the lymphocytes of small cervical lymph nodes in this anatomic location (see Figs. 20-1 and 20-2). The parenchymal cells are arranged in sheets, cords, and trabeculae. In contrast to the adult parathyroid gland, the fetal gland has no stromal fat and the connective tissue septa consist mainly of a vascular network with very little supporting collagen in the perivascular stroma (see Figs. 20-3 and 20-4). The cytoplasm of the chief cells is clear to lightly eosinophilic (see Figs. 20-5–20-7) and the chromatin of the nuclei has a vague “salt and pepper” appearance (see Fig. 20-8). Ultrastructural studies have shown that the chief cells are rich in glycogen particles, with occasional secretory granules, lipid bodies,

and multivesicular bodies [4], and immunostaining with anti-serum to bovine parathyroid hormone has identified immunoreactive parathyroid hormone in fetuses as early as at 10 weeks gestation [5].

With careful microscopic inspection of the cross sections of the neck organs, it is not unusual for a parathyroid gland to be found posterior to or within the thyroid gland (see Fig. 20-9) or with an associated undescended thymic lobule (see Figs. 20-10–20-12), given the common embryonic origin of the thymus and inferior parathyroid glands. Other sites where parathyroid glands can be found include within the thymus gland proper, pericardium, paratracheal, or paraesophageal tissues.

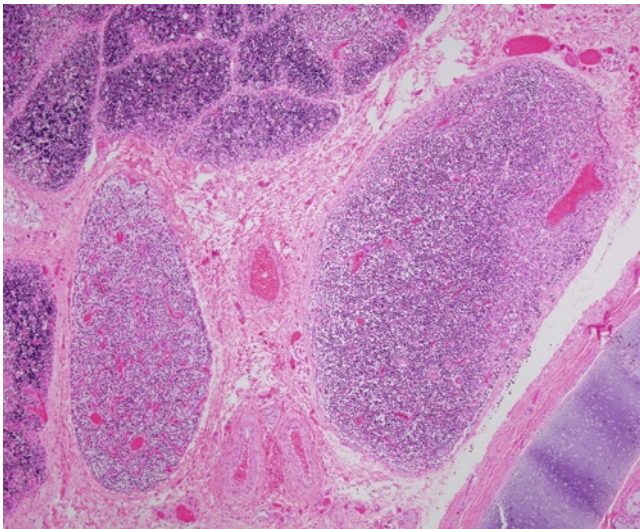


FIGURE 20-1. Parathyroid gland versus lymph node: low-power view of two nodules within the cervical tissues. At low power it may be difficult to distinguish parathyroid gland from lymph node or ectopic thymic tissue, especially in the setting of any significant autolysis. In this image, the nodule on the left is a parathyroid gland and the nodule on the right is a lymph node. Thymic tissue is above. See Figure 20-2 for a higher power view of cellular details (Hematoxylin and eosin [H&E], 4 \times .)

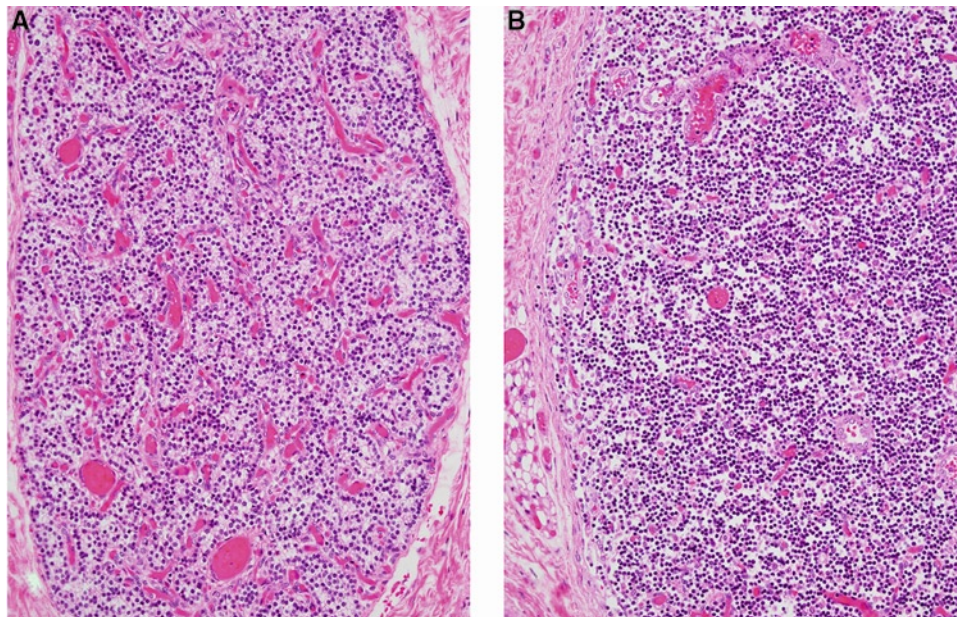


FIGURE 20-2. Parathyroid gland versus lymph node. Higher power view for comparison of parathyroid gland (**A**) and lymph node (**B**). **A**, The parathyroid gland shows a trabecular arrangement of epithelial cells with lightly eosinophilic cytoplasm and

well-defined cell borders. **B**, The lymph node shows a more diffuse population of small lymphocytes without significant cytoplasm or well-defined cell borders. (**A** and **B**, H&E 20 \times .)

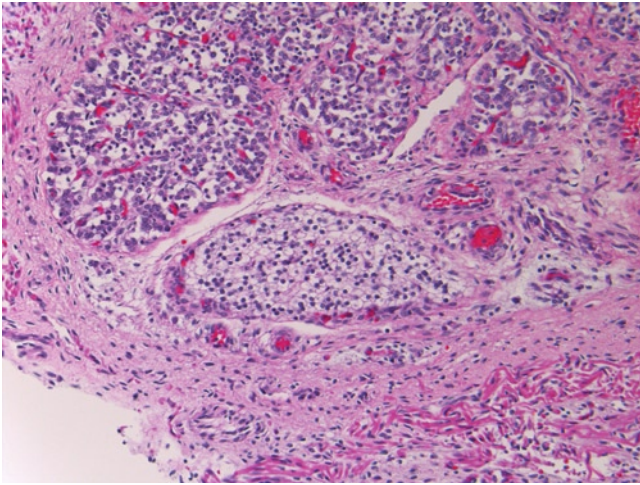


FIGURE 20-3. Medium-power view of the fetal parathyroid gland at 18 weeks gestation. This small parathyroid gland is located posterior to the thyroid lobe (above it). In contrast to the thyroid gland, the parathyroid gland is usually well preserved, as it undergoes autolysis more slowly. The cytoplasm of the parenchymal cells is clear and the nuclei are round and centrally placed. Cell borders are well demarcated and no stromal fat is present. (H&E, 20 \times .)

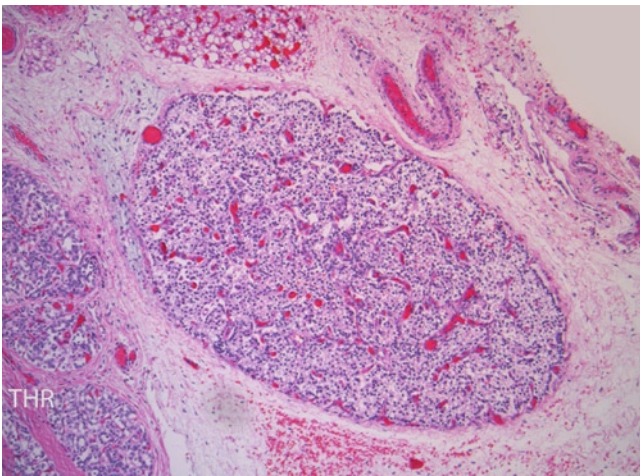


FIGURE 20-4. Lower power view of the fetal parathyroid gland at 24 weeks gestation. The gland shown here is larger than the one at 18 weeks (see [Figure 20-3](#)) and is also found adjacent to the thyroid gland (THR) in the perithyroidal fat and connective tissue. Note the thin fibrous capsule and rich vascular network that are visible at low power. (H&E 10 \times .)

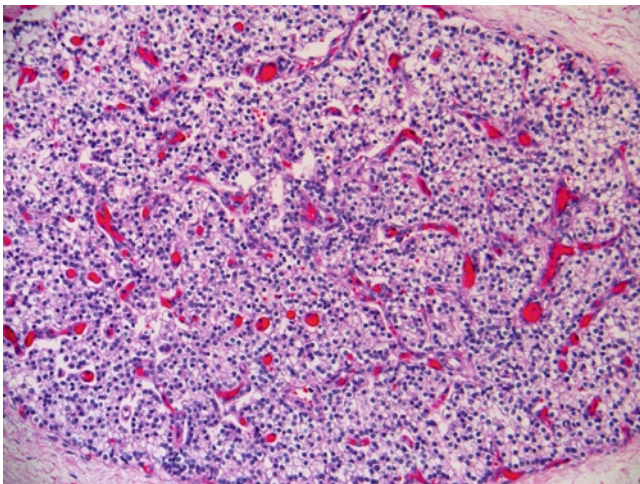


FIGURE 20-5. Higher power view of the fetal parathyroid gland at 24 weeks gestation. The parenchymal cells, chief cells, are fairly monotonous-appearing polygonal cells arranged in cords and trabeculae. Cell borders are well defined and the cytoplasm appears clear to lightly eosinophilic. (H&E, 20 \times .)

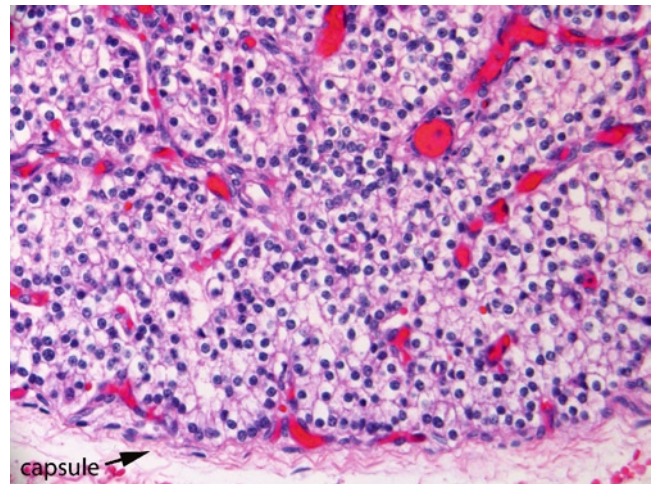


FIGURE 20-6. High-power view of the fetal parathyroid gland at 24 weeks gestation. Note the thin fibrous capsule and detail of the parenchymal chief cells. (H&E, 40 \times .)

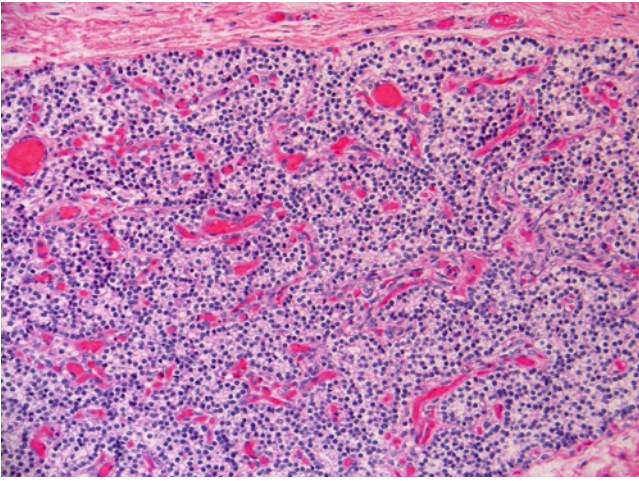


FIGURE 20-7. Fetal parathyroid gland at 39 weeks gestation. The gland is larger still and the parenchymal cells appear more tightly packed than in midgestation; compare with Figure 20-5. (H&E, 20x.)

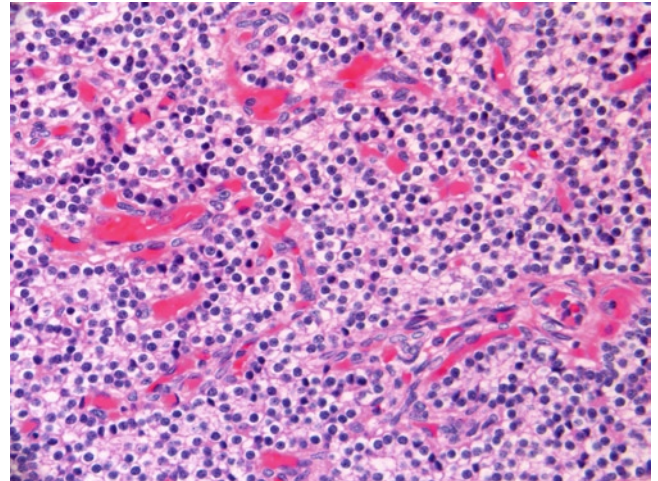


FIGURE 20-8. High-power view of the fetal parathyroid gland at 39 weeks gestation. (H&E, 40x.)

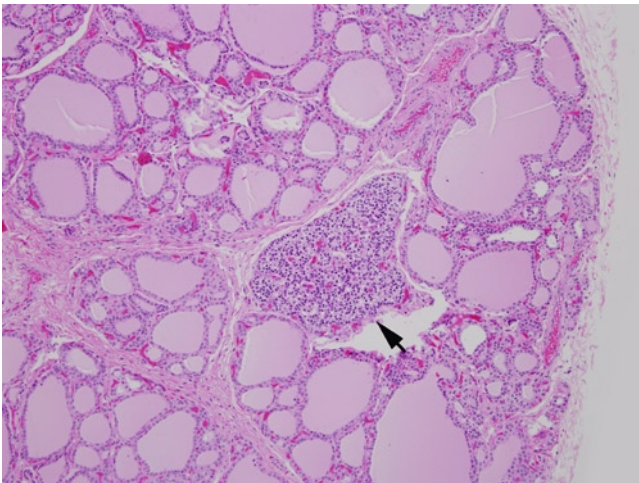


FIGURE 20-9. Intrathyroidal parathyroid gland (arrow) identified within the thyroid parenchyma at 34 weeks gestation. (H&E, 10x.)

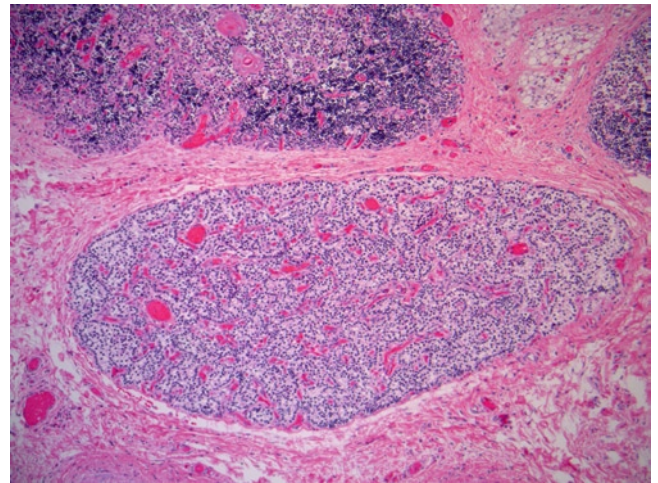


FIGURE 20-10. Term gestation with identification of parathyroid gland adjacent to an ectopic, undescended thymic lobule above it. (H&E, 4x.)

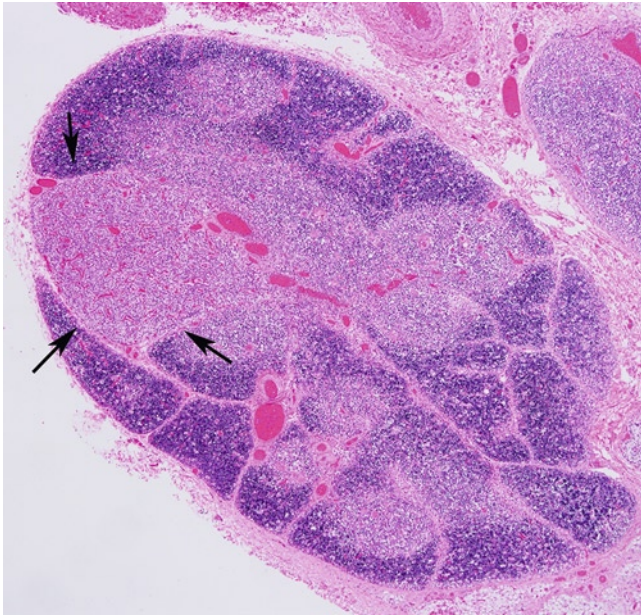


FIGURE 20-11. Ectopic, undescended thymic lobule with embedded parathyroid gland. This is a low-power view of an ectopic thymic lobule in the cervical region, intimately associated with parathyroid gland tissue, indicated by arrows. (H&E, 4 \times .)

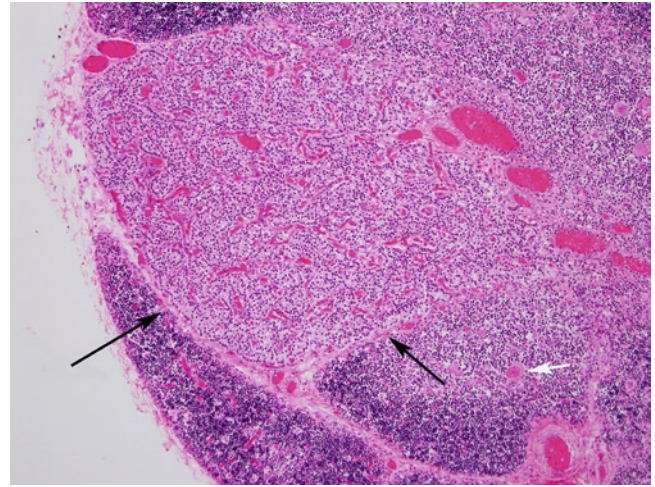


FIGURE 20-12. Parathyroid gland embedded within an ectopic, undescended thymic lobule. A higher magnification of parathyroid gland (black arrows) within the cervical thymic lobule is shown. The white arrow denotes a Hassall's corpuscle. (H&E, 10 \times .)

References

1. Maclsaac RJ, Heath JA, Rodda CP, *et al.*: Role of the fetal parathyroid glands and parathyroid hormone-related protein in the regulation of placental transport of calcium, magnesium and inorganic phosphate. *Reprod Fertil Dev* 1991, 3:447–457.
2. Valdes-Dapena MA: *Histology of the Fetus and Newborn*. Philadelphia, PA: Saunders; 1979.
3. Schoenwolf GC, Larsen WJ: *Larsen's Human Embryology*, 4th edn. Philadelphia, PA: Elsevier/Churchill Livingstone; 2009.
4. Nakagami K, Yamazaki Y, Tsunoda Y: An electron microscopic study of the human fetal parathyroid gland. *Z Zellforsch Mikrosk Anat* 1968, 85:89–95.
5. Leroyer-Alizon E, David L, Anast CS, Dubois PM: Immunocytochemical evidence for parathyroid hormone in human fetal parathyroid glands. *J Clin Endocrinol Metab* 1981, 52:513–516.

21

Pituitary Gland

Linda M. Ernst

Despite its small size, the fetal pituitary gland produces a variety of important hormones. Normal development of the human fetal pituitary gland is essential for fetal homeostasis, as well as for the appropriate differentiation and maturation of several organ systems required for extrauterine survival [1]. This chapter reviews the histological features of the adenohypophysis; the anterior lobe of the pituitary gland; and neurohypophysis, the posterior lobe of the pituitary gland. In addition, some features unique to the fetal and neonatal pituitary gland, such as laminated calcifications within the anterior lobe, will be discussed.

Embryology

The pituitary gland is formed from two different ectodermally derived structures: the Rathke's pouch and a portion of the diencephalon known as the infundibulum. These distinctive embryologic origins correlate with the two distinct histological compartments of the pituitary gland, the adenohypophysis (anterior lobe) derived from Rathke's pouch and the neurohypophysis (posterior lobe) derived from the infundibulum [2-4].

Rathke's pouch begins in the third week of gestation as an outgrowth of ectoderm from the stomodeum, the primitive mouth of the embryo. The epithelial outgrowth develops a lumen and forms an epithelial-lined diverticulum. This pouch extends dorsally toward the infundibulum, which is the small ventral extension of the floor of the diencephalon that will become the neurohypophysis. At approximately 6 weeks gestation, Rathke's pouch loses its connection with the surface ectoderm of the mouth and becomes an epithelial-lined cyst. The posterior wall of the cyst remains thin, is in close contact with the infundibulum, and will become the pars intermedia. The epithelium of the anterior wall of the cyst proliferates to form the rounded mass of the anterior lobe of the pituitary gland, the pars distalis (see Fig. 21-1). A small group of cells from the posterior portion of the anterior lobe grow up the stalk of the infundibulum and are known as the pars tuberalis. The lumen of the original Rathke's pouch becomes flattened in the anteroposterior direction and becomes a slit-like space between the pars distalis anteriorly and the pars intermedia posteriorly. Its remnants become the microscopic glandular structures of the pars intermedia [2-4].

The anterior lobe of the pituitary gland is responsible for elaboration of the pituitary hormones: growth hormone (GH), adrenal corticotropin hormone (ACTH), prolactin (PRL), thyroid-stimulating hormone (TSH), follicular-stimulating hormone (FSH), and luteinizing hormone (LH). Differentiation of the ectodermal cells from Rathke's pouch into the various

hormone-producing cells depends on gradients of growth factors, such as FGF8 and BMP2, that emanate from the ventral diencephalon and ventral pituitary organizing center, respectively. These overlapping gradients result in the expression of specific transcription factors that drive differentiation and the production of specific hormones [5–7].

The posterior lobe of the pituitary gland forms by the proliferation of neuroglial cells at the distal end of the infundibulum. The infundibulum remains the stalk of the pituitary gland and nerve fibers from the hypothalamus also grow into the posterior lobe via the infundibular stalk.

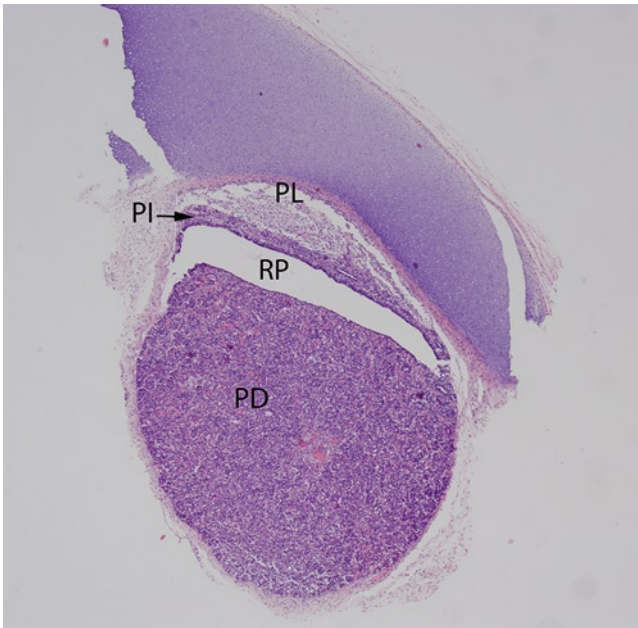


FIGURE 21-1. Low-power view of the entire fetal pituitary gland at 17 weeks gestation. The gland, removed with portions of the cartilaginous sella turcica (*upper right*), is shown here. The slit-like opening of Rathke's pouch (RP) is visible. The most anterior portion of the anterior lobe or pars distalis (PD) is the rounded mass anterior to Rathke's pouch. The thin rim of similar-appearing cells of the anterior pituitary on the opposite side of Rathke's pouch is known as the pars intermedia (PI). The posterior lobe (PL) is adjacent to the PI and has a generally paler staining appearance than the anterior lobe. (Hematoxylin and eosin [H&E], 2 \times .)

Histology

General Overview

Sampling the fetal pituitary gland for histological examination can be difficult since the tissues of the gland are extremely soft and easily compressed if they are grasped by forceps. After removing the brain, the pituitary gland can be removed intact by excising it along with the bony tissues of the sella turcica. Using this technique, the surrounding cartilaginous and bony tissues of the sella turcica protect the pituitary gland and serve as a "handle" to grasp the pituitary gland. The entire gland with the rim of the cartilaginous/bony tissue can be submitted in toto for histologic examination after brief decalcification.

Due to the separate embryologic origins of the anterior and posterior lobes of the pituitary gland, the histological appearances of these compartments are quite distinct in the fetus. The anterior lobe of the pituitary gland appears as an ovoid amphophilic mass of polygonal epithelial cells that are separated by a slit-like cavity from the thin layer of similar-appearing cells, forming the pars intermedia in the posterior aspect of the anterior lobe. Although well demarcated from the anterior lobe, the posterior lobe is in direct contact with the anterior lobe and stands in contrast with its pale staining, fibrous appearance (see Figs. 21-1–21-4).

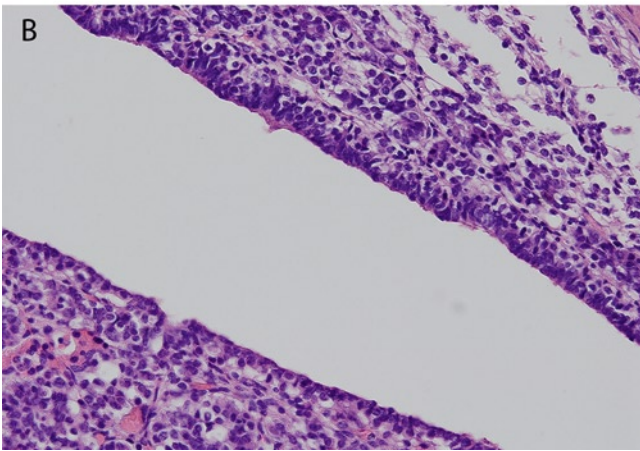
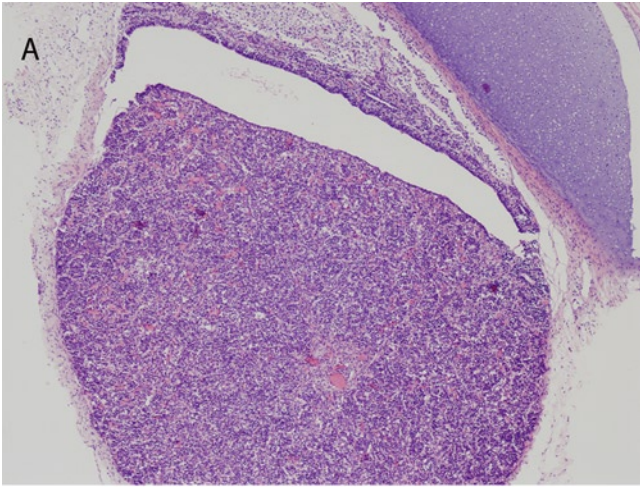


FIGURE 21-2. Higher power views of the anterior lobe of the pituitary gland at 17 weeks gestation. **A**, The anterior lobe is composed of pars distalis and pars intermedia separated by residual lumen of Rathke's pouch. **B**, This close-up view is of the cells lining the lumen of Rathke's pouch. Note the cuboidal to columnar palisading epithelial cells. (**A**, H&E, 4 \times and **B**, H&E, 20 \times .)

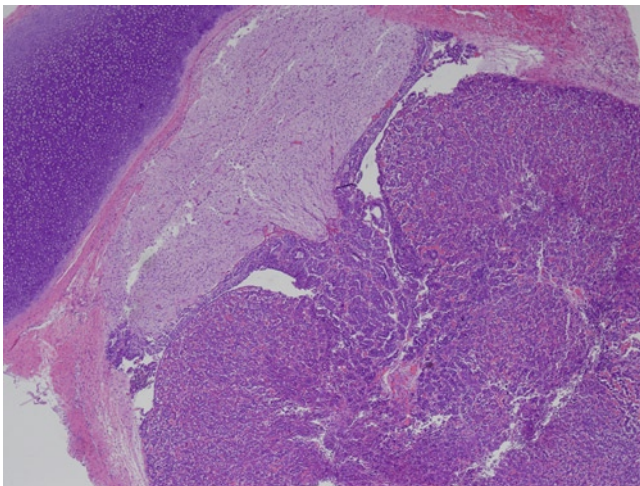


FIGURE 21-3. Low-power view of the pituitary gland at 26 weeks gestation. Note that the gland is larger, but the overall structure of the anterior and posterior lobes is identical. (H&E, 2 \times .)

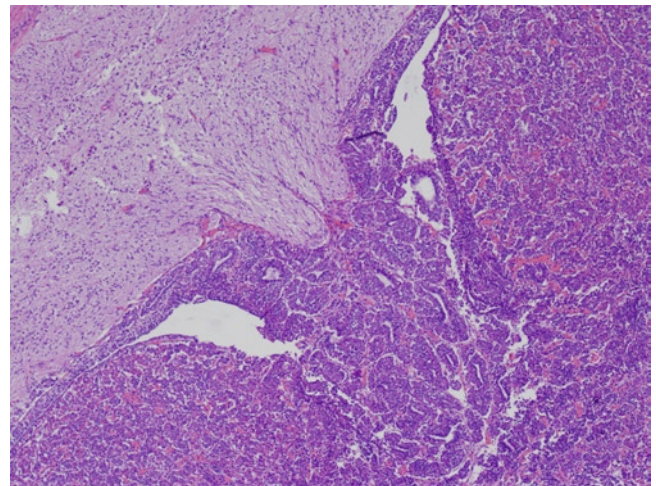


FIGURE 21-4. Closer view of the junction between anterior and posterior pituitary lobes at 26 weeks gestation. Note the residual lumen of Rathke's pouch and the lining epithelial cells. Glandular structures are formed within the pars intermedia. The posterior lobe (*upper left*) has a pale, fibrillary appearance. (H&E, 4 \times .)

Anterior Pituitary

The anterior lobe of the pituitary gland is composed of epithelial cells arranged in cords and nests with an intervening delicate capillary network. The epithelial cells have round, slightly eccentrically placed nuclei and fairly abundant cytoplasm, which is characterized by an affinity for either acidophilic dye (acidophils), basophilic dye (basophils), or neither (chromophobes) on H&E staining. The acidophil cells appear to be the most numerous in the fetal pituitary gland and have brightly eosinophilic cytoplasmic granules. As a general rule, acidophilic cells are considered to secrete GH and PRL, and are located primarily in the rounded lateral projections of the pars distalis. Basophil cells are also commonly present and have dark blue-stained cytoplasmic granules. Basophils that secrete ACTH and TSH are located primarily in the central region of the pars distalis, referred to as the mucoid wedge because the basophil cells are also positive using the periodic acid-Schiff method [8]. Basophil cells that secrete the gonadotropins FSH and LH are scattered throughout the pars distalis. Both cell types, acidophils and basophils, are generally arranged in clusters throughout the gland (see Fig. 21-5). Although chromophobe cells can represent up to 50% of cells in the adult pituitary gland [8], they are not very prominent in the fetal pituitary. They are seen as only small clusters of cells with poorly stained, inconspicuous cytoplasm.

Immunohistochemical studies in rats indicate that ACTH is the first pituitary hormone detectable on embryonic day 15 and that the other hormones become detectable in a predictable pattern over the next few days [9]. Immunohistochemical and ultrastructural studies of human fetal pituitary glands [10–12] have shown that ACTH-producing cells are seen as early as 6 to 8 weeks gestation. Features characteristic of somatotrophs, which secrete GH, are seen at 8 to 9 weeks and cells producing most other hormones are identifi-

able by 15 to 16 weeks gestation. Lactotrophs, PRL-producing cells, are somewhat variable in number in the first and second trimester, but are relatively numerous near term. In general practice, immunohistochemical stains for the pituitary hormones can be performed on the human fetal pituitary gland and reveal the presence of all the anterior pituitary hormones near term. The staining pattern for each hormone is different, varying in intensity and the number of cells stained, but is similar to adult control pituitary glands. The hormones with the most intense and widespread staining in the anterior lobe are ACTH (see Fig. 21-6) and GH (see Fig. 21-7).

A unique histological feature of the anterior lobe of the fetal and newborn pituitary is the presence of ovoid, calcified concretions (see Fig. 21-8). These laminated calcifications have been noted in a majority of fetal pituitaries from midgestation to term and generally disappear within the first 6 months of life [13,14]. Although the etiology of these calcifications is uncertain, hypotheses include a relationship to hormonal activity of the fetal pituitary gland or developmental processes associated with cell death [13,14].

By adulthood, the lumen of Rathke's pouch between the pars distalis and pars intermedia is no longer visible, but in the fetal and neonatal pituitary gland the space may be present and lined by cuboidal to columnar epithelial cells (see Fig. 21-2). Persistence of a so-called Rathke cleft cyst (see Fig. 21-9) is identified, as an incidental finding, in up to one-third of autopsy cases [15,16]. If large enough, in adults and children, the Rathke cleft cyst can become symptomatic and require surgical intervention. Embryonic epithelial remnants of the obliterated stalk connecting Rathke's pouch to the embryonic oral cavity may also persist in the submucosa of the nasopharynx as the "pharyngeal pituitary" or in the sphenoid bone along the embryonic path of the stalk; these embryonic rests may be functional [17].

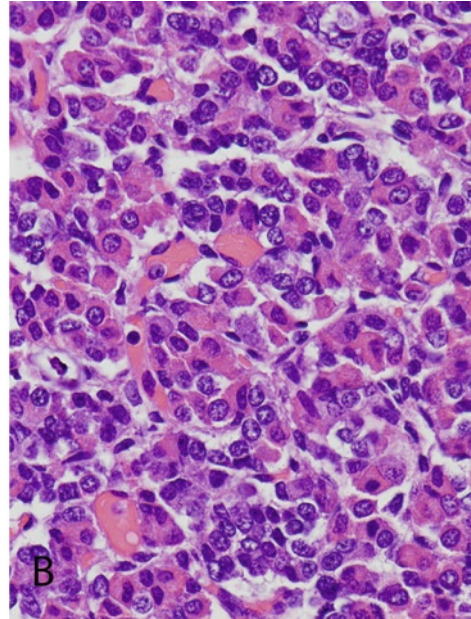
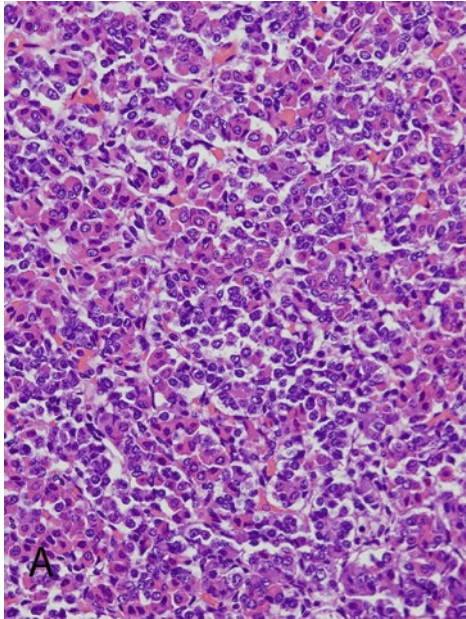


FIGURE 21-5. A and B, Views of the anterior lobe from the pars distalis region at 26 weeks gestation. Cells of the anterior lobe are arranged in small clusters, cords, and nests with intervening capillary network. Acidophil cells with eosinophilic cytoplasm

are easy to distinguish from the basophil cells with their dark, granular cytoplasm. Chromophobe cells are inconspicuous. (H&E: **A**, 20× and **B**, 40×.)

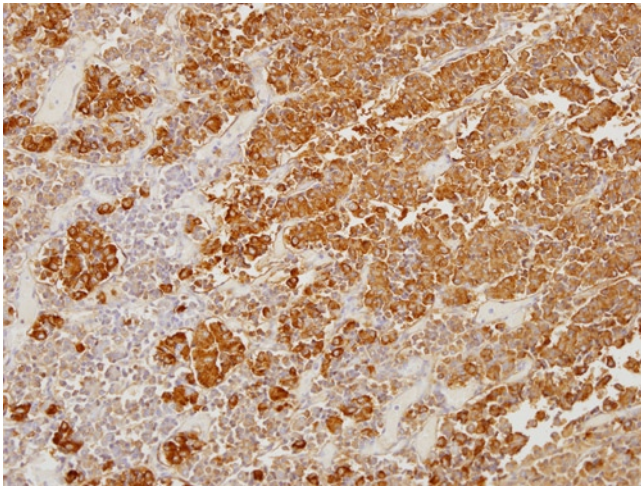


FIGURE 21-6. Anterior pituitary gland at 35 weeks gestation. Immunohistochemical stain for ACTH shows numerous anterior pituitary cells with positive staining. (ACTH immunohistochemistry, 20×.)

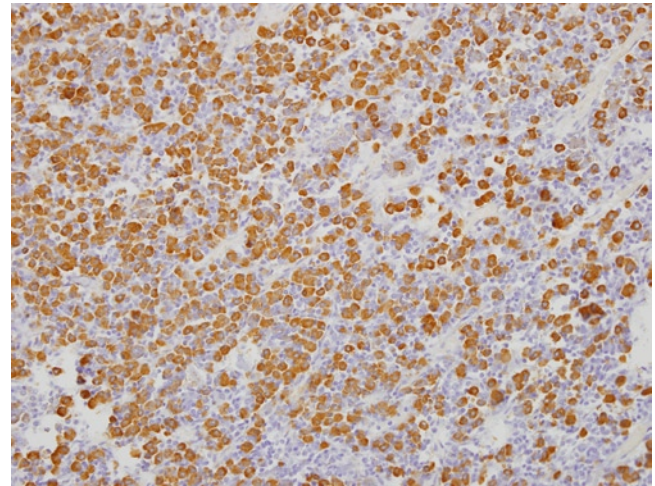


FIGURE 21-7. Anterior pituitary gland at 35 weeks gestation. Immunohistochemical stain for GH shows numerous anterior pituitary cells with positive staining. (GH immunohistochemistry, 20×.)

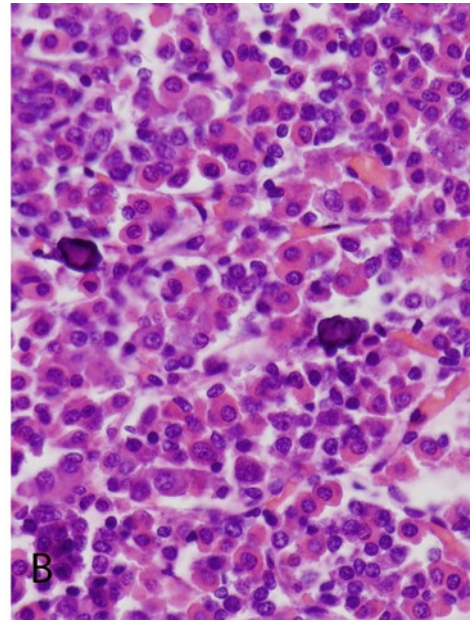
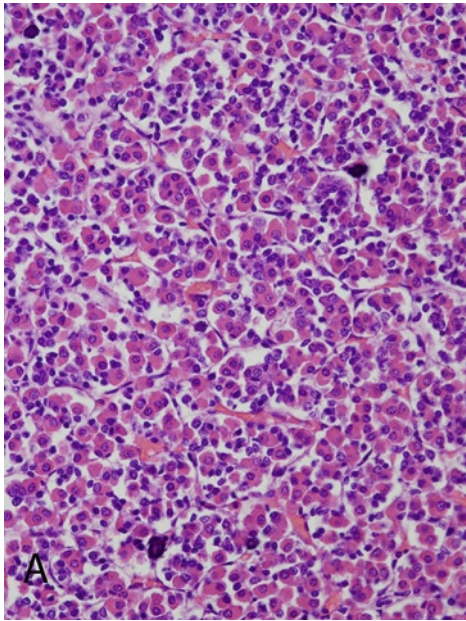


FIGURE 21-8. **A** and **B**, Anterior lobe of the pituitary gland at 35 weeks gestation. The overall architecture and cellular components are similar to 26 weeks gestation (compare with Fig. 21-5). Acidophil and basophil cells are easily distinguished by their cytoplasmic features. Chromophobe cells are still inconspic-

ous. Note the ovoid darkly basophilic concretions present in the anterior lobe. These calcified concretions, which appear partially laminated, are commonly seen in fetal and newborn pituitary glands, until approximately 6 months of age. (H&E: **A**, 20 \times and **B**, 40 \times .)

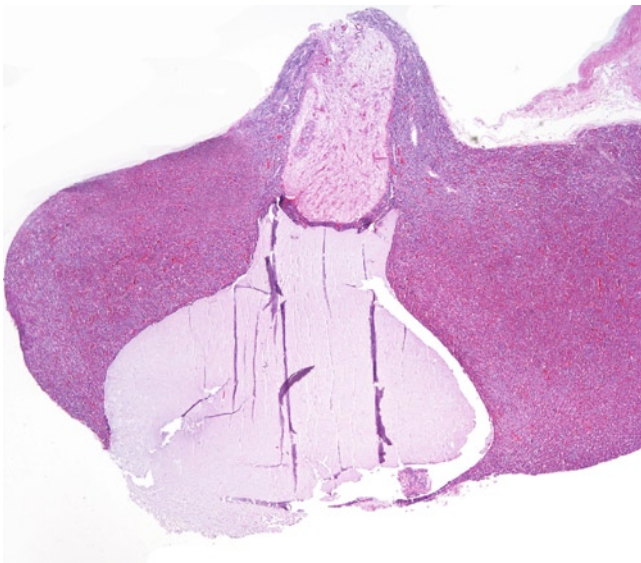


FIGURE 21-9. Rathke cleft cyst in a 1-year-old infant. Note the large cystic space involving the anterior pituitary gland. The cyst is lined by cuboidal to columnar epithelial cells, which can have cilia. (H&E, 1 \times .)

Posterior Pituitary

The main cell type seen in the posterior pituitary is the pituicyte, which is best classified as a subtype of the glial cell. Pituicytes have ovoid to elongate nuclei and most have fibrillary cytoplasmic processes (see Fig. 21-10, as well as Figs. 21-1, 21-3, and 21-4). In the adult pituitary gland, the posterior pituitary shows immunoreactivity for glial fibrillary acidic protein, vimentin, and S100 protein. However, in fetal life only very few glial fibrillary acidic protein positive fibers are seen (see Fig. 21-11). The morphologic features of pituicytes can vary and at least five different types have been described in the adult pituitary [8]. The second major constituent of the poste-

rior lobe is the nonmyelinated axons of neurosecretory neuronal cell bodies originating in the supraoptic and paraventricular nuclei of the hypothalamus. These axons store the two secretory products of those nuclei, vasopressin or antidiuretic hormone and oxytocin. These axons are easily identifiable in silver-stained sections of adult glands, but are not as easily identifiable, even with silver stains, in the fetal pituitary. The pituicytes surround the neurosecretory axons and a major function of the posterior lobe is to release the stored hormones into the circulation. The posterior pituitary also has a rich vascular network.

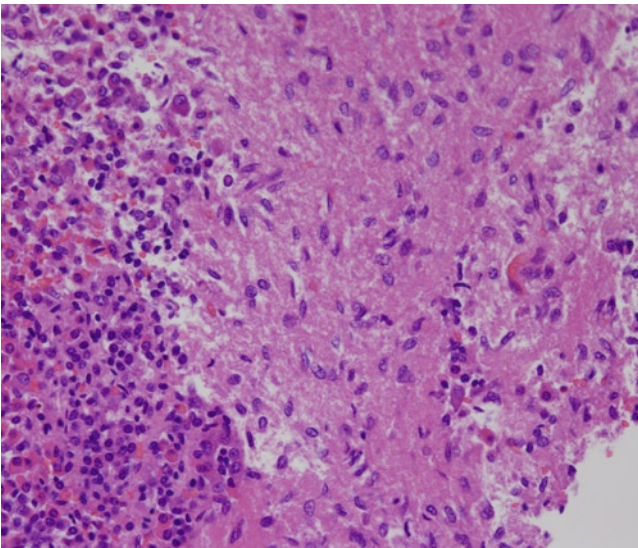


FIGURE 21-10. Posterior lobe of the pituitary gland at 35 weeks gestation. Posterior pituitary occupies most of the field with a small amount of anterior pituitary on the left for comparison. The posterior pituitary is less cellular and its pituicytes have ovoid to elongated nuclei and fibrillary cytoplasm. (H&E, 20 \times .)

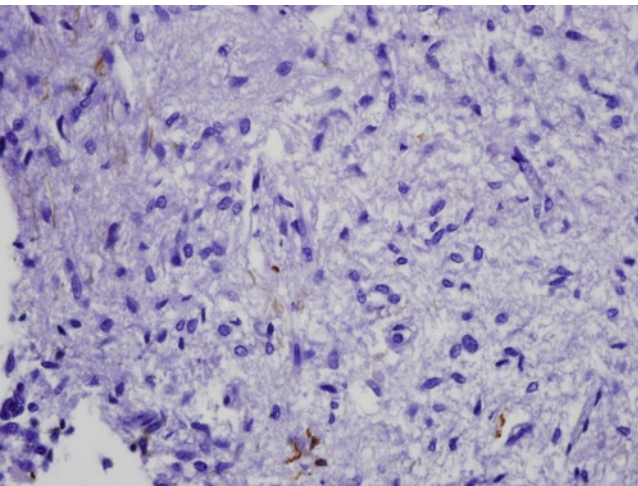


FIGURE 21-11. Posterior lobe of the pituitary gland at 35 weeks gestation. Stain for glial fibrillary acidic protein (GFAP) shows a few positive staining fibers. (GFAP immunohistochemistry, 40 \times .)

References

1. Ng PC: The fetal and neonatal hypothalamic-pituitary-adrenal axis. *Arch Dis Child Fetal Neonatal Ed* 2000, 82: F250–F254.
2. Valdes-Dapena MA: *Histology of the Fetus and Newborn*. Philadelphia, PA: Saunders; 1979.
3. Sadler TW, Langman J: *Langman's Medical Embryology*, edn 11. Philadelphia, PA: Wolters Kluwer Lippincott Williams & Wilkins; 2010.
4. Schoenwolf GC, Larsen WJ: *Larsen's Human Embryology*, edn 4. Philadelphia, PA: Elsevier/Churchill Livingstone; 2009.
5. Dasen JS, O'Connell SM, Flynn SE, et al.: Reciprocal interactions of Pit1 and GATA2 mediate signaling gradient-induced determination of pituitary cell types. *Cell* 1999, 97:587–598.
6. Nogami H, Hisano S: Functional maturation of growth hormone cells in the anterior pituitary gland of the fetus. *Growth Horm IGF Res* 2008, 18:379–388.
7. Treier M, Gleiberman AS, O'Connell SM, et al.: Multistep signaling requirements for pituitary organogenesis in vivo. *Genes Dev* 1998, 12:1691–1704.
8. Lopes MBS, Pernicone PJ, Scheithauer BW, et al.: Pituitary and sellar region. In *Histology for Pathologists*, edn 3. Edited by Mills SE. Philadelphia, PA: Lippincott Williams & Wilkins; 2007:321–344.
9. Watanabe YG, Daikoku S: An immunohistochemical study on the cytogenesis of adenohypophysial cells in fetal rats. *Dev Biol* 1979, 68:557–567.
10. Asa SL, Kovacs K, Horvath E, et al.: Human fetal adenohypophysis. Electron microscopic and ultrastructural immunocytochemical analysis. *Neuroendocrinology* 1988, 48:423–431.
11. Asa SL, Kovacs K, Laszlo FA, et al.: Human fetal adenohypophysis. Histologic and immunocytochemical analysis. *Neuroendocrinology* 1986, 43:308–316.
12. Asa SL, Kovacs K, Singer W: Human fetal adenohypophysis: morphologic and functional analysis in vitro. *Neuroendocrinology* 1991, 53:562–572.
13. Barson AJ, Symonds J: Calcified pituitary concretions in the newborn. *Arch Dis Child* 1977, 52:642–645.
14. Groisman GM, Kerner H, Polak-Charcon S. Calcified concretions in the anterior pituitary gland of the fetus and the newborn: a light and electron microscopic study. *Hum Pathol* 1996;27(11):1139–43.
15. Naylor MF, Scheithauer BW, Forbes GS, Tomlinson FH, Young WF. Rathke cleft cyst: CT, MR, and pathology of 23 cases. *J Comput Assist Tomogr* 1995;19(6):853–9.
16. Zada G, Ditty B, McNatt SA, McComb JG, Krieger MD. Surgical treatment of rathke cleft cysts in children. *Neurosurgery* 2009;64(6):1132–7; author reply 037–8.
17. Melchionna RH, Moore RA. The pharyngeal pituitary gland. *Am J Pathol* 1938;14(6):763–72 1.

SECTION VI

Hematolymphoid System

22

Thymus Gland

Linda M. Ernst

The normal thymus gland is not frequently encountered in the examination of adult histology due to its fatty involution after puberty. However, in the examination of fetal and neonatal tissues, the thymus gland is one of the major thoracic organs identified. Therefore, an understanding of its development and histological structure is important for anyone examining fetal and neonatal tissues. This chapter reviews the embryological origin and the major histological characteristics of the thymus gland throughout gestation, including the main components of the cortex and medulla and features of thymic involution.

Embryology

The thymus gland is a lymphoepithelial organ composed of two lobes of approximately equal size located beneath the sternum in the upper thorax, ventral to the great arteries, innominate vein, and superior portion of the pericardial sac. The bulk of the organ is derived from the ventral buds of the bilateral third pharyngeal pouches, which arise at the end of the fourth week after conception. These buds are initially hollow diverticula, but become solid cords of epithelial cells as their connection to the pharyngeal wall is lost by the seventh week. The cords migrate caudally and fuse to form the normally bilobed gland located inferior to the thyroid gland with the bulk of the gland in the anterior mediastinum [1,2]. In the fetus and newborn, it is usual for the gland to include thin cylinders of tissue extending superiorly from the superior edge of one or both thymic lobes into the neck region. These cervical extensions of the thymus are normal, indicative of the trail of the embryologic descent of the thymus. Additionally, ectopic lobules of thymic tissue can be found anywhere along the descent of the thymic buds from the pharynx. See further discussion below.

The endoderm of the pharyngeal pouch gives rise to the epithelial elements of the thymus gland, probably including Hassall's corpuscles, and the organ is secondarily populated with bone marrow-derived, precursor T-lymphocytes shortly after formation [3]. The distinction between cortex and medulla becomes visible in the embryologic period and is well established by the second trimester.

Histology

General Overview

The thymus is an encapsulated organ with a lobular architecture composed of a core of medullary tissue surrounded by cortical tissue (see Fig. 22-1). The capsule is comprised of loose connective tissue with short trabeculae that extend into the organ and carry blood vessels and nerves. The cortex is the outer dark-appearing region of the thymus, and the

medulla is the lighter central region. The main cell types within both the cortex and medulla of the thymus are the epithelial cells and lymphocytes, also known as thymocytes, derived from the bone marrow. The epithelial-reticular cells form the reticular framework or cytotreticulum of the cortex and medulla, and secrete thymic hormones such as thymulin, thymosin, thymopoietin, and thymic humoral factor [3]. The lymphocytes

are tightly packed in the interstices of the epithelial reticulum. Some epithelial cells, which are tightly joined together by desmosomes, form a continuous epithelial layer beneath the capsule, around the periphery of the entire gland, and investing the vascular trabeculae. This creates the blood-thymus barrier and isolates the thymus gland from much of the outside environment, which is important for development of the lymphocytes.

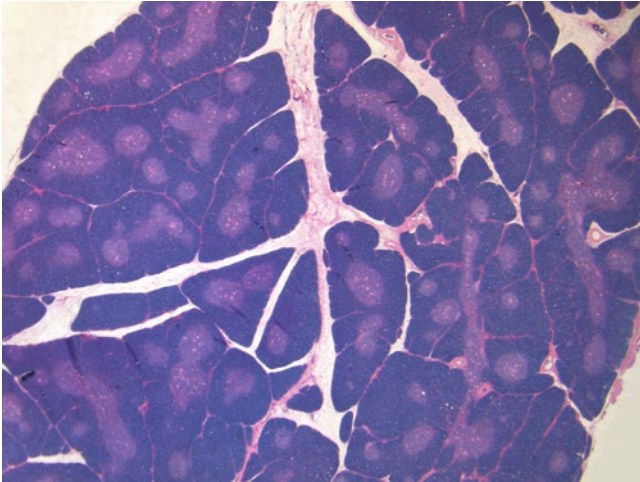


FIGURE 22-1. General overview of thymic architecture. Low-power view of the thymus at term. Note the lobular architecture with outer dark-appearing cortex and more central light-appearing medulla. (H&E, 1.25 \times .)

Capsule and Connective Tissue Trabeculae

The capsule consists of a thin layer of loose connective tissue containing blood vessels. Short connective tissue trabeculae extend into the organ carrying blood vessels. The capsule remains thin throughout gestation (see Fig. 22-2). Immunohistochemical studies have demonstrated tyrosine hydroxylase positive nerves in association with the large blood vessels beginning at 18 weeks

gestation, and these nerve fibers increase in density as gestation progresses [4]. The nerve branches penetrate the septa around 20 weeks gestation and reach the corticomedullary junction by 20 to 23 weeks. A few nerve fibers are also demonstrable within the medulla, closely associated with Hassall's corpuscles.

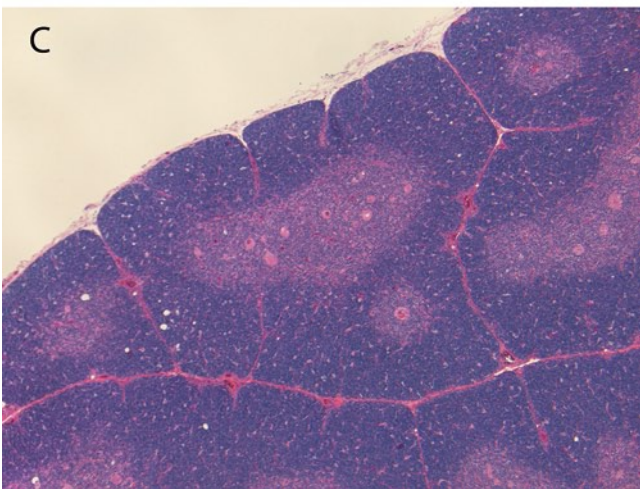
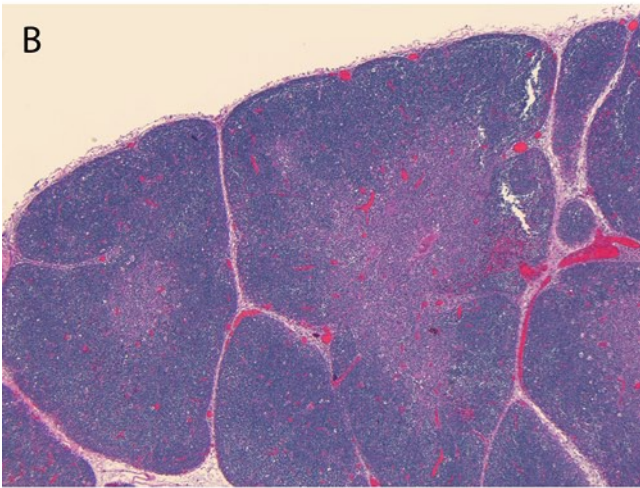
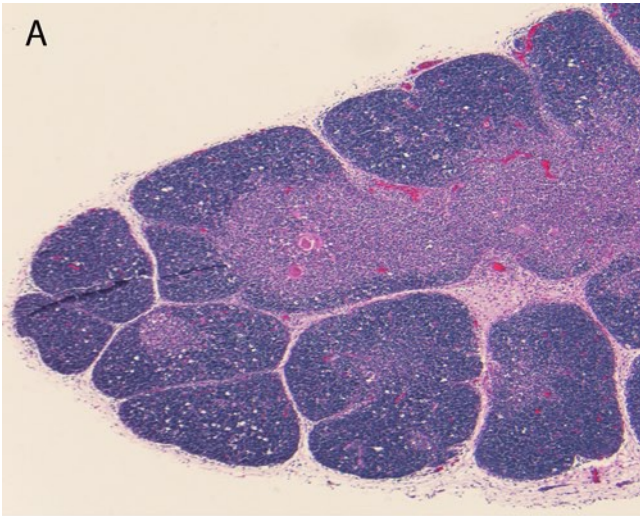


FIGURE 22-2. Thymus over gestation. Low-power view of the thymic development at 17 weeks (**A**), 22 weeks (**B**), and 40 weeks (**C**). Note the thin capsule with trabeculae of connective tissue creating the lobulated appearance. The cellular, dark-staining cortex surrounds the lighter-staining medulla within the lobule. In the early midtrimester, the interlobular septa are wider and the cortex is thinner. As gestation progresses, the interlobular septa become narrower and the cortex becomes thicker. (**A-C**, H&E, 5 \times .)

Cortex

The cortex is recognizable as the darker, more peripheral area of the gland arranged in lobules that are separated by connective tissue trabeculae (see Fig. 22-3). The overall architecture and histological appearance of the thymic cortex changes over gestation (see Figs. 22-2 and 22-3). When the bone marrow–derived precursor lymphoid cells first appear in the cortex, the lobules are small and widely spaced by interlobular septae, and the cortex is a small cap at the tips of the lobules. With increasing gestational age, the lobules become larger, interlobular septa become narrower, and the lobules appear more closely packed as the cortex extends along the edges of the each lobule. By the beginning of the third trimester, the lobule appears to be composed of equal thirds: one-third cortex on one side, one-third medulla, and one-third cortex on the opposite side of the lobule. By term, it is expected that approximately 85% of the thymus is composed of cortex and the remainder medulla [5].

Dark-staining of the cortex on hematoxylin and eosin (H&E) stain is due to densely packed lymphocytes. The density of the lymphocytes within the cortex obscures the underlying epithelial reticular framework, and thus cortical epithelial cells are difficult to identify. They can be recognized by cytokeratin stains and electron microscopy as larger, ovoid to polygonal cells with elongated cytoplasmic processes that appear to encircle the lymphocytes (see Figs. 22-4 and 22-5) [6]. Thymic epithelial cells can be subtyped using antibodies to the

thymic hormones. For example, subcapsular cortical cells are positive for thymosin α 1 and thymopoietin, and inner cortical cells are negative [3].

Lymphocytes in the cortex consist nearly exclusively of T-lymphocytes (see Figs. 22-6 and 22-7) that form a sheet without distinct follicle or germinal center formation. There is, however, some variability in the cytologic features and immunophenotype of the lymphocytes. Recently arrived precursor T-lymphocytes from the bone marrow populate a thin layer of the periphery of the cortex beneath the capsule. These immature thymocytes are large and actively proliferate. They undergo a series of maturational steps, and at each step they acquire distinctive immunophenotypic cytoplasmic and membrane markers. As the lymphocytes mature, they become smaller (see Fig. 22-8) and descend through the cortex and into the medulla. The fully differentiated thymocytes exit the medulla via the blood vessels and lymphatic channels. During this complex developmental process, some lymphocytes will undergo apoptosis. Macrophages are also present in the cortex and function as both antigen-presenting cells and phagocytic cells. After ingesting the debris of apoptotic lymphocytes, the macrophages are known as tingible body macrophages (see Fig. 22-9). Extramedullary hematopoiesis is common and is usually confined to the capsule, interlobular septa, and along the vessels. It may be composed of purely eosinophilic myeloid elements (see Fig. 22-10).

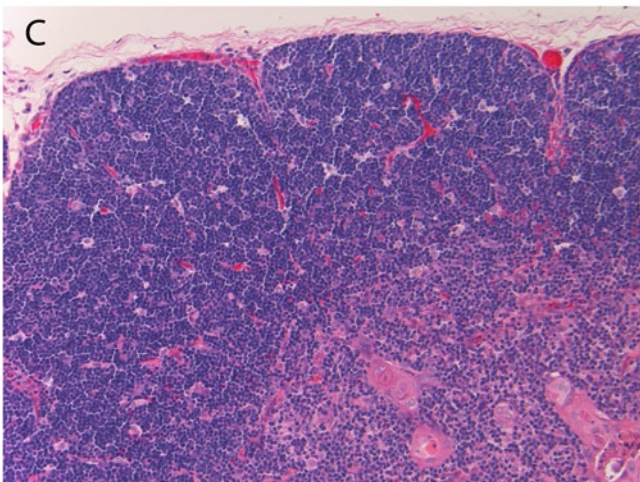
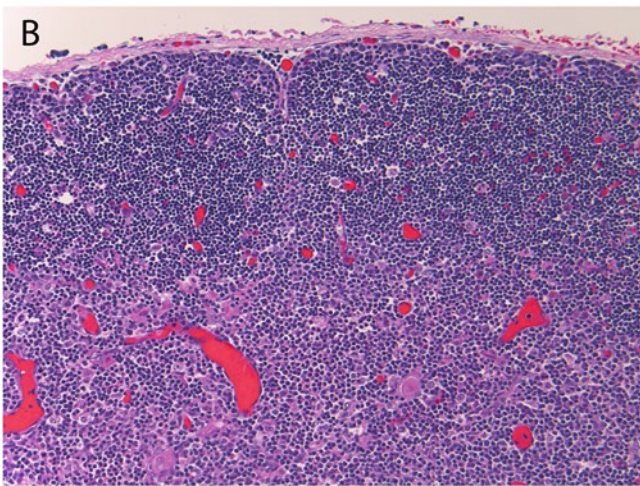
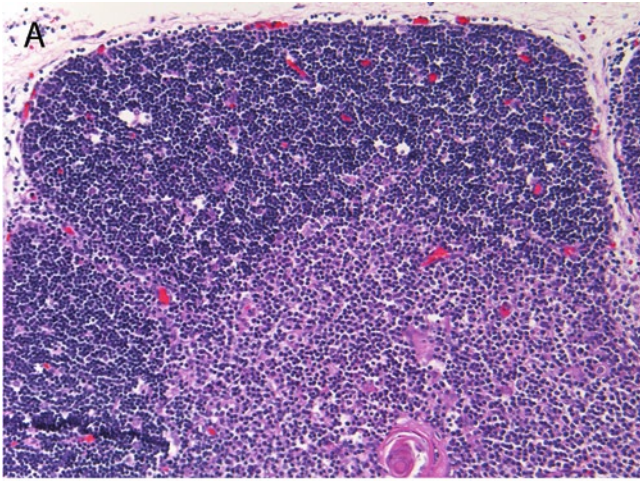


FIGURE 22-3. Thymic cortex over gestation. Medium-power views of the thymic capsule, cortex, and superficial medulla over gestation at 17 weeks (**A**), 22 weeks (**B**), and term (**C**). Note the architecture of the cortex as it changes over gestation and becomes thicker and more densely packed with lymphocytes. (**A-C**, H&E, 20 \times .)

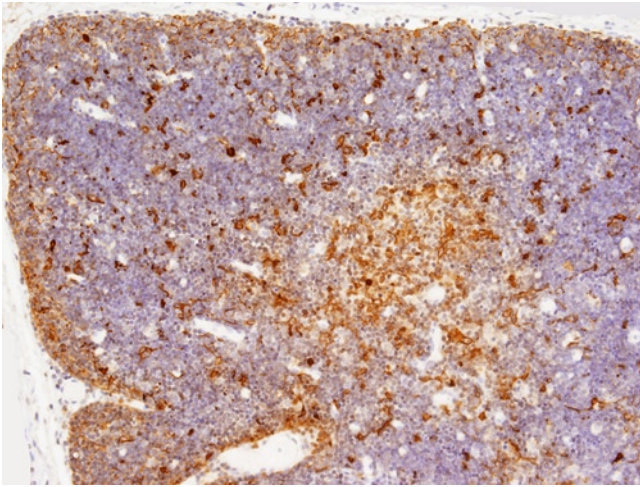


FIGURE 22-4. Thymic epithelial cells at 22 weeks gestation. Cytokeratin stain highlights scattered cortical epithelial cells, some with cytoplasmic processes. (Cytokeratin AE1/AE3 immunohistochemistry, 20 \times .)

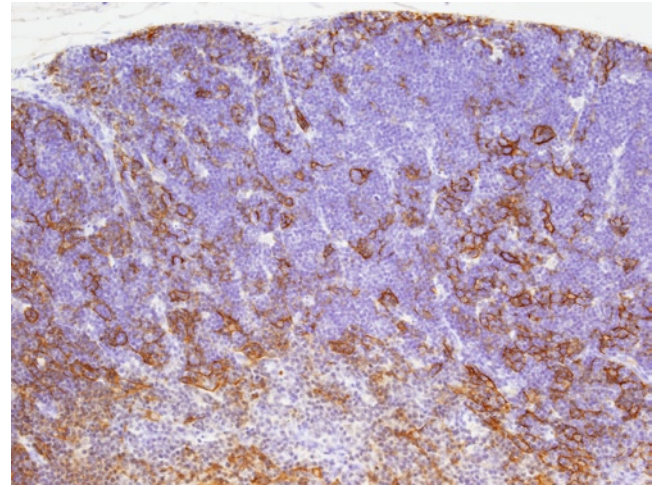


FIGURE 22-5. Thymic epithelial cells at term. Cytokeratin stain highlights scattered cortical epithelial cells, many with cytoplasmic processes, creating the reticular network of the thymus. (Cytokeratin AE1/AE3 immunohistochemistry, 20 \times .)

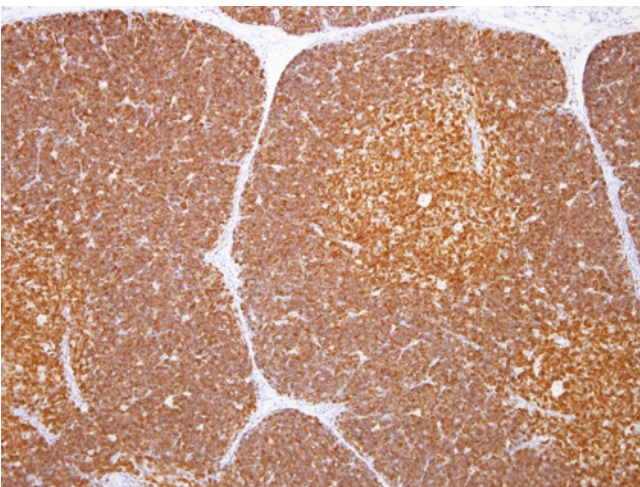


FIGURE 22-6. Thymic lymphocytes at term. CD3 stain highlights densely packed T-lymphocytes in the cortex, and still abundant, but slightly less packed in the medulla. (CD3 immunohistochemistry, 20 \times .)

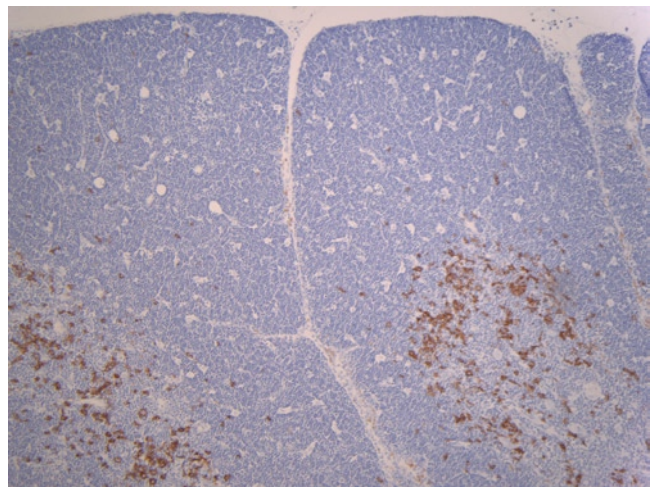


FIGURE 22-7. Thymic lymphocytes at term. CD20 stain showing near absence of B-lymphocytes in the cortex, and presence of scattered B-lymphocytes in the medulla. Compare with [Figure 22-6](#). (CD20 immunohistochemistry, 10 \times .)

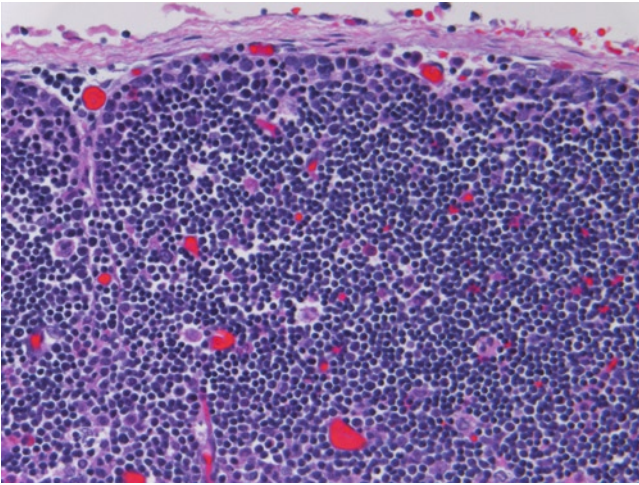


FIGURE 22-8. Thymic cortical lymphocytes. High-power view of thymic cortex at 23 weeks gestation. Note the lymphocytes are slightly larger near the periphery of the lobule and are smaller near the center. (H&E, 40 \times .)

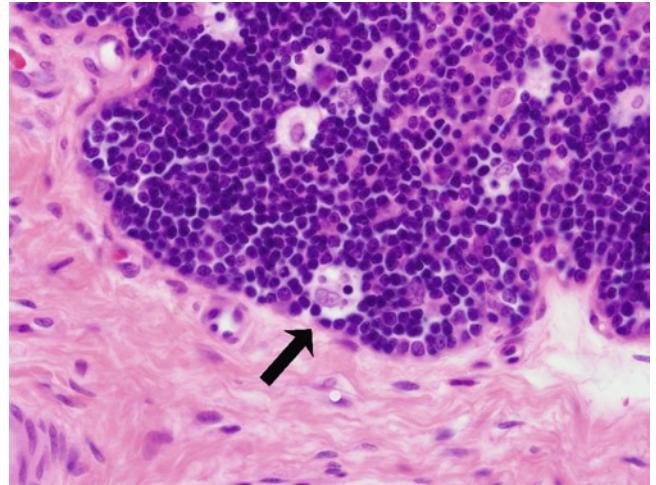


FIGURE 22-9. Tingible body macrophage in thymic cortex. Note the macrophage (*arrow*) with abundant cytoplasm containing apoptotic debris. (H&E, 60 \times .)

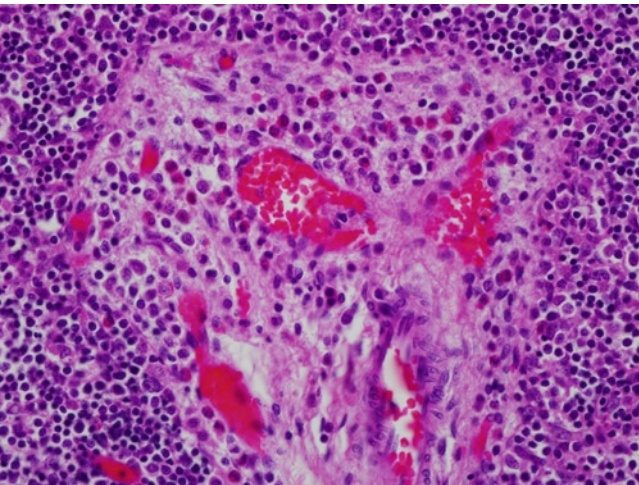


FIGURE 22-10. Extramedullary hematopoiesis in thymus. High-power view of connective tissue trabecula in thymic cortex with extramedullary hematopoiesis consisting mostly of perivascular eosinophilic myeloid precursors. (H&E, 40 \times .)

Medulla

In the medulla, the same lymphoid and epithelial components are present, but there are fewer lymphocytes in the medulla giving the medulla a "lighter" appearance by H&E stain (see Fig. 22-11). The reticular medullary epithelial cells are the predominant cells in the medulla, as they are no longer obscured by lymphocytes, and these cells are positive for thymosin $\alpha 1$ [3]. The epithelial cells of medulla are larger than those in the cortex. In addition, ovoid epithelial structures with concentric lamellated keratinization, known as Hassall's corpuscles are characteristic of the medulla (see Fig. 22-12-22-14).

These structures originate from a single medullary epithelial cell that undergoes degeneration characterized by enlargement of the cell, eosinophilia, and vacuolation of the cytoplasm. Adjacent epithelial cells become involved to form a lamellated hyaline mass.

Although the majority of the medullary lymphocytes are T-lymphocytes, isolated B-lymphocytes are seen along connective tissue trabeculae, around the small vessels at the corticomedullary junction and in the medulla around Hassall's corpuscles.

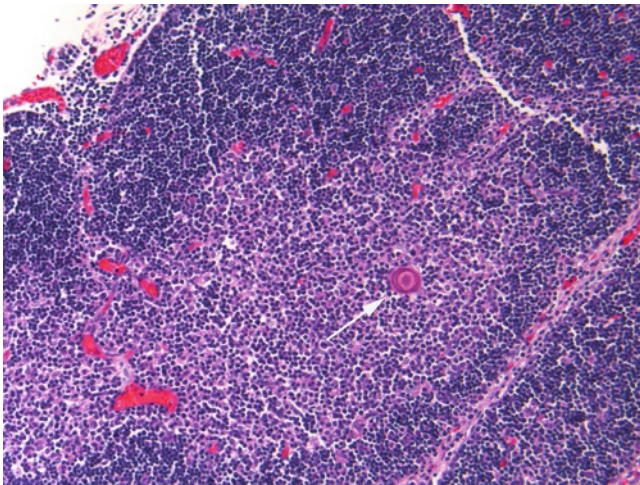


FIGURE 22-11. Thymic medulla at 17 weeks gestation. At 17 of weeks gestation, Hassall's corpuscles are visible as a few, small lamellated structures (arrow). (H&E, 20 \times .)

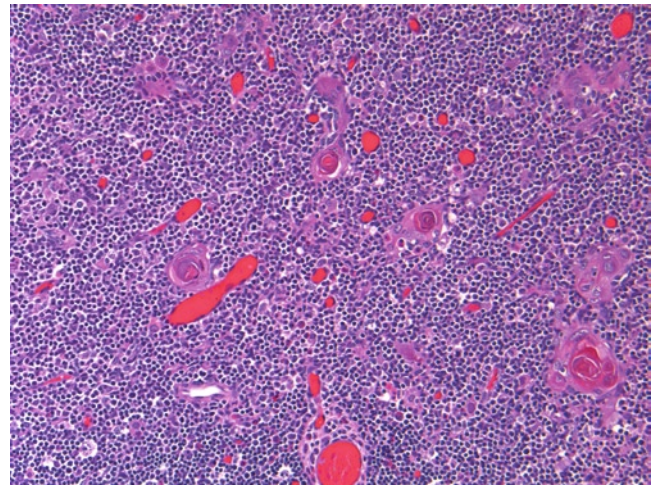


FIGURE 22-12. Thymic medulla at 22 weeks gestation. By 22 weeks gestation, Hassall's corpuscles are easily identified in the medulla and vary somewhat in size and shape. (H&E, 20 \times .)

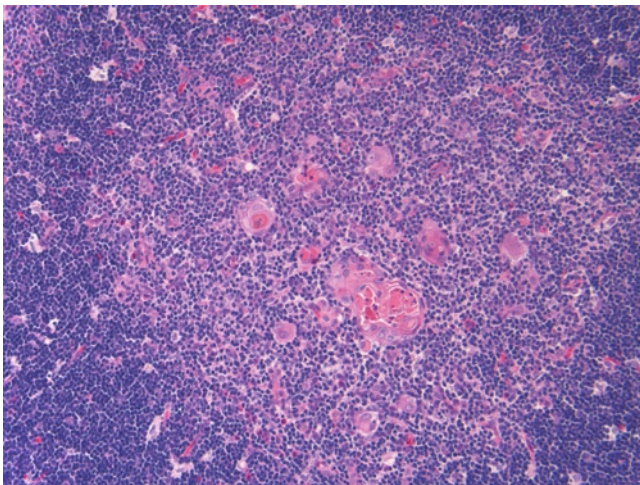


FIGURE 22-13. Thymic medulla at term. At term, numerous Hassall's corpuscles are visible in the medulla. (H&E, 20 \times .)

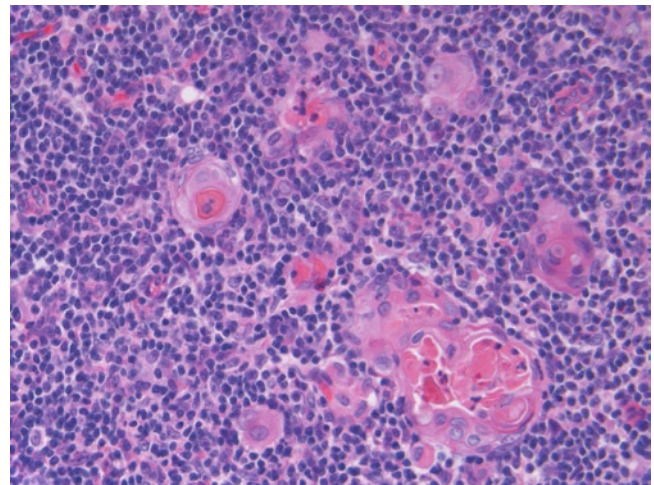


FIGURE 22-14. Thymic medulla at term. Higher-power view of Hassall's corpuscles at term. (H&E, 40 \times .)

Special Considerations

Thymic Tissue in Ectopic Sites

Thymic tissue can be found at any location along the embryologic path of descent of the thymus. It is normal for there to be cervical extensions of thymic tissue emanating from the most superior pole of each lobe. It is not unusual for the cervical extensions to reach the lower pole of the thyroid gland, but it is unusual for cervical extensions to reach the level of the isthmus or higher [7]. Nodules of thymic tissue not connected to the main

gland are a common finding in fetuses. They can be found near the lower pole of the thyroid gland (see Fig. 22-15), along the lateral lobes of the thyroid gland, adjacent to or admixed with parathyroid gland, within the thyroid gland (see Fig. 22-16), along and behind the carotid sheath, behind the pharynx and even as far superior as the base of the cranium.

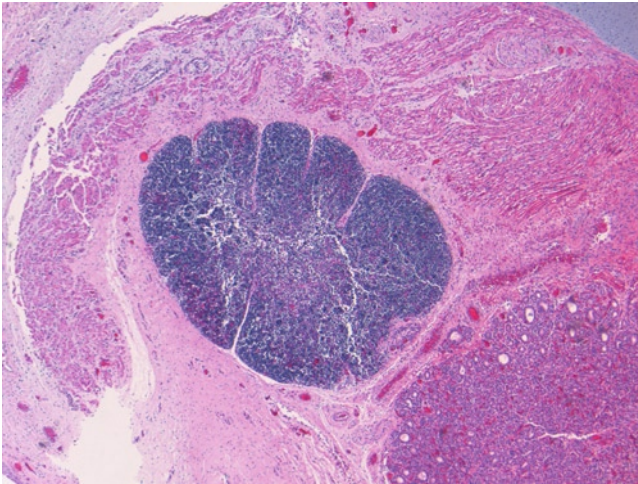


FIGURE 22-15. Thymic tissue in ectopic site. Ectopic thymic lobule is shown, located in the perithyroidal soft tissues near the lower pole of the thyroid gland, visible at the lower right. (H&E, 5 \times .)

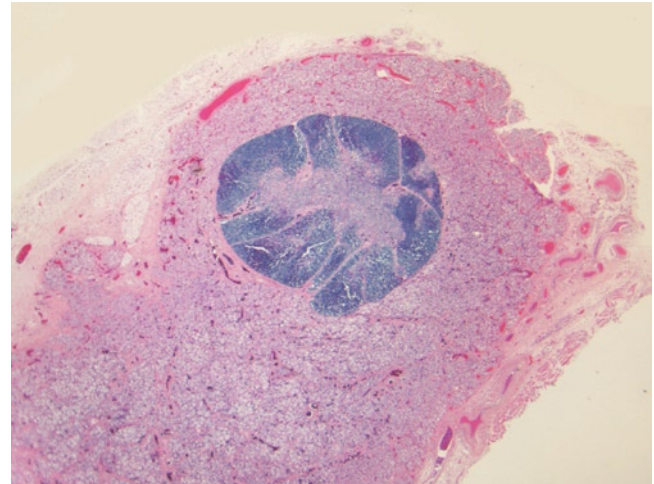


FIGURE 22-16. Thymic tissue in ectopic site. Ectopic thymic tissue is shown within the partially autolyzed thyroid gland. (H&E, 1.25 \times .)

Involution of the Thymus Gland

The thymus gland weight and histology can be useful markers of fetal stress in utero. Thymic stress involution is characterized by lysis or apoptosis of the many dark-staining cortical lymphocytes (see Figs. 22-17 and 22-18), which produces increasingly more severe histologic abnormalities: 1) a starry sky appearance to the cortex due to unmasking of tingible body macrophages and epithelial cells; 2) a less basophilic appearance

of the cortex; 3) narrowing of the cortex; 4) blurring of the corticomedullary distinction; 5) disappearance of the cortex; 6) crowding of Hassall's corpuscles in the medulla; and 7) reduction in thymic weight [5,8]. Caution should be used when interpreting changes of involution in the setting of intrauterine fetal death, as loss of nuclear basophilia in all organs is characteristic of fetuses retained in utero after death.

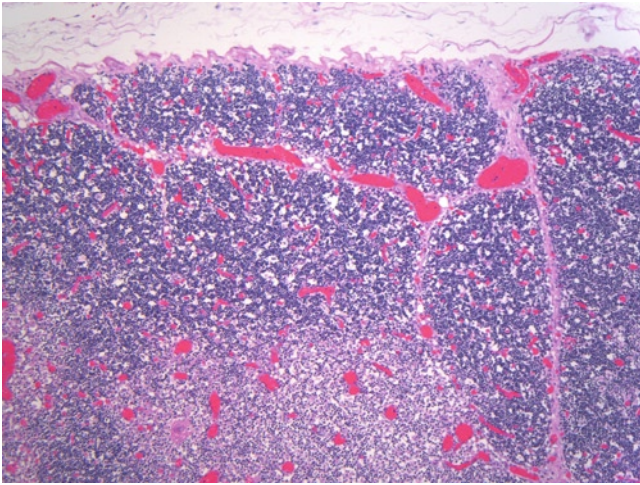


FIGURE 22-17. Stress involution of the thymus. Thymus gland at 32 weeks gestation is shown with starry sky appearance to the thymic cortex due to depletion of cortical lymphoid cells. (H&E, 10 \times .)

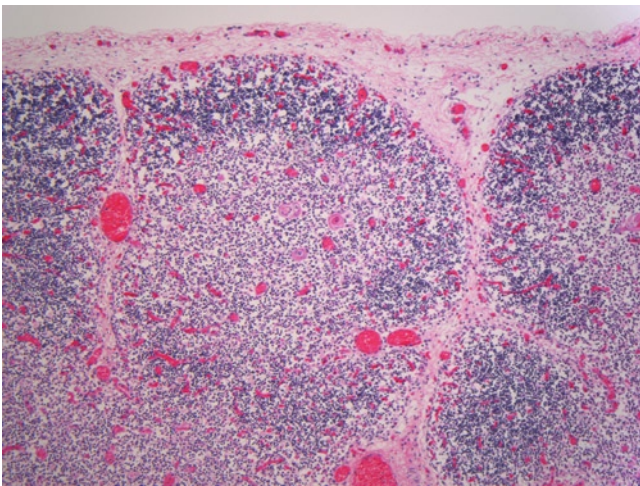


FIGURE 22-18. Stress involution of the thymus. Thymus gland at 30 weeks gestation is shown with more severe cortical lymphoid depletion, cortical thinning, and blurring of the distinction between cortex and medulla. Also note Hassall's corpuscles appear more crowded (H&E, 10 \times .)

References

1. Valdes-Dapena MA: Thymus. In *Histology of the Fetus and Newborn*. Philadelphia: Saunders; 1979:45-58.
2. Sadler TW, Langman J: Head and neck. In *Langman's Medical Embryology*, edn 11. Philadelphia: Wolters Kluwer Lippincott Williams & Wilkins; 2010:272.
3. Pearse G: Normal structure, function, and histology of the thymus. *Toxicol Pathol* 2006, 34:504-514.
4. Anagnostou VK, Doussis-Anagnostopoulou I, Tiniakos DG, et al.: Ontogeny of intrinsic innervation in the human thymus and spleen. *J Histochem Cytochem* 2007, 55:813-820.
5. Singer D: Disorders of the lymphoid tissue and immune system. In *Textbook of Fetal and Neonatal Pathology*, edn 2. Edited by Wigglesworth J, Singer D. Malden, MA : Blackwell Science; 1998:436-437.
6. Suster S, Rosai R: Thymus. In *Histology for Pathologists*, edn 3. Edited by Mills SE. Philadelphia: Lippincott Williams & Wilkins; 2007:509.
7. Gorlin R, Cohen M: The Orofacial region. In *Textbook of Fetal and Neonatal Pathology*, edn 2. Edited by Wigglesworth J, Singer D. Malden, MA: Blackwell Science; 1998:743-744.
8. van Baarlen J, Schuurman HJ, Huber J: Acute thymus involution in infancy and childhood: a reliable marker for duration of acute illness. *Hum Pathol* 1988, 19:1155-1160.

23

Spleen

Linda M. Ernst

The histological appearance of the spleen changes dramatically during fetal life. Since much of the architecture of the spleen is not fully formed in the embryonic period, significant development of the red and white pulp occurs during the second and third trimesters of fetal life with additional changes occurring postnatally. Unfortunately, there are only a few histological studies of the human fetal spleen in the literature, and while they provide some insight into prenatal splenic development, more comprehensive analyses are needed to fully understand the changes that occur in this complex organ during fetal life.

Nevertheless, a working knowledge of the normal splenic appearance at certain gestational ages can be helpful in recognizing abnormal development of the spleen that has been retarded or accelerated by a pathologic process. In this chapter, representations of the normal splenic architecture are provided throughout the second and third trimesters. The main components studied are the capsule, the vascular tree, and the white and red pulp.

Embryology

The spleen is derived from condensation of mesoderm within the dorsal mesogastrium around the fifth week of gestation. This mesoderm forms the capsule, connective tissue, and reticular framework of the spleen. The splenic mass takes its final position in the left upper quadrant of the peritoneal cavity after growth of the dorsal mesogastrium and rotation of the stomach. This rotation also establishes the splenorenal (renoleino) ligament. The gastrosplenic (gastroleino) ligament is formed by the portion of the dorsal mesentery that remains between the spleen and stomach [1,2].

At the end of the embryonic period, although the splenic anlage is formed and has assumed its appropriate anatomic position, splenic development is quite primitive. There is no distinct architectural organization at this time and the parenchyma of the splenic anlage consists predominantly of hematopoietic precursors and a few macrophages. Almost no lymphocytes are present at this stage [1,2].

Histology

Capsule

The fetal spleen is an encapsulated organ, and the capsule is composed of longitudinally arranged collagen and elastic fibers. In early gestation the capsule is a thin layer, but with increasing gestational age the capsule becomes slightly thicker. Trabeculae of connective tissue extend downward from the capsule, but generally do not contain blood vessels and extend only a short distance into the parenchyma.

Vascular Tree

The splenic artery enters the spleen at the hilum and gives rise to branches that become increasingly smaller with a decreasing collagenous cuff also containing veins and lymphatic channels. In the mature spleen, the central arteriole is identified because it no longer travels with an accompanying vein and its collagenous adventitia is replaced by lymphoid tissue [3,4]. Prior to significant lymphoid colonization of fetal spleen, these central arterioles or their precursors can be seen as small muscularized arterioles surrounded by delicate reticulin

fibers (see Fig. 23-1). In the mature spleen, the central arterioles terminate in a capillary bed formed within the lymphoid tissue of the white pulp. At the termination of these capillaries, the lining cells are replaced by macrophages, the so-called "sheathed" end of the capillary, and blood flowing through this capillary then passes into the splenic sinuses [3,4]. The splenic sinuses eventually merge with the veins that are traveling along with the larger arteries to the hilum.

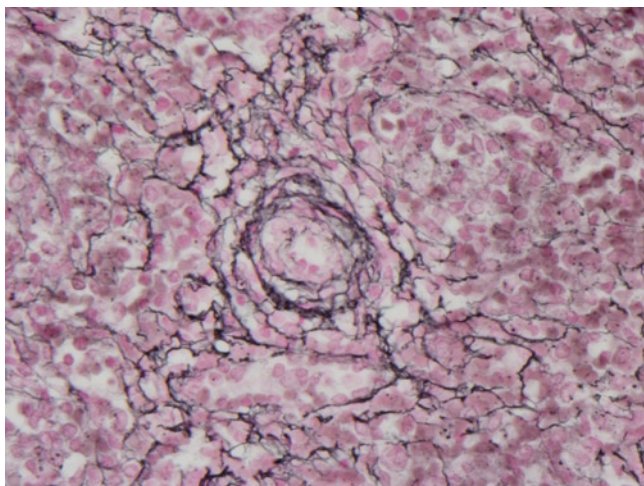


FIGURE 23-1. Fetal spleen at 16 weeks gestation. Note the early reticulin condensation around the small arteriole. (Reticulin stain, 40 \times .)

White Pulp

The white pulp of the spleen is essentially the lymphoid component of the organ, which in the adult spleen contains mature T- and B-lymphocyte compartments. The B-cell areas include the germinal center, mantle zone, and marginal zone and the T-cell area is the less well-organized parafollicular zone, but T-cells are also a component of the periarteriolar clusters.

In the fetal spleen, these lymphoid compartments are just beginning to develop and do not achieve the histological architecture that is recognizable in the mature, adult spleen, even by the end of full-term gestation. Figure 23-2 summarizes the time-dependent changes in the splenic lymphoid development and development of the splenic sinuses. Colonization of the spleen by lymphoid tissue is usually not visible until approximately 14 to 18 weeks gestation (see Figs. 23-3–23-5) and at first consists of scattered T- and B-lymphocytes [5,6]. Around 19 to 20 weeks gestation, lymphocytes begin to form small clusters around splenic arterioles (see Fig. 23-6). In this early stage there is no specific organization of lymphocytes into lymphoid follicles, and a mixture of B- and T-lymphocytes is present within the lymphoid aggregates (see Fig. 23-7). It has been shown that the early aggregates of B-lymphocytes accumulate around the more peripheral branches of the arterioles, whereas T-lymphocytes are

seen more centrally surrounding the larger arteriole trunks [6]. By the end of the second trimester, B-lymphocytes begin to form small primary follicular clusters (see Fig. 23-8), including the presence of follicular dendritic cells within the follicle [6]. These primary follicles can be recognized on hematoxylin and eosin (H&E) stain by the presence of an eccentric proliferation of small lymphocytes adjacent to the periarteriolar lymphoid cuff (see Figs. 23-9 and 23-10). Steiniger *et al.* have also demonstrated that these first fetal B-cell follicles do not arise from the initial B-cell clusters along the peripheral arterioles, but that they form more centrally where the periarteriolar T-cells sheaths are present [6]. These primary follicles enlarge throughout the third trimester (see Figs. 23-11, 23-12, and 23-13–23-16) [7]. However, germinal centers are not generally seen in the fetal spleen and may even be absent in the early neonatal period until sufficient antigen exposure and time is allowed for germinal center formation. Therefore, in summary, by the end of normal term gestation (see Figs. 23-17 and 23-18), splenic lymphoid tissue consists of primary follicles (B-lymphocyte zones) and the early formation of periarteriolar lymphoid sheaths (T-lymphocyte zones), but the reactive secondary follicles and formation of splenic mantle and marginal zones are absent.

After birth, there still is a lag time before the secondary follicles, mantle zone, and marginal zone lymphocytes are seen in the spleen. Secondary follicles form in the neonatal period after antigen exposure and contain a mixture of small B-lymphocytes and large transformed B-lymphocytes producing a characteristically more pale appearance than the primary follicles on H&E stain (see Fig. 23-19). In addition, follicular dendritic cells (CD21⁺, CD23⁺, and CD35⁺), occasional CD4⁺ T-cells, and macrophages are also seen within the secondary follicle [3]. In an infant autopsy series examining splenic lymphoid development, it has been shown that secondary follicles are consistently found at an age of 2.5 months or older [7]. The secondary follicle is surrounded by a more compact zone of small lymphocytes known as the mantle zone (bcl-2⁺, CD45RA⁺, IgM⁺, and

IgD⁺) and the marginal zone surrounds the mantle zone [3]. The splenic marginal zone is composed of medium-sized B-lymphocytes (bcl-2⁺, CD45RA⁻, and IgD⁻) in a dense, concentric meshwork of reticulin fibers that express smooth muscle actin [3]. The splenic marginal zone has been shown to be consistently present at an age of 8.5 months or older [7]. In addition, the lack of appropriate and timely mantle-zone development has been shown to be associated with sudden infant death or infectious causes of death [7].

As the splenic B-lymphocyte regions mature, the T-cell areas become more well defined and form a nodule of CD4⁺ T-lymphocytes around the splenic arterioles. These are usually seen at the edge of the secondary follicles and are surrounded by the concentric smooth muscle actin positive reticulin fibers.

Summary of Splenic Lymphoid and Sinus Development		
Gestational age	Lymphocytes	Splenic sinuses
0–12 wk	None	Not formed
14–18 wk	Scattered B- and T-lymphocytes	Not formed
19–23 wk	Lymphocyte condensations begin around arterioles	Beginning formation
23+ wk	Increasing number of B-lymphocytes around arterioles Primary follicle formation begins	Present
After birth	Formation of germinal centers with antigen exposure Formation of mantle and marginal zones	Present

FIGURE 23-2. Summary of splenic lymphoid and sinus development. Information regarding lymphocytes and splenic sinuses at various gestational ages is provided here.

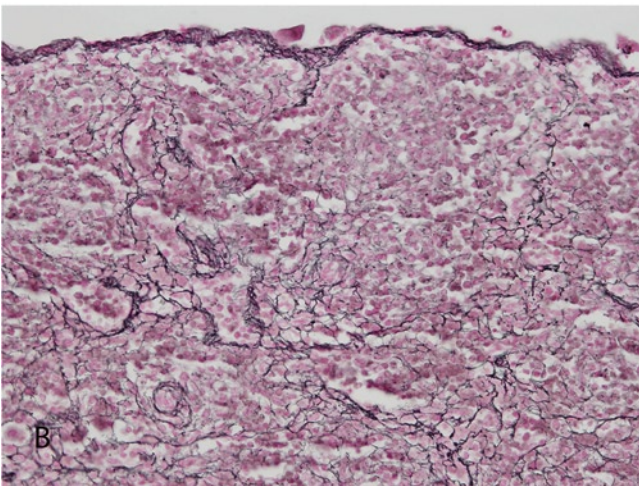
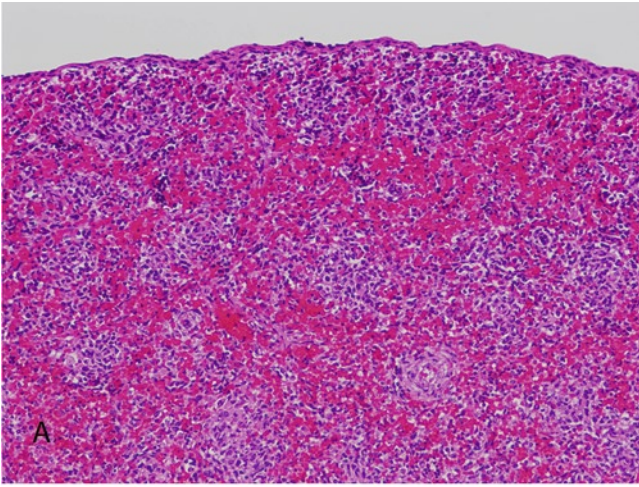


FIGURE 23-3. Fetal spleen at 16 weeks gestation. Note the absence of conspicuous lymphoid aggregates at this early gestational age. **A**, Very little lymphoid tissue appears to be present on H&E stain. Note the thin fibrous capsule. **B**, Reticulin stain highlights reticulin within the fibrous capsule and the very short trabeculae extending into the parenchyma. Also note that there is very little reticulin tissue within the splenic parenchyma at this gestational age, with only small concentric condensations of reticulin around arterioles. (**A**, H&E, 10 \times and **B**, reticulin stain, 10 \times .)

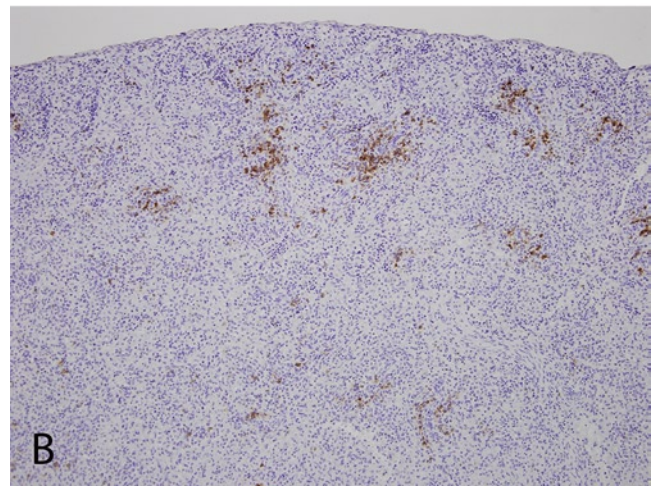
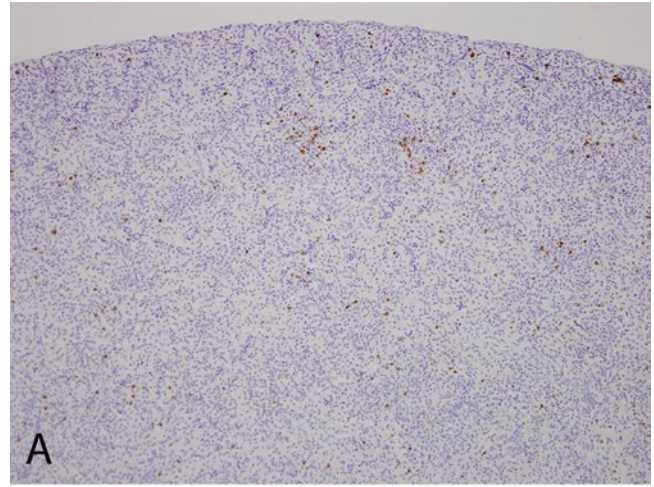


FIGURE 23-4. Fetal spleen at 16 weeks gestation. These images show the complement of CD3⁺ T-lymphocytes (**A**) and CD20⁺ B-lymphocytes (**B**). Note that the B-lymphocytes are beginning to form small aggregates and there also are scattered T-lymphocytes present. (**A**, CD3 immunohistochemistry, 10 \times and **B**, CD20 immunohistochemistry, 10 \times .)

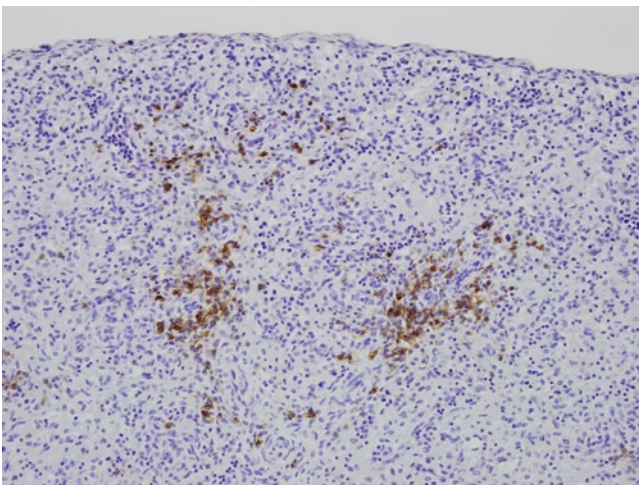


FIGURE 23-5. Fetal spleen at 16 weeks gestation. This higher power view shows the CD20⁺ cells aggregating around the central arteriole. (CD20 immunohistochemistry, 20 \times .)

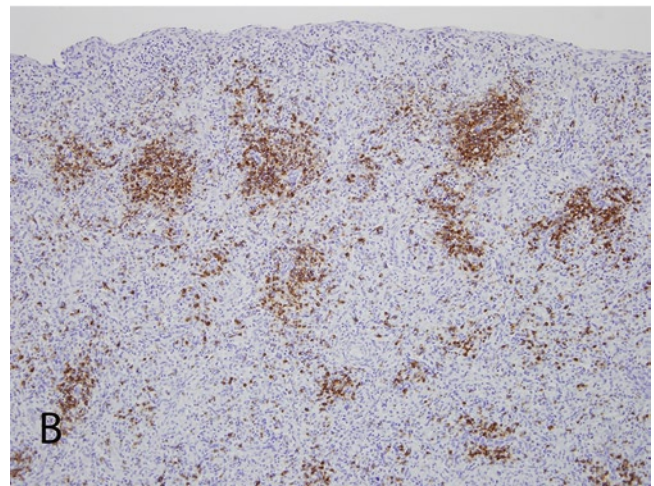
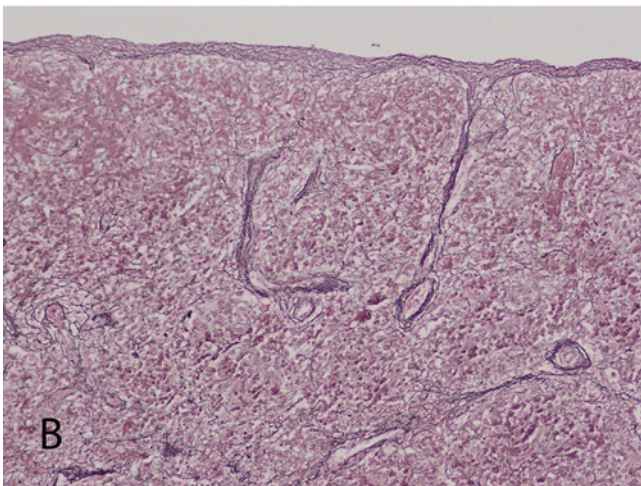
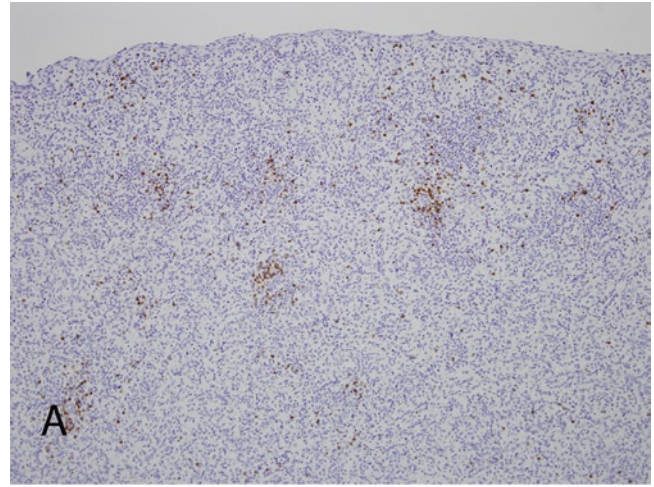
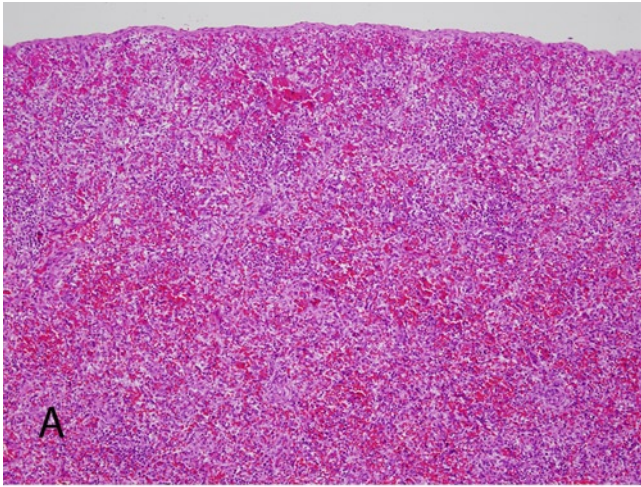


FIGURE 23-6. Fetal spleen at 21 weeks gestation. Early lymphoid aggregates are beginning to become visible on H&E stain (**A**). Note that the capsule is slightly thicker and that reticulin stain highlights lengthening trabeculae extending into the parenchyma (**B**). (**A**, H&E, 10× and **B**, reticulin stain, 10×.)

FIGURE 23-7. Fetal spleen at 21 weeks gestation. These images show the complement of CD3⁺ T-lymphocytes (**A**) and CD20⁺ B-lymphocytes (**B**). Note that the B-lymphocyte aggregates are larger and more well formed than at 16 weeks gestation. Also, slightly more scattered T-lymphocytes are present. (**A**, CD3 immunohistochemistry, 10× and **B**, CD20 immunohistochemistry, 10×.)

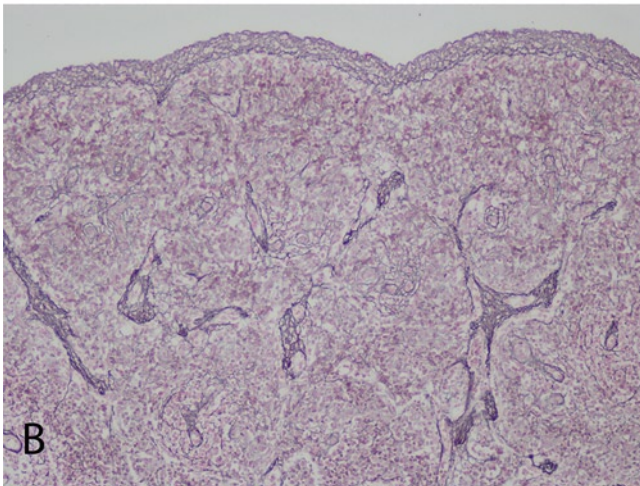
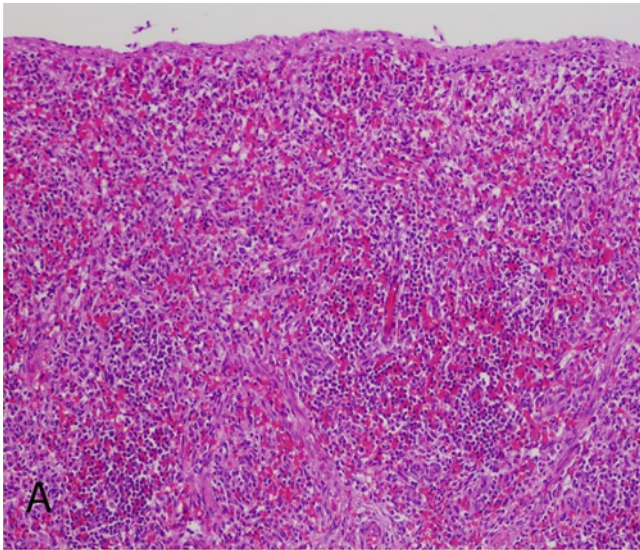


FIGURE 23-8. Fetal spleen at 23 weeks gestation. On the H&E-stained section (**A**), the lymphoid tissue is becoming more prominent. The reticulin stain (**B**) highlights the slightly increased thickness of the capsule and the increasing number and thickening of reticulin fibers extending into the parenchyma. (**A**, H&E, 10× and **B**, reticulin stain, 10×.)

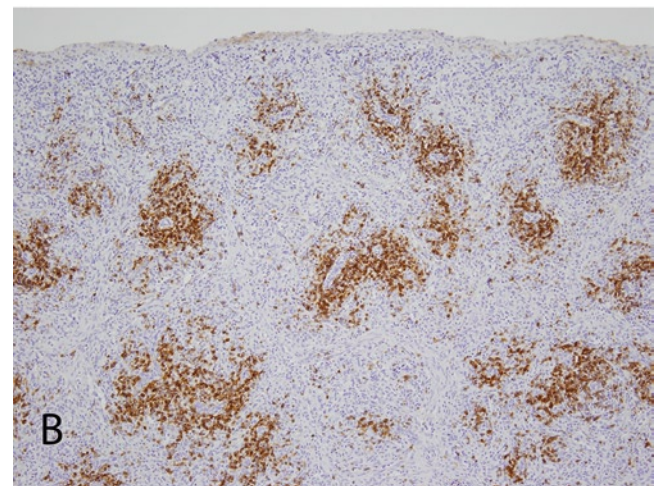
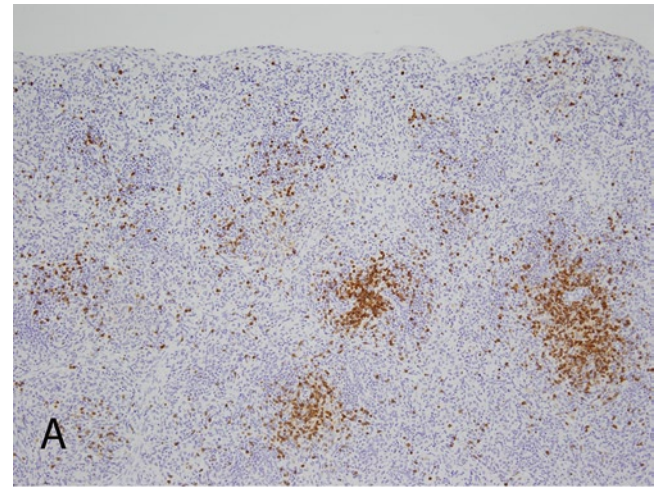
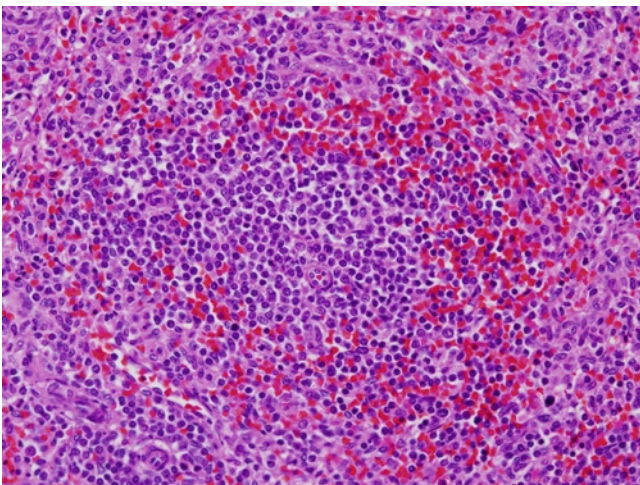


FIGURE 23-10. Fetal spleen at 24 weeks gestation. These images show the complement of CD3⁺ T-lymphocytes (**A**) and CD20⁺ B-lymphocytes (**B**). Note that the B-lymphocyte aggregates are well formed and are associated with scattered T-lymphocytes, which also begin to form small clusters. (**A**, CD3 immunohistochemistry, 10× and **B**, CD20 immunohistochemistry, 10×.)

FIGURE 23-9. Fetal spleen at 24 weeks gestation. This higher power view shows one of the lymphoid aggregates. (H&E, 20×.)

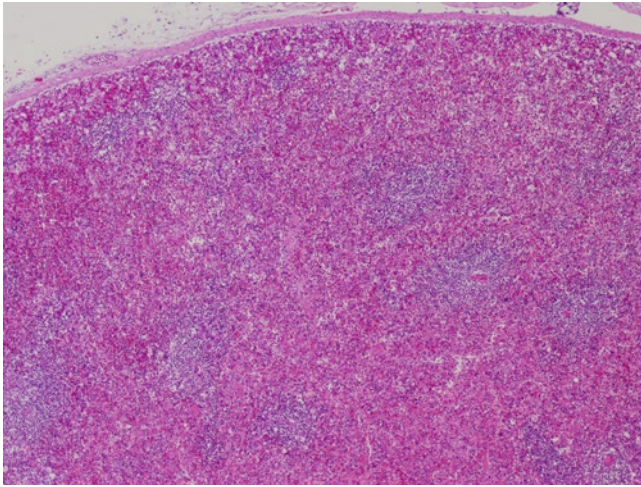


FIGURE 23-11. Fetal spleen at 32 weeks gestation. This low-power view shows the presence of clearly recognizable lymphoid aggregates at this gestational age. (H&E, 4 \times .)

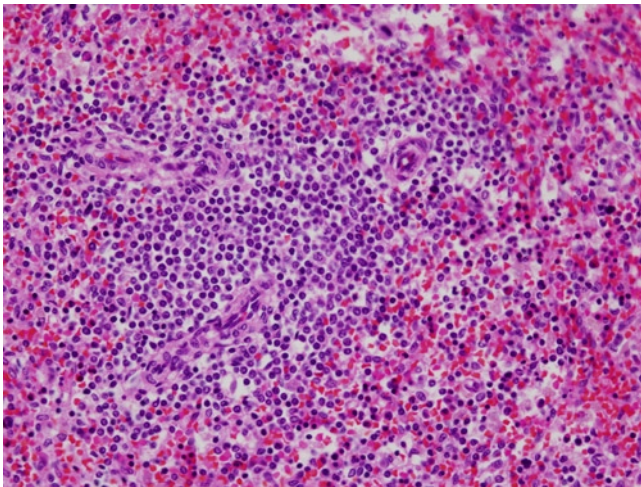


FIGURE 23-12. Fetal spleen at 32 weeks gestation. Note the eccentric proliferation of lymphocytes (primary follicle) adjacent to a central arteriole. (H&E, 20 \times .)

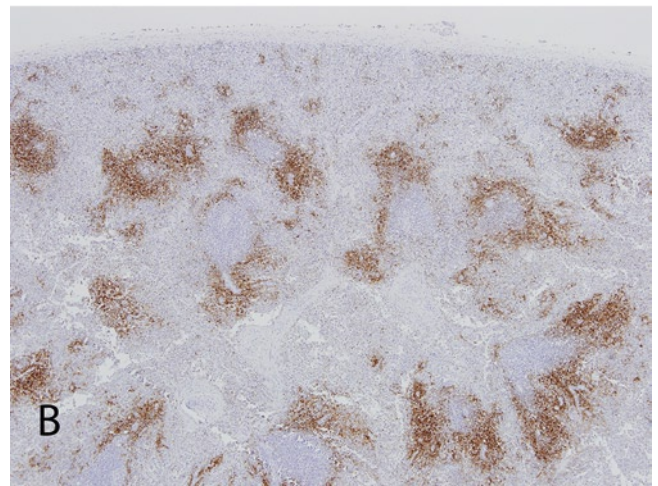
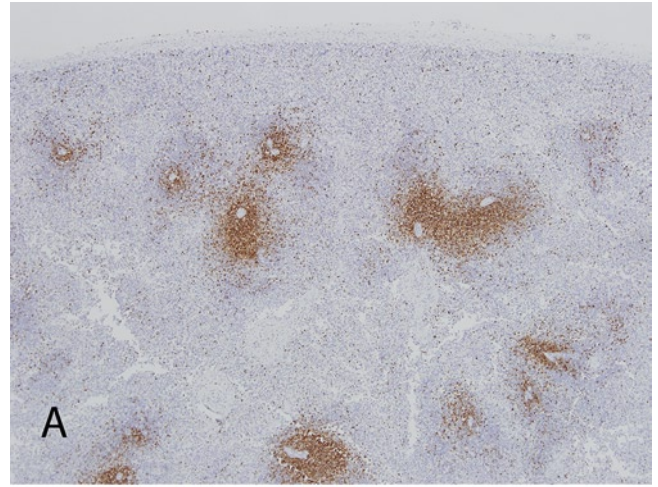


FIGURE 23-13. Fetal spleen at 32 weeks gestation. These images show the complement of CD3⁺ T-lymphocytes (**A**) and CD20⁺ B-lymphocytes (**B**). Note that B-lymphocyte aggregates now are seen adjacent to clusters of periarteriolar T-lymphocytes. (**A**, CD3 immunohistochemistry, 4 \times and **B**, CD20 immunohistochemistry, 4 \times .)

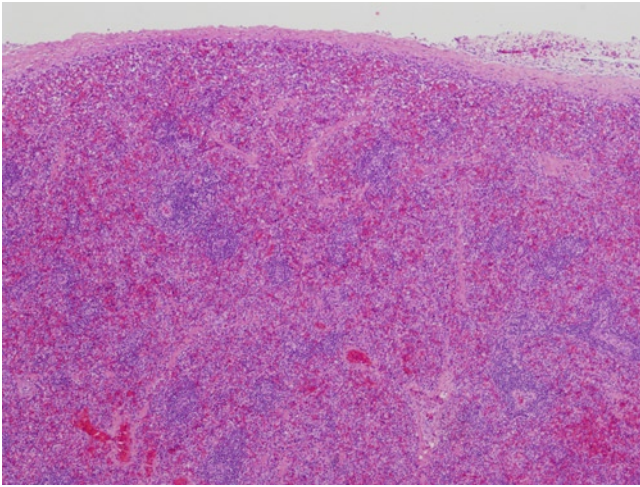


FIGURE 23-14. Fetal spleen at 35 weeks gestation. This low-power view shows numerous primary lymphoid follicles without germinal centers. (H&E, 4 \times .)

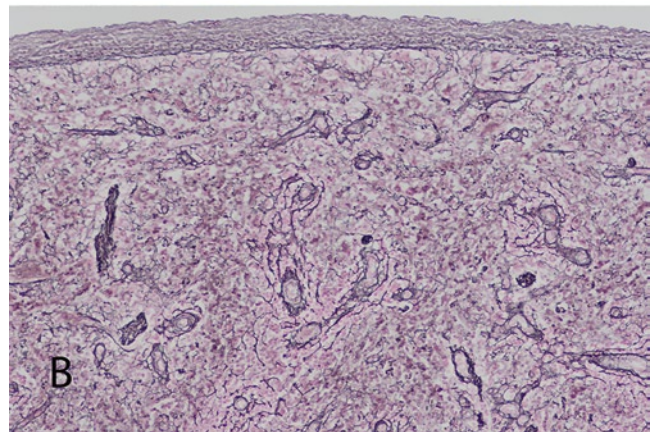
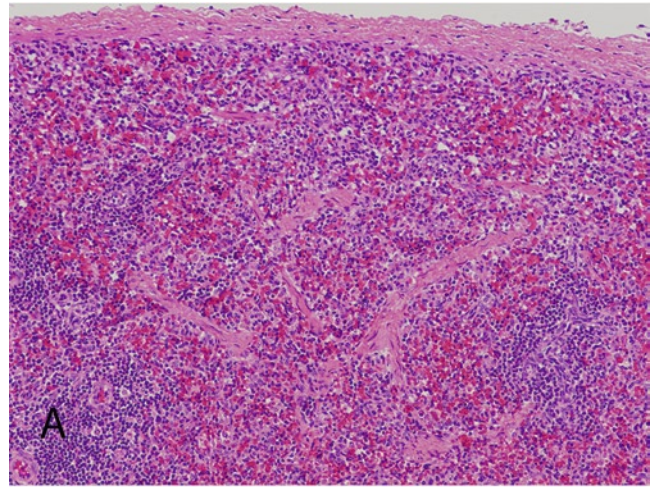


FIGURE 23-15. Fetal spleen at 35 weeks gestation. **A**, A slightly higher power of splenic capsule and a few of the underlying lymphoid follicles with H&E stain are shown. **B**, The reticulin stain highlights the capsular reticulin and increasing intraparenchymal reticulin. (**A**, H&E, 10 \times and **B**, reticulin stain, 10 \times .)

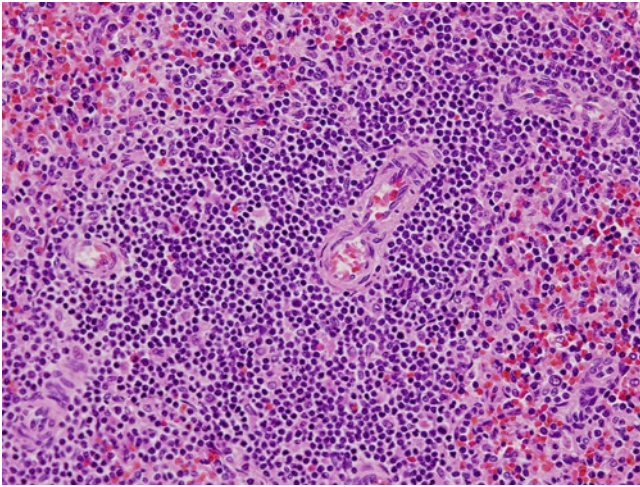


FIGURE 23-16. Fetal spleen at 35 weeks gestation. A higher power view of a primary lymphoid follicle is shown. (H&E, 20 \times .)

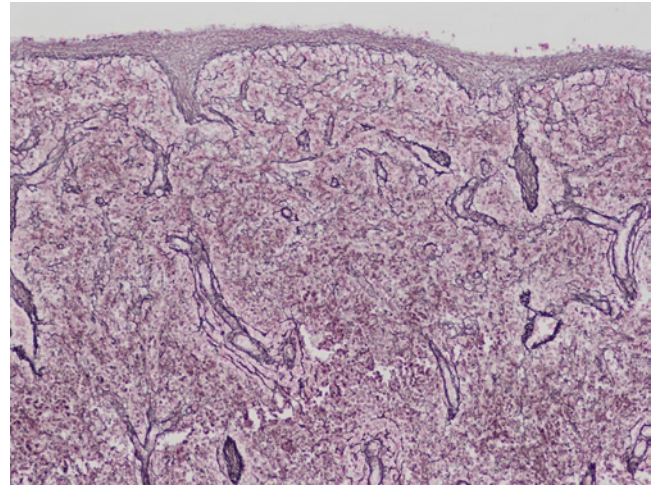


FIGURE 23-18. Fetal spleen at term showing the mature fetal reticulin pattern. (Reticulin stain, 10 \times .)

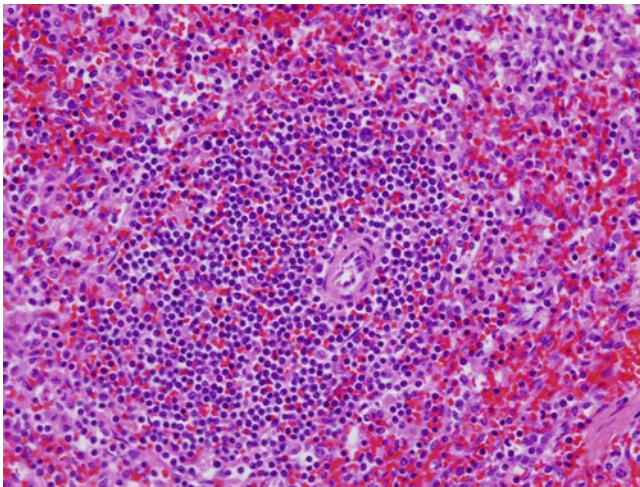


FIGURE 23-17. Fetal spleen at term showing primary lymphoid follicle. Germinal centers are not seen. (H&E, 20 \times .)

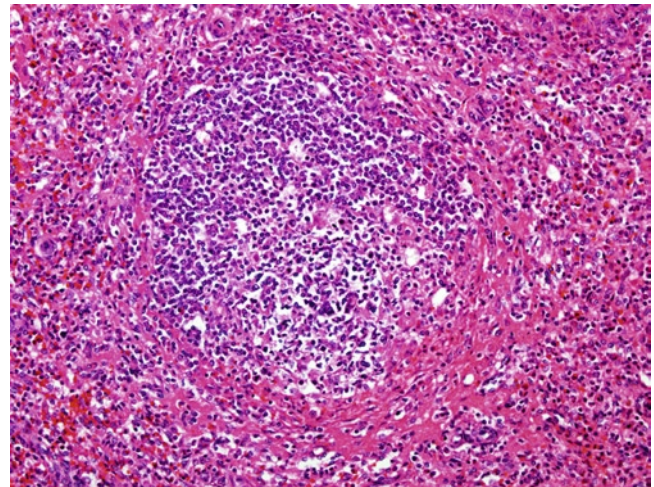


FIGURE 23-19. Postnatal spleen showing focal germinal center (secondary follicle) formation. (H&E, 20 \times .)

Red Pulp

The red pulp is the tissue intervening between the white pulp and is composed of a loose reticular stromal tissue, also known as the *cords of Billroth* , which contains lymphocytes, macrophages, and other blood cells. Reticulin stains of the fetal spleen show increasing amounts of reticulin within the red pulp as the spleen matures with advancing gestation (see Figs 23-3, 23-6, 23-8, 23-15, and 23-18). Between the splenic cords are the specialized sinuses of the spleen, which form as

outpouchings of the peripheral venules. The sinusoids have fenestrated basement membranes and are surrounded by transversely arranged reticulin fibers. Steiniger *et al.* have suggested that even in the early second trimester, splenic sinuses are not yet formed and begin formation at 19 to 23 weeks gestation (see Figure 23-2) [6]. The endothelium that lines the fetal splenic sinuses is recognized as weakly expressing CD34 antigen [6].

Special Considerations

Accessory Spleen(s)

Accessory spleens usually develop from smaller adjacent condensations of mesenchyme near the splenic

hilum. Their structure and histology is typically similar to the main spleen.

Fetal Spleen and Hematopoiesis

The fetal spleen has classically been considered a hematopoietic organ, but the exact role of the fetal spleen in hematopoiesis remains controversial. It is clear that hematopoietic cells are seen in the spleen beginning in the embryonic period, and throughout fetal life, but with far less density than in the fetal liver. In a study employing cell suspensions of human midtrimester fetal spleen, Calhoun *et al.* have shown that the hematopoietic cells present are predominantly polychromatic and orthochromatic normoblasts, and that the most immature myeloid and erythroid precursors are rare to absent

[8]. Also, they note that splenic normoblasts are seen predominantly in vessels and sinuses of the spleen in histological sections. In addition, the authors showed that the midtrimester fetal spleen lacks transcripts of the typical hematopoietic growth factors such as granulocyte colony-stimulating factor and erythropoietin. The role of the fetal spleen in prenatal hematopoiesis is still a controversial topic and designation of the spleen as a primary or secondary hematopoietic organ will require further debate and investigation.

References

1. Sadler TW, Langman J: *Langman's Medical Embryology*, edn 11th. Philadelphia, PA: Wolters Kluwer Lippincott Williams & Wilkins; 2010.
2. Schoenwolf GC, Larsen WJ: *Larsen's Human Embryology*, edn 4. Philadelphia, PA: Elsevier/Churchill Livingstone; 2009.
3. O'Malley DP, George TI, Orazi A, Abbondanzo SL, eds: *Embryology and histology of the lymph node and spleen. In Benign and Reactive Conditions of Lymph Node and Spleen.* Washington, DC: ARP; 2009.
4. van Krieken JHJ, Orazi A: Spleen. *In Histology for Pathologists.* Edited by Mills SE. Philadelphia, PA: Lippincott Williams & Wilkins; 2007.
5. Timens W, Rozeboom T, Poppema S: Fetal and neonatal development of human spleen: an immunohistological study. *Immunology* 1987, 60:603–609.
6. Steiniger B, Ulfing N, Risse M, Barth PJ: Fetal and early post-natal development of the human spleen: from primordial arterial B cell lobules to a non-segmented organ. *Histochem Cell Biol* 2007, 128:205–215.
7. Kruschinski C, Zidan M, Debertain AS, *et al.*: Age-dependent development of the splenic marginal zone in human infants is associated with different causes of death. *Hum Pathol* 2004, 35:113–121.
8. Calhoun DA, Li Y, Braylan RC, Christensen RD: Assessment of the contribution of the spleen to granulocytopoiesis and erythropoiesis of the mid-gestation human fetus. *Early Hum Dev* 1996, 46:217–227.

24

Lymph Nodes and Lymphatics

Michele E. Paessler

The function of the lymph nodes is to interact with and process antigens. Lymph nodes are found throughout the body and are usually located along blood vessels. Lymph nodes are numerous in areas that drain organs and in those that are in contact with the environment [1]. The respiratory and gastrointestinal tracts have large groups of lymph nodes: the hilar and mediastinal and mesenteric lymph nodes, respectively. This chapter focuses on the architecture of the developing lymph node throughout the second and third trimesters.

Embryology

The lymphatic vessels and lymph nodes arise from the lateral plate mesoderm. In order to understand the development of the lymph nodes, one must first discuss the lymphatics. The lymphatic system develops as discrete spaces in the mesenchyme, which form an endothelial lining. These spaces fuse, progressively grow, and branch into the lymphatic system [2]. The lymphatic system originally is distributed along the main venous trunks. The fusion and integration of these lymphatic networks give rise to six lymph sacs [3]. The first lymph sacs appear about the fifth week of gestation as the right and left jugular lymph sacs. Subsequently, the subclavian duct, thoracic duct, cistern chyli, and retroperitoneal lymph sacs develop [4]. It is from these primary sacs that endothelial sprouts grow, hollow out to form a lumen, and ultimately give rise to the peripheral lymphatic vessels [4].

Once the lymphatic system is established, primary lymph nodes start to develop at about 8 to 11 weeks gestation. The development of the lymph node starts with a lymphatic plexus in close association with strands of mesenchymal tissue. The mesenchymal cells condense at the base of the lymph sac and invaginate inward along with the endothelium [5]. In addition to the mesenchyme, the lymph sac is composed of capillaries, vascular loops, fibroblastic reticulum cells, and extracellular matrix [6,7]. By 13 weeks gestation, the lymph sac is composed predominantly of mesenchyme and the space between the endothelial lining and mesenchymal core develops into the marginal sinus [5]. At this point, the capillaries increase and the intermediate sinuses develop. The connective tissue on the outer side of the marginal sinus gives rise to the lymph node capsule [6,7]. The marginal sinus is first colonized by lymphoblasts and later repopulated by lymphocytes. A mass of smaller channels is formed by the growing lymphocytes and connective tissue; these small channels give rise to the efferent vessels. Blood vessels follow along the connective tissue framework in which the lymphocytes are proliferating.

Dense lymphoid tissue continues to develop in tandem with the vascular strands and this gives rise to the characteristic morphology seen in the medulla of the lymph node [4]. The cortex of the lymph node does not develop until much later in gestation and mature lymph nodes complete with germinal centers are not seen until the postnatal period [2].

Histology

In the developing fetus, the lymph nodes are basically a mass of lymphoid tissue that has a capsule and sinuses. In the early weeks of gestation, the lymph nodes are

small and appear to be depleted. As the gestational age increases, the lymph nodes become larger and contain more lymphocytes.

Blood Supply

Arteries enter the lymph node at the hilus, then branch and form a capillary network that supplies the paracortex and follicles. Venous drainage accompanies the arteriolar route and the veins leave the lymph node

through the hilus. The postcapillary venules are the entry site of circulating lymphocytes into the lymph node parenchyma [1].

Lymphatics

Lymphatic fluid enters the lymph node through the afferent lymphatic vessel, which penetrates the capsule, and then enters the subcapsular, intermediate, and medullary sinuses. Lymphatic fluid then exits the lymph node as the efferent lymphatic vessel. The intranodal sinuses are lined by sinus endothelial cells. Naïve B- and T-cells from the blood use specific receptors to recognize ligands on the high endothelial venules in the

lymph nodes and pass between these cells to enter the paracortex and then migrate to distinct B- and T-cell areas within the lymph node [8]. Under the influence of cytokines and chemokines, the T-cells localize in the paracortex and associate with dendritic cells, which aid in their differentiation. B-cells localize to follicles under the influence of cytokines secreted from follicular dendritic cells.

Lymph Nodes

On gross examination, fetal lymph nodes are typically small and round to bean shaped. On sectioning, the lymph nodes are tan–gray in appearance. Lymph nodes can be identified grossly by the middle of the second trimester, especially the mesenteric lymph nodes.

Microscopic sections of the fetal lymph node show that the lymphoid compartments are just beginning to develop and do not achieve the histologic architecture that is recognizable in the mature, adult lymph node, even at the end of full-term gestation. The demarcation of cortex and medulla becomes more distinct with the increase in gestational weeks [5]. Early in the second trimester, lymph nodes are usually quite small and are surrounded by a capsule and contain sinuses. Light and electron microscopy has shown that the marginal, intermediate, and medullary sinuses become developed with increasing gestational age [7]. By light microscopy, fetal lymph nodes have a diffuse pattern and are composed of small lymphocytes. There is often a paucity of lymphocytes as compared to adult nodes, imparting a “depleted” appearance (see Fig. 24-1). However, this should not be misinterpreted as a pathologic change.

From the 12th week of gestation until term, T-cells circulate in the periphery and settle into the growing lymph nodes [5,9]. This influx of lymphocytes from the circulation leads to enlargement of the lymph nodes. Early in the second trimester, the fetal lymph nodes are

composed predominantly of T-cells that are scattered throughout the primitive lymph node (see Fig. 24-2A); there is a predominance of CD4+ T-cells and only rare CD8+ T-cells [10]. At this point, B-cells are present in the outer cortex but do not yet form primary follicles [10]. After the 17th week of gestation, clearly defined B-cell follicles can be found. Although the primary follicles are formed, they may be difficult to see on morphologic grounds alone. Immunohistochemical stains for B-cell markers highlight these small primary follicles (see Fig. 24-2B).

As the fetus matures and approaches term, the lymph nodes enlarge, generally become more cellular, and appear less depleted (see Figs. 24-3–24-6). The demarcation of cortex and medulla becomes more apparent with increasing gestational age. The cortex is more cellular as compared to the medulla, which has a much looser structure [5]. Light as well as electron microscopy shows that the marginal, intermediate, and medullary sinuses also become more developed [7]. T-cells are still a major component of the lymph node (see Figs. 24-7 and 24-8) and localize to T-cell regions that are located in the cortex, where they are accompanied by interdigitating dendritic cells. Germinal centers are not apparent in any stage of gestation, even in the term fetus [7,9]. Normally, germinal center formation does not occur until the postnatal period, when their formation is driven by antigenic stimuli [11].

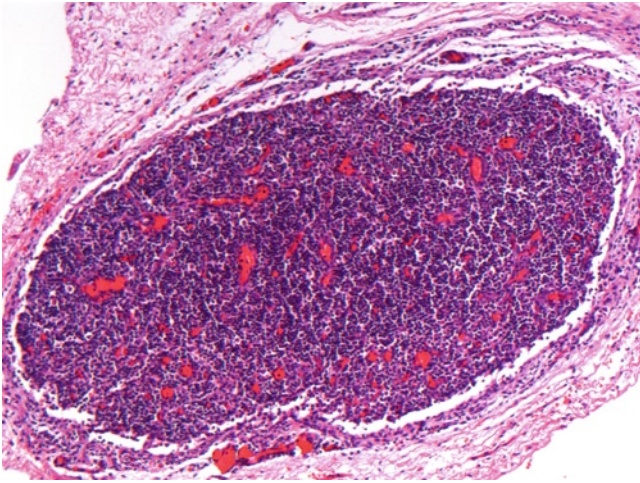


FIGURE 24-1. Lymph node at 19 weeks gestation. This lymph node is one of many small lymph nodes in the mesentery and is surrounded by a collagenous connective tissue capsule. Beneath the capsule the sinus is apparent. The lymph node has a diffuse pattern and is composed of small lymphocytes. No identifiable follicles are seen. (Hematoxylin and eosin. [H&E], 10 \times .)

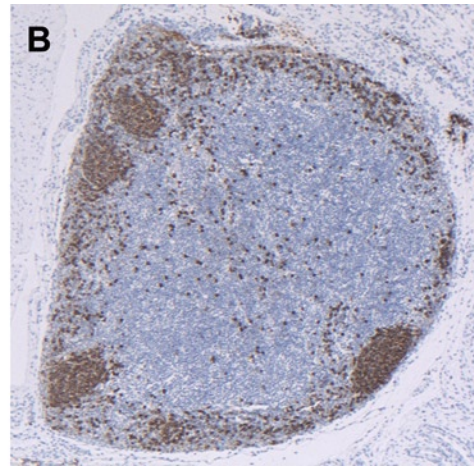
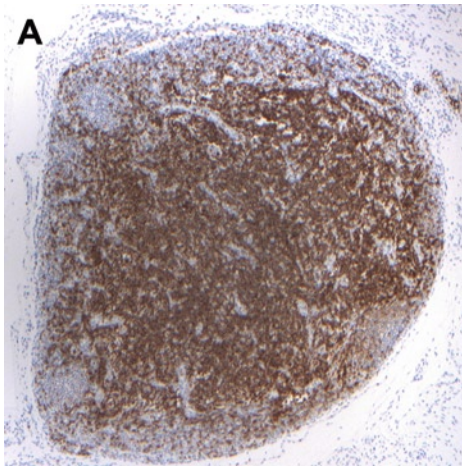


FIGURE 24-2. Lymph node at 19 weeks gestation. **A**, CD3 immunohistochemical stain shows that the lymph node is composed predominantly of T-cells. Primary follicles cannot be recognized by H&E but become evident with immunohistochemistry.

The follicles on the periphery of the lymph node do not stain with CD3. **B**, CD20 immunohistochemical stain highlighting B-cells in the primary follicles in the cortex. (2.5 \times .)

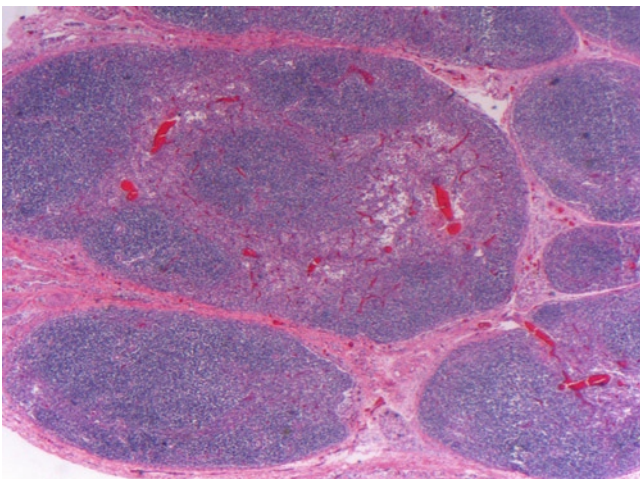


FIGURE 24-3. Mesenteric lymph nodes at 34 weeks gestation. The developing lymph nodes show a capsule and network of sinuses. No follicles are seen. (H&E, 2.5 \times .)

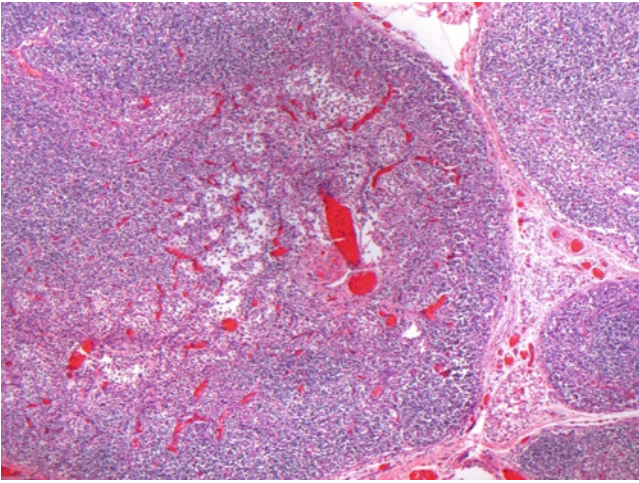


FIGURE 24-4. Mesenteric lymph nodes at 34 weeks gestation. This higher power view of mesenteric lymph node shows sinuses. (H&E, 5 \times .)

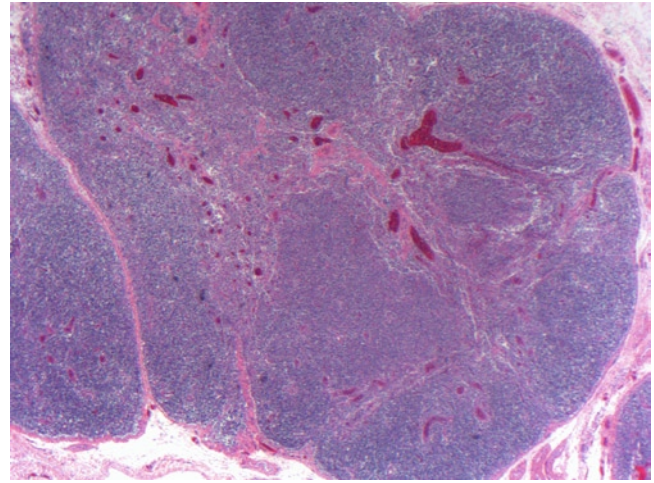


FIGURE 24-5. Lymph node at 41 weeks gestation. The lymph node is larger and more cellular than those seen earlier in gestation, and has a capsule and sinuses. Primary follicles are not readily seen. (H&E, 2.5 \times .)

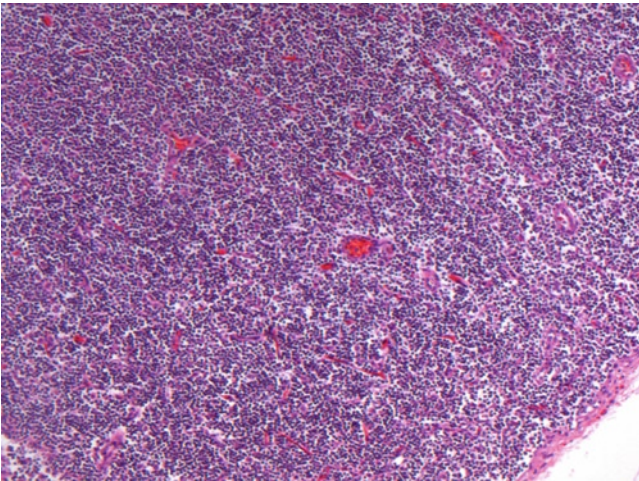


FIGURE 24-6. Lymph node at 41 weeks gestation. This higher power view shows that the lymph node is composed predominantly of sheets of small lymphocytes. (H&E, 10 \times .)

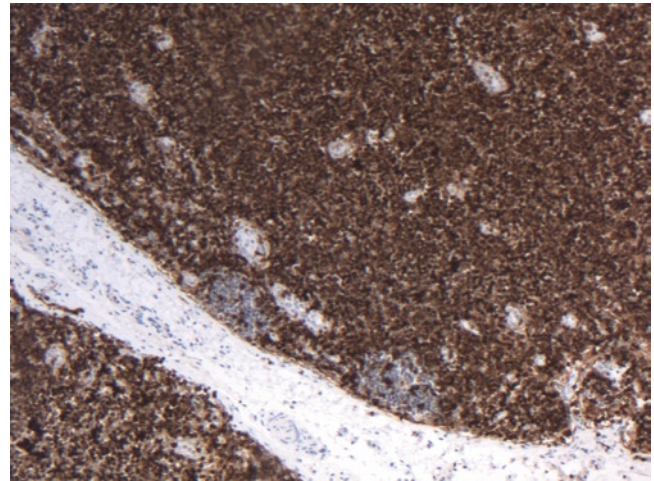


FIGURE 24-7. Lymph node at 41 weeks gestation. This CD3 immunohistochemical stain shows that the lymph node is composed predominantly of CD3 positive T-cells. (10 \times .)

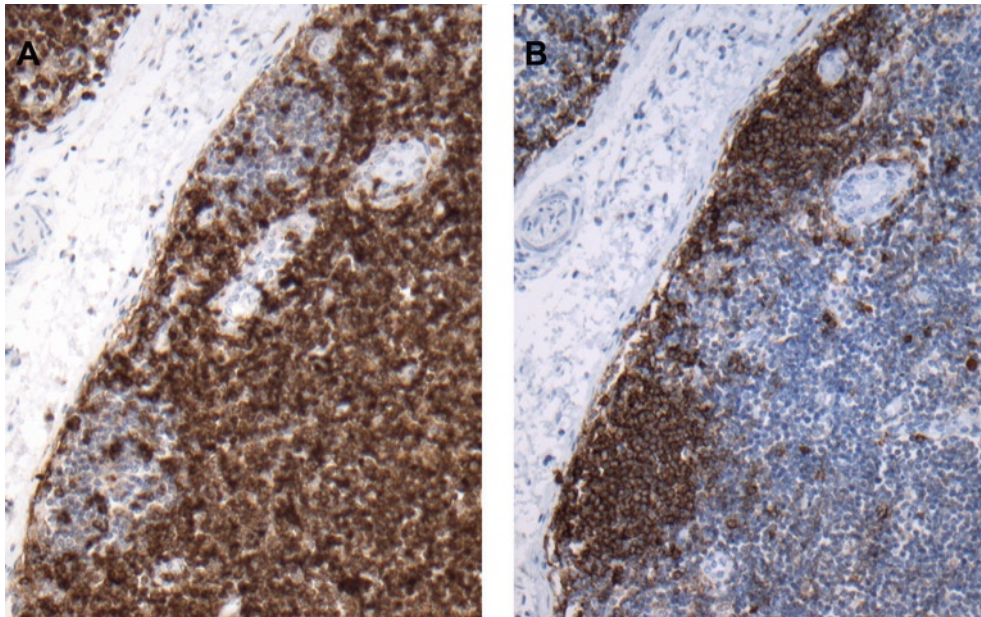


FIGURE 24-8. Lymph node at 41 weeks gestation. **A**, This higher power view of CD3 immunohistochemical stain shows the positive T-cells and small nodules of negative cells that represent

B-cell follicles. **B**, This CD20 immunohistochemical stain shows primary follicles composed of small B-lymphocytes. (20 \times .)

Special Considerations

Lymph Node and Hematopoiesis

The lymph node may be a site of hematopoiesis in the fetus. Cells from the erythropoietic and granulocytic

lineages may be seen. If present, they are usually located in the medulla of the lymph node.

Hemophagocytosis

Hemophagocytosis is commonly seen in lymph nodes from fetal autopsies. The presence of hemophagocytosis does not imply that the patient has hemophagocytic syndrome or hemophagocytic lymphohistiocytosis.

The significance of this finding is not known and may likely represent an agonal event. A clear etiology or source of infection for inciting this finding is not known.

References

1. Van der Valk P, Meijer CJLM: Lymph nodes. In *Histology for Pathologists*, edn 3. Edited by Mills SE. Philadelphia: Lippincott Williams & Wilkins; 2007:763–781.
2. Arey LB: *Developmental Anatomy*, rev edn 7. Philadelphia: W. B. Saunders; 1974:370–372.
3. Valdes-Dapena MA: *Histology of the Fetus and Newborn*. Philadelphia: W. B. Saunders; 1979:65–77.
4. Patten BM: *Human Embryology*, edn 2. New York: McGraw-Hill; 1953:649–655.
5. Hoorweg K, Cupedo T: Development of human lymph nodes and Peyer's patches. *Semin Immunol* 2008, 20:164–170.
6. Bailey RP, Weiss L: Light and electron microscopic studies of post capillary venules in developing human fetal lymph nodes. *Am J Anat* 1975, 143:43–58.
7. Markgraf R, Gaeueker B, Muller-Hermelink HK: The development of the human lymph node. *Cell Tissue Res* 1982, 225:387–413.
8. Crivellato E, Vacca A, Ribatti D: Setting the stage: the anatomists view of the immune system. *Trends Immunol* 2004, 25:210–217.
9. Kyriazis AA, Esterly JR: Development of lymphoid tissues in the human embryo and early fetus. *Arch Pathol* 1970, 90:348–353.
10. Asano S, Akaike Y, Muramatsu T, *et al.*: Immunohistologic detection of primary follicle in human fetal and newborn lymph node anlagen. *Pathol Res Pract* 1993, 189:921–927.
11. Veereman-Wauters G: Neonatal gut development and postnatal adaptation. *Eur J Pediatr* 1996, 155:627–632.

25

Palatine Tonsil

Linda M. Ernst

The palatine tonsils, representing a portion of the gut-associated lymphoid tissue, are usually the largest and most readily sampled tonsils in the human fetus. The palatine tonsils are located along the lateral walls of the oropharynx within the tonsillar fossa created by two tonsillar pillars. The anterior tonsillar pillar is also known as the palatoglossal arch and forms an arc of soft tissue and muscle between the tongue and soft palate. The posterior tonsillar pillar, also known as the palatopharyngeal arch, forms an arc of soft tissue and muscle between the soft palate and posterior pharynx [1,2]. Since there is little projection of the palatine tonsils into the pharynx during fetal life, they are easily overlooked grossly but can be sampled for microscopic study by carefully removing the soft palate and tonsillar fossae during removal of the tongue. Serial horizontal sections of the neck tissues, including the attached soft palate, will usually provide reasonable microscopic sections of the palatine tonsils. This chapter will review the histological changes in the palatine tonsil during fetal life.

Embryology

The epithelium of the palatine tonsils is derived from the bilateral endodermal buds of the second pharyngeal pouch. The mesodermal elements are derived from the second pharyngeal membrane and nearby tissues of the first and second pharyngeal arches. At approximately 12 weeks gestation, the epithelium of the second pharyngeal pouch proliferates and grows in a finger-like fashion into the surrounding mesenchyme. The central cells in these epithelial columns degenerate, forming the tonsillar crypts that are secondarily infiltrated by lymphoid tissue. The mesenchyme forms the remaining stromal elements of the tonsils [3,4].

Histology

In the early second trimester fetus, the palatine tonsillar tissue is recognized as infoldings of stratified squamous epithelium in close continuity with small lymphoid tissue congeries (see Figs. 25-1–25-3). Investigators have shown that as early as 14 weeks gestation, B-lymphoid cells are seen in association with follicular dendritic cells, representing the early formation of lymphoid follicles. In addition, parafollicular T cells are present in the early midtrimester [5,6]. Using routine hematoxylin and eosin (H&E) stains, the lymphoid cells in the early midtrimester appear to be mostly small lymphocytes with occasional larger forms seen (see Figs. 25-4 and 25-5); however, the formation of definitive lymphoid follicles is not well appreciated. Tonsillar crypts in early gestation are devoid of significant squamous debris.

In the late second and early third trimester, the tonsillar lymphoid tissue steadily increases and vague follicular aggregates can be seen (see Figs. 25-6–25-9). Germinal centers are not seen. In addition, keratin debris and sloughed epithelial cells can be seen in the crypts (see Figs. 25-6–25-9). Although the epithelial basement membrane in fetal and neonatal tonsillar crypts appears to be intact by immunochemical markers, transmission electron

microscopy demonstrates pores in the basement membrane that allow the passage of lymphocytes into the epithelium [7]. Therefore, it is not unusual to find numerous intraepithelial lymphocytes in the tonsillar crypt epithelium, even in the midtrimester (see Fig. 25-10).

By term, the palatine tonsils have obtained significant size and lymphoid tissue is well formed (see Figs. 25-11–25-13); however, germinal center formation is still not normally seen. As is the case in other lymphoid tissues, germinal center formation in the tonsil normally takes place postnatally, with exposure to environmental antigens [8].

Other related lymphoid organs in the Waldeyer ring, representing the pharyngeal lymphoid ring, are the adenoids in the nasopharynx, the tubal tonsils posterior to the opening of the pharyngotympanic or Eustachian tubes into the nasopharynx, and the lingual tonsil in the posterior tongue. Histologically, the main distinction between these different tonsillar tissues is the type of epithelium that lines the surface of the organ and the crypts or folds. The lingual tonsil shares the same stratified squamous epithelium as the palatine tonsil, while the adenoids and tubal tonsils have pseudostratified columnar, ciliated epithelium as seen in the respiratory tract [1].

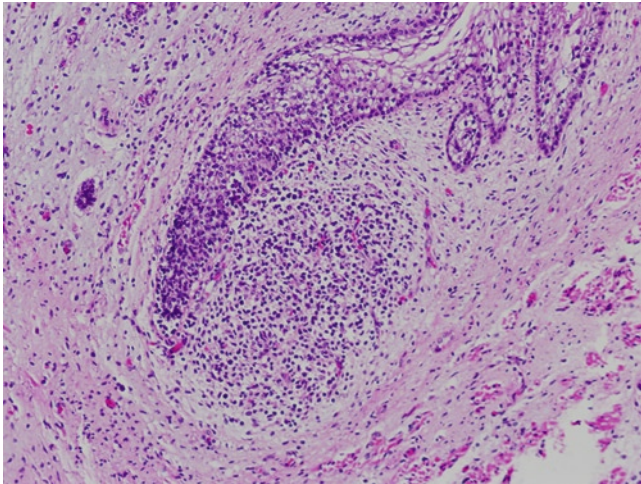


FIGURE 25-1. Palatine tonsil at 16 weeks gestation. This low-power view of palatine tonsil shows the finger-like extension of stratified squamous epithelium surrounded by a small collection of small lymphocytes. (H&E, 10 \times .)

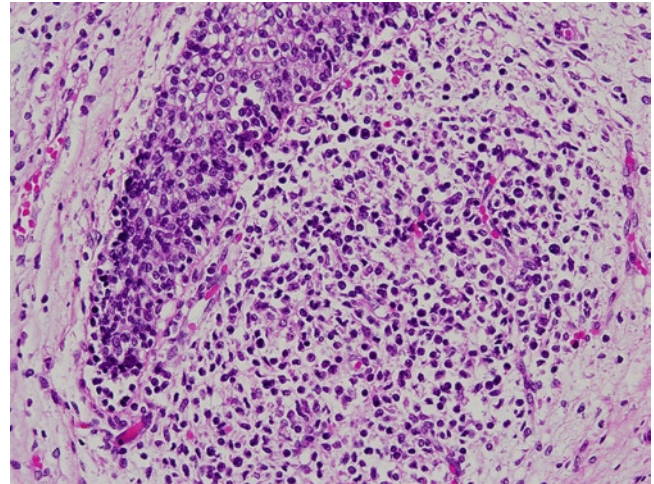


FIGURE 25-2. Palatine tonsil at 16 weeks gestation. This higher power view shows that the constituents of the lymphoid aggregate are small lymphocytes surrounding a delicate capillary network. (H&E, 20 \times .)

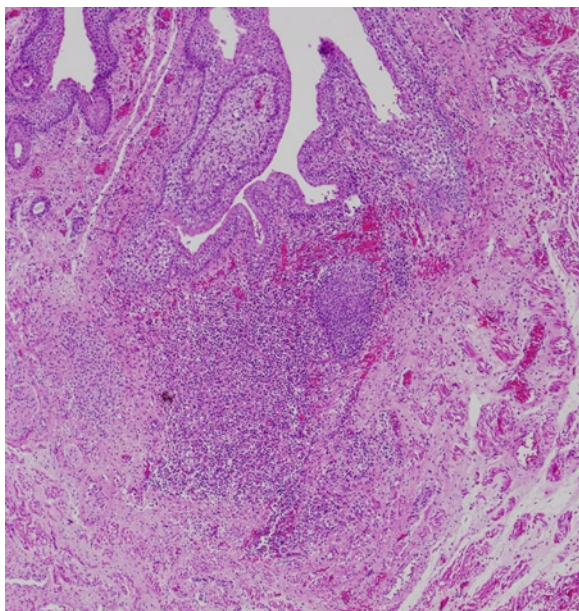


FIGURE 25-3. Palatine tonsil at 17 weeks gestation. This low-power view shows multiple infoldings of stratified squamous epithelium surrounded by a slightly larger collection of small lymphocytes. (H&E, 4 \times .)

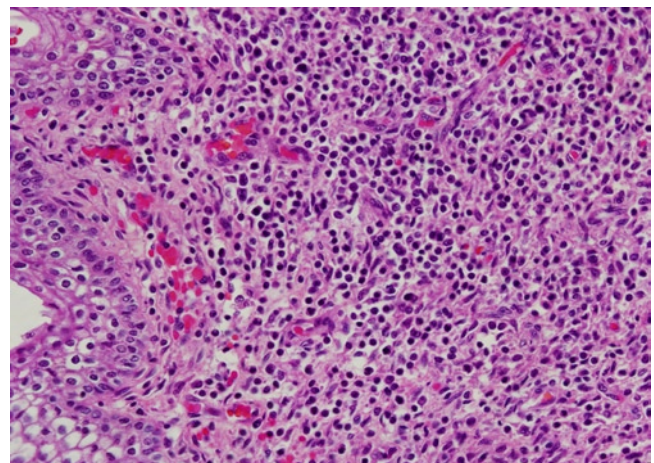


FIGURE 25-4. Palatine tonsil at 17 weeks gestation. This higher power view shows that the constituents of the lymphoid tissue are mostly small lymphocytes with a rich capillary network. (H&E, 20 \times .)

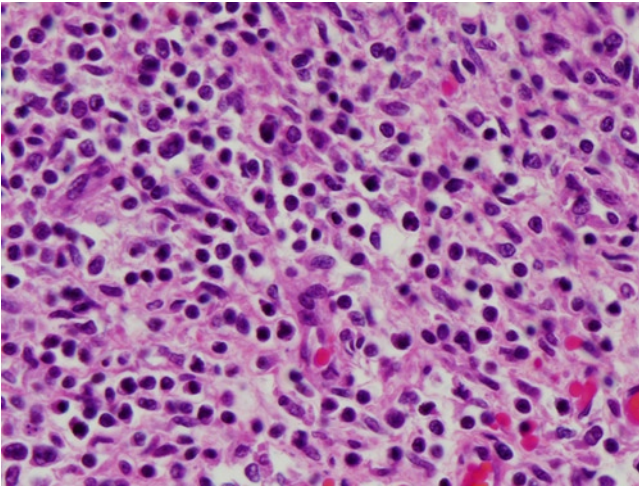


FIGURE 25-5. Palatine tonsil at 17 weeks gestation. This high-power view shows a monotonous population of small lymphocytes with occasional larger forms. (H&E, 40 \times .)

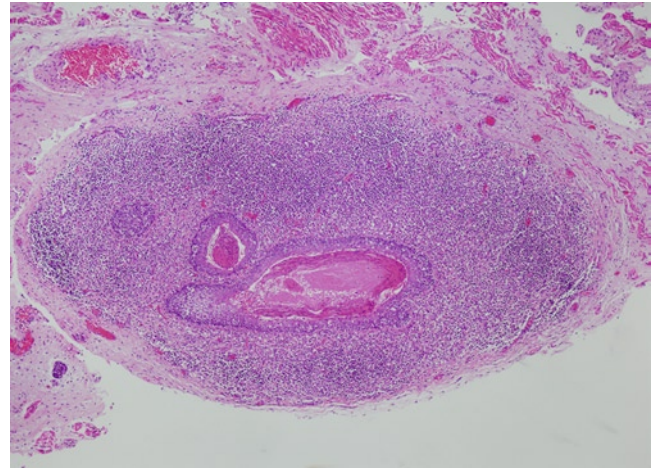


FIGURE 25-6. Palatine tonsil at 21 weeks gestation. Note the more robust lymphoid tissue with vague nodularity surrounding an epithelial infolding with central keratin debris and compare with [Figures 25-1](#) and [25-3](#). (H&E, 4 \times .)

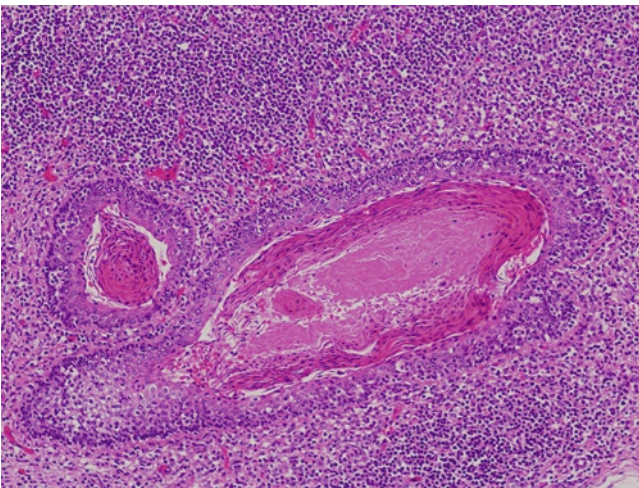


FIGURE 25-7. Palatine tonsil at 21 weeks gestation. This higher power view of tonsillar crypt contains sloughed and partially keratinized squamous epithelial cells. Bacterial elements are not seen in the crypts during fetal life. (H&E, 10 \times .)

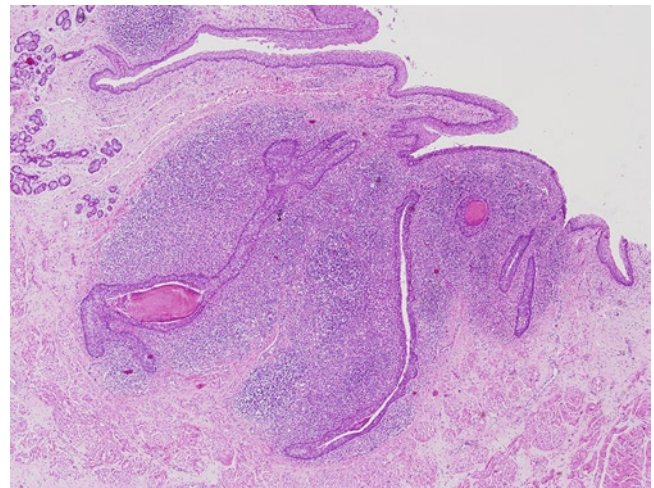


FIGURE 25-8. Palatine tonsil at 27 weeks gestation. This low-power view shows the increasing crypt formation and increased amount of lymphoid tissue. (H&E, 4 \times .)

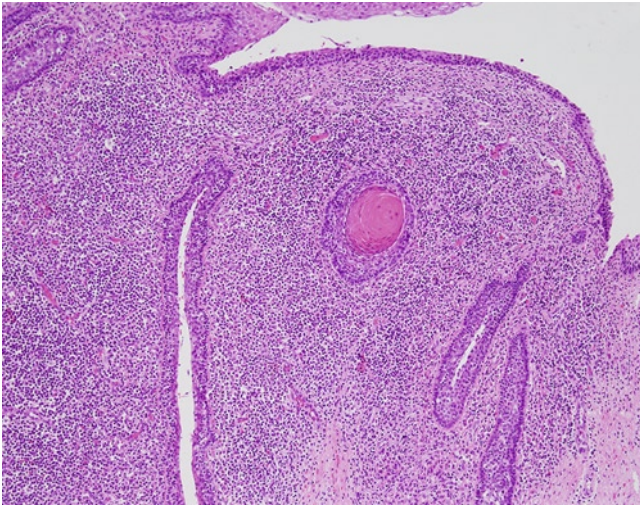


FIGURE 25-9. Palatine tonsil at 27 weeks gestation. Note the increasing crypt formation and increased amount of lymphoid tissue. (H&E, 10 \times .)

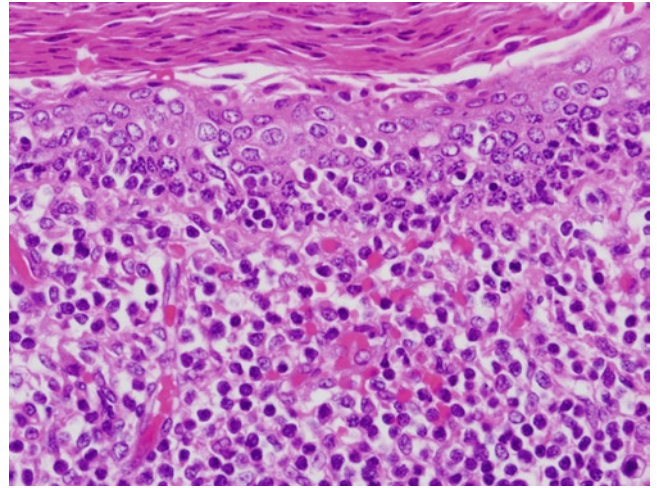


FIGURE 25-10. Palatine tonsil in the midtrimester with intraepithelial lymphocytes. This high-power view of palatine tonsil at 21 weeks gestation shows numerous lymphocytes within the tonsillar crypt epithelium. (H&E, 60 \times .)

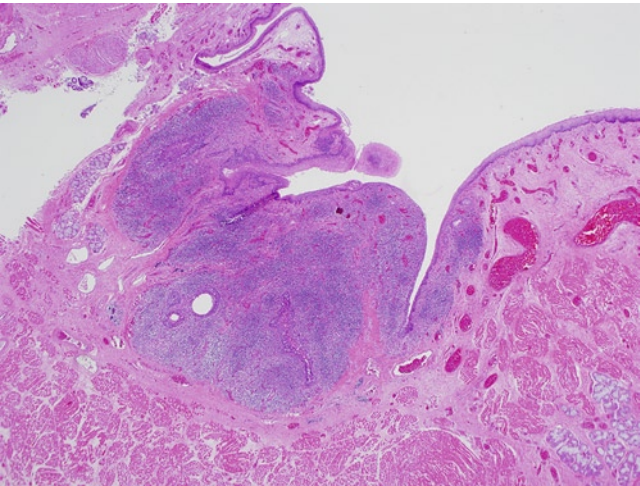


FIGURE 25-11. Palatine tonsil at term. This low-power view shows that the palatine tonsil is fairly large and displays crypt formation along with an increased amount of lymphoid tissue. (H&E, 2 \times .)

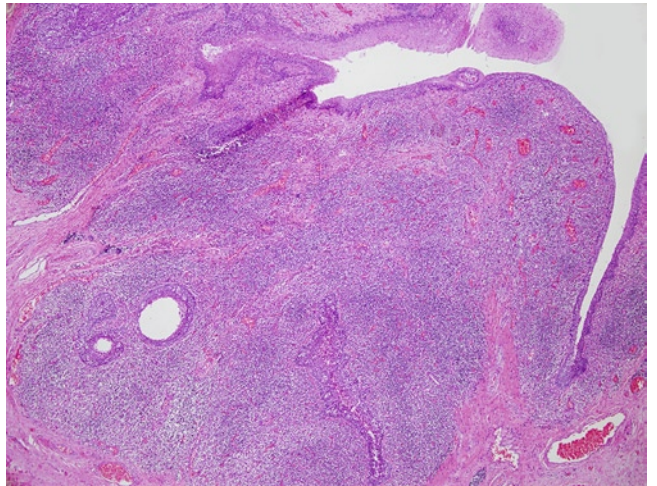


FIGURE 25-12. Palatine tonsil at term. This slightly higher power view shows the increased amount of lymphoid tissue. Note the normal lack of germinal center formation. (H&E, 4 \times .)

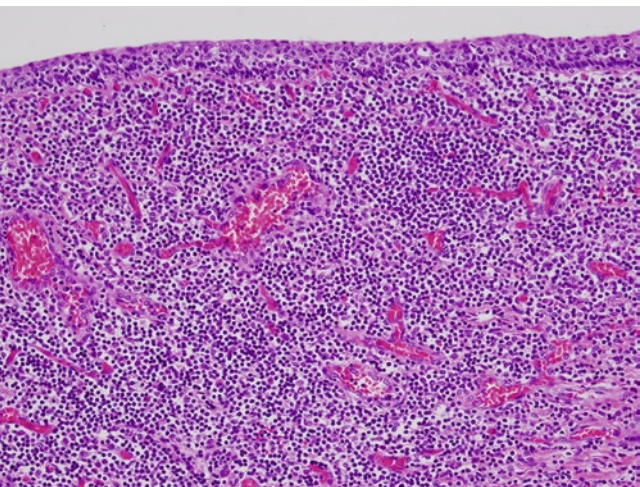


FIGURE 25-13. Palatine tonsil at term. This higher power view shows tonsillar epithelium and the presence of intraepithelial lymphocytes. (H&E, 20 \times .)

References

1. Balogh K, Pantanowitz L: Mouth, nose and paranasal sinuses. In *Histology for Pathologists*. Edited by Mills SE. Philadelphia, PA: Lippincott Williams & Wilkins; 2007:403–430.
2. Valdes-Dapena MA: *Histology of the Fetus and Newborn*. Philadelphia, PA: Saunders; 1979.
3. Sadler TW, Langman J: *Langman's Medical Embryology*, edn 11. Philadelphia, PA: Wolters Kluwer Lippincott Williams & Wilkins; 2010.
4. Schoenwolf GC, Larsen WJ: *Larsen's Human Embryology*, edn 4. Philadelphia PA: Elsevier/Churchill Livingstone; 2009.
5. von Gaudecker B: Development and functional anatomy of the human tonsilla palatina. *Acta Otolaryngol Suppl* 1988, 454:28–32.
6. von Gaudecker B, Muller-Hermelink HK: The development of the human tonsilla palatina. *Cell Tissue Res* 1982, 224:579–600.
7. Choi G, Suh YL, Lee HM, *et al.*: Prenatal and postnatal changes of the human tonsillar crypt epithelium. *Acta Otolaryngol Suppl* 1996, 523:28–33.
8. Wittenbrink N, Zemlin M, Bauer K, Berek C: Exposure to environmental antigens induces the development of germinal centers in premature neonates. *Dev Immunol* 2002, 9:177–179.

26

Bone Marrow

Michele E. Paessler and Scott Bourne

In the developing embryo and fetus, hematopoiesis is a dynamic process that starts in the yolk sac, continues in the liver, and finally stabilizes in the bone marrow. The role of the spleen in fetal hematopoiesis is controversial and is discussed in Chapter 23. Starting at 11 weeks gestation, hematopoiesis begins in the bone marrow and will remain there for the rest of adult life. Hematopoiesis begins with self-renewing multipotent stem cells that give rise to committed progenitor cells, which ultimately differentiate into the cells that circulate in the peripheral blood.

Since the peripheral blood elements are short lived, hematopoiesis must be a constant process in order to maintain homeostasis. Hematopoiesis is a highly complicated system that culminates in many well-orchestrated processes with the cooperation of stem cells, the supportive microenvironment, and numerous regulatory factors that provide stimulatory and inhibitory signals [1]. This chapter reviews the structure of the normal fetal bone marrow and discusses specific aspects of myelopoiesis, erythropoiesis, lymphopoiesis, and megakaryopoiesis.

Embryology

The primary sites of hematopoiesis change during human development, starting in the yolk sac, proceeding transiently to the liver, and finally stabilizing in the bone marrow. Interestingly, the only hematopoietic cells to be produced in the same tissue at all stages of human development are T-cells, which develop in the thymus.

Shortly after gastrulation, a network of extra-embryonic mesodermal cells serves as the site of origin of both the vascular and hematopoietic systems. Since both endothelial and hematopoietic cells are derived from the same cluster of mesodermal cells, the existence of a common precursor called a *hemangioblast* has been proposed [2]. These mesodermal cells have a spatial orientation such that the peripheral cells acquire the morphology and phenotype of endothelial cells and the central cells disappear to form the first vascular lumens. The birthplace of hematopoiesis lies in the mesodermally derived clusters of primitive hematopoietic cells, referred to as "blood islands," which develop adjacent to the newly formed vascular endothelium in the developing yolk sac blood vessels [2,3]. Hematopoiesis begins with the production of primitive red cells in the blood islands of the yolk sac shortly after implantation. The yolk sac is the primary site of erythropoiesis from 3 to 6 weeks gestation and maintains the viability of the embryo until hematopoiesis is established in the liver [2-4]. The blood islands are composed almost exclusively of erythroid cells; however, a few megakaryocytes have been identified [5]. Yolk sac erythropoiesis is megaloblastic and results in the production of nucleated red cells containing three embryonic hemoglobins Gower I ($\zeta_2\varepsilon_2$), Gower II ($\alpha_2\varepsilon_2$), and Portland I ($\zeta_2\gamma_2$), and in later embryos, hemoglobin F ($\alpha_2\gamma_2$) [5]. The onset of circulation allows yolk sac-derived primitive nucleated erythrocytes to enter embryonic tissues [2]. The first organ to be colonized is the liver, which is the principal site of hematopoiesis in the embryo from weeks 6 to 22 of gestation (see Chapter 4, Fig. 4-6) [2,6]. Stem cell migration to the liver gives rise to hepatic

hematopoiesis in which hematopoietic foci develop in the hepatic cords during the sixth week of gestation [7]. The fetal spleen also shows foci of hematopoiesis shortly following the liver, at about the seventh week of gestation [8]. Approximately half of the nucleated cells in the liver are erythroid cells, and only a few myeloid and megakaryocytic cells are identified. The erythroid cells at this stage are normoblastic and produce nucleated red cells that contain hemoglobin F. The population of erythroid cells in the liver progressively declines as the transition to the marrow approaches; however, occasional erythroid cells can still be detected at the end of gestation and in the early postnatal weeks.

After 22 weeks gestation, the bone marrow serves as the permanent site of hematopoiesis and remains so during the rest of gestation and postnatal life. Marrow hematopoiesis commences during the 11th week of gestation in specialized mesodermal structures termed "primary logettes", which are loose networks of mesenchymal cells that surround a central artery [2]. The marrow cavities are formed when bone or cartilage is eroded by blood vessels and cells from the periosteum

[1,9]. Once the marrow cavities are formed, the vascular connective tissue is organized and becomes colonized by hematopoietic cells [2]. The first blood cells that differentiate in the bone marrow proper are myeloid cells followed by erythroid cells [2]. Interestingly, the early hematopoietic precursor cells that colonize the marrow are not multipotent hematopoietic stem cells. It is thought that the hematopoiesis in the fetal bone marrow is initially established by committed progenitor cells that provide the essential myeloid and erythroid cells needed by the fetus. Multipotent self-renewing hematopoietic stem cells, in addition to their much-needed supporting stromal environment, are established later in gestation [2,3]. After the 22nd week of gestation, the marrow becomes the predominant site of hematopoiesis. The most active site of fetal bone marrow hematopoiesis is the vertebral column, followed by the femur, pelvis, fibula/tibia, and humerus. Fetal bone marrow erythropoiesis is normoblastic and produces non-nucleated red blood cells that contain hemoglobins F and A. Furthermore, it is the primary site for intrauterine granulopoiesis and megakaryopoiesis.

Histology

In living pediatric patients, the evaluation of bone marrow usually requires an aspirate as well as biopsy specimens. However, in fetal autopsies, aspirates are not commonly made. Therefore, the evaluation of the bone marrow is most often made on the morphologic review of sections of bones. These sections are most often taken from the rib or vertebral bodies. Less often, the iliac crest, long bones, clavicle, temporal bone, or other bones are studied. Ideally, for optimal evaluation of the marrow, the sample should be a thin-cut, well-stained section that has not undergone excessive decalcification. Optimal cytology is usually obtained in the first 3 hours postmortem but cellular detail can be retained for up to 15 hours postmortem [10]. Generally, evaluation of the bone marrow includes an estimate of the degree of cellularity, identification of the cell lineages that are present, assessment of the myeloid to erythroid (M:E) ratio, and evaluation of the maturation of the cell lines.

Throughout fetal life, the bone marrow is virtually 100% cellular (see Fig. 26-1). Occasional adipocytes can be seen. At birth, the marrow is approximately 80% to 100% cellular [1]. Another important aspect in bone marrow evaluation is the assessment of the M:E ratio. In the early second trimester, hematopoiesis transitions to the bone marrow from the liver and the M:E ratio can be variable (see Fig. 26-2); however, by the end of the second trimester, at about 26 weeks, the M:E ratio stabilizes at approximately 1 to 2:1 (see Figs. 26-3 and 26-4). A periodic acid-Schiff (PAS) stain may be useful in differentiating erythroid cells from myeloid and lymphoid cells, and for evaluating the M:E ratio. On a PAS stain, the myeloid cells have pink cytoplasm, erythroid cells have gray cytoplasm, and lymphoid cells have PAS negative cytoplasm (see Fig 26-5).

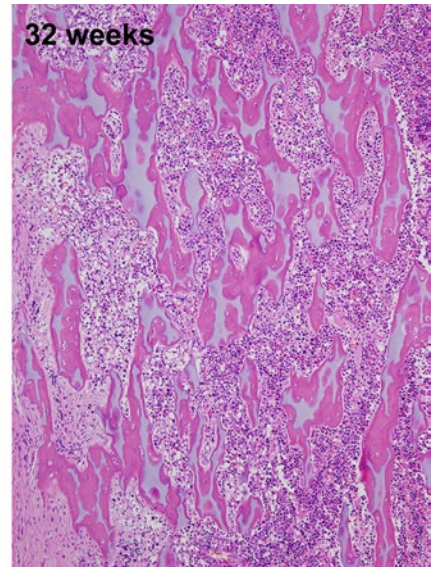
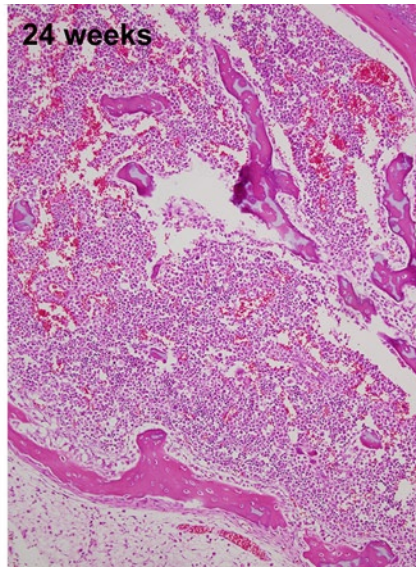
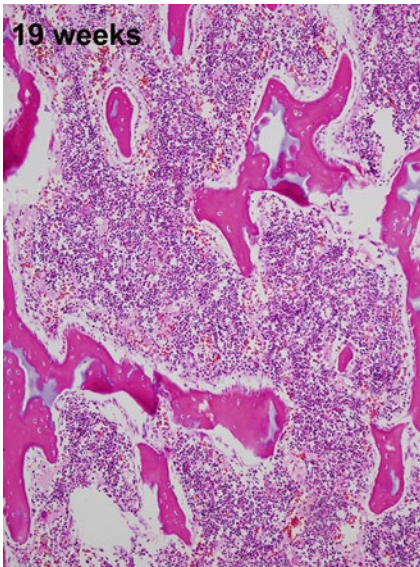


FIGURE 26-1. Bone marrow during fetal life. Note that the marrow is virtually 100% cellular in all samples from various gestational ages. Note the monotonous similarity of the bone marrow throughout the last half of prenatal life. (Hematoxylin and eosin [H&E], 10 \times .)

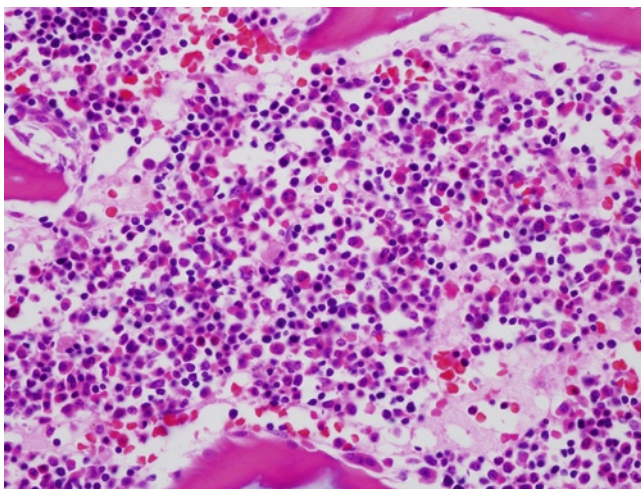


FIGURE 26-2. Bone marrow at 19 weeks gestation. Maturing myeloid progenitors and small clusters of erythroid progenitors are shown. An occasional megakaryocyte is seen. (H&E, 40 \times .)

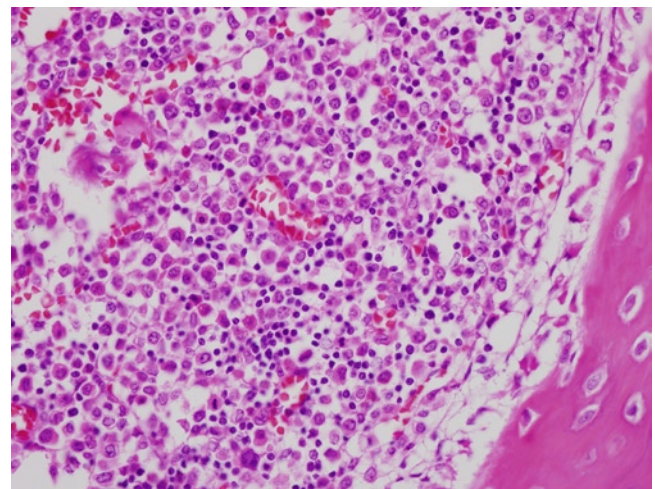


FIGURE 26-3. Bone marrow at 24 weeks gestation. The marrow shows trilineage hematopoiesis. This field shows myeloid progenitors with pink cytoplasm and a few small erythroid clusters. The M:E ratio is approximately 1 to 2:1. In addition, an occasional megakaryocyte is seen. (H&E, 40 \times .)

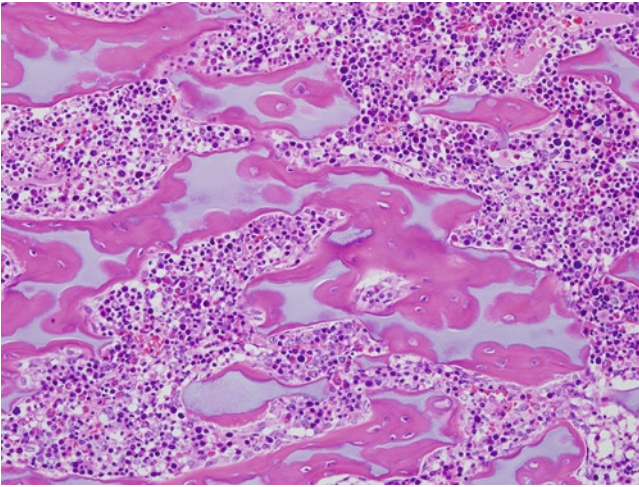


FIGURE 26-4. Bone marrow at 32 weeks gestation. The marrow remains virtually 100% cellular with small sheets of maturing myeloid progenitors and small clusters of erythroid progenitors. The M:E ratio is approximately 1 to 2:1. Occasional adipocytes are seen. (H&E, 20 \times .)

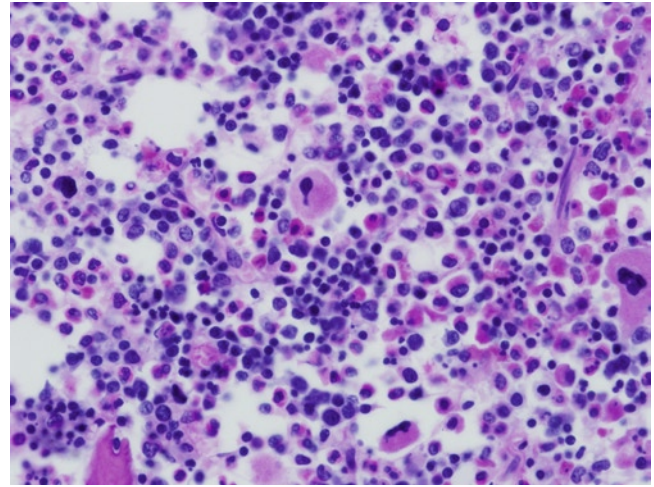


FIGURE 26-5. Bone marrow at 41 weeks gestation. PAS stain aids in the distinction between the myeloid and erythroid lineages. Myeloid cells have pink cytoplasm whereas erythroid cells have gray cytoplasm. Megakaryocytes are also easily identified. (PAS, 60 \times .)

Structure of the Bone Marrow

The bone marrow is encased by cortical bone, traversed by trabecular bone, and is composed of a network of capillary–venous sinuses that occupy the space between the bony trabeculae. The principal blood supply to the marrow is the nutrient artery and the periosteal capillary network. The nutrient artery supplies the bony trabeculae and branches to form the capillary venous sinus network, which is an integral component of hematopoiesis. Newly formed hematopoietic cells are released into the periphery via the capillary–venous sinus [1].

The bone marrow microenvironment is an essential factor in hematopoiesis. A key component in the

microenvironment is a heterogeneous group of cells, called stromal cells, which include adipose cells and fibroblasts, among others. These stromal cells play a key role in supporting hematopoiesis by secreting numerous proteins, adhesion molecules, and regulatory products that are necessary for stem cell survival and osteogenesis [1].

In addition to the myeloid, erythroid, lymphocytic, and megakaryocytic lineages, discussed in detail below, a variety of other cell types reside in the bone marrow, such as macrophages, mast cells, osteoblasts, and osteoclasts.

Trilineage Hematopoiesis

Hematopoiesis is a spectrum of development that spans from the stem cell to a committed precursor cell that progressively acquires specific lineage characteristics and culminates in the terminally differentiated cells that

are released into the circulation. This continuum of maturation is tightly regulated at every step by the coordinated expression of many genes [1].

Myelopoiesis

Granulopoiesis

Granulopoiesis has a geographic distribution in that granulocytic elements tend to mature adjacent to the bony trabeculae, where growth factors such as granulocyte colony-stimulating factor and granulocyte-macrophage colony-stimulating factor drive maturation down the granulocytic pathway (see Figs. 26-6 and 26-7). The most immature granulocyte is the myeloblast, which usually accounts for up to 3% to 5% of the marrow cells. The next stages of maturation are the promyelocyte, myelocyte, metamyelocyte, band, and finally the segmented form. At each successive stage, nuclear and cytoplasmic maturation changes occur. The nuclear chromatin condenses and progressively segments, while the cytoplasm develops secondary granules and becomes acidophilic. These specific nuclear

and cytoplasmic changes are best appreciated on bone marrow aspirates. In tissue specimens, immature myeloid cells with moderate amounts of pink cytoplasm are seen adjacent to the trabeculae (see Fig. 26-6) but the different stages of maturation are more difficult to visualize. As the granulocytes mature, they migrate from the bony trabeculae toward the interstitium. Mature granulocytes are identified by their segmented nuclei. Granulocytes are released through the sinus wall into the circulation.

In the fetal liver, hematopoiesis consists predominantly of intrasinusoidal erythropoiesis; granulopoiesis is a minor component seen in the portal tracts. The predominant site of granulopoiesis in the fetus is the bone marrow [11].

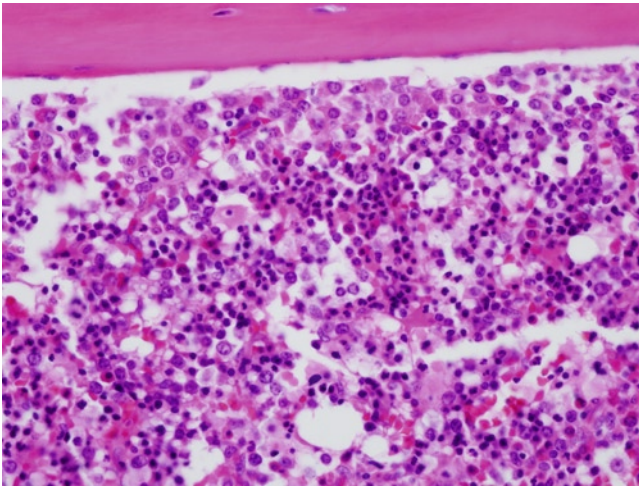


FIGURE 26-6. Granulopoiesis. The most immature myeloid cells are located adjacent to the bony trabeculae and the more mature cells are located away from the trabeculae. Bone marrow at 40 weeks gestation is shown. (H&E, 40 \times .)

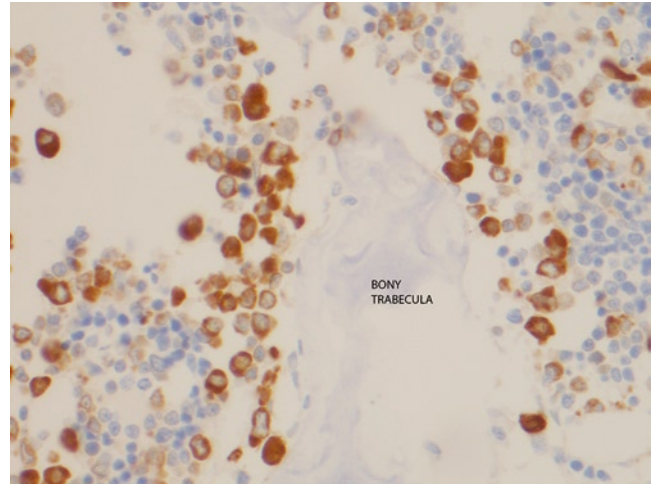


FIGURE 26-7. Granulopoiesis. Immunohistochemical stain for myeloperoxidase is shown, demonstrating the most immature myeloid progenitors adjacent to the bony trabeculae. Bone marrow at 40 weeks gestation is shown. (40 \times .)

Monopoiesis

The same myeloid precursor cell from which the granulocytic series differentiates also gives rise to the monocytic lineage. Monocyte differentiation consists of three stages: the monoblast, the promonocyte, and the mature monocyte. Monoblasts have open chromatin and linear condensations, discrete nucleoli, and

abundant cytoplasm. As the monoblast matures into a promonocyte and mature monocyte, the nucleus shows increased folding and the cytoplasm gains azurophilic granules. Maturing monocytes are often difficult to ascertain in postmortem fetal samples.

Erythropoiesis

The most important regulatory factor in erythropoiesis is erythropoietin (EPO). The hypoxic internal milieu of the fetus stimulates high EPO levels, which fall dramatically in postnatal life. Erythroid precursors usually mature in colonies throughout the bone marrow and do not have a specific geographic distribution like the granulocytic series. In the bone marrow, the earliest erythroid precursor is the pronormoblast and the successive maturational stages include the basophilic normoblast, polychromatic normoblast, orthochromatic normoblast, reticulocyte, and mature erythrocyte, which is non-nucleated. Each stage shows progressive nuclear and cytoplasmic changes. The nuclear chromatin shows progressive condensation and development of a pyknotic nucleus that is ultimately extruded. The cytoplasm initially is intensely basophilic and progressively acquires hemoglobin, imparting a polychromatophilic change to the cytoplasm and eventually an eosinophilic appearance. These stages in erythroid development are best identified on bone marrow aspirates. In bone marrow sections, the erythroid precursors are identified in colonies and the pronormoblasts are large with open chromatin and a prominent "box car-shaped" nucleolus. The more mature erythroid cells are smaller in size and show dark, round nuclei (see Figs. 26-2-26-4). Erythroid precursors are the predominant lineage in the fetal liver, whereas erythropoiesis is less prominent in the bone marrow where the myeloid to erythroid ratio is

approximately 1 to 2:1 after approximately 26 weeks of gestation [11]. It may be difficult to distinguish erythroid cells from maturing lymphoid cells (hematogones) in tissue sections. A specific immunohistochemical stain, such as glycophorin C or glycophorin A, may be necessary to assess the quantity of erythroid precursors (see Fig. 26-8). A PAS stain may also help to differentiate the two cell types (see Fig. 26-5). Red blood cells derived from the bone marrow are non-nucleated, unlike the red blood cells from the fetal liver. However, under conditions of extreme stress, nucleated red blood cells may be seen.

In sections of bone marrow from autopsies of fetuses and newborns, the nuclei of normoblasts are frequently abnormal. They may be multiple, irregular, multilobated, or have little blebs (see Fig. 26-9). The changes are referred to as dyserythropoiesis or erythroid dysplasia. Dyserythropoietic cells may be mistaken for segmented neutrophils in sections stained with H&E. A PAS stain helps to make the distinction (see Fig. 26-10). The changes of dyserythropoiesis in fetal autopsy material are almost always a nonspecific reactive change due to hypoxia or stress from other causes. However, these abnormalities are very similar to those seen in some forms of familial congenital dyserythropoietic anemia. The diagnosis of congenital dyserythropoietic anemia should be made only in the very rare clinical context of profound unexplained anemia, preferably with confirmation by identifying a diagnostic genetic defect.

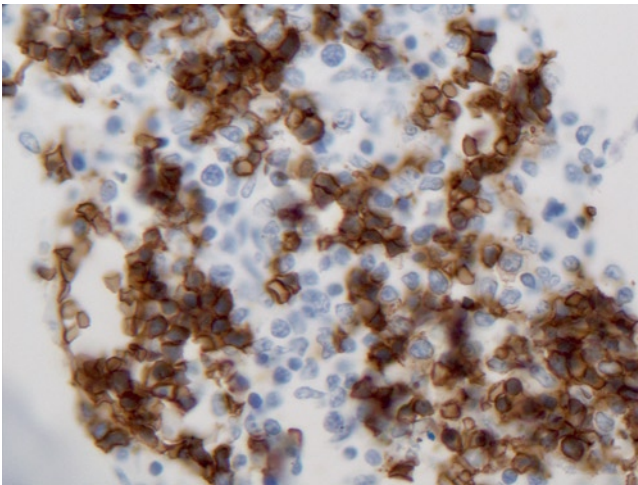


FIGURE 26-8. Erythropoiesis. Immunohistochemical stain for glycophorin C, which stains all red blood cells including nucleated and non-nucleated forms, is shown. When hematogones are numerous (see Figs. 26-11 and 26-12), this stain may be necessary to differentiate hematogones from erythroid cells. (50 \times).

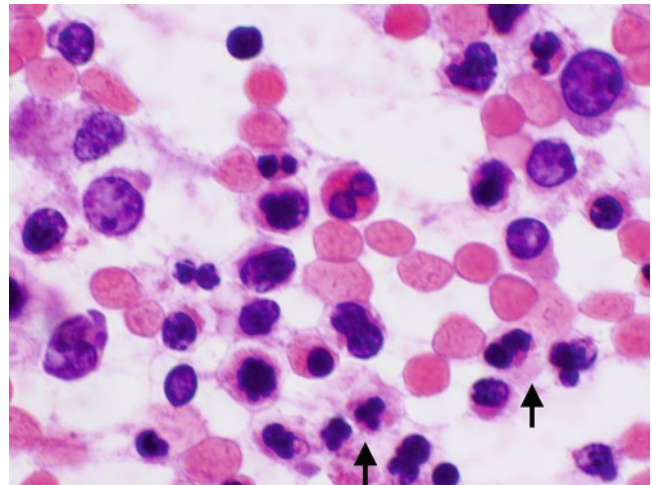


FIGURE 26-9. Dyserythropoiesis. Note the irregular and lobulated outlines of the erythroid nuclei and nuclear budding (arrows). While congenital dyserythropoietic anemias are a possibility in neonates with anemia and dysplasia, agonal hypoxic events are the most common cause of erythroid dysplasia seen at autopsy. Term bone marrow is shown. (H&E, 100 \times .)

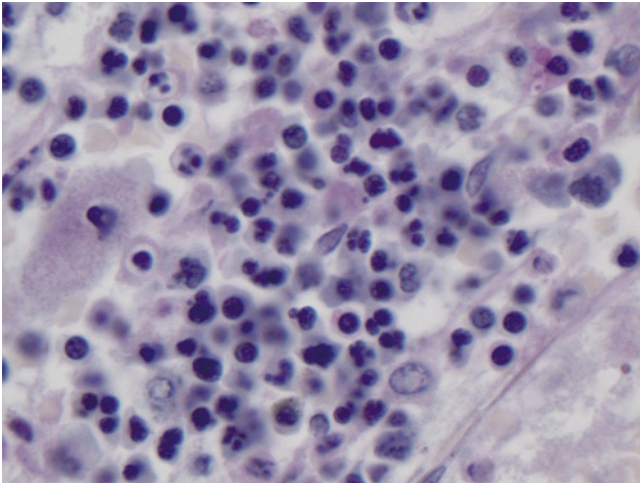


FIGURE 26-10. Dyserythropoiesis. This PAS stain shows sheets of red blood cell precursors with nuclear irregularities, including budding and lobations, that mimic neutrophils. The PAS stain confirms that the cells in question are dyserythropoietic red blood cells and not neutrophils, which have PAS positive cytoplasm. Note the gray-colored cytoplasm in the erythroid cells. (100 \times .)

Megakaryopoiesis

Megakaryopoiesis is regulated by many growth and regulatory factors and cytokines, thrombopoietin being one of the most important. Megakaryocytic differentiation is not associated with mitotic divisions such as the myeloid and erythropoietic lineages. Megakaryocytes mature by increasing nuclear lobations, a process termed *endomitosis* [1]. The most immature form is the megakaryoblast and maturation to a platelet-forming megakaryocyte is

marked by an increase in size and nuclear lobations. In addition, as the megakaryocyte matures it expresses specific platelet glycoproteins and von Willebrand factor, among other proteins. Megakaryocytes are the most infrequent of the hematopoietic lineages and usually account for less than 1% of the marrow cells. The megakaryocytes are usually seen scattered throughout the marrow adjacent to the sinuses (see Figs. 26-2 and 26-5).

Lymphopoiesis

Stem cells differentiate into committed lymphoid and myeloid progenitor cells. The myeloid progenitors give rise to the myeloid, erythroid, and megakaryocytic lineages. The lymphoid progenitors give rise to B, T, and NK cells. The development of B- and T-lymphocytes is highly dependent on the bone marrow microenvironment. T-cell precursors are derived in the bone marrow and home to the thymus, as this is the site of T-cell maturation. B-cell proliferation and differentiation occurs in the bone marrow and is dependent on numerous growth and regulatory factors such as interleukin IL-1 and IL-7. B- and T-cells cannot be distinguished on their morphologic features, but rather their specific immunophenotypic profile. T-cells characteristically express CD3 even in the earliest stages and B-cells express different antigens at specific stages of maturation. The most immature B-cells express CD19, CD79a, TdT, CD34, and HLA-DR and often coexpress CD10. As the B-cells mature, CD34, TdT, and CD10 are lost and CD20 and surface immunoglobulin

are expressed in the later stages of maturation. These immunophenotypic features are best appreciated on flow cytometric studies. Maturing B-cells are often abundant in fetal and postnatal specimens, as well as pediatric specimens, and are termed *hematogones* (see Figs. 26-11 and 26-12). Morphologically, hematogones show a spectrum of maturation from lymphoblasts to mature B-cells. These morphologic features are best seen on an aspirate. In tissue sections, hematogones are intermediate to small in size with round to slightly irregular nuclei and scant cytoplasm. Hematogones usually infiltrate through the marrow and may form small aggregates. The amount of hematogones seen in fetal and neonatal bone marrow is variable but they may compose up to 50% to 60% of the cells. Hematogones may often be difficult to distinguish from maturing erythroid precursors based on morphology alone. In such cases, a PAS or immunohistochemical stains should be used to distinguish erythroid elements from lymphoid elements.

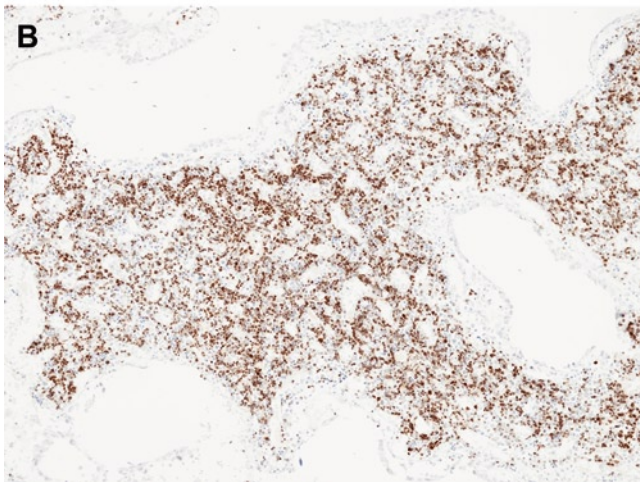
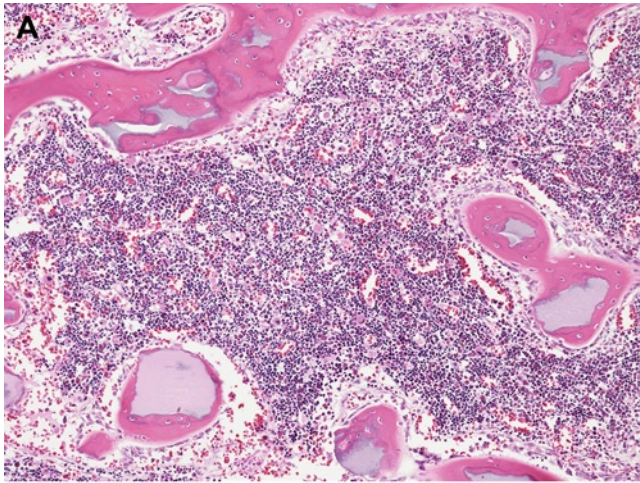


FIGURE 26-11. Hematogones. This low-power composite image shows H&E (A) of bone marrow at 38 weeks gestation compared with a PAX5 immunohistochemical stain (B) to show the abundance of maturing B-cells (hematogones) present within the fetal bone marrow. PAX5 is a marker that is positive in all stages of B-cell development. Note that the hematogones are difficult to discern from erythroid precursors by H&E examination alone. (10 \times .)

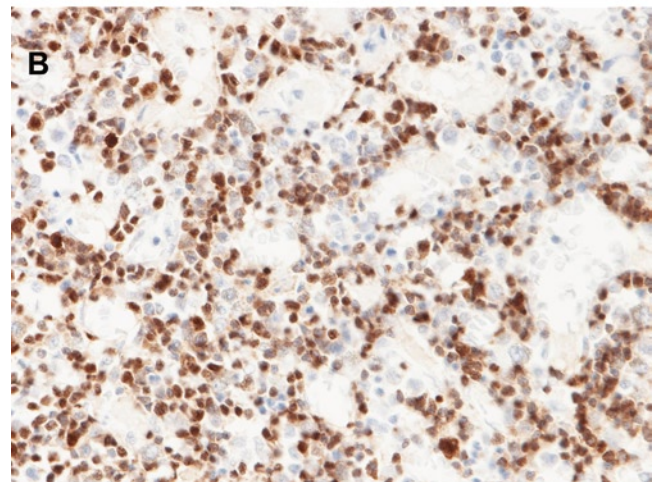
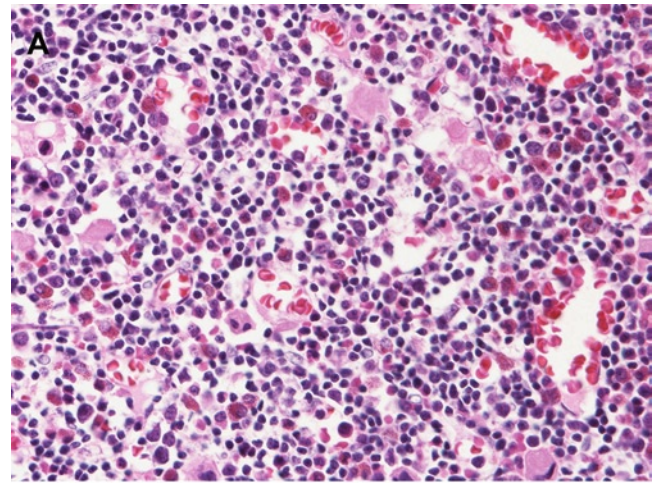


FIGURE 26-12. Hematogones. This higher power image compares H&E (A) and PAX5 immunohistochemical stain (B) of bone marrow at 38 weeks gestation. Hematogones may be so numerous that the diagnosis of leukemia may be raised. Immunohistochemical stains for all stages of B-cell maturation are positive in hematogones while in B-cell leukemias they are positive for only one stage of maturation. (40 \times .)

Special Considerations

Hemophagocytosis

Macrophages are present in the marrow and phagocytosis of cells and debris is a normal physiologic activity. An increased number of activated macrophages with phagocytosed red blood cells, granulocytes, and cellular debris are often found in fetal bone marrow (see Fig. 26-13). Hemophagocytosis is easier to appreciate on aspirate slides but can be apparent in formalin-fixed paraffin-embedded sections. An immunohistochemical stain specific for macrophages such as CD163, the hemoglobin scavenger receptor, is

useful to highlight macrophages and help discern the hemophagocytosis (see Fig. 26-14). Hemophagocytosis has many causes. Most cases are a nonspecific reactive change secondary to an underlying process such as infection and the inflammatory response. Morphology cannot distinguish between nonspecific reactive hemophagocytosis and familial hemophagocytic syndrome. The typical clinical picture and genetic testing are necessary for a definitive diagnosis of familial hemophagocytic syndrome.

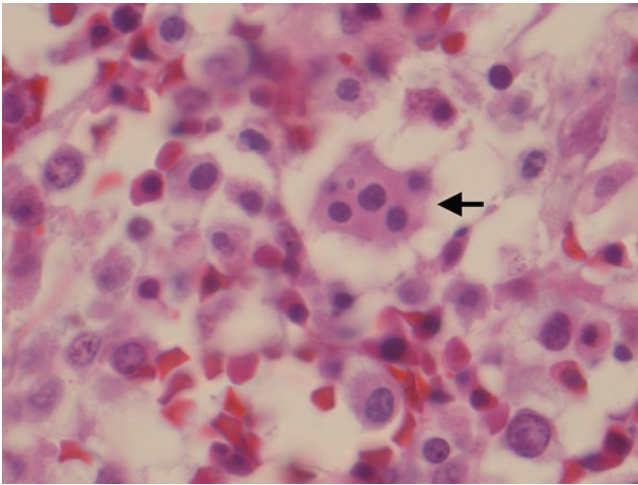


FIGURE 26-13. Hemophagocytosis. Note a macrophage (arrow) that has ingested several intact cells. Term bone marrow is shown. (H&E, 40 \times .)

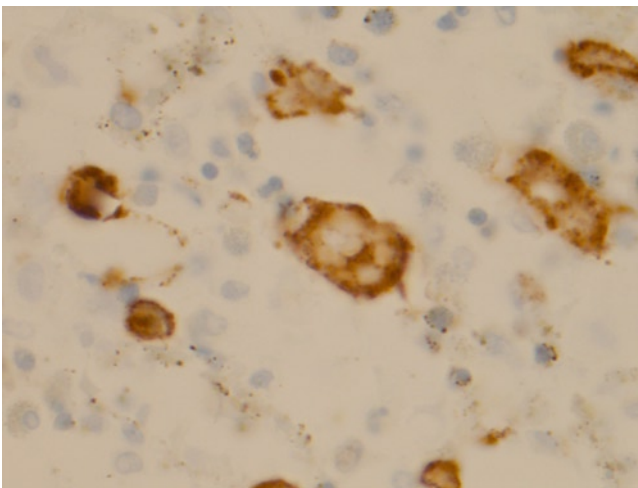


FIGURE 26-14. Hemophagocytosis. Shown is immunohistochemical stain for CD163, hemoglobin scavenger receptor, which is a macrophage marker. Note the cytoplasmic stain in the enlarged, activated, positive macrophages. The multiple round negative spots in the cytoplasm of the cell in the middle represent phagocytic vacuoles containing phagocytosed blood cells. The single round negative image in the cell in the center right could be the nucleus. (40 \times .)

References

1. Foucar K: *Bone Marrow Pathology*, edn 2. American Society for Clinical Pathology Press: Chicago; 2001.
2. Tavian M, Peault B: Embryonic development of the human hematopoietic system. *Int J Dev Biol* 2005, 49:243–250.
3. Peault B: Hematopoietic stem cell emergence in embryonic life: developmental hematology revisited. *J Hematother* 1996, 5:369–378.
4. Palis J, Yoder MC: Yolk-sac hematopoiesis: the first blood cells of mouse and man. *Exp Hematol* 2001, 29:927–936.
5. Wickramasinghe SN: Bone marrow. In *Histology for Pathologists*. Edited by Mills SE. Philadelphia: Lippincott Williams & Wilkins; 2007:799–836.
6. Gilmour JR: Normal haemopoiesis in intrauterine and neonatal life. *J Pathol Bacteriol* 1941, 52:25–55.
7. Emura I, Sekiya M, Ohnishi Y: Two types of immature erythrocytic series in the human liver. *Arch Histol Jpn* 1983, 46:631–643.
8. Foucar K, Viswanatha DS, Wilson CS: Non-neoplastic disorders of bone marrow. In *Atlas of Nontumor Pathology*, edn 1. Washington, DC: American Registry of Pathology Press; 2009.
9. Kelemen E, Calvo W, Fliedner TM: *Atlas of Human Hemopoietic Development*. Berlin: Springer-Verlag; 1979.
10. Gilbert-Barness E, Debich-Spicer D: *Handbook of Pediatric Autopsy Pathology*. Totowa, NJ: Humana; 2005.
11. Kalpaktoglou PK, Emery JL: Human bone marrow during the last three months of intrauterine life. A histological study. *Acta Haematol (Basel)* 1965, 34:228–238.

SECTION VII

Central Nervous System

27

Brain and Spinal Cord

Veena Rajaram

The brain and spinal cord can be easily identified from the embryonic period of life. They grow rapidly during early fetal life with different parts of the brain growing at different rates throughout gestation and early postnatal life. This chapter gives a brief summary of embryology and macroscopic changes in the central nervous system (CNS) with microscopic descriptions and examples of the normal histology of different parts of the brain and spinal cord at various gestational ages.

Embryology

Development of the CNS occurs in successive epochs, each with multiple phases and different mechanisms of morphogenesis. Initially, the CNS develops from the neural plate, a collection of superficial flat ectodermal plate cells (neuroepithelium matrix) seen at gestational week (GW) 2.5, which then folds to form the neural groove. The neural folds fuse to form the neural tube. This fusion begins at the future rhombencephalic and spinal regions at GW 3 (22 days, Carnegie Stage [CS] 10) and proceeds in a cranial and caudal direction. The anterior neuropore closes at around GW 4 (CS 11) and the posterior neuropore by GW 5 (CS 13). The ventricular system is then separated from the amniotic cavity and the cerebrospinal fluid is secreted by the lining ependymal cells. The rostral part of the neural tube forms the cranial vesicles (prosencephalic, mesencephalic, and rhombencephalic) and the caudal part forms the spinal cord. The cranial vesicles begin to expand from GW 3.5 throughout the first trimester, to form "superventricles." They then shrink gradually with a caudal to rostral gradient. Part of the prosencephalic vesicle evaginates bilaterally to form the telencephalic vesicles by late GW 5 (CS 14) and the medial ganglionic eminence becomes visible (future thalamus, subthalamus, and hypothalamus). By CS 15, the expanding cerebral vesicles are delineated externally by the di-telencephalic sulcus and the lateral ganglionic eminence can be identified (future cerebral cortex, basal ganglia, and olfactory bulb) [1]. The rhombencephalic superventricle is the first to expand; the ventral medullary flexure then divides the rhombencephalic superventricle into a metencephalic (cerebello-pontine) pool and a myelencephalic (medullary) pool. The dorsal medullary vellum invaginates to form the choroid plexus and this superventricle begins to shrink. The mesencephalic (future aqueduct) and the diencephalic (future third ventricle) superventricles do not significantly expand. The caudal part of the neural tube canal is thin and slit-like in the spinal cord. Between GW 4 to GW 5.5, the neuroepithelium in the spinal cord proliferates and reaches a peak. The lumen of the neural canal becomes diamond shaped and then oval, and its caudal end dilates to form the terminal ventricle [2].

The neuroepithelial matrix proliferates to give rise to neural stem cells and precursor cells that differentiate into neural and glial cells in the CNS. Due to the differential rate of growth of the different parts of the neural tube, the tube develops three flexures: the midbrain flexure, neck flexure, and pontine flexure. The midbrain flexure is the first ventral flexure between the forebrain and the midbrain; the second ventral flexure is between the hindbrain and the spinal cord (neck flexure); and the third, dorsal flexure (pontine flexure) develops between the above two ventral flexures [3].

The forebrain is initially a single cavity with a thin roof and floor. The lateral walls have a dorsal and ventral area internally separated by the hypothalamic sulcus. The optic vesicles are the first lateral diverticula from the forebrain. Their proximal part constricts to form the optic stalks. The telencephalic vesicles then evaginate from the prosencephalic vesicle and form the cerebral hemispheres with lateral ventricles that communicate with the central portion of the former through the foramen of Monro. The anterior part of the prosencephalic roof plate between the foramina and the recess of the optic stalk is the lamina terminalis. The floor plate anterior to the foramina and the lateral walls give rise to the anterior hypothalamus, optic chiasm, and optic recesses. During the fifth week, bilateral olfactory diverticula appear anteriorly, medially in the floor of the lateral ventricles. They form the olfactory bulbs and tracts. The cerebral hemispheres grow and enlarge anteriorly, superiorly, and posteriorly. The medial surfaces are separated from each other by the longitudinal fissure. The cranial end forms the frontal pole while the posterior end folds caudally and ventrally to form the temporal pole; the new posterior end forms the occipital pole. The temporal lobes expand to cover the brainstem laterally and the cerebral hemispheres gradually overlap the diencephalon, midbrain, and cerebellum successively [2].

Elevations develop in the floor and adjacent lateral wall of the lateral ventricles, representing the corpus striatum and caudate nuclei. Another internal elevation (future hippocampus) develops in the wall of the lateral ventricle anterior and inferior to the attachment of the olfactory stalk (pyriform area). The two hippocampi are connected by fibers crossing between the fornix in the upper part of the lamina terminalis, the commissure of the fornix. Commissures between the two hemispheres develop later and lie dorsal to the fornix; they expand to form the corpus callosum. Projection fibers from the neocortex develop near the end of the first trimester, and extend medially and downward, dividing the corpus striatum into medial caudate and lateral lentiform nucleus

and, externally, a slight depression on the superolateral surface of the cerebral hemispheres (lateral cerebral fossa) indicates the site of the corpus striatum [4]. By the fourth month, the adjacent temporal pole grows and converts this fossa into the lateral sulcus. Sulci start forming on the medial surface of the hemispheres and then on the superolateral and inferior surfaces. Most of the major sulci can be identified by the end of the seventh month (see Fig. 27-1) [2,5].

The diencephalon and the midbrain are gradually covered by the cerebral hemispheres. The hindbrain is initially longer than the combined length of the forebrain and midbrain. At the pontine flexure, the roof becomes thin and stretched, and the ventricular cavity becomes triangular, the lateral angles become the lateral recess of the fourth ventricle, and the dorsal and ventral surfaces are separated by the sulcus limitans. The cerebellar hemispheres project into the fourth ventricle as two small swellings at the rhombic lip of the dorsal lamina. They are initially separated by the most cranial part of the roof of the metencephalon, which then develops into the vermis. There is a gradual reduction of the intraventricular part of the cerebellar hemispheres with the development of the dorsal part (extroversion of the cerebellum). The cerebellum develops transverse grooves on its surface and stretches across the cranial part of the fourth ventricle. The rest of the metencephalon develops into the pons. The cranial part of the myelencephalon (medulla oblongata) forms part of the floor of the fourth ventricle [4]. The development of the lower part is similar to that of the spinal cord. The spinal cord initially occupies the entire length of the vertebral canal with spinal nerves emerging at right angles to the cord. By the seventh week, the vertebral column develops more rapidly and by the 25th week of gestation, the spinal cord extends to the third lumbar vertebra. The intermediate part of the terminal ventricle and its coverings form the filum terminale. The caudal end of this ventricle remains adherent to the overlying ectoderm and should disappear before birth; however, it may occasionally persist to form congenital cysts [2,6].

Sulcal Development			
Gestational age	Medial surface	Superolateral surface	Base/inferior surface
GW 8–11	Hippocampal	Interhemispheric Lateral fossa	
GW 12–15	Callosal	Lateral	
GW 16–19	Parieto-occipital Calcarine Cingulate		Olfactory
GW 20–23	Collateral	Rolandic/central Superior temporal	
GW 24–27		Precentral Postcentral Superior frontal Lateral occipital Intraparietal	
GW 28–31		Inferior temporal Inferior frontal	
GW 32–35	Marginal Insular	SECONDARY SULCI FROM: Superior and inferior frontal Superior temporal Intraparietal, occipital	
GW 36–39		SECONDARY SULCI FROM: Transverse and inferior temporal Cingulate TERTIARY SULCI FROM: Superior and inferior frontal Intraparietal	Orbital
GW 40–44	SECONDARY SULCI FROM: Callosomarginal Insular	TERTIARY SULCI FROM: Inferior temporal Occipital	SECONDARY SULCI FROM: Orbital

FIGURE 27-1. Sulcal development.

Histology

General Overview

Neurogenesis and gliogenesis are sequential processes that occur simultaneously from proliferating neuroepithelial cells. Neurogenesis is more prominent in early gestation and gliogenesis in late gestation [7]. Neocortical neurons proliferate in the ventricular zone and the subventricular zone with a rapid phase from GW 10 and a slower phase from GW 22. Following neuronal migration at GW 8, the cortical plate is formed from the preplate stage that consists of Cajal-Retzius cells and subplate cells between the ventricular zone and the pia mater [8]. The subplate cells are neurons that arise early, form connections, and help establish the cortical lamination. They form the cell and fiber compartment for migratory cells and fibers between the cortical plate and the intermediate zone. The intermediate zone constitutes the white matter in the adult brain and contains the migrating cells and fibers in the developing fetal brain. The cortical plate along with the marginal zone develops into the six-layered adult cortex and is the final destination of the migrating neurons. Axonal formation can be identi-

fied soon after neurogenesis commences. By GW 12, the fibers forming the external capsule, internal capsule, and limbic bundles can be identified. By GW 15 to 16, afferent axons from the thalamus and basal forebrain approach the cortical plate but enter the cortical plate at GW 26 to 28. Between GW 17 to 19, the periventricular and callosal fibers are seen and there are increased fibers in the subplate and marginal zone [1,9].

Radial glia arise from the ventricular zone during early gestation and play a role in neuronal migration. They mature into astrocytes at the end of neurogenesis. During the second half of gestation and early postnatal life, the subventricular zone is the proliferative zone and the source of astrocytes and oligodendrocytes. The postnatal subventricular zone cells give rise to the protoplasmic astrocytes in the gray matter [10]. Oligodendrocyte precursor cells are prominent at midgestation, and proliferate in the subventricular zone in the telencephalon in late gestation and the early postnatal period. They transform to mitotically active preoligodendrocytes that give rise to post-

mitotic oligodendrocytes [11]. Germinal matrices with proliferating neuroglial precursors (glioepithelia) may persist in the subventricular zone after the cessation of neurogenesis and gliogenesis, even throughout adult life [1]. "Myelination gliosis" is seen in the white matter before the onset of myelination. Unlike the astrocytes seen in reactive gliosis, the "myelination glial cells" have large, pale nuclei and scant cytoplasm. They are glial fibrillary acidic protein (GFAP) positive but, following the onset of myelination, these cells assume the characteristics of mature oligodendrocytes. Myelination begins by the end of first trimester

in the spinal cord and by term the brainstem contains myelinated tracts while almost no myelin is seen in the cerebral hemispheres. Only the posterior limb of the internal capsule, corona radiata, optic tract and chiasm, ansa lenticularis, and pallidal and commissural fibers contain microscopic myelin. Myelination occurs mostly in the first postnatal year and may continue for decades in some systems in the cortex. It progresses from caudal to rostral parts in some systems (white matter tracts in the spinal cord) but may begin simultaneously in other systems (internal capsule and superior cerebellar peduncle) [1,12-14].

First Trimester

Neural tube

At the time of closure (GW 3), the neural tube is lined by a single layer of short columnar to cuboidal, ciliated epithelial cells with closely associated rapidly proliferating neuroepithelial cells and early preplate. The neuroepithelial cells have large, hyperchromatic nuclei and scant cytoplasm in a background of minimal supportive mesenchyme. They consist of multipotential precursor cells that express multiple glial and neuronal markers. In areas that produce large cortical structures with similar neuronal population (*ie*, neocortex, tectum, and cerebellum), neuroepithelial cells lining the ventricular surface are in sheets and form a smooth surface. They form small, irregular aggregates in areas with future multiple distinctive, neuronal populations

(*ie*, hippocampal, thalamic, and hypothalamic nuclei) (see Fig. 27-2) [4].

The surrounding meningeal tissue is spongy and transiently thick between the pial surface of the brain and the adjacent dural membrane. The pia mater is seen early, adherent to the neural tissue, and consists of a network of reticulum and elastic fibers. The arachnoid is the most prominent space with "super-arachnoid reticulum." It is spongy and contains granulations, villi, and septa with circulating cerebrospinal fluid. The dura is seen later and consists of dense connective tissue [2]. Glycogen-rich cells with abundant clear cytoplasm can be seen in the dura and arachnoid. By GW 9, the super-arachnoid reticulum decreases in size (see Fig. 27-2).

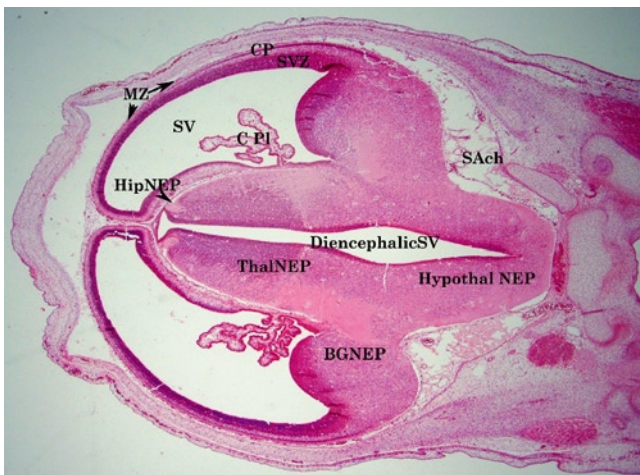


FIGURE 27-2. Coronal sections of a GW 8 fetal brain showing the telencephalic superventricle, future lateral ventricle (SV), and diencephalic superventricle (Diencephalic SV). The hippocampal neuroepithelium (HipNEP), thalamic neuroepithelium (ThalNEP), basal ganglia neuroepithelium (BGNEP), and hypothalamic neuroepithelium (Hypothal NEP) are well defined. The marginal zone (MZ) can be seen and the early cortical plate (CP) with subventricular zone (SVZ) can be identified. The meningeal layers consist of loose mesenchyme, the superarachnoid (SAch). The fetal choroid plexus (C PI) is identified in the super ventricle. (Hematoxylin and eosin [H&E], 2×.)

Cerebral cortex

A thick proliferative ventricular zone is seen at GW 6 with a narrow, cell-sparse marginal zone. By GW 7, an additional proliferative zone, the subventricular zone, begins to form between these two layers (see Fig. 27-3). This layer is thickest at the ganglionic eminence and is narrow medially. Fate-restricted progenitor cells with mitotic ability and differentiating neurons migrate along radial glia from the ventricular lumen to the subventricular zone and the early gray matter of the incipient cortical plate below the narrow, cell-sparse marginal zone (see Figs. 27-2 and 27-3). Three cell types can be identified at

this time: 1) round "globular" cells with end-feet attached to ventricular lumen; 2) oval "fibrous" cells with end-feet at the ventricular surface and a thin, radial fiber reaching the pial surface; and 3) "detached" cells with their processes reaching the pial surface [4]. The primary neuroepithelial cell matrix generates macroneurons that are large neurons with long axons. These macroneurons, also known as Cajal-Retzius neurons, migrate radially to the primordial plexiform layer (preplate). Between GW 7.5 to 8, radially organized neurons form the initial cortical plate below the marginal zone. An intermediate zone (fetal white matter) is seen containing transient migratory cells and afferent axonal

fibers from the thalamus [1]. Stratified transitional fields where the migrating cells/fibers from the subventricular zone to the cortical plate sojourn begin appearing by GW 9 but are best identified in the second trimester [4]. In the hippocampus, macroneurons forming the pyramidal cells of Ammon's horn and dentate neuroepithelial cells are present by GW 9 but dentate gyrus is seen in the second trimester [15].

Basal ganglia neurons are derived from the basal ganglia neuroepithelium (see Figs. 27-4 and 27-5) and the internal capsule is recognized by GW 8 [16]. The

choroid plexus in the ventricular cavity has a "budding" appearance with smooth pseudostratified epithelium (see Figs. 27-4 and 27-6) [4]. The cells lining the choroid plexus frequently have a clear, glycogen-rich cytoplasm. The cerebral peduncle forms by GW 10 to GW 13.5. Axons from the thalamus establish synaptic contact in the subplate by GW 11. Pioneer fibers are seen in the anterior commissure by GW 10. The hippocampal commissure is seen by GW 11 and the earliest fibers of the corpus callosum are seen by GW 11 to GW 13 [17].

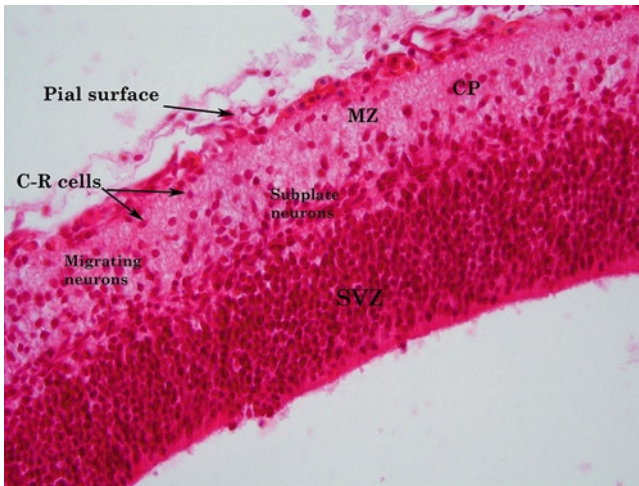


FIGURE 27-3. Cerebral cortex at GW 8. The cerebral cortex shows a thick layer of neuroepithelium in the ventricular/subventricular zone (SVZ). Migrating Cajal-Retzius cells are seen in the subplate and settling Cajal-Retzius cells (C-R cells) are present in the marginal zone (MZ). Early cortical plate (CP) formation is seen. The pial surface with loose mesenchyme and blood vessels is present. (H&E, 40 \times .)



FIGURE 27-4. Basal ganglia at GW 8. Basal ganglia neuroepithelium in the subventricular zone (SVZ) with migrating and sojourning basal ganglia neurons (BG) and adjacent fetal choroid plexus (C PI) are shown. The glioependymal cells (GEP) are identified adjacent to the ventricular lining and the choroid plexus stem cells (C PI SC). Early axonal processes can be seen (AF). (H&E, 10 \times .)

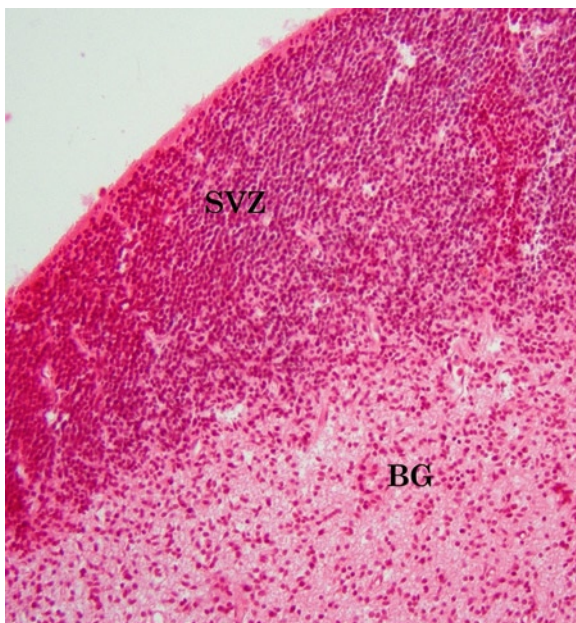


FIGURE 27-5. Basal ganglia at GW 8. This higher power view is of the basal ganglia neuroepithelium in the subventricular zone (SVZ) and neurons of the basal ganglia (BG). (H&E, 20 \times .)

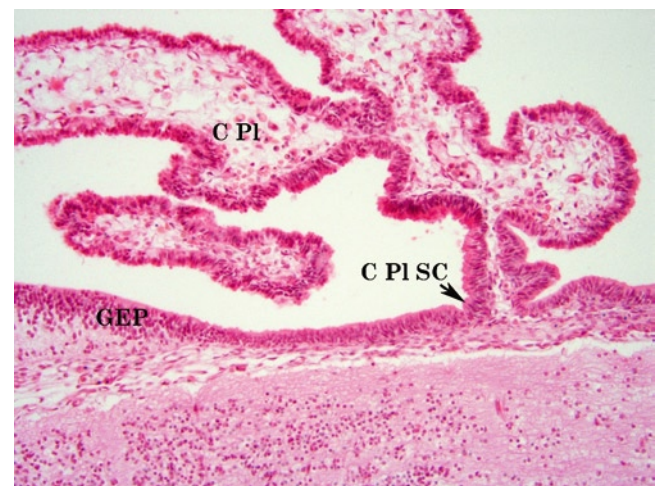


FIGURE 27-6. Choroid plexus at GW 8. This higher power image is of the glioependymal cells (GEP) adjacent to the ventricular lining and the choroid plexus stem cells (C PI SC). Pseudostratified, spindled/elongated cells of the fetal choroid plexus (C PI) are seen. (H&E, 20 \times .)

Brainstem and cerebellum

Rhombencephalic neuroepithelium has several components: upper rhombic lip region, lower rhombic lip region, ventromedial region, and ventrolateral region. Lower rhombic lip region neuroepithelial cells are the source of precerebellar nuclei neurons, progenitors of the inferior olivary nucleus and pontine neurons [18]. The inferior olivary nucleus can be seen at GW 7.5 and the pontine nucleus by GW 11. The earliest descending axonal fibers can be seen at this time.

Upper rhombic lip region neuroepithelial cells are the source of neurons of the cerebellum. Cerebellar neuroepithelial cells are well identified by GW 5. From GW 6.5 to GW 7.5, neurons migrate to the deep cerebellar nuclei (fastigial nucleus) and at GW 8.5 axons from these

neurons cross the midline in the fused vermis. Radial migration of Purkinje cells begins at the same time and peaks at GW 7.5. The cells are seen as a densely packed mass of darkly staining cells over the neuroepithelial cells in the anterior and posterior cerebellum and start dispersing and migrating to the surface by GW 9. The formation of the secondary germinal matrix, the external granular layer in the subpial area of the dorsal rhombic lip, begins by GW 7.5 to 8.5. By the end of first trimester (GW 11), the external granular layer covers the entire formative cerebellar cortex, the Purkinje cells form a crescent-shaped mass superficially, and the deep cerebellar nuclei (dentate, interpository, and fastigial) are formed [19,20].

Spinal cord

Spinal neuroepithelial cells around a slit-shaped ventricle change shape with ventro-dorsal compartmentalization under the influence of the neural crest and peripheral structures. By GW 4.5, differentiating neurons are seen in the earliest maturing areas of the spinal cord (motor neurons). The dorsal horn expands between early GW 7 and GW 8.5. Dorsal root fibers can be seen entering the spinal cord by GW 5.5 and bifurcation of the dorsal root is identified by GW 5.5. The dorsal funiculus appears by early GW 5 and is formed by GW 8.5. The ventral funiculus also appears at the same time (early GW 5). The lateral funiculus begins to grow by GW 5.5.

Increased cellularity due to glial proliferation is seen in the dorsal funiculus and myelination glia can be seen as cells with large, pale nuclei with fine, stippled chromatin; prominent nucleoli; and scant cytoplasm. Myelination may have begun in the medial lemniscus but myelination can be identified using special stains only in the second trimester, as most of the myelin lipids are extracted from the tissue during processing. The dorsal, ventral, and lateral funiculi continue to expand. By the end of first trimester, the gray matter resembles that of the adult spinal cord and all components of the white matter are expanding and better defined [6].

Second and Third Trimesters

GW 13 to GW 15

By GW 13, the cortical plate, just beneath the marginal zone, has a bilaminar appearance with an outer darker area and inner lighter area (see Fig. 27-7). The subpial granular layer, a transient cell layer containing Cajal-Retzius cells, appears below the pia mater in the lateral cortex and extends over the dorsal and medial areas. During this period, the subplate is seen to have an upper cell fiber-rich layer and a lower cell-sparse zone. Migrating cells can be seen in the stratified transitional fields with neurons stopping and aggregating in layers 2, 4, and 5. Stratified transitional field layer 1 contains the superficial fibrous layer (future subcortical white matter) and stratified transitional field layer 6 contains the deep layer of callosal fibers (see Fig. 27-8) [21]. The neuroepithelial layer and subventricular zone is prominent in the basal ganglia at GW 14. Caudate and putamen can be identified, separated by the internal capsule (see Fig. 27-9). The neurons in the diencephalic

region are maturing (see Fig. 27-10) and the ventricular region is lined by a thin layer of glioepithelium/ependyma. There is outflow of cortico-fugal efferent fibers by GW 13.5 and the cerebral peduncles are formed [16].

In the brainstem (see Fig. 27-11), the fourth ventricle is also lined by glioepithelial/ependymal lining and the medulla has two active germinal sites. The cochlear neuroepithelium in the lateral recess of the fourth ventricle and the precerebellar neuroepithelium producing the pontine neurons may be present in the medulla [18]. The cerebellar surface is covered by the external granular layer. Purkinje cells are not visible at this time (see Fig. 27-12). The gray matter in the spinal cord shows maturing neurons in the ventral horn with a columnar arrangement of these cells. The roof plate is receding and white matter is increasing along the dorsal midline (see Fig. 27-13) [6,21].



FIGURE 27-7. Cerebral cortex at GW 14. This low-power view of the cerebral cortex shows the cortical plate (CP) and subplate (SP). Migrating cells are seen in the stratified transitional fields (STF) 1, 2, 4, 5, and 6; layer 3 is absent (seen in granular cortex only). The subventricular zone (SVZ) is seen surrounding the lateral ventricle (LV). (H&E, 2 \times .)



FIGURE 27-8. Cerebral cortex at GW 14. This higher magnification shows the following layers: stratified transitional field (STF) of the migrating cells layers 1, 2, 4, 5, and 6 (layer 3 is absent; it is seen in the granular cortex only); the subpia granular layer (SGL); and the marginal zone (MZ), which will become layer I of the cortical plate. CP—cortical plate; LV—lateral ventricle; NEP—neuroepithelium; SP—subplate; SVZ—subventricular zone. (H&E, 10 \times .)

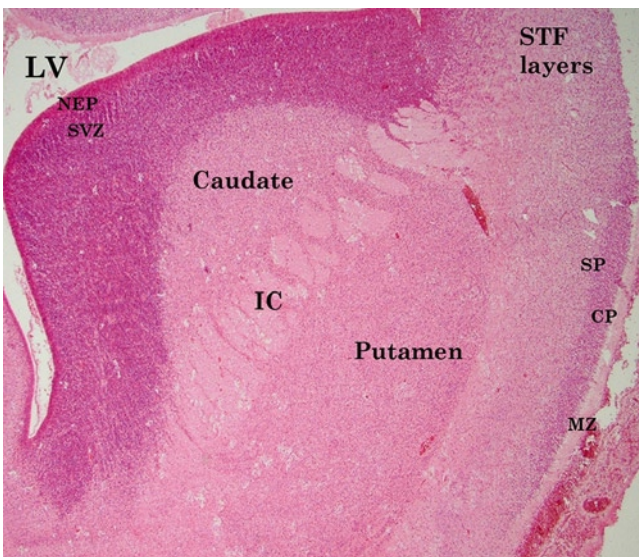


FIGURE 27-9. Basal ganglia at GW 14. Basal ganglia neuroepithelium (NEP) and subventricular zone (SVZ) with caudate, internal capsule (IC), and putamen are shown. The adjacent cortex shows the stratified transitional fields (STF) 1, 2, 4, 5, and 6; subplate (SP) and cortical plate (CP) with marginal zone (MZ). LV—lateral ventricle. (H&E, 4 \times .)

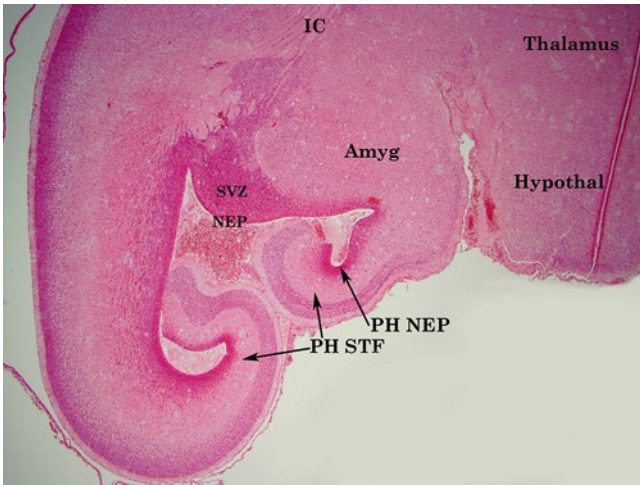


FIGURE 27-10. Diencephalon at GW 14. Thalamus, hypothalamus (Hypothal), amygdala (Amyg), striatal neuroepithelium (NEP) and subventricular zone (SVZ), parahippocampal neuroepithelium (PH NEP), parahippocampal stratified transitional fields (PH STF), and internal capsule (IC) are shown. (H&E, 4 \times .)

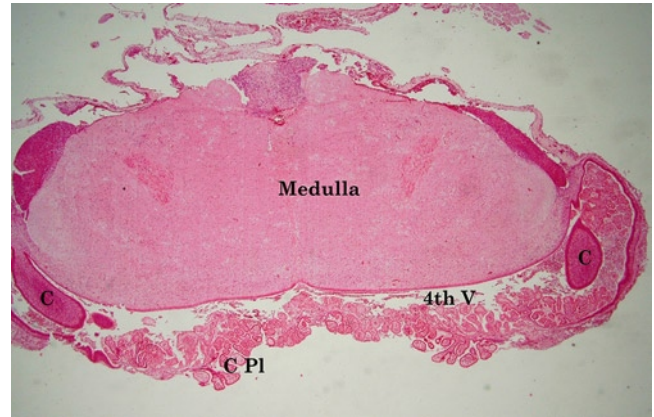


FIGURE 27-11. Brain stem and cerebellum at GW 14. Medulla, cerebellum (C), and choroid plexus (C PI) with the fourth ventricle (4th V) are shown. (H&E, 4 \times .)

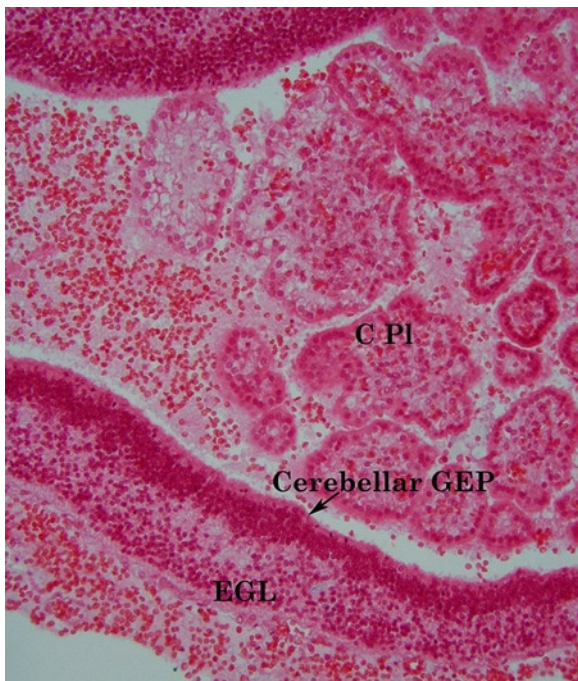


FIGURE 27-12. Cerebellum at GW 14. The cerebellar gliopendymal layer (GEP) and the external germinal layer (EGL) are shown with an adjacent choroid plexus containing a simple cuboidal to columnar cell lining (C PI). Purkinje cells are not yet visible. (H&E, 20 \times .)

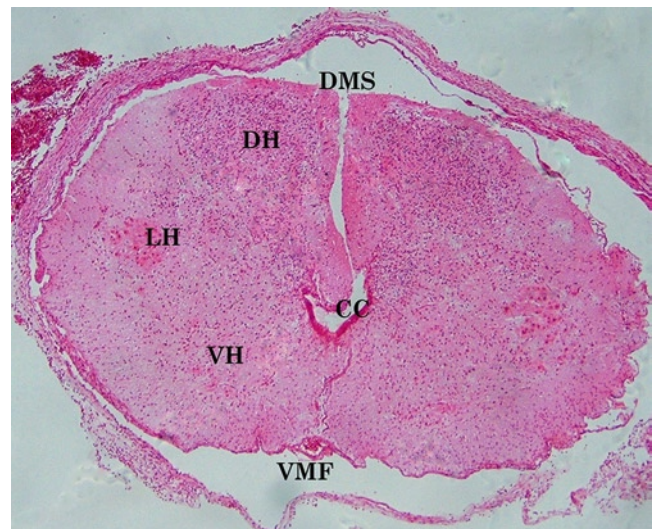


FIGURE 27-13. Spinal cord at GW 14. The spinal cord is shown with a well-identified ventral horn (VH), lateral horn neurons (LH), and a dorsal horn (DH). There is scant neuroepithelium around the central canal (CC). The ventral median fissure (VMF) and disrupted dorsal median septum (DMS) are seen. (H&E, 4 \times .)

GW 16 to GW 18

At this gestational age, the thickness of the cortical plate is increased compared to an earlier gestational age. Cajal-Retzius cells lie in the subpial granular layer with early migration into the marginal zone at GW 14 to GW 18 (see Fig. 27-14). At GW 15, the subplate increases in thickness so that it is greater than four times the thickness of the cortical plate. Migrating neurons are seen in the stratified transitional field layers (see Fig. 27-14). Stratified transitional layer 3 is seen only in the granular cortical areas (future sensory cortex). In the hippocampus, the granule cell layer in the dentate fascia is seen by GW 13 and the pyramidal neurons in the Ammon's horn can be seen by GW 15 (see Figs. 27-15 and 27-16). The neuronal migration to Ammon's horn and dentate is striking; cellularity in the precursor cell subgranular zone is prominent below the dentate layer. The choroid plexus

shows maturation with a simple cuboidal epithelium lining the fibrovascular cores (see Fig. 27-17). The striatal neuroepithelium is still prominent, and the caudate and putamen are larger than that seen at GW 14 (see Fig. 27-18). The neurons in the thalamus appear mature and there is a thin layer of gliependymal cells lining the third ventricle (see Fig. 27-19). In the brainstem, the gliependymal cell lining is convoluted around the aqueduct and fourth ventricle with persistent neuroepithelium in the medulla and migrating neurons in the pons (see Fig. 27-20). The cerebellar external granular layer is actively producing basket, stellate, and granule cells. Purkinje cells may be seen migrating from the ventricular zone, but have not formed a discrete layer yet (see Fig. 27-21). The spinal cord is enlarging with the accumulation of white matter tracts [21].

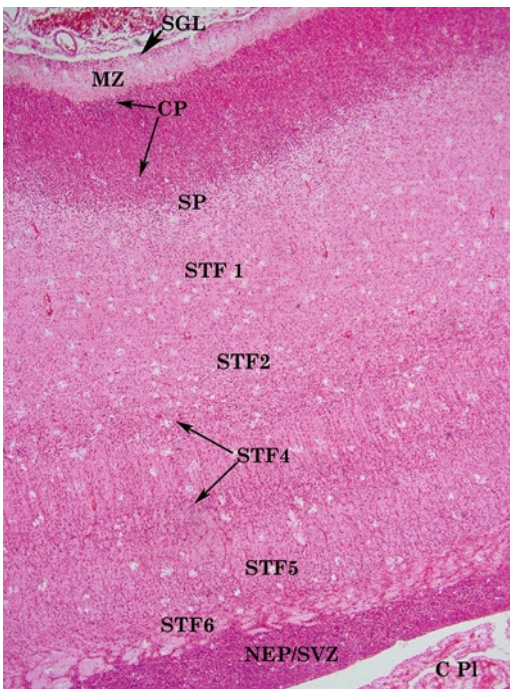


FIGURE 27-14. Cerebral cortex at GW 17. The cortical layers are better identified with the subpial granular layer (SGL) containing the glioepithelium. There are a few Cajal-Retzius cells in the marginal zone (MZ) or layer I. The cortical plate (CP) is thicker with more neurons. The subplate (SP) and the stratified transitional fields (STF) 2, 4, and 5 contain sojourning neurons, while STF 1 is the superficial fibrous layer that persists as the subcortical white matter. STF 6 contains the deep layer of callosal fibers outside the germinal matrix with neuroepithelium and subventricular zone (NEP/SVZ). The choroid plexus (C Pl) is seen in the lateral ventricle. (H&E, 4 \times .)

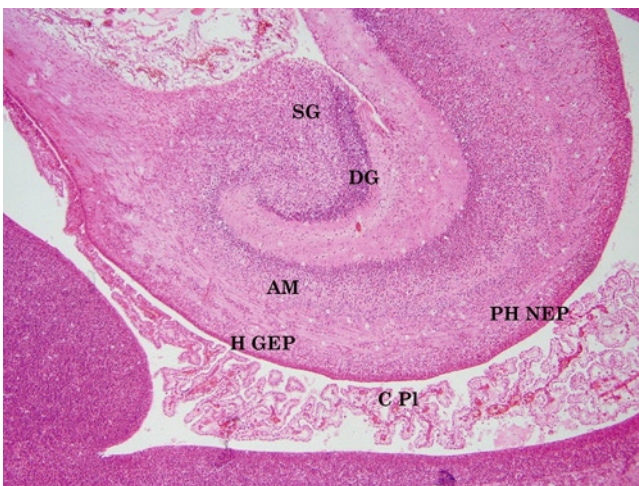


FIGURE 27-15. Hippocampus at GW 17. Granule cells of the dentate gyrus (DG) are seen migrating from the subgranular zone (SG). Ammonic migration and the sojourn zone (AM) are seen adjacent to the hippocampal glioepithelium (H GEP). Parahippocampal neuroepithelium and subventricular zone (PH NEP) is adjacent to the lateral ventricle with the choroid plexus (C Pl). (H&E, 4 \times .)

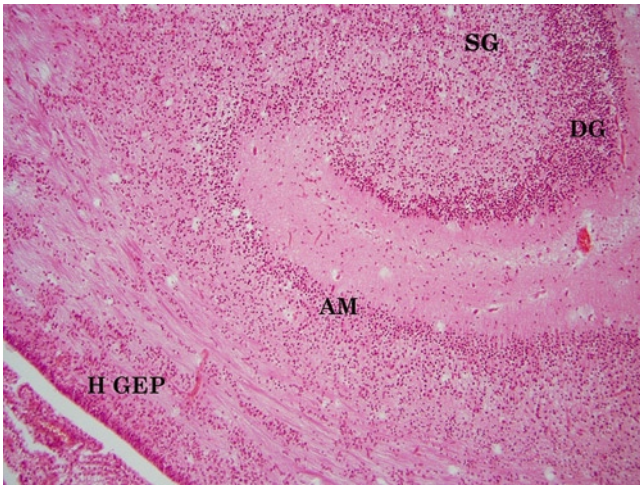


FIGURE 27-16. Hippocampus at GW 17. A higher magnification of Figure 27-15 is shown here. Granule cells of the dentate gyrus (DG) are seen migrating from the subgranular zone (SG). Ammonic migration and the sojourn zone (AM) are seen adjacent to the hippocampal glioepithelium (H GEP). (H&E, 10 \times .)

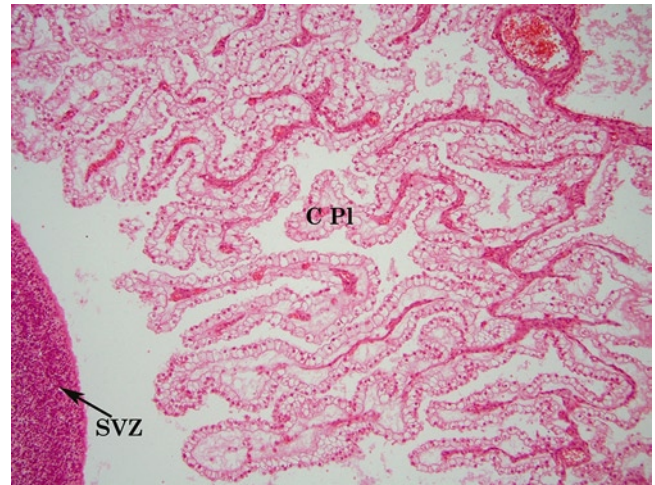


FIGURE 27-17. Choroid plexus at GW 17. The simple cuboidal cells with abundant clear (glycogenated) cytoplasm lining the fibrovascular cores of the maturing choroid plexus (C Pl) are shown. The adjacent neuroepithelium/subventricular zone (SVZ) is also seen. (H&E, 10 \times .)

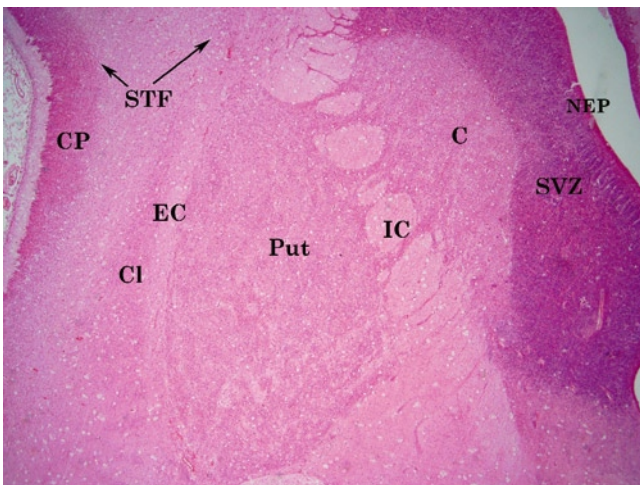


FIGURE 27-18. Corpus striatum at GW 17. The striatal neuroepithelium (NEP) and subventricular zone (SVZ) persist. The neurons in the head of caudate (C) and the putamen (Put) are better defined and the white matter tracts, internal capsule (IC) and external capsule (EC), are easily identified. The claustrum (Cl) is seen below the cortical plate/subplate (CP) and the stratified transitional fields (STF). (H&E, 2 \times .)

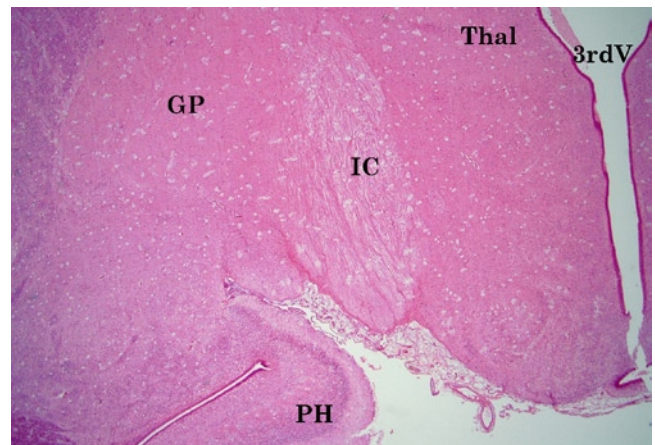


FIGURE 27-19. Thalamus (Thal) with the adjacent third ventricle (3rdV) and parahippocampal gyrus (PH) at GW 17. The globus pallidus (GP) is seen adjacent to the internal capsule (IC), which continues as the cerebral peduncle. (H&E, 2 \times .)

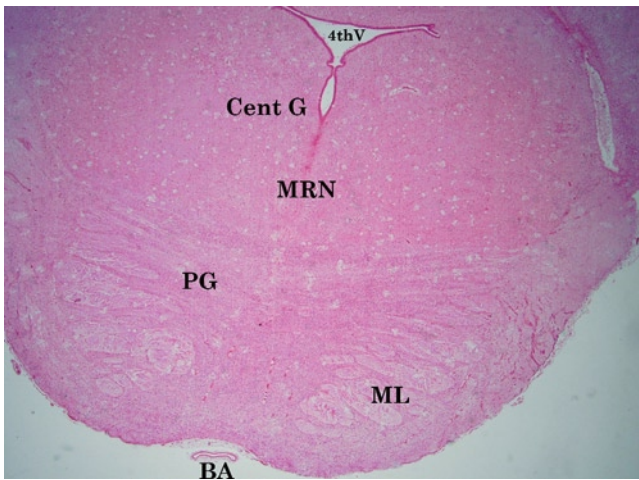


FIGURE 27-20. Brainstem at GW 17. The pons is shown with central gray and reticular formation (Cent G), raphe nuclear complex (MRN), fourth ventricle (4thV), and pontine gray matter (PG). The medial lemniscus and trapezoid body (ML) are present. A cross-section of the basilar artery (BA) is also seen. (H&E, 2 \times .)

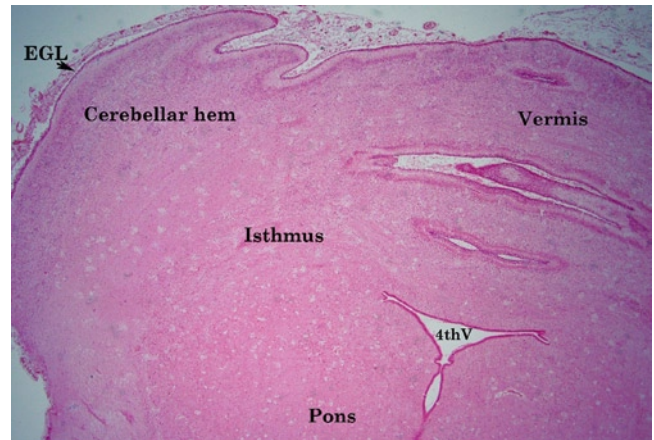


FIGURE 27-21. Cerebellum at GW 17. The external germinal layer (EGL) is seen in the vermis and cerebellar hemisphere. The fourth ventricle (4thV) is also shown. (H&E, 2 \times .)

GW 19 to GW 22

The thickness of the cortical plate continues to increase and a thicker neuroepithelial cell layer is seen generating neurons for definitive cortical layers II, III, and IV. Stratified transitional fields are more defined with an easily observable difference between granular (future sensory) and agranular (future motor) regions. The thickness of the subpial granular layer varies in the different regions of the cortex. The subpial granular layer covers the whole neocortex as a uniform layer by GW 20/21 (see Figs. 27-22–27-24). This layer is composed of cells with round or ovoid nuclei and scant cytoplasm with one or two processes. No mitotic figures are seen. Cajal-Retzius cells move deeper into the marginal zone (molecular layer/cortical layer I) by GW 21/22. In the cortical plate, neurons to the definitive layers II, III, and IV accumulate in the granular/supragranular layer and neurons to layers V and VI are seen in the infragranular layer. By GW 20 to GW 24, thalamic and basal forebrain afferents accumulate in the subplate. In the hippocampus, the ammonic migration of pyramidal neurons is well defined and granule cells are seen migrating to the dentate gyrus. Stem cells settle in the subgranular zone beneath the granular layer, at the periphery of the dentate hilus (see Figs. 27-25 and 27-26). In the basal ganglia, the neuroepithelial cell layer is larger and neurons are being generated and migrating to the striatum (see Fig. 27-27). Neurons in the thalamus are well settled and a very thin layer of gliopendymal cells lines the third ventricle (see Fig. 27-28). The neurons are well settled in

the midbrain, pons, and medulla with a very thin layer of gliopendymal cells lining the aqueduct and fourth ventricle [21].

By the second trimester, the periventricular/aqueductal neuroepithelium is almost absent throughout the midbrain, pons, medulla, and cerebellum, as most of the neurons are produced in the first trimester (see Figs. 27-29 and 27-30). The cerebellar cortex is covered by the external granular layer. There is a thin rim of molecular layer and the Purkinje layer is beginning to form. The dentate nucleus in the cerebellum is not laminated at GW 20 but begins to show differentiation by GW 21. The germinal trigone with neuronal and gliopendymal/gliopendymal precursors is seen adjacent to the tela choroidea (see Figs. 27-31 and 27-32). The external granular layer, molecular layer, Purkinje cell layer, and granular cell layer are all recognizable (see Fig. 27-33) [21]. The most prominent finding in the spinal cord by GW 19 is an increase in glial cells in the white matter, corresponding to myelination glia. Their density varies in the different tracts, being very sparse in the ventral and lateral corticospinal tracts, and very densely populated adjacent to the ventral gray matter. The dorsal funiculus has a relatively dense glial cellularity. The glial cell density is high in the cervical region and lower in the lumbosacral levels. In the gray matter, the ventral motoneurons are easily identified (see Figs. 27-34 and 27-35); the lateral horn motoneurons and the large neurons in Clarke's column can be identified in the thoracic level [6].

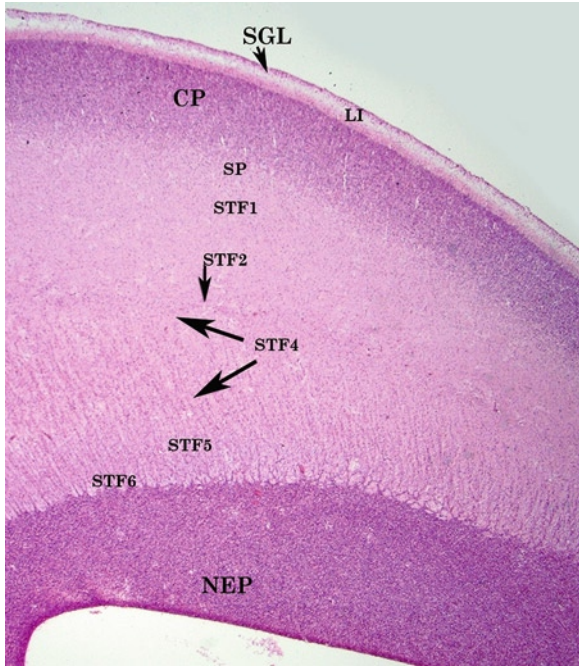


FIGURE 27-22. Cerebral cortex at GW 20. Shown is the frontal cortex with thicker cortical plate (CP) containing the supragranular and infragranular layers. The subpial granular layer (SGL) and subplate (SP) are present. The stratified transitional fields (STF) 5 and 6 are not well visualized. The periventricular neuroepithelium and subventricular zone (NEP) are still prominent. LI—layer I. (H&E, 2×.)

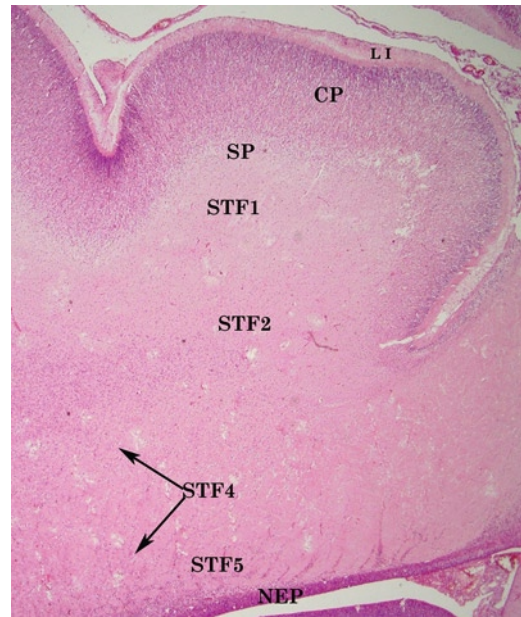


FIGURE 27-23. Cerebral cortex at GW 21. The parietal cortex with a thicker cortical plate (CP) and minimal subpial granular layer is shown. Layer I (LI) is well defined. The thickness of the neuroepithelium/subventricular zone (NEP) is less as compared to GW 20. SP—subplate; STF—stratified transitional field. (H&E, 2×.)

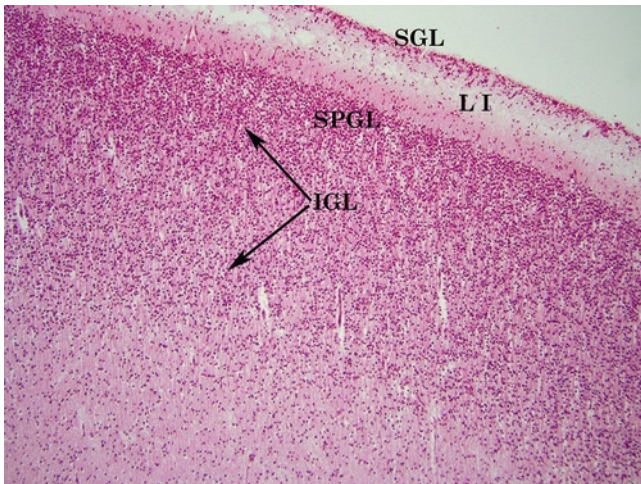


FIGURE 27-24. Cerebral cortex at GW 21. This higher magnification of the cortex shows the subpial granular layer/glioepithelium (SGL), layer I of the cortex (LI), cortical plate with supragranular (SPGL), and infragranular layers (IGL). (H&E, 10×.)

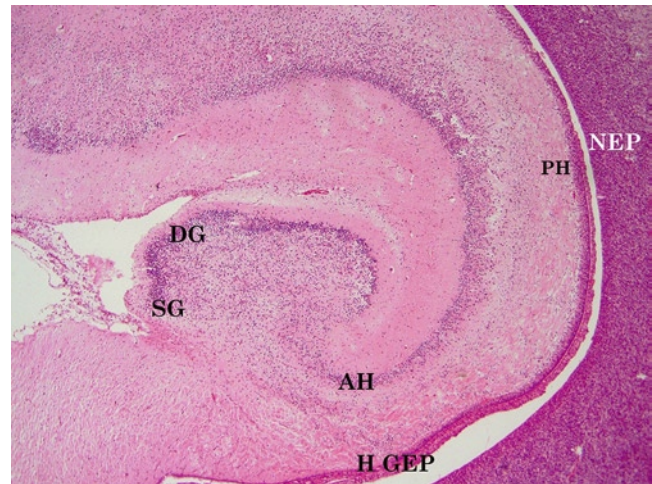


FIGURE 27-25. Hippocampus at GW 21. The hippocampus-granular cells of the dentate gyrus (DG) are seen migrating from the subgranular zone (SG). Ammonic migration and the sojourn zone (AH) are seen adjacent to the hippocampal glioepithelium (H GEP). The parahippocampal gyrus with thinner neuroepithelium and subventricular zone (PH) is shown, as is the adjacent neuroepithelium and subventricular zone of the temporal lobe (NEP). (H&E, 2×.)

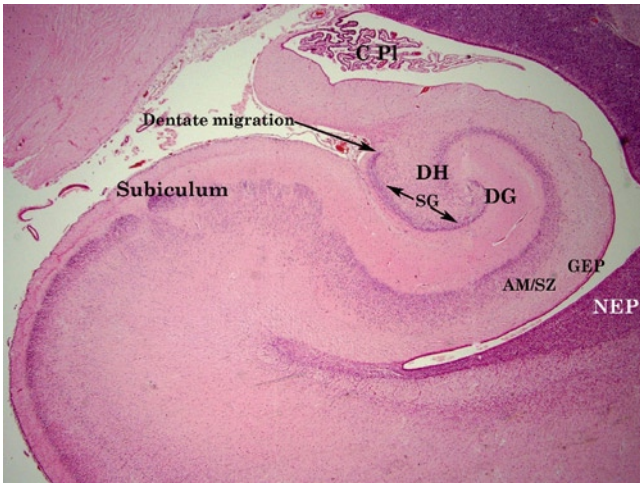


FIGURE 27-26. Hippocampus at GW 22. This image of the hippocampus shows dentate migration, ammonic migration and sojourn zone (AM/SZ), hippocampal glioepithelium/ependymal (GEP), and the parahippocampal neuroepithelium/subventricular zone (NEP). The dentate hilus (DH), granular layer (DG) adjacent to the molecular layer, and the subgranular zone (SG) are well defined. The choroid plexus (C PI) is seen in the lateral ventricle. (H&E, 2 \times .)

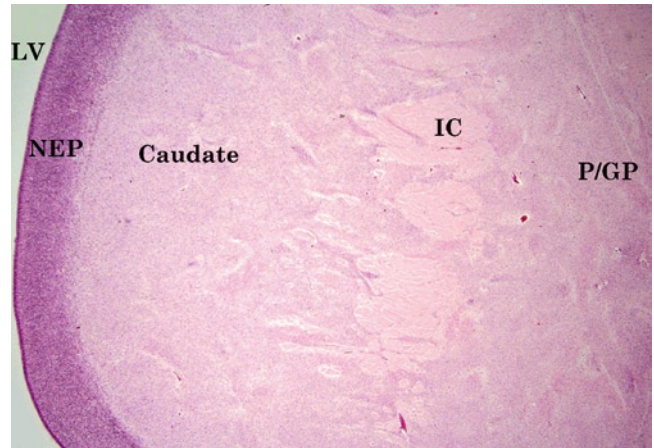


FIGURE 27-27. Basal ganglia at GW 22. Shown are basal ganglia with ventricular lining cells/neuroepithelium (NEP) adjacent to the lateral ventricle (LV). The caudate, putamen, and globus pallidus (P/GP) contain maturing neurons. The internal capsule (IC) is easily identified. (H&E, 2 \times .)



FIGURE 27-28. Thalamus at GW 21. The thalamus with minimal glioepithelium (GEP) is shown. The third ventricle (3rdV) has an ependymal lining with choroid plexus visible focally. (H&E, 2 \times .)

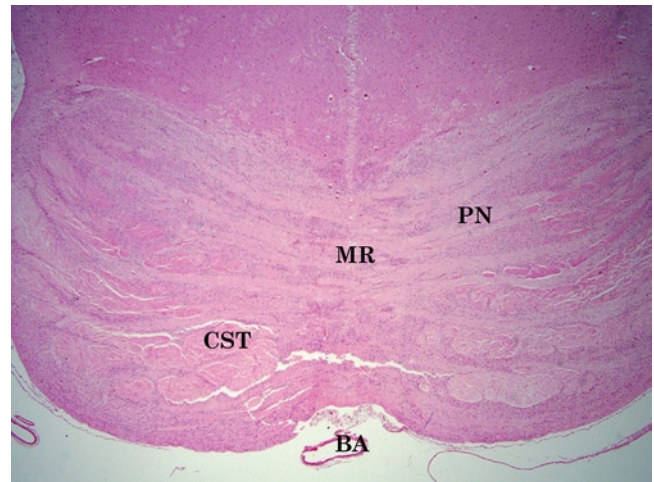


FIGURE 27-29. Brainstem at GW 20. The pons is shown with pontine nuclei and fibers (PN), median raphe (MR) with pontocerebellar tract, descending corticospinal tract (CST), and basilar artery (BA). (H&E, 2 \times .)

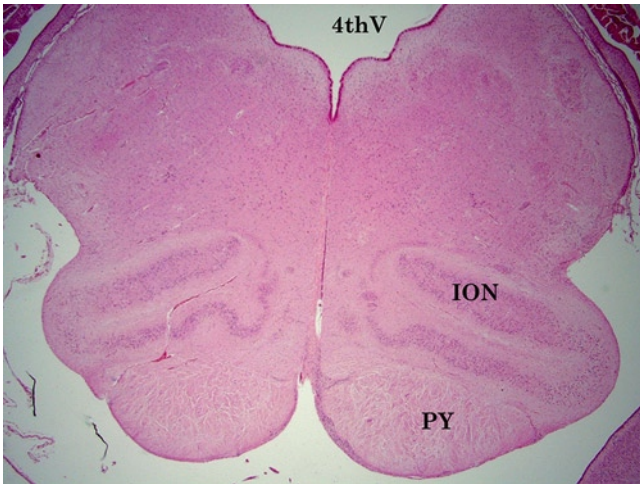


FIGURE 27-30. Brainstem at GW 21. The medulla with well-formed inferior olivary nucleus (ION) and pyramids (PY) is shown. 4th V—fourth ventricle. (H&E, 2 \times .)

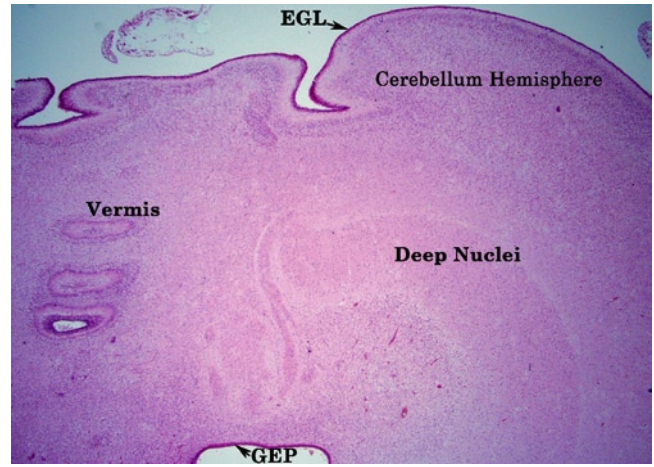


FIGURE 27-31. Cerebellum at GW 20. The cerebellum is shown with vermis, deep gray nuclei, external granular layer (EGL), and gliopithelium/ependymal (GEP) lining the fourth ventricle. (H&E, 2 \times .)

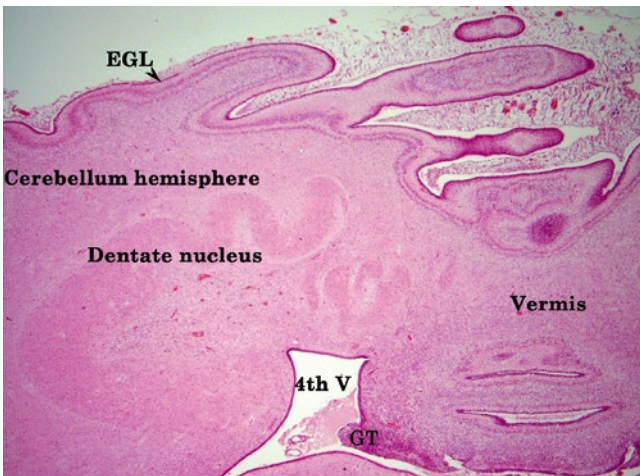


FIGURE 27-32. Cerebellum at GW 21. The cerebellum is shown with better differentiated dentate nucleus and germinal trigone (GT) adjacent to the fourth ventricle (4thV). EGL—external granular layer. (H&E, 2 \times .)

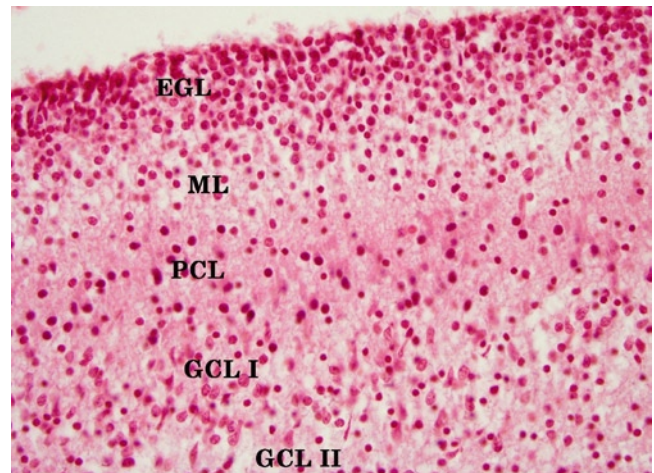


FIGURE 27-33. Higher magnification of cerebellar cortex showing the layers. EGL—external granular layer; GCL I—granule cell layer, dense superficial part; GCL II—granule cell layer, sparse deep part; ML—molecular layer with migrating granule cells; PCL—Purkinje cell layer containing migrating and settling Purkinje cells. (H&E, 20 \times .)

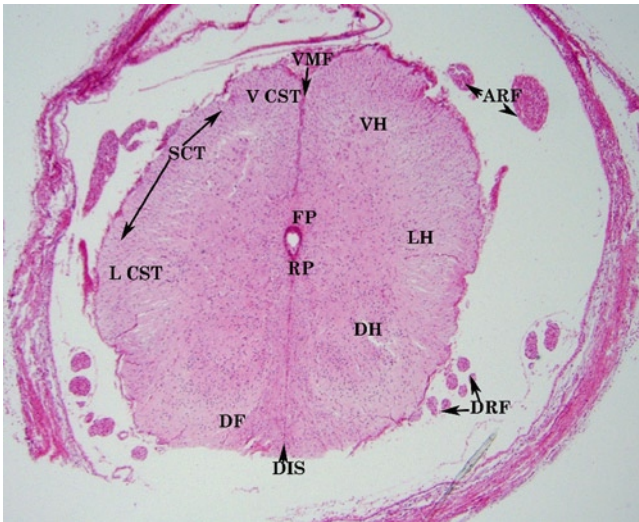


FIGURE 27-34. Spinal cord at GW 20. This image of the spinal cord shows the ventral median fissure (VMF); dorsal intermediate septum (DIS); the central canal with roof plate (RP) and floor plate (FP); neurons in the anterior/ventral horn (VH), lateral horn (LH), and dorsal horn (DH); the ascending and descending fiber tracts, spinocephalic and spinocerebellar tracts (SCT); ventral/anterior and lateral corticospinal tracts (V CST, L CST), and the dorsal funiculus (DF). The anterior root fibers (ARF) and dorsal root fibers (DRF) are also seen. (H&E, 4×.)

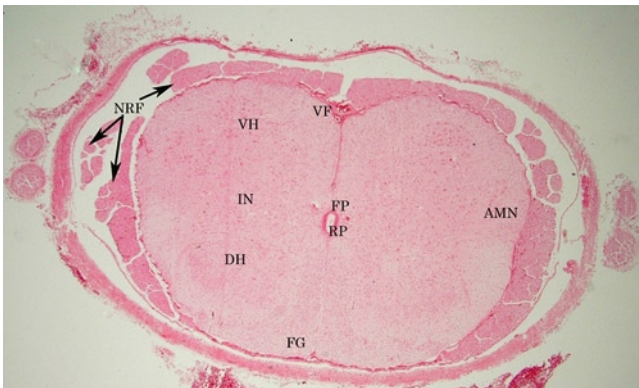


FIGURE 27-35. Spinal cord at GW 22. The spinal cord is shown with the roof plate (RP) and floor plate (FP) adjacent to the central canal, neurons in the anterior/ventral horn (VH), intermediate interneurons (IN), autonomic motoneurons (AMN), and the dorsal horn (DH). The white matter tracts are seen in the ventral funiculus (VF) adjacent to the ventral median fissure and the fasciculus gracilis (FG) adjacent to the dorsal median septum. Cross-sections of the anterior and dorsal nerve root fibers (NRF) are seen adjacent to the cord. (H&E, 2×.)

GW 23 to GW 28

The cortical periventricular neuroepithelial cell layer is thick and produces neurons and glia in all the lobes. Migrating cells are visible in all the lobes (see Fig. 27-36). The basic six layers of the cortex are seen by GW 26 to GW 29 (see Fig. 27-37). The subpial granular layer increases in thickness in some areas up to GW 26, while it disappears almost entirely in other areas. The cells of the subpial granular layer give rise to neurons and glia while a significant number undergo developmental cell death. The thalamic and basal forebrain efferents penetrate the cortical plate and assume a columnar distribution by GW 24 to GW 28. Glial hypercellularity can be seen by GW 24 in the hemispheric white matter. It continues to increase during late gestation into the early postnatal period. The proliferative glia can be highlighted on a glial fibrillary acidic protein (GFAP) immunostain (see Figs. 27-38 and 27-39) [21]. Myelination is mostly absent in the white matter at this gestational age (see Fig. 27-40) [13]. In the hippocampus, most of the pyramidal neurons in Ammon's horn are formed by GW 24. The cytoarchitectural pattern of pyramidal neurons in the Ammon's horn is well established by GW 23 to 25 [15]. In the basal ganglia, the neuroepithelial cell layer over some portions of the caudate nucleus is scant (see Fig. 27-41) while that overlying the striatum and nucleus accumbens is

thick. Glial hypercellularity is seen in the internal capsule (see Fig. 27-42). Neurons in the thalamus appear to be mature. The external granular layer covering the cerebellar cortex is actively proliferating and producing basket, stellate, and granule cells (see Fig. 27-43). Descent of cells from this layer to form the internal granular layer begins after the Purkinje cells begin to have dendrites. Purkinje cells have their typical appearance by GW 28 and they continue to migrate through the internal granular layer. The dentate nuclei are well formed by GW 25. The gliependymal lining of the cerebral aqueduct in the midbrain and anterior fourth ventricle is convoluted, while that of the remaining fourth ventricle is smooth. In the pons, before GW 27, the cells of the pontine nuclei are immature progenitor cells with scant cytoplasm and indistinct nucleoli. By GW 28, the cells are larger and more differentiated with a pale nucleus and distinct large nucleolus. The medulla shows well-formed corticospinal tracts and inferior olivary nucleus complex (see Fig. 27-44). By GW 24 to 28, myelination can be seen in some of the tracts in the tectum and tegmentum [21]. The spinal cord shows expansion of the dorsal funiculus with increased cellularity in the cuneate fasciculus (see Fig. 27-45 and Fig. 27-46). Some myelination can be seen in the dorsal funiculus (see Fig. 27-47) [6, 14].

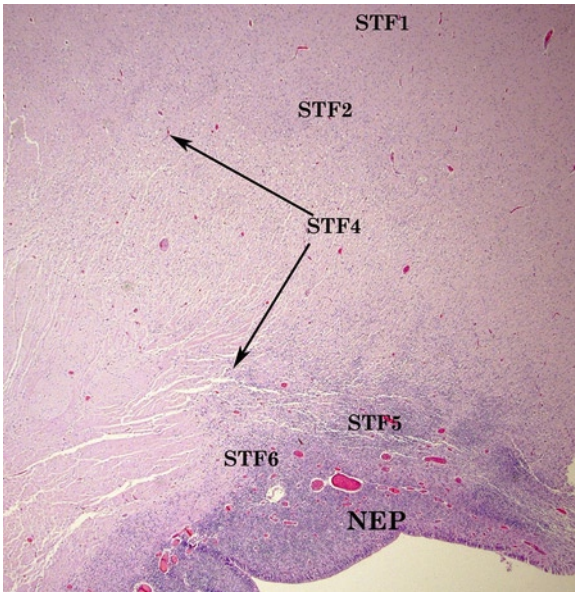


FIGURE 27-36. Cerebral cortex at GW 25. Periventricular region at GW25. Persistent germinal matrix containing cells of the neuroepithelium and subventricular zone (NEP) is shown. The layers of stratified transitional fields (STF) can be identified as follows: STF6—deep layer adjacent to the germinal matrix containing callosal fibers; STF5—deep cellular layer that is the first sojourn for migrating cells; STF4—cells and fibers intermingle to form striations; STF2—upper cellular layer that is the last sojourn before cells move into the cortical plate; STF1—superficial fibrous layer with cells migrating through to the cortical plate. (H&E, 2×.)

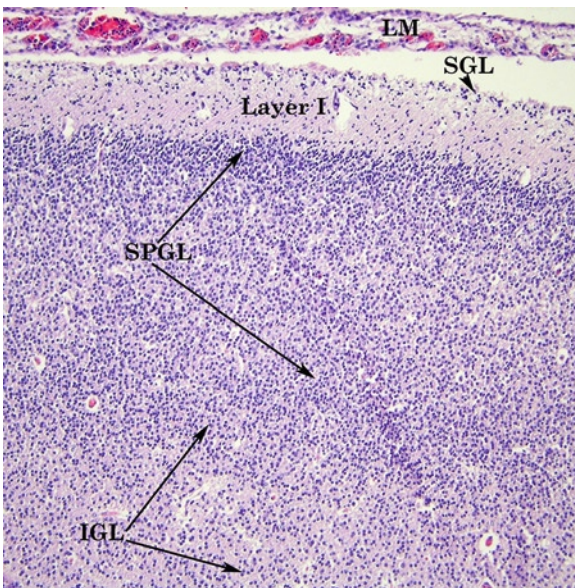


FIGURE 27-37. Cerebral cortex at GW 25. This higher magnification is of the cortical plate with scant subpial granular layer (SGL) below the leptomeninges (LM). The adjacent molecular layer (Layer I) contains occasional Cajal-Retzius neurons. The granular/supragranular (SPGL) layers contain the recently migrated neurons of layers II, III, and IV. The infragranular layer (IGL) contains layers V (darker) and VI neurons. (H&E, 10×.)

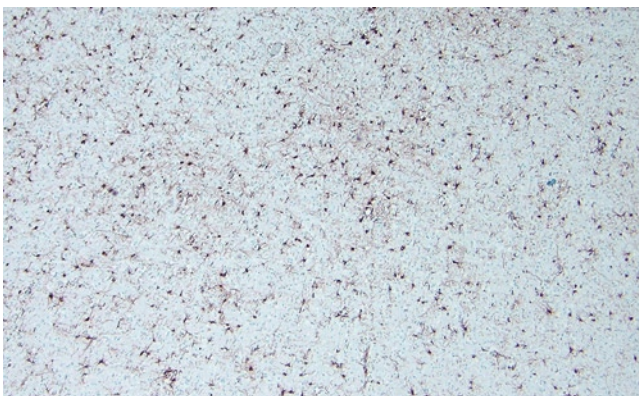


FIGURE 27-38. White matter at GW 25. GFAP immunostain highlights the proliferating glia in the cortical white matter. (GFAP, 4×.)

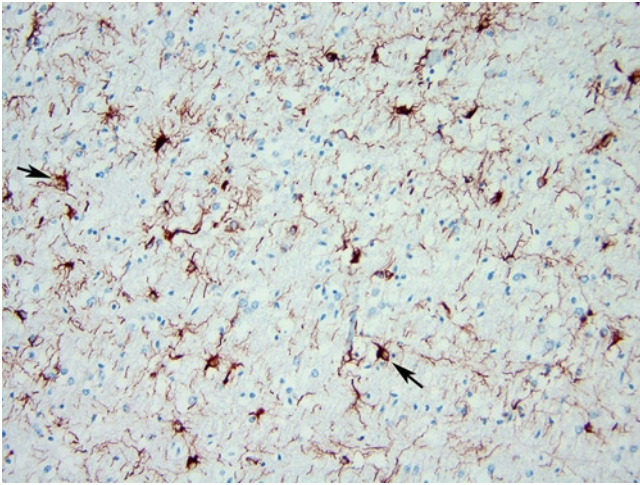


FIGURE 27-39. White matter at GW 25. This higher magnification shows some of the cells with larger, pale nuclei and scant cytoplasm, consistent with myelination glia (arrows). (GFAP, 20 \times .)

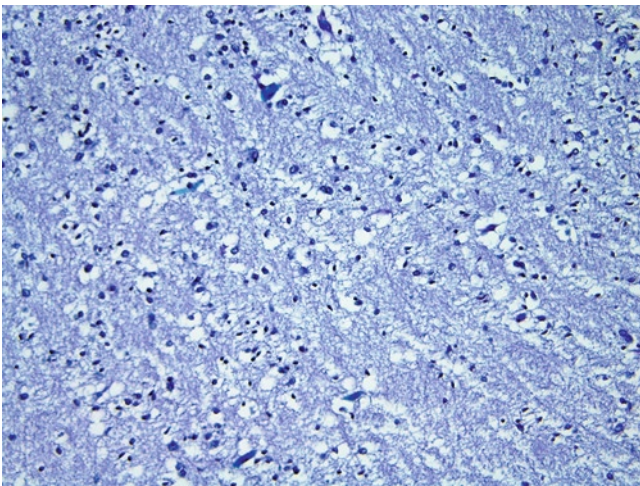


FIGURE 27-40. White matter at GW 25. This Luxol fast blue (LFB) image shows a lack of myelination. (LFB/periodic acid-Schiff [PAS], 20 \times .)

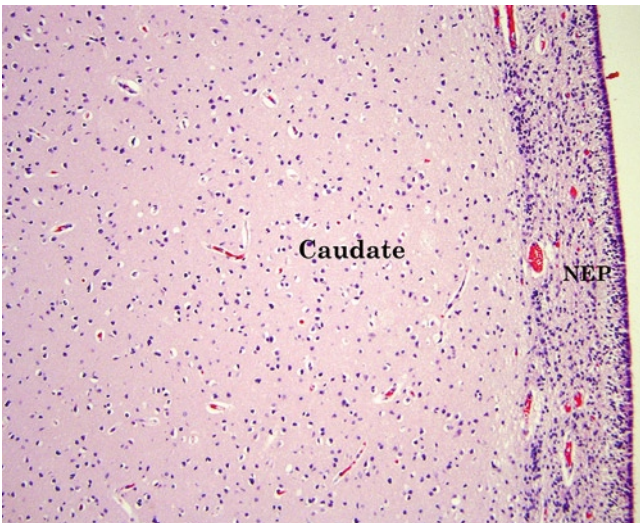


FIGURE 27-41. Basal ganglia at GW 27. This basal ganglia section shows scant cellularity of the neuroepithelium (NEP) and sub-ventricular zone with maturing neurons in the caudate nucleus. (H&E, 2 \times .)

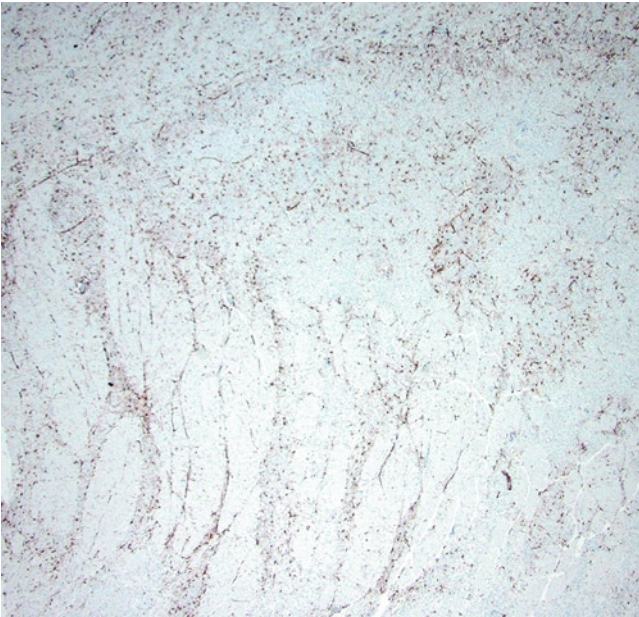


FIGURE 27-42. Proliferating glia. This GFAP immunostain highlights the proliferating glia in the internal capsule and basal ganglia matter. (GFAP, 2 \times .)

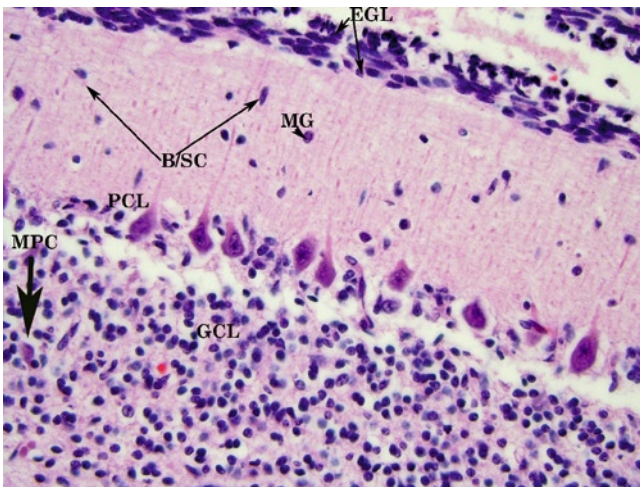


FIGURE 27-43. Cerebellar cortex at GW 25. Cerebellar cortex has an external germinal/granular layer (EGL) containing proliferative and migrating cells, migrating granule cells (MG), settled granule cells in the internal granular layer (GCL), migrating Purkinje cells (MPC), and settled Purkinje cells in the Purkinje cell layer (PCL). The molecular layer contains settling basket and stellate cells (B/SC). (H&E, 40 \times .)

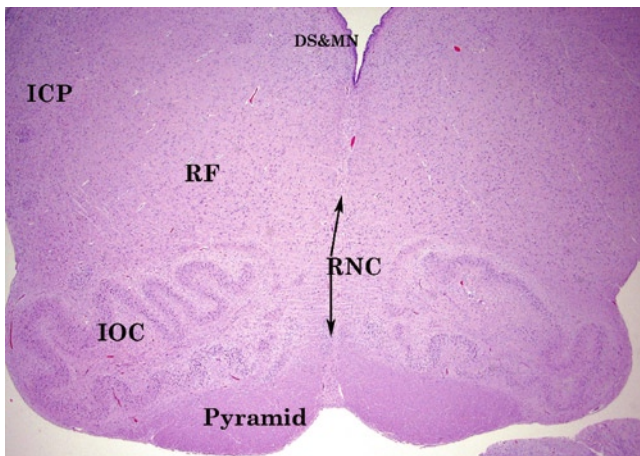


FIGURE 27-44. Medulla at GW 25. This section of medulla shows well-formed corticospinal tracts (pyramids) and inferior olivary complex/nucleus (IOC). Other structures that can be identified are the raphe nuclear complex (RNC), dorsal sensory and motor nucleus (DS&MN) of the Xth nerve, the reticular formation (RF), and the inferior cerebellar peduncle (ICP). (H&E, 2 \times .)

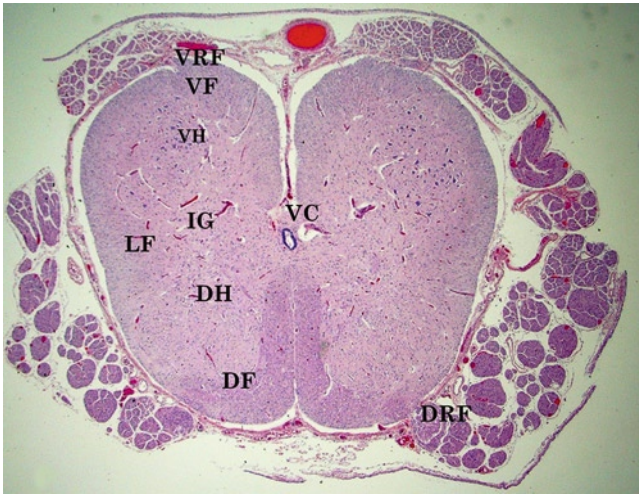


FIGURE 27-45. Spinal cord at GW 25. Spinal cord section showing well-formed ventral (VH), intermediate (IG), and dorsal (DH) gray matter containing mature neurons. The white matter tracts are easily identified in the ventral funiculus (VF) containing the ventral corticospinal tract, vestibulospinal tract, and some of the spinocephalic tracts; the lateral funiculus (LF) contains the rest of the spinocephalic and spinocerebellar tracts, and the lateral corticospinal tracts; the dorsal funiculus (DF) contains the fasciculus gracilis and cuneatus. The ventral commissure (VC) contains gray matter adjacent to the central canal and crossing fibers of the white matter superficially. The ventral (VRF) and dorsal root fibers (DRF) are seen exiting/entering the cord. (H&E, 2 \times .)

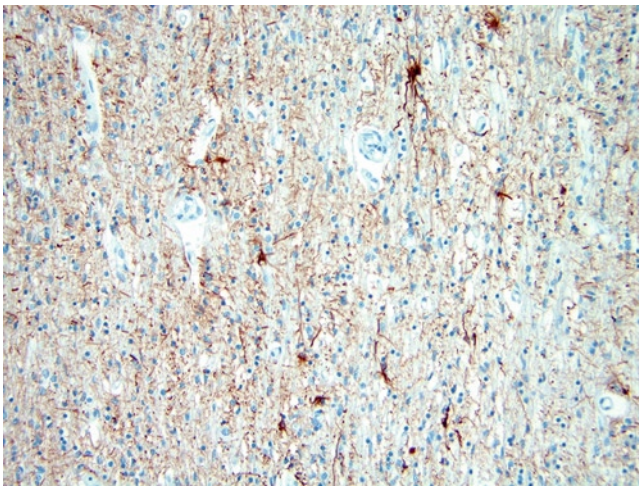


FIGURE 27-46. Spinal cord at GW 25. This GFAP immunostain highlights a few proliferating glia in the spinal cord. (GFAP, 20 \times .)

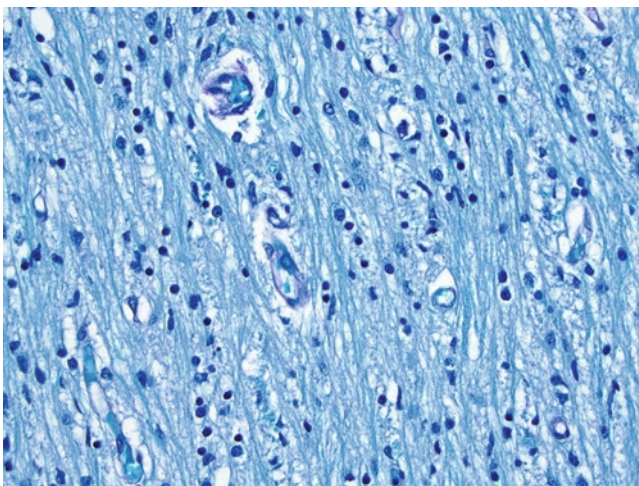


FIGURE 27-47. Spinal cord at GW 25. This LFB stain shows myelination around some of the axonal fibers (longitudinal section). (LFB/PAS, 40 \times .)

GW 29 to GW 33

In this gestational period, the subpial granular layer is scant or absent over the cerebral cortex. Cajal-Retzius cells disappear from the marginal zone by GW 30. A few migrating and sojourning neurons are seen in the stratified transitional fields. The basic six layers of the cortex are well established by GW 32 (see Fig. 27-48) [22]. There is increased cellularity in the white matter secondary to "myelination gliosis" (see Figs. 27-49 and 27-50), but a paucity of myelination in the cerebral cortex (see Fig. 27-51) [13]. In the basal ganglia, the neuroepithelial cell layer is thick over the striatum (see Fig. 27-52) and nucleus accumbens. There is increased cellularity in the internal capsule with myelination gliosis that is highlighted by GFAP immunostain (see Fig. 27-53) and a paucity of myelination as highlighted by LFB/PAS stain (see Fig. 27-54). The choroid plexus shows the characteristic "hob-nail" pattern of

the lining cells. The cells themselves show a decrease in glycogen content and have an "adult-type" appearance (see Fig. 27-55). Neurons in the thalamus are settled and maturing. The midbrain, pons, and medulla show a slightly convoluted glioependymal layer around the aqueduct and anterior part of the fourth ventricle while the rest of the fourth ventricle has a smooth lining. [22]. In the cerebellum, the external granular layer has the highest proliferation of cells between GW 28 and GW 34. The cerebellar cortex itself is less defined between the hemispheric lobules. The Purkinje cell layer can be identified though the Purkinje cells continue to migrate through the internal granular layer (see Fig. 27-56). The molecular layer is better defined (see Fig. 27-57) [19,20]. The spinal cord shows expansion and increased myelination in the dorsal funiculus (see Fig. 27-58) [6].

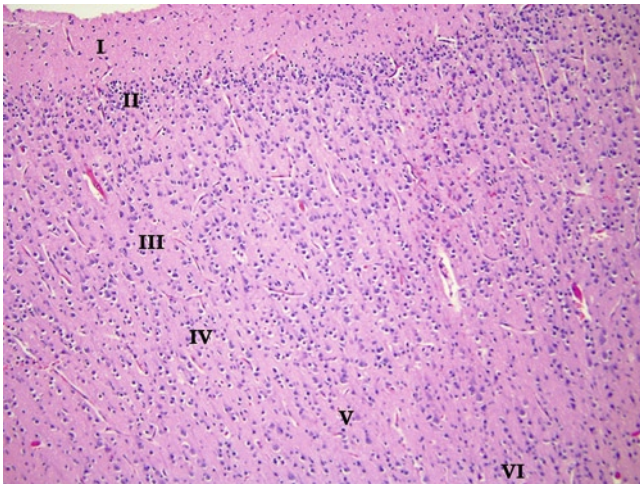


FIGURE 27-48. Cerebral cortex at GW 32. The cerebral cortex shows scant or absent subpial granular layer. The six layers of the cerebral cortex can be identified with maturation of the neurons in most of the layers. The latest arriving immature neurons are seen settling in layer II. (H&E, 10 \times .)

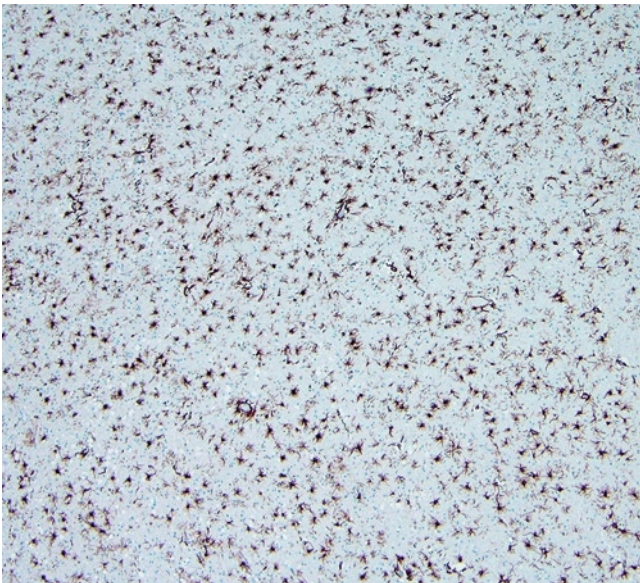


FIGURE 27-49. Cerebral cortex at GW 32. This GFAP immunostain highlights an increase in proliferating glia in the cortical white matter. (GFAP, 4 \times .)

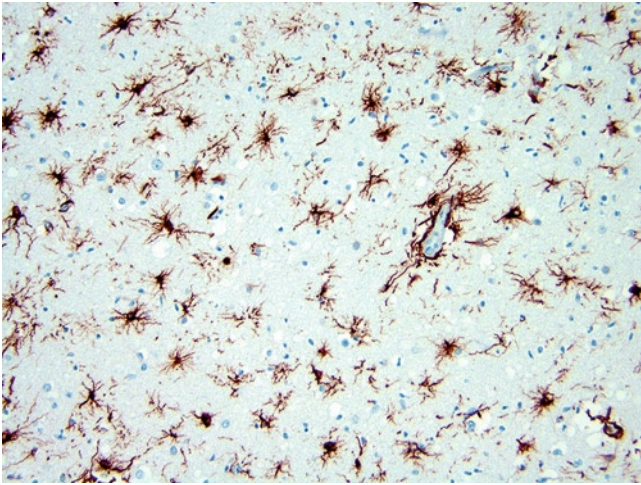


FIGURE 27-50. Cerebral cortex at GW 32. This higher magnification of a GFAP stain shows a relative increase in "myelination glia" compared to Figure 27-38. (GFAP, 20 \times .)

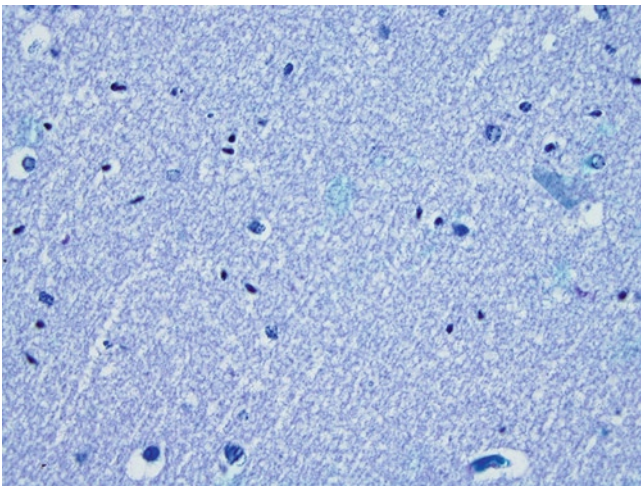


FIGURE 27-51. Cerebral cortex at GW 32. This LFB stain shows the lack of myelination. (LFB/PAS, 40 \times .)



FIGURE 27-52. Basal ganglia at GW 32. Persistent neuroepithelium/subventricular zone cells (NEP) are adjacent to the caudate nucleus with maturing neurons and the internal capsule (IC). (H&E 2 \times .)



FIGURE 27-53. Basal ganglia at GW 32. This GFAP stain shows an increase in proliferating glial cells in the basal ganglia. (GFAP, 2 \times .)

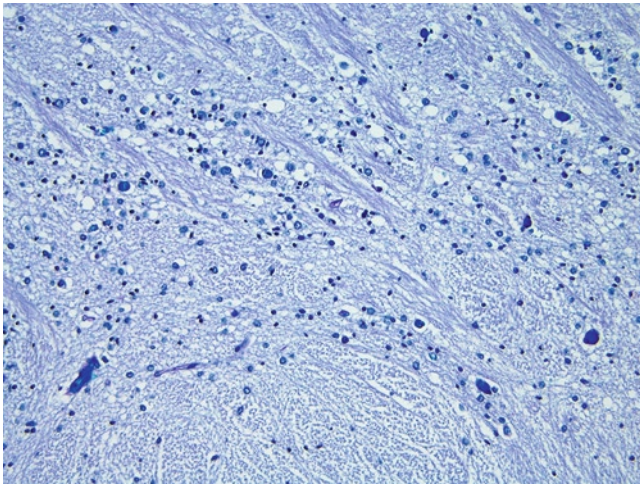


FIGURE 27-54. Basal ganglia at GW 32. This LFB/PAS stain shows the lack of onset of myelination. (LFB/PAS, 20 \times .)

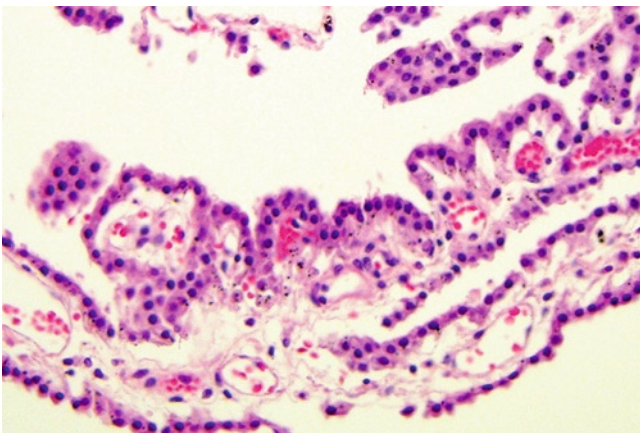


FIGURE 27-55. Choroid plexus at GW 32. The choroid plexus shows a decrease in glycogen content of the lining cells with some "hob-nailed" appearance of the surface. (H&E, 20 \times .)

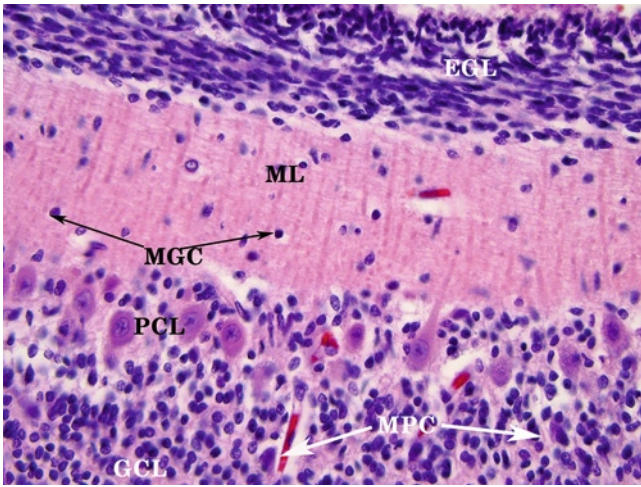


FIGURE 27-56. Cerebellum at GW 30. The cerebellar cortex shows a predominantly well-formed Purkinje cell layer (PCL) and internal granular layer (GCL). A few migrating Purkinje cells (MPC) can still be identified in the GCL. There are migrating granule cells (MGC) from the external germinal/granular layer (EGL) in the molecular layer (ML). (H&E, 40 \times .)

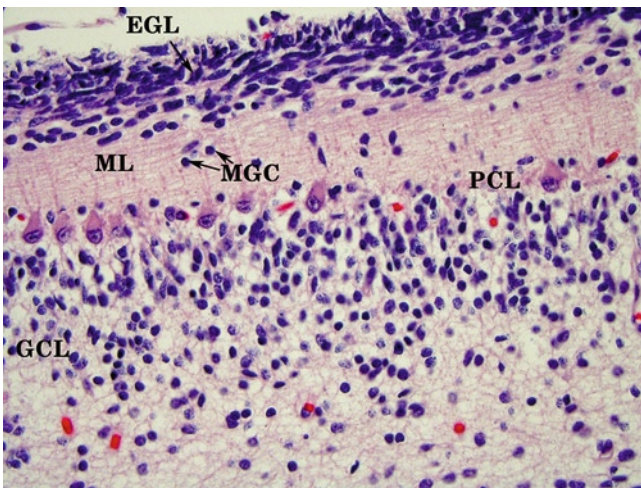


FIGURE 27-57. Cerebellum at GW 32. The cerebellar cortex shows a persisting external germinal/granular layer (EGL) with migrating granule cells (MGC) in the molecular layer (ML). The Purkinje cell layer (PCL) shows well-settled Purkinje cells with apical caps and migrating Purkinje cells are seen in the granular layer (GCL). (H&E, 40 \times .)

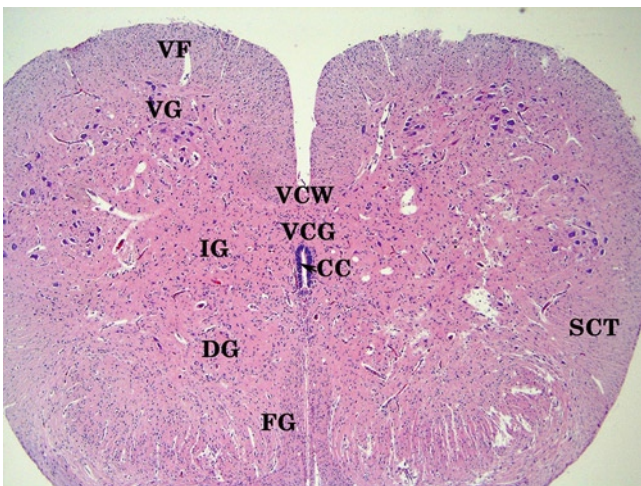


FIGURE 27-58. Spinal cord at GW 30. Spinal cord is shown with anterior/ventral (VG), intermediate (IG), and dorsal gray matter (DG), as well as the central canal (CC) with ventral gray (VCG) and white matter commissures (VCW). The white matter tracts in the ventral funiculus (VF) (ventral corticospinal tract and vestibulospinal tracts, some spinocephalic tracts), lateral (SCT) spinocephalic, spinocerebellar, and lateral corticospinal tracts. The posterior (FG) superficial and deep fasciculus gracilis are better defined with increase in myelination. (H&E, 4 \times .)

GW 34 to GW 38

The subpial granular layer of the cerebral cortex is scant or absent over most of the lobes (see Figs. 27-59–Fig. 27-61). The marginal zone is still cellular but the Cajal-Retzius cells are absent. There is a persistent neuroepithelial layer in all the lobes generating neurons and glial cells. There are migrating and sojourning neurons in the stratified transitional fields. The subplate is highly developed in the somatosensory cortex and is small in the primary visual cortex. After GW 35 the subplate decreases in thickness [22]. The white matter shows increased cellularity due to “myelination gliosis” (see Figs. 27-62 and 27-63) but myelination has not begun (see Fig. 27-64). In the hippocampus, most of the granule cells are formed by GW 34 but granule cell proliferation and migration continues (see Fig. 27-65) [15]. The neuroepithelial cell layer over the basal ganglia is scant, but remains visible over the striatum (see Fig. 27-66) and nucleus accumbens. There is an increase in myelination glia in the internal capsule and there may be the onset of myelination in some of the fibers in the internal capsule (see Figs. 27-67 and 27-68). Neurons

in the thalamus are settled and maturing [9,22]. In the midbrain, pons, and medulla, there is a slightly thicker gliependymal layer lining the posterior aqueduct and anterior fourth ventricle than the posterior part of the fourth ventricle. Myelination is seen in the trapezoid body and auditory system, medial longitudinal fasciculi, ansa lenticularis, optic chiasm and tract, and cranial nerves toward the end of final trimester [6]. In the cerebellum after GW 34, most of the granule cell proliferation occurs in the internal granular layer. The external granular layer is still prominent over the entire cerebellar cortex (see Figs. 27-69 and 27-70) [22]. In the spinal cord, the ventral motoneurons are well segregated, the lateral motoneurons and Clarke's column are prominent, and clusters of small neurons are identified in the substantia gelatinosa (dorsal horn). Penetrating myelinated fibers can be seen in the dorsal horn. Myelinated fibers can be seen on special stains (LFB with PAS) in the dorsal funiculus and some myelination is seen in the ventral and lateral funiculi (see Figs. 27-71 and 27-72) [6,13].

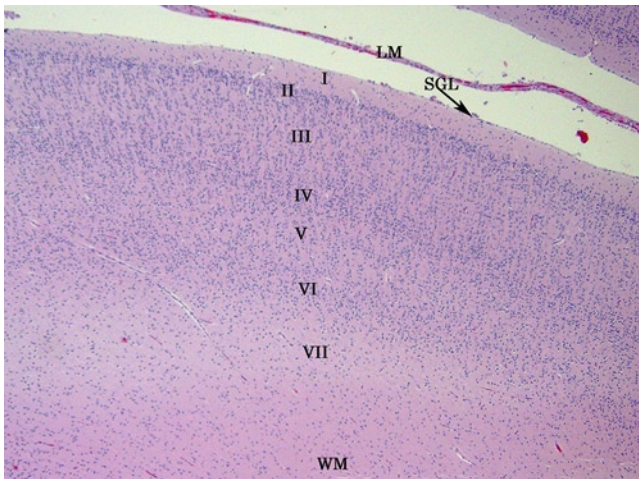


FIGURE 27-59. Cerebral cortex at GW 35, frontal cortex. This section shows the leptomeninges (LM), underlying scant, interrupted subpial granular layer (SGL) in the frontal cortex with well-defined cortical layers I to VI. Layer VII represents the subplate and WM the adjacent white matter. (H&E, 2 \times .)

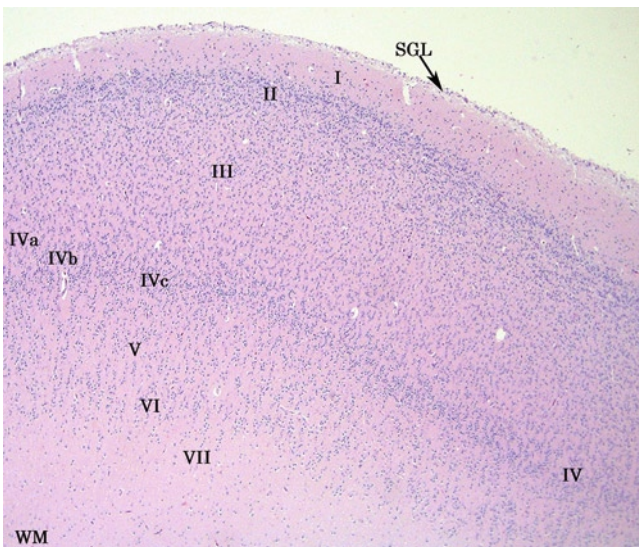


FIGURE 27-60. Cerebral cortex at GW 35, occipital/striate cortex. The cortical layers (I–VII) are well defined and early separation of layer IV into three layers by the optic radiation is seen in the striate cortex. The subpial granular layer (SGL) is seen as a very thin continuous layer. WM—white matter. (H&E, 2 \times .)

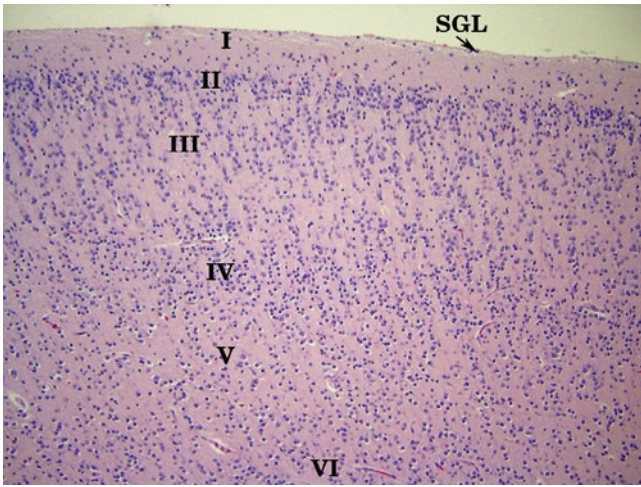


FIGURE 27-61. Cerebral cortex at GW 35, frontal cortex. This higher power image shows a scant, interrupted subpial granular layer (SGL) in the frontal cortex and well-defined cortical layers (I–VI). (H&E, 10×.)

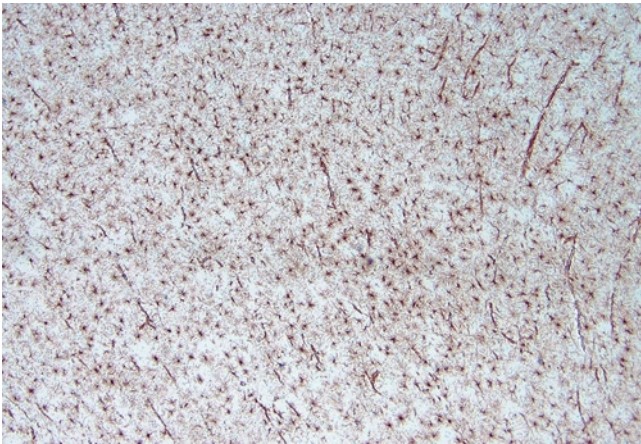


FIGURE 27-62. Cerebral cortex white matter at GW 35. This GFAP immunostain shows increased "myelination" gliosis. (GFAP, 4×.)

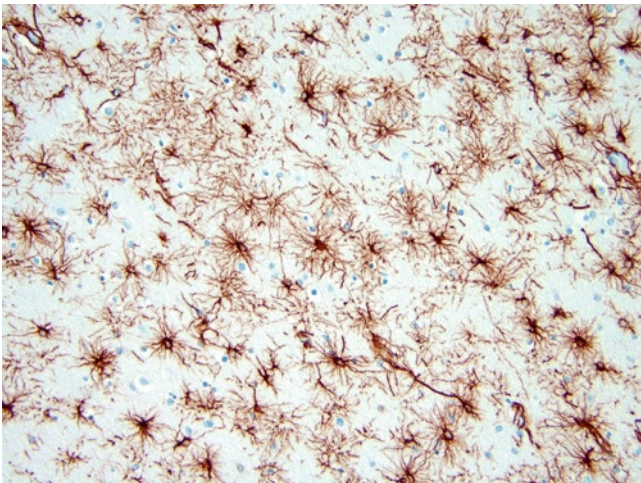


FIGURE 27-63. Cerebral cortex white matter at GW 35. This higher magnification of a GFAP immunostain showing the "myelination" glial cell with large pale nuclei and scant cytoplasm. (GFAP, 20×.)

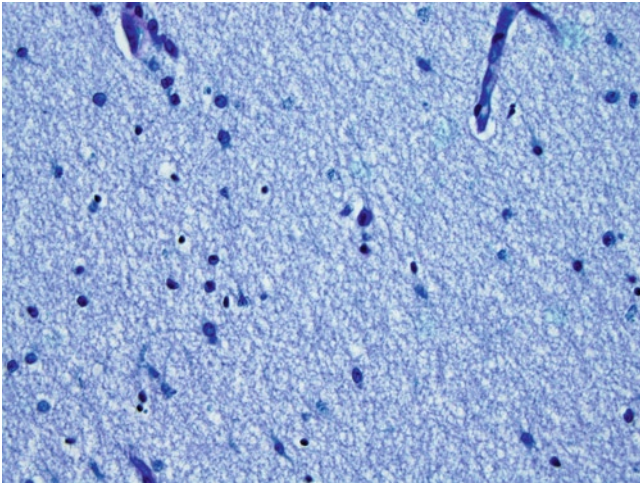


FIGURE 27-64. Cerebral cortex white matter at GW 35. This LFB stain image shows a lack of onset of myelination. (LFB/PAS, 40 \times .)

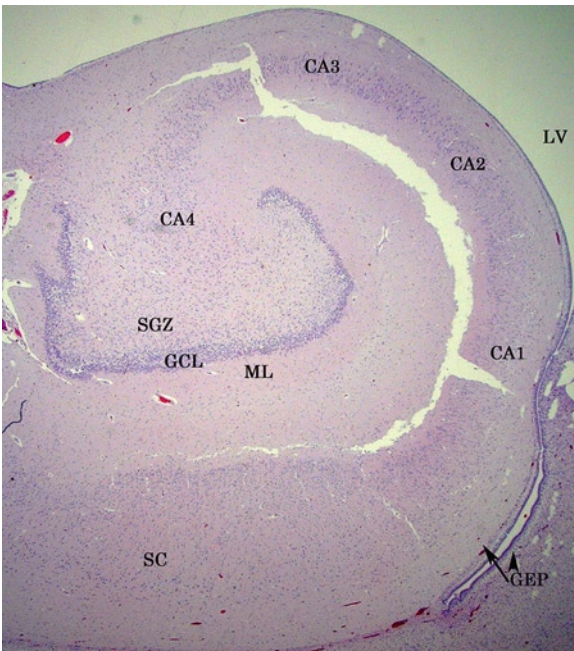


FIGURE 27-65. Hippocampus at GW 35. This section of the hippocampus shows the granular cells in the dentate fascia (GCL) with the subgranular zone (SGZ) still identified. The molecular layer (ML) and the pyramidal layer of the hippocampus with CA4, CA3, CA2, and CA1 can be identified, along with part of the subiculum (SC). There is scant subventricular neuroepithelium/glioependymal layer (GEP) adjacent to the lateral ventricle (LV). CA—Cornu Ammonis. (H&E, 2 \times .)

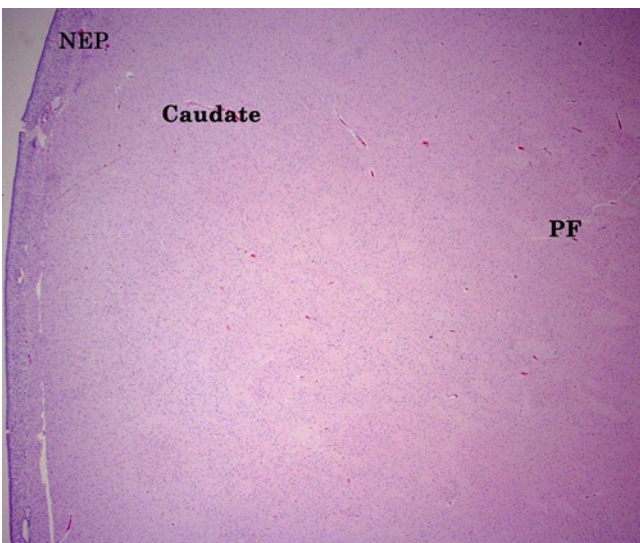


FIGURE 27-66. Basal ganglia at GW 35. Basal ganglia is shown with scant neuroepithelial cells (NEP) in the subventricular zone and pencil fibers (PF) traversing the caudate nucleus. (H&E, 2 \times .)

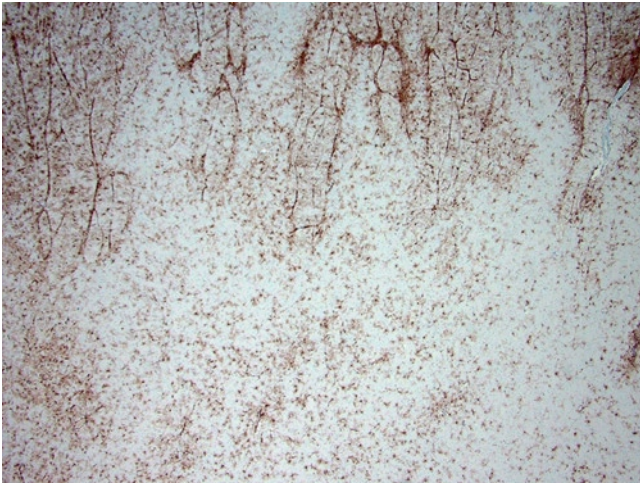


FIGURE 27-67. Basal ganglia at GW 35. This GFAP immunostain shows increased glial proliferation in the internal capsule. (GFAP, 2 \times .)

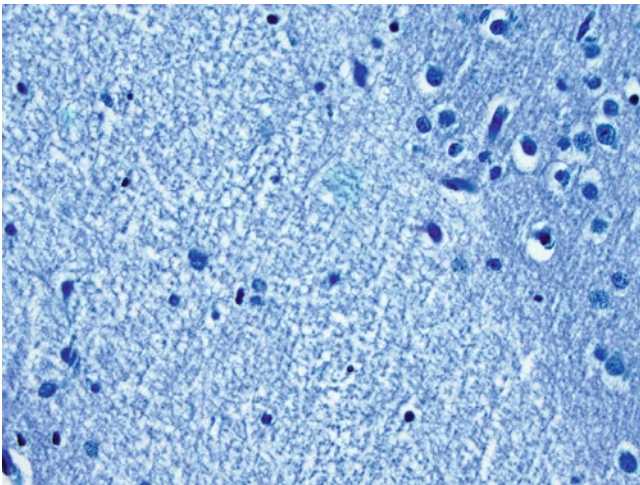


FIGURE 27-68. Basal ganglia at GW 35. This LFB stain image shows the possible onset of myelination in the internal capsule. (LFB/PAS, 40 \times .)

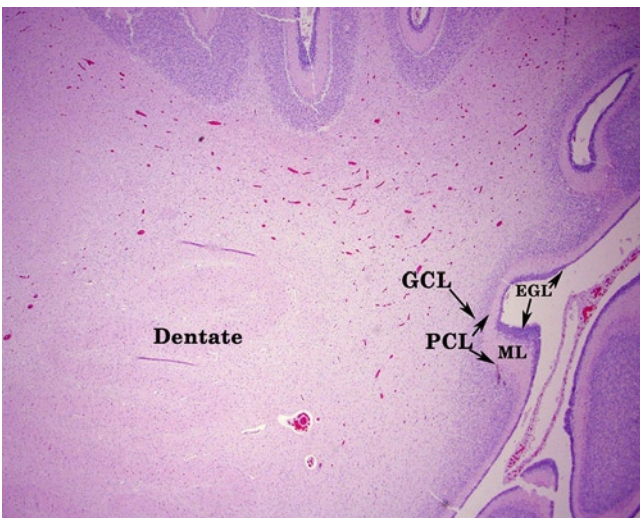


FIGURE 27-69. Cerebellum at GW 35. This image of the cerebellum with well-formed folia shows persistent external granular/germinal layer (EGL), molecular layer (ML), Purkinje cell layer (PCL), and internal granular layer (GCL). The dentate nucleus is easily identified and the white matter shows normal vascular pattern. (H&E, 2 \times .)

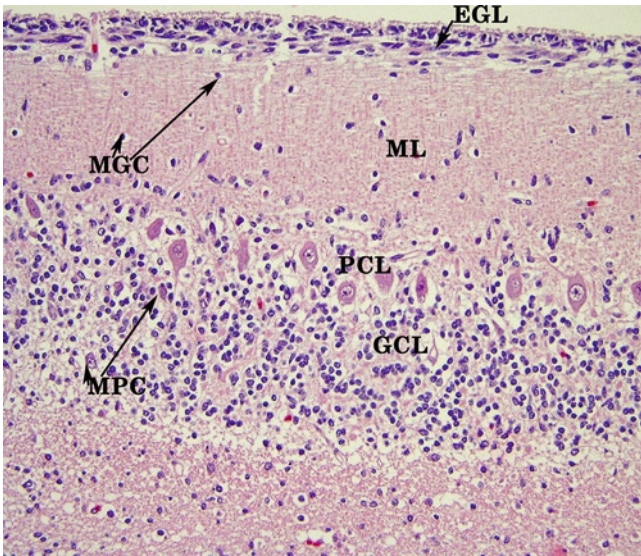


FIGURE 27-70. Cerebellum at GW 35. This higher magnification shows the layers with migrating granule cells (MGC) in the molecular layer and migrating Purkinje cells (MPC) in the internal granular layer. EGL—external granular/germinal layer; GCL—internal granular layer; ML—molecular layer; PCL—Purkinje cell layer. (H&E, 20 \times .)

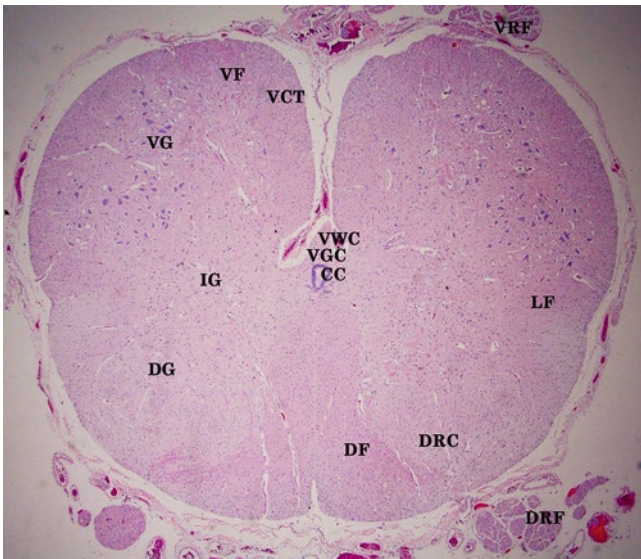


FIGURE 27-71. Spinal cord at GW 35. This image of the spinal cord shows the ventral (VG), intermediate (IG), and dorsal gray (DG) matter with the ventral gray commissure (VGC) adjacent to the central canal (CC) and the ventral white commissure (VWC). The ventral corticospinal tracts (VCT), vestibulospinal tracts, and part of the spinocephalic tracts are seen in the ventral funiculus (VF). The lateral funiculus (LF) contains the lateral corticospinal tracts, intraspinal tracts, and the spinocephalic tracts. The dorsal funiculus (DF) contains the fasciculus gracilis and fasciculus cuneatus, and the dorsal root collateralization zone (DRC). The dorsal root fibers (DRF) and ventral root fibers (VRF) can be seen. (H&E, 2 \times .)



FIGURE 27-72. Spinal cord at GW 35. **A**, This GFAP immunostain shows relatively increased glial cells in the ventral funiculi (darker staining) compared to the dorsal funiculi. (GFAP, 2 \times .) **B**, This LFB stained image with PAS shows myelination in the dorsal funiculi and some of the ventral and lateral tracts. The ventral and dorsal root fibers are myelinated. (LFB/PAS, 2 \times .)

Term

By term the marginal zone in the cerebral cortex is sparsely cellular in most areas. The cortical layers are well established (see Fig. 27-73). The subplate continues to decrease in thickness and disappears by the first postnatal month. A reduction in the thickness of the subplate begins in the depth of sulci and later in the crown of gyri [1,7]. The hemispheric white matter increases in thickness (see Figs. 27-74 and 27-75) but myelination has not begun. A prominent neuroepithelium/subventricular zone may still be present over the striatum (see Fig. 27-76) and nucleus accumbens. Streams of migrating neurons and glia can be seen in the lateral migratory stream. Most of the neurons and glia in the diencephalon are settled. Near term, myelination can be seen in the central portions of the hemispheric white matter under the sensory-motor strip and in the posterior limb of the internal capsule associated with a slight decrease in cellularity of the myelination glia (see Fig. 27-77). The dentate granular layer is better formed in the hippocampus, though proliferation in the

granular layer is still ongoing (see Fig. 27-78). In the cerebellum the thickness of external granular layer remains constant from GW 28. The internal granular layer and central white matter increase in thickness consistently through gestation. The Purkinje cell layer is well defined (see Fig. 27-79) [22]. The nuclear groups of the brainstem nuclei are well established and the neurons are well differentiated, including those in the pons. Myelination of many of the fiber tracts can be identified. In the spinal cord gray matter, the ventral motoneurons are well segregated, the lateral motoneurons and Clarke's column are prominent, and clusters of small neurons are identified in the substantia gelatinosa (dorsal horn). Penetrating myelinated fibers can be seen in the dorsal horn. By the end of this trimester, myelination is almost complete in the dorsal funiculus and is progressing well in the rest of the tracts [6]. The glial cellularity starts to decrease in these tracts. The ventral and lateral corticospinal tracts are still sparsely cellular and not myelinated [12,13].

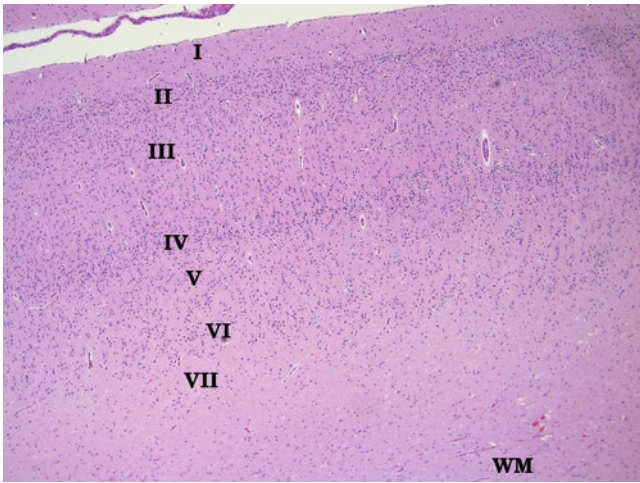


FIGURE 27-73. Cerebral cortex at term. Shown is the cerebral cortex showing the cortical layers (I–VI) with sparse cellularity in the molecular layer (I) and the subplate (VII). WM—white matter. (H&E, 2 \times .)

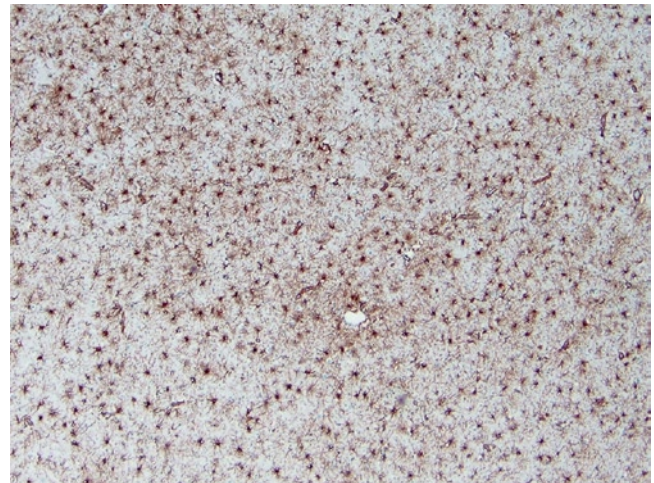


FIGURE 27-74. White matter at term. This GFAP immunostain shows some decrease in cellularity in the white matter compared to Figure 27-62. (GFAP, 2 \times .)

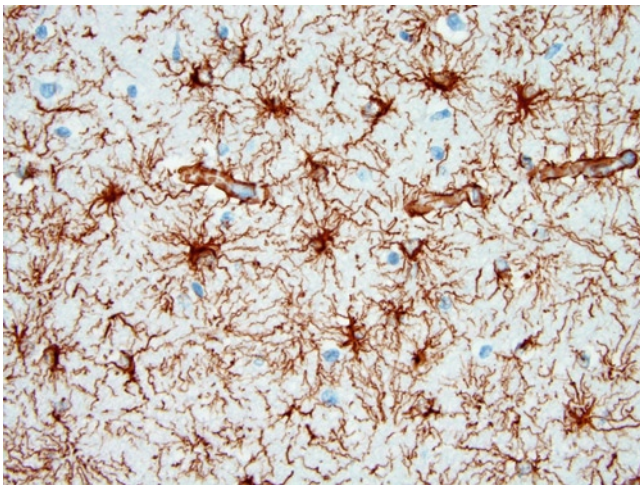


FIGURE 27-75. White matter at term. This higher magnification shows a predominance of "myelination" glia with large pale nuclei and scant cytoplasm. (GFAP, 40 \times .)

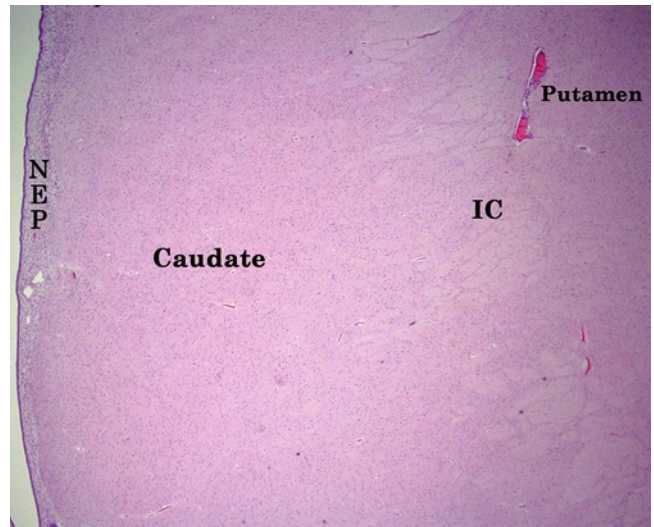


FIGURE 27-76. Basal ganglia at term. Basal ganglia with sparse proliferating neuroepithelial cells (NEP) are shown in the sub-ventricular zone. The internal capsule (IC) is separating the caudate from putamen with crossing fibers seen between the two. (H&E, 2 \times .)

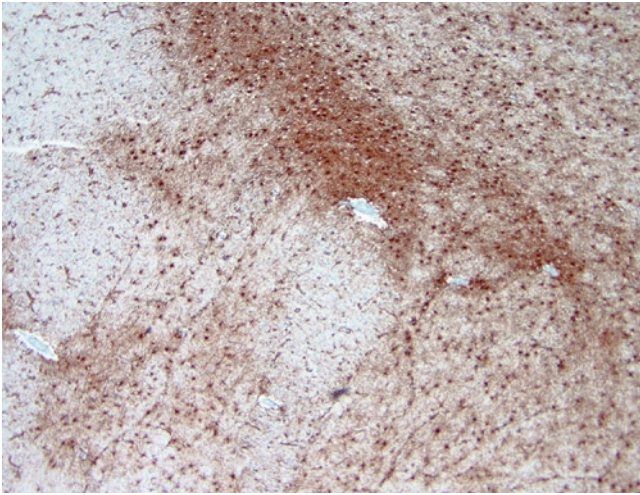


FIGURE 27-77. Basal ganglia at term. This GFAP immunostain shows some decrease in cellularity in the internal capsule and basal ganglia. (GFAP, 4 \times .)

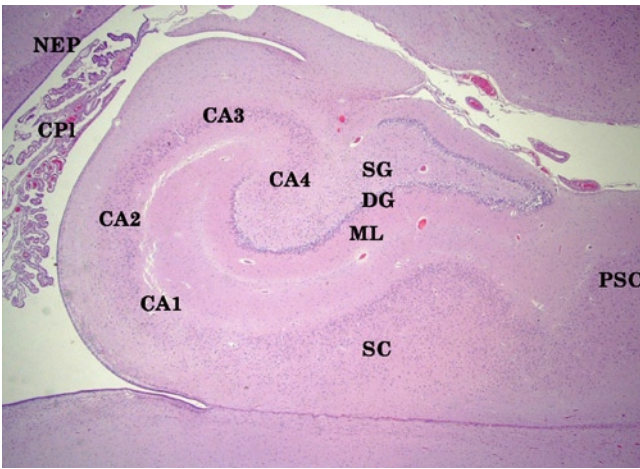


FIGURE 27-78. Hippocampus at term. The hippocampus with the dentate granule layer (DG) is better formed as compared to that seen at GW 35. The subgranular zone (SG) and molecular layer (ML) are present and the pyramidal cells of the hippocampus and Ammon's horn (CA1 to 4) are well developed. The subiculum (SC) and presubiculum (PSC) is seen. The choroid plexus (CPI) is seen in the lateral ventricle and the adjacent neuroepithelium/glioependymal layer (NEP) is sparsely cellular. (H&E 2 \times .)

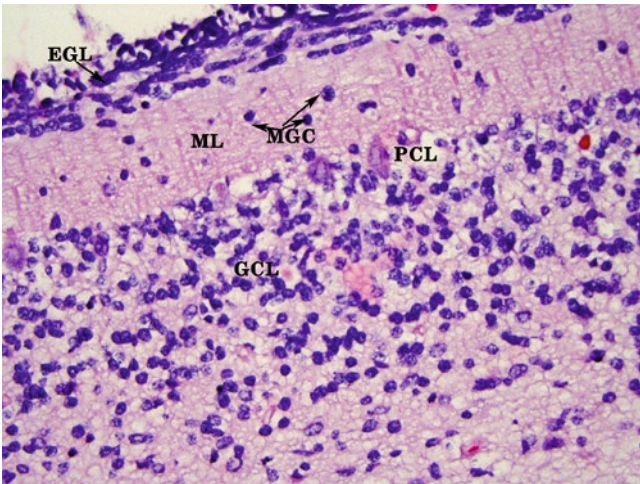


FIGURE 27-79. Term: cerebellum with persistent external granular layer (EGL) with migrating granular cell (MGC) in the molecular layer (ML). The Purkinje cell layer (PCL) and the internal granular cell layer (GCL) are well demarcated. (H&E, 40 \times .)

Postnatal

The marginal zone is sparsely cellular at birth and the cortical layers are well formed (see Figs. 27-80 and 27-81). Neurons in the cortical layers are maturing and migrating neurons/glia cells are seen in the stratified transitional fields for the first few months postnatally. The subplate disappears by the first postnatal month and subplate neurons persist in adult brain white matter as interstitial neurons. Active neurogenesis persists in adults in the subventricular zone around the lateral ventricles [1]. In the hippocampus, granule cell proliferation and migration continues throughout gestation and postnatally up to 8 months of age [15]. Neurogenesis persists in the granular layer throughout adult life. By the end of first postnatal month, myelination can be seen in the cingulum and optic radiation. White matter cellularity seems to decrease with the onset of myelination (see Figs. 27-82 and 27-83). Myelination in the hemispheric white matter proceeds frontally and occipitally from the areas subjacent to the central sulcus. Myelination in the temporal cortex may be seen near the end of the first postnatal year and is similar to that seen in adults by the end of the second year of life (see Fig. 27-84). The basal ganglia and diencephalic neurons are well settled and myelination of the internal capsule is complete by 6 months postnatally (see Figs. 27-85–27-87) [13,14]. The midbrain, pons, and medulla are fully formed and neurogenesis is

not identified by the end of first postnatal month. Pigmentation of the neurons in the substantia nigra, locus ceruleus, and dorsal vagal nucleus is not visible for the first 5 years of postnatal life. In the cerebellum, external granular layer continues to proliferate at a lower rate up to 8 months postnatally. The thickness of external granular layer then decreases (see Fig. 27-88) and completely disappears by 1 year after birth (see Fig. 27-89). The internal granular layer and central white matter increase in thickness consistently throughout gestation and during the first year of life [22]. Myelination of the white matter in the parasagittal areas can be seen toward term. Following birth, there is maturation of the spinal cord and early myelination with increased glial cellularity in the corticospinal tracts can be seen a few days after birth. By 4 weeks of age, a medial to lateral gradient of myelination is identified in the lateral corticospinal tracts and by 4 months of age, the myelination pattern is almost similar to that seen in adults. All parts of the dorsal funiculus are myelinated. Myelination in the lateral corticospinal tract is advanced and the ventral corticospinal tract, if present, is entirely myelinated. Large fascicles of myelinated fibers can be seen in the dorsal horn of the gray matter while there is ongoing myelination in the substantia gelatinosa and the reticulated areas (see Figs. 27-90 and 27-91) [6,13].

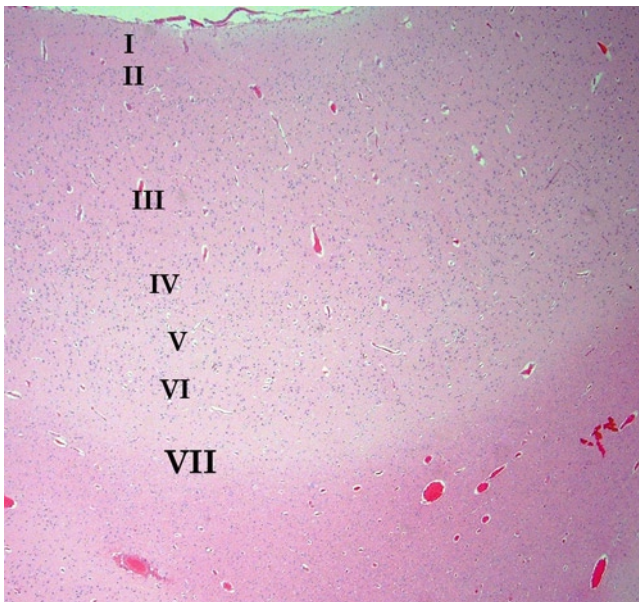


FIGURE 27-80. Frontal cortex 2 years postnatal. The frontal cerebral cortex shows the cortical layers with sparse cellularity in the molecular layer and the subcortical plate/subplate (VII). The white matter appears to be myelinated. (H&E, 2 \times .)

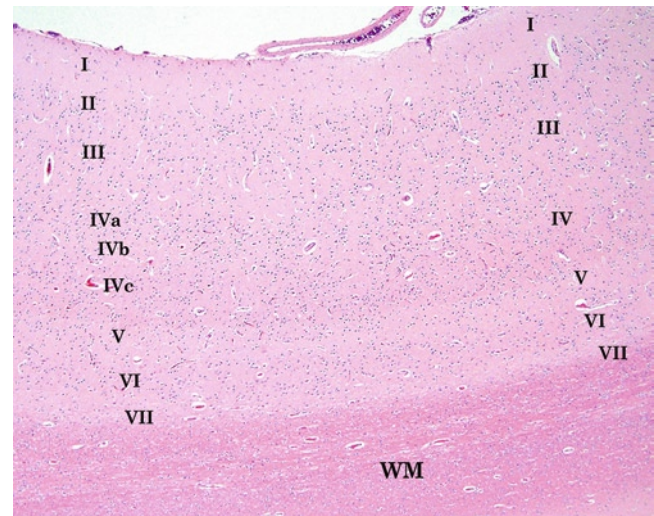


FIGURE 27-81. Occipital cortex, 2 years postnatal. The occipital cerebral cortex shows the cortical layers with the band of Gennari (IVb) in the peristriate cortex, the subcortical plate/subplate (VII), and myelinated white matter (WM). (H&E, 4 \times .)



FIGURE 27-82. White matter, 2 years postnatal. This GFAP immunostain of cerebral cortex shows a decrease in GFAP-positive glial cells in the white matter. (GFAP, 4×.)

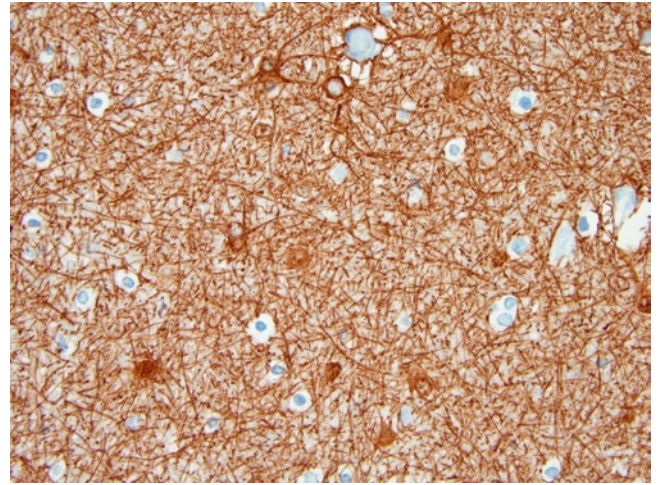


FIGURE 27-83. White matter, 2 years postnatal. This higher magnification of white matter is shown with rare "myelination" glia. (GFAP, 40×.)

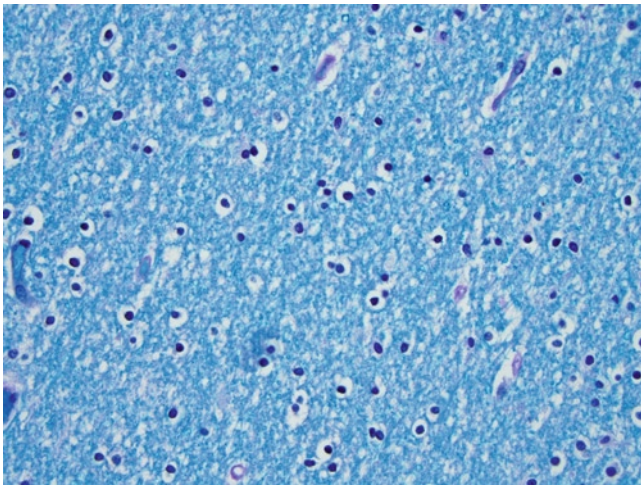


FIGURE 27-84. White matter, 2 years postnatal. This LFB stain with PAS shows myelination of the hemispheric white matter. (LFB/PAS, 40×.)

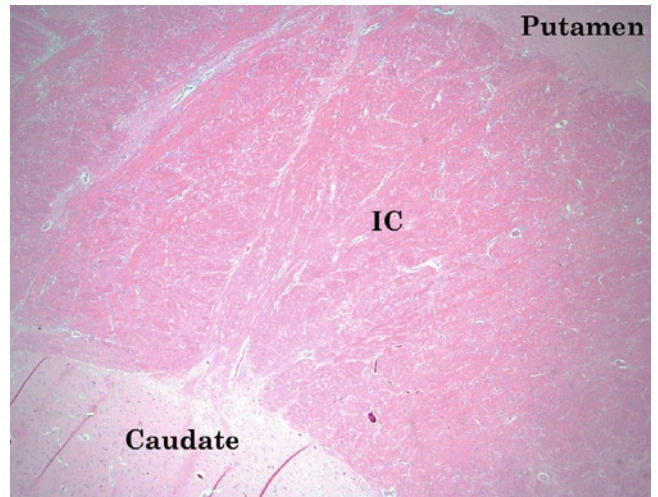


FIGURE 27-85. Basal ganglia, 2 years postnatal. Basal ganglia with mature neurons in the caudate and putamen with the internal capsule (IC) is separating them appearing myelinated. (H&E, 2×.)

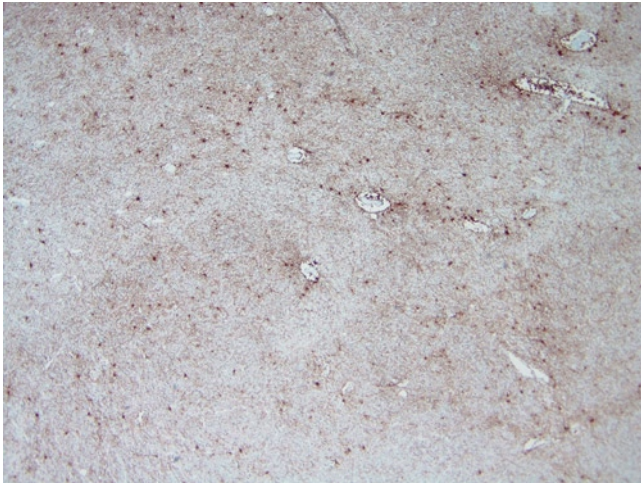


FIGURE 27-86. Basal ganglia, 2 years postnatal. This GFAP immunostain shows a decrease in GFAP-positive glial cells in the internal capsule. (GFAP, 4 \times .)

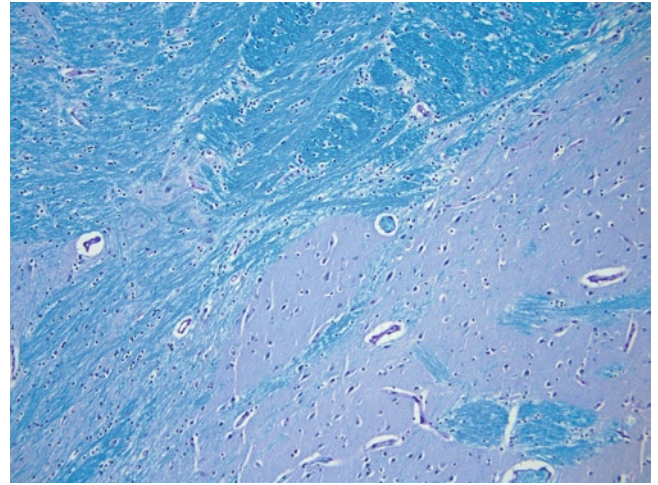


FIGURE 27-87. Basal ganglia, 2 years postnatal. This LFB stain with PAS shows myelinated internal capsule and fibers in the basal ganglia. (LFB/PAS, 10 \times .)

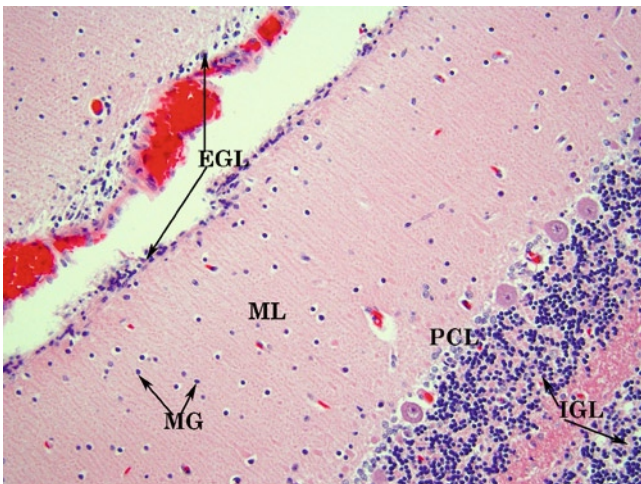


FIGURE 27-88. Postnatal cerebellum, 6 months. The cerebellum shows a persistent external granular cell/germinal layer (EGL), well-formed Purkinje cell layer (PCL), and an internal granular layer (IGL) with migrating granule cells (MG) in the molecular layer (ML). The white matter is thin but appears to be myelinated. (H&E, 40 \times .)

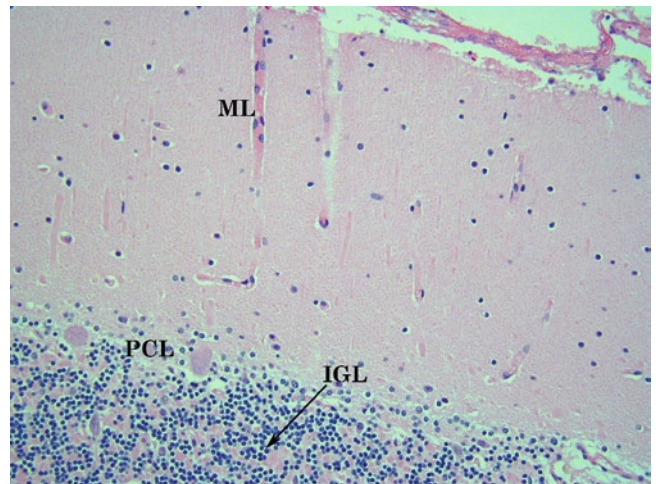


FIGURE 27-89. Postnatal cerebellum, 2 years. The cerebellum shows an absent external granular layer, well-formed Purkinje cell layer (PCL), and internal granular layer (IGL) with sparse cellularity in the molecular layer (ML). (H&E, 40 \times .)

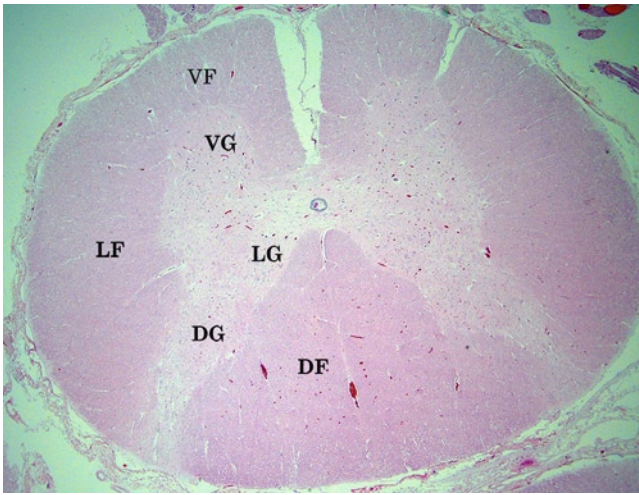


FIGURE 27-90. Spinal cord, 2 years postnatal. The spinal cord shows the ventral (VG), intermediate (LG), and dorsal gray (DG) matter. The ventral corticospinal tracts, vestibulospinal tracts, and part of the spinocephalic tracts are seen in the ventral funiculus (VF). The lateral funiculus (LF) contains the lateral corticospinal tracts, intraspinal tracts, and the spinocephalic tracts. The dorsal funiculus (DF) contains the fasciculus gracilis and fasciculus cuneatus and the dorsal root collateralization zone. (H&E, 2 \times .)



FIGURE 27-91. Spinal cord, 2 years postnatal. **A**, This GFAP immunostain shows a decrease in GFAP-positive cells in ventral and dorsal funiculi. (GFAP, 2 \times .) **B**, This LFB with PAS image showing myelination in all the tracts. (LFB/PAS, 2 \times .)

References

1. Meyer G: Genetic control of neuronal migrations in human cortical development. *Adv Anat Embryol Cell Biol* 2007, 189:1–111.
2. Valdés-Dapena MA: *Histology of the Fetus and Newborn*. Philadelphia: Saunders; 1979.
3. O'Rahilly R, Muller F: Significant features in the early prenatal development of the human brain. *Ann Anat* 2008, 190:105–118.
4. Bayer SAAJ: *Atlas of the Human Central Nervous System Development*, vol 5. Boca Raton, FL: CRC; 2002.
5. Chi JG, Dooling EC, Gilles FH: Gyral development of the human brain. *Ann Neurol* 1977, 1:86–93.
6. Bayer SAAJ: *Atlas of the Human Central Nervous System Development*, vol 1. Boca Raton, FL: CRC; 2002.
7. Jacobson M, Rao MS: Developmental neurobiology. In Kluwer Academic/Plenum; 2005:129–150.
8. Herschkowitz N: Brain development in the fetus, neonate and infant. *Biol Neonate* 1988, 54:1–19.
9. Vasung L, Huang H, Jovanov-Milosevic N, et al.: Development of axonal pathways in the human fetal fronto-limbic brain: histochemical characterization and diffusion tensor imaging. *J Anat* 2010, 217:400–417.
10. Jacobson M, Rao MS: Developmental neurobiology. In Kluwer Academic/Plenum; 2005:197–222.
11. Jacobson M, Rao MS: Developmental neurobiology. In Kluwer Academic/Plenum; 2005:151–96.
12. Kinney HC, Back SA: Human oligodendroglial development: relationship to periventricular leukomalacia. *Semin Pediatr Neurol* 1998, 5:180–189.
13. Gilles FH: Myelination in the neonatal brain. *Hum Pathol* 1976, 7:244–248.
14. Bodhireddy SR, Lyman WD, Rashbaum WK, Weidenheim KM: Immunohistochemical detection of myelin basic protein is a sensitive marker of myelination in second trimester human fetal spinal cord. *J Neuropathol Exp Neurol* 1994, 53:144–149.
15. Seress L, Abraham H, Tornoczky T, Kosztolanyi G: Cell formation in the human hippocampal formation from mid-gestation to the late postnatal period. *Neuroscience* 2001, 105: 831–843.
16. Vuksic M, Rados M, Kostovic I: Structural basis of developmental plasticity in the corticostriatal system. *Coll Antropol* 2008, 32(Suppl 1):155–159.
17. Bayer SAAJ: *Atlas of the Human Central Nervous System Development*, vol 4. Boca Raton, FL: CRC; 2002.
18. Hatta T, Satow F, Hatta J, et al.: Development of the pons in human fetuses. *Congenit Anom (Kyoto)* 2007, 47:63–67.
19. Bell JE, Sandison A, Boddy J, et al.: Development of the cerebellum with particular reference to cellular differentiation in the external granular layer. *Early Hum Dev* 1989, 19: 199–211.
20. Abraham H, Tornoczky T, Kosztolanyi G, Seress L: Cell formation in the cortical layers of the developing human cerebellum. *Int J Dev Neurosci* 2001, 19:53–62.
21. Bayer SAAJ: *Atlas of Human Central Nervous System Development*, vol 3. Boca Raton, FL: CRC; 2002.
22. Bayer SAAJ: *Atlas of the Human Central Nervous System Development*, vol 2. Boca Raton, FL: CRC; 2002.

SECTION VIII

Musculoskeletal System

28

Bone

Linda M. Ernst

The skeletal system is developing throughout fetal life and continues to develop well into postnatal life. The changes in embryonic and fetal life in the skeleton are dramatic, and the study of the normal histological changes in bone development can be important for understanding abnormalities encountered in such disease states as intrauterine growth restriction, skeletal dysplasia, and metabolic disturbances. This chapter reviews the normal development of the skeletal system and the histological components of bone throughout gestation.

Embryology

The bones of the skeletal system are derived from paraxial mesoderm, lateral plate mesoderm, and neural crest cells. After gastrulation, the mesodermal cells that migrated from the primitive streak begin to form three condensations lateral to the notochord: the paraxial mesoderm, the intermediate mesoderm, and the lateral plate mesoderm. The most medial, known as the paraxial mesoderm, is destined to contribute to the axial skeleton, the skeletal muscles of the trunk and limbs, and the dermis of the skin [1,2]. In the vertebrate embryo, the paraxial mesoderm begins to further divide into adjacent, rounded somitomeres, which first appear in the cranial region and extend as paired structures along the length of the embryo [1]. It should be noted that the existence of somitomeres in human embryos is not universally accepted [3].

From the eighth somitomere to the caudal end of the embryo, the somitomeres continue to show further segmentation into somites, which are paired block-like condensations of primitive mesenchymal cells clearly seen in human embryos. The first somites form around day 20 and continue to form in a cranial-to-caudal direction until approximately day 30. Approximately 42 to 44 pairs of somites are formed with eventual regression of the caudal-most somites [1]. Somites are extremely important in the developing embryo because they establish the initial segmentation of the body and provide the mesenchymal tissue for skeletal and muscular elements of the majority of the body (see Fig. 28-1).

The somitic mesoderm is further subdivided in the fourth week of gestation into the ventromedial portion known as the sclerotome, which will form vertebrae and ribs, and the more lateral segment known as the dermomyotome, which will give rise to the precursors of the skeletal muscles and dermis of the skin. Within each sclerotome, the ventral cells migrate to surround the notochord and form the vertebral bodies. The dorsal cells surround the neural tube and become the vertebral arches and spinous processes. Cells in the lateral portion of the sclerotome will form the transverse processes and ribs. The formation of ribs begins on day 35 with the first endochondral ossification in the ribs seen about 6 weeks of development [2].

The sternum develops from the lateral plate mesoderm, specifically from structures known as the sternal bars, which are two, paired longitudinal mesenchymal condensations in the ventrolateral body wall. The sternal bars begin to fuse around the seventh

week of development in a cranial to caudal fashion. Ossification centers begin to form on the sixtieth day, with multiple ossification centers forming in a cranial-to-caudal progression [2].

The skeletal elements of the limbs are derived from the parietal layer of the lateral plate mesoderm, which gives rise to the limb buds at the end of the fourth week. The mesenchyme of the limb bud is under the inductive influence of an ectodermal thickening at the tip of the bud known as the apical ectodermal ridge [1,2], which arises from the ectodermal ring. The inductive influences of the apical ectodermal ridge promote proliferation and differentiation of the limb bud. Bone formation within the long bones occurs in the center of the diaphysis, with an initial condensation of mesenchymal cells that differentiate into chondrocytes. Formation of a primary center of ossification (see Figs. 28-2 and 28-3) begins when stem cells in the perichondrium produce a layer of osteoblasts that fabricate a thin layer of woven bone on the surface of the condensation of chondrocytes. These chondrocytes then become organized into progressive layers of resting, proliferating, pre-hypertrophic and hypertrophic chondrocytes. Once the nutrient vessel of the long bone enters this cartilaginous model near the end of the embryonic period, osteoblasts derived from perivascular stem cells enter the region and begin replacing the chondrocytes and forming the mineralized trabeculae of the bone

centrally. The cartilaginous tissue is resorbed and ossification by osteoblasts then spreads toward the ends of the bone. Most of the long bones of the extremities have primary ossification centers by the midtrimester but retain cartilaginous caps at their epiphyseal ends (see Fig. 28-4). Ossified cortical bone is formed from the primary bone collar in all the long bones by birth, and ossification centers can be seen in the distal femoral epiphyses by approximately 35 weeks of gestation (see Fig. 28-5) and in the proximal tibial epiphyses at term (see Figs. 28-6 and 28-7) [4].

The bones of the skull and face develop from neural crest cells, paraxial/somitic mesoderm, and from the pharyngeal arches [1,2]. The membranous neurocranium, composed of flat bones that surround the brain, is derived from both neural crest cells and somitic mesoderm. The bones ossify by membranous ossification and show bony spicules radiating from the central area to the periphery of the bone. Growth occurs by resorption of the central area and new bone formation at the periphery. The chondrocranium, the bones at the base of the skull, forms from cartilaginous precursors derived from neural crest and paraxial mesoderm. Ossification of the bones of the chondrocranium occurs by endochondral ossification. Lastly, bones of the face (also known as the viscerocranium) develop from the first two pharyngeal arches and neural crest cells. These bones ossify by membranous ossification.

Skeletal and Muscular Derivatives of Somites		
Somite pairs	Skeletal derivatives	Muscular derivatives
1-4, occipital	Occipital skull bones of nose, eyes, inner ears	Extrinsic ocular muscles Muscle of tongue
5-12, cervical	Portion of occipital bone Cervical vertebrae	Cervical paraspinal muscle Upper limb muscles
13-24, thoracic	Thoracic vertebrae Ribs Sternum	Thoracic paraspinal muscle Intercostal muscles Abdominal wall musculature Upper limb muscles
25-29, lumbar	Lumbar vertebrae	Lumbar paraspinal muscle Abdominal wall musculature Lower limb muscles
30-34, sacral	Sacral vertebrae	Sacral paraspinal muscle
35-37, coccyx	Coccyx	Paracoccygeal muscle

FIGURE 28-1. Skeletal and muscular derivatives of somites.

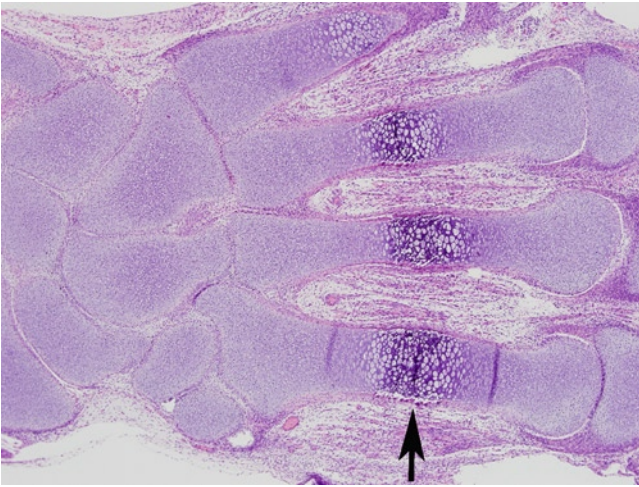


FIGURE 28-2. Metacarpal bone ossification in late first trimester of gestation. Metacarpal bones of the hand show central primary ossification centers recognized by the proliferating cartilaginous tissue showing early ossification (*arrow*). (Hematoxylin and eosin [H&E], 4 \times)

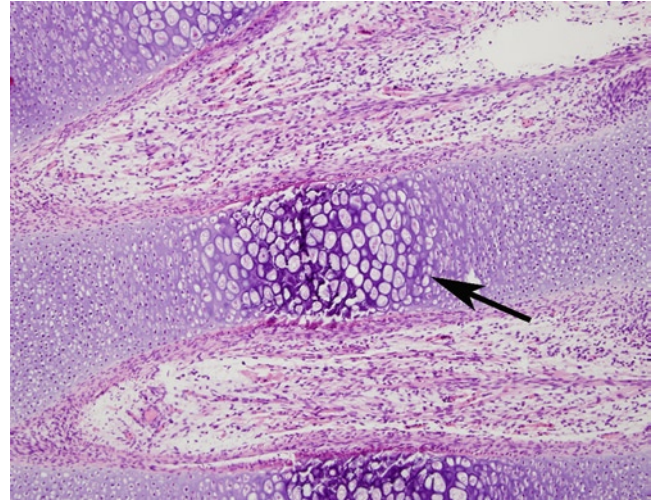


FIGURE 28-3. Metacarpal bone ossification in late first trimester of gestation. Higher-power view of primary ossification center in central area of metacarpal bone (*arrow*). Note the thin rim of woven bone over the surface of the cartilaginous condensation. (H&E, 10 \times .)

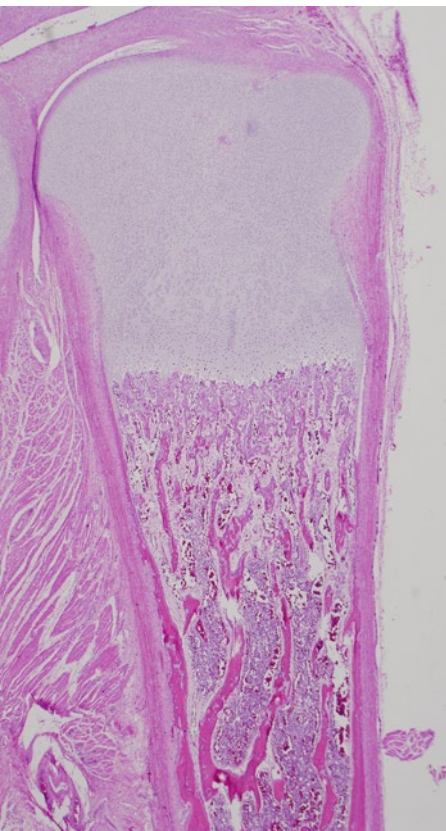


FIGURE 28-4. Long bone ossification at 20 weeks of gestation. Low-power view of the long bone showing central ossification and formation of trabeculae in the medullary cavity. Note the end of the bone consists of a rounded cartilaginous cap that allows for continued growth. (H&E, 2 \times .)



FIGURE 28-5. Radiograph of the lower limb of a 38-week fetus. Note ossification of the distal femoral epiphysis (*arrow*).



FIGURE 28-6. Radiograph of the lower limb of a 40-week fetus. Note ossification of the distal femoral epiphysis and proximal tibia epiphysis (*arrows*).

Ossification in the Fetus

Body Region	Week
Head	
Mandible	7
Occipital bone	8–10
Maxilla	8
Temporal bone	9
Sphenoid	9–14
Nasal bone	10
Frontal bone	9–10
Bony labyrinth	17–20
Neck	
Hyoid bone	28–32
Thorax	
Clavicle	7
Scapula	8–9
Ribs, 2 nd –11 th	8–9
Ribs, 1 st and 12 th	10
Vertebra	
Cervical, thoracic, lumbar, upper sacral arches	9–12
Cervical, thoracic, lumbar and upper sacral bodies	10–12
4 th sacral arches	19–25
5 th sacral body	13–28
Coccyx	37–40
Odontoid process of axis	17–20
Pelvis	
Ilium	9
Ischium	16–17
Pubis	21–28
Upper extremity	
Humerus	8
Proximal humeral epiphysis	37–42
Radius	8
Ulna	8
Metacarpals, 2 nd and 3 rd	9
Metacarpals, 1 st , 4 th , and 5 th	10–12
Distal phalanges	9
Proximal phalanges, 2 nd and 3 rd	9
Proximal phalanges, 1 st and 4 th	10
Proximal phalanx, 5 th	11–12
Middle phalanges, 2 nd , 3 rd , and 4 th	12
Middle phalanx, 5 th	13–16
Lower extremity	
Femur	8–9
Distal femoral epiphysis	35–40
Tibia	8–9
Proximal tibial epiphysis	40
Fibula	9
Metatarsals, 2 nd and 3 rd	9
Metatarsals, 1 st , 4 th , 5 th	10–12
Calcaneus	21–29
Talus	24–32
Cuboid	40
Distal phalanx, 1 st	9
Distal phalanges, 2 nd , 3 rd , 4 th	10–12
Distal phalanx, 5 th	13–14
Proximal phalanges	13–14
Middle phalanx, 2 nd	20–25
Middle phalanx, 3 rd	21–26
Middle phalanx, 4 th	29–32
Middle phalanx, 5 th	33–36

(Data from Siebert [4].)

FIGURE 28-7. Ossification in the fetus.

Histology

Structure of Bone

Periosteum

The periosteum is a thin connective tissue layer that covers the outer surface of the bone (see Figs. 28-8 and 28-9). It is composed of a fibrocollagenous outer layer

and a more cellular inner layer known as the cambium layer. The cells in the cambium layer are osteoprogenitor cells.

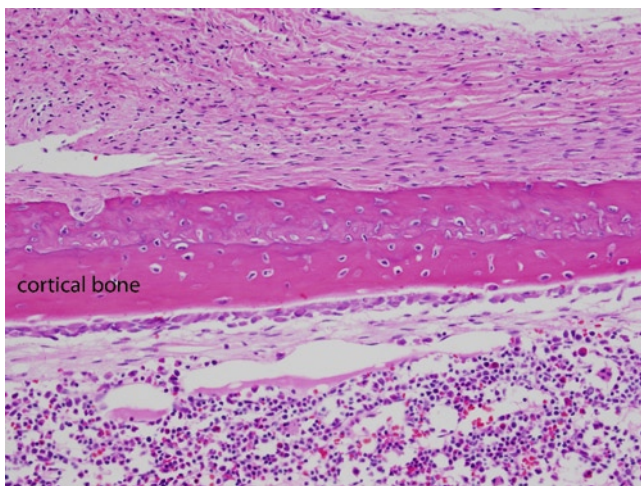


FIGURE 28-8. Periosteum and cortical bone at 20 weeks of gestation. Medium-power view of the surface of a fetal long bone showing the periosteum composed of two layers. The top layer is slightly less cellular than the bottom layer. Also note the woven bone of the cortical bone and deeper medullary cavity. (H&E, 10 \times .)

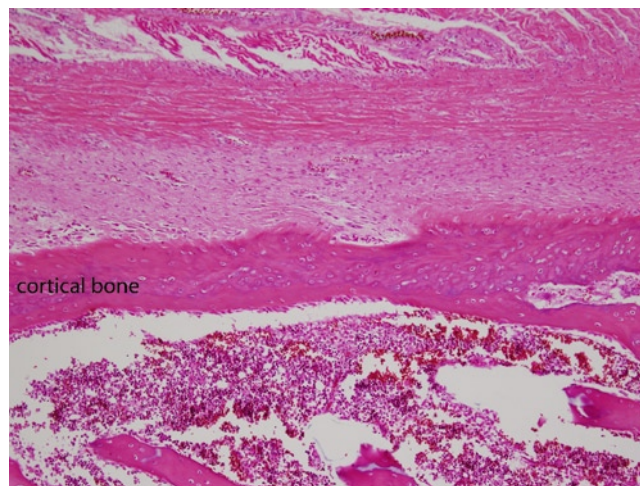


FIGURE 28-9. Periosteum and cortical bone at 36 weeks of gestation. This image illustrates the surface of a fetal long bone showing the periosteum that appears slightly thicker than in the midtrimester. The top layer shows dense collagenous tissue and the lower cambium layer is more cellular. Also note the woven bone of the cortical bone and the deeper medullary cavity. (H&E, 10 \times .)

Cortical bone

The cortex of long bones of the fetus is composed predominantly of dense woven bone (see Figs. 28-8 and 28-9). In the first trimester, ossification centers are just beginning to form and cortical bone is just beginning to be present by the end of the first trimester. In the

midtrimester, cortical bone is seen and is thickest in the middle of the diaphysis. The cortex thickens over gestation, but may be very thin to absent near the growth plate (see Fig. 28-10).

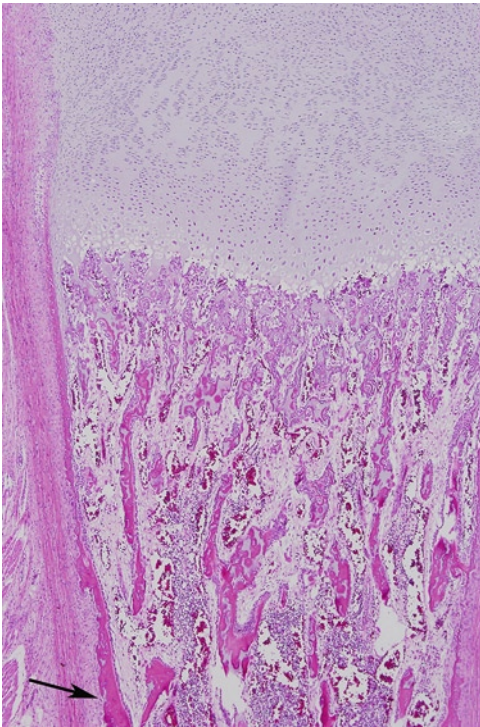


FIGURE 28-10. Cortical bone near growth plate at 20 weeks of gestation. This image is a low-power view of the end of a long bone. Note the woven bone of the cortical bone (arrow) that becomes extremely thin to nonexistent at the growth plate. (H&E, 4 \times .)

Medullary canal

The bone of the medullary cavity is not composed of solid bone, but is formed by trabeculae of bone, with bone marrow spaces interspersed between the bony trabeculae (see Figs. 28-11 and 28-12). In developing

bone, the trabeculae are composed of woven bone, but in mature bone the bony trabeculae are comprised of lamellar bone.

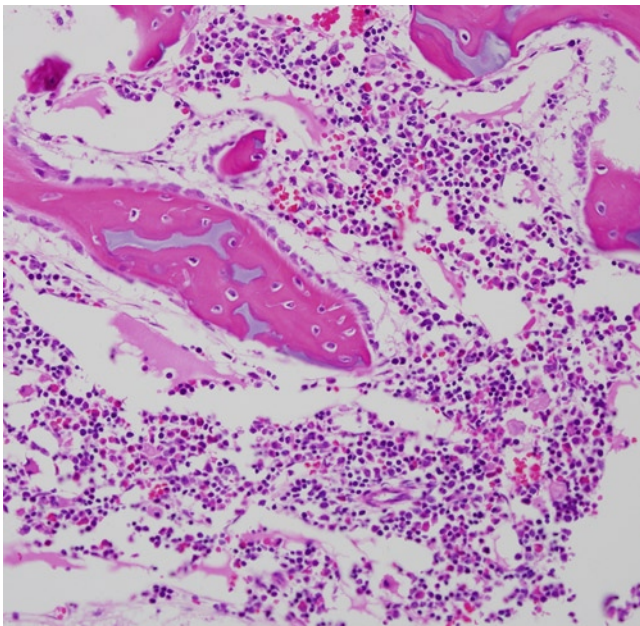


FIGURE 28-11. Medullary bone at 20 weeks of gestation. Note the partially ossified trabeculae of woven bone rimmed by osteoclasts. Osteocytes are present within the woven bone. Bone marrow spaces are present between the trabeculae. (H&E, 20 \times .)

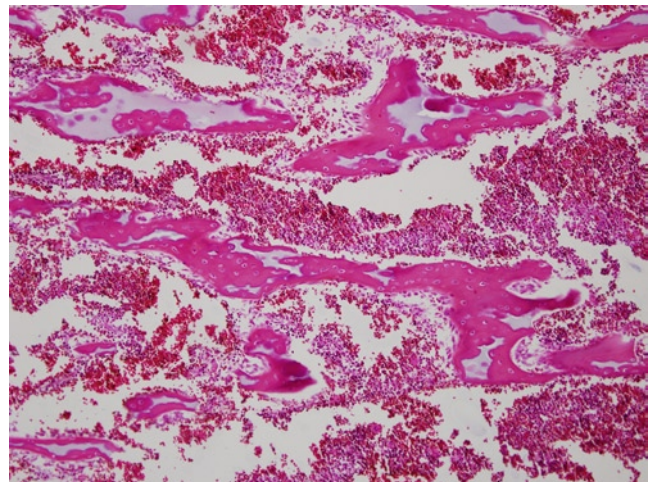


FIGURE 28-12. Medullary bone at 36 weeks of gestation. Note the partially ossified trabeculae of woven bone with central areas composed of basophilic cartilaginous tissue. Osteocytes are present within the woven bone. Bone marrow spaces are present between the trabeculae and appear congested in this image. (H&E, 10 \times .)

Histological types of bone

Bone is a mixture of organic and inorganic materials. The main organic components are the bone's cellular elements and the organic matrix consisting predominately of type I collagen. The inorganic component of bone is a calcium deficient variant of hydroxyapatite [5].

Lamellar bone

Lamellar bone is composed of parallel-oriented type I collagen fibers. It is typically produced more slowly than woven bone and is seen in mature bone. Using routine H&E stains, lamellar bone is eosinophilic and appears

less cellular than woven bone. The lacunae are more evenly distributed along the lamellae consisting of parallel-oriented collagen fibers that can be highlighted by examination under polarized light (see Fig. 28-13).

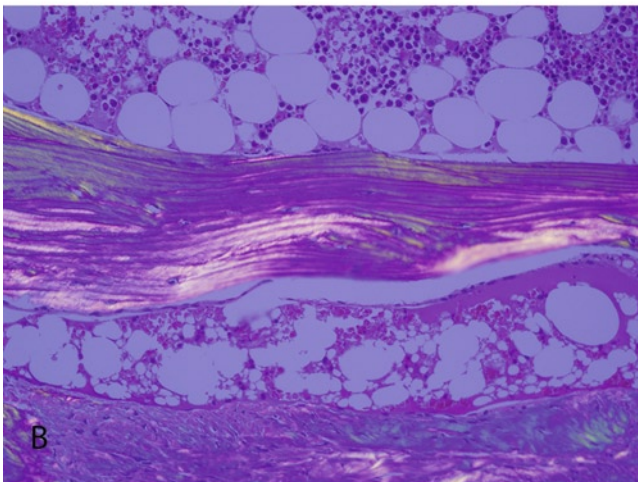
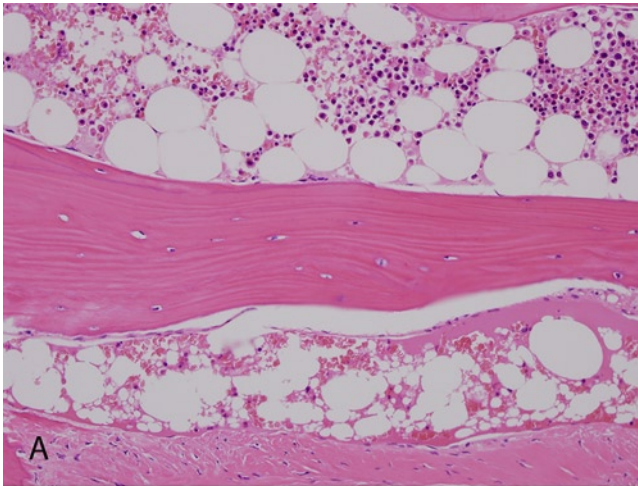


FIGURE 28-13. Lamellar bone. In the center of each field is a bony trabecula composed of lamellar bone from an adult specimen. **A**, Note the organized parallel-oriented collagen fibers and osteocytes with small pyknotic nuclei. **B**, The parallel-oriented collagen fibers are highlighted by the examination under polarized light (**A** and **B**, H&E, 20 \times .)

Woven bone

Woven bone is characterized by type I collagen fibers arranged in an irregular meshwork. In embryonic and fetal development, woven bone predominates because woven bone can be produced and resorbed more quickly than the more organized lamellar bone.

In H&E-stained sections, woven bone appears hypercellular, with lacunae arranged in a haphazard pattern. Examination with polarized light reveals collagen fibers arranged in nonparallel, random directions (see Fig. 28-14).

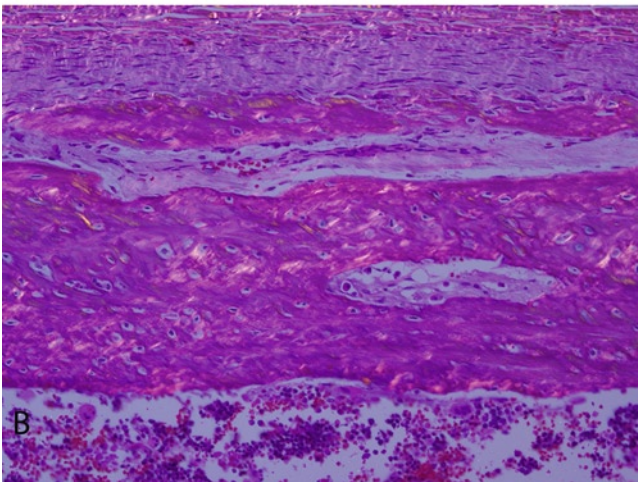
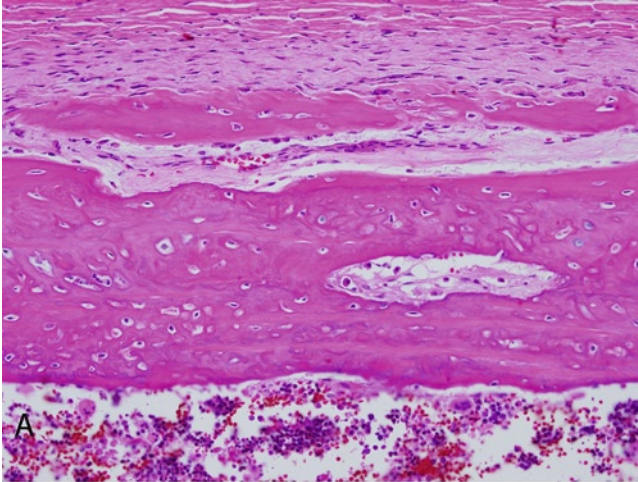


FIGURE 28-14. Woven bone. In the center of each field is cortical bone from a 20-week fetus. **A**, Woven bone in general appears more disorganized than lamellar bone. Note the haphazard arrangement of collagen fibers and osteocytes. **B**, The haphazardly oriented collagen fibers are highlighted by the examination under polarized light (**A** and **B**, H&E, 20 \times .)

Cell Types in Bone

Osteoprogenitor cells

Osteoprogenitor cells are committed mesenchymal cells that under the influence of proper growth and transcription factors will form osteoblasts [5]. In fetal

bone, they are most easily recognized in the periosteum as spindle- to stellate-shaped cells in the inner/cambium layer (see Figs. 28-8 and 28-9).

Osteoblasts

Osteoblasts are the main cell involved in bone production. Osteoblasts produce and arrange the organic matrix of the bone, and are responsible for the regulation of the mineralization of the bone [5]. Osteoblasts are present on the surfaces of bone and their appearance varies with their metabolic activity. When inactive, they have a benign spindle cell appearance similar to

fibroblasts. When active, osteoblasts become larger and adopt a polygonal shape with abundant amphophilic to basophilic cytoplasm (see Fig. 28-15). The nucleus is typically positioned eccentrically away from the surface of the matrix and shows prominent nucleoli. Perinuclear halos representing the active Golgi apparatus can be seen [5].

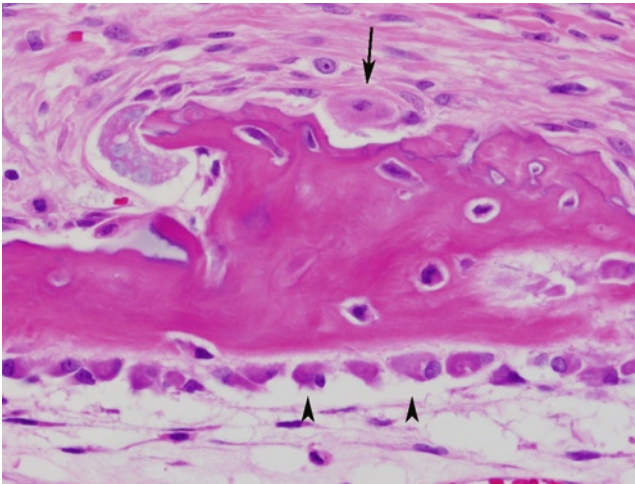


FIGURE 28-15. Woven bone with prominent osteoblasts. This is cortical bone from a 20-week fetus. The osteoblasts are lining the bottom surface of the bone (*arrowheads*). Osteoblasts have abundant cytoplasm and the nucleus is oriented away from the surface of the bone. Note the plump-appearing osteocytes within lacunae of the woven bone. An osteoclast is present on the opposite surface of the bone (*arrow*). (H&E, 60 \times .)

Osteocytes

As an individual osteoblast produces matrix, it surrounds itself with matrix, and inhabits a small lacunar space within the matrix becoming an osteocyte (see Fig. 28-15). In mature lamellar bone, osteocyte nuclei within the lacunae are generally smaller and more pyknotic than osteoblasts. In addition, the mature osteocyte is oriented in the direction of its surrounding lamellae. In the fetus, because most of the bone is woven bone,

osteocytes are more plump and their orientation is more random (compare Figs. 28-13 and 28-14). Although not well-appreciated in H&E-stained sections, osteocytes have numerous long cytoplasmic processes throughout the canaliculi of the matrix. These cellular processes are important for intercellular communication between osteocytes and with osteoblasts, and aid with the osteocyte function of maintaining the bone.

Osteoclasts

Osteoclasts are the cells responsible for resorption of bone by release of their lysosomal contents in the resorption pit [5]. Osteoclasts appear as multinucleated, large cells on the surface of the bone (see Fig. 28-16). As the

matrix is resorbed by the osteoclast, a small resorption pit is formed known as Howship's lacunae within which the osteoclast is found.

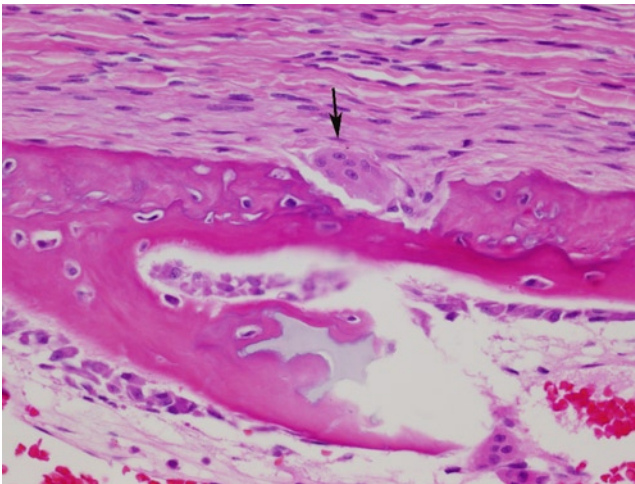


FIGURE 28-16. Woven bone with osteoclast. This is cortical bone from a 20-week fetus. Note the multinucleated osteoclast (arrow) within the resorption pit. (H&E, 40 \times .)

Types of Bone Formation

Endochondral ossification

Histological assessment of the growth plate is important to determine that bone formation and growth is occurring normally. Routine samples of the long bones may be difficult to acquire, but a sample of rib that includes the costochondral junction typically demonstrates the growth plate nicely.

The growth plate has five poorly delimited, recognizable histological zones [5-7]. These zones demonstrate the morphologic changes as chondrocytes mature at the growth plate. The zones from the distal end of the bone toward the ossified central bone are: 1) Zone of resting cartilage: resting chondrocytes are present in lacunae in this zone. 2) Zone of proliferating cartilage: chondrocytes multiply in this region and appear as

aggregates of small cells in small longitudinal columns. 3) Zone of hypertrophic cartilage: chondrocytes in this zone remain arranged in columns, but the cytoplasm expands and appears clear on H&E-stained sections. The cytoplasm of these chondrocytes is loaded with glycogen. 4) Zone of cartilage degeneration with cartilage matrix mineralization. In this zone, the chondrocytes lose their nuclei and appear as "degenerated" cells, although the exact nature of these morphologic changes is not clear [6,7]. The cartilage matrix also begins to undergo mineralization in this zone. 5) Zone of woven bone formation on mineralized cartilage matrix. In the zone closest to the metaphysis, woven bone is deposited on the mineralized cartilage matrix (see Figs. 28-17-28-21).

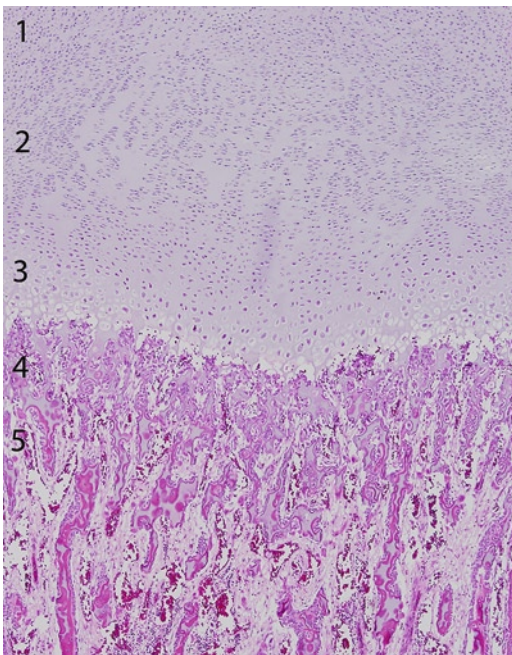


FIGURE 28-17. Growth plate at 20 weeks of gestation. Low-power view of the five zones of endochondral ossification: 1) zone of resting cartilage; 2) zone of proliferating cartilage; 3) zone of hypertrophic cartilage; 4) zone of cartilage degeneration with cartilage matrix mineralization; and 5) zone of woven bone formation on mineralized cartilage matrix. (H&E, 4 \times .)

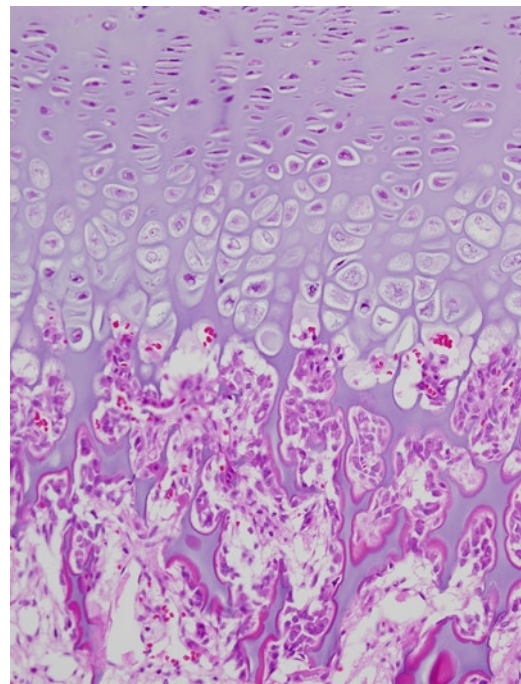


FIGURE 28-18. Growth plate at 20 weeks of gestation. Higher-power view of the physal area. At the top of the image, chondrocytes appear as aggregates of small cells in small longitudinal columns. In the middle, the hypertrophic zone, the cytoplasm of the chondrocytes balloons and appears clear with abundant glycogen. In the lower zone, the cartilage matrix appears basophilic and acellular with thin pink rims of ossification. (H&E, 20 \times .)



FIGURE 28-19. Growth plate at 36 weeks of gestation. Low-power view of end of a long bone in the third trimester. The overall organization of the growth plate is unchanged. (H&E, 2 \times .)

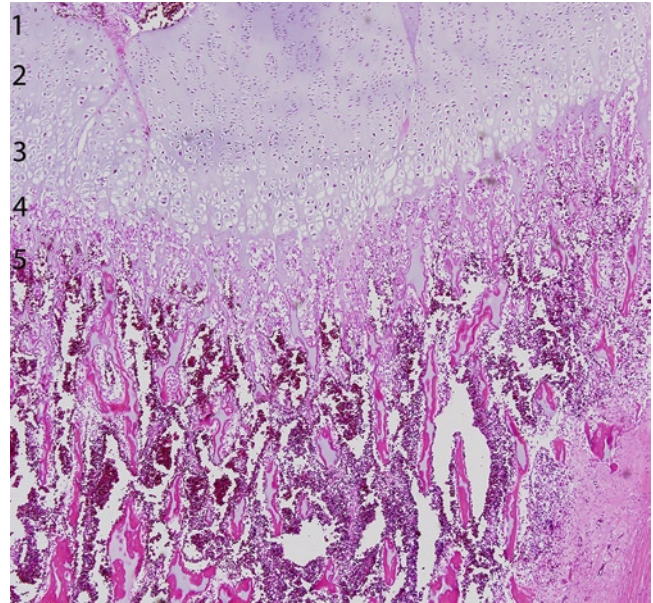


FIGURE 28-20. Growth plate at 36 weeks of gestation. Low-power view of the five zones of endochondral ossification: 1) zone of resting cartilage; 2) zone of proliferating cartilage; 3) zone of hypertrophic cartilage; 4) zone of cartilage degeneration with cartilage matrix mineralization; and 5) zone of woven bone formation on mineralized cartilage matrix. (H&E, 4 \times .)

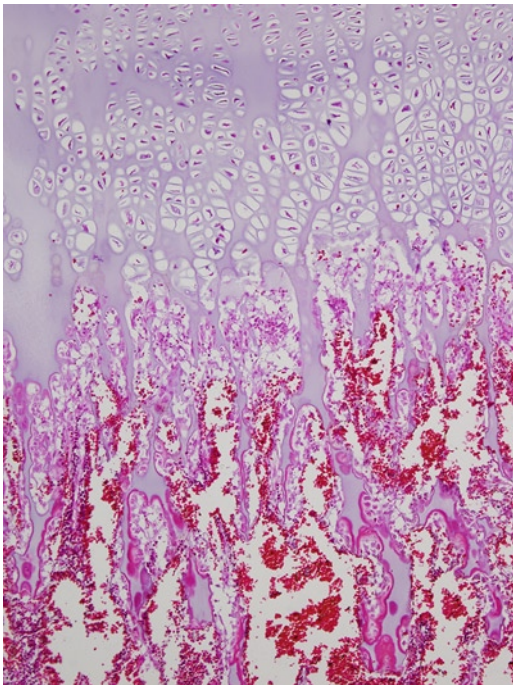


FIGURE 28-21. Growth plate at 36 weeks of gestation. Higher-power view of the physal area. At the top of the image, chondrocytes appear as aggregates of small cells in small longitudinal columns. In the middle, the hypertrophic zone, the cytoplasm of the chondrocytes balloons and appears clear with abundant glycogen. In the lower zone the cartilage matrix appears basophilic and acellular with thin pink rims of ossification. (H&E, 10 \times .)

Membranous ossification

As mentioned in the embryology section of this chapter, the bones of the skull and face ossify by membranous ossification, a process of bone formation along a fibrous lining membrane. In the fetus, the lining membrane is typically the periosteum, which contains osteoprogenitor cells that differentiate into osteoblasts. These osteoblasts

directly deposit bone matrix. Membranous bone formation is also important in cortical bone formation of the long bones, so nearly all bones undergo membranous ossification [5]. Growth occurs by resorption of the central area and new bone formation at the periphery.

References

1. Sadler TW, Langman J: *Langman's Medical Embryology*, edn 11. Philadelphia: Wolters Kluwer Lippincott Williams & Wilkins; 2010.
2. Schoenwolf GC, Larsen WJ: *Larsen's Human Embryology*, edn 4. Philadelphia, PA: Elsevier/Churchill Livingstone; 2009.
3. The skeletal system and the limbs. In *Human Embryology & Teratology*, edn 3. Edited by O'Rahilly R, Mèuller F. New York: Wiley-Liss; 2001:360.
4. Siebert J: Perinatal, fetal and embryonic autopsy. In *Potter's Pathology of the Fetus, Infant, and Child*, edn 2. Edited by Gilbert-Barness E. Philadelphia, PA: Mosby Elsevier; 2007:712.
5. Rosenberg AE, Roth SI: Bone. In *Histology for Pathologists*, edn 3. Edited by Mills SE Philadelphia: Lippincott Williams & Wilkins; 2007:75–95.
6. Gilbert-Barness E: Osteochondrodysplasia—constitutional diseases of bone. In *Potter's Pathology of the Fetus, Infant, and Child*, edn 2. Edited by Gilbert-Barness E. Philadelphia, PA: Mosby Elsevier; 2007:1836–1897.
7. Yang SS: The skeletal system. In *Textbook of Fetal and Perinatal Pathology*, edn 2. Edited by Wigglesworth JS, Singer DB. Malden, MA: Blackwell Science; 1998:1039–1082.

29

Skeletal Muscle

Linda M. Ernst

Fetal movements in utero are an important part of the developmental process, and normal fetal movements are a marker of fetal well-being. The muscular system of the fetus provides the contractile apparatus necessary to move the extremities, trunk, and head, and produce fetal breathing movements. Primary abnormalities in the development of skeletal muscle or secondary conditions that reduce fetal movements can produce pathologic changes in skeletal muscle and lead to abnormalities in the development of other organ systems. Therefore, an understanding of the normal development and histological appearance of skeletal muscle is necessary to interpret fetal pathology. This chapter reviews the developmental changes in skeletal muscle from the embryo to the term fetus/neonate.

Embryology

Skeletal muscle is mesodermal in origin [1–3]. After gastrulation, the mesodermal cells that migrated from the primitive streak begin to form three condensations lateral to the notochord: the paraxial mesoderm, the intermediate mesoderm, and the lateral plate mesoderm. The most medial condensation, known as the paraxial mesoderm, is destined to contribute to the axial skeleton, the skeletal muscles of the trunk and limbs, and the dermis of the skin [2,3]. In the vertebrate embryo, the paraxial mesoderm begins to further divide into adjacent, rounded somitomeres, which first appear in the cranial region and extend as paired structures along the length of the embryo [2]. It should be noted that the existence of somitomeres in human embryos is not universally accepted [4]. By electron microscopy, the somitomeres consist of whorled mesenchymal cells without further differentiation [1]. The skeletal muscles of the cervical and cranial structures are derived from the first seven cranial pairs of somitomeres, which become the mesenchyme of the branchial arches [2].

From the eighth somitomere to the caudal end of the embryo, the somitomeres continue to show further segmentation into somites, which are paired block-like condensations of primitive mesenchymal cells clearly seen in human embryos. The first somites form around day 20 and continue to form in a cranial-to-caudal direction until approximately day 30. Approximately 42 to 44 pairs of somites are formed with eventual regression of several of the most caudal somites [2]. Somites are extremely important in the developing embryo because they establish the initial segmentation of the body and provide the mesenchymal tissue for skeletal and muscular elements of the majority of the body (see Fig. 28-1).

The somitic mesoderm is further subdivided in the fourth week of gestation into the ventromedial portion known as the sclerotome, which will form vertebrae and ribs, and the more lateral segment known as the dermomyotome, which will give rise to the precursors of the skeletal muscles and dermis of the skin. Within the dermomyotome, two muscle-forming areas are identified, the ventrolateral compartment and the dorsomedial compartment. Cells in the ventrolateral compartment migrate into the parietal layer of the lateral plate mesoderm and form infrahyoid, abdominal wall, and limb muscles. Cells in the dorsomedial area form the muscles of the back, shoulder girdle, and intercostal spaces [2,3].

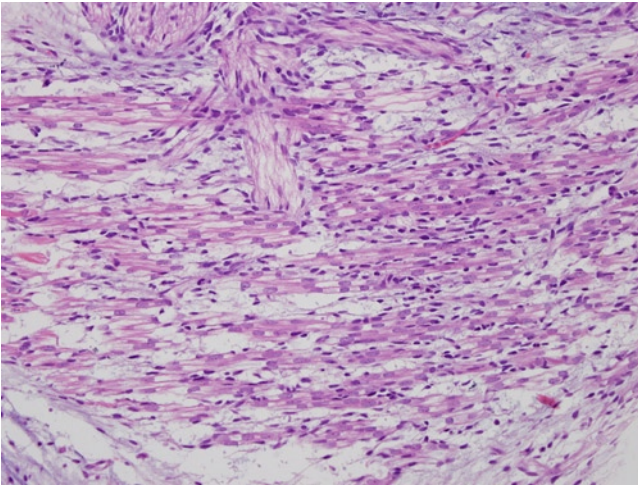


FIGURE 29-1. Embryonic skeletal muscle. Note the formation of primary myotubes characterized by longitudinally arranged nuclei with open chromatin and nucleoli. The cytoplasm is eosinophilic and cross-striations are not seen. (Hematoxylin and eosin [H&E], 20 \times .)

Histology

Early Histogenesis of Muscle

During early embryogenesis, some primitive mesenchymal cells differentiate into “pre-myoblasts,” so-named because these cells lack definitive histological features to distinguish them from the other mesenchymal cells, but have begun differentiation toward myogenesis. Once these cells achieve some phenotypic features of muscle such as presence of desmin and myofilaments in the cytoplasm, they are known as myoblasts [1]. These are spindle-shaped, elongated cells with fine granular cytoplasm and ovoid nuclei with prominent nucleoli [5].

Muscle fibers are formed by the fusion of multiple muscle cells, and mature muscle fibers are recognized

by their peripheral nuclei and organization of filaments into sarcomeres. The first step toward the formation of muscle fibers begins around 7 weeks gestation with the formation of primary myotubes, formed by the fusion of embryonic myoblasts. Primary myotubes have both immature-appearing cytoplasm and nuclei. They are characterized by chains of large central nuclei, each with prominent central nucleoli (see Figs. 29-1–29-4), surrounded by cytoplasm containing myofibrils, glycogen, and mitochondria [1].

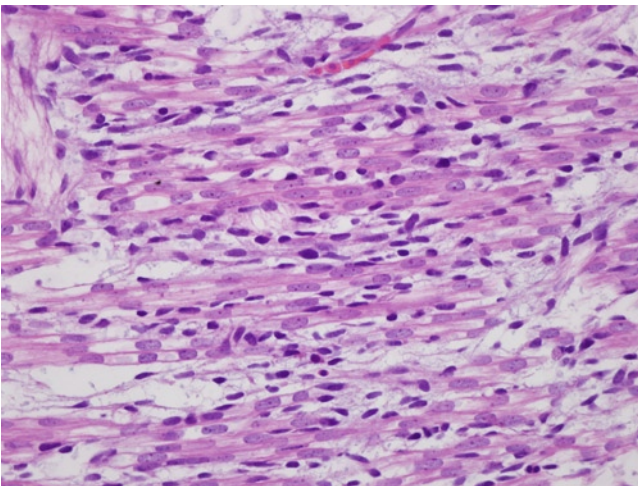


FIGURE 29-2. Embryonic skeletal muscle. A higher-power view of the primary myotubes with long chains of immature-appearing nuclei with prominent nucleoli. The cytoplasm appears clear to filamentous. (H&E, 40 \times .)

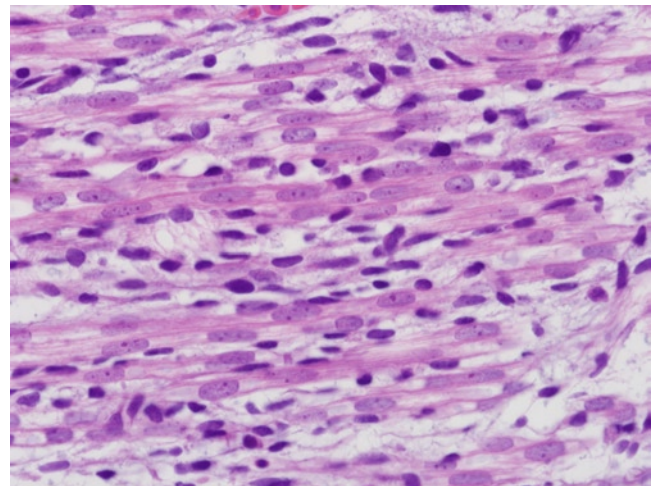


FIGURE 29-3. Embryonic skeletal muscle. High-power view of longitudinally arranged primary myotubes. Note nuclear detail and cytoplasm of primary myotubes. (H&E, 60 \times .)

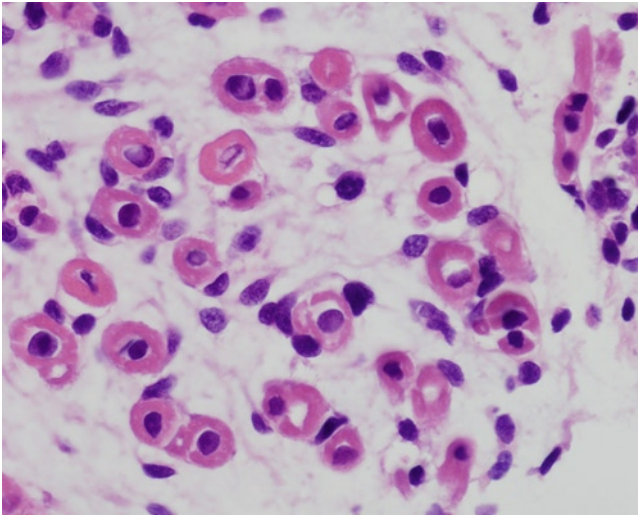


FIGURE 29-4. Embryonic skeletal muscle. High-power view of cross-section of primary myotubes. The nuclei are placed centrally within the myotube and central clearing is seen. (H&E, 60 \times .)

Fetal Muscle Development

In the early fetal period, secondary myotubes begin to form in a similar manner to primary myotubes. Secondary myotube development is characterized by the fusion of fetally derived myoblasts, which are larger in diameter than embryonic myoblasts and contain more myofilaments. Therefore, physiologically, secondary myotubes begin to show contractility [5]. Histologically, secondary myotubes also show central nuclei similar to primary myotubes. Secondary myotube formation continues throughout the early midtrimester but begins to decline at midgestation [5], although some myoblasts continue to divide and fuse until 30 weeks gestation [1]. Secondary myotubes mature into myofibers recognizable in the midtrimester (Figs. 29-5–29-7). With further maturation, myofibers develop an increasing number of myofibrils with easily visible cross-striations, and more nuclei

become peripherally located along the muscle fiber (Figs. 29-8–29-10). By term, most of the myofibers have peripherally placed nuclei (Figs. 29-11–29-13), but occasional central nuclei (up to 5%) is still considered within the range of normal.

Early muscle fibers are considered to be undifferentiated type 2c fibers. Further muscle fiber-type differentiation occurs at approximately 18 or 19 weeks gestation (16–20-week range) [1,6]. Type 1 fibers are the first to appear at this time. Later, type 2 fibers appear [1,7], with type 2b fibers present at approximately 25 weeks gestation, and type 2a fibers recognizable at approximately 35 weeks gestation [6]. By term, nearly 80% of muscle fibers are identified as either type 1 or type 2 (Figs. 29-14 and 29-15) [5]. Type 2c fibers are normally absent in postnatal infants beyond 1 to 2 weeks [7].

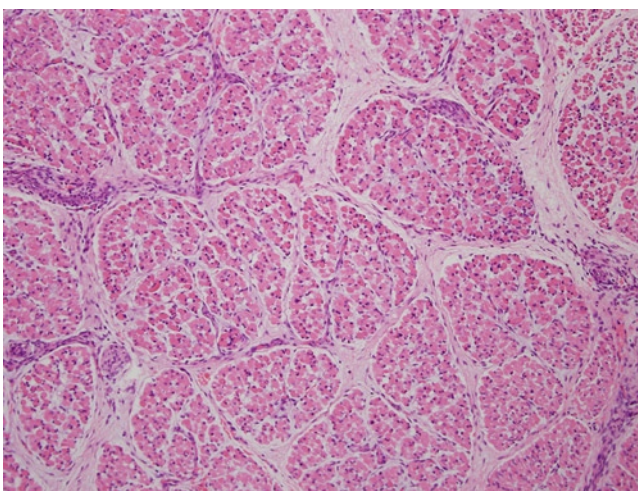


FIGURE 29-5. Fetal skeletal muscle at 17 weeks gestation. Low-power view of fascicular arrangement of muscle fibers. Note the interstitial connective tissue containing nerves and blood vessels. The muscle fibers shown are seen in cross-section and the majority of the fibers have peripherally placed nuclei. (H&E, 10 \times .)

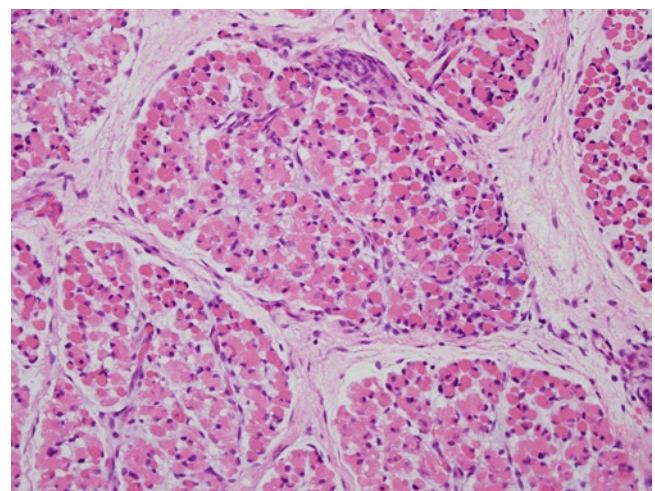


FIGURE 29-6. Fetal skeletal muscle at 17 weeks gestation. Medium-power view of muscle fascicles. The muscle fibers have fairly uniform polygonal shape and the majority of the fibers have peripherally placed nuclei. Occasional central nuclei are seen at this gestational age. (H&E, 20 \times .)

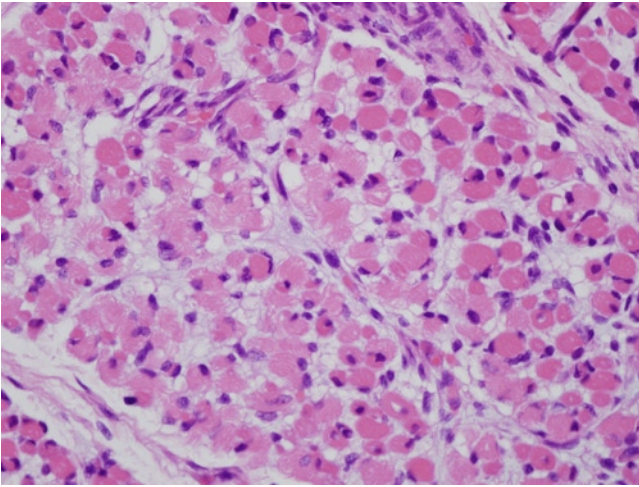


FIGURE 29-7. Fetal skeletal muscle at 17 weeks gestation. High-power view of fetal muscle fibers in cross-section, highlighting the polygonal shape and mostly peripherally placed nuclei. (H&E, 40 \times .)

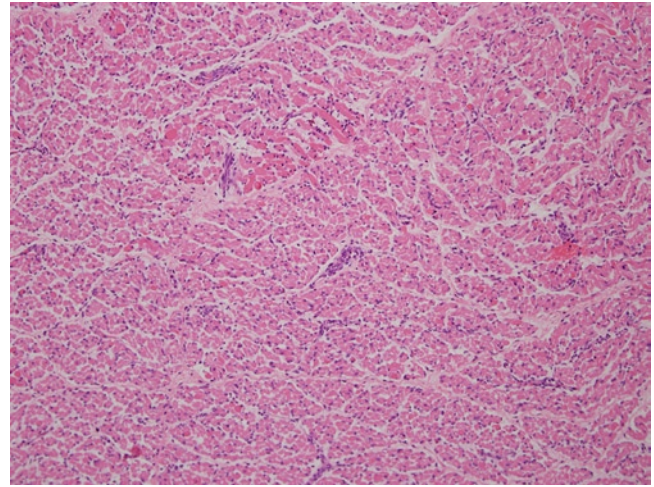


FIGURE 29-8. Fetal skeletal muscle at 23 weeks gestation. Low-power view of cross-section of skeletal muscle. Note the tight fascicular arrangement of muscle fibers. There is less interstitial connective tissue compared with 17 weeks gestation (see Fig. 29-5). (H&E, 10 \times .)

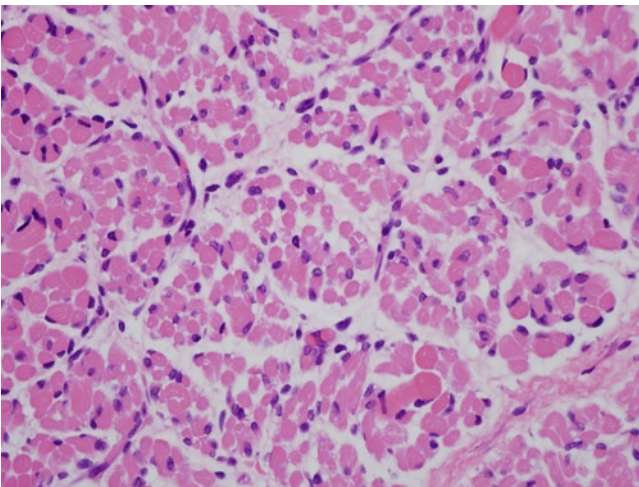


FIGURE 29-9. Fetal skeletal muscle at 23 weeks gestation. High-power view of cross-section of skeletal muscle showing fairly uniform polygonal shape of muscle fibers. By this gestational age, nearly all the fibers have peripherally placed nuclei. (H&E, 40 \times .)

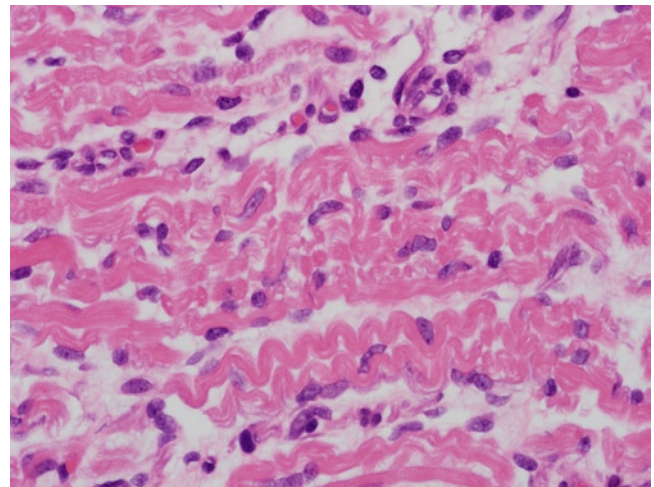


FIGURE 29-10. Fetal skeletal muscle at 23 weeks gestation. High-power view of longitudinally arranged fibers skeletal muscle. Longitudinal sections do not show the shape of the muscle fiber as well, but cross-striations of myofibrils are seen more easily. By this gestational age, nearly all the fibers have peripherally placed nuclei. (H&E, 60 \times .)

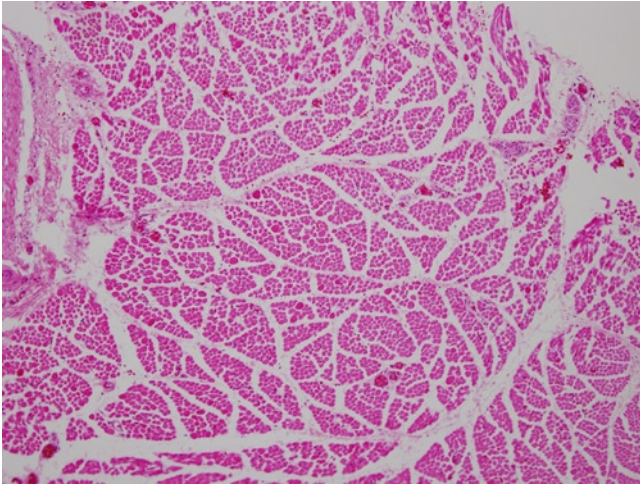


FIGURE 29-11. Skeletal muscle at term. Low-power view of cross-section of muscle fibers showing fascicular arrangement of the fibers at term. Note the interstitial connective tissue containing nerves and blood vessels. The muscle fibers are larger than earlier in gestational and have rounded polygonal shapes that are relatively uniform. The majority of the fibers have peripherally placed nuclei in this cross-section. (H&E, 10 \times .)

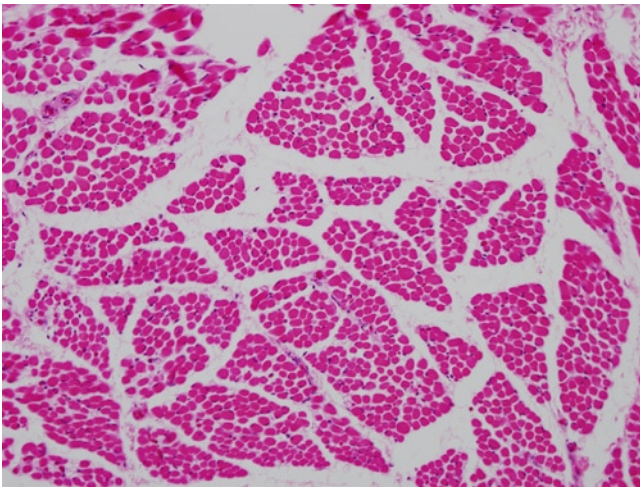


FIGURE 29-12. Skeletal muscle at term. Medium-power view of cross-section of muscle fascicles. The muscle fibers have fairly uniform, rounded polygonal shape, and the majority of the fibers have peripherally placed nuclei. Occasional central nuclei can be seen at this gestational age. (H&E, 20 \times .)

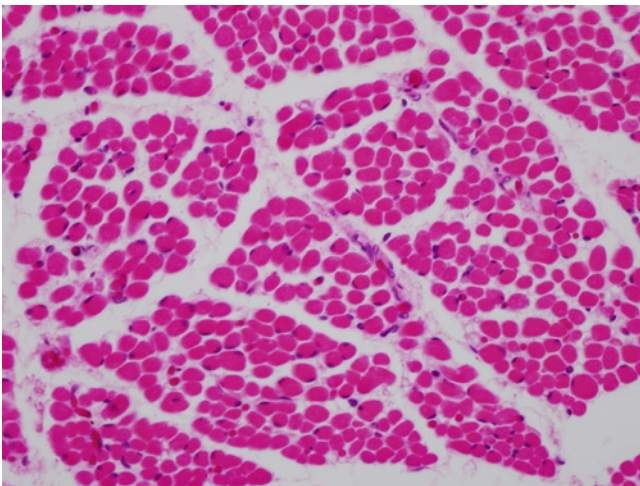


FIGURE 29-13. Skeletal muscle at term. High-power view of muscle fibers in cross-section, highlighting the rounded, polygonal shape and mostly peripherally placed nuclei. (H&E, 40 \times .)

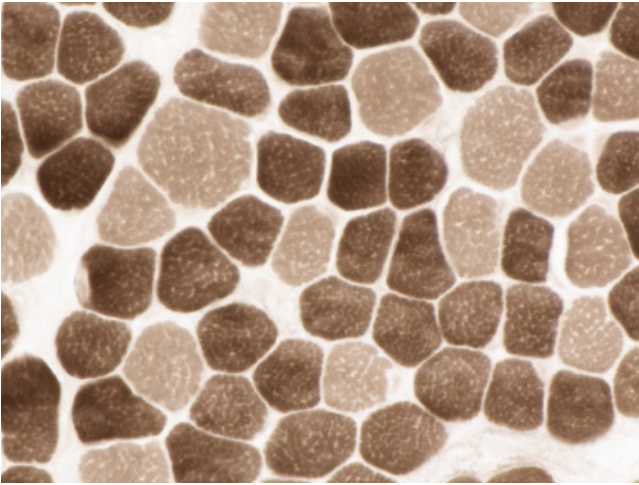


FIGURE 29-14. Skeletal muscle fiber types in full-term neonate. Frozen section muscle biopsy examined after ATPase reaction at pH 9.4 demonstrating type 1 fibers (*light brown*) and type 2a and 2b fibers (*dark brown*). Note the presence of both type 1 and type 2 fibers by this method. (Frozen section, ATPase pH 9.4, 60 \times .)

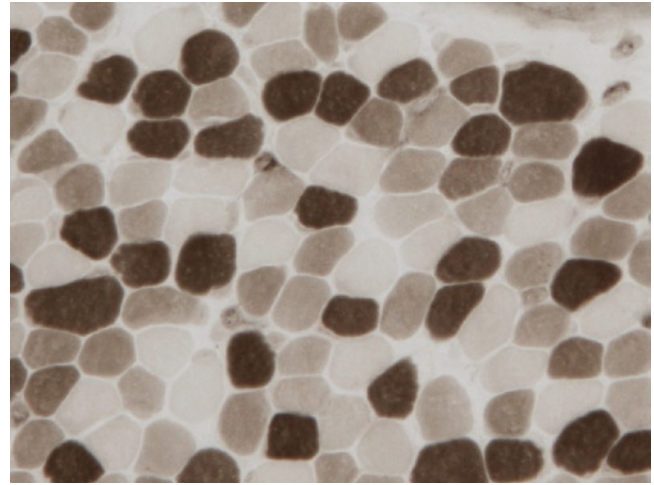


FIGURE 29-15. Skeletal muscle fiber types in full-term neonate. Frozen section muscle biopsy examined after ATPase reaction at pH 4.6 demonstrating type 1 fibers (*dark brown*), type 2b fibers (*light brown*), and type 2a fibers (*unstained*). Note the presence of both type 2a and type 2b fibers at this gestational age. (Frozen section, ATPase pH 4.7, 60 \times .)

Postnatal Muscle Development

Newborn muscle fibers have polygonal shapes, but appear more rounded than the typical angulated polygonal fibers seen in older children and adults (see Fig. 29-16) [7]. Usually muscle fibers are tightly packed together, but there is a variable amount of perimysial connective tissue consisting of collagen fibers with blood vessels and nerve tissue. Postnatal growth of mus-

cle fibers occurs by increasing the length of sarcomeres and by adding new sarcomeres. There is also some evidence of a gradual rise in fiber number after birth [8]. Satellite cells are quiescent myoblast cells with regenerative capacity and are present beneath the basement membrane of the myofiber [3,6]. These cells can be called upon to regenerate myofibers if needed.

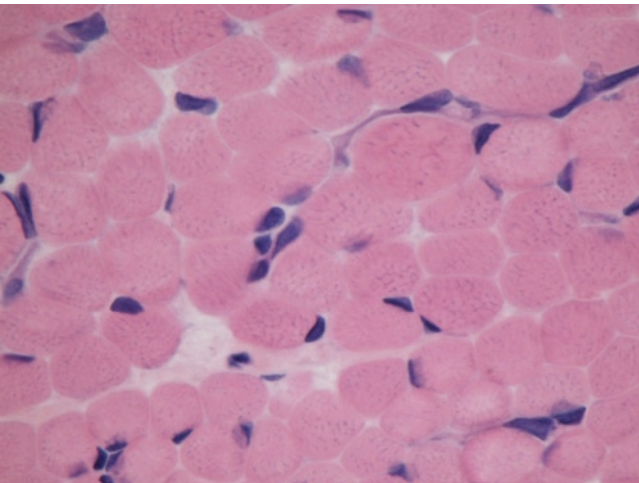


FIGURE 29-16. Newborn skeletal muscle. Note the rounded, polygonal fibers with peripheral nuclei. (Frozen section, H&E, 60 \times .)

Special Considerations

Supporting Framework of Muscle

The epimysium is the collagenous tissue that surrounds groups of fascicles and forms the outer fascia of the entire muscle. At the muscle ends, the epimysium merges with the dense connective tissue of the tendon. The muscle fascicles are each surrounded by a connective tissue sheath called the perimysium. The perimysium

contains the nerves and blood vessels to and from the muscle unit. Each individual fiber is invested, either fully or partially, by the endomysium, which is a connective tissue layer composed of collagen, elastic fibers, and reticulin fibers [5]. The terminal blood supply to the muscle fiber is found within the endomysium (see Fig. 29-17).

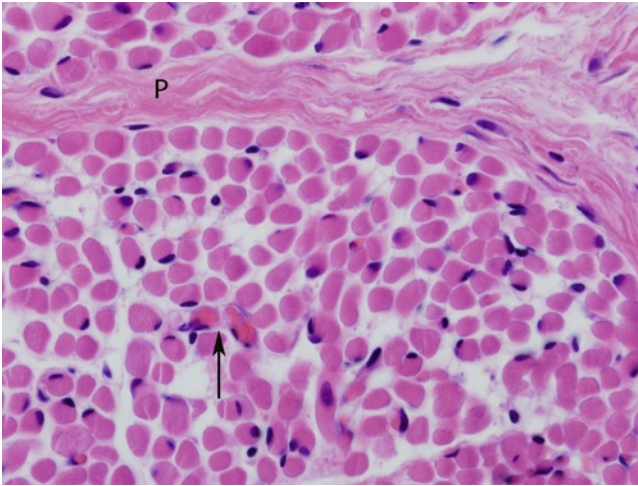


FIGURE 29-17. Perimysium and endomysium. This image of term muscle demonstrates the edge of a muscle fascicle with its surrounding perimysium (P). Note the wispy connective tissue, the endomysium, surrounding the individual muscle fibers and containing capillaries (arrow). (H&E, 60 \times .)

Muscle Spindles

Muscle spindles are mechanoreceptors that sense length and tension in the muscle. Histologically, the muscle spindle appears as an encapsulated structure within the perimysium. The capsule is composed of multiple thin layers of collagen-containing flattened specialized fibroblasts. Contained within the capsule are several intrafusal fibers, known as bag fibers and chain fibers. The bag fibers are generally larger and longer than the chain fibers [5].

The first histological evidence of the muscle spindle appears at 11 weeks gestation as a network of nerve fibrils around a few young muscle cells. The intrafusal fibers of the muscle spindle begin to differentiate from the extrafusal fibers in the twelfth week of gestation, and the formation of the capsule also begins around that

time [9]. By the fifteenth week of gestation, it appears that most, if not all, muscle spindles have formed [9]. Over gestation, the size of the muscle spindles increases and the capsule thickens (compare Figs. 29-18–Figs. 29-20). At 12 to 14 weeks, the capsule is only a single layer, and by 15 weeks it begins to have two layers (see Fig. 29-18). The layers increase over gestation with up to a maximum of five noted at 31 weeks gestation (see Figs. 29-19) and Figs. 29-20) [9]. The capsule of the mature, adult muscle spindle generally has 10 to 15 layers [5]. The intrafusal fibers enlarge over gestation and the number of intrafusal fibers within a muscle spindle increases by splitting or by incorporation of adjacent fibers up until approximately 31 weeks gestation [9]. Adult muscle spindle usually contains 3 to 15 intrafusal fibers [5].

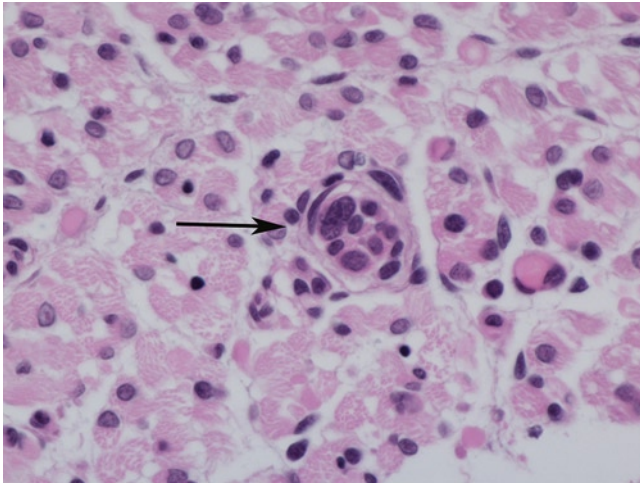


FIGURE 29-18. Muscle spindle at 16 weeks gestation. In the center of the image is an encapsulated muscle spindle (arrow) housing intrafusal fibers of varying sizes with central nuclei. Note, at this gestational age, the capsule is only a few layers thick and the muscle spindle is small in this high-power image. (H&E, 60 \times .)

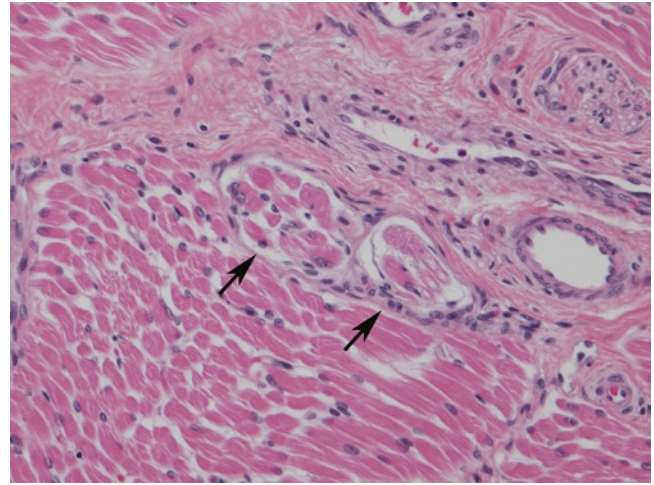


FIGURE 29-19. Muscle spindle at 34 weeks gestation. In the center of the image is a longitudinally oriented muscle spindle (arrows). The connective tissue capsule is slightly thicker and the muscle spindle is larger (compare with Fig. 29-18). Intrafusal fibers of varying sizes with central and peripheral nuclei are noted. (H&E, 20 \times .)

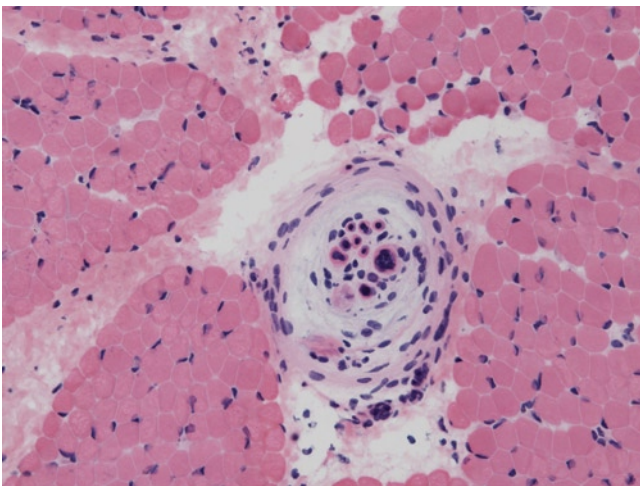


FIGURE 29-20. Muscle spindle in newborn. In the center of this frozen section, muscle biopsy of a newborn is an encapsulated muscle spindle. Note the larger size of this muscle spindle and several concentric thin layers of collagen forming the capsule, with specialized fibroblasts within the capsule. Within the capsule are several intrafusal fibers cut in cross-section. (Frozen section, H&E, 20 \times .)

References

1. Carpenter S, Karpati G: *Pathology of Skeletal Muscle*, edn 2. New York: Oxford University Press; 2001.
2. Sadler TW, Langman J: *Langman's Medical Embryology*, edn 11. Philadelphia: Wolters Kluwer Lippincott Williams & Wilkins; 2010.
3. Schoenwolf GC, Larsen WJ: *Larsen's Human Embryology*, edn 4. Philadelphia, PA: Elsevier/Churchill Livingstone; 2009.
4. The skeletal system and the limbs. In *Human Embryology & Teratology*, edn 3. Edited by O'Rahilly R, Mèuller F. New York: Wiley-Liss; 2001:360.
5. Heffner RR, Balos LL: Skeletal muscle. In *Histology for Pathologists*. Edited by Mills SE. Philadelphia: Lippincott Williams & Wilkins; 2007:195–198.
6. Romansky SG: Neuromuscular diseases. In *Potter's Pathology of the Fetus, Infant, and Child*, edn 2. Edited by Gilbert-Barness E. Philadelphia, PA: Mosby Elsevier; 2007:1889–1957.
7. Lake BD, Barbet JP: Skeletal musculature. In *Textbook of Fetal and Perinatal Pathology*, edn 2. Edited by Wigglesworth JS, Singer DB. Malden, MA: Blackwell Science; 1998:1083–1109.
8. Adams RD, DeReuck J: Metrics of muscle. In *Basic Research in Myology*. Amsterdam: Excerpta Medica; 1972.
9. Cuajunco F: Development of the neuromuscular spindle in human fetuses. *Contributions to Embryology* 1940, 28:95–128.

SECTION IX

Mammary Gland

30

Mammary Gland

Dale S. Huff

The prenatal and neonatal development of the mammary gland occurs in three stages: 1) the primordia from 6 to 8 weeks postmenstrual age; 2) the nipple from 8 to 19 weeks; and 3) the ducts of the mammary gland proper from 19 weeks to the neonatal period. The developing breast is composed of specialized epithelium and mesenchyme. The specialized epithelium will form the ectodermal nipple and the mammary ducts. The specialized mesenchyme will form the stroma and smooth muscle of the nipple and areola, the intralobular stroma, and the interlobular septa, as well as the supporting connective tissues including the capsule, Cooper ligaments, and pectoral ligaments. Cooper ligaments anchor the breast to the overlying dermis. Pectoral ligaments anchor the breast to the underlying pectoralis fascia. Interactions between the mesenchyme and epithelium result in the synchronous differentiation of the epithelial basal cells into myoepithelium and the mesenchyme into its various components.

The early development of the specialized mesenchyme may be androgen dependent. The prenatal development of the nipple and mammary ducts is independent of hormonal control until maternal and placental hormones stimulate the hyperplasia and secretory activity of the ducts, beginning at 35 weeks. Fetal prolactin stimulates the neonatal secretion of milk, which can lead to a transient discharge of a thin milky liquid sometimes referred to as "witches' milk" from the nipple at 5 to 7 days of age. The prenatal and neonatal mammary gland is similar in females and males.

The postmenstrual gestational ages given for the timing of the developmental events are estimates. The ages at which the events occur vary widely among published series and studies large enough to define the range of gestational ages at which specific features normally appear are not available. Therefore, the definitions of normal, delayed, or advanced development for a given gestational age have not been established.

Embryology

The Primordia: 6 2/7 to 8 0/7 Weeks

The primordia of the breast are the mammary band, mammary crest, and primordial nipple. The mammary band is also known as the intermembral segment of the ectodermal ring [1]. See the section entitled The Early Embryology of the Genitourinary Tract for a description of the ectodermal ring.

The mammary band is the segment of the ectodermal ring between the upper and lower limb buds. It appears early in the sixth week. Since the mammary band is present in nonmammalian as well as mammalian vertebrates, it is not specific for the mammary gland.

The mammary crest is the primordium that is specific for the mammary gland and develops within the mammary band [1,2]. The mammary crest appears at 7 weeks as a narrow, microscopic thickening of the ectoderm within the mammary band adjacent to the caudal edge of the upper limb bud. It grows caudally as a narrow, linear crest for a variable

distance toward the lower limb bud. The mammary crest stops its caudal growth then shortens by regression beginning at its caudal end and extending cranially. By 8 weeks all that remains of the crest is a round, lens-shaped placode of thickened ectoderm near the upper limb bud in the region that will become the axilla.

The mesoderm under the ectodermal placode becomes specialized and differentiates into two layers, a dense band under the ectodermal basement membrane and a deeper, looser, well-vascularized layer. This ectodermal placode and the underlying specialized mesoderm are the primordium of the nipple [1,2].

Histology

The Nipple: 8 to 19 Weeks

During the 8th week, the nipple is a microscopic, lens-shaped, nodular placode in the lateral ectoderm at the caudal edge of the upper limb bud. It bulges upward above the surface of the surrounding epidermis and downward into the underlying specialized mesoderm. The low, cuboidal basal cells of the surrounding epidermis differentiate into the specialized basal cells of the nipple, which are tall, columnar cells with apical nuclei and subnuclear vacuoles. The other cells of the nipple, the central cells, are large, polygonal, and vacuolated and have small, eccentric nuclei. The two-layered, specialized mesenchyme differentiates further into four concentric layers stretched around the deep surface of the nipple. The most superficial layer will become the dense, dermis-like stroma of the nipple and areola. The second layer will become the layer of smooth muscle of the nipple and areola. The third layer will become the intralobular stroma. The deepest layer will form the dense, supporting connective tissues of the breast including the interlobular septa, the capsule of the breast, Cooper ligaments, and the pectoralis ligaments [2]. In routine autopsy material, some of these layers may be indistinct.

During the 9th week, the position of the nipple begins to shift from the lateral to the ventral aspect of the body. The surface of the nipple flattens and becomes flush with the surrounding epidermal surface. The deep portion of the nipple enlarges and pushes into the underlying mesenchyme, forming an enlarging hemispheric ectodermal nodule. The specialized mesoderm completely surrounds the globular nipple and extends laterally

under the immediately adjacent epidermis that will become the areola [2].

During the 10th week, the specialized mesenchyme becomes more distinct and proliferates, pushing the nipple up above the level of the adjacent epidermis. A shallow pit, the mammary pit, appears in the center of the ectodermal surface of the nipple, forming the inverted nipple characteristic of the prenatal breast. By the 14th week, the immunohistochemical phenotypes of the basal and central cells of the nipple are distinct from each other and from their counterparts in the adjacent epidermis [3]. The nipple is in its final position on the ventral body wall.

Beginning at the 15th week, the deep border of the nipple becomes irregular and lobulated (see Figs. 30-1 and 30-2). The specialized mesenchyme continues to proliferate, forming a mound at the top of which sits the inverted nipple. The mammary pit deepens. The tall columnar basal cells of the nipple remain distinct from the small, cuboidal basal cells of the adjacent epidermis. The areola becomes identifiable grossly and microscopically because it lacks the pilosebaceous units and sweat glands that appear in the adjacent skin at this time. Lobules of fat appear in the subcutaneous tissue of the adjacent skin but not in the specialized mesoderm of the nipple and areola. At 16 weeks, keratinization begins and the mammary pit becomes filled with keratin. By 17 weeks, the basal cells of the nipple are immunophenotypically incompletely differentiated epithelial precursor cells [3,4]. Sensory end organs appear in the specialized mesenchyme.

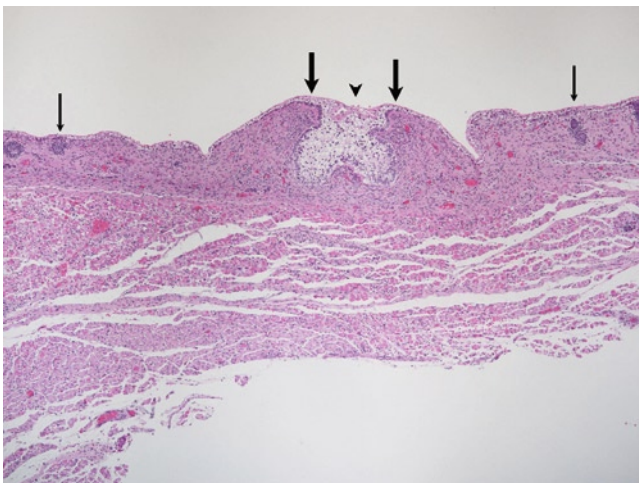


FIGURE 30-1. Lobular phase of the development of the nipple: gestational age 16 weeks. The diameter of the ectodermal nipple is 0.25 mm. The *narrow arrows* close to the edges point to pilosebaceous units at the junction of the areola and adjacent epidermis. The *thick arrows* point to the edges of the ectodermal nipple. The *arrow head* points to the shallow mammary pit. The ectodermal nipple sits on top of the mound of specialized mesenchyme and this picture persists throughout prenatal development. Note the irregular indentations of the deep border of the nipple, the absence of pilosebaceous units in the areola, the presence of pilosebaceous units in the adjacent skin, the concentric layers of specialized mesenchyme around the nipple and under the areola, and the underlying pectoralis muscle. Figures 30-1 and 30-2 are from the same breast. (Hematoxylin and eosin [H&E], 4 \times .)

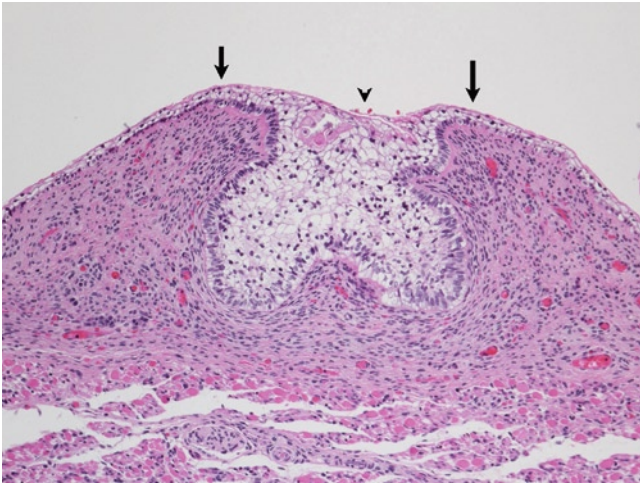


FIGURE 30-2. Lobular phase of the development of the nipple: gestational age 16 weeks: higher magnification of Figure 30-1. The *arrows* point to the edges of the nipple. The *arrow head* points to the mammary pit. Keratinization of the mammary pit is beginning. The small, inconspicuous basal cells of the adjacent epidermis differentiate into the specialized tall, columnar basal cells of the nipple. Note the large, clear central cells. The concentric layers of the specialized mesenchyme around the nipple and under the areola are easily seen. (H&E, 10 \times .)

The Mammary Ducts: 19 Weeks to the Neonatal Period

Until the 19th week, the development of the breast has involved only the nipple, areola, and specialized mesoderm. The development of the mammary ducts begins at 19 weeks when the basal cells of the nipple at a few discrete foci differentiate into pseudostratified placodes of thin, columnar cells with scant cytoplasm and long, hyperchromatic nuclei. These placodes are the beginnings of the primary mammary ducts (see Figs. 30-3 and 30-4). A thick layer of smooth muscle appears in the second layer of the specialized mesoderm under the nipple and areola (see Fig. 30-5). The orientation of the muscle is predominately circular, but vertically oriented fibers are also present, most noticeably parallel to the primary ducts under the nipple. Glands of Montgomery, sometimes called *tubercles of Montgomery*, appear in the areola. Glands of Montgomery are composed of a large complex of sebaceous units associated with a single duct that is similar to a lactiferous duct, which opens onto the surface of the areola often near its periphery. Although the ducts are difficult to distinguish from lactiferous ducts, the glands of Montgomery end blindly and do not contribute to the ductal-lobular parenchyma of the mammary gland. At 19 weeks the immunophenotype of the basal cells has differentiated into myoepithelial cell precursors and that of the central cells into luminal epithelial cell precursors [3,4].

As the first mammary duct placodes elongate into solid primary mammary ducts, new placodes form and then elongate until a total 15 to 20 solid, straight primary ducts are present. These are the future lactiferous ducts of the major segments of the adult breast and they penetrate perpendicularly into the first two layers of dense, specialized mesenchyme. Each has a long, straight stem or stalk and an end bud. The end buds are bulbous and solid. The stalks develop lumens and are lined by two layers of cells, basal cells and luminal cells. The basal cells are cuboidal in contrast to the tall, columnar basal cells of the nipple and they lie upon a thick, continuous basement membrane. The luminal cells are small and non-vacuolated in contrast to the large, vacuolated central cells of the nipple. The solid end buds lack a distinct basement membrane and are composed of undifferentiated

basal and central epithelium (see Figs. 30-6–30-8). By 22 weeks, basal cells at the junction of the stalks and end buds differentiate into smooth muscle actin-positive, terminally differentiated myoepithelial cells and the central cells differentiate into terminally differentiated luminal epithelial cells [3–5].

By the 24th week, the end buds of the elongating ducts penetrate through the dense layer of smooth muscle and into the underlying layer of loose mesenchyme. A sheath of the loose mesenchyme surrounds each duct and will become the intralobular stroma. The ducts with their loose stromal sheaths are separated by septa, the interlobular septa, arising from the fourth dense, deep layer of specialized mesenchyme. The end buds begin to grow by branching morphogenesis within the loose intralobular stroma [6]. The end buds are the active sites of proliferation, invasion, branching, and differentiation of the ducts. Sebaceous glands appear at the origins of the ducts and glands of Montgomery (see Figs. 30-9 and 30-10). Lumens extend into the end buds, the mammary pit becomes wider and shallower, and the inverted nipple becomes cup shaped (see Figs. 30-11–30-13).

By 26 weeks, continued branching morphogenesis results in a complex ductal tree, a lobular pattern, and an enlarging breast bud. Secretions appear in the lumens of the end buds. Maturing interlobular septa accentuate the lobular-like architecture and Cooper ligaments and pectoralis ligaments become more conspicuous. Adipose tissue appears within the intralobular stroma and interlobular septa, and the inverted nipple becomes larger and deeper. By 32 to 35 weeks, the breast bud becomes palpable but is usually only a few millimeters in diameter (see Figs. 30-14–30-17).

By 35 weeks gestation, ductal elongation, end bud branching, and secretion accelerate, causing enlargement of the breast bud (see Figs. 30-18–30-20). Extramedullary hematopoiesis is commonly seen in the intralobular stroma and less often in the interlobular septa. The amount varies widely and tends to be more extensive near term than earlier in development. In some cases, the myoepithelial cells assume the phenotype of mature smooth muscle cells (see Fig. 30-21).

Squamous metaplasia of large ducts, apocrine metaplasia (see Fig. 30-22), and giant cells in the interlobular stroma may be seen as have been described in adults (see Figure 30-23). At term, the breast bud is usually 8 mm in diameter. Secretion of "witches' milk" and oozing of milk from the nipple may be apparent by 5 to 7 days of life. The lobular architecture, branching end buds, and secretory changes mimic but are probably not identical to the terminal duct lobular unit and alveolae of the adult. Some ducts become cystic (see Figure 30-24). The breast continues to enlarge for 2 weeks or longer after a term birth and may attain a diameter of a few or more centimeters. The nipple may remain inverted.

Beginning at approximately 2 weeks postnatal age, the distal branches of the ductal tree begin to regress and secretion decreases. The intralobular stroma begins

to disappear. Cystic change may become extensive prior to complete regression (see Figs. 30-25 and 30-26). The dense interlobular stroma becomes more prominent and the breast is reduced to the 15 to 20 segmental lactiferous ducts and a few major branches (see Fig. 30-27). The breast decreases in size but may be palpable and up to 1 cm in diameter at 6 months of age [7,8].

The definitions of the normal size of the breast bud, the duration of the stage of hyperplasia and secretion, and duration and severity of cystic change are not well established. Cystic change may become severe and persistent, and secretory changes may persist in the thin epithelial linings of the cysts. The distinction between persistent cystic regression and galactocele may be difficult. After neonatal regression is complete, the breast remains inactive until thelarche.

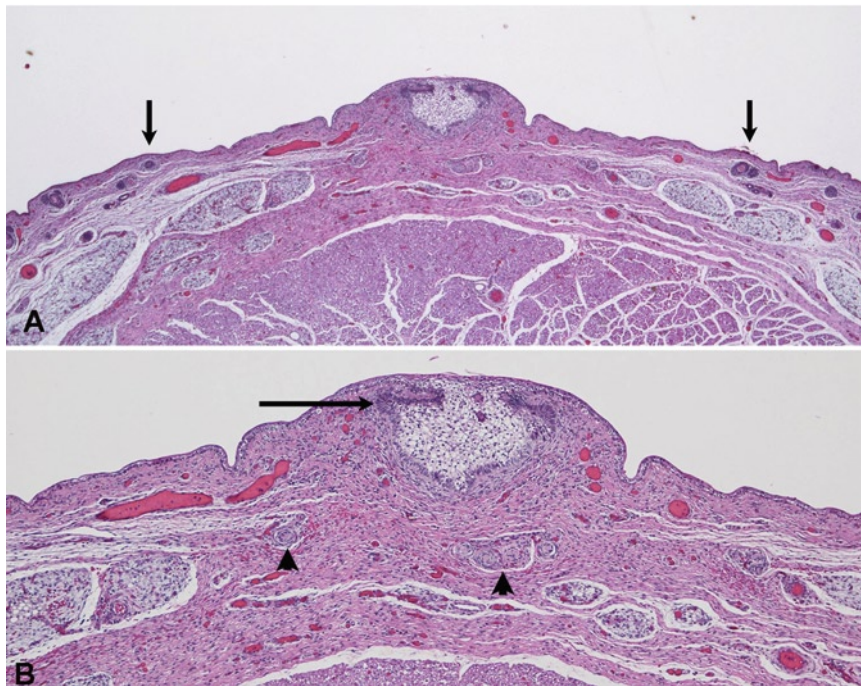


FIGURE 30-3. Earliest appearance of the buds of the mammary ducts: gestational age 21 3/7 weeks. The diameter of the ectodermal nipple has not enlarged and is 0.25 mm. Figures 30-3 and 30-4 are from the same breast. **A**, Buds of mammary ducts. This breast is very similar to that shown in Figures 30-1 and 30-2, except for the presence of the buds of the mammary ducts. The arrows point to pilosebaceous units at the junction of the areola and adjacent epidermis. The differences between the adjacent skin and the areola are depicted with numerous pilosebaceous units in the adjacent skin, but none in the areola. Fetal fat is now abundant in the subcutaneous tissue

under the adjacent skin but is sparse under the periphery of the areola and absent under the nipple and central areola. The dense, specialized mesenchyme extends to the pectoralis fascia. Sensory end organs have appeared in the specialized mesenchyme of the nipple and areola and dilated capillaries surround the nipple. (H&E, 2 \times .) **B**, Higher magnification of **A**. The mammary pit is tangentially sectioned and appears as tubular cross sections. Two early buds of mammary ducts are seen, one arising from each shoulder of the nipple. The horizontal arrow points to the bud on the left. The arrow heads point to sensory end organs. (H&E, 4 \times .)

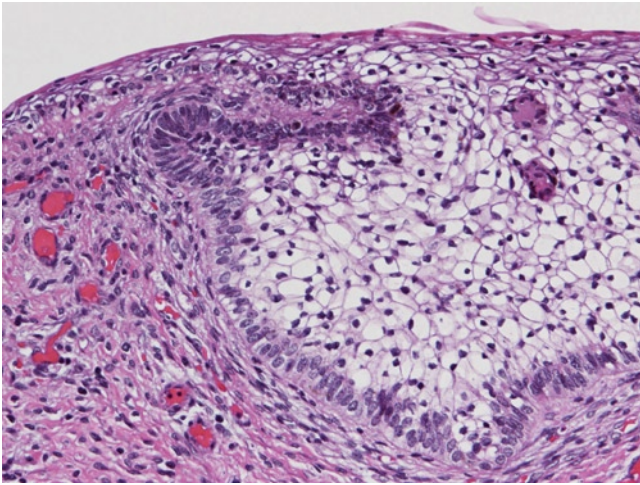


FIGURE 30-4. Earliest appearance of the buds of the mammary ducts: gestational age 21 3/7 weeks: higher magnification of Figure 30-3. Note the details of the differentiation of the basal cells from the low, inconspicuous cells of the adjacent epidermis to the tall, specialized basal cells of the nipple and then to the pseudostratified, columnar, hyperchromatic cells of the bud of the mammary duct on the left. The large, vacuolated central cells of the nipple blend into the midzone of the epidermis. (H&E, 20 \times .)

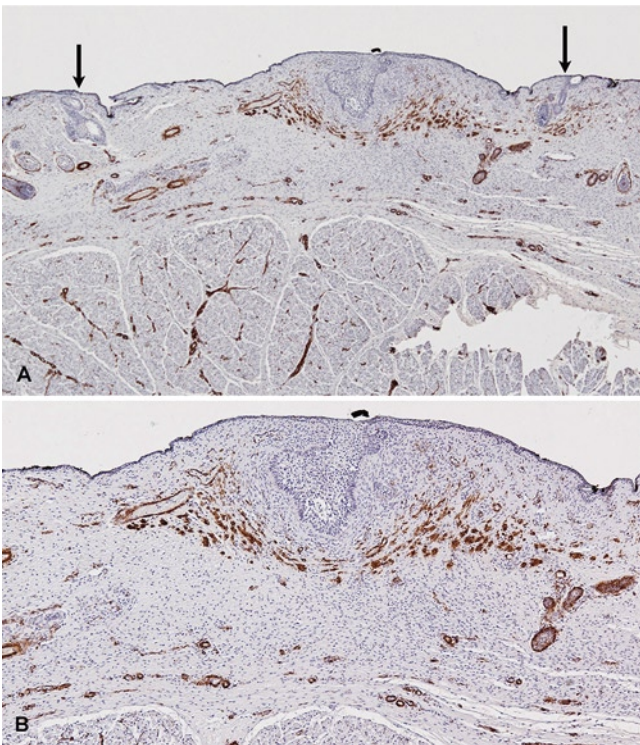


FIGURE 30-5. Smooth muscle in the second layer of specialized mesenchyme: gestational age 23 0/7 weeks. The diameter of the ectodermal nipple is still 0.25 mm. **A**, Concentric rings of smooth muscle surround the nipple and extend like wings into the mesenchyme of the central areola. The arrows point to pilosebaceous units at the junction of the areola and adjacent epidermis. One bud of a mammary duct arises from the top right side of the nipple. Fetal fat is not seen under the nipple and areola. (Smooth muscle actin immunostain, 2 \times .) **B**, Higher magnification of **A**. Note the first layer of dense mesenchyme under the nipple and areola, the smooth muscle in the second layer, and the undifferentiated deeper layers of mesenchyme extending to the pectoralis fascia. (Smooth muscle actin immunostain, 4 \times .)

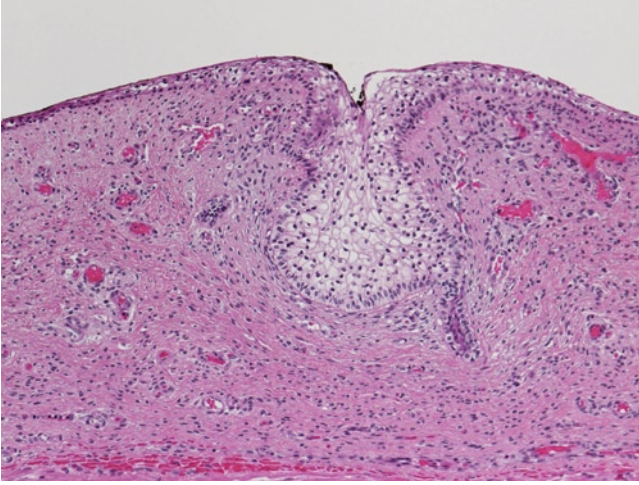


FIGURE 30-6. Ducts penetrating into the first two layers of specialized mesenchyme: gestational age 21 5/7 weeks. The diameter of the nipple is 0.25 mm. This photograph includes the ectodermal nipple, the specialized mesenchyme, and the central areola, but not the periphery of the areola. A corona of dilated capillaries surrounds the nipple and the mammary pit is deepening. The histologic phenotype of the basal cells of the nipple remains distinct from that of the adjacent epidermis. An elongating duct arising from the lower right corner of the nipple is pushing into the mesenchyme. Figures 30-6 to 30-8 are from the same breast. (H&E, 10 \times .)

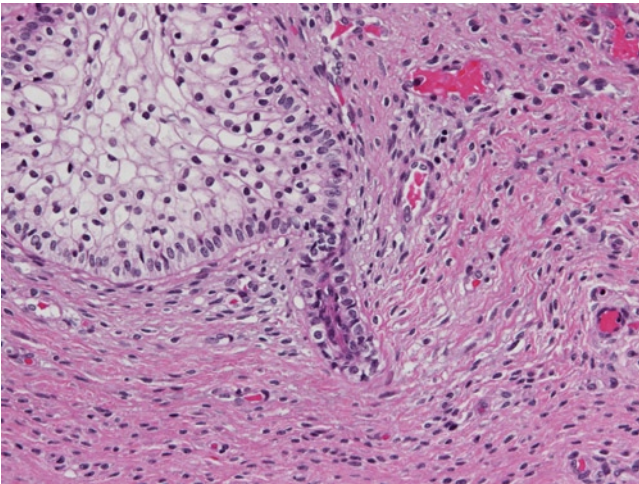


FIGURE 30-7. Ducts penetrating into the first two layers of specialized mesenchyme: gestational age 21 5/7 weeks: higher magnification of Figure 30-6. This solid duct is composed of basal and luminal epithelial cells. The cuboidal basal cells are precursors of myoepithelial cells and are distinct from the columnar basal cells of the nipple. The luminal cells are squamous-like. (H&E, 20 \times .)

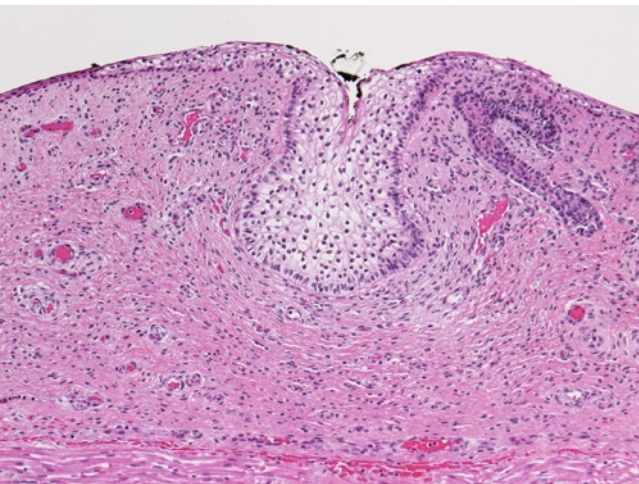


FIGURE 30-8. Ducts penetrating into the first two layers of specialized mesenchyme: gestational age 21 5/7 weeks: deeper section. Two penetrating ducts join before entering the nipple. Each has a bulbous solid end bud that is the site of ductal differentiation, proliferation, and elongation. The concentric layers of mesenchyme extend to the fascia of the pectoralis muscle at the bottom of the picture. (H&E, 10 \times .)

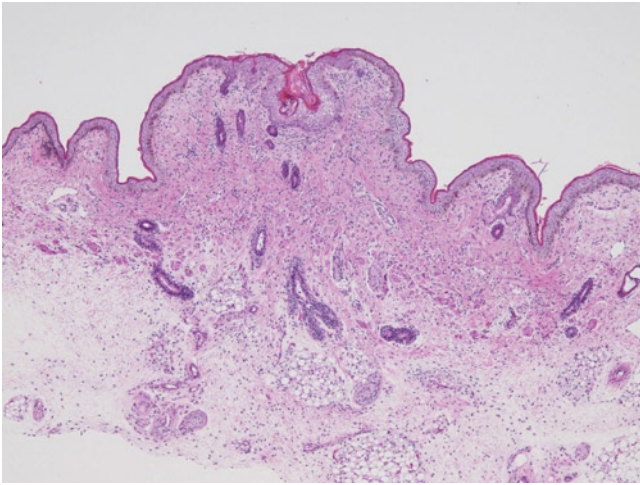


FIGURE 30-9. Early branching morphogenesis of mammary ducts: gestational age 24 4/7 weeks. The enlarging nipple has a diameter of 1 mm. The inverted nipple sits atop a mound of specialized mesenchyme and most of the areola is included. The ducts have pushed through the layer of smooth muscle, penetrated into the underlying layer of loose mesenchyme that will become the intralobular stroma and are elongating by branching morphogenesis. Glands of Montgomery arise from the areola lateral to the nipple. They are nearly identical to the major mammary ducts but do not have end buds and do not branch. One is associated with sebaceous glands. Figures 30-9 and 30-10 are from the same breast. (H&E, 4 \times .)

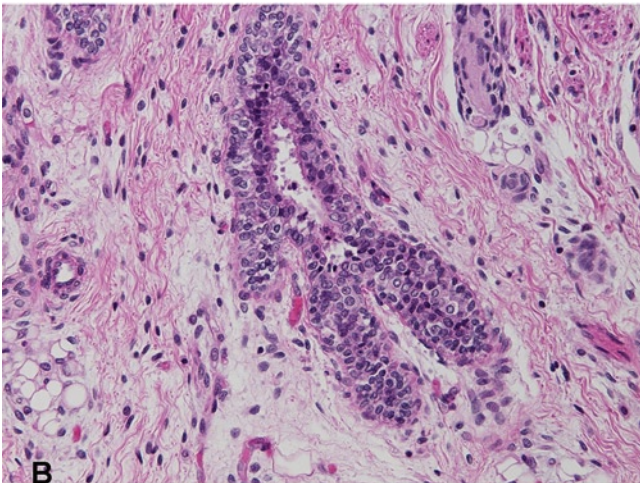
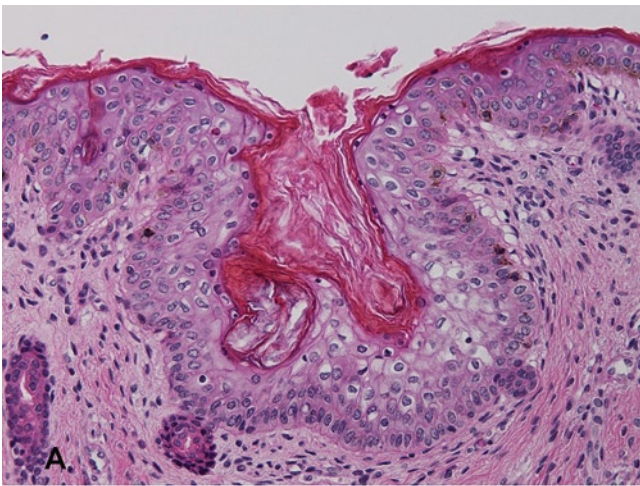


FIGURE 30-10. Early branching morphogenesis of mammary ducts: gestational age 24 4/7 weeks: higher magnifications of Figure 30-9. **A**, The enlarging crater of the inverted nipple is filled with keratin. The major ducts are lined by a layer of cuboidal basal cells and a layer of flat luminal cells with eosinophilic cytoplasm. (H&E, 10 \times .) **B**, The terminal ducts enter the intralobular stroma and branch into solid terminal end buds. The terminal ducts are lined by a basal layer of terminally differentiated myoepithelial cells and a luminal layer of terminally differentiated luminal epithelial cells. The solid end buds are lined by basal precursors of myoepithelial cells and central precursors of luminal epithelial cells. Epithelial differentiation occurs at the junction of the terminal duct and end bud. Note the difference in the phenotypes of the epithelial cells of the primary ducts, terminal ducts, and end buds. (H&E, 20 \times .)

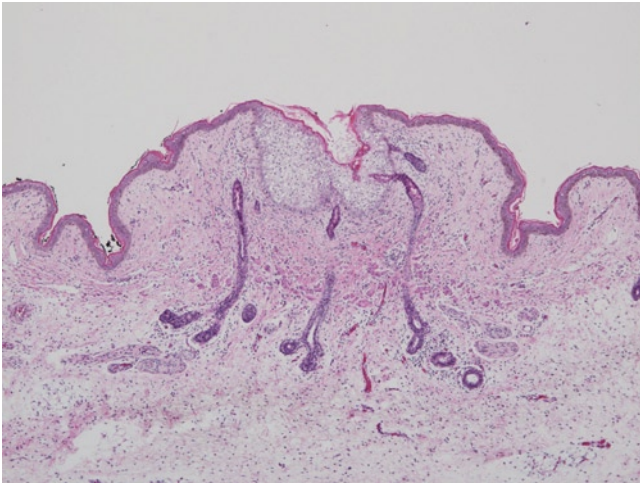


FIGURE 30-11. Progressive branching morphogenesis. The breast shown is only slightly more advanced than the one shown in Figure 30-10. The gestational age is 26 5/7 weeks and the diameter of the nipple is 1 mm. After this nipple becomes everted sometime after birth, the orifice of the duct entering the middle of the nipple in this image will be located at the tip of the everted nipple while those entering the lateral border here will be located at sides of the everted nipple. The layer of smooth muscle is prominent. Figures 30-11 to 30-13 are from the same breast. (H&E, 4 \times .)

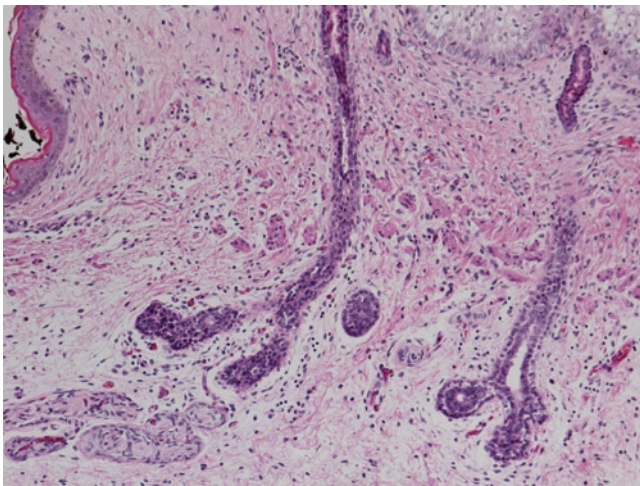


FIGURE 30-12. Progressive branching morphogenesis: higher magnification of Figure 30-11. The branches of each primary duct form a simple lobule invested in loose intralobular stroma. The lobules are separated by slightly more dense interlobular connective tissue that is derived from the fourth layer of the specialized mesenchyme. Undifferentiated end buds are seen on the left and sensory end organs are prominent. (H&E, 10 \times .)

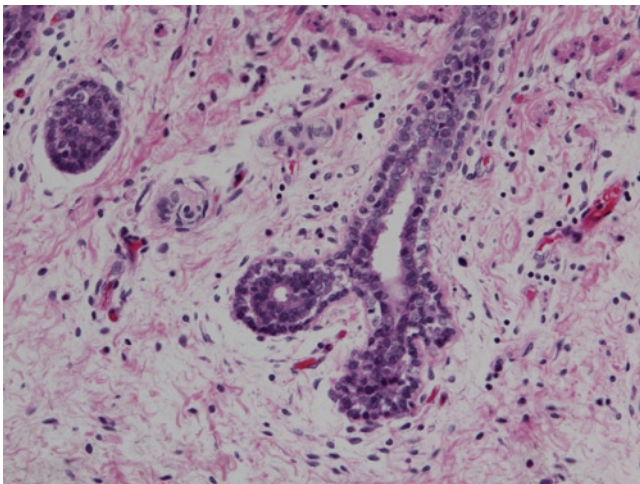


FIGURE 30-13. Progressive branching morphogenesis: higher magnification of the lobule on the right in Figure 30-12. The lumen extends into the terminal branches of the duct. The myoepithelial and luminal epithelial cells demonstrate progressive differentiation. (H&E, 20 \times .)

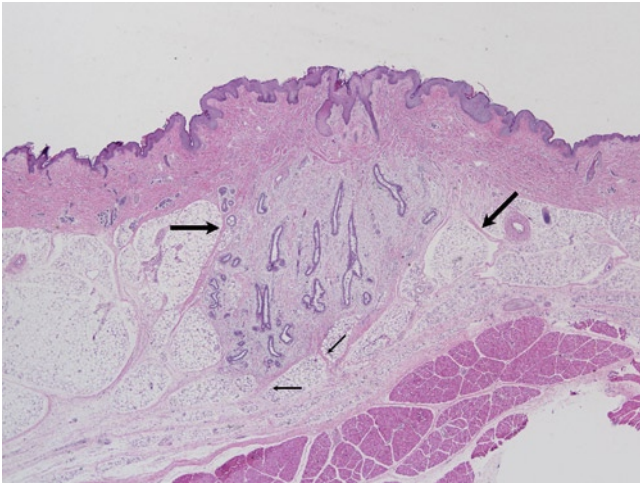


FIGURE 30-14. Complex branching of mammary ducts: gestational age 34 4/7 weeks. The diameter of the breast bud is 3 mm. The complex branching results in an enlarging, palpable breast bud and the primary ducts entering the nipple are lined by squamous epithelium. Each primary duct has several generations of branches that form complex lobules surrounded by intralobular stroma. The interlobular septa are becoming more dense and the irregular capsule, Cooper ligaments, and pectoral ligaments are becoming defined. The *large arrows* point to Cooper ligaments and the *small arrows* point to pectoral ligaments. Figures 30-14 to 30-17 are from the same breast. (H&E, 2 \times .)

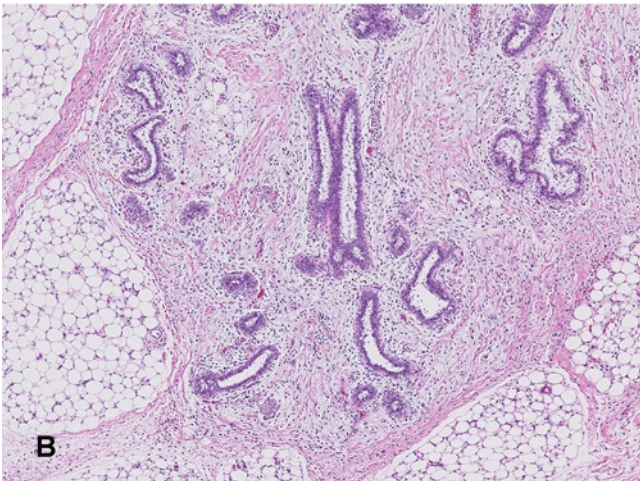
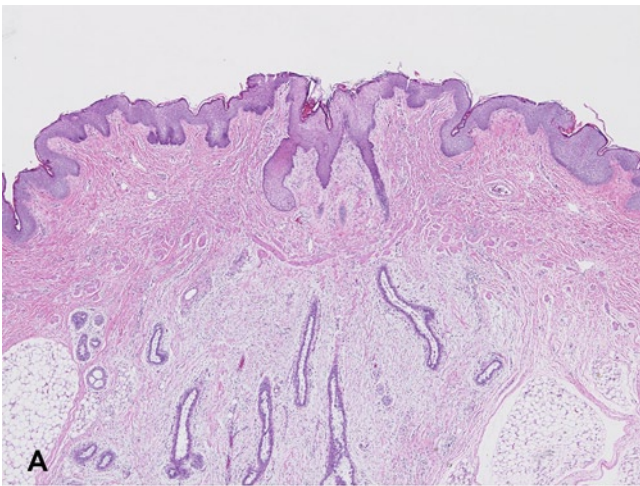


FIGURE 30-15. Complex branching of mammary ducts: gestational age 34 4/7 weeks: higher magnifications of Figure 30-14. Note the continuing differentiation of the loose intralobular stroma and wisps of denser interlobular stroma in this figure and the following figures. (A, H&E, 4 \times and B, H&E, 10 \times .)

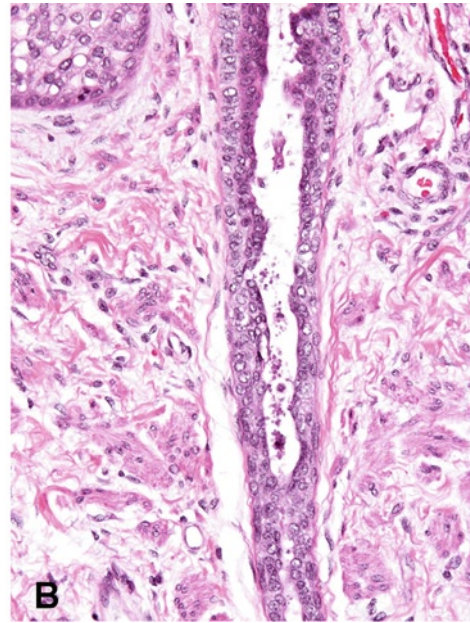
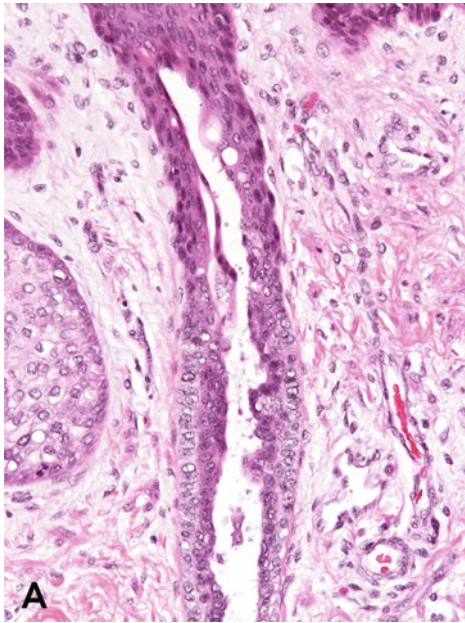


FIGURE 30-16. Higher magnification of primary ducts. **A**, This segment of the primary duct is superficial to the layer of smooth muscle. The proximal end of the duct (*top*) is lined by squamous epithelium. Distally (*bottom*), the myoepithelium transforms from an inconspicuous layer of flattened cells to a prominent layer of cuboidal cells while the luminal epithelium is composed

of one or more layers of flattened eosinophilic cells. (H&E, 20 \times .) **B**, This is the same duct as it penetrates through the layer of smooth muscle. Its proximal end (*top*) overlaps the distal end of the duct in **A**. The myoepithelial cells transform from the cuboidal cells in **A** to inconspicuous flat cells, while the luminal epithelial cells become prominent cuboidal cells. (H&E, 20 \times .)

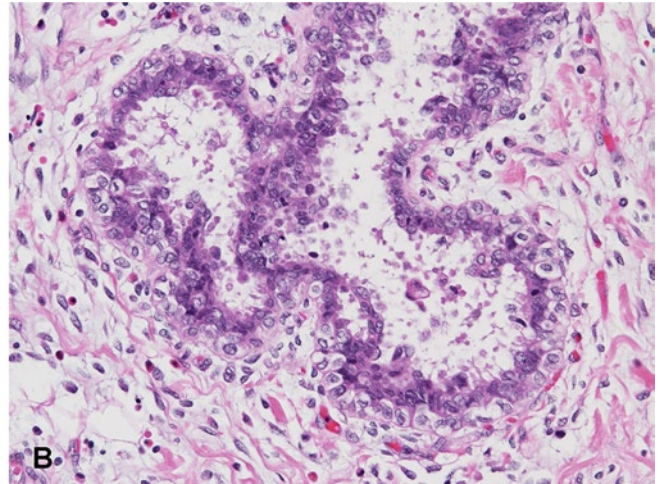
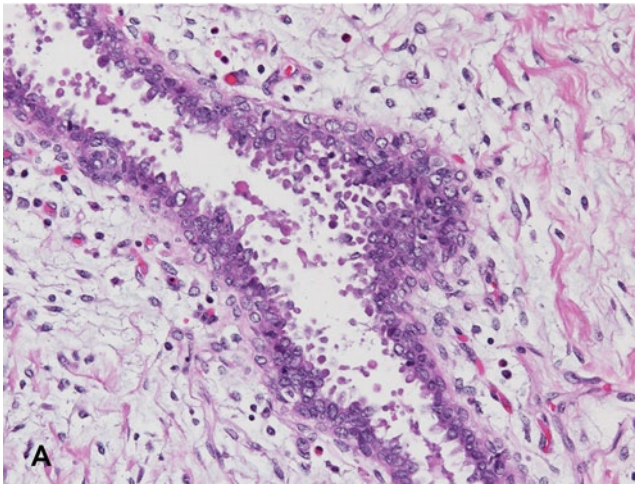


FIGURE 30-17. Primary duct entering the intralobular stroma. **A**, Primary duct deep to the layer of smooth muscle is shown. The morphology of the duct changes dramatically as it enters the intralobular stroma beneath the layer of smooth muscle. The myoepithelial cells are flat and inconspicuous while the luminal epithelial cells are tall and columnar, and demonstrate apical

projections and blebs. The lumen contains secretory material. There is mild extramedullary hematopoiesis in the intralobular stroma. (H&E, 20 \times .) **B**, Branching ends of an intralobular duct. The end buds have lumens containing secretions and the myoepithelial cells are prominent. (H&E, 20 \times .)

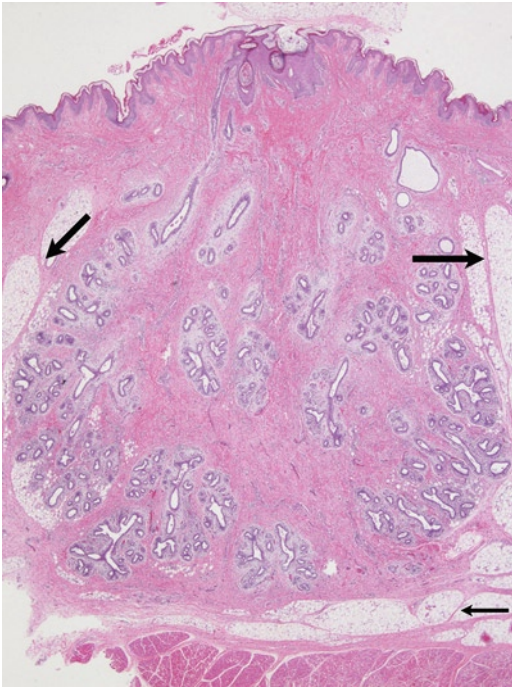


FIGURE 30-18. Neonatal hyperplasia and secretion: gestational age 38 6/7 weeks. The diameter of the breast bud is 7 mm. The lobular appearance is exaggerated by the enlargement of the lobules and the broad, dense bands of interlobular stroma. The capsule of the breast, Cooper ligaments, and pectoral ligaments are more prominent. Fat is present in the lobules and interlobular septa. The *large arrows* point to Cooper ligaments and the *small arrows* point to pectoral ligaments. Figures 30-18 to 30-20 are from the same breast. (H&E, 1×.)

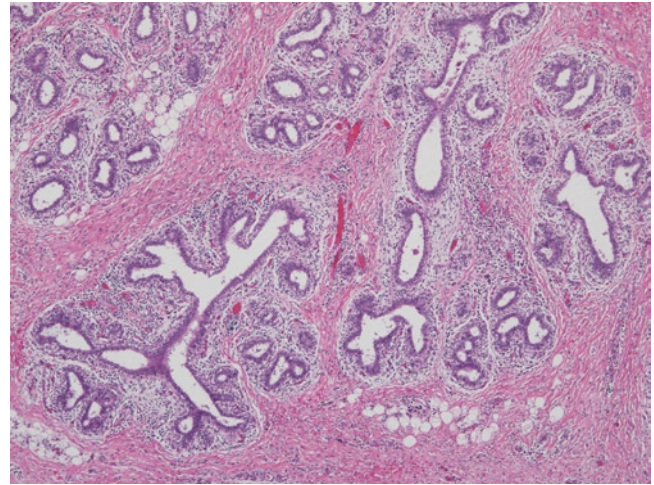


FIGURE 30-19. Neonatal hyperplasia and secretion: gestational age 38 6/7 weeks: higher magnification of Figure 30-18. Intralobular branching of the ducts is extensive and complex. Extramedullary hematopoiesis is prominent in the intralobular stroma. (H&E, 10×.)

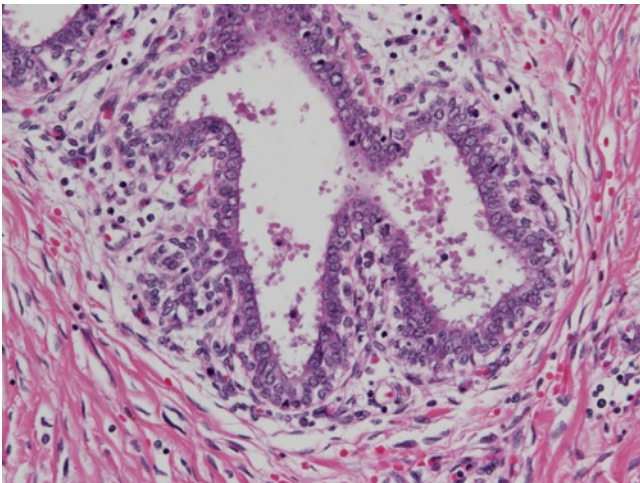


FIGURE 30-20. Neonatal hyperplasia and secretion: gestational age 38 6/7 weeks: higher magnification of the terminal branches of the intralobular ducts shown in Figure 30-19. Secretory changes are prominent. (H&E, 20×.)

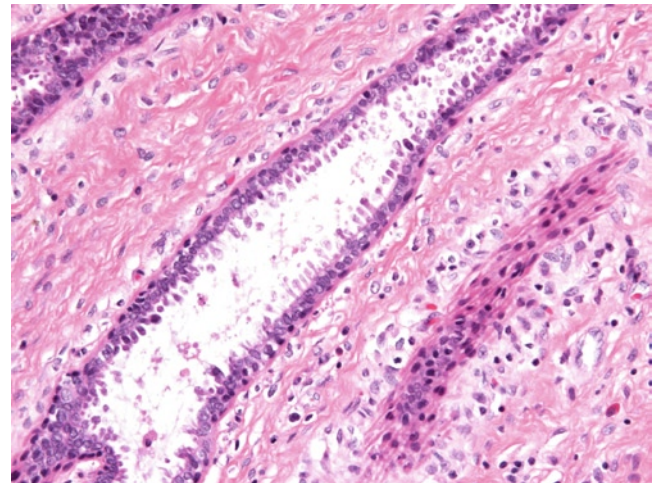


FIGURE 30-21. Additional variation of the morphology of myoepithelial cells: gestational age 35 0/7 weeks. This primary duct is deep to the layer of smooth muscle of the nipple and areola. The spindle-shaped myoepithelial cells with eosinophilic cytoplasm display distinct myoid differentiation. To the right of and parallel to the duct is a band of myoid myoepithelial cells from the adjacent duct cut en face. (H&E, 20×.)

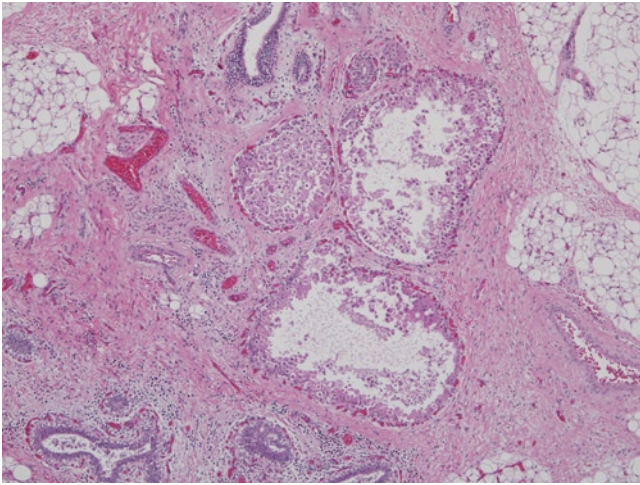


FIGURE 30-22. Apocrine metaplasia: gestational age 36 5/7 weeks. Apocrine metaplasia of mammary ducts is common in near-term breasts and becomes more extensive prior to and during regression. (H&E, 4 \times .)

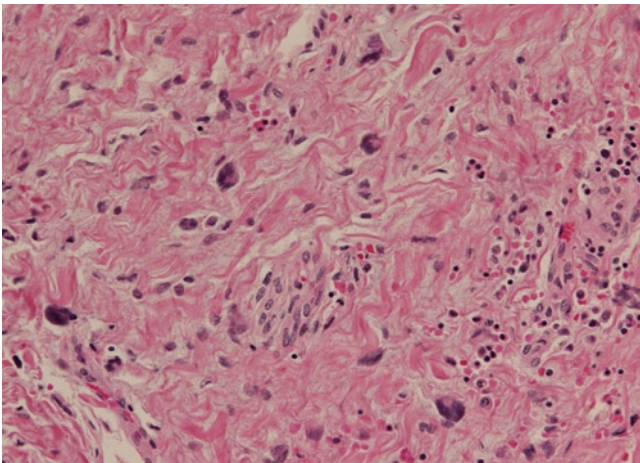


FIGURE 30-23. Atypical giant cells in the interlobular stroma: gestational age 41 2/7 weeks. The frequency and significance of this change is not known. Extramedullary hematopoiesis is also present. (H&E, 20 \times .)

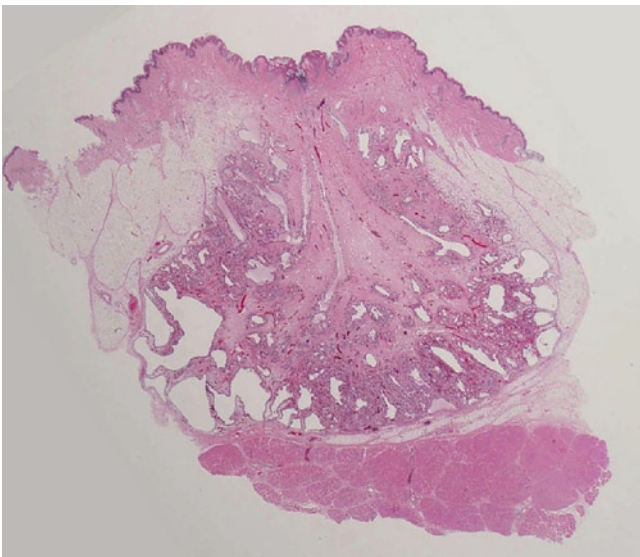


FIGURE 30-24. Near-term hyperplasia with early regression: gestational age 41 0/7 weeks. The baby lived 9 days. The diameter of the breast bud is 1.5 cm. Cystic change is an early indication of regression. (H&E, 0.5 \times .)

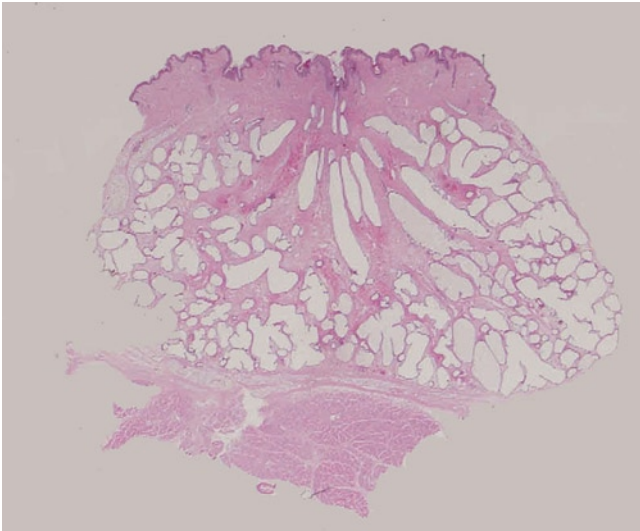


FIGURE 30-25. Neonatal regression: gestational age 42 0/7 weeks. The baby lived 9 days. The diameter of the breast bud is 1.2 cm. Diffuse cystic change is common during regression. (H&E, 0.5 \times .)

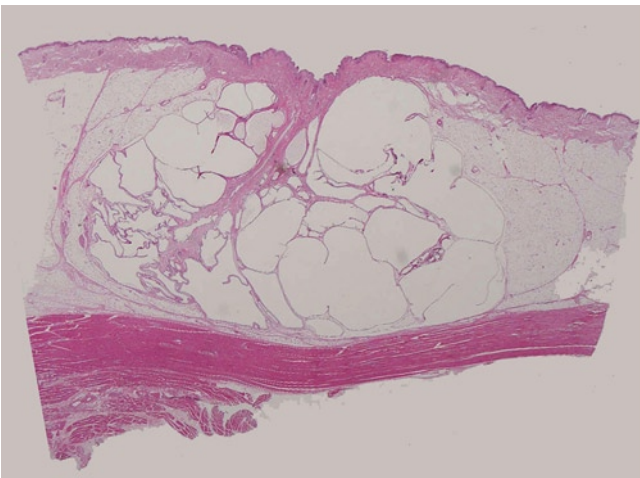


FIGURE 30-26. Exaggerated cystic change during regression: gestational age 39 0/7 weeks. The baby lived 39 days. The diameter of the breast bud is 1.7 cm. The difference between normal and abnormally exaggerated cystic change during regression is not well defined, but this case is unusual in both the severity and duration of the cystic change. This degree of exaggerated cystic change of regression may be difficult to distinguish from a galactocele. (H&E, 0.5 \times .)

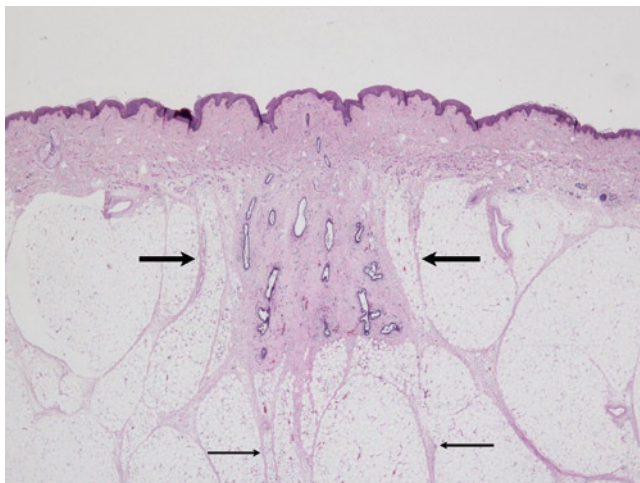


FIGURE 30-27. Neonatal regression: gestational age 25 5/7 weeks. The baby lived 7 months. The diameter of the breast bud is 2 mm. The distal branches, end buds, and intralobular stroma disappear, leaving only primary lobular ducts and dense interlobular stroma. Cooper and pectoral ligaments remain. The *large arrows* point to Cooper ligaments and the *small arrows* point to pectoral ligaments. (H&E, 1 \times .)

References

1. O'Rahilly R, Muller F: The origin of the ectodermal ring in staged human embryos of the first five weeks. *Acta Anat* 1958, 122: 145–157.
2. Hughes ESR: The development of the mammary gland. *Ann R Coll Surg* 1950, 6:3–23.
3. Friedrichs N, Steiner S, Buettner R, Knoepfle G: Immunohistochemical expression patterns of AP2a and AP2g in the developing fetal human breast. *Histopathology* 2007, 51: 814–823.
4. Sternlicht MD: Key stages in mammary gland development. The cues that regulate ductal branching morphogenesis. *Breast Cancer Res* 2006, 8:201–211.
5. Jolicouer F, Gaboury LA, Oligny LL: Basal cells of second trimester fetal breasts: immunohistochemical study of myoepithelial precursors. *Pediatr Dev Pathol* 2003, 6:398–413.
6. Jolicouer F: Intrauterine breast development and mammary myoepithelial lineage. *J Mammary Gland Biol Neoplasia* 2006, 10: 199–210.
7. McKiernan JF, Hull D: Breast development in the newborn. *Arch Dis Child* 1981, 56:525–529.
8. Anbazhagan R, Bartek J, Monaghan P, Gusterson BA: Growth and development of the human infant breast. *Am J Anat* 1995, 192:407–417.

SECTION X
Placenta

31

Placenta

Linda M. Ernst

The placenta is the organ of fetal–maternal exchange during gestation. It is a fetal organ by embryologic origin, but has close association with the maternal tissues of the endometrium. Thus, it is unique among the fetal organs in that maternal tissues are also a significant part of the histological component of the placenta.

An examination of the placenta is an important component of a thorough investigation into the cause of fetal death and may help with an understanding of neonatal morbidities. The histology and pathology of the placenta are best understood using a systematic approach to the several anatomic/histological compartments of the placenta. These include the extraplacental membranes, the umbilical cord, the chorionic plate or fetal surface, the basal plate, and the villous parenchyma. These regions correspond to the usual samples of the placenta submitted for microscopic examination in a thoroughly studied placenta. Knowledge of the normal histological appearance of each of these compartments at a variety of gestational ages is necessary to interpret any pathologic changes.

Embryology

The earliest trophoblastic cells of the placenta are recognizable by the 12 to 16 cell stage as the outer cell mass of the developing cellular sphere known as the *morula* (see Fig. 31-1A). By the blastocyst stage, the trophoblast cells of the outer cell mass expand and flatten to form the outer layer of the blastocyst that encloses the inner cell mass, now referred to as the *embryoblast*, at one pole (see Fig. 31-1B). At the end of the first week of gestation, the trophoblast cells situated along the embryonic pole of the blastocyst reach and begin to invade the endometrial lining. Shortly after beginning to invade the endometrium, differentiation of cellular phenotypes is seen within the trophoblast layer (see Fig. 31-1C). An outer layer of syncytiotrophoblast and inner layer of cytotrophoblast are formed [1,2]. The cytotrophoblast cells represent the replicative layer of trophoblast and maintain a simple layer of epithelial cells, whereas the syncytiotrophoblast layer is a multinucleated syncytium formed by fusion of numerous trophoblastic cells. The syncytiotrophoblast layer is thickest at the embryonic pole and decreases in thickness around the circumference of the blastocyst (see Fig. 31-1C).

With continued blastocyst invasion into the endometrium, lacunae begin to form within the syncytiotrophoblast layer (see Fig. 31-1D). These lacunae begin to coalesce and form an anastomosing network of sinusoidal spaces that become filled with maternal blood as the leading invasive trophoblast cells reach and invade maternal endometrial blood vessels. Thus, the beginning of the maternal circulation to the placental tissues is established at approximately 12 days gestation [1,2]. By the end of the second week of development, the formation of primary chorionic villi begins as cytotrophoblast cells proliferate as short columns protruding outward, still covered by the syncytiotrophoblast. In the third week of development, mesodermal cells, derived from the extraembryonic mesoderm,

infiltrate the cytotrophoblastic cores of the primary villi and produce structures known as secondary villi, which are characterized by a mesodermal core lined by cytotrophoblast cells, all covered by syncytiotrophoblast. The next step in villous development is the formation of a vascular network within the mesodermal core, the characteristic of tertiary villi (see Fig. 31-2). The blood vessels formed within the tertiary villi become linked to blood vessels developing in the chorionic plate and connecting stalk to complete the formation of the fetoplacental circulation.

The formation of the amniotic and chorionic cavities (see Fig. 31-3) occurs simultaneously with villous development. At the beginning of the second week of development, the amniotic cavity begins as a small cavity within the epiblast layer of the bilaminar germ disc formed from the embryoblast [1,2]. The cells lining the roof of the amniotic cavity are in continuity with the cytotrophoblast shell surrounding the embryo and are called *amnioblasts*. The cells of the other layer of the bilaminar embryo, the hypoblast, form the lining of a second cavity, the primitive yolk sac. The lining of the primitive yolk sac is also initially in contact with the cytotrophoblast. Subsequently, mesodermal cells derived from the primitive yolk sac begin to proliferate and fill the space between the two existing sacs (amniotic and primitive yolk sac) and the cytotrophoblast (see Fig. 31-3A). This mesodermal layer is known as the extraembryonic mesoderm. Later, cavities begin to form within the extraembryonic mesoderm, and these numerous cavities coalesce to form a new cavity, the chorionic cavity (or

extraembryonic coelom), which surrounds the amniotic cavity and yolk sac cavity except where the connecting stalk, the future umbilical cord linking fetal and placental circulations, is present (see Fig. 31-3B). With this development, both the amniotic and chorionic linings contain a mesodermal layer of connective tissue derived from the extraembryonic mesoderm, also referred to as the *extraembryonic somatopleuric mesoderm*. This mesoderm will form the definitive connective tissue layers of the membranes and chorionic plate. As the amniotic sac expands to fill the chorionic cavity, the mesodermal tissues of the amnion and chorion are in close contact (see Fig. 31-3C).

The primitive yolk sac is replaced by the smaller definitive or secondary yolk sac, and in the process small exocoelomic cysts are produced and persist in the chorionic cavity between the chorion mesoderm and the amnion mesoderm. Around the fifth week of gestation, the yolk sac stalk containing the vitelline vessels becomes incorporated into the connecting stalk, the future umbilical cord along with the allantois, and the umbilical vessels (see Fig. 31-3D) [1,2]. In embryonic life, intestinal loops also protrude into the connecting stalk along the opening between the midgut and the yolk sac, the omphalomesenteric duct. By the end of the embryonic period, however, the yolk sac is obliterated and the intestines return to the abdomen. The umbilical cord then contains the umbilical vessels surrounded by Wharton's jelly. However, remnants of the embryonic structures within the umbilical cord are seen commonly in fetal life.

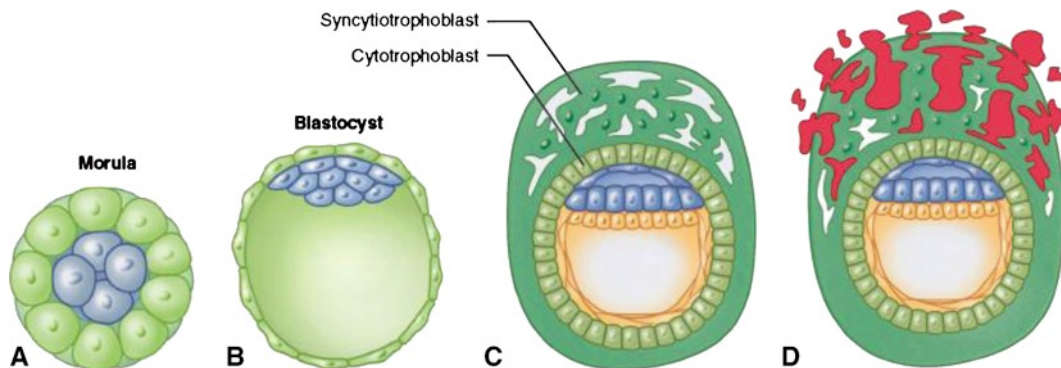


FIGURE 31-1. Early placental development. **A.** The morula at 3 to 4 days after fertilization is characterized by an inner cell mass that will form the embryo (blue) and outer cell mass that will form the placenta (green). **B.** During the blastocyst stage, the cells of the outer cell mass (green), the trophoblast, will form the placenta. **C.** Trophoblast differentiation occurs shortly after

the blastocyst implants on the endometrium. The outer layer is the syncytiotrophoblast (dark green) and the inner layer is the cytotrophoblast (light green). **D.** As the blastocyst continues to invade the endometrium, lacunae form within the syncytiotrophoblast layer and contain maternal blood (red).

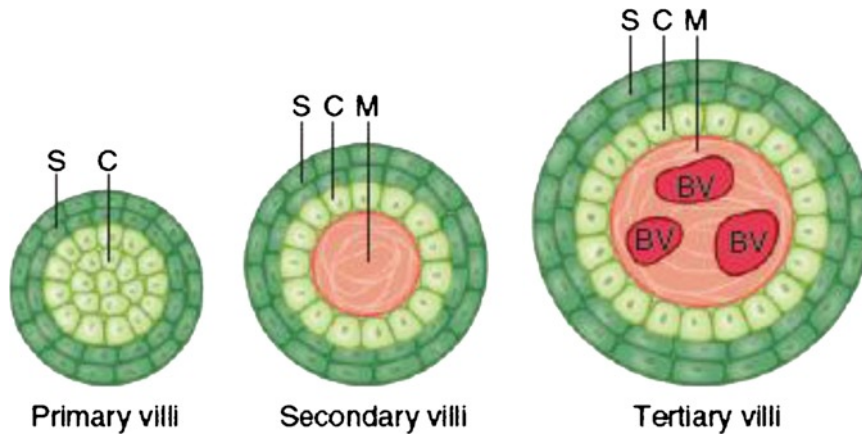


FIGURE 31-2. Comparison of the components of primary, secondary, and tertiary villi. BV—fetal blood vessels; C—cytotrophoblast; M—mesenchyme; S—syncytiotrophoblast.

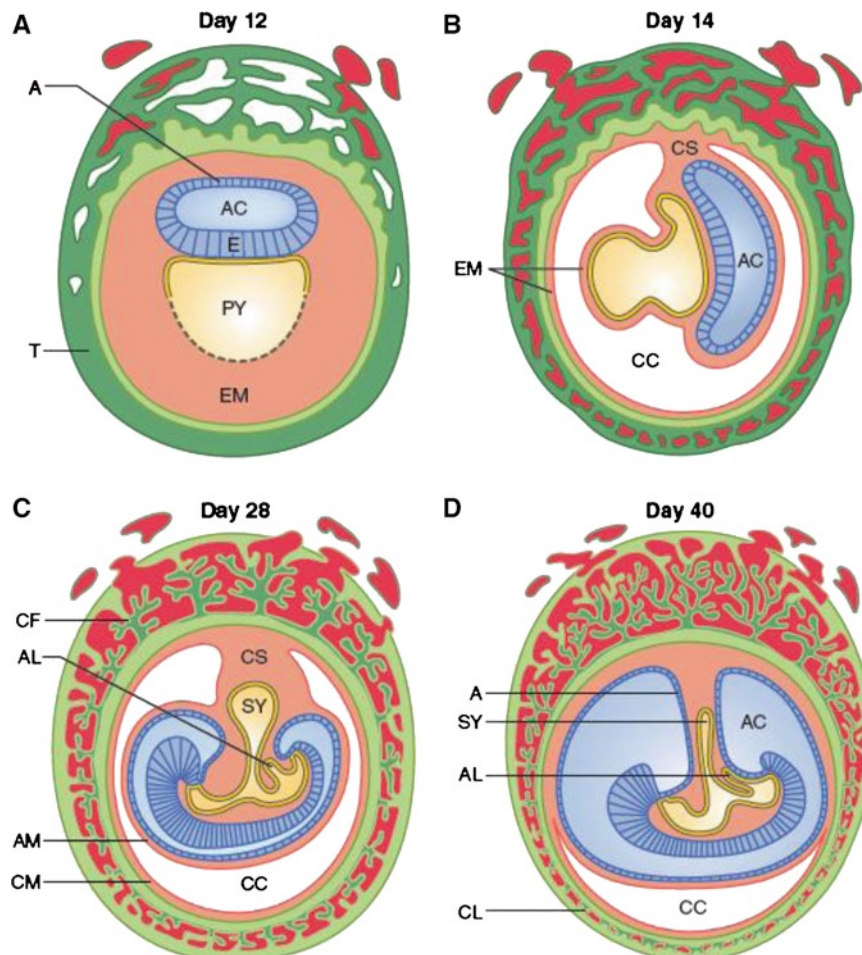


FIGURE 31-3. Formation of the amniotic cavity, chorionic cavity, and umbilical cord. **A**, Day 12. The amniotic cavity (AC) begins as a small cavity within the epiblast layer (E). The cells lining the cavity will form the amnion (A). The cells of the hypoblast form the lining the primitive yolk sac (PY). The extraembryonic mesoderm (EM) fills in the space between the two existing sacs (amniotic and primitive yolk sac) and the cytotrophoblast (T). **B**, Day 14. A cavity has now formed within the extraembryonic mesoderm, the chorionic cavity (CC) or extraembryonic coelom, and the extraembryonic mesoderm (EM) is present on the inner surface of the trophoblast and surrounds the yolk sac and amniotic

sac (AC). The connecting stalk (CS) is also beginning to develop. **C**, Day 28. As the amniotic sac expands to fill the chorionic cavity, the mesodermal tissues of the amnion (AM) and chorion (CM) come in close contact. The secondary yolk sac (SY), allantois (AL), and connecting stalk (CS) are developing. The placental tissue is forming villous structures in the chorion frondosum (CF). **D**, Day 40. As the trophoblast continue to develop and invade the endometrium, the placental disc is becoming more obvious and the villi of the chorion laeve (CL) atrophy. Note the continued maturation of the amniotic (AM) and chorionic (CC) cavities that surround the connecting stalk as the embryo folds.

Histology

By the beginning of the midtrimester, the placental anatomy is established, but the tissues continue to undergo maturational changes throughout the fetal period. The structural anatomy of the compartments of

the placenta: the extraplacental membranes, the umbilical cord, the chorionic plate, the basal plate, and the villous parenchyma, is reviewed in [Figure 31-4](#).

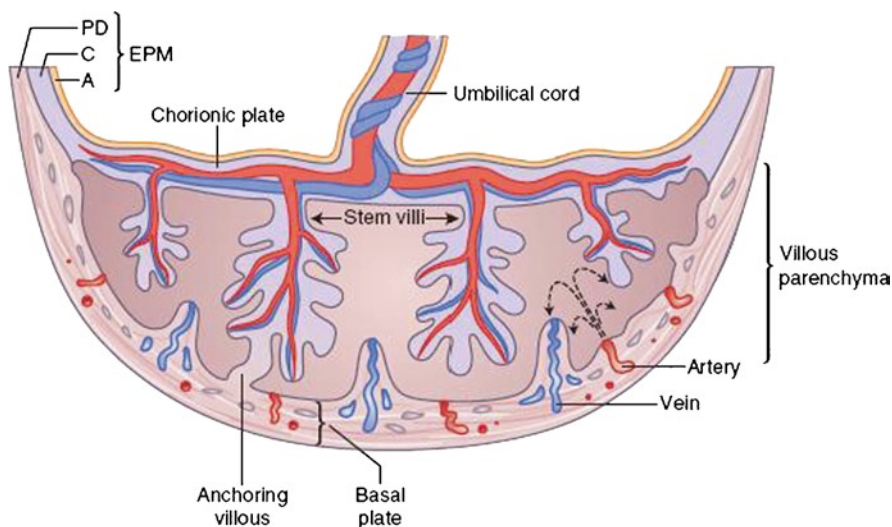


FIGURE 31-4. Placenta anatomy. Anatomy of the placenta including the extraplacental membranes (EPM) composed of amnion (A), chorion (C), and parietal decidua (PD), the umbilical cord, the chorionic plate, the basal plate, and the villous parenchyma.

Extraplacental Membranes

Histological sections of the human extraplacental membranes are composed of three main tissue layers that surround the amniotic sac: the fetally derived amnion, the fetally derived chorion, and the maternally derived decidua. Over the gestational period, all three layers remain present with only minor changes in thickness or epithelial appearance (see Figs. 31-5–31-7).

The amnion consists of a simple squamous to cuboidal epithelial layer, which is in contact with the amniotic fluid. The epithelium has an underlying basement membrane, and a thin connective tissue layer is present beneath the basement membrane. The paucicellular connective tissue layer of the amnion is composed of collagen and elastic fibers with a few identifiable fibroblasts and occasional macrophages. These macrophages will ingest pigment in abnormal situations such as intra-amniotic meconium or blood. No vessels, nerves, or lymphatics are present in the connective tissue of the amnion. As gestation approaches term, the amnion epithelial cells may appear slightly more columnar and reactive. Intra-amniotic irritants, such as meconium, will cause marked and bizarre amnion epithelial cell alterations (see Figs. 31-8 and 31-9).

The amnion and chorion are imperfectly fused [3,4], and a potential space exists between the two, which can be seen histologically as a gap between the amnion and chorion connective tissue layers. Embryologically,

this space represents the remnant of the extraembryonic coelom. This potential space is referred to as the spongy layer and is composed of loosely arranged collagen fibers (see Fig. 31-7) that sometimes have a myxoid or edematous appearance and contain scattered fibroblasts and macrophages [3].

The chorionic layer of the membranes is known as the chorion leave. The chorion leave, in general, is also composed of epithelial and connective tissue layers. However, in contrast to the amnion, these layers in the chorion are reversed in orientation. Therefore, the connective tissue layer of the chorion is adjacent to the connective tissue layer of the amnion. The chorionic connective tissue is slightly thicker than the amnion connective tissue but has a similar appearance of paucicellular connective tissue composed of collagen and elastic fibers with occasional macrophages. Although the chorion leave is in continuity with the vascular chorionic plate, the chorion leave itself is avascular. Therefore, all fetally derived tissues in the extraplacental membranes are avascular.

The epithelial layer of the chorion has several layers of trophoblastic cells and the thickness of the trophoblastic cells is variable. In addition, the chorionic epithelial layer contains atrophied villi that appear as well-circumscribed, slightly basophilic nodules throughout the layer (see Figs. 31-5 and 31-6).

The maternally derived tissue layer of the extraplacental membranes is the decidua. Until about 20 weeks, this layer is referred to as decidua capsularis, the initial abembryonic decidual covering of the implanted blastocyst. When the decidua capsularis fuses with the decidua parietalis of the opposite side of the uterus, the decidua is then referred to as decidua parietalis. However, histologically, there is no distinct difference [3]. The decidua of the membranes is the only vascularized tissue of the membranes and has both a superficial and deep vascular component. The maternal vasculature in the decidua parietalis does not undergo invasion and remodeling by extravillous trophoblast cells. Therefore,

parietal decidual vessels can and frequently do contain smooth muscle (see Fig. 31-10). However, excessive mural thickening/hypertrophy of these membranous maternal vessels, defined as mean wall diameter more than 30% of mean circumference, is considered one of the pathologic features of maternal vascular underperfusion [5]. Other changes such as fibrinoid necrosis, acute atherosclerosis, and thrombosis should not be considered normal within the parietal decidual vessels. Lastly, inflammatory cells are also seen in the decidua with occasional macrophages and foci of lymphocytes as normal components of the decidua (see Fig. 31-11). However, plasma cells are not a normal component of the decidua.

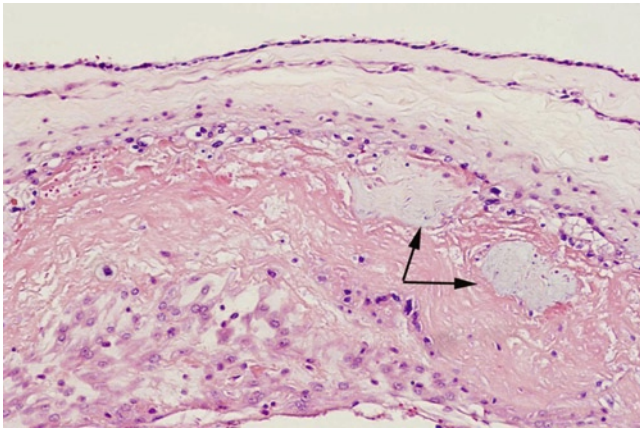


FIGURE 31-5. Membranes at 15 weeks gestation. Note the simple, nearly squamous epithelial layer of the amnion at the upper limit of the image. The amnion and chorionic connective tissues are back-to-back and there is a somewhat thin trophoblastic layer in the chorion. Note the atrophic villi of the chorion laeve (arrows). The decidua is the layer at the lower edge of the image. (Hematoxylin and eosin [H&E], 10 \times .)

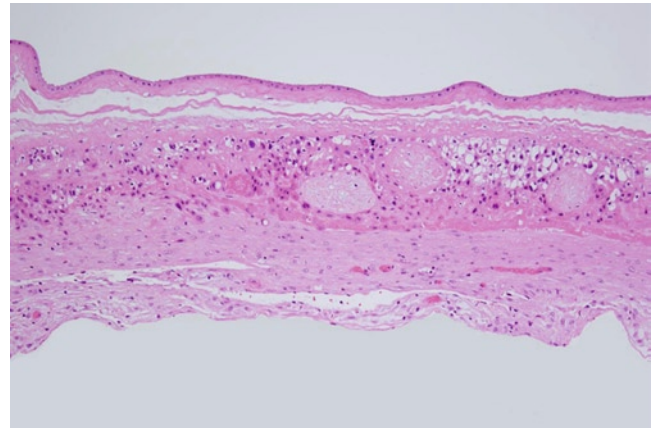


FIGURE 31-6. Membranes at term. The amnion is slightly more cuboidal at this gestational age, but still relatively flattened. The chorionic trophoblast is somewhat thicker, but still shows the atrophic villi of the chorion laeve. A clear distinction can be made between the decidual cells with polygonal, pale cytoplasm and the more amphophilic cytoplasm of the chorionic trophoblast. (H&E, 10 \times .)

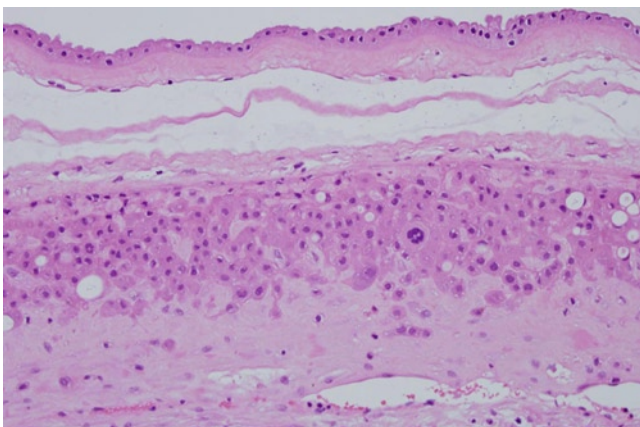


FIGURE 31-7. Membranes at term. Higher-power view of the membrane components. Note the potential space between the amnion and chorion with the spongy layer containing loose collagen fibers. Trophoblast cells of the chorion have variable sizes and shapes and occasional multinucleated cells are seen. (H&E, 20 \times .)

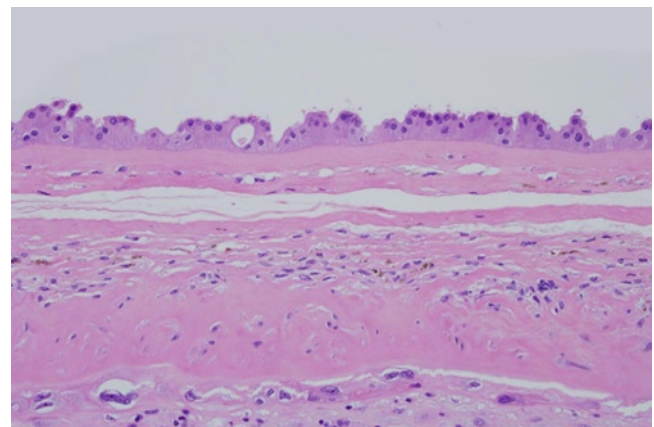


FIGURE 31-8. Membranes at 32 weeks gestation with reactive amniotic changes. Note the amnion epithelium is columnar, and many of the amniotic nuclei are apically placed, instead of the normal basal location. This is a reactive change that is commonly seen in the amnion, and in this case numerous hemosiderin-laden macrophages, indicative of previous hemorrhage, are noted in the amnion and chorionic connective tissue. (H&E, 20 \times .)

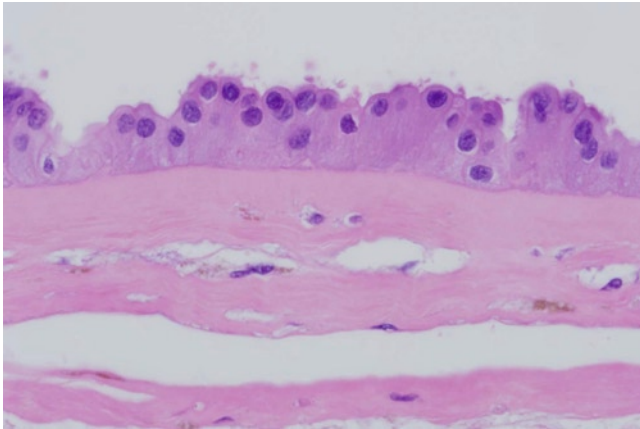


FIGURE 31-9. Higher-power view of reactive amnionic changes. Note that several of the nuclei are apically placed whereas others remain at the basal aspect of the cell, giving a somewhat pseudostratified appearance to the epithelium. (H&E, 60 \times .)

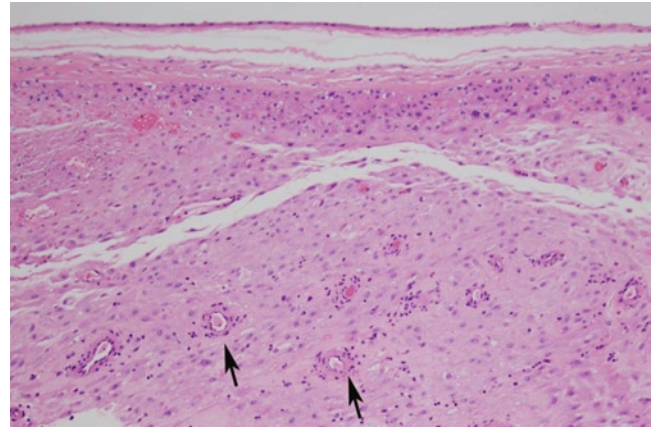


FIGURE 31-10. Decidua parietalis at term. Note the muscularized decidual vessels present (arrows). Because these vessels are not normally remodeled by trophoblast, they frequently retain a thin coat of smooth muscle. (H&E, 10 \times .)

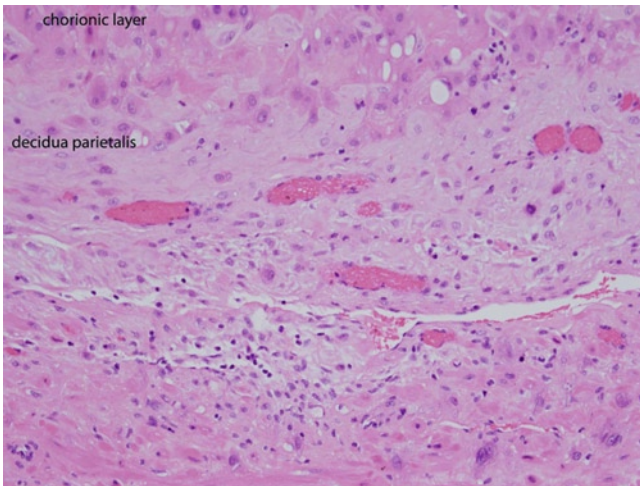


FIGURE 31-11. Decidua parietalis at term. Medium-power view of the decidua in the membranes. Note the fairly thin-walled vessels both in the superficial and deep layers of the decidua. Also note the scattered lymphocytes that are a normal component of the decidua. The lower edge of the image contains a few adherent myometrial fibers. (H&E, 20 \times .)

Umbilical Cord

The umbilical cord is the conduit for the fetal vasculature between the placenta and the fetus. The main components of the umbilical cord are the fetal umbilical vessels, two umbilical arteries and a vein, surrounded by a gelatinous, shock-absorbing substance known as Wharton's jelly (see Fig. 31-12). The outermost covering of the umbilical cord, which is in contact with amniotic fluid and firmly attached to the cord [6], is histologically the same as amnion epithelium with its underlying basement membrane (see Fig. 31-13). However, squamous metaplasia of the umbilical cord epithelium is considered normal (see Fig. 31-14), and is especially common near the fetal body wall. The Wharton's jelly (see Figs. 31-13 and 31-14) consists of mucopolysaccharides, such as hyaluronic acid and chondroitin sulfate, which give a slightly basophilic appearance to the jelly on H&E-stained sections. Sparse collagen fibers and other microfibrils are also present,

produced predominantly by myofibroblasts located at the periphery of the umbilical vessels and beneath the basement membrane of the epithelium [6]. Scattered macrophages and mast cells are present within the substance of Wharton's jelly [6].

The umbilical arteries possess two smooth muscle layers, an outer circular and an inner spiral longitudinal layer, and thus have generally thicker walls than the vein, which has only a single layer of circular smooth muscle (see Figs. 31-15 and 31-16). Occasional elastic fibers may be seen in the media of the arteries, but, generally, the umbilical arteries lack a well-formed internal elastic lamina. The vein, however, has a well-formed internal elastic lamina (see Figs. 31-17–31-19) [6,7]. There are no vasa vasorum, lymphatic channels, or nerves within the umbilical cord [6]. However, at the fetal end of the cord, there have been descriptions of ganglion cells [8] and nerve fibers [8,9].

The normal umbilical cord commonly contains embryonic remnants of either the allantoic duct or the vitelline duct. Vitelline (omphalomesenteric) duct remnants are present at the fetal end of the cord, and can be composed of the endodermally derived epithelial elements or of the vessels associated with the vitelline duct. Epithelial remnants usually possess a lumen lined by mucin-producing cuboidal to columnar epithelial cells, sometimes accompanied by a muscular wall (see Figs. 31-20 and 31-21), but other endodermally derived

tissues such as hepatocytes may be seen [10]. Vitelline vessel remnants may also accompany the vitelline duct remnant near the fetal end of the cord, and may appear as a single thin-walled vessel or sometimes as a plexus of vessels (see Figs. 31-22 and 31-23).

Allantoic remnants are also typically present at the fetal end of the cord between the two arteries (see Fig. 31-24). They are composed of transitional-type epithelial cells arranged in a spherical configuration usually without a recognizable lumen.

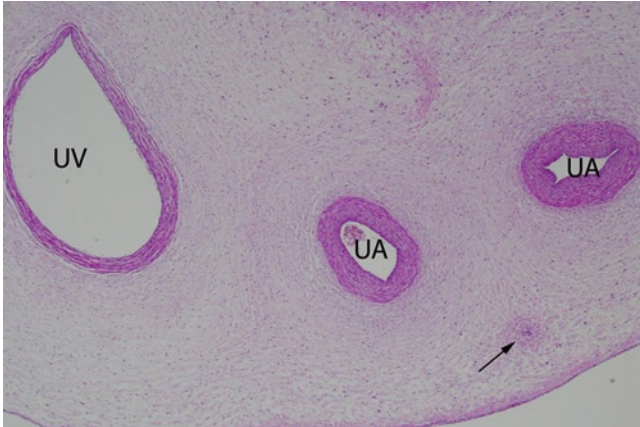


FIGURE 31-12. Umbilical cord at 16 weeks gestation. Low-power view showing the single umbilical vein (UV) and two umbilical arteries (UA). A small allantoic remnant is also present between the two arteries (arrow). (H&E, 2 \times .)

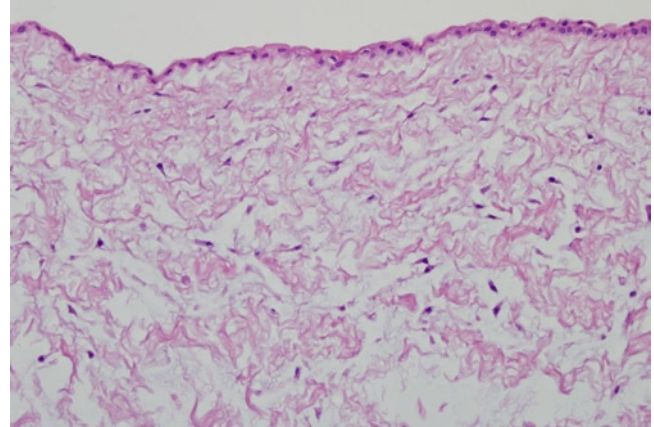


FIGURE 31-13. Umbilical cord at 24 weeks gestation. Medium-power view of external surface of the cord showing the amnion epithelium lining the cord and the paucicellular Wharton's jelly beneath it (H&E, 20 \times .)

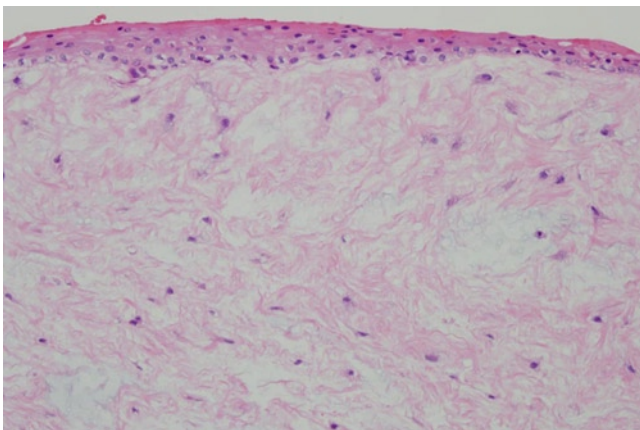


FIGURE 31-14. Umbilical cord at 36 weeks gestation. Medium-power view of external surface of the cord showing squamous metaplasia of the external surface of the umbilical cord and the paucicellular Wharton's jelly beneath it (H&E, 20 \times .)

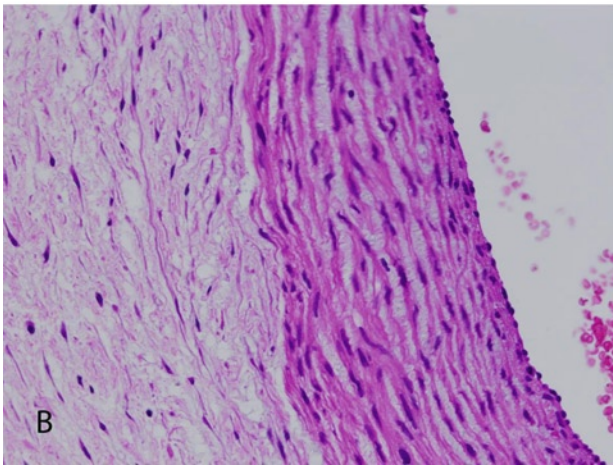
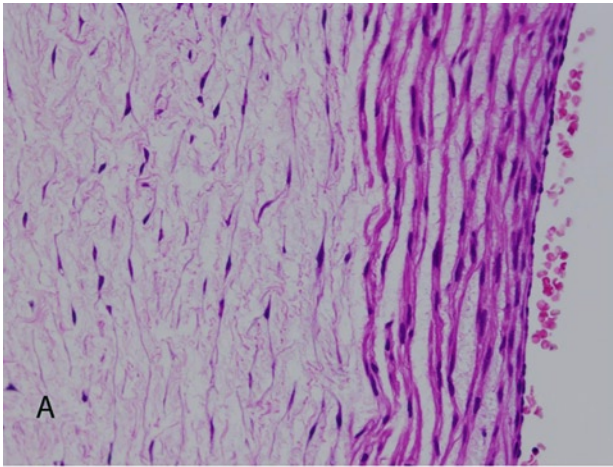


FIGURE 31-15. Umbilical cord at 16 weeks gestation. Comparison of the layers of umbilical vein (**A**) and umbilical artery (**B**). Note that, at this gestational age, the muscle layer is relatively thin and distinction between vein and artery can be difficult. (**A** and **B**, H&E, 10 \times .)

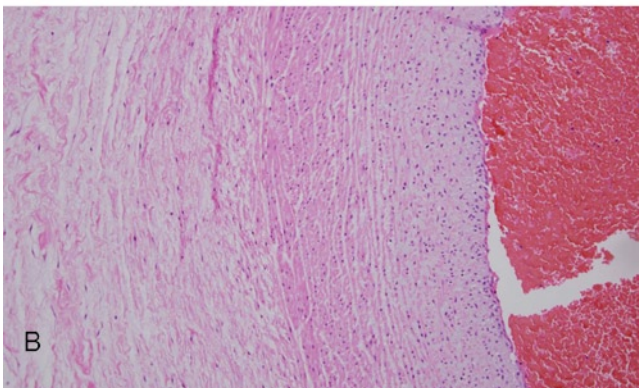
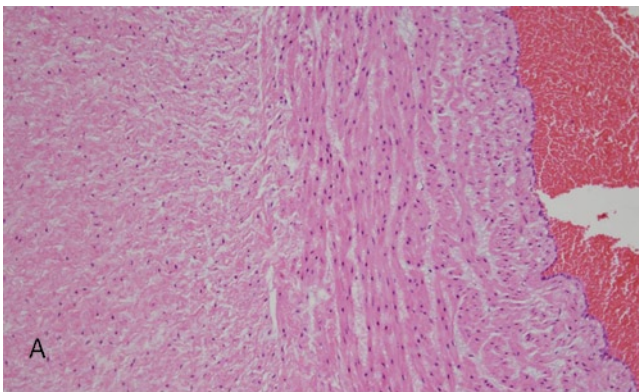


FIGURE 31-16. Umbilical cord at 35 weeks gestation. Comparison of the layers of umbilical vein (**A**) and umbilical artery (**B**). The umbilical artery has two smooth muscle layers and a slightly thicker wall than the vein, which has single layer of circular smooth muscle. (**A** and **B**, H&E, 10 \times .)

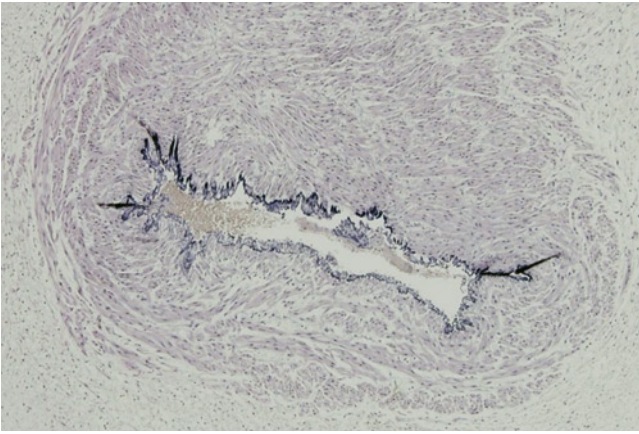


FIGURE 31-17. Umbilical vein at term. Umbilical vein showing prominent internal elastic lamina. (Verhoeff Van Gieson, 4×.)

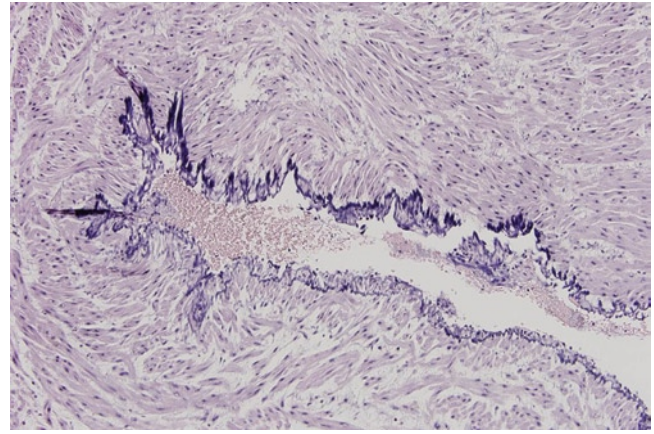


FIGURE 31-18. Umbilical vein at term. Higher power view of the umbilical vein showing prominent internal elastic lamina. (Verhoeff Van Gieson, 10×.)

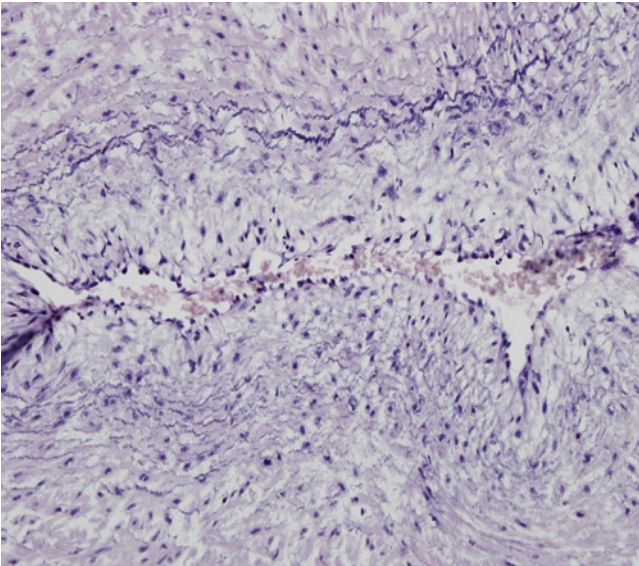


FIGURE 31-19. Umbilical artery at term. Umbilical artery with scattered peripheral elastic fibers but lack of internal elastic lamina. (Verhoeff Van Gieson, 20×.)

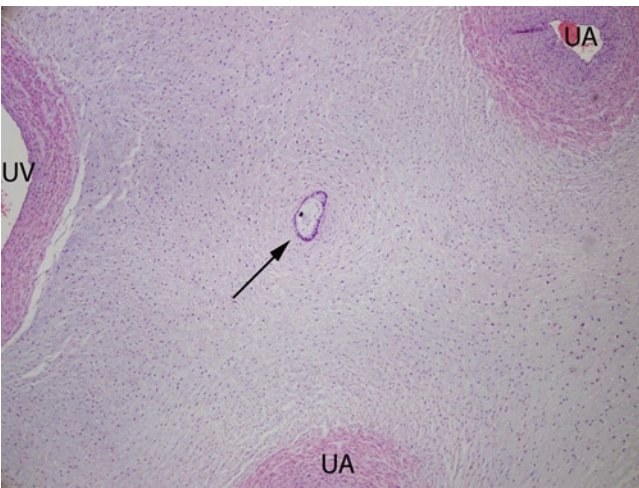


FIGURE 31-20. Umbilical vitelline duct remnant. Low-power view of umbilical cord demonstrating remnant of the vitelline/omphalomesenteric duct (arrow) located centrally in the cord between the umbilical vein (UV) and two umbilical arteries (UA). (H&E, 4×.)

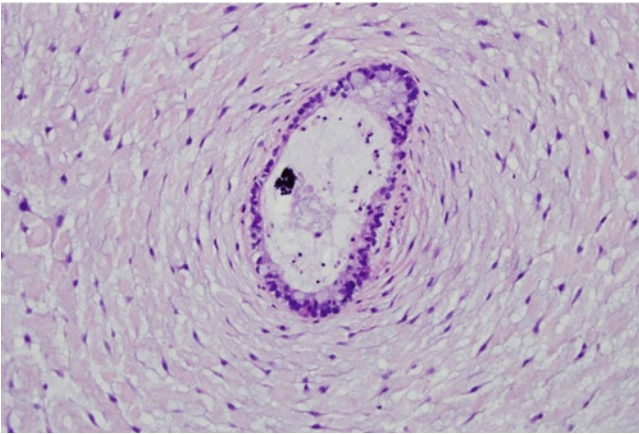


FIGURE 31-21. Umbilical vitelline duct remnant. Higher-power view of the vitelline/omphalomesenteric duct remnant showing the cuboidal to columnar lining cells with focal mucin production resembling the epithelium of the gut. (H&E, 20 \times .)

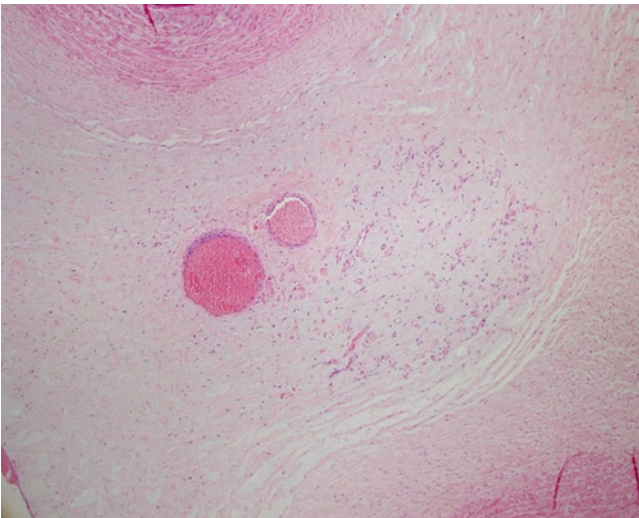


FIGURE 31-22. Umbilical vitelline vessel remnant. Low-power view of the vitelline/omphalomesenteric vessel remnant showing two large thin-walled vascular structures and a plexus of smaller vessels. (H&E, 10 \times .)

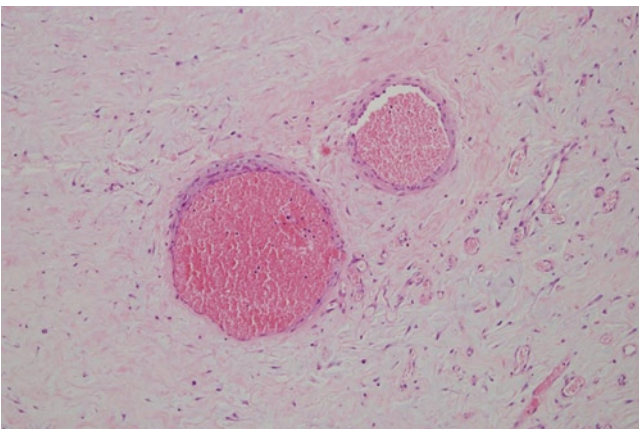


FIGURE 31-23. Umbilical vitelline vessel remnant. Higher-power view of the vitelline duct vascular remnant present at term. (H&E, 40 \times .)

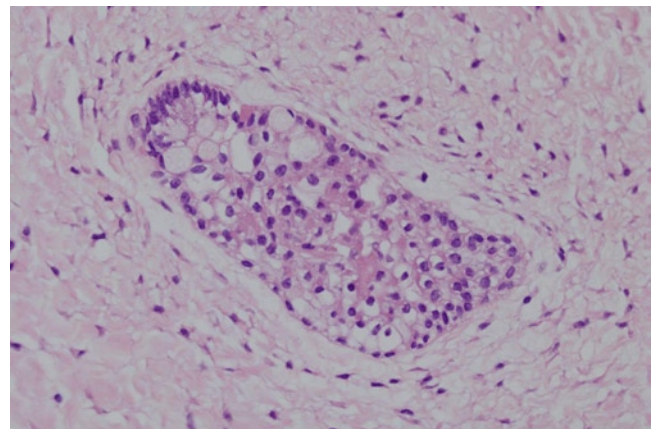


FIGURE 31-24. Allantoic remnant of the umbilical cord. (H&E, 20 \times .)

Chorionic Plate

The chorionic plate, or fetal surface of the placenta, is covered by a layer of amnionic tissue that is identical to the amnion of the extraplacental membranes. This amnion layer is easily stripped from the surface of the chorionic plate and is sometimes not present in histological sections taken from the fetal surface.

The chorionic plate represents a segment of the continuous layer of chorionic tissue surrounding the fetus. It differs from the chorion laeve because the chorionic plate has a thicker connective tissue containing fetal vessels that ramify from the umbilical cord onto the fetal surface (see Figs. 31-25–31-30). The fetal vasculature of the chorionic plate consists of muscularized fetal vessels, but distinguishing arteries from veins based on morphologic histological features on routine H&E stains is not consistently possible [4]. Fetal vessels of the chorionic plate frequently have asymmetrical thinning of the muscular coat, especially in superficial segments of the vessels (see Fig. 31-27). In addition, it is not unusual to see myxoid intimal cushions in fetal chorionic vessels.

However, in the absence of subendothelial fibrin or fibrin deposition or calcification, these myxoid cushions are not considered histological evidence of fetal vascular obstruction [11]. The connective tissue of the chorionic plate, which surrounds the fetal vessels, is composed of collagen layers and is generally paucicellular-containing fibroblasts and occasional macrophages.

Beneath the connective tissue of the chorionic plate, a layer of trophoblastic cells is found that varies in thickness but is usually just a few cells thick. These trophoblastic cells line the subchorionic intervillous space. A subchorionic fibrin layer (known as Langhans' fibrin), also of variable thickness, forms beneath the trophoblastic layer [12]. In general, with increasing gestational age, the subchorionic fibrin layer shows areas of increasing thickness forming subchorionic fibrin plaques (see Figs. 31-28 and 31-29; compare with Figs. 31-26 and 31-27). Stem villi arise from the lower surface of the chorionic plate (see Fig. 31-30) and give rise to the remainder of the villous parenchyma beneath the chorionic plate.

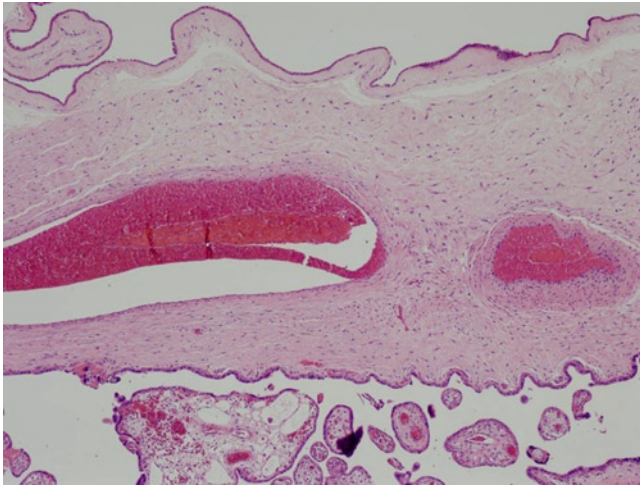


FIGURE 31-25. Chorionic plate at 21 weeks gestation. The amnionic layer is present (*top*). The chorionic connective tissue layer is thicker than in the membranes and contains the fetal chorionic vessels. (H&E, 4 \times .)

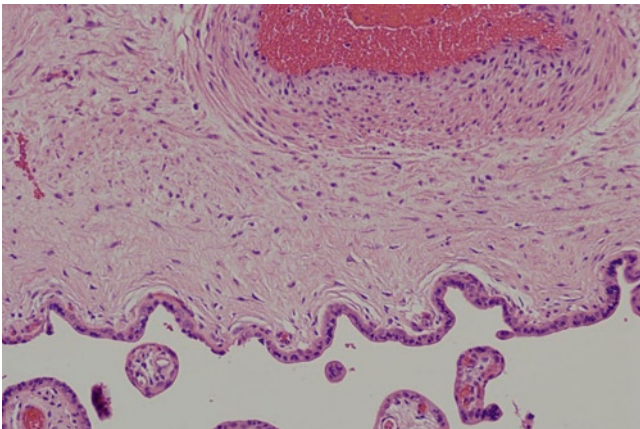


FIGURE 31-26. Chorionic plate at 21 weeks gestation. Higher-power image to show the trophoblastic lining of the lower border of the chorionic plate at the interface with intervillous space. Subchorionic fibrin is not prominent at this gestational age. (H&E, 10 \times .)

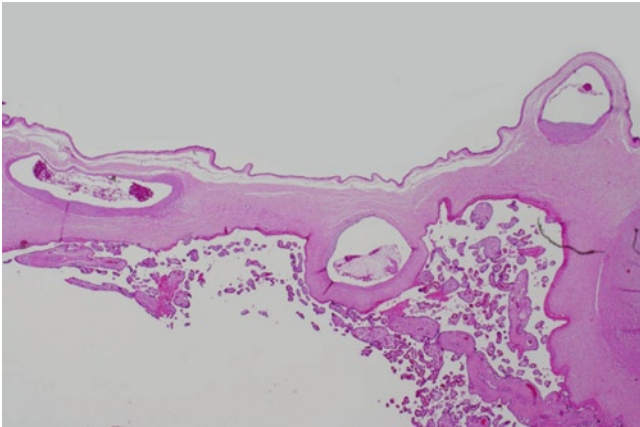


FIGURE 31-27. Chorionic plate at 32 weeks gestation. Low-power view of the chorionic plate (fetal surface of the placenta). The amnionic layer is present, and subchorionic fibrin is more prominent. Note there is frequently asymmetry of the chorionic vessel wall, with thinning noted along the upper surface of the vessels. (H&E, 2 \times .)

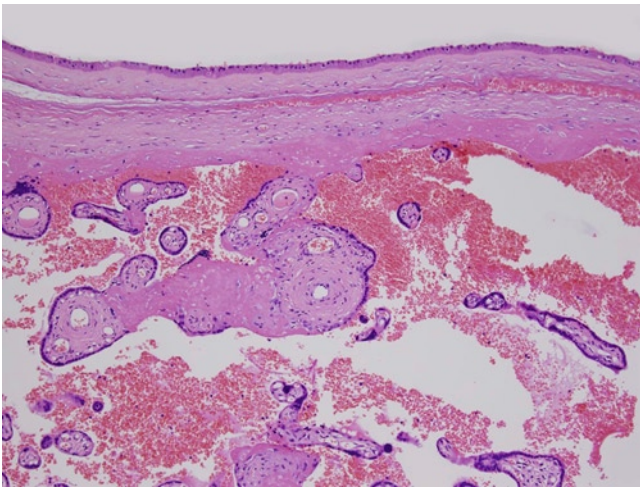


FIGURE 31-28. Chorionic plate at term. Low-power view of the chorionic plate between fetal vessels. Note the fairly thick layer of subchorionic fibrin present. (H&E, 10 \times .)

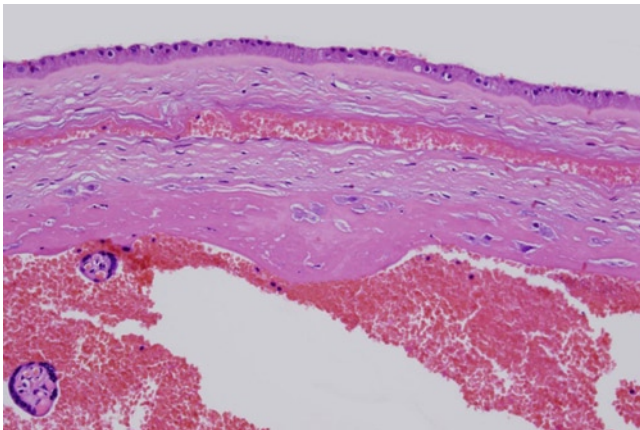


FIGURE 31-29. Chorionic plate at term. Higher-power view of the chorionic plate between fetal vessels. Note the fairly thick layer of subchorionic fibrin present and the trophoblastic cells present within the fibrin. Inflammatory cells are not normally present within this fibrin layer. (H&E, 20 \times .)

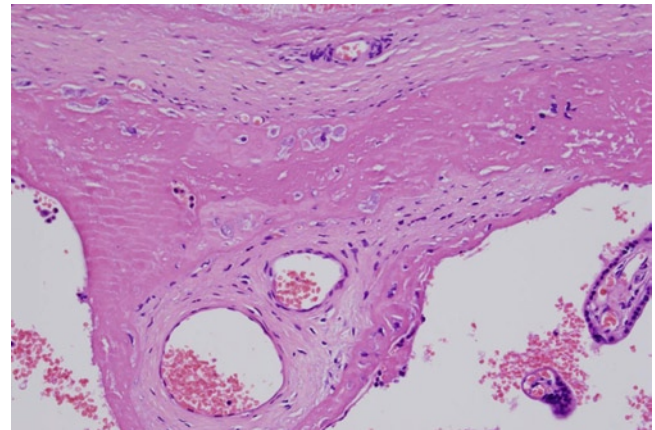


FIGURE 31-30. Chorionic plate at term. Higher-power view of the lower chorionic plate showing the origin of a stem villous from the chorionic plate. (H&E, 20 \times .)

Basal Plate

The basal plate is present on the maternal aspect of the delivered placenta. It is the relatively thin layer, measuring up to 0.15 mm [12], covering the maternal aspect of the placenta and has a smooth grayish gross appearance. This thin layer represents an intimate mixture of both maternal and fetal tissue at their closest point of contact. Therefore, an understanding of the normal components of the basal plate is important for understanding and interpreting pathologic alterations in this region. The main components or layers of the basal plate are listed in Fig. 31-31 and shown in Fig. 31-32.

The inner layer of the basal plate is adjacent to the intervillous space and is lined by syncytiotrophoblast cells focally and maternal endothelial cells where the trophoblasts are absent. There are two layers of fibrin on either side of the principal layer of the basal plate. Both of these layers appear as discontinuous or interrupted pale eosinophilic acellular layers in routine H&E-stained sections at term. The inner-most fibrin layer is known as Rohr's fibrin and the outer layer is Nitabuch's fibrin [12]. In some areas of the inner surface of the basal plate, Rohr's fibrin is exposed and in contact with the components of the intervillous space, and is therefore continuous with perivillous fibrin (see Fig. 31-33). Nitabuch's fibrin is on the opposite side of the principal layer and is considered the boundary between maternal and fetal tissues of the placenta because it separates the most superficial extravillous trophoblast of the principal layer from the maternal decidual cells. Although Nitabuch's fibrin represents the maternal-fetal boundary, it is by no means a blockade to fetal extravillous trophoblast cells. Trophoblast cells are frequently seen well beyond Nitabuch's layer [12]. Additional tissue is usually attached to the delivered placenta deep to Nitabuch's fibrin, and this tissue is known as the separation zone [12]. It contains predominantly decidualized endometrial stromal cells with occasional extravillous trophoblast cells (see Fig. 31-34).

The principal layer of the basal plate is the thickest layer, occupying 50% to 75% of the basal plate at term [12]. Within this layer, the anchoring villi are seen as somewhat atrophic-appearing villous structures embedded in fibrin. Anchoring villi are the most distal extensions of stem villi, and their "heads" are anchored in the basal plate. From the abembryonic surface of anchoring villi, trophoblast cells proliferate and extend into the basal plate as the so-called trophoblast cell columns.

Extravillous trophoblast cells emanate from these cell columns and then migrate through the basal plate, endometrium, and myometrium to perform their main duty of maternal vascular remodeling (see Fig. 31-34). Maternal tissues are also a component of the principal layer of the basal plate with the main cell consisting of the decidualized endometrial stromal cells. Other endometrial stromal cells are also present including the vasculature of the endometrial stroma, fibroblasts, and occasional macrophages. Scattered lymphoid and natural killer cells are also seen in the normal basal plate [12]. However, plasma cells are not considered a normal component of the decidua.

The process of maternal vascular remodeling by the trophoblast is essential for obtaining adequate perfusion to the intervillous space and, thus, the fetus. The effects of this remodeling process are evident in histological samples of the basal plate, and alterations from the normally expected appearance of these vessels may be indicative of a pathologic process. Extravillous trophoblast cells first reach the spiral arterioles of the endometrium in the first trimester between 6 to 12 weeks gestation (the first wave of invasion) [13-15]. Trophoblast cells enter the vascular lumen and produce factors that degrade the smooth muscle and elastic tissue of the vascular media. During the fetal period, especially in the midtrimester, the process of vascular remodeling is ongoing, with the second wave of trophoblast invasion occurring in the early midtrimester (16-22 weeks; see Fig. 31-35) [13-15]. The extravillous trophoblast cells reach as far as the myometrial segments of the spiral arterioles by this time [15]. Therefore, in the midtrimester, it is not unusual to see partially remodeled arterioles or arterial lumens containing endovascular trophoblast (see Fig. 31-36). However, as gestation progresses, evidence of such ongoing remodeling should be less frequent, and most maternal vessels should appear as completely remodeled spiral arterioles (see Fig. 31-37). The degraded medial tissues are replaced by a fibrin paucicellular material containing embedded extravillous trophoblast cells, but devoid of smooth muscle or elastic tissue. With the degradation of the medial tissues, there is also a marked increase in the diameter of the vascular lumen. The cells lining of these vascular channels are extravascular trophoblast cells, which acquire an endothelial phenotype (see Fig. 31-38) [12,13].

Components of the Basal Plate from Intervillous Space to Endometrium

Lining of maternal endothelial cells and syncytiotrophoblast

Rohr's fibrin

Principal layer

Fetal tissues:

Extravillous trophoblast

Nonproliferative trophoblast emanating from cell columns

Anchoring villi

Buried cell columns

Maternal tissues:

Decidual cells

Connective tissue (endometrial stroma, vessels, fibroblasts, macrophages)

Nitabuch fibrin's

Separation zone

Decidua and other components of endometrial stroma,

Occasional extravillous trophoblasts

Multinucleated extravillous trophoblast (placental site giant cells)

FIGURE 31-31. Components of the basal plate from intervillous space to endometrium.

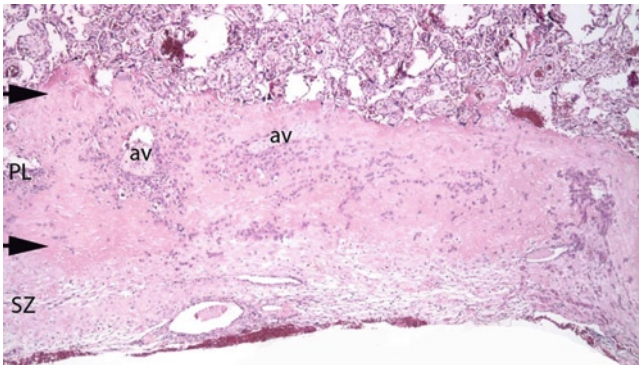


FIGURE 31-32. Basal plate at term. Low-power view of the basal plate showing the major constituents of the maternal-fetal interface. The intervillous space (*top of basal plate*) is lined by maternal endothelial cells and syncytiotrophoblast. *Top arrow* indicates Rohr's fibrin. The principal layer (PL; *between the two arrows*), contains anchoring villi (av) with trophoblast emanating from cell columns. Other cells present include fibroblasts, macrophages, and decidua. *Lower arrow* indicates Nitabuch's fibrin. The separation zone (SZ) contains decidua and other stromal components with occasional trophoblasts. (H&E, 4 \times .)

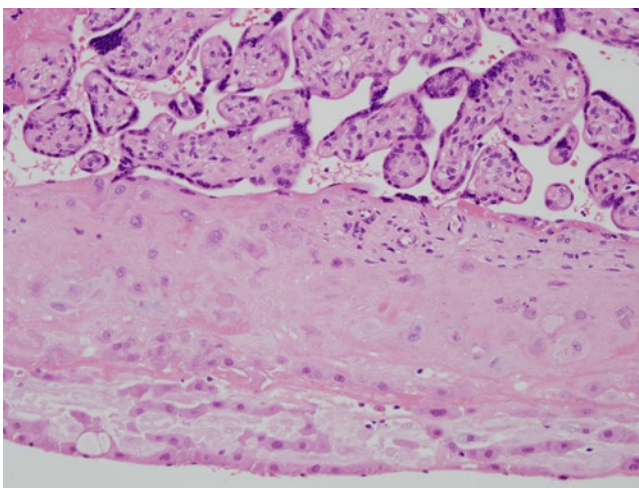


FIGURE 31-33. Basal plate at term. Inner aspect of the basal plate showing the lining of the intervillous space ranges from maternal endothelial cells, syncytiotrophoblast, and bare Rohr's fibrin/intervillous fibrin. (H&E, 20 \times .)

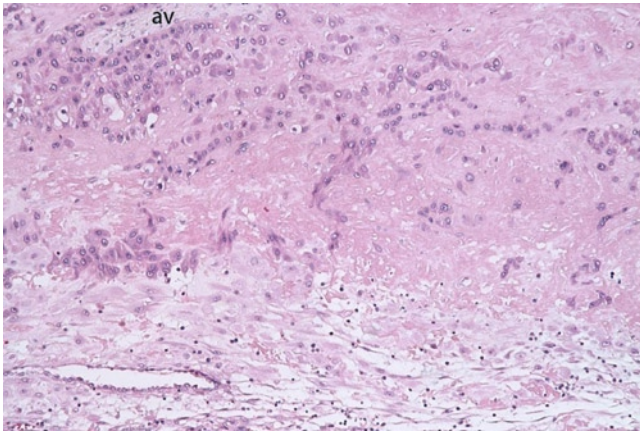


FIGURE 31-34. Basal plate at term. Medium-power view of basal plate showing the main constituents of the principal layer and separation zone. Note the extravillous trophoblast cells emanating from the anchoring villous (av). The cytoplasm of the trophoblast is more amphophilic than the cytoplasm of the decidua, which can aid in the distinction of the two cell types. Note that extravillous trophoblast cells are seen beyond Nitabuch's fibrin. (H&E, 10 \times .)

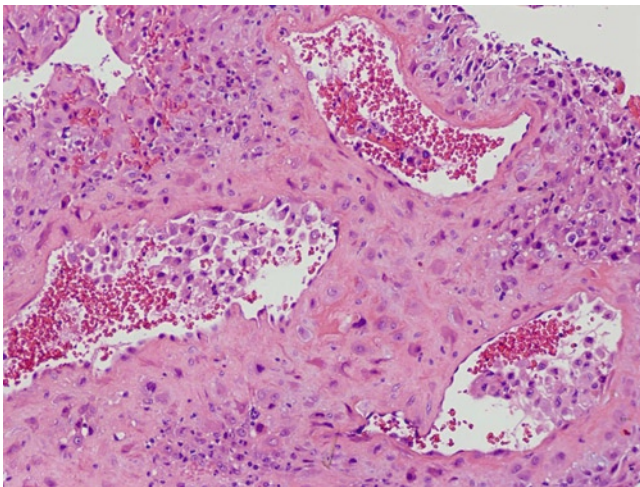


FIGURE 31-35. Basal plate at 14 weeks gestation. Note the ongoing remodeling of maternal vasculature by extravillous trophoblast. The media of the spiral arterioles has been predominantly destroyed, but numerous extravillous trophoblast cells remain in the vascular lumina. (H&E, 10 \times .)

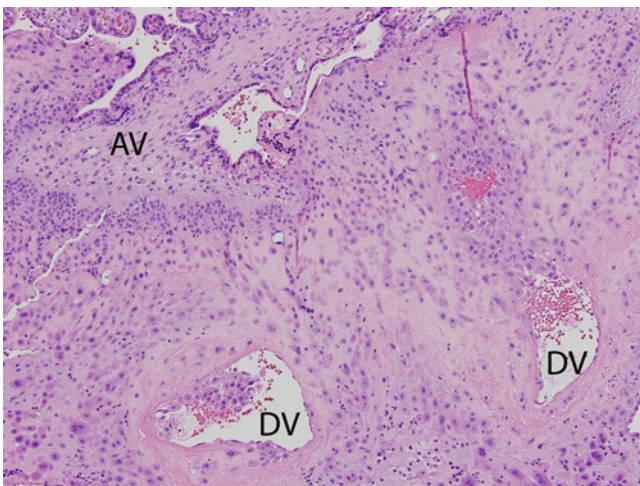


FIGURE 31-36. Basal plate at 23 weeks gestation. Note the extravillous trophoblast cells emanating from the anchoring villous (AV) and the extravillous trophoblast cells within the principal layer of the basal plate. The media of the spiral arterioles has been predominantly destroyed, and a few extravillous trophoblast cells remain in the decidual vessel (DV) lumina. (H&E, 10 \times .)

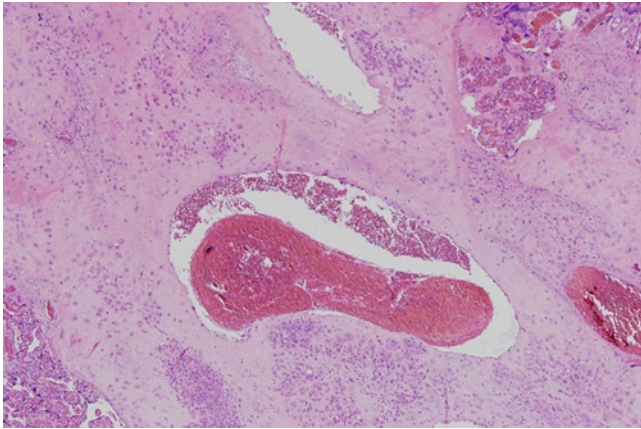


FIGURE 31-37. Basal plate at term. Fully remodeled maternal vessel with large luminal size, and wall composed of fibrin lacking smooth muscle. No residual intravascular trophoblast cells are seen. (H&E, 4 \times .)

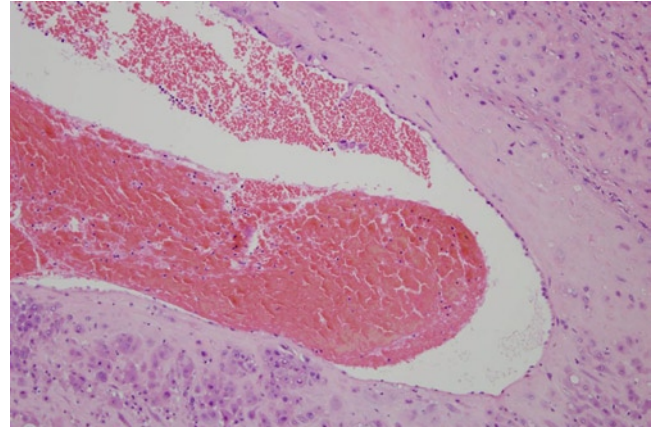


FIGURE 31-38. Basal plate at term. Higher-power view of the remodeled maternal vessel. Note the flattened lining cells and extravillous trophoblast embedded in the fibrin wall. (H&E, 10 \times .)

Villous Parenchyma

The tissues between the chorionic plate (fetal surface) and basal plate (maternal surface) comprise the villous parenchyma. The villous parenchyma is surrounded by the intervillous space, which contains maternal blood, but the remainder of the tissue between the two placental surfaces is fetally derived chorionic villi. The basic components of all chorionic villi are an outer trophoblastic covering, villous stroma, and fetal vessels. These components vary in character depending on the developmental stage of the placenta, which accounts for the dramatic histological changes seen in cut sections of the villous parenchyma over the course of normal gestation. The main alterations over time occur in the types of chorionic villi present at each developmental stage and the percentage of the various types of villi. The types of chorionic villi and the major characteristics of their basic components are listed in Fig. 31-39 [16,17]. The types and distribution of chorionic villi at various gestational ages are listed in Fig. 31-40 [16,17]. In summary, the main villous types are: mesenchymal villi, immature intermediate villi, mature intermediate villi, terminal villi, and stem villi. Mesenchymal villi are present throughout gestation but predominate in the first trimester. Mesenchymal villi give rise to immature and mature intermediate villi. Immature intermediate villi become stem villi and also give rise to new mesenchymal villi. Terminal villi, the mature functional end of the villous tree, arise from mature intermediate villi.

Each of the different types of chorionic villi present in the fetal period develop from the mesenchymal villous, which is the tertiary villous of the embryologic period (see Fig. 31-2) and predominates in the embryonic placenta. Mesenchymal villi are present in smaller numbers throughout gestation and act as the reservoir for continued villous growth and development [17]. Mesenchymal villi appear as long slender villous structures with primitive-appearing reticular stroma with centrally placed blood vessels and a double layer of trophoblast: inner

cytotrophoblast and outer syncytiotrophoblast (Figs. 31-41–31-43). In the fetal period, they are found at the tips and along the surfaces of immature and mature intermediate villi.

Stem villi are also present at all gestational stages and represent the conduits for the larger fetal vessels as well as serving as the support structure for the villous tree. They extend from the main trunks beneath the chorionic plate (truncus chorii) to the basal plate where they form the anchoring villi. Stem villi also send out side branches (rami and ramuli chorii) that extend into the placental lobule [17]. All stem villi are characterized by densely collagenized stroma and the presence of arteries and veins containing media and/or adventitia. The large stem villous trunks have the largest arteries and veins with the thickest muscular walls. The outer layer of trophoblast is typically thick and in many instances is replaced by fibrin.

In the early midtrimester, the most numerous villous type is the immature intermediate villous, which represents the first generation of villi with vessels lacking vascular media or adventitia arising from the stem villi (see Fig. 31-44). Immature intermediate villi typically have a thick trophoblast layer with cytotrophoblast present over more than 50% of the circumference (see Fig. 31-45) [17]. The stroma is described as reticular with numerous fluid-filled spaces, many containing placental macrophages or Hofbauer cells [17]. These villi generally contain centrally placed fetal vessels without the formation of vasculosyncytial membranes (see Fig. 31-46).

By the late midtrimester (see Figs. 31-47–31-53), many of the immature intermediate villi have transformed into stem villi, and mature intermediate villi are formed. Mature intermediate villi exhibit a more fibrous stroma than immature intermediate villi and are generally slightly smaller. They also have better vascularization than immature intermediate villi, but still have less than 50% of their stroma occupied by capillaries.

Terminal villi also begin to form at the surface of mature intermediate villi in the late midtrimester. Terminal villi represent the end of the villous tree and have the greatest capacity of maternal–fetal exchange because they are highly vascularized with more than 50% of their stroma occupied by capillaries. The number of terminal villi in a cross-section of placental parenchyma increases, with increasing gestational time throughout the third trimester. For instance, at 27 to 28 weeks gestation, mature intermediate villi still predominate, whereas terminal villi occupy less than 50% of the villous volume (see Figs. 31-54–31-57). By 32 weeks gestation, the number of terminal villi is roughly equal to the number of mature intermediate villi (see Figs. 31-58–31-61). By the late third trimester, terminal villi are the most numerous villous type; at term, terminal villi represent 60% of the placental cross-section (Figs. 31-62–31-65) [17]. In addition to the numerous capillaries in the villous stroma, terminal villi have significant thinning of the trophoblastic layer accompanied by sinusoidal dilation of fetal capillaries, allowing for reduction of the diffusion distance between the fetal and maternal circulations. Vasculosyncytial membranes, which represent the diffusion barrier in terminal villi, are composed of syncytiotrophoblast cytoplasm, fused syncytiotrophoblast and fetal capillary basement membrane, and fetal capillary endothelial cell cytoplasm. Vasculosyncytial membranes appear as the thin eosinophilic barrier, devoid of nuclei, between the dilated fetal capillary and intervillous space in H&E-stained sections (see Figs. 31-59 and 31-63). Vasculosyncytial membranes begin to become noticeable in the early third trimester, and increase in number as the pregnancy approaches term. At term, approximately 40% of the villous surface is composed of vasculosyncytial membranes [17].

Syncytiotrophoblastic knots or syncytial knots, defined as clumps of syncytiotrophoblastic nuclei along the villous perimeter can be noted throughout the fetal

period. Their etiology and pathogenesis is not clear, but the accumulation of these syncytial nuclei does increase with increasing gestational age (see Fig. 31-40) [18]. The peripheral displacement of these nuclei may aid in the formation and functional significance of the fetomaternal diffusion barrier.

Perivillous fibrin, the product of blood clotting on the villous surface, can be noted as a normal feature throughout gestation (see Figs. 31-47, 31-50, 31-51, 31-54, 31-55, 31-58). The deposition of perivillous fibrin increases with increasing gestational age, and is normally more prominent around stem villi, in the subchorionic region, and at the placental margin [19]. Therefore, caution should be exercised when interpreting the amount of perivillous fibrin in histological sections taken from these areas. Generally, the normal deposition of perivillous fibrin has an evenly distributed pattern. The deposition of perivillous fibrin should be considered abnormal when there are macroscopically visible deposits involving larger parts of the villous tree [19].

The fetal vessels of the placenta contain the elements of fetal blood. Nucleated red blood cells (NRBC) in the villous circulation are seen commonly in the first trimester (see Fig. 31-43), and there is a correlation between the number of nucleated and anucleate erythrocytes seen in the fetal circulation and the number of gestational days in the first trimester [20]. However, as gestation progresses, NRBC are seen less frequently in the fetal circulation, and are rare in the third trimester. Redline [21] correlated elevated NRBC counts ($2.5 \times 10^3/\text{mm}^3$) with placental findings, and found a threshold of 10 NRBC per 10 high-power fields (40 \times) in the fetal circulation of the placenta distinguished infants with elevated NRBC counts. Therefore, the finding of at least one definitive NRBC in most high-power fields of the villous parenchyma is a reasonable indicator of an increased NRBC count in the infant [21], and should be considered above the normal range.

Villous Types and Characteristics					
Villous type	Size, mm	Trophoblast	Stroma	Vessels/capillary density	Fate
Mesenchymal villi	60–100	Thick, double layer	Primitive stroma	Few vessels	Immature and mature intermediate villi
Immature intermediate villi	100–400	ST = 100% CT > 50%	Reticular stroma; Numerous macrophages	Poorly developed capillaries	Become stem villi by 21–24 wk Mesenchymal villi
Mature intermediate villi	80–150	ST = 100% CT < 50%	Begin fibrous stroma	< 50% capillaries	Terminal villi
Terminal villi	60	Thin layer with formation of VSM	Scant fibrous stroma	> 50% capillaries	End of villous tree
Stem villi	150–500	Thick layer, frequently replaced by fibrin	Fibrous stroma	Large muscularized arteries and veins, few capillaries	Important support of villous tree

CT—cytotrophoblast; ST—syncytiotrophoblast; VSM—vasculosyncytial membranes.
(Data from Benirschke et al. [16,17].)

FIGURE 31-39. Villous types and characteristics.

Villous Types and Other Characteristics by Gestational Age

Gestational age	Major types of villi present	Villi with cytotrophoblast, %	Villi with syncytial knots, average %
15–16 wk	IMMATURE INTERMEDIATE VILLI PREDOMINATE Mesenchymal villi Stem villi	80	–
20 wk	IMMATURE INTERMEDIATE VILLI WANING Mesenchymal villi Stem villi	60	5.8
24 wk	MATURE INTERMEDIATE VILLI FORM Few terminal villi form Stem villi Mesenchymal villi	50	8.6
28 wk	MATURE INTERMEDIATE VILLI AND INCREASING TERMINAL VILLI Stem villi Mesenchymal villi	45	13.2
32 wk	EQUAL NUMBERS OF TERMINAL VILLI AND MATURE INTERMEDIATE VILLI Stem villi Mesenchymal villi	35	13.1
36 wk	TERMINAL VILLI > MATURE INTERMEDIATE VILLI Stem villi Mesenchymal villi	25	22.5
Term	TERMINAL VILLI 60% OF CROSS-SECTION Stem villi Mesenchymal villi	20	29

(Data from Benirschke *et al.* [16] and Loukeris *et al.* [18].)

FIGURE 31-40. Villous types and other characteristics by gestational age.

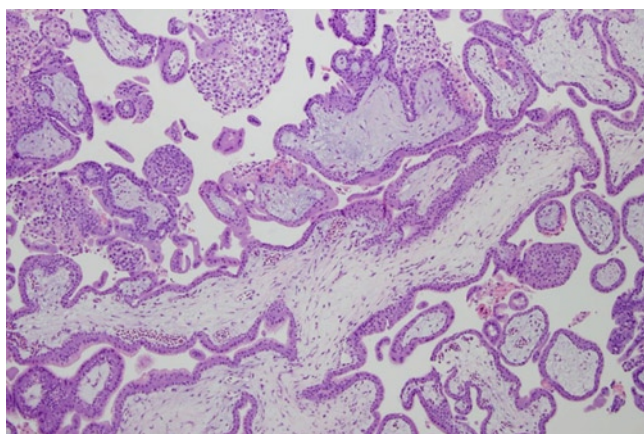


FIGURE 31-41. Placental tissue at 6 weeks gestation. Note abundance of mesenchymal villi with sparse vascularity and primitive mesenchymal stroma. (H&E, 4 \times .)

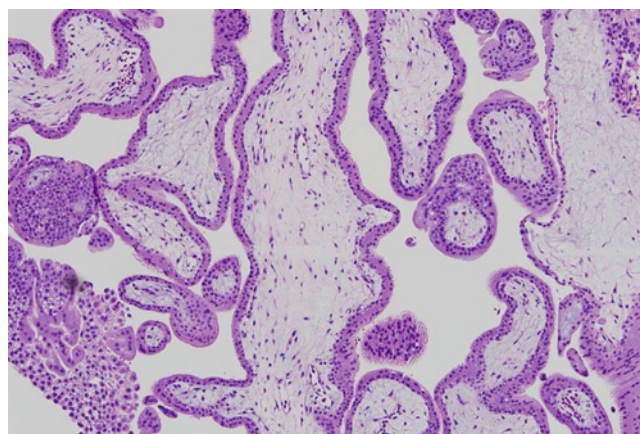


FIGURE 31-42. Placental tissue at 6 weeks gestation. Note abundance of mesenchymal villi with sparse vascularity and primitive mesenchymal stroma. (H&E, 10 \times .)

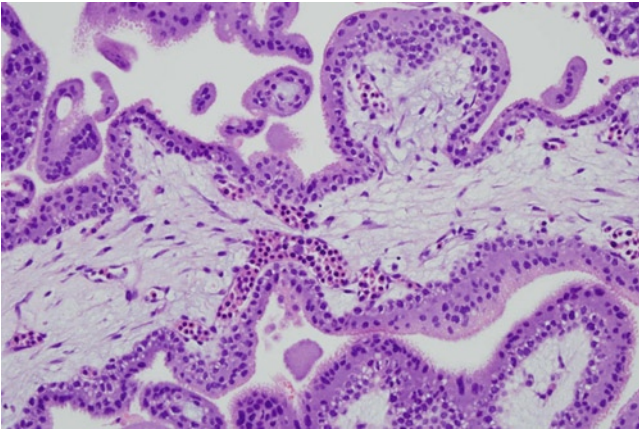


FIGURE 31-43. Placental tissue at 6 weeks gestation. Close up of mesenchymal villous showing double layer of inner cytotrophoblasts and outer syncytiotrophoblasts. Note the primitive-appearing stroma with thin-walled vessels showing numerous nucleated erythrocytes in the fetal circulation at this gestational age. (H&E, 20 \times .)

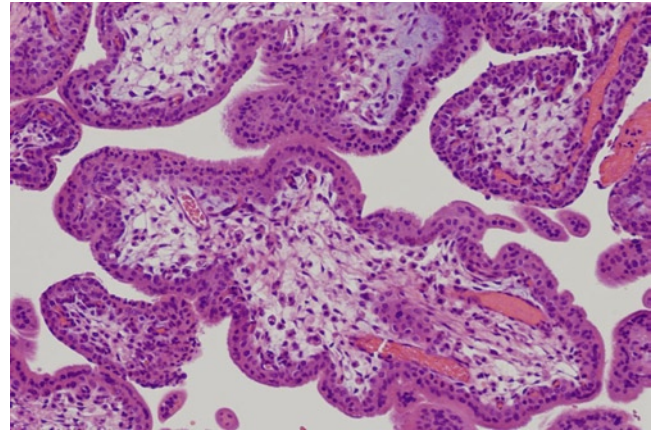


FIGURE 31-44. Placental villi at 14 weeks gestation. Immature intermediate villous shown here with thick double layer of trophoblast and reticular stroma with numerous macrophages. The stroma here is more cellular than in mesenchymal villi. There are only occasional capillaries seen within the villous stroma (H&E, 10 \times .)

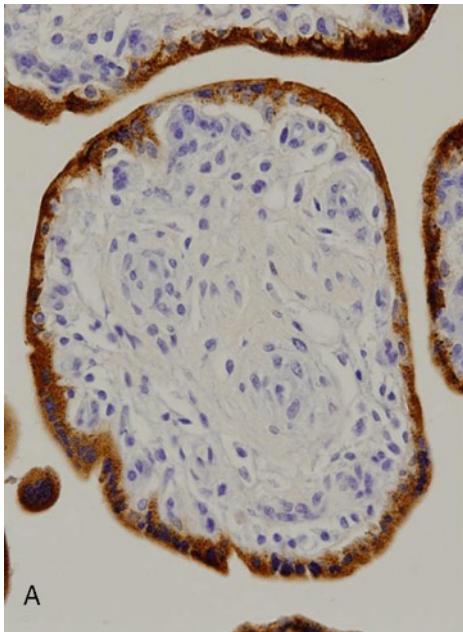
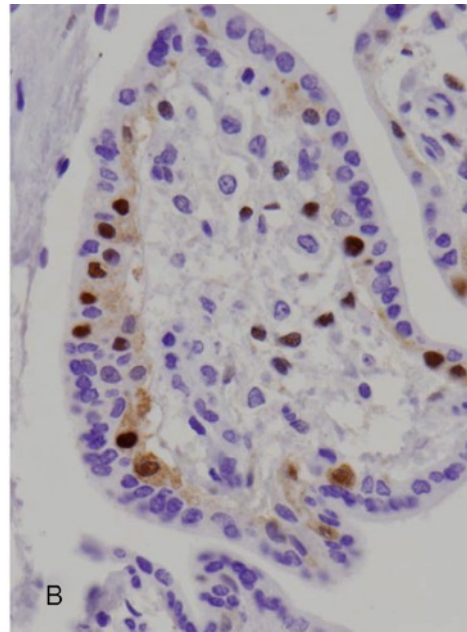


FIGURE 31-45. Chorionic villous at 16 weeks gestation. **A**, Note the continuous layer of syncytiotrophoblast highlighted by stain for human chorionic gonadotropin (HCG immunohistochemistry,



20 \times). **B**, Cytotrophoblast layer is discontinuous, but still fairly prominent as demonstrated by P57(KIP2) staining (P57[KIP2] immunohistochemistry, 40 \times .)

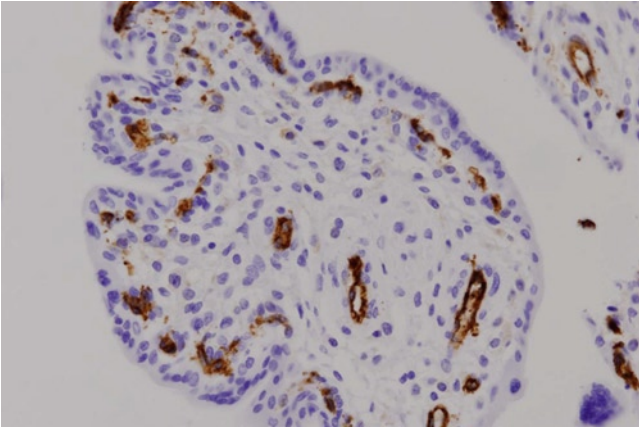


FIGURE 31-46. Placental villi at 16 weeks gestation. The vasculature of the villous is highlighted with CD31 immunohistochemical stain. Note the ratio of capillaries to stroma is quite low and the capillaries are fairly centrally placed. The stroma appears cellular. This villous appearance is appropriate for an immature intermediate villous (CD31 immunohistochemistry, 20 \times .)

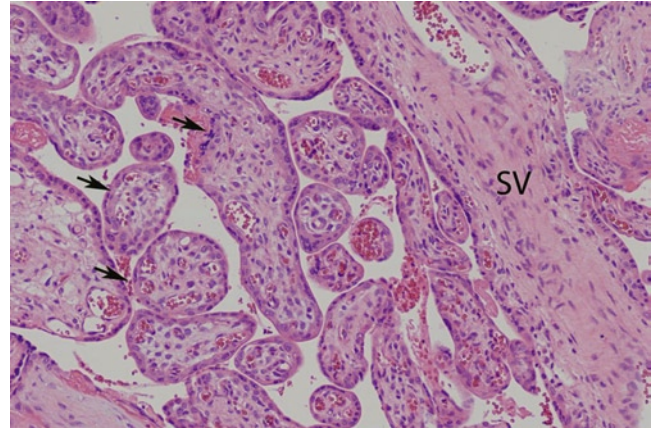


FIGURE 31-47. Placental villi at 21 weeks gestation. Note the formation of early stem villous (SV; right) and presence of mature intermediate villi (arrows) with a more fibrous stroma than immature intermediate villi. Capillary formation does not occupy a large percentage of the stroma. (H&E, 10 \times .)

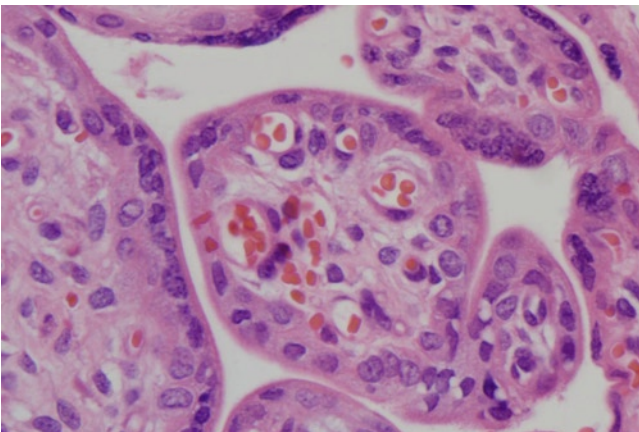


FIGURE 31-48. Placental villi at 21 weeks gestation. Mature intermediate villous with a more fibrous stroma than immature intermediate villi. Capillary formation does not occupy a large percentage of the stroma. (H&E, 40 \times .)

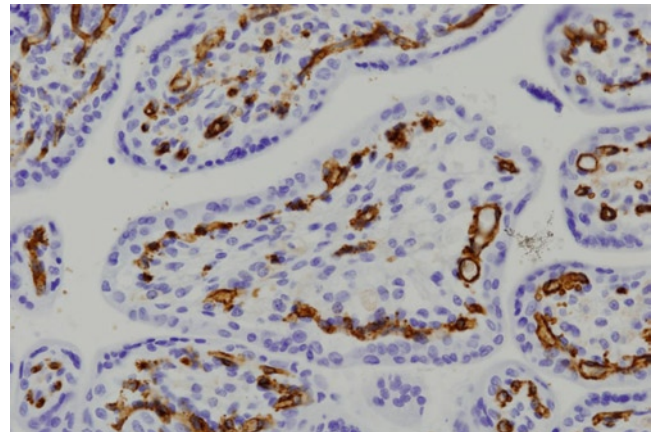


FIGURE 31-49. Placental villi at 20 weeks gestation. CD31 stain highlighting capillary formation occupying less than 50% of the stroma. (CD31 immunohistochemistry, 20 \times .)

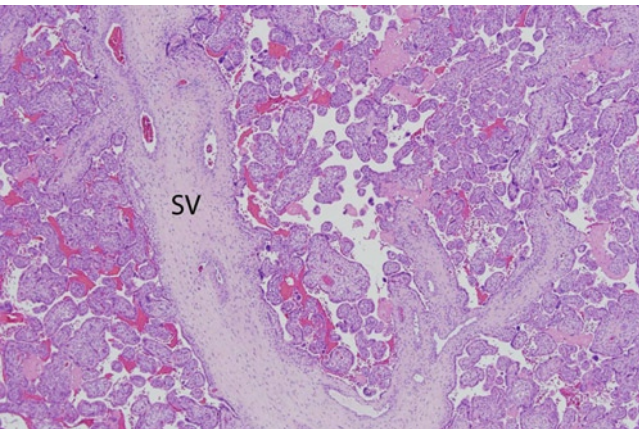


FIGURE 31-50. Placental villi at 23 to 24 weeks gestation. Low-power view stem villous (SV) surrounded predominantly by mature intermediate villi. Capillary formation is not prominent at this low power. (H&E, 4 \times .)

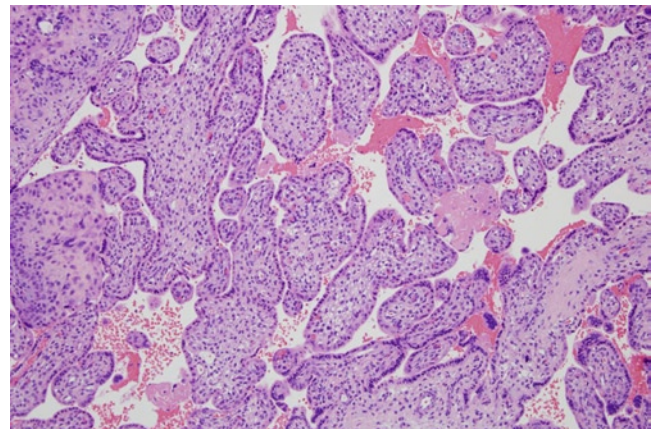


FIGURE 31-51. Placental villi at 23 to 24 weeks gestation. Mostly mature intermediate villi seen. Terminal villi are not a prominent feature in this image, although a few may be present at this gestational age. (H&E, 10 \times .)

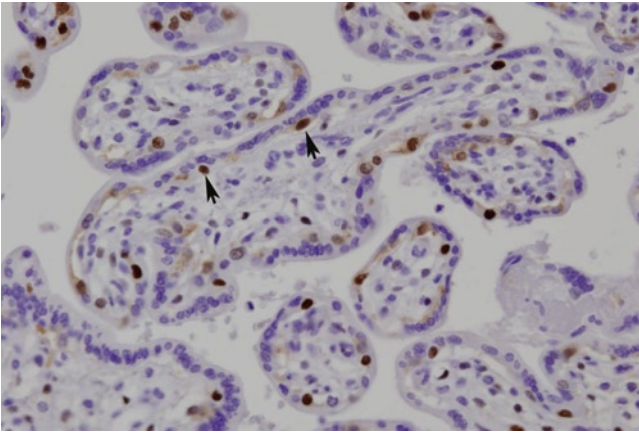


FIGURE 31-52. Chorionic villi at 23 to 24 weeks gestation. P57 (KIP2) stain highlighting villous cytotrophoblast cells (arrows). The cytotrophoblast of mature intermediate villi occupy less than 50% of the surface. (P57 [KIP2] immunohistochemistry, 20 \times .)

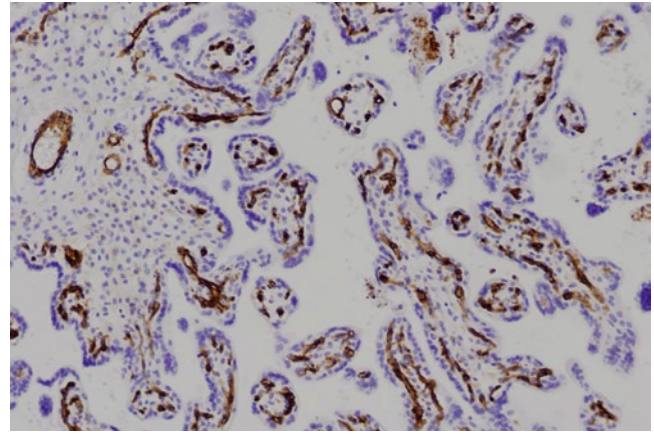


FIGURE 31-53. Chorionic villi at 23 to 24 weeks gestation. CD31 stain highlighting villous vessels. Note that most villi have less than 50% stroma occupied by capillaries. (CD31 immunohistochemistry, 10 \times .)

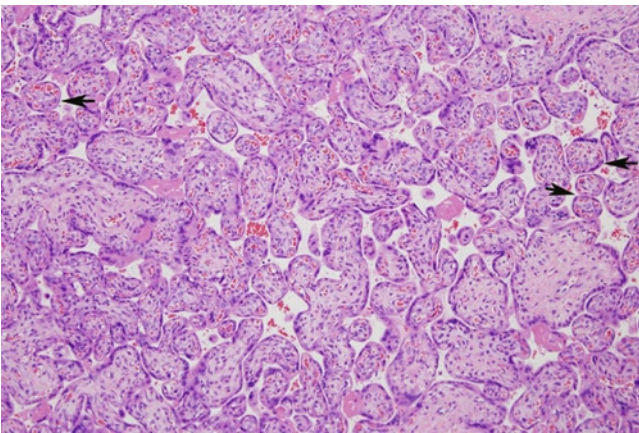


FIGURE 31-54. Chorionic villi at 27 weeks gestation. Mature intermediate villi still predominate, but terminal villi (arrows), characterized as smaller villi with more than 50% capillaries, are seen occasionally. (H&E, 10 \times .)

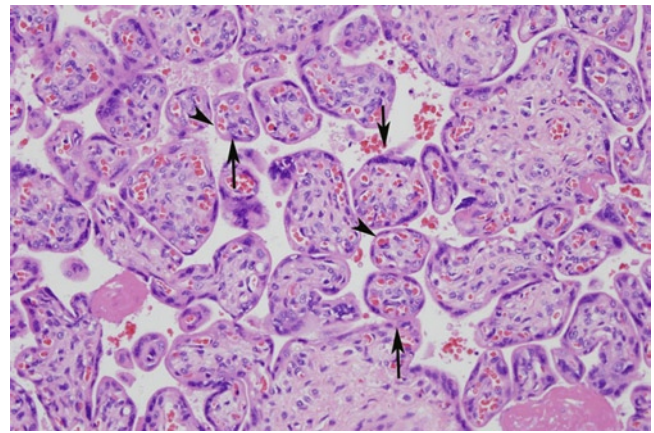


FIGURE 31-55. Chorionic villi at 27 weeks gestation. Mature intermediate villi with occasional smaller terminal villi (arrows). Vasculosyncytial membranes are just beginning to form (arrow-head). Perivillous fibrin is present, but not excessive. (H&E, 20 \times .)

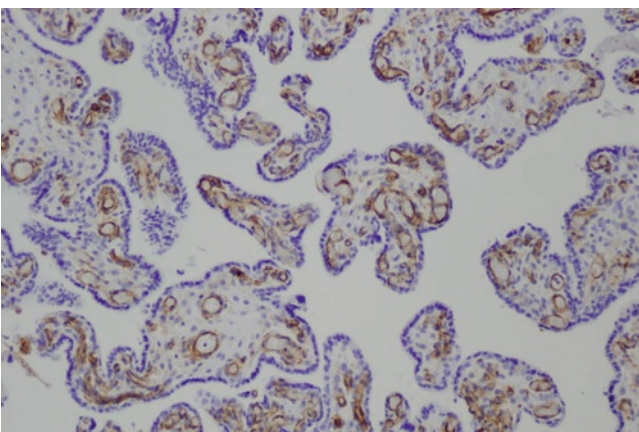


FIGURE 31-56. Placental villi at 28 weeks gestation with CD31 stain highlighting villous vessels. Note the villi in the center of the image have more than 50% of their stroma occupied by capillaries, a feature of terminal villi. (CD31 immunohistochemistry, 10 \times .)

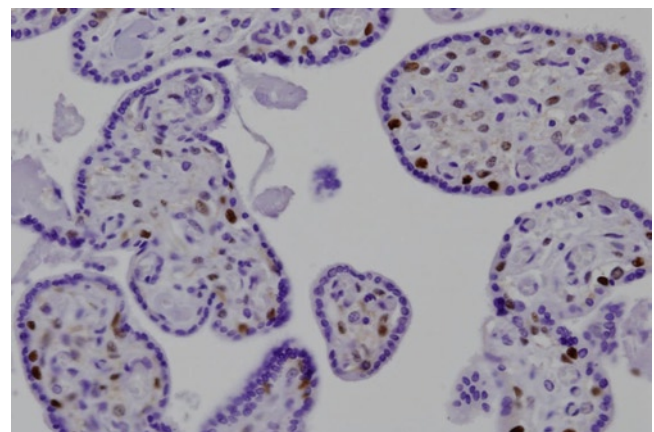


FIGURE 31-57. Chorionic villi at 28 weeks gestation. P57 (KIP2) stain highlighting discontinuous villous cytotrophoblast. (P57 [KIP2] immunohistochemistry, 20 \times .)

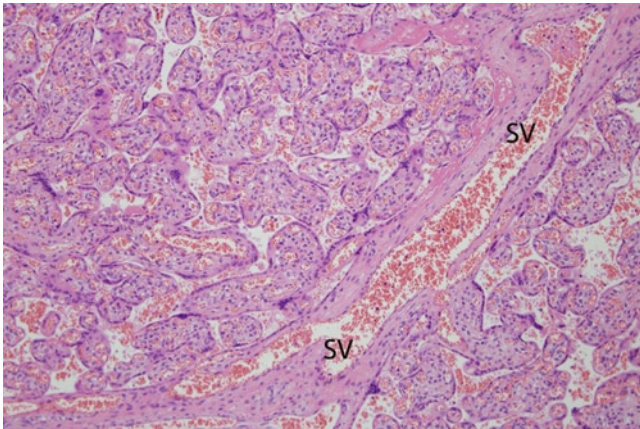


FIGURE 31-58. Chorionic villi at 32 weeks gestation. Villi are smaller and more vascular than at 27 to 28 weeks (compare with Fig. 31-51). Stem villous (SV) is present (right). (H&E, 10 \times .)

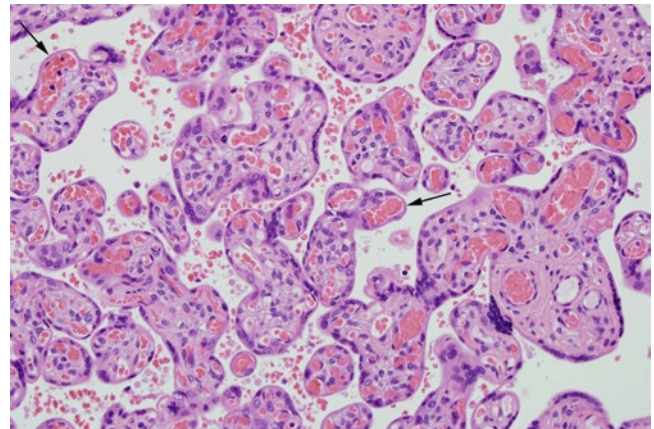


FIGURE 31-59. Chorionic villi at 32 weeks gestation. Note presence of more terminal villi and vasculosyncytial membranes (arrows) than at earlier gestation. (H&E, 20 \times .)

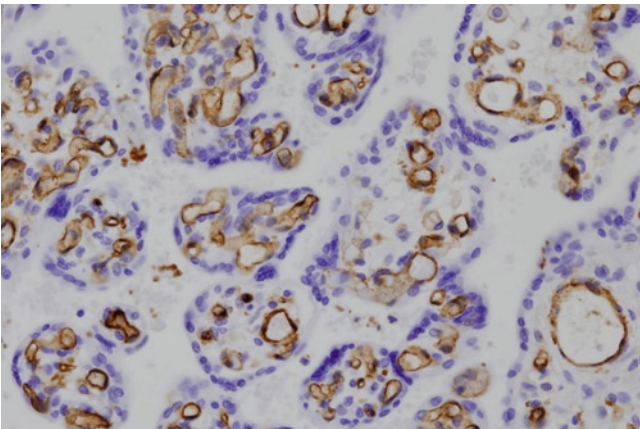


FIGURE 31-60. Placental villi at 32 weeks gestation with CD31 stain highlighting villous vessels. Note that many villi have more than 50% stroma occupied by capillaries, a feature of terminal villi. (CD31 immunohistochemistry, 20 \times .)

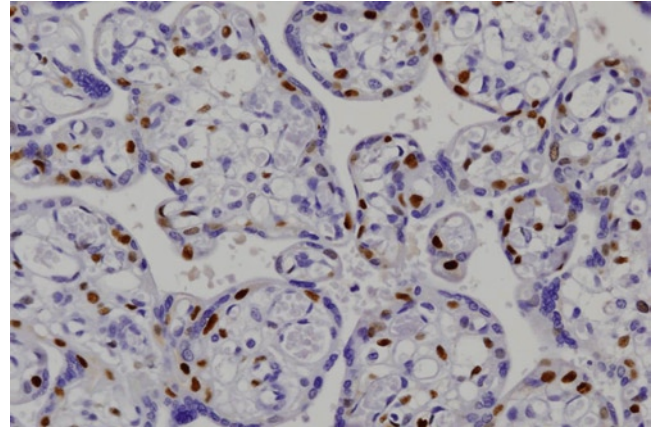


FIGURE 31-61. Placental villi at 32 weeks gestation with P57(KIP2) stain highlighting villous cytotrophoblast. (P57[KIP2] immunohistochemistry, 20 \times .)

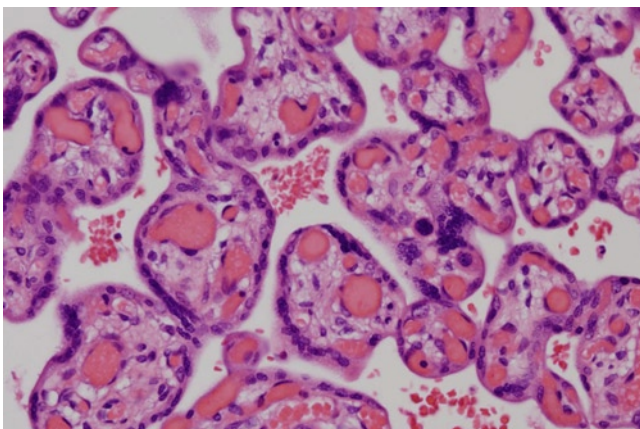


FIGURE 31-62. Placental villi at 39 weeks gestation. Note the still increasing number of terminal villi and well-formed vasculosyncytial membranes. (H&E, 20 \times .)

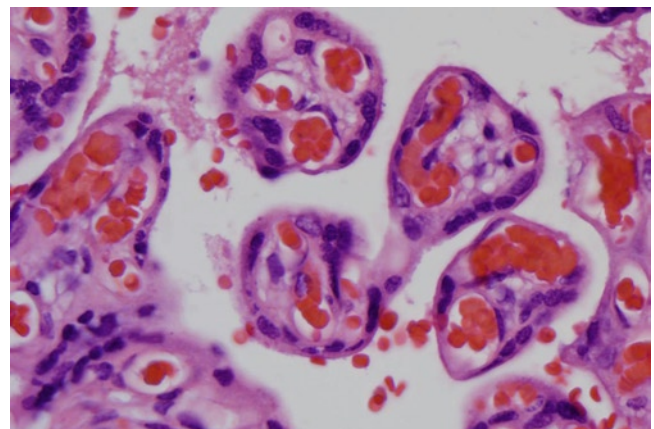


FIGURE 31-63. Placental villi at 39 weeks gestation. Higher-power view of villi highlighting vasculosyncytial membranes of terminal villi. (H&E, 40 \times .)

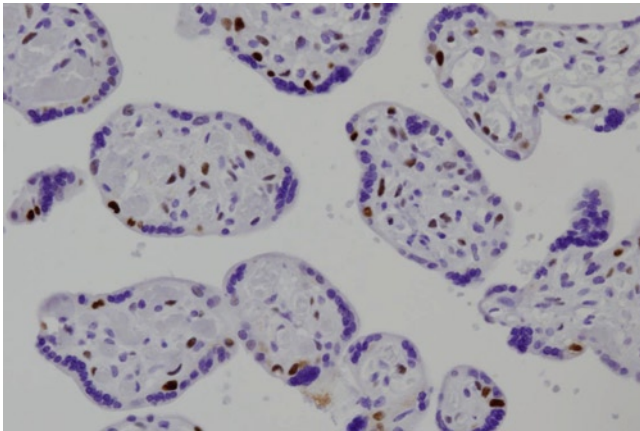


FIGURE 31-64. Placental villi at 39 weeks gestation with P57 (KIP2) stain highlighting villous cytotrophoblast, which is not very prominent at this gestational age. (P57[KIP2] immunohistochemistry, 20 \times .)

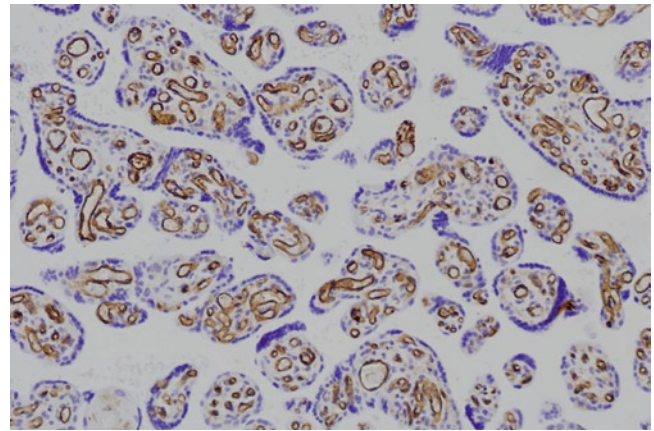


FIGURE 31-65. Placental villi at 39 weeks gestation with CD31 stain highlighting villous vessels. Note that many villi have more than 50% stroma occupied by capillaries, a feature of terminal villi. (CD31 immunohistochemistry, 10 \times .)

Special Considerations

Multiple Gestations

Microscopic anatomy of placentas of twin pregnancies and higher order multiple births does not differ significantly from singleton placentas in the main basic compartments of the placenta. In fact, in some multiple gestation pregnancies, completely separate placentas are found. However, if there is an area of connection between any two placentas of a multiple gestation pregnancy, histological sampling of this area is required to classify and document the type of placentation. Considering twin placentas for simplicity, there are three types of twin placentas: dichorionic diamniotic, monochorionic diamniotic, and monochorionic monoamniotic. The presence or absence of a dividing membrane, the portion of membranes that separates the two twin sacs, and the character of that membrane will define the type of twin placenta present.

Dichorionic diamniotic twin placentas can present as two completely separate placentas (no connection between the twin placentas; no dividing membrane present), or there can be a membranous connection between the twins (dividing membrane present on extraplacental membranes) or there can

be fusion of the placenta discs with presence of a dividing membrane on the chorionic plate.

Monochorionic diamniotic twins essentially always present as a single placental disc, and the dividing membrane is typically found on the fetal surface. If no dividing membrane is seen, the examiner should be suspicious of monochorionic monoamniotic placentation. However, be aware that the dividing membrane of the monochorionic diamniotic twin is very delicate and easily avulsed from the fetal surface before examination. Other data supportive of monoamniotic placentation should be sought such as cord entanglement, short intercordal distance, or conjoined fetuses.

The gross characteristics of the dividing membrane are described in Fig. 31-66. Histologically, the monochorionic diamniotic dividing membrane is characterized simply by two amnions in back-to-back orientation (see Fig. 31-67). In comparison, the dichorionic diamniotic dividing membrane is characterized by the addition of chorionic tissue between the two back-to-back amnions (see Figs. 31-68 and 31-69).

Gross Characteristics of Twin Dividing Membranes		
	Dichorionic	Monochorionic
MEMBRANE THICKNESS	Thick/4 layers	Thin/2 layers
MEMBRANE CHARACTER	Atrophied villi of chorion visible	Smooth and transparent, no atrophied villi
ATTACHMENT TO CHORIONIC PLATE (T-ZONE)	Well attached, thickened ridge visible at attachment	Not well attached, easily torn away, no ridge visible at attachment
CHORIONIC VESSELS	Stop at dividing membrane	Traverse beneath dividing membrane

FIGURE 31-66. Gross characteristics of twin dividing membranes.

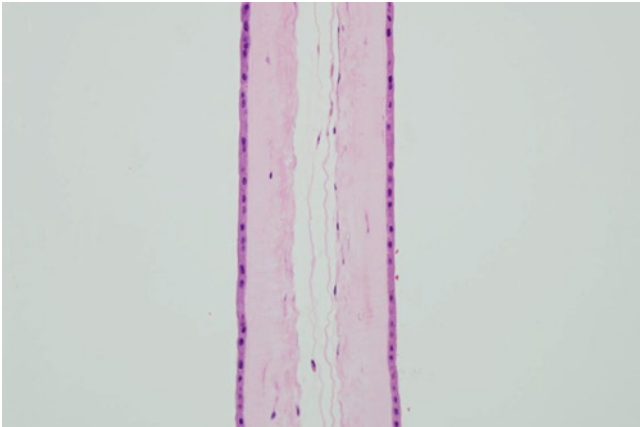


FIGURE 31-67. Monochorionic dividing membrane from a twin placenta. The dividing membrane consists of two back-to-back amnion membranes. (H&E, 200 \times .)

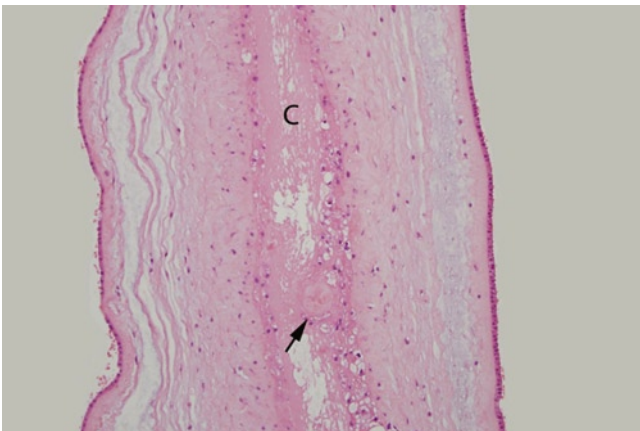


FIGURE 31-68. Dichorionic dividing membrane from a twin placenta. This is the typical appearance of the fused membranes with back-to-back fused chorions (C). Note that there is no significant parietal decidua between the two chorions and an atrophied villous of the chorion laeve is seen (arrow). The amnions of each twin are adjacent to the fused chorions with their connective tissue facing the central fused chorions. (H&E, 10 \times .)

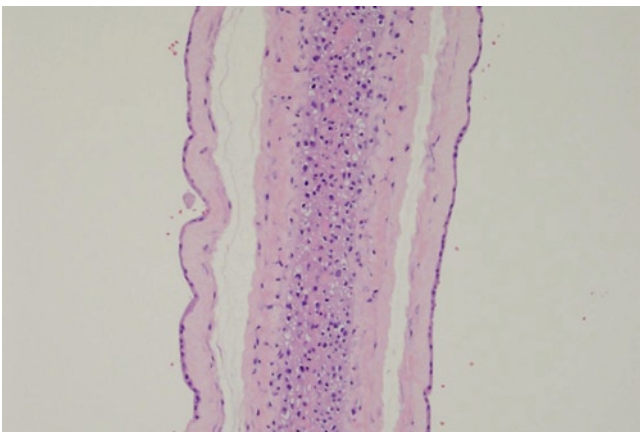


FIGURE 31-69. Dichorionic dividing membrane from a twin placenta. Fused membranes with back-to-back chorions. In this figure, there are no visible atrophied villi of the chorion laeve, which are seen in a patchy fashion in dichorionic dividing membranes. (H&E, 20 \times .)

Fetus Papyraceous

In some multiple gestations, one of the fetuses may either be selectively reduced or die spontaneously and be retained until the full term of pregnancy's gestation. Regardless of the mechanism of death, when a fetus dies in utero and is retained in utero, it will undergo involutional changes. With prolonged periods of retention in utero, the fetal tissue becomes atrophied and flattened, and is known as a fetus papyraceous. It is usually recognized as a somewhat thickened, ovoid area on the extraplacental membranes. Features that distinguish fetus papyraceous from thickened decidua

or mere decidual necrosis include the presence of a small speck of retinal pigment in the region of the eye or the presence of parallel-oriented ribs of the thoracic cage (see Fig. 31-70). If the fetus papyraceous is examined histologically, it shows variable degrees of loss of nuclear basophilia in fetal tissue, but with prolonged retention nearly all the visceral organs show loss of nuclear basophilia. Skeletal elements, such as cartilage and bone, are the easiest to recognize because of longer retention of nuclear detail in those tissues (see Fig. 31-71).

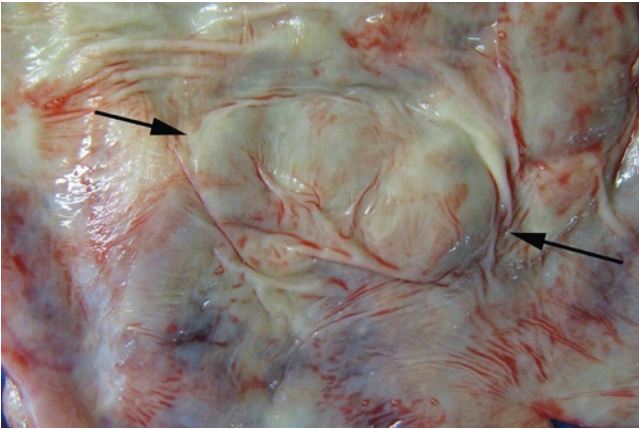


FIGURE 31-70. Gross image of fetus papyraceus within the extra-placental membranes. Note the flattened and rounded appearance of the macerated fetal tissue. Fetal rib cage can be seen faintly and is a clue to the presence of a fetus papyraceus.

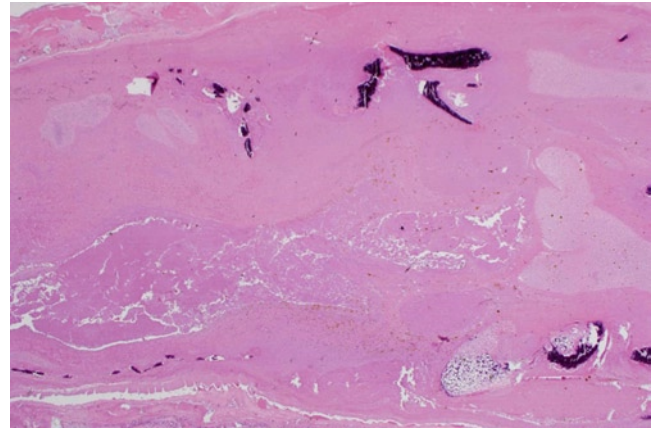


FIGURE 31-71. Microscopic appearance of fetus papyraceus. Note the macerated fetal tissues with significant loss of nuclear basophilia. Skeletal elements tend to retain nuclear detail the longest (H&E, 2 \times .)

Yolk Sac Remnant

Not infrequently, a small ovoid, flattened calcification can be noted between the chorion and amnion either in the extraplacental membranes or on the chorionic plate (see Fig. 31-72). This represents the calcified remnant of

the yolk sac, which atrophies in the embryonic period. Histological sections usually show an ovoid calcification without other epithelial elements located between the chorion and amnion (see Fig. 31-73).

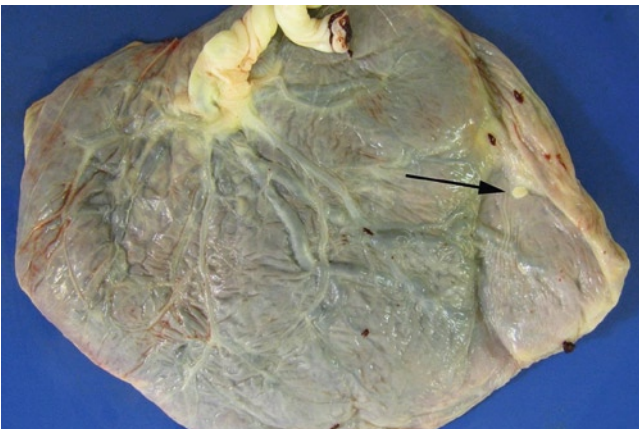


FIGURE 31-72. Gross image of yolk sac remnant. Small, ovoid, yellow-white structure (arrow) noted on the chorionic plate.

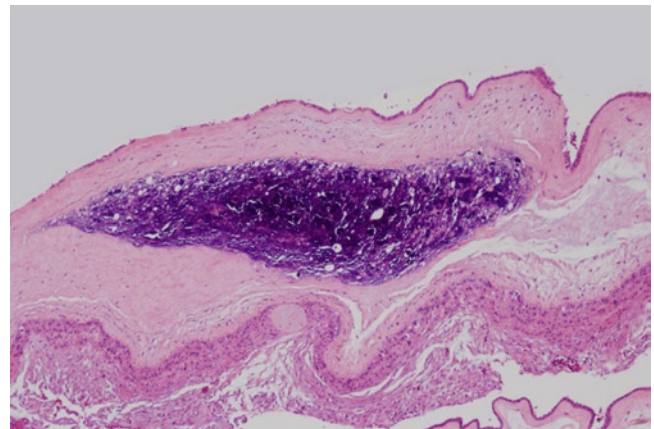


FIGURE 31-73. Calcified yolk sac remnant. Low-power image of the yolk sac remnant located between the amnion and chorion of the membranes. (H&E, 4 \times .)

References

1. Sadler TW, Langman J: *Langman's Medical Embryology*, edn 11. Philadelphia: Wolters Kluwer Lippincott Williams & Wilkins; 2010.
2. Schoenwolf GC, Larsen WJ: *Larsen's Human Embryology*, edn 4. Philadelphia: Elsevier/Churchill Livingstone; 2009.
3. Anatomy and pathology of the placental membranes. In *Pathology of the Human Placenta*. Edited by Benirschke K, Kaufmann P, Baergen RN. New York: Springer; 2006:321–379.
4. Benirschke K: Remarkable placenta. *Clin Anat* 1998, 11:194–205.
5. Redline RW, Boyd T, Campbell V, et al.: Maternal vascular underperfusion: nosology and reproducibility of placental reaction patterns. *Pediatr Dev Pathol* 2004, 7:237–249.
6. Anatomy and pathology of the umbilical cord. In *Pathology of the Human Placenta*. Edited by Benirschke K, Kaufmann P, Baergen RN. New York: Springer; 2006:380–451.
7. Stehbens WE, Wakefield JS, Gilbert-Barness E, Zuccollo JM: Histopathology and ultrastructure of human umbilical blood vessels. *Fetal Pediatr Pathol* 2005, 24:297–315.
8. Drut R, Quijano G: Heterotopic neurons in the umbilical cord. *Pediatr Dev Pathol* 2005, 8:124–127.
9. Ellison JP: The nerves of the umbilical cord in man and the rat. *Am J Anat* 1971, 132:53–60.
10. Preminger A, Udassin R, Pappo O, Arad I: Ectopic liver tissue within the umbilical cord. *J Pediatr Surg* 2001, 36:1085–1086.
11. Redline RW, Ariel I, Baergen RN, et al.: Fetal vascular obstructive lesions: nosology and reproducibility of placental reaction patterns. *Pediatr Dev Pathol* 2004, 7:443–452.
12. Frank HG, Kaufmann P: Nonvillous parts and trophoblast invasion. In *Pathology of the Human Placenta*. Edited by Benirschke K, Kaufmann P, Baergen RN. New York: Springer; 2006:191–312.
13. Salafia CM: The normal placenta immune anatomy and function. *Immunol Allergy Clin North Am* 1998, 18:271–289.
14. Khong TY, Sawyer IH: The human placental bed in health and disease. *Reprod Fertil Dev* 1991, 3:373–377.
15. Khong TY: The Robertson-Brosens-Dixon hypothesis: evidence for the role of haemochorial placentation in pregnancy success. *Br J Obstet Gynaecol* 1991, 98:1195–1199.
16. Characterization of the developmental stages. In *Pathology of the Human Placenta*, edn 5. Edited by Benirschke K, Kaufmann P, Baergen RN. New York: Springer; 2006:121–173.
17. Architecture of normal villous trees. In *Pathology of the Human Placenta*, edn 5. Edited by Benirschke K, Kaufmann P, Baergen RN. New York: Springer; 2006:121–173.
18. Loukeris K, Sela R, Baergen RN: Syncytial knots as a reflection of placental maturity: reference values for 20 to 40 weeks' gestational age. *Pediatr Dev Pathol* 2010, 13:305–309.
19. Histologic approach to villous alterations. In *Pathology of the Human Placenta*, edn 5. Edited by Benirschke K, Kaufmann P, Baergen RN. New York: Springer; 2006:482–483.
20. Salafia CM, Weigl CA, Foye GJ: Correlation of placental erythrocyte morphology and gestational age. *Pediatr Pathol* 1988, 8:495–502.
21. Redline RW: Elevated circulating fetal nucleated red blood cells and placental pathology in term infants who develop cerebral palsy. *Hum Pathol* 2008, 39:1378–1384.

Appendix

Trimming of Blocks for Microscopic Study

The following description of microscopic sections represents a general guideline for an appropriate sampling of autopsy tissues. However, the number, site, and size of sections should be tailored to the individual case.

Since the morphology of fetal tissues changes throughout gestation, it is important for the pathologist to become familiar with their normal appearance in order to evaluate possible abnormalities. Therefore, even when organs are grossly normal or maceration is present, sections should be obtained in the same manner.

I. Head and neck

A. Tongue, Hyoid Bone, and Epiglottis

Sagittal section of base of tongue along midline including foramen cecum.

B. Neck Soft Tissues, Larynx, Upper Esophagus, Thyroid, and Parathyroid Glands

Serial cross-sections at 3-mm intervals of entire larynx and thyroid gland.

C. Submandibular Salivary Gland

II. Respiratory system

A. Trachea (in patients who have been ventilated)

Longitudinal coronal section of distal trachea, carina, and main stem bronchi.

B. Lungs

One section of each lobe including the hilum and major bronchus and extending into peripheral lung and pleura.

III. Cardiovascular System

A. Heart

1. Normal heart: one longitudinal section of each ventricle including a papillary muscle, full-thickness free wall, atrioventricular valve, and base of atrium.

2. Anomalous heart: sections of right and left ventricles along cuts made to examine the chambers. Gross specimen is preserved for teaching and should remain as intact as possible.

B. Aorta (if considered necessary)

IV. Digestive system

A. Esophagus and Stomach

1. Longitudinal section of distal esophagus and proximal stomach across the G–E junction and cross-sections of distal and proximal esophagus.

2. Cross-section(s) of body of stomach.

3. Longitudinal section of antrum and duodenum across the pylorus.

B. Small and Large Bowel

Random cross-sections if no lesions are seen. Include ileocecal valve and appendix.

C. Rectum

Longitudinal section of the rectum with anal skin, if present. A cross-section of distal end of rectum and attached prostate or vagina is also acceptable.

D. Liver

One section from each lobe (gallbladder can be included to identify right lobe).

E. Pancreas

One section of head including adjacent duodenum and one or two cross-sections of body and tail.

V. Urogenital system

A. **Kidneys**

One section of each kidney including at least one well-oriented medullary pyramid with papilla and overlying cortex (renal lobe).

B. **Bladder**

A strip of bladder mucosa and wall. Include cross-section of prostate if not already sampled.

C. **Uterus**

Cross-section of fundus and longitudinal midsagittal section of cervix and vagina (if no septation is seen on cross-section).

D. **Ovaries**

Longitudinal section including hilum and broad ligament.

E. **Testes**

Longitudinal section including epididymis.

VI. Lymphoreticular system

A. **Spleen and Thymus**

One section of each.

B. **Lymph Nodes**

Sample as necessary according to gross findings. For routine sampling of lymph nodes the small bowel mesentery provides a good source.

VII. Endocrine system

A. **Thyroid and Parathyroid Glands**

Usually not separated from larynx and trachea. See head and neck section.

B. **Adrenal Glands**

One cross-section of each gland perpendicular to long axis for better orientation of cortex and medulla.

C. **Pituitary Gland**

Usually submitted in toto within the sella turcica. If larger, one transverse section showing anterior and posterior lobes is desirable.

VIII. Musculoskeletal system

A. **Psoas and Diaphragm**

Longitudinal and cross-sections of each.

B. **Rib and Vertebral Body**

Longitudinal section of rib including the costochondral junction and midsagittal section of vertebral body. Decalcify very gently and for a minimal period of time. Do not decalcify overnight.

Index

A

- Accessory spleens, 260
- Adrenal cortical rests, 139
- Adrenal corticotropin hormone (ACTH), 234
- Adrenal cytomegaly, 210
- Adrenal gland
 - adrenal cytomegaly, 210
 - areas and zones, 203
 - calcifications, 211
 - definitive cortical zone, adenoid change, 211
 - embryology, 203
 - extramedullary hematopoiesis, 211
 - heterotopic adrenal tissue, 209–210
 - histology
 - capsule, 204
 - cortex, 205
 - medulla, 208
 - at 12 weeks gestation, 204, 206
 - at 17 weeks gestation, 204
 - at 20 weeks gestation, 204, 206
 - at 26 weeks gestation, 204
 - at 35 weeks gestation, 205, 206
 - at 39 weeks gestation, 206
- Adventitia, 40, 118, 119
- Alveolar stage, 32–33
- Alveoli, 23, 26
- Anal canal
 - less than 14 weeks, 59
 - 14 to 30 weeks, 60, 63
- Anitschkow nuclear structure, 6
- Anterior pituitary gland
 - ACTH, 234
 - histological feature of, 234
 - Rathke cleft cyst, 234, 236
 - at 26 weeks gestation, 234, 235
 - at 35 weeks gestation, 234–236
- Antral follicles, 176
- Aorta, 15
- Apocrine metaplasia, 358
- Appendix
 - less than 14 weeks, 59
 - 14 to 30 weeks, 59–63
- Auerbach's plexus, in small intestine, 57

B

- Basal ganglia
 - at term, 314–315
 - at 8 weeks, 289
 - at 14 weeks, 291
 - at 22 weeks, 297
 - at 27 weeks, 301
 - at 32 weeks, 305–306
 - at 35 weeks, 310–311
 - at 2 years postnatal, 317–318
- Basal plate
 - components of, from intervillous space to endometrium, 376
 - layers, 375, 376

- maternal vascular remodeling, 375
- at term, 375–378
- 14 weeks gestation, 377
- at 23 weeks gestation, 377
- Basophils, 234
- Bilateral bulbourethral glands, 163
- Biliary tract
 - hepatic duct, transverse section of, 73, 76
 - at 16-weeks, 73, 74
 - at 17-weeks, 73, 74
 - at 24-weeks, 73, 75
 - at 36-weeks, 73, 75
- Bipotential genitourinary tract
 - bipotential gonads, 100, 101
 - mesonephric and paramesonephric ducts, 102, 103
 - paramesonephric duct, in male, 102
- Bipotential gonads, 100, 101
- Bipotential paramesonephric ducts, 102, 103
- Blood islands, 273
- Blood supply, lymph nodes, 262
- Blood vessels
 - aorta, 15
 - ductus arteriosus, 16–17
 - umbilical vein, 17
- Bone
 - cell types in
 - osteoblasts, 332
 - osteoclasts, 333
 - osteocytes, 333
 - osteoprogenitor cells, 332
 - embryology
 - long bone ossification, 324, 325
 - lower limb, 324, 326
 - metacarpal bone ossification, 324, 325
 - ossification, in fetus, 324, 327
 - paraxial mesoderm, 323
 - somites, skeletal and muscular derivatives of, 323, 324
 - somatic mesoderm, 323
 - sternum, 323–324
 - formation, types
 - endochondral ossification, 334–335
 - membranous ossification, 336
 - histology
 - cell types, 332–333
 - formation, 334–336
 - structure, 328–329
 - types, 330–331
 - organic components, 330
 - structure of
 - cortical bone, 328–329
 - medullary canal, 329
 - periosteum, 328
 - types of
 - lamellar bone, 330
 - woven bone, 331
- Bone marrow
 - embryology, 273–274

- during fetal life, 275
 - hematopoiesis, 273
 - hemophagocytosis, 280–281
 - histology, 274–280
 - myelopoiesis
 - dyserythropoiesis, 278–279
 - erythropoiesis, 278
 - granulopoiesis, 277
 - hematogones, 279–280
 - lymphopoiesis, 279–280
 - megakaryopoiesis, 279
 - monopoiesis, 277
 - structure of, 276
 - trilineage hematopoiesis, 276
 - at 19 weeks gestation, 275
 - at 24 weeks gestation, 275
 - at 32 weeks gestation, 276
 - at 41 weeks gestation, 276
 - Brain. *See* Central nervous system (CNS)
 - Brainstem, 290
 - Branching morphogenesis, 163
 - Bronchi, 23, 25
 - Bronchioles, 23, 26
 - Bronchus-associated lymphoid tissue (BALT), 23, 26
 - Brunner's glands, 54–55, 58
- C**
- Calcification, yolk sac, 387
 - Calcitonin immunohistochemistry, 222
 - Canalicular stage, 29–30
 - Capsule, fetal spleen, 251
 - Caudal gonadal ligaments, 98–100
 - Central nervous system (CNS)
 - embryology, 285–286
 - first trimester
 - brainstem and cerebellum, 290
 - cerebral cortex, 288–289
 - neural tube, 288
 - spinal cord, 290
 - histology
 - first trimester, 288–290
 - myelination gliosis, 288
 - neurogenesis, 287
 - second and third trimesters, 290–313
 - postnatal
 - basal ganglia, 316–318
 - cerebellum, 316, 318
 - frontal cortex, 316
 - occipital cortex, 316
 - spinal cord, 316, 319
 - white matter, 316, 317
 - second and third trimesters
 - 13 to 15 weeks, 290–292
 - 16 to 18 weeks, 293–295
 - 19 to 22 weeks, 295–303
 - 29 to 33 weeks, 304–307
 - 34 to 38 weeks, 308–313
 - sulcal development, 287
 - term
 - basal ganglia at, 313–315
 - cerebellum, 313, 315
 - cerebral cortex at, 313, 314
 - hippocampus at, 313, 315
 - white matter at, 313, 314
 - Centroacinar cells, 80, 81
 - Cerebellum
 - in first trimester, 290
 - postnatal, 318
 - at term, 315
 - at 14 weeks, 292
 - at 17 weeks, 295
 - 20 and 21 weeks gestation, 298
 - 30 and 31 weeks, gestation, 307
 - at 35 weeks, 311–312
 - Cerebral cortex
 - at postnatal, 316
 - at term, 313, 314
 - at 8 weeks, 289
 - at 14 weeks, 291
 - at 17 weeks, 293
 - at 20 weeks, 296
 - at 21 weeks, 296
 - at 25 weeks, 300
 - at 32 weeks, 304–305
 - at 35 weeks, 308–309
 - white matter, 309–310
 - Chorionic plate, 373–374
 - Choroid plexus
 - at 8 weeks, 289
 - at 17 weeks, 294
 - at 32 weeks, 306
 - Conduction system, heart, 13–14
 - Congenital blood cyst, 10, 12
 - Congenital erosion, 193
 - Connective tissue trabeculae, 242–243
 - Cordae tendineae, 10
 - Corpus striatum, 294
 - Cortical bone, 328–329
 - Cowper's glands. *See* Bilateral bulbourethral glands
- D**
- Definitive urogenital sinus, 117
 - Dichorionic diamniotic twin placentas, 385
 - Diencephalon, 286, 292
 - Ductus arteriosus, 16–17
 - Ductus deferens. *See* Vas deferens
 - Ductus venosus, 68, 69
 - Duodenum, 54–55, 58
 - Dyserythropoiesis, 278–279
- E**
- Ectodermal ring, 97, 98
 - Embryology
 - adrenal gland, 203
 - bone
 - long bone ossification, 324, 325
 - lower limb, 324, 326
 - metacarpal bone ossification, 324, 325

- ossification, in fetus, 324, 327
 - paraxial mesoderm, 323
 - somites, skeletal and muscular derivatives of, 323, 324
 - somitic mesoderm, 323
 - sternum, 323–324
 - bone marrow, 273–274
 - epididymis
 - efferent ductules and head of, 143–144
 - mesonephric duct, 143
 - urogenital union, 144
 - fallopian tubes, 181
 - of genitourinary tract
 - bipotential, 101–103
 - primitive, 95–100
 - lymph nodes, 261
 - mammary gland, 347–348
 - ovary
 - central zone and peripheral zone, 173–174
 - 7th week postfertilization, 173
 - 8th week postfertilization, 174
 - palatine tonsil, 267
 - parathyroid gland, 225
 - pituitary gland, 231–232
 - placenta
 - amniotic and chorionic cavities, formation of, 364–365
 - early placental development, 363, 364
 - primary, secondary, and tertiary villi, 364, 365
 - prostate gland, 163
 - of salivary glands, 87
 - seminal vesicle, 157
 - skeletal muscle, 337–338
 - of spleen, 251
 - testis
 - primordial germ cells, maturation process, 122
 - seminiferous tubules, 121
 - tunica albuginea, 122
 - thymus gland, 241
 - thyroid gland, 213
 - uterus, 187
 - vagina, 195
 - vas deferens, 153
 - Embryonic skeletal muscle, 338–339
 - Embryonic stage, lung, 27
 - Endocardium, 8–9
 - Endochondral ossification, 334–335
 - Endocrine cell nucleomegaly, 82, 84
 - Endocrine pancreas, 82–84
 - Endometrium
 - at 28 and 32 weeks, 190
 - at 21 weeks, 190
 - at 35 weeks, 191
 - Endomysium, 343
 - Epicardium, 5–6
 - Epididymis
 - coni vasculosi, 147
 - embryology
 - efferent ductules and head of, 143–144
 - mesonephric duct, 143
 - urogenital union, 144
 - fetal histology, 145
 - coni vasculosi, 22 weeks gestation, 147
 - at 17 weeks gestation, 146
 - at 22 weeks gestation, 147–148
 - at 34 weeks gestation, 149–150
 - at 39 weeks gestation, 150–152
 - function, 143
 - histology, 144
 - EPM. *See* Extraplacental membranes (EPM)
 - Epoophoron, 180
 - Erythropoiesis, 278
 - Esophagus
 - Auerbach's plexus in, 46
 - ectopic gastric cardiac in, 44
 - less than 14 weeks, 41–43
 - pyloric mucosa in, 44
 - 14 to 30 weeks, 43–44
 - 30 to 40 weeks, 45–46
 - at 34 weeks, 45
 - at 35 weeks, 46
 - Exocrine pancreas, 80–81
 - Extramedullary hematopoiesis, 211
 - Extraplacental membranes (EPM)
 - decidua parietalis, 367–368
 - reactive amniotic changes, 366, 368
 - at term, 366, 367
 - at 15 weeks gestation, 366, 367
 - at 32 weeks gestation, 366, 367
- ## F
- Fallopian tubes
 - anatomic organization, 181
 - embryology, 181
 - histology, 182–184
 - muscularis (myosalpinx) layer
 - 23 weeks, 183
 - 32 weeks, 184
 - 38 weeks, 184
 - serosa layer
 - 19 weeks, 182
 - 21 weeks, 183
 - 38 weeks, 184
 - tubal mucosa layer
 - 19 weeks, 182, 183
 - 21 weeks, 183
 - 23 weeks, 182
 - Fetal Leydig cells
 - definition, 121
 - maturation, 123
 - regression and dedifferentiation, 128
 - Fetal muscle development
 - muscle fibers, full-term neonate, 339, 342
 - at term, 341
 - at 17 weeks gestation, 339–340
 - at 23 weeks gestation, 340
 - Fetal pulmonary developmental stages
 - alveolar stage, 32–33
 - canalicular stage, 29–30
 - embryonic stage, 27

- pseudoglandular stage, 28–29
- saccular stage, 31–32
- Fetal spermatogonia, 121
- Fetal spleen. *See* Spleen
- Fetal vs. adult myocardium, 4
- Fetus papyraceous, 386–387
- Follicles, 176
- Follicular atresia, 179
- Folliculogenesis
 - Graafian follicle, 32 weeks gestation, 178
 - primary follicles, 30 weeks gestation, 177
 - primordial follicles, 28 weeks gestation, 177
 - secondary or preantral follicles
 - 32 weeks gestation, 177
 - 38 weeks gestation, 178
 - tertiary or antral follicles, 38 weeks gestation, 178
 - 28 weeks gestation, 177
- Foramen ovale, 3
- Forebrain, 286
- Fused paramesonephric ducts, 195

G

- Gastrointestinal tract
 - definition and function, 39
 - embryology, 39
 - histology
 - anal canal, 59–60, 63–64
 - appendix, 59–63
 - esophagus, 41–46
 - large intestine, 59–61
 - small intestine, 52–58
 - stomach, 47–51
 - timing and sequence, developmental events, 40–41
 - wall, organization of, 40
 - segments, 39
- Genitourinary tract
 - bipotential
 - bipotential gonads, 100, 101
 - mesonephric and paramesonephric ducts, 102, 103
 - paramesonephric duct, in male, 102
 - phases of, 95
 - primitive
 - described, 95
 - ectodermal ring, 97, 98
 - inguinal region and caudal gonadal ligaments, 98–100
 - mesonephros and mesonephric duct, 96–97
- Graafian follicle, 176
- Granulopoiesis, 277
- Gut-associated lymphoid tissue
 - in appendix, 61
 - in small intestine, 57

H

- Hassall's corpuscles, 248
- Heart
 - embryology, 3–4
 - histology
 - endocardium, 8–9
 - epicardium, 5–6
 - fetal vs. adult myocardium, 4

- myocardium, 6–8
- pericardium, 5
- specialized structures
 - conduction system, 13–14
 - papillary muscles and cordae tendineae, 10
 - valve leaflets and cusps, 10–13

Hematogones, 279–280

Hematopoiesis

- bone marrow, 273
- extramedullary, 211
- fetal spleen and, 260
- liver, 70, 72
- lymph nodes and, 265
- pancreas, 84
- trilineage, 276

Hemophagocytosis, 265, 280–281

Hemosiderin, 70, 73

Hepatic lobule

- endothelial sinusoids, 69, 71
- hematopoiesis, 70, 72
- hemosiderin, 70, 73
- hepatocyte cords, 69, 70
- Kupffer cells, 69–70
- 20-weeks, 69, 71

Hepatic vasculature, development of, 68–69

Hepatobiliary morphogenesis, 67–68

Heterotopic adrenal tissue, 209–210

Hilus cells, 179

Hippocampus

- at term, 315
- at 17 weeks, 293–294
- at 21 weeks, 296
- at 22 weeks, 297
- at 35 weeks, 310

I

Inguinal region, 98–100

Interlobular stroma, 358

Intra-acinar pulmonary arterioles, 33

Intracytoplasmic hyaline globules, 55

Intrapulmonary karyorrhectic cells, 34

Intrapulmonary squamous cells, 34–35

Intrathyroidal inclusions, 223

J

Juxtaglomerular apparatus, 108, 113

K

Karyorrhectic cells, intrapulmonary, 34

Kidney

embryology

- common excretory duct, 105
- eighth week, 106–107
- seventh week, 106
- sixth week, 105–106
- 19 weeks, 107

histology

- collecting ducts, 108, 115
- glomeruli, development of, 108, 111, 112
- juxtaglomerular apparatus, 108, 113

- medulla, 108, 114–115
- nephrogenesis, 108, 111–112
- nephrogenic zone, 107–108, 110
- proximal convoluted tubules, 108, 113
- renal cortex, 107, 109
- renal lobe, 107
- renin-expressing cells, 108, 114
- tubular growth and maturation, 108, 113
- at 19 weeks gestation, 107

Kupffer cells, 69–70

L

Lamellar bone, 330

Lamina propria, 118, 119

Large intestine

- 14 to 30 weeks, 59–61
- 30 to 40 weeks, 64
- at 12 weeks, 59

Liver

- embryology
 - development mechanisms, 67–68
 - hepatic morphogenesis, 68
 - hepatic vasculature, development of, 68–69
- hematopoiesis in, 70, 72
- hemosiderin in, 70, 73
- histology
 - biliary tract, 73–76
 - hepatic lobule, 69–73

Long bone ossification, 324, 325

Loops of Henle, 106, 108, 114

Lung

- embryology, 22
- formation, stages of, 21–22
- histology
 - fetal pulmonary developmental stages, 27–33
 - postnatal pulmonary, 23–26
- intra-acinar pulmonary arterioles, 33
- intrapulmonary karyorrhectic cells, 34
- intrapulmonary squamous cells, 34–35

Lymphatics, 264. *See also* Lymph nodes

Lymph nodes

- embryology, 261
- and hematopoiesis, 265
- hemophagocytosis, 265
- histology, 262–265
- lymphatics, 262
- mesenteric, at 34 weeks gestation, 262–264
- vs. parathyroid gland, 225–226
- 41 weeks gestation, 262, 264–265
- at 19 weeks gestation, 262–263

Lymphopoiesis, 279–280

M

Mammary gland

- development stages, 347
- ducts
 - apocrine metaplasia, 358
 - appearance of, buds, 350, 351
 - atypical giant cells, interlobular stroma, 358
 - complex branching, 355

- early branching morphogenesis, 353
- exaggerated cystic change, 359
- near-term hyperplasia, early regression, 358
- neonatal hyperplasia and secretion, 357
- neonatal regression, 359
- penetratoins, 352
- primary ducts, 356
- progressive branching morphogenesis, 354
- smooth muscle, specialized mesenchyme, 351

embryology, 347–348

histology, 348–350

mammary band, 347

mammary crest, 347–348

nipple, 16 weeks gestation, 348, 349

witches' milk, 347

Medulla

- adrenal gland, 208–209
- kidney, 106–108, 114–115
- thymus gland, 248

Medullary canal, 329

Megakaryopoiesis, 279

Membranous ossification, 336

Membranous septum, 4

Mesenteric lymph nodes, 262–264

Mesonephric ducts, 96–97, 102, 103

Mesonephric remnants duct, 180

Mesonephros ducts, 96–97

Metacarpal bone ossification, 324, 325

Monochorionic diamniotic twins, 385

Monopoiesis, 277

Mucosa, 40

Müllerian ducts, 102, 103

Multiple gestations, 385–386

Muscle development

- early histogenesis, 338–339
- fetal, 339–342
- postnatal, 342

Muscle spindles, 343–344

Muscularis propria, 40, 119–120

Myelination, 288

Myelopoiesis

- dyserythropoiesis, 278–279
- erythropoiesis, 278
- granulopoiesis, 277
- hematogones, 279–280
- lymphopoiesis, 279–280
- megakaryopoiesis, 279
- monopoiesis, 277

Myocardium, 6–8

Myometrium, 189, 190

N

Nephrogenesis, 105, 108, 111–112

Nephron

- diagrammatic fate map of, 106
- at eighth week, 107

Nesidioblastosis, 79, 83

Neural tube, 288

Nodular splenic heterotopia, 84, 85

Nucleated red blood cells (NRBC), 379

O

Oogonia, 174
Osteoblasts, 332
Osteoclasts, 333
Osteocytes, 333
Osteoprogenitor cells, 332
Ostium primum, 3
Ostium secundum, 3
Ovary
 embryology
 central zone and peripheral zone, 173–174
 7th week postfertilization, 173
 8th week postfertilization, 174
 follicular atresia, 179
 folliculogenesis
 follicles, maturational stages, 28 weeks gestation, 177
 Graafian follicle, 32 weeks gestation, 178
 primary follicles, 30 weeks gestation, 177
 primordial follicles, 28 weeks gestation, 177
 secondary or preantral follicles
 32 weeks gestation, 177
 38 weeks gestation, 178
 tertiary or antral follicles, 38 weeks gestation, 178
 hilus cells, 35 weeks gestation, 179
 histology
 oocytes and follicles, 24 weeks gestation, 176
 oogonia, 16 weeks gestation, 176
 stroma, 19 and 35 weeks gestation, 175
 surface epithelium, 21 weeks gestation, 174
 tunica albuginea (TA), 28 weeks gestation, 175
 19 weeks gestation, 174
 mesonephric duct remnants, 19 weeks gestation, 180
 rete ovarii, 180

P

Palatine tonsil
 embryology, 267
 histology, 267–270
 with intraepithelial lymphocytes, 268, 270
 location of, 267
 at term, 268, 270
 at 16 weeks gestation, 267, 268
 at 17 weeks gestation, 267–269
 at 21 weeks gestation, 267, 269
 at 27 weeks gestation, 267, 269–270
Pancreas
 embryology, 79–80
 histology
 endocrine pancreas, 82–84
 exocrine pancreas, 80–81
 hematopoiesis, 84
 lymphoid tissue, 84
 nodular splenic heterotopia, 84, 85
 pancreatic stroma, 80
 small bowel pancreatic heterotopia, 84, 85
Papillary muscles, 10
Parafollicular C cells
 fetal thyroid gland, close-up view, 222
 lateral lobe, thyroid gland, 222

Parathyroid gland
 embryology, 225
 histology
 ectopic, undescended thymic lobule, 229
 vs. lymph node, 225–226
 term gestation, 228
 at 18 weeks gestation, 227
 at 24 weeks gestation, 227
 at 34 weeks gestation, 228
 at 39 weeks gestation, 228
 vs. lymph node, 225–226
Paraxial mesoderm, 323
Pericardium, 5
Perimysium, 343
Periosteum, 328
Perivillous fibrin, 379
Pituicytes, 237
Pituitary gland
 anterior
 ACTH, 234
 histological feature of, 234
 Rathke cleft cyst, 234, 236
 at 26 weeks gestation, 234, 235
 at 35 weeks gestation, 234–236
 embryology, 231–232
 histology, 232–237
 posterior, 237
Placenta
 anatomy of, 366
 basal plate
 components of, from intervillous space to endometrium, 376
 layers, 375
 at term, 375–378
 14 weeks gestation, 377
 at 23 weeks gestation, 377
 chorionic plate, 373–374
 definition, 363
 dichorionic dividing membrane, 386
 embryology
 amnionic and chorionic cavities, formation of, 364–365
 early placental development, 363, 364
 villous development, 364, 365
 extraplacental membranes
 decidua parietalis, 367–368
 reactive amnionic changes, 366, 368
 at term, 366, 367
 at 15 weeks gestation, 366, 367
 at 32 weeks gestation, 366, 367
 fetus papyraceous, 386–387
 histology, 366–385
 monochorionic dividing membrane, 386
 multiple gestations, 385–386
 twin dividing membranes, 385
 umbilical cord
 allantoic remnants, 369, 372
 arteries, 368, 370
 components of, 368
 vein and artery, at term, 371
 vitelline duct remnant, 369, 371–372

- at 16 weeks gestation, 369, 370
- at 24 weeks gestation, 369
- at 35 weeks gestation, 370
- at 36 weeks gestation, 369
- Wharton's jelly, 368, 369
- villous parenchyma
 - chorionic villi, 381, 383–384
 - gestational age, types and characteristics by, 380
 - mesenchymal villi, 378
 - nucleated red blood cells, 379
 - perivillous fibrin, 379
 - placental tissue, at 6 weeks, 380–381
 - placental villi, 381–385
 - stem villi, 378
 - syncytiotrophoblastic knots or syncytial knots, 379
 - terminal villi, 379
 - types and characteristics, 378, 379
 - yolk sac remnant, 387
- Posterior pituitary gland, 237
- Postnatal cerebellum, 318
- Preantral follicles, 176
- Primary follicles, 176
- Primordia, 347–348
- Primordial follicles, 176
- Prostate gland
 - embryology, 163
 - epithelial elements
 - ejaculatory ducts, 17 weeks gestation, 165
 - prostatic ducts, squamous metaplasia of, 166
 - prostatic utricle, verumontanum, 166
 - squamous metaplasia, prostatic urethra with, 166
 - verumontanum, 17 weeks gestation, 165
 - 17 weeks gestation, 165
 - 20 weeks gestation, 167
 - 24 weeks gestation, 167, 168
 - 29 weeks gestation, 168
 - 34 weeks gestation, 169
 - 39 weeks gestation, 169, 170
 - histology, 164
 - male genital system, accessory glands
 - prostatic utricle
 - purpose, 163
 - stromal elements, 170
 - 17 weeks gestation, 164
- Prostatic utricle, 163
- Pseudoglandular stage, 28–29
- Pulmonary acinus, 23, 24

R

- Radial glia, 287
- Rathke cleft cyst, 234, 236
- Rathke's pouch, 231
- Red pulp, in spleen, 260
- Renal lobe, 107
- Rete ovarii, 180
- Rete testis
 - 15 weeks gestation, 124
 - 26 weeks gestation, 131, 132
 - 39 weeks gestation, 133–134
 - 41 weeks gestation, 135

- Rostral neural crest cells, 41

S

- Saccular stage, 31–32
- Salivary glands
 - embryology, 87
 - submandibular gland, histology of
 - at 16 weeks, 88
 - at 19 weeks, 88, 89
 - at 23 weeks, 88, 89
 - at 27 weeks, 88, 90–91
 - at 35 weeks, 88, 91
 - at 41 weeks, 88, 92
- Secondary follicles, 176
- Seminal colliculus. *See* Verumontanum
- Seminal vesicle
 - appearance of, 157–158
 - embryology, 157
 - fetal development
 - 17 weeks gestation, 158
 - 24 weeks gestation, 159
 - 29 weeks gestation, 159–160
 - 34 weeks gestation, 160
 - 38 weeks gestation, 161
 - functions, 157
 - histology, 157–161
- Seminiferous tubule
 - definition, 121
 - 15 weeks gestation, 125
 - 17 weeks gestation, 126
 - 21 weeks gestation, 129
 - 26 weeks gestation, 131
 - 39 weeks gestation, 132, 133
 - 41 weeks gestation, 135
- Sertoli cells, 121
- Skeletal muscle
 - early histogenesis, 338–339
 - embryology, 337–338
 - fetal muscle development, 339–342
 - histology, 338–342
 - muscle spindles, 343–344
 - postnatal muscle development, 342
 - supporting framework, 343
- Small bowel pancreatic heterotopia, 84, 85
- Small intestine
 - Auerbach's plexus in, 57
 - Brunner's glands, 54–55, 58
 - duodenum, 54–55, 58
 - gut-associated lymphoid tissue in, 57
 - intracytoplasmic hyaline globules, 55
 - less than 14 weeks, 52–53
 - 14 to 30 weeks, 54–57
 - 30 to 40 weeks, 58
- Solid cell nests. *See* Ultimobranchial body remnants
- Somitic mesoderm, 323
- Spermatid duct. *See* Vas deferens
- Spinal cord. *See also* Central nervous system (CNS)
 - in first trimester, 290
 - at 14 weeks, 292
 - at 19 weeks, 295

- at 20 weeks, 299
 - at 22 weeks, 299
 - at 25 weeks, 303
 - at 30 weeks, 307
 - at 35 weeks, 312–313
 - 2 years postnatal, 319
 - Spleen
 - accessory, 260
 - capsule, 251
 - embryology, 251
 - and hematopoiesis, 260
 - histology of, 251–260
 - postnatal, 259
 - red pulp, 260
 - at term, 259–260
 - vascular tree, 252
 - at 16 weeks gestation, 252, 254
 - at 21 weeks gestation, 255
 - at 23 weeks gestation, 256
 - at 24 weeks gestation, 256
 - at 32 weeks gestation, 257
 - at 35 weeks gestation, 258–259
 - white pulp
 - follicular dendritic cells, 252, 253
 - splenic lymphoid and sinus development, 252, 253
 - splenic marginal zone, 253
 - T-and B-lymphocytes, 252, 255–256
 - Squamous cells, intrapulmonary, 34–35
 - Stem villi, 373, 374, 378–380
 - Stomach
 - esophago-gastric junction, 48
 - gastric cardiac mucosa, 49
 - gastric pyloric mucosa, 51
 - at 12 weeks, 49
 - at 24 weeks, 49
 - at 35 weeks, 51
 - less than 14 weeks, 47–49
 - muscularis propria, 47, 49
 - oxyntic mucosa, 51
 - 14 to 30 weeks, 49–50
 - 30 to 40 weeks, 51
 - Stress involution, thymus gland, 249–250
 - Stroma, thyroid gland, 222
 - Submandibular gland
 - at 16 weeks, 88
 - at 19 weeks, 88, 89
 - at 23 weeks, 88, 89
 - at 27 weeks, 88, 90–91
 - at 35 weeks, 88, 91
 - at 41 weeks, 88, 92
 - Submucosa, 40
 - Subserosa, 40
 - Sulcal development, 287
 - Syncytial knots. *See* Syncytiotrophoblastic knots
 - Syncytiotrophoblastic knots, 379
- T**
- Terminal villi, 379
 - Tertiary follicles, 176
 - Testicular embryonic remnants, 140
 - Testis
 - adrenal cortical rests, 139
 - embryology
 - primordial germ cells, maturation process, 122
 - seminiferous tubules, 121
 - tunica albuginea, 122
 - embryonic remnants, 140
 - histology
 - capsule layers, 123
 - fetal Leydig cells maturation, 123
 - fetal Leydig cells regression and dedifferentiation, 128
 - germ cells maturation, 122, 127–128
 - gonocytes fetal spermatogonia transformation, 10–13
 - mini puberty, 135–136
 - rete testis, 15 weeks gestation, 124
 - 20 to 40 weeks postmenstrual age, 128–135
 - 15 weeks gestation, 123–125
 - 17 weeks gestation, 125–126
 - 21 weeks gestation, 129
 - 23 weeks gestation, 129–130
 - 26 weeks gestation, 130, 131
 - 39 weeks gestation, 132, 133
 - 41 weeks gestation, 134, 135
 - 26 weeks gestation, rete testis, 131, 132
 - 39 weeks gestation, rete testis, 133–134
 - 41 weeks gestation, rete testis, 135
 - mesonephric remnants
 - cystic, sessile appendix epididymis, 138
 - embryonic rests, 139
 - solid, pedunculated appendix epididymis, 138
 - surface epithelium appendix epididymis, 139
 - paramesonephric remnants, 137
 - Thalamus, 294, 297
 - Thymic medulla, 248
 - Thymus gland
 - architecture, 241–242
 - capsule and connective tissue trabeculae, 242–243
 - cortex
 - architecture and histological appearance, 244, 245
 - extramedullary hematopoiesis, 247
 - lymphocytes in, 244, 246–247
 - staining of, 244, 246
 - tingible body macrophages, 247
 - embryology, 241
 - histology, 241–248
 - medulla, 248
 - stress involution of, 249–250
 - thymic tissue, in ectopic sites, 249
 - Thyroid follicles
 - cuboidal epithelial cells, 215
 - at term, 221
 - at 15 weeks gestation, 216
 - at 18 weeks gestation, 217
 - at 21 weeks gestation, 218
 - at 26 weeks gestation, 219
 - at 34 weeks gestation, 220
 - Thyroid gland
 - embryology, 213

functional components
 parafollicular C cells, 221–222
 stroma, 222
 thyroid follicles, 215–221
histology
 fetal neck organs, 214
 fetal/neonatal thyroid gland, 215
intrathyroidal inclusions, 223
ultimobranial body remnants, 223
Trilineage hematopoiesis, 276

U

Ultimobranial body remnants, 223

Umbilical cord

 allantoic remnants, 369, 372
 arteries, 368, 370
 components of, 368
 vein and artery at term, 371
 vitelline duct remnant, 369, 371–372
 at 16 weeks gestation, 369, 370
 at 24 weeks gestation, 369
 at 35 weeks gestation, 370
 at 36 weeks gestation, 369
 Wharton's jelly, 368, 369

Umbilical vein, 17

Urinary bladder

 adventitia, 118, 119
 bladder wall, 118
 embryology, 117–118
 histology, 118
 lamina propria, 118, 119
 muscularis propria, 119–120
 urothelium, 118, 119
 vesico-urethral canal, 117

Urogenital union, 144

Urothelium, 118, 119

Uterine cervix

 at 23 weeks, 192
 at 24 weeks, 192
 at 32 weeks, 192, 193
 at 35 weeks, 193
 at 37 weeks, 193
 at 38 weeks, 193

Uterine corpus

 18 days after birth, 191
 endometrium
 at 28 and 32 weeks, 190
 at 21 weeks, 190
 at 35 weeks, 191
 eosinophilic cytoplasm, 191
 myometrium, 189, 190
 at 19 weeks, 188
 at 21 weeks, 189
 at 35 weeks, 191
 at 38 weeks, 191

Uterus

embryology, 187
histology
 uterine cervix, 192–193
 uterine corpus, 188–191
 at 19 weeks, 188

V

Vagina

 embryology, 195
 histology
 at 18 days, postnatal life, 198
 at 23 weeks, 197
 at 25 weeks, 197
 at 32 weeks, 197, 198
 at 18 weeks gestation, 196
 layers, 195
 Valve leaflets and cusps, fetal, 10–13
 Vascular tree, of spleen, 252
 Vas deferens
 embryology, 153
 histology, 153–154
 ampulla, 34 weeks gestation, 156
 at 17 and 20 weeks gestation, 154
 at 24 and 29 weeks gestation, 154
 at 34 weeks gestation, 155
 at 38 weeks gestation, 155

Verumontanum, 164

Vesico-urethral canal, 117

Villous parenchyma

 chorionic villi, 381, 383–384
 by gestational age, 380
 mesenchymal villi, 378
 nucleated red blood cells, 379
 perivillous fibrin, 379
 placental tissue, at 6 weeks, 380–381
 placental villi, 381–385
 stem villi, 378
 syncytiotrophoblastic knots or syncytial knots, 379
 terminal villi, 379
 types and characteristics, 378, 379
 Visceral pericardium. *See* Epicardium
 Visceral pleura, 23

W

Wharton's jelly, 368, 369

White matter

 cerebral cortex, 308–310
 myelination gliosis in, 288
 at term, 313, 314
 at 34 to 38 weeks, 308
 at 25 weeks, 300–301
 at 2 years postnatal, 316, 317
Woven bone, 331

Y

Yolk sac remnant, 387